ISSN 2039-6651
anno 2019 numero 49

MISCELLANEA INGV

15th International Conference on Gas Geochemistry- ICGG15

ISTITUTO NAZIONALE DI GEOFISICA E VULCANOLOGIA

49

REGISTRAZIONE AL TRIBUNALE DI ROMA N.174 | 2014, 23 LUGLIO

Rappresentante legale: Carlo DOGLIONI
Sede: Via di Vigna Murata, 605 | Roma

ISTITUTO NAZIONALE DI GEOFISICA E VULCANOLOGIA

ISSN 2039-6651
anno **2019** numero **49**

MISCELLANEA INGV

15th International Conference on Gas Geochemistry- ICGG15

Editors: Francesco Italiano[1], Cinzia G. Caruso[1], Rossella Celi[2]

[1]INGV | Istituto Nazionale di Geofisica e Vulcanologia, Sezione di Palermo
[2]INGV | Istituto Nazionale di Geofisica e Vulcanologia, Amministrazione Centrale

Accepted *8 August 2019* | Accettato 8 agosto 2019

How to cite | Come citare AA. VV., (2019). 15th International Conference on Gas Geochemistry- ICGG15, Palermo & Milazzo, 30 September - 5 October 2019. Edited by F. Italiano, C.G. Caruso, R. Celi. Misc. INGV, 49: 1-338.

Cover | In copertina Sicily map (by Barbara Angioni)

49

INTERNATIONAL CONFERENCE ON GAS GEOCHEMISTRY 2019

Organized by

ISTITUTO NAZIONALE DI GEOFISICA E VULCANOLOGIA

Under the patronage of

UNESCO – Organizzazione delle Nazioni Unite per l'Educazione, la Scienza e la Cultura

Con il patrocinio della Commissione Nazionale Italiana per l'UNESCO

REGIONE SICILIANA

ARS

Comune di Milazzo

emso ERIC

EPOS ERIC

KM3NeT

Sponsorship

HIDEN ANALYTICAL

ThermoFisher SCIENTIFIC

SRA INSTRUMENTS ANALYTICAL SOLUTIONS

delisa Soluzioni per P.A.L. e Sanità

Ordine Regionale Geologi Sicilia

ISTITUTO ISTRUZIONE SUPERIORE RENATO GUTTUSO MILAZZO

ITET LEONARDO DAVINCI MILAZZO

SARAD

icgg15.pa.ingv.it/

+39 0916809281

icgg15@ingv.it

Palermo INGV headquarters
Lat 38°9'54.41"N | Long 13°18'34.43"E

Milazzo Castle
Lat 38°13'48.61"N | Long 15°14'31.46"E

Graphics: barbara.angioni@ingv.it

Organizer

Francesco Italiano	INGV

Local Organizing Committee

Cinzia Giuseppina Caruso	INGV
Felicia Rita Corsale	INGV
Alessandro Gattuso	INGV
Gianluca Lazzaro	INGV
Sergio Scirè Scappuzzo	INGV

Local Scientific committee

Antonio Caracausi	INGV
Walter D'Alessandro	INGV
Fausto Grassa	INGV
Marcello Liotta	INGV
Manfredi Longo	INGV
Marco Liuzzo	INGV
Antonio Paonita	INGV
Andrea Rizzo	INGV

International Scientific Committee

Calin Baciu	Romania
Stanley Chałupnik	Poland
Giuseppe Etiope	Italy
Chin Chou Fu	Taiwan
Jens Heinicke	Germany
Francesco Italiano	Italy
Antoine Kies	Luxembourg
Giovanni Martinelli	Italy
Bernard Marty	France
George Papatheodorou	Greece
Nemesio Pérez	Spain
Singh, S.	India
Andrzej Solecki	Poland
Hajimu Tamura	Japan
Yuri Taran	Mexico
Wang, Y. P.	China
Heiko Woith	Germany
Galip Yuce	Turkey

With the collaboration of

Filippo Altavilla	INGV
Roberta Barresi	INGV
Gabriella Busalacchi	INGV
Paolo Cosenza	INGV
Concetta Felli	INGV
Francesca Leone	INGV
Andrea Mastrolia	INGV
Giuseppe Messina	INGV
Isabella Munda	INGV
Margherita Nuccio	INGV
Sergio Simone Scirè Scappuzzo	INGV
Alessandra Vaianella	INGV

INDEX

ST01

GASES IN VOLCANIC AND GEOTHERMAL SYSTEMS

REFERENCE: ANTONIO PAONITA

Heat and Helium-3 Fluxes from Fogo volcano, Cape Verde

Alonso M.[1,5], Padrón E.[1,2,3], Hernández P.A.[1,2,3], Sumino H.[4], Pérez N.M.[1,2,3], Dionis S.M.[2,6], Melián G.V.[1,2,3], Fernandes P.[7], Padilla G.[1,2], Rodríguez F.[2], Asensio-Ramos M.[2], Silva S.[7], Albertos V.T.[2], Amonte C.[2], Pereira J.M.[8] and Recio G.[2]

[1]*Instituto Tecnológico y de Energías Renovables (ITER), Tenerife*
[2]*Instituto Volcanológico de Canarias (INVOLCAN), Tenerife*
[3]*Agencia Insular de la Energía de Tenerife (AIET), Tenerife*
[4]*The University of Tokyo, Department of Basic Science, Graduate School of Arts and Sciences, Japan*
[5]*Universidad Complutense de Madrid (UCM), Madrid, Spain*
[6]*Instituto Tecnológico de Canarias (ITC), Tenerife*
[7]*Universidade de Cabo Verde (UNICV), Santiago, Cape Verde*
[8]*Laboratório de Engenharia Civil (LEC) de Cabo Verde, Santiago Island, Cape Verde*

Corresponding Author: *mar@iter.es*

Earth's mantle is an important reservoir of compounds that are in a gaseous state, captured during the accretion of the planet and accumulated later through nuclear reactions and recycled from the surface [Alonso et. al., 2019]. The main pathway of mantle degassing thorough volcanic activity is accompanied by an important amount of heat flow transported to the surface by means of advective and diffusive mechanisms. In continental terranes, high temperature geothermal reservoirs acquire heat either from active or recently active magmatic systems or by deep fluid circulation in regions with elevated thermal gradients [Kennedy et al., 2000]. The measurement of the total thermal energy flux through the surface in volcanic areas is used to determinate changes in the magmatic activity and detecting changes in the energy balance of the volcanic system as a result of magmatic and tectonic processes [Dionis et al., 2015; Fridriksson et al., 2006; Hernández et al., 2012]. Accurate measurements of both heat and gas fluxes from active volcanoes contributes to a better understanding of the mantle-atmosphere link [Alonso et. al., 2019]. In this study we present the first estimation of heat and helium-3 fluxes from Pico do Fogo volcano in Cape Verde.

Helium (He) is considered an excellent geochemical indicator because it is chemically inert, physically stable, barely soluble in water under environmental conditions and practically non-adsorbable. He has two isotopes that occur naturally, ^{3}He and ^{4}He, with an atmospheric ratio $^{3}He/^{4}He = 1.384 \times 10^{-6}$ [Clarke et. al., 1976]. ^{4}He is produced as alpha particles during the radioactive decay of ^{238}U, ^{235}U and ^{232}Th, while ^{3}He is primordial He caught during the formation of the Earth. $^{3}He/^{4}He$ ratio varies from 10^{-8} in continental regions up to 10^{-5} in mantle-derived lavas [Graham, 2002]. Heat transport from the Earth interior to the surface is closely related to the mantle fluids ascent, and thus to the ^{3}He emission [Torgersen and Jenkins, 1982; Kennedy et al., 2000]. The measurement of that heat flux trough the surface is used to determinate changes in the energy balance of the volcanic system as well as in volcano monitoring [Hernández et al., 1998; Marrero Díaz et al., 2015; Padrón et al., 2012; 2013].
Cape Verde archipelago belongs to the Macaronesia and was generated by a mantle plume under the moving oceanic plate [Holm et al., 2008]. Fogo Island (476 km^2) is located in the Sotavento (leeward) alignment, in the southwest of the Cabo Verde archipelago. Its characterized by a 9 km-north-to-south caldera delimited by a vertical rim walls rising 1,000 m. from the bottom of the caldera (Cha

das Caldeiras), where Pico do Fogo (2,829 m.a.s.l.) is hosted. Pico do Fogo is one of the world's most active volcanoes with about 27 eruptions since its discovery in ~1500 A.D., with the last in 2014-2015 period [Worsley, 2015]. Volcanic activity since 1785 migrated from the summit crater to the lower flanks of the edifice creating secondary cones [Worsley, 2015], but remaining high temperature fumaroles and intense diffuse degassing inside the main crater. As it has been shown during several years by lot of authors, volcanic eruptions are frequently preceded by variations in the chemical composition of fluids from fumaroles and diffuse degassing, both increasing or decreasing in unrest and quiescence periods.

Since 1999, several geochemical surveys have been performed at Pico do Fogo main crater in order to strength the volcano monitoring program. About 63 measurements are performed at each survey covering an area of 0.142 km^2, with an average distance between points of 30 m. Surveys include also sampling of fumarolic discharges with temperature up to 200°C. At each sampling point, diffuse CO_2 measurements are conducted following the accumulation chamber method [Parkinson 1981], and soil and atmospheric temperatures are determined by means of a type-K thermocouple. Soil gas is collected in 20 cc glass vials inserting a 50 cm stainless probe 40 cm depth into the ground connected to a hypodermic syringe. ^4He is analysed with a quadrupole mass spectrometer and ^4He flux is determined combining diffusive and advective emission values following Fick's and Darcy's laws, respectively. ^3He and heat fluxes are determined following the methods described by Alonso et al., [2019] and Dawson, [1964], respectively. Sequential Gaussian Simulations are used to construct spatial distribution maps allowing us to interpolate unsampled areas and to calculate the uncertainty of the emissions. Fumarolic gas samples have been collected in a pre-evacuated glass flask filled with 50 ml of KOH 4N and CO_2/H_2O molar ratio analyzed by titration following the method described by Giggenbach and Goguel, [1989]. Lead-glass containers were filled with fumarolic gas discharge for helium isotopes analysis. Helium concentration and $^3He/^4He$ isotopic ratios are expressed as $R_A = R/R_{air}$, where R is the measured $^3He/^4He$ ratio and R_{air} is that of the air; 1.384×10^{-6} [Clarke et al., 1976] were analyzed using a high-precision noble gas mass spectrometer (modified-VG5400), following the procedure of Sumino et al. [Sumino et al., 2001]. The correction factor for the helium isotope ratio was determined by measurements of inter-laboratory helium standard named HESJ, with an established $^3He/^4He$ value of $20.63 \pm 0.10R_A$ [Mishima et al., 2002]. The analytical error for R_A was <2%. The measured $^3He/^4He$ ratios were corrected for air contamination based on the $^4He/^{20}Ne$ ratios measured with the mass spectrometer, assuming that all the neon has an atmospheric origin [Sano et al., 1985; Craig and Lupton, 1976].

^3He/heat ratios for Fogo volcanic system ranged between $3.32x10^{-11}$ and $5.13x10^{-10}$ cm^3 STP J^{-1}, with an average value of $2.24x10^{-10}$ cm^3 STP J^{-1} during the period of study [Table 1]. These values are higher than the calculated by Alonso et al., [2019] for Teide volcanic system ($0.37x10^{-12}$ cm^3 STP J^{-1}) and much higher than the value calculated by Elderfield and Schultz, [1996] for hydrothermal activity associated with hot spots from the lower and upper mantle, respectively ($24x10^{-12}$ and $0.5x10^{-12}$ cm^3 STP J^{-1}, respectively). In the temporal evolution of ^3He/heat relationship (Figure 1) it can be seen a significant increase of the parameters, close to the onset of 2014-2015 eruption pointing out the magma uprise to the surface. During the 8 years of geochemical monitoring at the summit crater of Pico do Fogo, two pulses in the diffuse CO_2 emission were observed, first one on November 2008 - February 2010 and a second one on March - August 2014, with maximum values of 339 and 337 t d^{-1}, respectively. The first anomalous period was characterized by a sharp increase on diffuse CO_2 emission, suggesting the first magma intrusion beneath Pico do Fogo volcano. This observation is also supported by a significant change on the $\delta^{13}C$-CO_2 signature from May 2009 (-10.2‰) to February 2010 (-6.1‰) of the diffuse CO_2 degassing, indicating an enrichment on the magmatic CO_2 component. On February 2010, the diffuse CO_2 emission rate was 219 ± 36 t d^{-1} [Dionis et al., 2015].

The second anomalous period started on March 2014, eight months before the 2014-15 Fogo eruption onset, and reached a relatively high value of 337 ± 119 t d^{-1} on August 30, 2014. It was likely caused by rising of magmatic gases from a second magma intrusion which ended on an eruption [Pérez et al., 2015]. ^{3}He/heat ratios for Fogo show a similar behaviour than the observed changes on the diffuse CO_2 emission rate and δ^{13}C-CO_2. These geochemical and geophysical evidences are clearly precursory signals of the 2014-15 Fogo eruption and evidence that this ratio is a powerful tool to monitor changes in the magmatic activity and in the energy balance of volcanic systems to strength volcano monitoring programs.

Table 1 Calculated ^{3}He and Heat fluxes for different surveys during the study period.

Date	^{3}He (mol y^{-1})	Heat Flux (MW)	^{3}He/Heat (cm^3 J^{-1})
Nov-2018	1.24	36	3.32 x 10-11
Mar-2014	3.25	16	5.13 x 10^{-10}
Oct-2013	0.83	4	1.35 x 10^{-10}
Abr-2013	1.22	10	1.15 x 10^{-10}
Feb-2012	0.63	7	4.40 x 10^{-11}
Dic-2010	1.27	4	3.15 x 10^{-10}
Feb-2010	2.35	10.3*	4.17 x 10^{-10}

*[Dionis et. al., 2015]

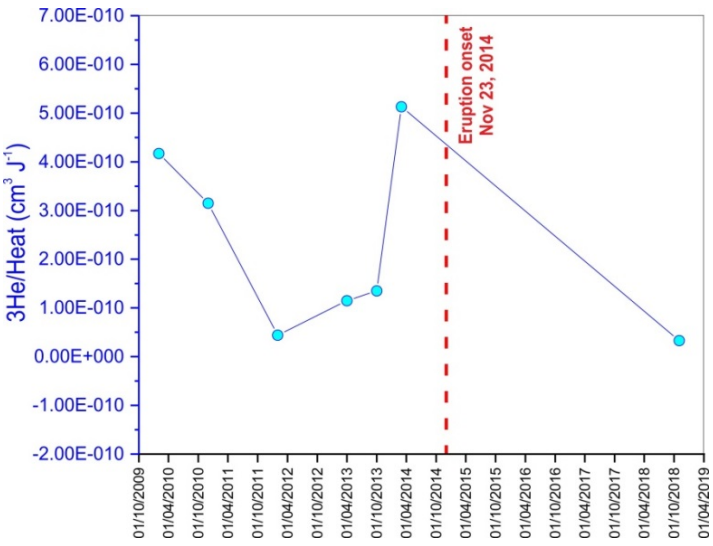

Figure 1 Temporal evolution of ^{3}He/Heat relationship from 2010 to 2018 for Pico do Fogo.

References

Alonso M., Padrón E., Sumino H., Hernández P.A., Melián G.V., Asensio-Ramos M., Rodríguez F., Padilla G., García-Merino M. Amonte C. and Pérez N.M., (2019). *Heat and Helium-3 fluxes from Teide Volcano, Canary Islands, Spain*. Geofluids. doi.org/10.1155/2019/3983864.

Clarke W.B., Jenkins W.J. and Top Z., (1976). *Determination of tritium by mass spectrometric measurement of ^{3}He.* International Journal of Applied Radiation and Isotopes, 27, 9, 515-522. doi.org/10.1016/0020-708X(76)90082-X.

Craig H. and Lupton J.E., (1976). *Primordial neon, helium and hydrogen in oceanic basalts*. Earth and Planetary Science Letters, 31(3), 369-385.

Dawson G.B., (1964). *The nature and assessment of heat flow from hydrothermal areas, New Zealand*. Journal of Geology and Geophysics, 7(1), 155-171.doi.org/10.1080/00288306.1964.10420167.

Dionis S.M., Melián G., Rodríguez F. Hernández P.A., Padrón E., Pérez N.M., Barrancos J., Padilla G., Sumino H., Fernandes P., Bandomo Z., Silva S., Pereira J.M. and Semedo H., (2015). *Diffuse volcanic gas emission and thermal energy release from the summit crater of Pico do Fogo, Cape Verde*. Bulletin of Volcanology, doi.org/10.1007/s00445-014-0897-4.

Elderfield H. and Schultz A., (1996). *Mid-ocean ridge hydrothermal fluxes and the chemical composition of the ocean*. Annual Review of Earth and Planetary Sciences. 24(1), 191-224.

Fridriksson T., Kristjánsson B.R., Ármannsson H., Margrétardóttir E., Ólafsdóttir S. and Chiodini G., (2006). *CO_2 emissions and heat flow through soil, fumaroles and steam heated mud pools at the Reykjanes geothermal area, SW Iceland*. Applied Geochemistry, 21(9), 1551-1569.

Giggenbach W.F. and Goguel R.L., (1989). *Collection and Analysis of Geothermal and Volcanic Water and Gas Discharges*. 4th Edition. Petone, New Zealand: Department of Scientific and Industrial Research, Chemistry Division. Report No.: CD 2401.

Graham D.W., (2002). *Noble gas isotope geochemistry of mid-ocean ridge and ocean island basalts: characterization of mantle source reservoirs*. Reviews in Mineralogy and Geochemistry, 47 (1), 247-317.

Hernández P.A., Pérez N.M., Salazar J.M.L., Notsu K. and Wakita H., (1998). *Diffuse emission of carbon dioxide, methane, and helium-3 from Teide volcano, Tenerife, Canary Islands*. Geophysical Research Letters, 25, 3311-3314.

Hernández P.A., Pérez N.M., Fridriksson T., Egbert J., Ilyinskaya E., Thorhallsson A., Ivarsson G., Gislason G., Gunnarsson G., Padrón E., Melián G., Mori T. and Notsu K., (2012). *Diffuse volcanic degassing and thermal energy release from Hengill volcanic system, Iceland*. Bulletin of Volcanology, 74(10), 2435-2448. doi.org/10.1007/s00445-012-0673-2.

Holm P.M., Grandvuinet T., Friis J., Wilson R., Barker A.K., Plesner S., (2008). *An ^{40}Ar-^{39}Ar study of the Cape Verde hot spot: temporal evolution in a semi-stationary plate environment*. Journal of Geophysical Research, 113: B08201. doi: 08210.01029/02007JB005339.

Mack Kennedy B., Fischer T.P. and Shuster D.L., (2000). *Twenty-Fifth Workshop on Geothermal Reservoir Engineering*. Heat and Helium in Geothermal Systems, Stanford University, Stanford, California, January 24-26, 2000 SGP-TR-165.

Marrero-Diaz R., López D., Pérez N.M., Custodio E., Sumino H., Melián G.V., Padrón E., Hernández P.A., Calvo D., Barrancos J., Padilla G. and Sortino F., (2015). *Carbon dioxide and helium dissolved gases in groundwater at central Tenerife Island, Canary Islands: chemical and isotopic characterization*. Bulletin of Volcanology, 77(10). doi:10.1007/s00445-015-0969-0.

Mishima K., Sumino H., Yamada T., Ieki S., Nagakura N., Otono H., and Oide H., (2002). *Accurate determination of the absolute $^{3}He/^{4}He$ ratio of a synthesized helium standard gas (Helium Standard of Japan, HESJ): Towards revision of the atmospheric $^{3}He/^{4}He$ ratio*. Geochemistry, Geophysics, Geosystems, 36(2), 191-195. doi: 10.1029/2018GC007554.

Padrón E., Pérez N.M., Hernández P.A., Sumino H., Melián G., Barrancos J., Nolasco D. and Padilla G., (2012). *Helium emission at Cumbre Vieja volcano, La Palma, Canary Islands*. Chemical Geology, 312-313, 138-147. doi: 10.1016/j.chemgeo.2012.04.018.

Padrón E., Pérez N.M., Hernández P.A., Sumino H., Melián G.V., Barrancos J., Nolasco D., Padilla G., Dionis S., Rodríguez F., Hernández I., Calvo D., Peraza M.D. and Nagao K., (2013). *Diffusive helium emissions as a precursory sign of volcanic unrest*. Geology, 41(5), 539-542. doi:10.1130/G34027.1.

Pérez N.M., Dionis S., Fernandes P., Barrancos J., Rodríguez F., Bandomo Z., Hernández P.A., Melián G.V., Silva S., Padilla G., Padrón E., Cabral J., Calvo D., Asensio-Ramos M., Pereira J.M., Gonçalves A.A., Barros I. and Semedo H., (2015). *Precursory signals of the 2014-15 Fogo eruption (Cape Verde) detected by surface CO_2 emission and heat flow observations*. Geophysical Research Abstracts, Vol. 17, EGU2015-10644, 2015 EGU General Assembly 2015 © Author(s) 2015. CC Attribution 3.0 License.

Parkinson K.J., (1981). *An improved method for measuring soil respiration in the field*. Journal of Applied Ecology, 18, 1, 221-228.

Sano Y. and Wakita H., (1985). *Geographical distribution of $^3He/^4He$ ratios in Japan: implications for arc tectonics and incipient magmatism*. Journal of Geophysical Research, 90(B10), 8729-8741.

Sumino H., Nagao K., and Notsu K., (2001). *Highly sensitive and precise measurement of helium isotopes using a mass spectrometer with double collector system*. Journal of the Mass Spectrometry Society of Japan, 49(2), 61-68.

Torgersen T. and Jenkins W.J., (1982). *Helium isotopes in geothermal systems: Iceland, The Geysers, Raft River and Steamboat Springs*. Geochimica et Cosmochimica Acta, 46, 5, 739-748. doi.org/10.1016/0016-7037(82)90025-4.

Worsley P., (2015). *Physical geology of the Fogo volcano (Cape Verde Islands) and its 2014-2015 eruption*. Geology Today, 31(4), 153-159. doi: org/10.1111/gto.12102.

Thermal Changes on a mild thermal anomaly during explosive activity of Mt. Etna

Diliberto I.S., Gennaro E.

Istituto Nazionale di Geofisica e Vulcanologia, Sezione Palermo, Italy

Corresponding Author: *iole.diliberto@ingv.it*

Introduction

In a volcanic system, lava flows and explosive paroxysms are two episodic expressions of the energy deriving directly from the magma, while hot springs, fumaroles and volcanic clouds are diverse manifestations of the continuous impacts of magmatic heat release on the Earth's surface. During paroxysms, the magma is driven to the surface by the expansion of its gas phase and the surface thermal release is channeled by the eruptive conduits. Even during inter-eruptive periods, the gas phase is continuously spreading, released by diffuse outgassing of the volatile emanations around the volcanic edifice. The convective release emanating through the eruptive vents and fumaroles degrades towards diffuse degassing around the fumaroles and is dispersed along the active fractures. In this case the main variable directly related to changes of the diffuse heat release is the temperature gradient of the ground. A lot of robust monitoring devices are commercially available for direct measures of temperature, moreover the environmental conditions for diffuse degassing get these measures much more feasible, if compared to the thermal monitoring of fumaroles vents.

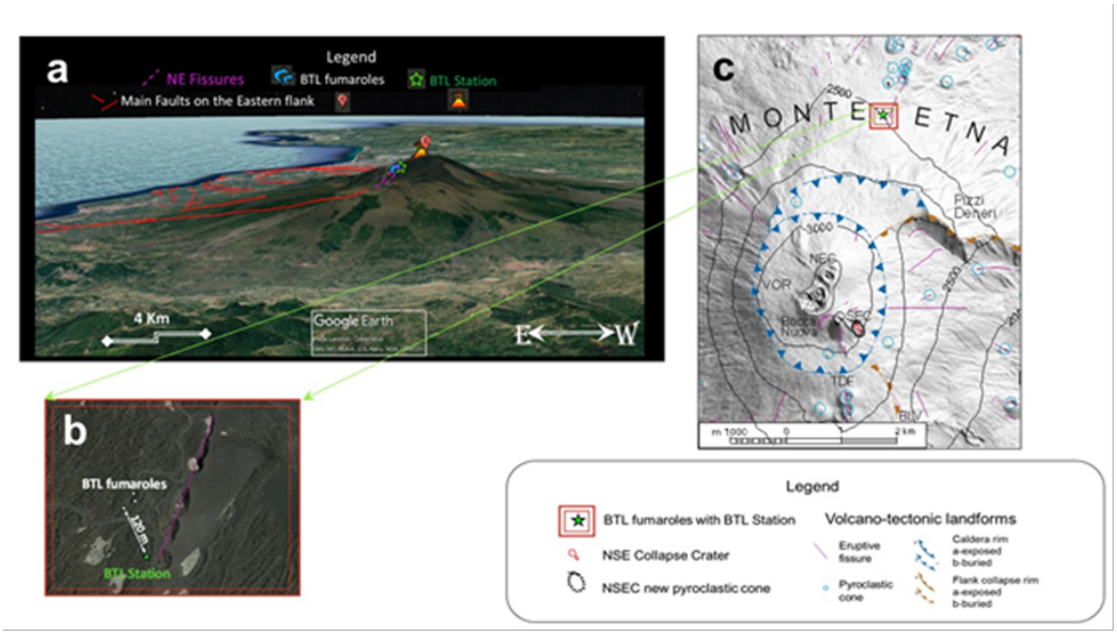

Figure 1 a) Detail of the satellite image (Landsat, Google Earth, June 2014) with the eruptive fracture locally named as the Bottoniera line b) Satellite view (Landsat, Google Earth, June 2017) of Mt. Etna volcano c) Digital elevation model of Mt. Etna volcano, showing the locations of the sites mentioned in the text and the main volcano - tectonic landforms. [Modified from Diliberto et al., 2018].

The problematic aspects with monitoring the diffuse emanations consist of (i) the length of the time series to be analyzed, (ii) the high resolution required for the accuracy of the measurement, and (iii) the time interval between two measurements. Regardless, both the volatile emanations and their associated thermal anomalies can be detected and monitored on the ground during any volcanic phase [Alparone et al., 2004; Cannata et al., 2010; Chiodini et al., 2001; D'Alessandro et al., 1997; Girona et al., 2018; Granieri et al., 2010; Epiard et al., 2017; Liotta et al., 2010; Liuzzo et al., 2013; Madonia et al., 2013; Mattia et al., 2015; Maucourant et al., 2014; Paonita et al., 2016; Tabbagh & Trezeguet, 1987].

The following discussion focuses on the hourly-recorded data from January to September 2012 in a mild thermal anomaly near the top of the North-East Rift of Mt. Etna, (2474 m a.s.l., Figure 1 a-c), which has been monitored for three years.

On the North-East Rift, the steam condensation depth has fluctuated with in the ground, from depths of a couple of meters to more than thirty meters. The purpose of this study is to explore the relationship between the hot fluid circulation dispersed through one of the main eruptive fractures of Mt. Etna, and the eruptive activity channeled at distance, through a different conduit. An outstanding feature of this paper is that we compare the results from two monitoring applications of the thermal release that have been working in the same interval at two different locations on Mt. Etna, one has been dispersed by the ground and the other has been channelized directly to the eruptive vents, during the last sustained lava fountains. The channelized heat release has been evaluated by Bombrun et al., [2016] during the explosive activity. Instead, the diffusive heat flux monitored at a particular site, namely the Bottoniera Line Station (BTL station, Figure 1 a-c) represents the residual heat, continuously stemmed by volatile emanations (vapor and gases of hydrothermal and/or magmatic origin) towards the NE Rift. Two different thermal variables, under very different local conditions, have both represented a part of the energy output linked to the main (magmatic) source.

We retain that the hot fluid circulation monitored by the low enthalpy fluid emanated at distance from the eruptive vents, could indicate transient conditions in the subsurface and possibly highlight the relationships among different causes of the time variations (volcanic and of external origin). The SHSFlux data from the BTL station of Mt. Etna is just one very local trace of the thermal effect of changing hot gas circulation below the North-East Rift system (hereafter "NE Rift").

References about the eruptive activity

In the last century, Mt. Etna erupted every 1.5 years on average (Mattia et al., 2015), offering considerable opportunities for experimental geochemical monitoring. Many transitions, from lava flow to strombolian activity to explosive paroxysms, have been observed in the eruptive activity (ref to INGV reports). Figure 1a shows the eastern flank of Mt. Etna, where many fault systems are present. According to Barreca et al., [2013], the relationship between the volcanic and seismic risk on this flank is particularly important to assess the local hazard. The NE Rift system, located on the northeastern flank of the volcano (Figure 1a, b), represents a network of north- northeast-striking eruptive fissures that have frequently erupted [e.g., in 1978, 1979, 2002; Alparone et al., 2004; Andronico et al., 2005]. Many aligned parasitic cones - known as the Bottoniera line (BTL) have been raised by the eruptive activity on the northern slope of Mt. Etna, with some of them being visible in Landsat images (Figure 1b. 1c). After 2002, a persistent hydrothermal activity has fed a low temperature fumarole area located at the top of the NE rift [Giammanco et al., 2016; Liotta et al., 2010]. From 2010 to 2012, Mt. Etna volcano showed a change in the eruptive style [e.g., Behncke et al., 2016; Bonnaccorso et Calvari, 2013; Cannata et al., 2010; Viccaro et al., 2014]. The explosive activity, associated with intense lava flows, began at the Southeast Crater (SEC) and on January 12,

2011, moved eastward on its flank (Figure 1c). It resulted in the building up of a new summit cone, named the New Southeast Crater [NSEC, Figure 1a, 1c; Behncke et al., 2016]. Many authors [e.g. Bonaccorso and Calvari, 2013; Calvari et al., 2018; Viccaro et al., 2014] have described the eruptions occurring during 2010-2012, underlining the difference compared to what was observed in previous decades. The main features of this last period have been the high rates of erupted lava and the high explosive activity, with energetic lava fountains. Viccaro et al., [2014] suggested that the principal site of structural conjunction between the active plumbing systems was an open-conduit system located at shallow levels (1-2 km a.s.l.) beneath the NEC. Both Viccaro et al., [2014] and Carbone et al., [2015] suggested the occurrence of magmatic fluids transfer from a reservoir shifted northeast relative to the conduit erupting in this period. Specifically, the volcanic activity occurred from 2009 to 2012 and so many available references raised the questions that guided our research: Could the thermal release diffused at the top of the NE Rift be influenced by the gas dynamics described by Viccaro et al., [2014]? How could the thermal monitoring data from a mild thermal anomaly augment the actual observation network? Is there any relation between the volatile emanations which are continuously spreading around the volcanic edifice and the paroxysms displayed from the eruptive conduits?

Monitoring Methods

Thermal monitoring of the steam heated soil (SHS)

The SHS is a permeable ground where low steam flux condenses inside the ground and the thermal anomaly reaching the surface zone is so low to be of difficult detection. Changes of external origin, like barometric perturbations, sun radiation and rainfall greatly influence the flux of volatiles. So external changes cannot be negliged and in some instances, they have been a specific object of study [e.g., Gaudin et al., 2015]. This SHS monitoring method evaluates the heat flux (SHSFlux data) from the diffuse degassing zone in a porous ground surrounding the low temperature fumaroles of the NE rift. SHS temperatures are measured at the BTL monitoring station (Figure 1c) and the SHS heat flux (SHSFlux) is evaluated using the SHS method developed by Aubert et al., [1999], which has already been described by different authors [e.g., Gaudin et al., 2015]. This method measures continuously the shallow vertical temperature profile in a zone of the SHS. The number of thermal sensors, depth of the monitored profile, and distance from fumaroles are closely dependent on the local conditions and the background thermal flux. Therefore, the BTL station was located at a marginal position with respect to the surface manifestation of steam advection. Following previous experiences at other monitoring stations, we recorded the temperature changes in porous ground (loose volcanic breccia) at a short distance (about 120 m, Figure 1b) from low-temperature fumarole vents and from the Bottoniera line of craters (“eruptive fissure”, Figure 1b, c). The total depth of the monitored profile was 0.60 m and we placed four sensors vertically in the ground at 0.15 m intervals. At the best condition, the monitored profile is almost dry (low humidity and absence of a liquid phase and steam) and the condensation zone of the steam ascending from the deep magmatic source stands at a short distance from the bottom of the monitored profile along the z-axis.

The instrumental system consisted of four PT1000 sensors (range -40°C to 150°C, accuracy ±0.2°C, resolution ±0.1°C) connected to data logger (model EBRO EBI 2T-313 four-channel stored in a watertight protector case. The temperature variations were recorded hourly for about three years and the stored data file was downloaded once, at the end of the monitoring period. The simple technology and the easy parametrization required for this monitoring method have low energy consumption and technical maintenance, which facilitated uninterrupted and long-term data acquisition. Therefore, we were able to avoid any widespread interpolation of missing data and rejected some low-quality data,

without losing information. We calculated the best linear fit with least squares methods and obtain the coefficient of determination or R2; for R2> 0.99 we assume a linear relationship between temperature and depth. To avoid estimation errors, from evaluations of SHSFlux we excluded the hourly temperature profiles showing a correlation coefficient lower than 0.99.

Radiative transfer from the explosive activity

Ground-based thermal cameras and radiometers are widely used to track plume emissions dynamics and characterize explosive eruptions [e.g., Harris, 2013; Spampinato et al., 2015]. A permanent radiometer station located in the Belvedere area (Figure 1c, BLV) recorded each fountain episode occurring on Mt. Etna, from the end of 2011 to February 2013. The radiometer registers the power radiated by a volcanic feature in terms of the difference detected in the field of view between the apparent temperature of hot surface and the apparent temperature of the background. Bombrun et al., [2016] analyzed the sequence of frames and evaluated the radiative thermal energy for each fountaining episode registered by the radiometer. We recommend those references for the technical description and a detailed explanation of the methodologies applied by the authors [Bombrun et al., 2016]. Among the various parameters, Bombrun et al., [2016] calculated the flux from the radiant surface captured by the radiometer during the emissions of gas and particles composing the hot clouds targeted by the optical sensor. The radiant flux, integrated through time for each lava fountain episode, resulted in the total radiant energy (TRE) value. In the discussion, the TRE values are compared to the time variations of SHSFlux, recorded during the same hours.

Discussion and Conclusions

Over three years (2010-2012), the range of diffuse heat from the ground, monitored on the NE Rift, varied in response to different perturbations. The record of ground temperatures tracked the vertical oscillations of the depth reached by the front of the vapor ascending to the top of the NE Rif (Figure 3), providing, at the same time, an easy evaluation of heat flux released by the steam heated soil (SHSFlux). Before April 2010, the front of the vapor ascending to the top of the NE Rift raised to shallow depths. The same front was stable during the eruptive period. Finally, tens of days before the end of the last active lava flow, we observed unstable conditions of the deepening convective front, and the depletion of diffused heat release, recorded by the BTL station. The time variations of SHSFlux from the ground partially depended on changes in atmospheric conditions (e.g., the seasonal modulation of air temperature; [Diliberto et al., 2018]), but they were also related to the changes of magma conditions in the shallow plumbing system (1-2 km a.s.l.), occurring in the monitoring period. A seasonal modulation resulting from cyclic variation of the solar radiation of the ground surface caused an inverse correlation between the SHSFlux and the air temperature. The long time series of hourly data, including the eruptive cycle, showed also that Near the Bottoniera line of craters (BTL station on the NE Rift), several peaks of SHSFlux occurred before and during the eruptive period, defining a wide range of SHSFlux values. In the last stage, after April 2012, we registered the lowest range of SHSFlux and the variations of external origin seem the main cause of variation of SHSFlux. Before and during the eruptive period the upper threshold's value was triplicated. Focusing on the last period of activity, the record of ground temperatures could have provided some precursory signals on the transient behavior of the volcanic system towards the standstill of the eruptive activity, regardless several sustained lava fountaining episodes were still characterizing the eruption stile of the NSEC. The thermal monitoring clearly shows that the power of the convective circulation on the NE Rift decreased several hours before the onset of the last lava fountains (the two most energetic paroxysms, TRE >5 x1010 J). The decrease of heat flux was irreversible after the end

of the eruption, and the backward of the convective front on the ground surface lasted throughout the following months. The diffuse heat released in the thermal site of the NE Rift appear in these cases inversely related to the heat release channeled through the NSEC during the major paroxysms. The short-term paroxysms considered in this paper are still too few to define significant correlations between the energy radiated by lava fountains from the NSEC and the SHSFlux diffused from a thermal spot located along another active Rift. Nonetheless, the new data acquired by SHSFlux monitoring could encourage the development of networks based on temperature monitoring to follow the state of active volcanoes. These in situ temperature measurements provide a wide set of direct data which, based on the high mobility of the volatile emanations, are able to track diffuse thermal effects on the ground surface throughout the different phases of activity (rest, lava flows, passive degassing, explosive activity). We conclude that time variations of SHSFlux from the ground partially depended on changes in atmospheric conditions (e.g., the seasonal modulation of air temperature showed by Diliberto et al., 2018), but they were also related to the changes of magma conditions in the shallow plumbing system (1-2 km a.s.l.), occurring in the monitoring period. Therefore, we suggest that thermal monitoring in the steam-heated grounds around fumaroles and volcanic vents could be a new systematic tool for volcanic surveillance, since the time-series analysis of these monitoring data could yield up-to-date information about a volcanic system, both before and during eruptions.

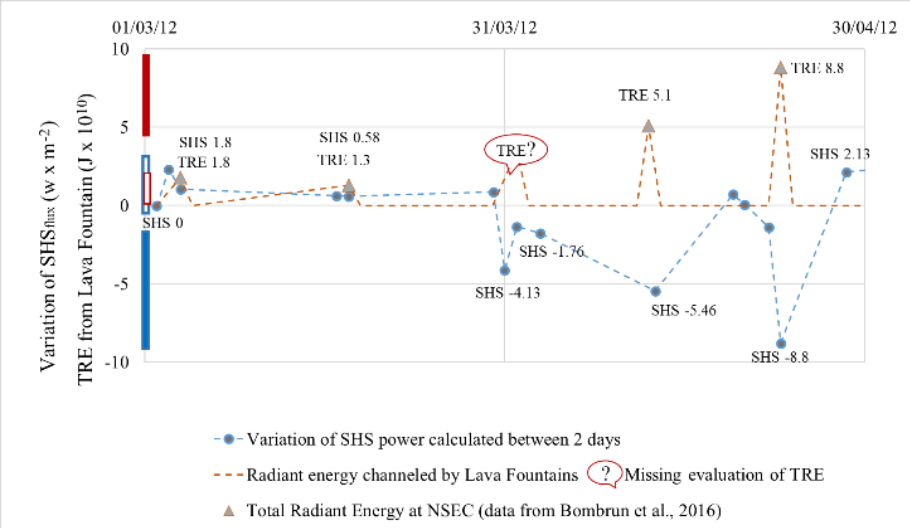

Figure 2 Day variations of SHSFlux recorded at the BTL station during the Lava Fountains (LFs) episodes and Total Radiant Energy of the lava fountains episodes as evaluated by Bombrun et al., [2016].

References

Andronico D., Branca S., Calvari S., Burton M., Caltabiano T., Corsaro R.A. et al., (2005). *A multi-disciplinary study of the 2002-03 Etna eruption: insights into a complex plumbing system.* Bull. Volcanol., 67, 314-330. doi: 10.1007/s00445-004-0372-8.

Aubert M., (1999). *Practical evaluation of steady heat discharge from dormant active volcanoes: case study of Vulcarolo fissure (Mount Etna, Italy).* Journal of Volcanology and Geothermal Research, 92, 413-429.

Barreca G., Bonforte A. and Neri M., (2013). *A pilot GIS database of active faults of Mt. Etna (Sicily): a tool for integrated hazard evaluation.* J. Volcanol. Geotherm. Res., 251,170-186. doi:

10.1016/j.jvolgeores.2012.08.013.

Behncke B., Branca S., Corsaro R.A., De Beni E., Miraglia L. and Proietti C., (2014). *The 2011-2012 summit activity of Mount Etna: birth, growth and products of the new SE crater*. J. Volcanol. Geotherm. Res., 270:10-21. doi: 10.1016/j.jvolgeores.2013.11.012.

Bombrun M., Spampinato L., Harris A., Barra V. and Caltabiano T., (2016). *On the transition from strombolian to fountaining activity: a thermal energy-based driver*. Bulletin of Volcanology, Volume 78, article id.15, 13 pp. doi: 10.1007/s00445-016-1009-4.

Bonaccorso A. and Calvari S., (2013). *Major effusive eruptions and recent lava fountains: Balance between expected and erupted magma volumes at Etna volcano*. G.R.L., 40, 6069-6073, doi: 10.1002/2013GL058291.

Calvari S., Cannavò F., Bonaccorso A., Spampinato L. and Pellegrino A.G., (2018). *Paroxysmal Explosions, Lava Fountains and Ash Plumes at Etna Volcano: Eruptive Processes and Hazard Implications*. Front. Earth Sci., 6:107. doi: 10.3389/feart.2018.00107.

Cannata A., Giudice G., Gurrieri S., Montalto P., Alparone S., Di Grazia G., Favara R., Gresta S. and Liuzzo M., (2010). *Relationship between soil CO_2 flux and volcanic tremor at Mt Etna: Implications for magma dynamics*. Environ. Earth Sci., 61, 477-489, doi:10.1007/s12665-009-0359-z.

Carbone D., Zuccarello L., Messina A., Scollo S. and Rymer H., (2015). *Balancing bulk gas accumulation and gas output before and during lava fountaining episodes at Mt. Etna*. Scientific Reports, 5:18049. doi: 10.1038/srep18049.

Chiodini G., Frondini F., Cardellini C., Granieri D., Marini L., Ventura G., (2001). *CO_2 degassing and energy release at Solfatara volcano, Campi Flegrei, Italy*. J. Geophys. Res. Solid Earth., 106(B8):16213-21.

D'Alessandro W., Giammanco S., Parello F. and Valenza M., (1997). *CO_2 output and δ13C (CO_2) from Mount Etna as indicators of degassing of shallow asthenosphere*. Bullettin. Volcanol., 58(6):455-458. https://doi.org/10.1007/s004450050154.

Diliberto I.S., Gagliano Candela E., Morici S., Pecoraino G., Bellomo S., Bitetto M. and Longo M., (2018). *Changes in heat released by hydrothermal circulation monitored during an eruptive cycle at Mt. Etna (Italy)*. Bulletin of Volcanology, 80 (31) https://doi.org/10.1007/s00445-018-1198-0.

Epiard M., Avard G., de Moor J.M., Martínez Cruz M., Barrantes Castillo G., Bakkar H., (2017). *Relationship between Diffuse CO_2 Degassing and Volcanic Activity. Case Study of the Poás, Irazú, and Turrialba Volcanoes, Costa Rica*. Front. Earth Sci., 5(October):1-14.

Giammanco S., Melián G., Neri M., Hernández P.A., Sortino F., Barrancos J., López M., Pecoraino G., Perez N.M., (2016). *Active tectonic features and structural dynamics of the summit area of Mt. Etna (Italy) revealed by soil CO_2 and soil temperature surveying* Journal of Volcanology and Geothermal Research, 311, 79-98.

Girona T., Realmuto V., (2018). *Satellite-based thermal precursors of volcanic eruptions*. Abstracts Volume of the International meeting "Cities on Volcanoes 10", 2-7 September 2018, Napoli, Italy, Miscellanea INGV, 43: 758.

Granieri D., Avino R., Chiodini G., (2010) *Carbon dioxide diffuse emission from the soil: Ten years of observations at Vesuvio and Campi Flegrei (Pozzuoli), and linkages with volcanic activity*. Bull. Volcanol., 72(1):103-18.

Harris A.J.L., (2013). *Thermal remote sensing of active volcanoes: a user's manual*. Cambridge University Press, doi: 10.1017CBO9781139029346.

Liotta M., Paonita A., Caracausi A., Martelli M., Rizzo A.L. and Favara R., (2010). *Hydrothermal processes governing the geochemistry of the crater fumaroles at Mount Etna volcano (Italy)*. Chem. Geol., 278:92-104 htpp//doi.org/10.1016/jchemgeo201009004.

Liuzzo M., Gurrieri S., Giudice G., Giuffrida G., (2013). *Ten years of soil CO_2 continuous monitoring on Mt. Etna: Exploring the relationship between processes of soil degassing and volcanic activity*. Geochem. Geophys. Geosyst., 14, doi:10.1002/ggge.20196.

Madonia P., Rizzo A., Diliberto I.S. and Favara R., (2013). *Continuous monitoring of fumarole temperatures at Mount Etna (Italy)*. Journal of Volcanology and Geothermal Research, 257, 12-20.

Mattia M., Bruno V., Caltabiano T., Cannata A., Cannavo F., D'Alessandro W., Di Grazia G., Federico C., Giammanco S., La Spina A., Liuzzo M., Longo M., Monaco C., Patanè D. and Salerno G., (2015). *A comprehensive interpretative model of slow slip events on Mt. Etna's eastern flank*. Geochem. Geophys. Geosyst., 16, 635-658, doi:10.1002/2014GC005585.

Maucourant S., Giammanco S., Greco F., Dorizon S. and Del Negro C., (2014). *Geophysical and geochemical methods applied to investigate fissure-related hydrothermal systems on the summit area of Mt. Etna volcano (Italy)*. Journal of Volcanology and Geothermal Research, 280, 111125 doi.org/10.1016/j.jvolgeores.2014.05.014.

Paonita A., Caracausi A., Martelli M., Rizzo A.L., (2016). *Temporal variations of helium isotopes in volcanic gases quantify pre-eruptive refill and pressurization in magma reservoirs: The Mount Etna case*. Geology, 44-7, 499-502, doi: 10.1130/G37807.1

Spampinato L., Sciotto M., Cannata A., Cannavò F. et al., (2015). *Multi-parametric study of the February - April 2013 paroxysmal phase of Mt. Etna. New South East Crater*. Geochemistry, Geophysics, Geosystems, doi: 10.1002/2015GC005795.

Tabbagh A. and Trezeguet D., (1987). *Determination of sensible heat flux in volcanic areas from ground temperature measurements along vertical profiles: the case study of Mount Etna Sicily, Italy*. J. Geophys. Res., 92, B5:3635-3644 https://doi.org/10.1029/JB092iB05p03635.

Viccaro M., Garozzo I., Cannata A., Di Grazia G. and Gresta S., (2014). *Gas burst vs. gas-rich magma recharge: A multidisciplinary study to reveal factors controlling triggering of the recent paroxysmal eruptions at Mt. Etna*. Journal of Volcanology and Geothermal Research, 278-279, 1-13.

C-He isotope signature of Larderello (Italy) geothermal gases

Gherardi F., Droghieri E. and Magro G.

Consiglio Nazionale delle Ricerche (CNR), Istituto di Geoscienze e Georisorse (IGG), Pisa, Italy

Corresponding Author: *f.gherardi@igg.cnr.it*

Introduction

The geothermal community is now facing the scientific and technological challenges of producing geothermal energy from very hot rocks, and finding/exploiting supercritical fluids. This increasing scientific interest is further boosted by a number of recent experiments and models for crustal permeability indicating that brittle-ductile transition is not a key factor control on permeability, and that potentially exploitable resources may occur up to temperatures in excess of 450 °C at depths up to 6 km b.g.l. [Watanabe et al., 2017].

At Larderello, granitic intrusions into a thinned continental crust act as the heat source for the regional thermal anomaly, and a major seismic reflector (K-horizon) extends all over the field at 3 to 6 km depth. The K-horizon is supposed to be the top of the brittle-ductile transition, and/or the top of one or more permeable reservoirs possibly containing high-P, supercritical fluids [Batini et al., 1978; 1985].

In this framework, on late 2017, a deep well was deepened at Larderello in the search of supercritical fluids (UE DESCRAMBLE project). An extremely high temperature of more than 500 °C was estimated at bottom hole, associated with a leak-off pressure of about 300 bar, though the existence of an exploitable reservoir was not proven [Bertani et al., 2018].

The fact that no relevant fluid entries were recorded during the deepening of this well, in concomitance with the crossing of the local major seismic reflectors, raised fundamental questions about the geothermal significance of this type of seismic reflectors, starting from their relevance as possible targets for drilling and industrial exploitation of supercritical fluids.

To gain some insight on the super-hot horizons of the Larderello geothermal field, we thus present new data on the isotope composition of noble gases and CO_2 from productive wells approaching the K-horizon, and/or closely related to granitic bodies in the southern margin (Monterotondo and Lago) and the Radicondoli-Montieri sectors of the geothermal field. Wells from the southern margin were located in the surroundings of the test site of the DESCRAMBLE project.

Methods

Gas samples were collected with standard sampling methods [Giggenbach and Goguel, 1989]. The dry gas fraction was obtained by means of a cyclone separator. Noble gases analyses were stored in copper pinched-off tubes and in glass vials equipped with two full glass stopcocks.

The CO_2 was separated in the laboratory from water vapour and other components by means of cold traps at liquid N_2 and ethanol dry ice temperatures. The CO_2 was used for determining its carbon isotope composition. The analyses were performed on a Finnigan MAT 250 mass spectrometer.

Noble gases were processed on a stainless steel high-vacuum line equipped with hot traps (Ti getter) to separate noble gases from reactive gases. Noble gases are then separated each other by means of traps cooled at variable temperatures by a cryostat pump.

The extraction line is connected to both a magnetic mass spectrometer (MAP 215-50) and a quadrupole mass spectrometer (Spectralab 200, VG-Micromass). ^{3}He and ^{4}He were determined by peak jumping and detected on ion counting and faraday cup device, respectively. Resolution for ^{3}He was higher than 600 AMU for HD-^{3}He at 5% of the peak. The air standard was introduced into the extraction line and treated in the same way as the samples to check reproducibility. The air ^{3}He/^{4}He and ^{4}He/^{20}Ne ratios exhibited a reproducibility better than 10% over the analysis period.

Results and Discussion

A large dataset of helium and neon isotopic compositions and relative abundances [Magro et al., 2003; and references therein], and of carbon isotope composition of CO_2 [Gherardi et al., 2005; and references therein] is available for the geothermal fluids of Larderello. Here we complemented such database with new ^{3}He/^{4}He and δ^{13}C(CO_2) data coming from the southern (Monterotondo and Lago) and the Radicondoli-Montieri sectors of the field (Figure 1). The wells from the southern sector were sampled in the framework of the DESCRAMBLE project [Bertani et al 2018], in an area where the K-horizon culminates at shallow depth (up to 3 km depth), and where the presence of ^{3}He-enriched deep mantle derived fluids was witnessed by ^{3}He/^{4}He ratios up to 3.2 Ra (with Ra = ^{3}He/^{4}He reference value for the air).

The new data reinforced on the available statistics of the Larderello geothermal field, and plotted on the range of highest frequency values between 0.6 to 2.6 Ra (^{3}He/^{4}He, Figure 1A), and between -5.5 to -4.5‰ vs V-PDB (δ^{13}C-CO_2; Figure 1B). Only two samples deriving from shallow, non-metamorphic productive layers, plotted out of this range, showing δ^{13}C-CO_2 values in the order of -3‰.

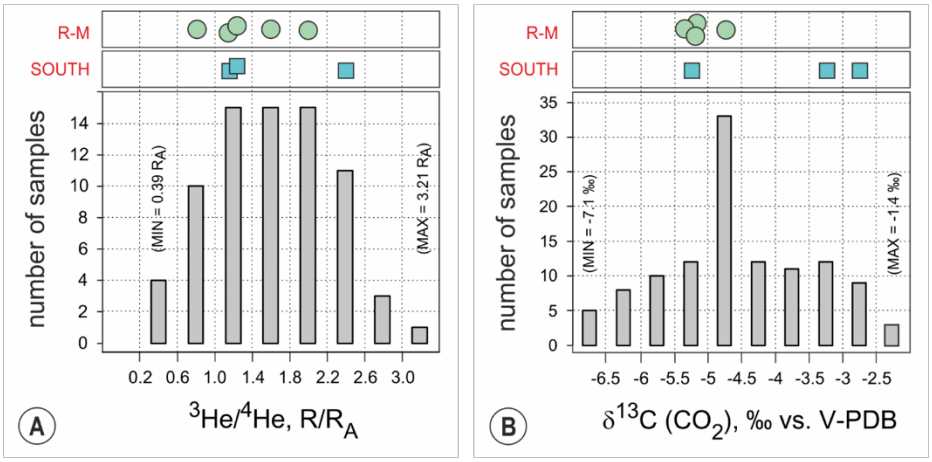

Figure 1 Histograms of ^{3}He/^{4}He (box A) and δ^{13}C(CO_2) (box B) in Larderello geothermal discharges. New data from Southern (squares, box "South") and Radicondoli-Montieri (circles, box "R-M") sectors are also shown.

Inspection of the whole dataset, inclusive of the new data presented here, revealed the following major features:

(i) No evident correlation was observed between the depth of the productive horizons and ^{3}He/^{4}He values. For instance, relatively low ^{3}He/^{4}He values were measured in the Radicondoli and Montieri wells, despite their depth in excess of ~2070 m, down to ~4300 m b.g.l. Similarly, in the southern margin of the field, a well with a producing level at ~2200 m b.g.l., showed a relatively low ^{3}He/^{4}He value of 1.2 Ra.

(ii) Conversely, a strict inverse correlation was noticed between $^3He/^4He$ values and K-horizon depth (i.e., the more surficial the top of the K-horizon, the higher is the value of $^3He/^4He$ ratio). For instance, the relatively low $^3He/^4He$ values measured at Radicondoli and Montieri corresponded to a local deepening of the K-horizon depth down to more than -5 km b.g.l.

(iii) $^3He/^4He$ values were directly correlated with heat flux. In particular, short-wavelength thermal perturbations were associated to an increase of radiogenic ^4He, derived from long-term water-rock interaction. The largest ^4He contribution was estimated for the oldest, U- and Th-enriched granites (>2.3 MA; [Gianelli and Laurenzi, 2001]) of the Radicondoli-Montieri area. On the contrary, long-wavelength thermal perturbations were related to ^3He-enriched fluid rising from the mantle [Magro et al., 2009].

(iv) ^3He-enriched fluids were hypothesized to be conveyed at the surface along preferential channels [Magro et al., 2009]. This was further supported by the relatively high $^3He/^4He$ value (>2.5 Ra) measured in a shallow well (<800 m b.g.l.) from the southern part of the field.

(v) No clear-cut correlations were observed between $\delta^{13}C\text{-}CO_2$ values and both (i) well and (ii) K-horizon culmination depths. The stable carbon isotopic composition of carbon dioxide mirrored instead the predominant lithology of the different production layers. In particular, the CO_2 derived from metamorphic rocks of the deeper reservoir was generally depleted in C-13 ($\delta^{13}C\text{-}CO_2$ < −4‰), compared to the CO_2 from carbonates, dolostones and anhydrites of the upper reservoir ($\delta^{13}C\text{-}CO_2$ generally > −4‰). Accordingly, the deep wells draining the metamorphic rocks of the Radicondoli-Montieri basin plotted at ~ −5‰, whereas the fluids collected (in southern zone) from the carbonate and anhydritic layers of the upper reservoir plotted at ~ −3‰.

Conclusions

C-He systematics emerged as an efficient tool to decipher the source of deep fluids at Larderello. The $\delta^{13}C\text{-}CO_2$ data supported the hypothesis of a predominantly crustal origin of the geothermal CO_2. Areal variations in the $\delta^{13}C$ signal appeared largely controlled by the lithological heterogeneity of the productive reservoir, with values < -4‰ generally associated with calc-silicate rocks of the metamorphic basement. The He isotope distribution at surface mirrored a dynamic balance between crustal- and mantle-derived fluids, while the geometry and the extension of the vertical permeability rule the deep, ^3He-enriched fluid transfer towards the surface. The widespread occurrence of granite bodies contributes to a dilution of the deep, ^3He-bearing signal, by release of variable ^4He amounts made available to circulating fluids via water-rock interaction. The oldest the age of the pluton, the largest was the estimated ^4He contribution.

References

Batini F., Burgassi P.D., Cameli G.M., Nicolich R., Squarci P., (1978). *Contribution to the study of deep lithospheric profiles: deep horizons in the Larderello - Travale geothermal field*. Mem. Soc. Geol. It., 19, 477-484.

Batini F., Bertini G., Gianelli G., Pandeli E., Puxeddu M., Villa I.M., (1985). *Deep structure, age and evolution of the Larderello-Travale geothermal field*. GRC Transactions, 9, 253-259.

Bertani R. and the DESCRAMBLE Science and Technology Team, (2018). *The First Results of the DESCRAMBLE Project*. Proceedings, 43rd Workshop on Geothermal Reservoir Engineering Stanford University, Stanford, California, February 12-14, 2018 SGP-TR-213.

Gherardi F., Panichi C., Gonfiantini R., Magro G., Scandiffio G., (2005). *Isotope systematics of C-bearing gas compounds in the geothermal fluids of Larderello, Italy*. Geothermics, 34, 442-470.

Gianelli G., Laurenzi M.A., (2001). *Age and cooling rate of the geothermal system of Larderello*. GRC Transactions 25, 731-735.

Giggenbach W.F., Goguel R.L., (1989). *Collection and analysis of geothermal and volcanic water and gas discharges*. Report n. CD 2401. Chemistry Division DSIR, New Zealand, p. 81.

Magro G., Ruggieri G., Gianelli G., Bellani S., Scandiffio G., (2003). *Helium isotopes in paleofluids and present-day fluids of the Larderello geothermal field: Constraints on the heat source*. J. Geophys. Res., 108 (B1), doi: 10.1029/2001JB00159.

Magro G., Bellani S., Della Vedova B., (2009). *The deep roots of the Larderello geothermal field (Italy) from heat flux and ^{3}He anomalies*. GRC Transactions, 33, 405-410.

Watanabe N., Numakura T., Sakaguchi K., Saishu H., Okamoto A., Ingebtritsen S.E., Tsuchiya N., (2017). *Potentially exploitable supercritical geothermal resources in the ductile crust*. Nature Geoscience, 10, 140-145.

The effect of thermochemical sulfate reduction on chemical and carbon isotopic characteristics of gas

Huijuan Guo, Yunpeng Wang, Jinzhong Liu

Guangzhou Institute of Geochemistry, Chinese Academy of Sciences, China

Corresponding Author: *guohuijuan@gig.ac.cn*

Introduction

The chemical and carbon isotopic data of gas hydrocarbons have been used as a critical indication to differentiate gas hydrocarbon sources, generative manners, thermal maturity levels and filling history of reservoirs. However, the chemical and carbon isotope of gas hydrocarbons could be influenced by other processes like thermochemical sulfate reduction (TSR) proven by laboratory experiments and geological observations [Hao et al., 2015; Worden and Smalley, 1996]. The influence of TSR on the chemical and carbon isotopic composition of gas has rarely been studied in the lab [Pan et al., 2006]. As the amount of hydrocarbon gases could be altered by thermal maturation and H_2S/CO_2 could react with the surrounding minerals or ions, it is difficult to assess the extent of TSR reaction on carbon isotope and when or how did the TSR change the chemical and carbon isotope of the original gases from geological observation. Therefore, the equation for the oxidation of gas hydrocarbons into CO_2 and H_2S deducted from geological gas composition is controversial [Worden and Smalley, 1996; Pan et al., 2006]. From controlled laboratory experiment, the relationship between the ratio of hydrocarbon gases and H_2S/CO_2 could be established providing basic information for the amount of H_2S assessment and how TSR could affect the composition and carbon isotope of gas.

A mixed gas sample which is mainly composed of methane (25%), ethane (30%), propane (25%) and nitrogen (20%, internal standard) was used to investigate the effect of TSR on composition and carbon isotope of gas by using high pressure gold tube thermal simulation equipment. The composition and carbon isotope of gas products were analyzed by GC and GC -IRMS after thermal simulation with isothermal pyrolysis temperature of 360℃ and a pressure of 50Mpa.

Magnesium sulfate heptahydrate, water and the mixed gas were loaded into gold tubes. As prior works show that water could promote the cracking of hydrocarbons, a control group which was only composed of mixed gas and water was conducted. What's more, the influence of sodium chloride which is common in ionized water on hydrocarbon gas TSR was also investigated.

Results

During 48-288 hour, the controlled group show no variation with respect to gas composition and carbon isotope. In contrast, the group with magnesium sulfate heptahydrate show the increase of methane content and decrease of propane and ethane. Moreover, the amount of H_2S and CO_2 increased with increasing pyrolysis time in a nonlinear pattern. The TSR reaction of hydrocarbon gas can be described by two primary stages termed as the initial stage and H_2S self-catalysis stage (Figure 1a-b). In the initial stage, the generation rate of H_2S is slow and hydrocarbon gases has small variation. At the H_2S self-catalysis stage, the volume of H_2S increased in a larger rate and the consumption of propane and ethane leads to the generation of methane and CO_2.

In accordance with gas composition, the variation of carbon isotope of hydrocarbon gases in the two

different stages are also different. In the initial stage, the carbon isotope of ethane and propane get heavier in a quite slow rate (Figure 1d-f). In the self-catalysis stage, methane, ethane and propane become heavier in a faster rate. When comparing the carbon isotope variation of different gas, different features of the two stages were shown. The carbon isotope of methane and propane get heavier in a greater rate than ethane in the initial stage. While, at H_2S self-catalysis stage, a reverse trend is present, i.e. carbon isotope of ethane get heavier in a greater rate than methane and propane.

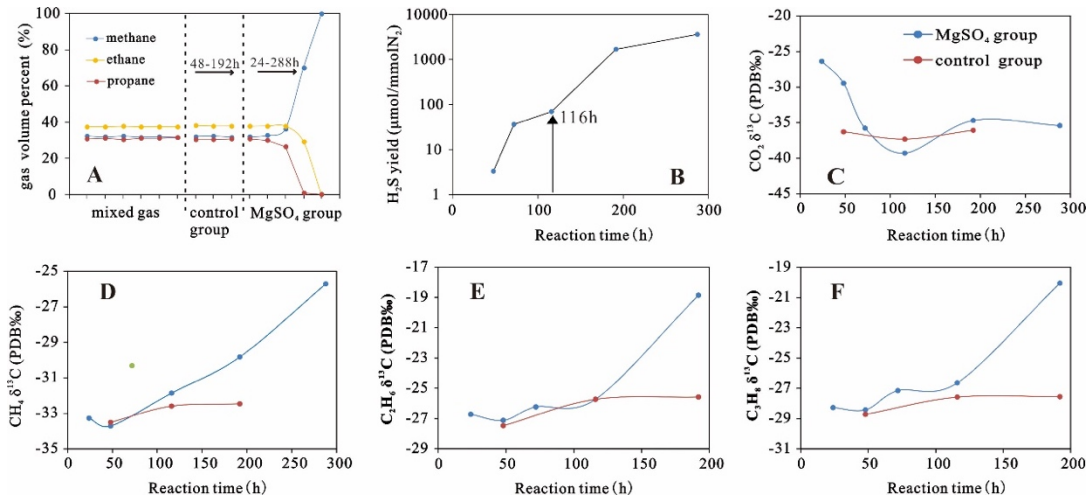

Figure 1 (A) the variation of gas volume percent of control group and $MgSO_4$ group with pyrolysis time, parallel measurement of mixed gas in gold tube before pyrolysis were analyzed to make sure that the gas infilling method was of good consistency. (B) H2S yield with reaction time. (C-F) variation of carbon isotope of carbon dioxide, methane, ethane and propane with pyrolysis time.

Conclusions

1. TSR of gaseous hydrocarbon including methane, ethane and propane proves that the consumption of propane and ethane lead to the increase of the amount of methane, carbon dioxide and hydrogen sulfide.
2. At the initial stage of TSR, the cracking of propane leads to heavier $\delta^{13}C$ of propane and methane showing that $\delta^{13}C$ of propane and methane get heavier in a faster rate than ethane, whereas, at the hydrogen sulfide self-catalytic stage, ethane cracking rate increased and $\delta^{13}C$ of ethane get heavier in a faster rate than methane and propane.
3. Sodium chloride could accelerate the TSR reaction of hydrocarbon gases and therefore present drier gas and heavier carbon isotope compared with the group without sodium chloride.

References

Hao F., Zhang X., Wang C., Li P., Guo T., Zou H., Zhu Y., Liu J., Cai Z., (2015). *The fate of CO_2 derived from thermochemical sulfate reduction (TSR) and effect of TSR on carbonate porosity and permeability, Sichuan Basin, China*. Earth-Science Reviews, 141, 154-177.

Pan C., Yu L., Liu J., Fu J., (2006). *Chemical and carbon isotopic fractionations of gaseous hydrocarbons during abiogenic oxidation*. Earth and Planetary Science Letters, 246, 70-89.

Worden R., Smalley P., (1996). *H_2S-producing reactions in deep carbonate gas reservoirs: Khuff Formation, Abu Dhabi*. Chemical Geology, 133, 157-171.

Mantle degassing through continental crust triggered by active faults: the case of the Baja California Peninsula

Grassa F.[1], Rizzo A.L.[1], Cruz R.Y.B.[2], Romero R.B.[3], Fernández A.G.[2], Kretzschmar T.G.[2], Gómez-Arias E.[4]

[1]*Istituto Nazionale di Geofisica e Vulcanologia, Sezione di Palermo, Italy*
[2]*Centro de Investigación Científica y de Educación Superior de Ensenada (CICESE), Baja California, México*
[3]*Instituto Nacional de Electricidad y Energías Limpias (INEEL), Cuernavaca, Morelos, México*
[4]*CONACYT-Centro de Investigación Científica y de Educación Superior de Ensenada (CICESE), Baja California, México*

Corresponding Author: *fausto.grassa@ingv.it*

The degassing of mantle fluids normally occurs in environments where magmatic activity is present. Occasionally it occurs also in some continental areas, where active volcanism is absent and an active geothermal regime exists [Mamyrin & Tolstikhin, 1984; Poreda & Craig, 1989; Caracausi et al., 2005; Caracausi & Paternoster, 2015]. In the Baja California Peninsula (BCP) and in the nearby Gulf of California (GoC), the degassing of volatiles is widespread and occurs within two different geodynamic contexts: 1) the cessation of the eastward subduction of the Farallón plate beneath the BC peninsula ~12 Ma ago [Atwater, 1970; Stock & Lee, 1994] and 2) the formation and development of the rift in the GoC which is associated with the thinning of the lithosphere and partial melting [Calmus et al., 2011]. In this complex regional geodynamic setting there are numerous gas manifestations: fumaroles and mud pools with temperatures between 30 and 100°C are principally located within continental crust along the eastern coast of the BCP and almost parallel to the rift fracture. Submarine hydrothermal manifestations have been found at in the GoC (e.g. in the Guaymas, Pescadero and Alarcon basins), where oceanic crust is being formed [Lonsdale, 1989; Fenby & Gastil, 1991] and high-temperature fluids (>240°C) are discharged [Von Damm et al., 1985; MBARI, 2012; Spelz et al., 2015]. Here we report new chemical and isotopic data ($^3He/^4He$, $\delta^{13}C_{CO2}$, $\delta^{13}C_{CH4}$, and δD_{CH4}) from poorly or previously unstudied hydrothermal and volcanic gases that are emitted along the eastern coast of the Baja California Peninsula (BCP), elucidating, for the first time, the geochemistry of gas emissions that occur along the eastern coast of the BCP.

By integrating our data with existing data from the other BCP and GoC gas manifestations, we constrain the origin of these gases, identify the main processes that modify their pristine compositions and evaluate the geotectonic implications. A comprehensive conceptual model to explain the nature of the gases that are emitted from the BCP is proposed to rationalize the relationship between the continental degassing of mantle-derived fluids and the lack of active volcanism.

The chemistry of the collected gases significantly varies among the sites. We distinguish three main groups: 1) CO_2-dominated, with CO_2 concentrations from 51.5 to almost 100%; 2) N_2-dominated, with an N_2 content between 47.8 and 89.5%; and 3) CH_4-dominated with CH_4 contents up to 82%. The $\delta^{13}C_{CO2}$ values range from around -5.0‰ to -18.4‰ at C without any systematic correlation with CO_2 concentration. The stable isotope signature of CH_4 shows a wide range of compositions from negative values towards unusually positive values. Finally high $^3He/^4He$ values (up to ~7 Ra) are found in volcanic gases, while lower ratios (≤1.6 Ra) characterize hydrothermal springs.

Thus, based on these results, we infer that the mantle beneath the BCP has MORB-like features, as in the rift within the Gulf of California, and we reconstruct the ascent of mantle/magmatic gases.

Both volcanic and hydrothermal gases are contaminated by two crustal-derived C-rich fluids. After contamination within the crust, these gases experience the partial dissolution of CO_2 in shallow waters, which further modifies their pristine composition.
Thermogenic and possibly abiogenic sources of methane are present only in volcanic gases from the BCP. Secondary methane oxidation (microbial/inorganic) processes are proposed for some hydrothermal gases, which are extremely enriched in heavy isotopes.
Finally, we argue that the hydrothermal gases that are emitted from the BCP have variable percentages of mantle contribution, indicating the presence of lithospheric faults enhancing the rise of mantle fluids also in areas where volcanism is absent.

References

Atwater T.M., (1970). *Implications of Plate Tectonics for the Cenozoic Tectonic Evolution of Western North America*. Geological Society of America Bulletin, 81, 3513-3536.

Calmus T., Pallares C., Maury R.C., Aguillón-Robles A., Bellon H., Benoit M. & Michaud F., (2011). *Volcanic markers of the post-subduction evolution of Baja California and Sonora, México: Slab tearing versus lithospheric rupture of the Gulf of California*. Pure Apply Geophysics, 168(8-9), 1303-1330. https://doi.org/10.1007/s00024-010-0204-z.

Caracausi A. & Paternoster M., (2015). *Radiogenic helium degassing and rock fracturing: A case study of the southern Apennines active tectonic region.* Journal of Geophysical Research, Solid Earth, 120, 2200-2211. https://doi.org/10.1002/2014JB011462.

Caracausi A., Favara R., Italiano F., Nuccio P.M., Paonita A. & Rizzo A., (2005). *Active geodynamics of the central Mediterranean Sea: Tensional tectonic evidences in western Sicily from mantle-derived helium.* Geophysical Research Letters, 32(4), 1-5. https://doi.org/10.1029/2004GL021608.

Fenby S.S. & Gastil R.G., (1991). *Geologic-tectonic map of the Gulf of California and surrounding areas*. In J.P. Dauphin & B.R.T. Simoneit (Eds.), The Gulf and Peninsular Provinces of the Californias, American Association of Petroleum Geologists, Memoir (Vol. 47, pp. 79-83).

Lonsdale P.F., (1989). *Geology and Tectonic History of the Gulf of California*. In E.L. Winterer, D.M. Hussong, & R. W. Decker (Eds.), The eastern Pacific Ocean and Hawaii, Geological Society of America, (pp. 499-521). Boulder, Colorado.

Mamyrin B.A. & Tolstikhin I.N., (1984). *Helium Isotopes in Nature*. New York: Elsevier MBARI. (273. pp.), (2012). Cruise report: Leg 7: Volcanoes and Seamounts April 21 - May 1, http://www.mbari.org/expeditions/goc12/legs/leg7/L7 index.html.

Poreda R. & Craig H., (1989). *Helium isotope ratios in Circum-Pacific volcanic arcs.* Nature, 338(6215), 473-478. https://doi.org.10.1038/338473a0.

Spelz R.M., Lupton J.E., Evans L.J., Zierenberg A., Clague D.A., Neumann F. & Paduan J.B., (2015). *Noble Gas geochemistry of the newly discovered hydrothermal fields in the Gulf of California: preliminary He-isotope ratios from the Alarcon Rise and Pescadero basin vent sites*. Fall AGU Meeting, San Francisco, Dic. 14-18, Abstract OS23C-2028.

Stock J.M. & Lee J., (1994). *Do microplates in subduction zones leave a geological record?* Tectonics, 13, 1472-1487.

Von Damm K.L., Edmond J.M., Grant B. & Measures C.I., (1985). *Chemistry of submarine hydrothermal solutions at Guaymas Basin, Gulf of California.* Geochimica et Cosmochimica Acta, 49, 2221-2237.

Preliminary study on the geochemistry of fluid discharges from Guallatiri volcano (northern Chile)

Inostroza M.[1,2], Tassi F.[3,4], Aguilera F.[2,5], Sepúlveda J.[2,5], Capecchiacci F.[6], Venturi S.[3,4], Capasso G.[7]

[1]*Universidad Católica del Norte, Chile*
[2]*Núcleo de Investigación en Riesgo Volcánico, Chile*
[3]*Dipartimento di Scienze della Terra, Università di Firenze, Italy*
[4]*CNR-IGG Istituto di Geoscienze e Georisorse, Firenze, Italy*
[5]*Departamento de Ciencias Geológicas, Universidad Católica del Norte, Chile*
[6]*Istituto Nazionale di Geofisica e Vulcanologia, Sezione di Napoli - Osservatorio Vesuviano, Italy*
[7]*Istituto Nazionale di Geofisica e Vulcanologia, Sezione di Palermo, Italy*

Corresponding Author: *manuel.inostroza@alumnos.ucn.cl*

Introduction

Guallatiri (18°25'S, 69°05'W; 6,073 m a.s.l.; Figure 1a) is a remote volcano located in the Central Andean Volcanic Zone (CAVZ; [Thorpe et al., 1982]), extending from south of Peru, west of Bolivia and northern Chile. Guallatiri volcano is considered the second most active volcano in the north of Chile (after Lascar volcano; [SERNAGEOMIN, 2015]). Geological evidences (recent pyroclastic deposits in Guallatiri village), recent eruptive events (e.g. small explosions and phreatic eruptions in 1913, 1959 and 1960; [Casertano, 1963]) and current fumarolic activity [González-Ferrán, 1995; Global Volcanism Program, 2013] suggest the occurrence of an active magmatic system. Likewise, a reactivation of the volcano might cause the melting of the thick glacial cap on the summit area (over 5,800 m a.s.l.), possibly generating devastating lahars. Despite those antecedents, few information is available about its geological evolution [e.g. García et al., 2004; Sepúlveda, 2018] and seismic activity (e.g. reports of volcanic activity from Sernageomin, Chile).

This work presents the first chemical and isotopic characterization of fumarolic gases and fluid discharges from cold and thermal springs of Guallatiri volcano. At this preliminary phase, the aim of the present is to investigate the fluid source region(s).

Case of Study

Guallatiri has been built over an Upper Oligocene to Pleistocene basement, consisting of volcanic rocks and continental sedimentary successions interbedded with ignimbritic flows that fill the Lauca basin [García et al., 2004]. Geological evolution of Guallatiri can be divided in 7 stages, consisting of superposition of lava flows, lava domes, laharic and pyroclastic flows [Sepúlveda, 2018]. Chemical composition of its products varies from trachyandesites to dacites, with a calc-alkaline affinity [Sepúlveda, 2018].

Currently, Guallatiri volcano shows a persistent and vigorous fumarolic activity from the volcano summit and southwestern flank (SF and SWF respectively, Figure 1c). Both SF and SWF display chimneys and cone-like vents (up to 50 cm diameter), and strong jet-type fumarolic emissions. Thermal springs (two of them with gas bubbles) are placed in the Chirigualla area (Figure 1b), 12 km northwest from the volcano, reaching temperatures up to 48 °C [Aguilera, 2008] whilst numerous cold springs are scattered on the southwest, west and north flanks, at distances 4.7 to 13.5 km from the volcano summit. Historical activity from Guallatiri has been poorly documented. Tephra ejection and gas

incandescence were reported to occur in 1913 and 1959, while a small phreatic eruption was recorded in 1960; all episodes had a VEI 2 [Casertano, 1963]. Increasing fumarolic activity was reported in 1985, when the plume reached a height up to 500 meters above the summit [González-Ferrán, 1995; Global Volcanism Program, 2013].

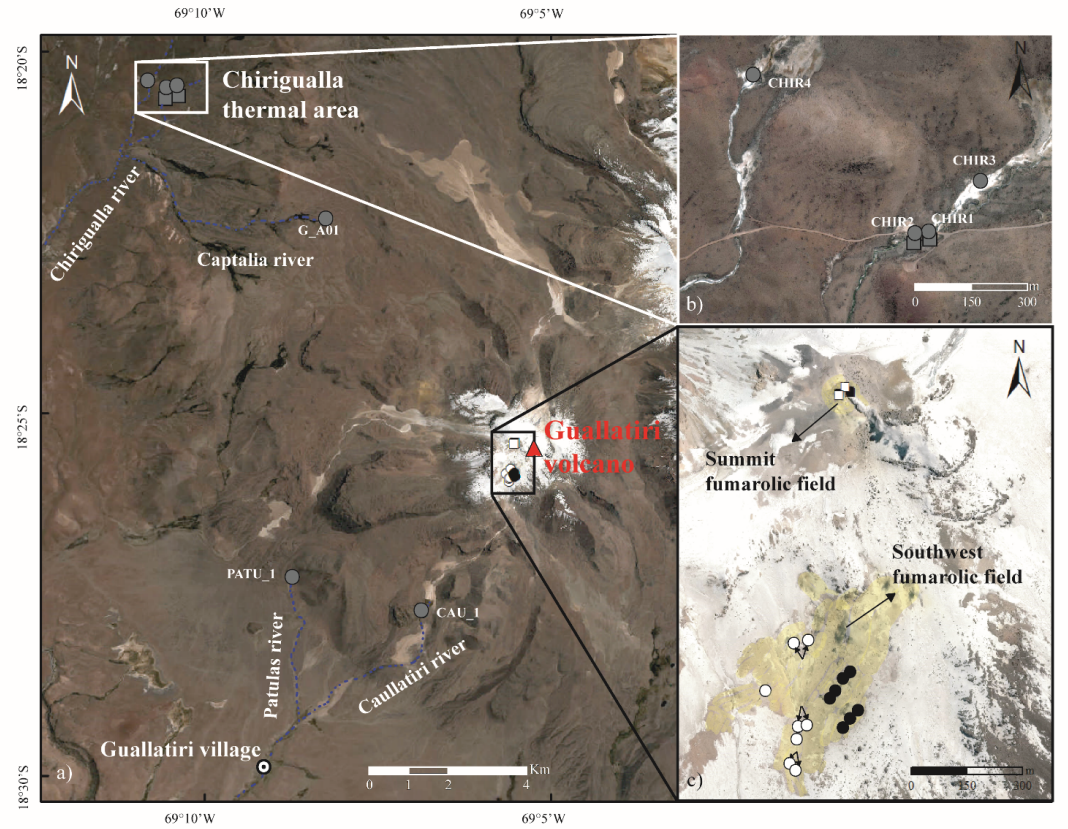

Figure 1 Location of samples taken from fumarolic fields and cold/thermal areas around the volcano. a) Satellite image showing the study area and sample sites, b) zoom-in at the Chirigualla thermal area and c) general view of summit and southwest fumarolic fields (SF and SWF respectively). SF samples are squares, SWF samples are circles, black symbols are high temperature (between 177 to 265 °C) gas emissions, white symbols are low temperature gas emissions (T < 91.4 °C). Grey symbols represent water (*circles*) and gas (*squares*) samples associated to thermal/cold emissions.

Methodology

Fumarolic gases and gases from bubbling pools were collected using a sampling line described by [Montegrossi et al., 2001]. Temperature of gas emissions were measured in the field.

Temperature, pH and EC were measured *in situ*. One unfiltered and one filtered (0.45 µm Sartorius®)-acidified (suprapur HCl at 1%) water samples were collected in polyethylene bottles for the analysis of major anions and cations respectively. Water samples for O and H isotopic analysis were collected and stored unfiltered in 100-ml dark glass bottles. Analytical errors were < 5 %.

Carbon isotopic composition of CO_2 and CH_4 ($\delta^{13}C$-CO_2 and $\delta^{13}C$-CH_4 respectively, expressed as ‰ vs. V-PDB) was measured by Cavity Ring-Down Spectroscopy (Picarro G2201-i). The R/Ra ratios (where R is the $^3He/^4He$ in the sample and Ra the $^3He/^4He$ in the air: $1.39 \cdot 10^{-6}$ [Mamytin and Tolstikhin, 1984]) and ^{20}Ne were analyzed using two Mass Spectrometers (Helix SFT-Thermo). Analysis were performed following internal protocols [e.g Di Piazza et al., 2015]. Analytical error was < 1 %. The R/Ra ratios were corrected using the $^{20}Ne/^4He$ ratios and expressed as Rc/Ra according

Poreda and Craig, [1989]. The $^{18}O/^{16}O$ and $^{2}H/^{1}H$ ratios (expressed as $\delta^{18}O$ and δD ‰ vs. V-SMOW, respectively) were determine by Laser Spectroscopy (LGR DT-100 Liquid Water Stable Isotope Analyzer) according the protocol proposed by International Atomic Energy Agency (2009).

Results

Temperature of fumarolic gases vary from 80.1 to 265 °C. The chemical composition is dominated by H_2O (up to ~ 93 %), followed by CO_2, SO_2 and H_2S respectively. Other typical magmatic-related compounds (e.g. HCl, HF) are in relatively low concentrations. Significant amounts of N_2 and H_2 whereas also measured, whereas CH_4, CO and He are relatively low.

Thermal springs from Chirigualla area have temperatures between 49.5 and 50.1 °C. Bubbles are rich in CO_2, whereas N_2 is the second component in abundance. Methane and H_2S are in significant concentrations, whereas SO_2, HCl and HF are absent.

Water discharges located around Guallatiri volcano have variable temperatures between 7.9 and 50.1 °C, being those of higher temperature focused in the Chirigualla thermal area. Cold waters are slightly basic (pH from 8.3 to 9.05), whereas thermal waters are more neutral (pH between 7.5 and 7.8). Chemical composition of waters varies from Ca^{+2}-SO_4^{-2} to Na^{+}-HCO_3^{-}.

Values of $\delta^{13}C$-CO_2 are up to -7.02 ‰ vs. V-PDB, whereas values of $\delta^{13}C$-CH_4 are up to -16.72 ‰ vs. V-PDB. The Rc/Ra values are ≤ 3.2, whereas $^{40}Ar/^{36}Ar$ ratios are close to typical atmospheric values [295.5; Ozima and Podosek, 2002]. Low values of $^{4}He/^{20}Ne$ ratios (≤9.2) suggest an appreciable air contamination ($^{4}He/^{20}Ne$ for air is 0.318; [Sano and Wakita, 1988]). The $\delta^{18}O$ and δD values of gas condensates are from -0.3 to 0.6 ‰ from -52 to -47 ‰ vs. V-SMOW, respectively. The $\delta^{18}O$ and δD values of cold springs range from -16.3 to -15.8 and -115 to -109 ‰ V-SMOW respectively.

Discussions

Origin of fumarolic gases

The N_2/Ar ratios (between 96 and 407) of the fumarolic gases are in the range for suggesting an extra-atmospheric N_2 source, typical in gases from subduction related volcanoes [Fischer, 2008 and references therein]. On the contrary, the $^{40}Ar/^{36}Ar$ ratios indicate that Ar is mainly sourced from air.

Low temperature (T < 91.4 °C) and high temperature (between 177 and 265 °C) fumaroles can be recognized. Low temperature gas emissions from SWF show relatively high abundances of hydrothermal-related species (e.g. H_2S, CH_4), whereas high temperature fumaroles from this sector of the volcano are enriched in magmatic-related species (e.g. SO_2). Gases emitted from SF show no significant difference between high and low temperature fumaroles, being both dominated by the magmatic component. Scrubbing processes are likely responsible for the hydrothermal-type features of the low temperature SWF fumaroles. These processes are likely triggered by freshwater addition from the glacial cap close to this fumarolic area, favoring reactions involving magmatic gases, host rocks and meteoric water. The $\delta^{18}O$ and δD values of water vapor are shifted from the Local Meteoric Water Line [Chaffaut et al., 1998], approaching at the “andesitic field” [Taran et al., 1989]. These findings indicate that gases have important contributions from fluids released during magma degassing. Noteworthy, the Rc/Ra ratios are mostly below the typical range of gases from active arc-volcanoes (between 3 and 8; [Poreda and Craig, 1989; Hilton et al., 2002]), suggesting strong addition of ^{4}He possibly derived from (i) radiogenic decay within the magma (magma aging) or (ii) interaction with ^{4}He-rich country rock [Hilton et al 1993]. On the contrary, the $\delta^{13}C$-CO_2 are typical for arc-related volcanoes [Sano and Marty, 1995]). However, the high $CO_2/^{3}He$ ratios, at least one order of magnitude from the typical MORB gases, indicate that CO_2 mainly originate from crustal source. According to the $\delta^{13}C$-CH_4

values, CH_4 derive from a biogenic source, related to both microbial activity and thermogenic processes, although a more detailed investigation is needed to definitely assess the origin of this gas compound.

Chemistry of gases from Chirigualla

Gases from bubbling pools in Chirigualla include abundant components from air, as supported by the N_2/Ar ratios slightly higher than the ASW value. The isotopic features of CO_2, as well as the occurrence of H_2S and CH_4 testifies a dominant hydrothermal-related source. The contribution of magmatic degassing is relatively low.

Water geochemistry

Cold waters located near the volcano are immature and have a Ca^{+2}-SO_4^{-2} composition (e.g. Captalia or Patuias rivers), suggesting interaction with magmatic-hydrothermal gases. Contrarily, Na^{+}-HCO^{3-} waters from the Chirigualla thermal area evidence the lateral migration of volcanic fluids causing prolonged fluid-rock interaction. The $\delta^{18}O$ and δD values of these springs is similar to the LMWL suggest major contributions from a meteoric source.

Conclusions

Chemical and isotopic analysis of gas discharges from fumarolic fields in the Guallatiri volcano show, at a first approximation, the typical features of arc-related volcanoes, produced by mixing, at different degrees, of magmatic- and, hydrothermal-type fluids. Scrubbing processes modify the original composition of gases, especially in gases from fumaroles affected by melting of the glacial cap. The relatively low He mantle fraction measured in these gases merits further investigation to explain the effective origin of ^{4}He-rich contribution.

The chemical composition of waters in the Chirigualla thermal area suggests the occurrence of a hydrothermal system, whereas the SO_4-rich cold spring are produced by shallow interaction between meteoric water and volcanic gases.

References

Aguilera F., (2008). *Origen y naturaleza de los fluidos en los sistemas volcánicos, geotermales y termales de baja entalpía de la zona volcánica central (ZVC) entre los 17 43'S y 25 10'S*. PhD Thesis, Antofagasta.

Casertano L., (1963). *General characteristics of active Andean volcanoes and a summary of their activities during recent centurias*. Bull. Seism. Soc. Am., 53:1415-1433.

Chaffaut I. Coudrain-Ribstein A. Michelot J.L. Pouyaud B., (1998). *Précipitations d'altitude du Nord-Chile, origine des sources de vapeur et données isotopiques*. Bull. Inst. Fr. Etudes Andines, 27:367-384.

Di Piazza A., Rizzo A.L., Barberi F., Carapezza M.L., De Astis G., Romano C., Sortino F., (2015). *Geochemistry of the mantle source and magma feeding system beneath Turrialba volcano, Costa Rica*. Lithos, 232, 319-335.

Fischer T.P., (2008). *Fluxes of volatiles (H_2O, CO_2, N_2, Cl, F) from arc volcanoes*. Geochem. J., 42(1), 21-38.

García G., Gardeweg M., Clavero J., Hérail G., (2004). *Hoja Arica, Región de Tarapacá*. Servicio Nacional Geología y Minas.

Global Volcanism Program, (2013). *Guallatiri (355020) in Volcanoes of the World*. v. 4.8.2. Venzke E., (ed.). Smithsonian Institution.

González-Ferrán O., (1995). *Volcanes de Chile*. Instituto Geográfico Militar.

Hilton D.R., Fischer T.P., Marty B., (2002). *Noble gases and volatile recycling at subduction zones*. Rev. Mineral. Geochem., 47:319-370.

Hilton D.R., Hammerschmidt K., Teufel S., Friedrichsen H., (1993). *Helium isotope characteristics of Andean geothermal fluids and lavas*. Earth Planet Sc. Lett., 120(3-4), 265-282.

Mamyrin B.A. and Tolstikhin I.N., (1984). *Helium isotopes in nature*. In: Fyfe W.S., (Ed.), Development in Geochemistry, Elsevier, Amsterdam.

Montegrossi G., Tassi F., Vaselli O., Buccianti A., Garofalo K., (2001). *Sulfur species in volcanic gases*. Analytical Chem., 73:3709-3715.

Ozima M. and Podosek F.A., (2002). *Noble gas geochemistry*. 2nd edn. Cambridge University Press, Cambridge.

International Atomic Energy Agency, (2009). *Laser spectroscopic analysis of liquid water samples for stable hydrogen and oxygen isotopes*. Training course series 35, Vienna.

Poreda R. and Craig H., (1989). *Helium isotope ratios in circum-Pacific volcanic arcs*. Nature, 338:473-478.

Sano Y. and Marty B., (1995). *Origin of carbon in fumarolic gas from island arcs*. Chem. Geol., 119(1-4), 265-274.

Sano Y. and Wakita H., (1985). *Geographical distribution of 3He/4He ratios in Japan: Implications for arc tectonics and incipient magmatism*. J. Geophys. Res.-Sol. Ea, 90(B10), 8729-8741.

Sepúlveda J.P., (2018). *Evolución geológica del Complejo Volcánico Guallatiri, región de Arica y Parinacota, Norte de Chile*. Undergraduate Thesis Thesis, Antofagasta.

SERNAGEOMIN, (2015). *Ranking de peligrosidad de los volcanes activos de Chile*. In: S.N.d.G.y. Minería (Editor), Santiago.

Taran Y.A., Pokrovsky B.G., Esikov A.D., (1989). *Deuterium and oxygen-18 in fumarolic steam and amphiboles from some Kamchatka volcanoes: "andesitic waters"*. Doklady Akademii, nauk SSSR, 304:440-443.

Thorpe R.S., (1982). *The Andes*. In Andesites: orogenic andesites and related rocks, 187-205.

"Thermal Karts of Herculane": new insights on the fluid geochemistry of the thermomineral waters of the Herculane area (Southwestern Romania)

Ionescu A.[1,2], Daskalopoulou K.[3], Temosvki M.[4], Persoiu A.[5], D'Alessandro W.[6], Caracausi A.[6], Roba C.[2], Baciu C.[2], Cardellini C.[1], Traian Brad[5], Pop C.[2], Alin Nicula[2], Molnar Kata[4], Laszlo Palcsu[4]

[1]*Università di Perugia, Dipartimento di Fisica e Geologia, Perugia, Italy*
[2]*Babeş-Bolyai University, Faculty of Environmental Science and Engineering, Cluj-Napoca, Romania*
[3]*Helmholzt Center Postdam, GFZ German Research Center for Geosciences, Postdam, Germany*
[4]*Isotope Climatology and Environmental Research Centre (ICER), Hungarian Academy of Sciences (ATOMKI), Debrecen, Hungary*
[5]*Emil Racovita Institute of Speleology, Romanian Academy, Cluj-Napoca, Romania*
[6]*Istituto Nazionale di Geofisica e Vulcanologia, Sezione di Palermo, Italy*

Corresponding Author: *arturkiralycj@yahoo.com*

In the Cerna Valley basin, located southwest of the Southern Carpathians and upstream from the confluence of Cerna with Belareca, an aquifer complex has developed. The basin is strongly influenced by hydrogeothermal phenomena, acting within two major geological structures, the Cerna Syncline and the Cerna Graben. The complex consists mainly of Jurassic and Cretaceous carbonate rocks, as well as the upper part of the Cerna Granite that is highly fractured, tectonically sunken into the graben. The geothermal investigations have shown the existence of some areas with values of the geothermal gradient falling into the 110-200°C/km interval. The zone with the maximal flux intensity is situated between the Baile Herculane railway station and the Crucea Ghizelei Well, an area where 24 sources (10 wells and 14 springs) are known. The geothermal anomaly is also extended to the south (Toplet), north (Mehadia) and NE (Piatra Puscata), a fact, which is stressed by the existence of hypothermal springs with low mineralization.

Lot of studies have investigated these manifestations although always from different point of views, separating the waters from the gases. In the case of the waters, many authors discussed the geochemistry of the waters, although generally taking into consideration only the chemistry and the physico-chemical parameters. A detailed description can be found in Povara et al., [2008]. Later in the 2000's, Wynn et al., [2010] tried to investigate sulphur in the waters and minerals of the area using stable isotopic data. In Ionescu et al., [2017] measured for the first time the isotopic composition of carbon-13 from dissolved methane from the springs and wells. In the case of the gas geochemistry, the first data on the composition of the gases was from Mastan 1987. In the 2000's slowly new data appeared on the isotopic compositions on the noble gases [Cosma et al., 2003].

The physical-chemical parameters of the sources show a strong N-S variability. At the entire thermo-mineral reservoir scale, the temperature of the water sources, the total mineralization, and the H2S quantity are increasing from the north to the south, and the pH and natural radioactivity are following the same trend.

The geothermal water sources (springs and drillings), always accompanied by large amounts of gases, are located where these fissures cross. Nitrogen and methane are the main components of emanated gases, and high helium and radon concentrations are present. Due to the high helium content, the

springs being comparable to the extreme case of the Homorod mud volcano (Romania). Based on the isotopic data methane is of thermogenic origin, with some samples being enriched in carbon-13. Based on these data, methane found in the Herculane gas-bearing springs, could have o geothermal origin.
In 2019 a new field campaign was organized in order to constrain the origin and the interaction of the fluids, this time in a more holistic point of view, combining not just the water geochemistry but also the gas geochemistry for the first time. The field camping was entitled "Thermal Karts of Herculane".

Photo 1 The field team at the statue of Hercules in Baile Herculane (Romania). From left to right: Aurel Persoiu, Alin Nicula, Artur Ionescu, Kyriaki Daskalopoulou, Cristian Pop, Kata Molnar, Marjan Temovski and Traian Bard.

Acknowledgments
The authors acknowledge support from the Deep Carbon Observatory, DCO grant n. 10759-1254. The team would also like to thank Socrate Bucur for helping in having access to some of the thermal manifestation.

References

Cosma C., Italiano F., Baciu C., Ristoiu D., Etiope G., (2003). *Gas composition and helium isotope ratios in geothermal sources from Cerna Valley (Romania)*. Proceedings of ICGG7: 22-23.

Ionescu A., Baciu C., Kis B.-M., Sauer P.E., (2015). *Evaluation of dissolved light hydrocarbons in different geological settings in Romania*. Chemical Geology, 469, 230-245.

Mastan I., (1987). *Helium in Geothermal Water Sources*. Ph.D. Thesis, University Babes-Bolyai, Cluj-Napoca, Romania.

Povara I., Simion G., Marin C., (2008). *Thermo-mineral waters from the Cerna Valley Basin (Romania)*. Studia Universitatis Babes-Bolyai, Geologia, 53(2), 41-54.

Wynn J.G., Sumrall J.B., Onac B.P., (2010). *Sulphur isotopic composition and the source of dissolved sulphur species in thermos-mineral springs of the Cerna Valley, Romania*. Chemical Geology, 271, 31-43.

Gas geochemistry of the seemingly inactive Ciomadul volcano (eastern Carpathians, Romania)

Kis Boglárka Mercédesz[1,2,3], Harangi Szabolcs[2], Caracausi A.[4], Palcsu László[3], Baciu C.[5], Ionescu A.[5,2], Sciarra A.[6], István Futó[3]

[1]*Institute of Geology, Babes-Bolyai University, Cluj-Napoca, Romania*
[2]*MTA-ELTE Volcanology Research Group, Eötvös University, Budapest, Hungary*
[3]*Isotope Climatology and Environmental Research Centre (ICER), (ATOMKI), Debrecen, Hungary*
[4]*Istituto Nazionale di Geofisica e Vulcanologia, Sezione di Palermo, Italy*
[5]*Faculty of Environmental Science and Engineering, Babes-Bolyai University, Cluj-Napoca, Romania*
[6]*Istituto Nazionale di Geofisica e Vulcanologia, Sezione di Sismologia e Tettonofisica, Roma, Italy*

Corresponding Author: *kis.boglarka@ubbcluj.ro*

Ciomadul is the youngest volcano in the Carpathian-Pannonian Region, Eastern-Central Europe, which last erupted 30 ka. This volcano is considered to be inactive, however, combined evidence from petrologic and magnetotelluric data, as well as seismic tomography studies suggest the existence of a subvolcanic crystal mush with variable melt content. Recently a multidisciplinary approach, involving petrology and thermobarometry on amphiboles reveal different crystallization conditions beneath the volcano suggesting the transcrustal magmatic system beneath Ciomadul. Numerical simulations on the thermal evolution of the magmatic system show that the upper crustal magmatic reservoir of the volcano may containg up to 58% melt, that is also consistent with previous geophysical anomalies on the in situ electrical conductivity [Harangi et al., 2015; Laumonier et al., 2019].

Gas emanations in the form of bubbling pools and low-temperature (T~8-10°C) dry mofettes are characteristic of the Ciomadul volcano. These gas emissions are often used for "curative effects" by the local people. CO_2-bubbling peat bogs and bubbling creeks can be also found, mainly at the north-eastern and southern parts of the Puturosul Mts. an older lava-dome of the volcanic complex. The minimum total CO_2 flux was estimated to be 8.7×10^3 t yr^{-1} calculated by summing the fluxes from focused emissions and diffuse degassing from the soil. The aquifers of this area are represented by CO_2-rich sparkling mineral water, with surface temperature up to 22.5 °C [Kis et al., 2017; 2019].

We investigated 31 gas emissions (dry mofettes as well as bubbling pools) at Ciomadul to constrain the origin of the volatiles. The CO_2 concentration in the collected gases ranges from 6.40 to 98.36%. Besides CO_2, H_2S (2.7×10^{-4} to 1.72×10^{-1} %), He (5.91×10^{-5} to 1.66×10^{-2} %), Ne (6.39×10^{-7} to 5.80×10^{-3} %), H_2 (1×10^{-5} to 2.3×10^{-1} %) CO (6×10^{-5} to 5×10^{-4} %), CH_4 (3.5×10^{-2} to 1.69 %), N_2 (1.5×10^{-1} to 74.5 %), and O_2 (2×10^{-3} to 18.99 %) are present in the gas samples. The $^3He/^4He$ ratios range between 0.77 to 3.10 R_a and the $^4He/^{20}Ne$ ratios from 0.36 and 1700, which show that some of the collected gases are affected by air contamination. The $^3He/^4He$ ratios after corrections for the air contamination (R/R_{ac}) are up to 3.25. The $\delta^{13}C_{CO2}$ ranges between -1.40‰ and -17.2‰ vs. V-PDB. The $\delta^{13}C$-CO_2 and $^3He/^4He$ compositions suggest the outgassing of a significant component of mantle-derived fluids. The He isotope signature in the outgassing fluids (up to 3.10 R_a) is lower than the values in the peridotite xenoliths of the nearby alkaline basalt volcanic field (R/R_a 5.95Ra±0.01) which are representative of a continental lithospheric mantle and significantly lower than MORB values.

Considering the chemical characteristics of the Ciomadul dacite, including trace element and Sr-Nd and O isotope compositions, an upper crustal contamination is less probable, whereas the primary

magmas could have been derived from an enriched mantle source. The low He isotopic ratios could indicate a strongly metasomatized mantle lithosphere. This could be due to infiltration of subduction-related fluids and postmetasomatic ingrowth of radiogenic He. The metasomatic fluids are inferred to have contained subducted carbonate material resulting in a heavier carbon isotope composition ($\delta^{13}C$ is in the range of -1.4 to -4.6 ‰) and an increase of $CO_2/^3He$ ratio. Our study shows the magmatic contribution to the emitted gases up to 80% [Kis et al., 2019].

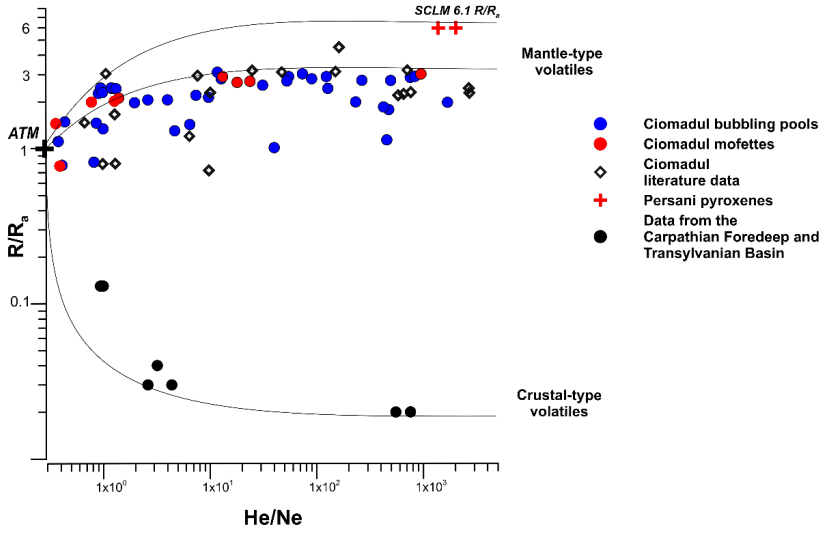

Figure 1 Noble gas composition of the studied gas-emissions of Ciomadul volcano and surroundings.

References

Harangi Sz., Novák A., Kiss B., Seghedi I., Lukács R., Szarka L., Wesztergom V., Metwaly M. & Gribovszki K., (2015). *Combined magnetotelluric and petrologic constrains for the nature of the magma storage system beneath the Late Pleistocene Ciomadul volcano (SE Carpathians*. Journal of Volcanology and Geothermal Research, 290, 82-96.

Kis B.M., Ionescu A., Cardellini C., Harangi Sz., Baciu C., Caracausi C. & Viveiros F., (2017). *Quantification of carbon dioxide emissions of Ciomadul, the youngest volcano of the Carpathian-Pannonian Region (Eastern-Central Europe, Romania).* Journal of Volcanology and Geothermal Research, 341, 119-130.

Kis B.M., Caracusi A., Palcsu L., Baciu C., Ionescu A., Futó I., Sciarra A., Harangi Sz., (2019). *Noble Gas and Carbon Isotope Systematics at the Seemingly Inactive Ciomadul Volcano (Eastern-Central Europe, Romania): Evidence for Volcanic Degassing*. Geochemistry, Geophysics, Geosystems, 20, 6, 3019-3043.

Laumonier M., Karakas O., Bachmann O., Gaillard F., Lukács R., Seghedi I., Menand T., Harangi, Sz., (2019). *Evidence for a persistent magma reservoir with large melt content beneath an apparently extinct volcano*. Earth and Planetary Science Letters, 521, 79-90.

Estimation of CO_2 release from thermal springs to the atmosphere

Li Vigni L.[1], D'Alessandro W.[1], Daskalopoulou K.[2], Gagliano A.L.[1], Calabrese S.[1,3]

[1]*Istituto Nazionale di Geofisica e Vulcanologia, Sezione di Palermo, Italy*
[2]*GFZ, German Research Centre for Geosciences, Potsdam, Germany*
[3]*Università degli Studi di Palermo, Dipartimento delle Scienze della Terra e del Mare, Palermo, Italy*

Corresponding Author: *livignilorenza@gmail.com*

Introduction

Geodynamically active regions have long been recognized as areas of anomalous Earth degassing [Irwin and Barnes, 1980]. Areas found at plate boundaries are characterized by seismic, volcanic and geothermal activity as well as ore deposition. These processes are enhanced by the circulation of hydrothermal fluids in the crust, which transport volatiles from the deep crust or mantle to the surface [King, 1986]. Kerrick and Caldera, [1998], were the first to indicate the significant contribution of the CO_2 degassing by extensional tectonic and hydrothermal activity in metamorphic belts during the Phanerozoic. Moreover, further studies concerning gas emissions from diffuse degassing tectonic structures on various geological regimes suggested in their majority elevated CO_2 concentrations [Klusman, 1993]. In fact, it is worth noting that the estimated global hydrothermal CO_2 flux from subaerial geothermal environments can be comparable to that of direct volcanic discharges [Kerrick et al., 1995; Seward and Kerrick, 1996].

Study Area

The back-arc geothermal fields of Greece include, among others, the Tertiary sedimentary basins of both Sperchios Basin and north Euboea, which are located in central Greece. Their tectonic activity contributes in crust thinning [Papadakis at al., 2016 and references therein] and elevated heat flow values [Fytikas and Kolios, 1979]. These geothermal anomalies due to the tectonic activity and the geological and volcanic regime are expressed as hot springs (Ypatis, Psoroneria, Thermopyles and Kamena Vourla in Sperchios Basin and Edipsos and Ilion in north Euboea). Tectonics of central Greece seems to be of particular interest as major fault structures are found in the area. Sperchios Basin was formed through the activity of WNW-ESE trending faults [Georgalas and Papakis, 1966; Marinos et al., 1973], whilst the Sperchios tectonic graben itself is considered to be the extension of the North Anatolia strike-slip fault. Moreover, in the north Euboean Gulf, the major fault structures are those of the Atalanti Fault Zone (AFZ) that consist of several segments of normal faults, trending about NW-SE [Pavlides et al., 2004].

Materials and Methods

Six groups of springs (Ypatis, Psoroneria, Thermopyles, Kamena Vourla, Edipsos and Ilion) were investigated in this study. Bubbling gases were sampled using an inverted funnel positioned above the bubbles and stored in glass flasks equipped with two stopcocks until analysis. Samples for dissolved gas analyses were collected in glass vials and were sealed underwater. In the laboratory, the concentrations of He, H_2, H_2S, O_2, N_2, CO_2 and CH_4, on the samples were analysed by an Agilent 7890B gas chromatograph with Ar as carrier.
The total CO_2 emitted through bubbling was measured at 6 different pools (Psoroneria, Psoroneria 2,

Thermopyles, Leonidas, Kamena Vourla and Ilion), whereas at other springs (Koniavitis-Sperchios Basin, Edipsos-Damaria and Edipsos-Thermopotamos) an estimation of the release was made by visual inspection. The CO_2 fluxes were measured using the floating chamber method [Mazot and Bernard, 2015] that was equipped with a portable fluxmeter (WEST Systems, Italy) based on the accumulation chamber method as suggested by Chiodini et al., [1998]. The flux data were processed with both the Graphical Statistical Approach (GSA) and the Stochastic Simulation Approach (SSA), with the latter being based on the algorithm of sequential Gaussian simulation [Deutsch and Journal 1998; Cardellini et al., 2003]. Zonal Statistics on the final CO_2 flux maps was obtained using the ArcMap 10.3 (ESRI) Spatial Analyst tool and were used to estimate the total CO_2 output to the atmosphere.

Results and Conclusions

Carbon dioxide is the prevailing gas species for the great majority of the under investigation sites, with only gases collected in the area of Kamena Vourla (Kamena Vourla and Koniavitis) being rich in N_2. The total bubbling CO_2 emission from the pools to the atmosphere ranged from 314 to 44,800 g/m^2/day. At sites with greater surfaces, the CO_2 release was estimated after performing direct measurements (28-Thermopyles, 74-Psoroneria) with the most elevated values being found in the areas of Thermopyles and Psoroneria (1 and 2 t/d, respectively) (Tab. 1); the maps were drawn following the SSA (Figure 1).

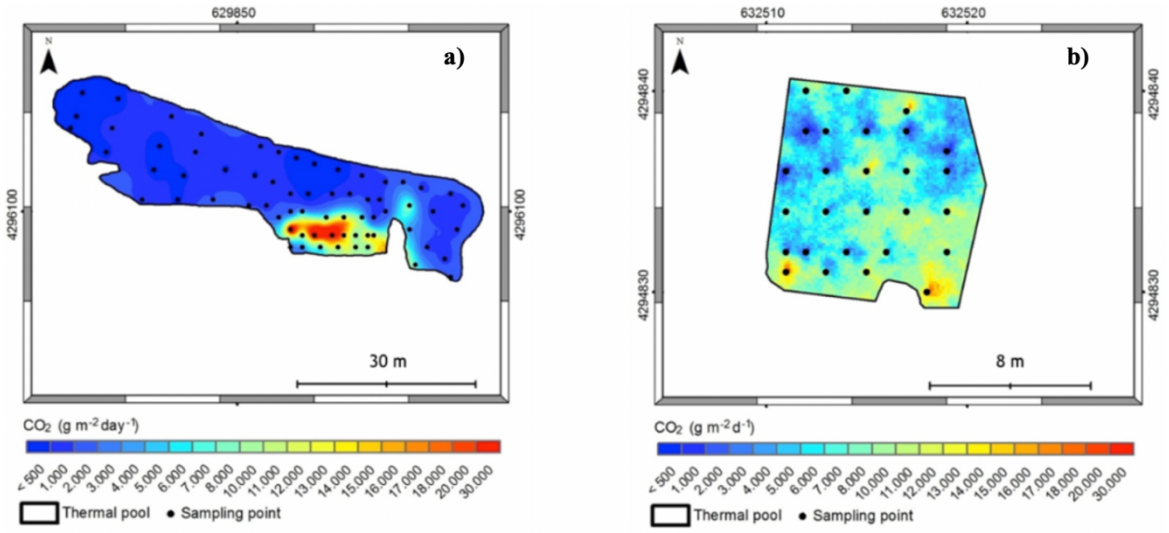

Figure 1 Maps of CO_2 output from Psoroneria (a) and Thermopyles (b) bubbling pools. Red areas represent the elevated free degassing.

The outgoing channels of the springs showed an elevated flow (> 250 l/s) of gas-charged water (> 15 mmol/l of dissolved CO_2). Even though no bubbling was visible along the stream, the dissolved CO_2 content sampled at different distances from springs of Psoroneria and Thermopyles, decreased up to an order of magnitude after few hundreds of metres, indicating an evident and intense, although not visible, CO_2 degassing versus the atmosphere. Physico-chemical parameters (temperature and pH) along the outlet channels were also measured at the same sampling points showing correlations (negative in terms of temperature; T decreased from 33.1 to 30.3 and 40.8 to 39 °C, respectively and positive in terms of pH; pH increased from 6.11 to 7.05 and 6.05 to 7.70, respectively) with the distance. The CO_2 output of the outgoing channels to the atmosphere was quantified considering the

difference between the initial and the final content of the dissolved CO_2 as well as the water flow, obtaining values of > 10 t/d for Thermopyles and ~9 t/d for Psoroneria. Estimations were also made at Ypatis, Kamena Vourla, Koniavitis and Edipsos, where the mean values reached 1 t/d of CO_2 for each spring.

Spring *Methods*	**Degassing pool** *Accumulation chamber* t/d	**Outflow channel** *Dissolved gases* t/d	**Total** t/d
Ypatis	0.2	0.54	0.74
Psoroneria	**2.3**	**9.23**	11.53
Thermopyles	**0.67**	**12.5**	13.17
Leonidas	**0.12**		0.12
Koniavitis	0.2	1.5	1.7
Kamena Vourla	**0.02**	0.1	0.12
Ediposos	0.15	**0.69**	0.84
Ilion	**0.07**	**0.08**	0.15
Total	3.73	24.64	28.37

Table 1 CO_2 output of bubbling pools, outgoing channels and the total amount released. Measured values are found in bold. The remaining part was estimated.

The obtained CO_2 released from the bubbling pools to the atmosphere was directly compared with the one estimated from the outgoing channels (Tab. 1).

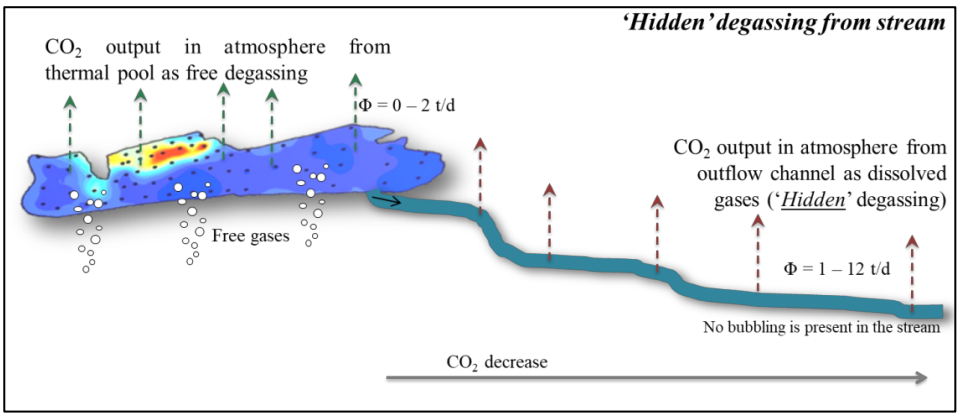

Figure 2 Concept model of total CO_2 output from spring to the atmosphere - stream system.

The degassing along the outflow channel was almost always higher than the corresponding bubbling pool, sometimes even an order of magnitude, suggesting that most of the degassing is "hidden". For each site the amount of CO_2 released versus the atmosphere was calculated as (Figure 2):

$$\Phi_{totCO_2} = \Phi_{pool} + \Phi_{stream} \quad (1)$$

The total CO_2 released to the atmosphere as estimated for the study area is at ~ 30 t/d, with the major contribution deriving from the degassing along the outflow channels of the thermal springs. Such output is comparable and sometimes higher than that of each single active volcanic system along the South Aegean Volcanic Arc (15 - 38 t/d) and highlights the importance of "hidden" degassing along CO_2 - oversaturated streams.

References

Cardellini C., Chiodini G., Frondini F., (2003). *Application of stochastic simulation to CO_2 flux from soil: mapping and quantification of gas release*. J. Geophys. Res., 108 (B9), 2425.

Chiodini G., Cioni R., Guidi M., Raco B., Marini L., (1998). *Soil CO_2 flux measurements in volcanic and geothermal areas*. Appl. Geochem., 13, 543-552.

Deutsh C.V. and Journel A.G., (1998). *GSLIB: Geostatistical Software Library and Users Guide*. Oxford University Press, New York.

Fytikas M. and Kolios N., (1979). *Preliminary heat flow map of Greece*. In: Cermak V., Rybach L., (Eds.), Terrestrial Heat Flow in Europe. Springer-Verlag, pp. 197-205.

Ganas A., (1997). *Fault segmentation and seismic hazard assessment in the Gulf of Evia Rift, central Greece*. Unpublished PhD thesis, University of Reading, 369 pp.

Georgalas G., Papakis N., (1966). *Observations sur les sources ordinaries et thermominerales radioactives de la region karstique de Kammena Vourla (Grece Centrale)*. In: N. Knjiga (ed): Proc. Int. Assoc. Hydrogeologists, Athens, Greece, 221-227.

Irwin W.P. and Barnes I., (1980). *Tectonic relations of carbon dioxide discharges and earthquakes*. Journal of Geophysical Research, 85, 3115-3121.

Kerrick D.M., McKibben M.A., Seward T.M. & Caldera K., (1995). *Convective hydrothermal CO_2 emission from high heat flow regions*. Chemical Geology, 121, 285- 293.

Kerrick D.M. and Caldera K., (1998). *Metamorphic CO_2 degassing from orogenic belts*. Chemical Geology, 145, 213- 232.

King C.Y., (1986). *Gas Geochemistry Applied to Earthquake Prediction: An Overview*. Journal of Geophysical Research, 91, 12,269-12,281.

Klusman R.W., (1993). *Soil Gas and Related Methods for Natural Resource Exploration*. Wiley, Chichester, 483.

Kranis H.D., (1999). *Neotectonic activity of fault zones in central-eastern mainland Greece (Lokris)*. Ph.D. Thesis.

Marinos P., Frangopoulos J., Stournaras G., (1973). *The thermomineral spring of Hypati (Central Greece): hydrogeological, hydrodynamical, geochemical and geotechnical study of the spring and the surrounding area*. Ann. Geol. Pays Hellen., 1:25, 105-214 (in Greek).

Mazot A. and Bernard A., (2015). *CO_2 Degassing from Volcanic Lakes*. In: Rouwet D., Christenson B., Tassi F., Vandemeulebrouck J., (Eds.), Volcanic Lakes, Advances in Volcanology, Springer, Heidelberg, pp. 341-354.

Papadakis G., Vallianatos F., Sammonds P., (2016). *Non-extensive statistical physics applied to heat flow and theearthquake frequency-magnitude distribution in Greece*. Physica, A 456, 135-144.

Pavlides S.B., Valkaniotis S., Ganas A., Keramydas D., Sboras S., (2004). *The active fault of Atalanti - re-evaluation with new geological data*. Bulletin of the Geological Society of Greece, 36, 1560-1567 (in Greek).

Seward T.M. and Kerrick D.M., (1996). *Hydrothermal CO_2 emission from the Taupo Volcanic zone, New Zealand*. Earth and Planetary Science Letters, 139, 105-113.

Volcanic CO_2 emissions in continental collision and rifting settings: A case study on active volcanoes in China

Maoliang Zhang[1], Zhengfu Guo[2], Wenbin Zhao[2] and Sheng Xu[1]

[1]*Institute of Surface-Earth System Science, Tianjin University, China*
[2]*Institute of Geology and Geophysics, Chinese Academy of Sciences, China*

Corresponding Author: *mzhang@tju.edu.cn*

Huge amounts of greenhouse gases (mainly CO_2) can be released into the atmosphere by volcanoes during eruptive stage and also quiescent stage. The relationship between volcanic CO_2 emissions and global climate change has drawn considerable attention from worldwide scientists for studying deep carbon cycle and geological carbon budget. Previous studies [e.g., Brune et al., 2017; McKenzie et al., 2016] suggest different contributions of volcanic CO_2 emissions to the past climate change for volcanism in different tectonic settings. In particular, continental volcanoes are believed to have played a dominant role in modulating atmospheric CO_2 concentrations, possibly due to the CO_2 contributions from (i) sedimentary carbonate rocks stored in the crust [McKenzie et al., 2016] and (ii) the continental lithospheric mantle metasomatized by CO_2-rich fluids/melts [Brune et al., 2017]. The continental volcanoes mainly refer to those from continental arcs and continental rifts. However, volcanoes in continental collision zones are rarely focused. Moreover, the characteristics of volcanic CO_2 emissions during quiescent stage remain less understood.

Here we focus on the Changbaishan volcanoes in continental rifting setting of eastern China and the Tengchong volcanoes in the India-Asia continental collision zone, in order to constrain the nature of volcanic CO_2 emissions in continental collision and rifting settings. Estimated CO_2 fluxes indicate that the CO_2 fluxes of Changbaishan and Tengchong volcanoes are 8.48×10^5 t a^{-1} and 4.5×10^6 t a^{-1} [Zhang et al., 2015; 2016; 2018], respectively. In addition, Tengchong volcanoes have higher carbon release rates that those of Changbaishan volcanoes, which corresponds well with the intensity of hydrothermal activities. Major controlling factors of carbon degassing in volcanic field include (i) distribution of sedimentary carbonate rocks in continental crust, (ii) the enrichment degree of carbon-rich components in mantle source and (iii) heat flow related to regional volcanic and tectonic activities. Evidence from field observations and carbon flux measurements indicate that the India-Asia continental collision zone has higher carbon degassing capacity that that of eastern Asian continental rifts. The interaction between magma and sedimentary carbonate rocks plays an important role in CO_2 degassing from volcanic field [Zhang et al. 2016]. Thus continental collision zone is an important CO_2 source for geological carbon budget and requires further study.

References

Brune S. et al., (2017). *Potential links between continental rifting, CO_2 degassing and climate change through time*. Nat. Geosci., 10, 941-946.

McKenzie N.R. et al., (2016). *Continental arc volcanism as the principal driver of icehouse-greenhouse variability*. Science, 352, 444-447.

Zhang M. et al., (2015). *Stagnant subducted Pacific slab-derived CO_2 emissions: Insights into magma degassing at Changbaishan volcano, NE China*. J. Asian Earth Sci., 106, 49-63.

Zhang M. et al., (2016). *Magma-derived CO_2 emissions in the Tengchong volcanic field, SE Tibet: Implications for deep carbon cycle at intra-continent subduction zone*. J. Asian Earth Sci., 127, 76-90.

Zhang M. et al., (2018). *The intraplate Changbaishan volcanic field (China/North Korea): A review on eruptive history, magma genesis, geodynamic significance, recent dynamics and potential hazards*. Earth-Sci. Rev., 187, 19-52.

Anomalous diffuse H_2 degassing prior to the recent magmatic intrusion at Cumbre Vieja volcano, La Palma, Canary Islands

Melián G.[1,2,3], Padrón E.[1,2,3], Pérez N.M.[1,2,3], Hernández P.A.[1,2,3], Asensio-Ramos M.[1], Amonte C.[1] and Martín-Lorenzo A.[1,2]

[1]*Instituto Volcanológico de Canarias (INVOLCAN), San Cristobal de La Laguna, Spain*
[2]*Instituto Tecnológico y de Energías Renovables (ITER), Granadilla de Abona, Spain*
[3]*Agencia Insular de la Energía de Tenerife (AIET), Granadilla de Abona, Spain*

Corresponding Author: *gladys@iter.es*

Introduction

Cumbre Vieja volcano (La Palma, Canary Islands, Figure 1) is the most active basaltic volcano in the Canaries with seven historical eruptions being Teneguía eruption (1971) the most recent one. Cumbre Vieja volcano is characterized by a main north-south rift zone 20 km long, up to 1950 m in elevation and covering an area of 220 km^2 with vents located at the northwest and northeast.

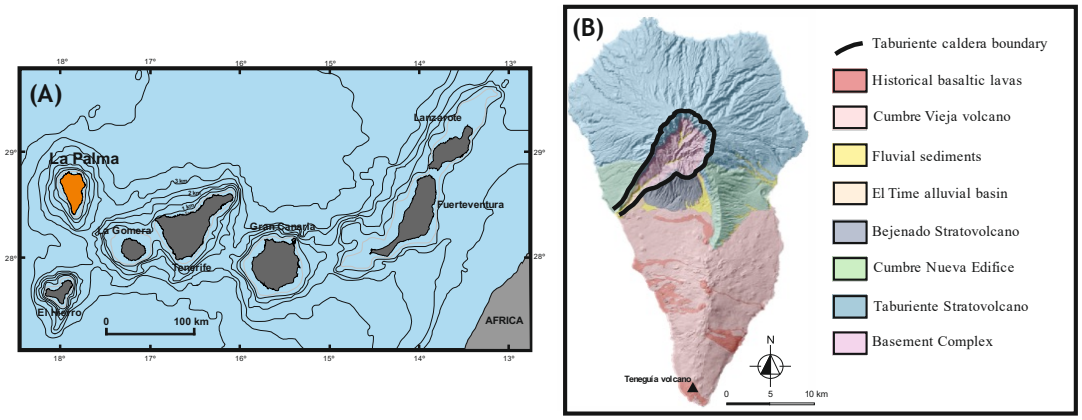

Figure 1 Geographic location of La Palma Island in the Canarian Archipelago (A) and simplified geologic map of La Palma Island (B).

On October 7th, 2017, a remarkable seismic swarm interrupted a seismic silence of 46 years in Cumbre Vieja volcano with more than 75 earthquakes located beneath Cumbre Vieja volcano at depths ranging between 15 and 28 km with a maximum magnitude of 2.7 (Figure 2). On October 13rd a second seismic swarm, lasting about 14 hours, was registered with more than 47 earthquakes at depths ranging between 14 and 25 km and with a maximum magnitude of 2.1. Here we show the results of soil H_2 emission surveys that have been carried out regularly since 2001. Soil H_2 emission was studied because: (1) Cumbre Vieja does not show any visible degassing (fumaroles, etc.), and thus the geochemical volcano monitoring program at this volcano has been focused on soil degassing surveys; and (2) H_2 generated within the crust moves rapidly and escapes to the atmosphere due to its geochemical characteristics, which make this gas an excellent geochemical tracer for the processes occurring within the volcano. H_2 is one of the most abundant trace species in volcano-hydrothermal systems and is a key participant in many redox reactions

occurring in the hydrothermal reservoir gas [Chiodini and Marini, 1998]. Although H_2 can be produced in soils by N_2-fixing and fertilizing bacteria, soils are considered nowadays as sinks of molecular hydrogen [Smith-Downey et al., 2006].

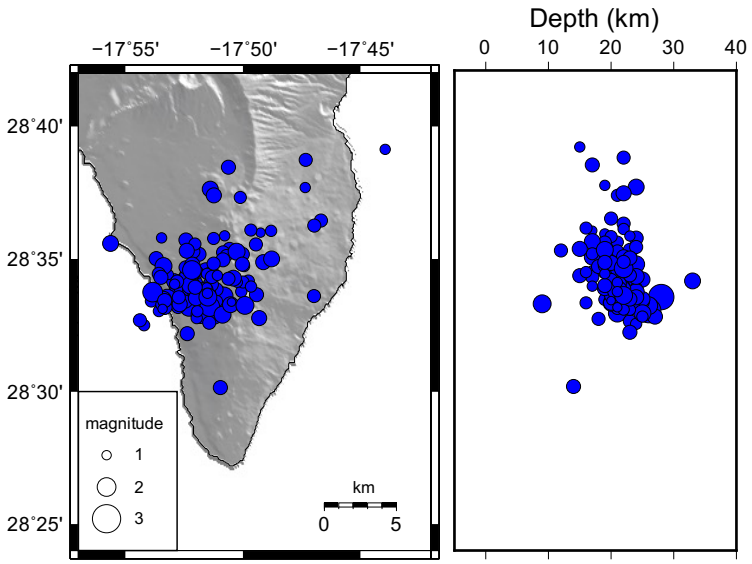

Figure 2 Epicentral location of the seismic events registered in October 7 and 13, 2017 (Source: IGN).

Soil gas samples were collected in about 600 selected sampling sites to obtain a homogeneous distribution at about 40 cm depth using a metallic probe and 60 cc hypodermic syringes and stored in 10 cc glass vials. Ten H_2 surveys were carried out between 2002 and 2017. After October 2017, in order to obtain an almost daily value, the H_2 emission rate was daily computed by means of integrating the new last day 50-70 measurements to the previous 550-530 ones. With this rotation method, we were able to estimate daily H_2 emission rates. H_2 content was analysed in the laboratory by a VARIAN CP4900 micro-GC. The results were used in a simple diffusive emission mechanism to compute the emission rate of H_2 at each survey. Finally, H_2 emission values were used to construct spatial distribution maps by using sequential Gaussian simulation (sGs) algorithm, allowing the estimation of the emission rate from the volcano.

In the period 2001-2003, three surveys were performed with an average H_2 emission rate of ~2.5 $kg \cdot d^{-1}$. This parameter increased significantly during the 2013-2017 period, showing an average value of ~16.6 $kg \cdot d^{-1}$. The maximum value of the series in the period 2001-2017 was measured in June 2017, reaching a value of 36 $kg \cdot d^{-1}$. This maximum value was measured 4 months before the seismic swarms. Figure 3 depicts the spatial distribution of the soil H_2 emission values for June 2016, June 2017 and October 2017 surveys. The emission values observed prior to the sismic unrest show warmer colors, according to the higher H_2 content values observed. No structural control has been observed in the emission values in any of the spatial distribution maps, nor in the one corresponding to the 13th of October 2017.

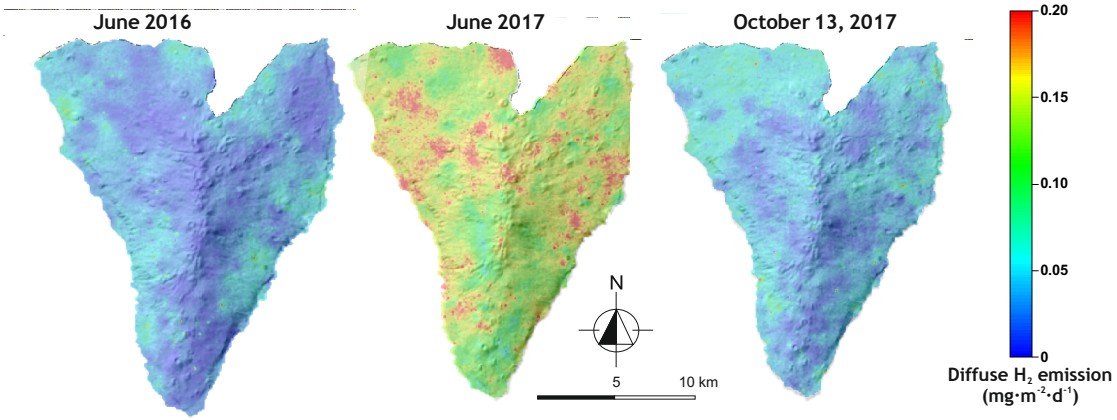

Figure 3 Spatial distribution maps of soil H_2 efflux measurements constructed from an average of 100 realizations using the sGs method.

Figure 4 shows the temporal evolution of the H_2 emission rate calculated for the entire volcanic system, with a relative maximum in 2013 and an absolute maximum in June 2017. It is worth noting that the relatively stable diffuse CO_2 emission reported by Padrón et al., [2015], emissions was broken by sudden increases during 2011 and 2013. The increase observed in 2013 in the soil H_2 emission agrees with the one measured in the CO_2 emission and reported by Padrón et al., [2015]. The daily emission values measured from October 18 to December 18, shows a relatively constant range of values between 8 and 14 kg·d^{-1}. The probability plot of the diffusive H_2 emission values estimated for the June and October 13 surveys (Figure 5) shows that both emission values are represented by single geochemical population, which suggest a single origin for the emission values and a negligible biogenic contribution. H_2 emission surveys have demonstrated to be sensitive and excellent precursors of magmatic processes occurring at depth in Cumbre Vieja. Periodic H_2 emission surveys provide valuable information to improve and optimize the detection of early warning signals of future volcanic unrest at Cumbre Vieja volcano.

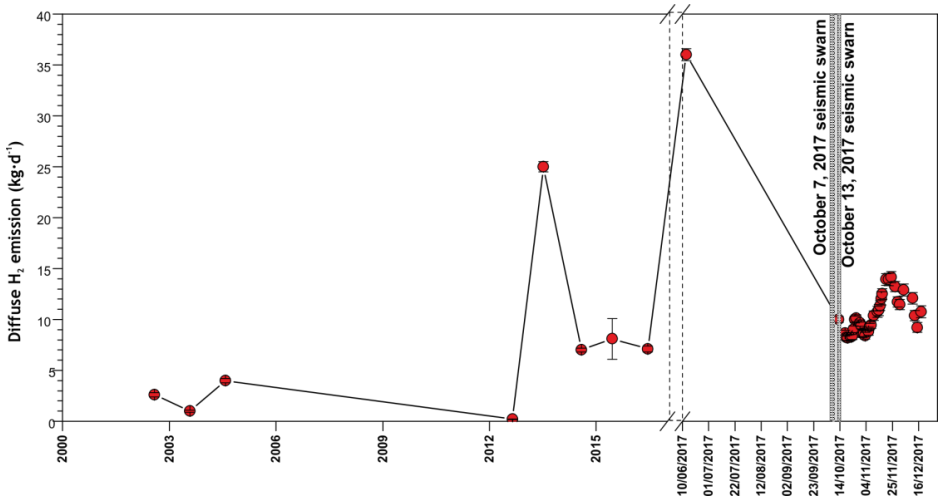

Figure 4 Temporal evolution of the estimated diffuse H_2 emission rate estimated from Cumbre Vieja volcano during the period 2002-2017.

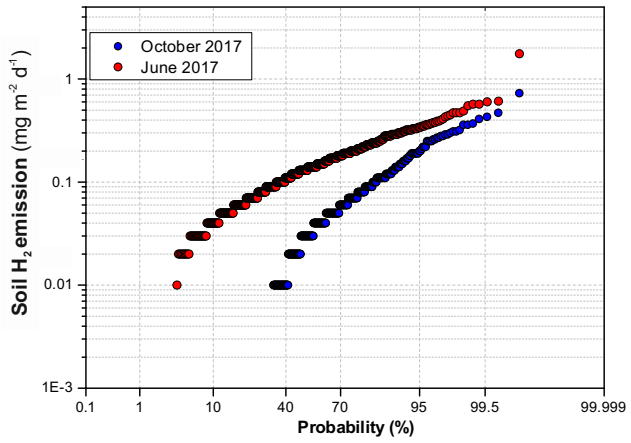

Figure 5 Statistical-graphic analysis of the soil H_2 efflux measurements performed at Cumbre Vieja volcano related to the June and October 2017 surveys.

References

Chiodini G. and Marini L., (1998). *Hydrothermal gas equilibria: the H_2O-H_2-CO_2-CO-CH_4 system*. Geochim. Cosmochim. Acta, 62, 2673-2687.

Padrón E., Pérez N.M., Rodríguez F., Melián G., Hernández P-A., Sumino H., Padilla G., Barrancos J., Dionis S., Notsu K., Calvo D., (2015). *Dynamics of diffuse carbon dioxide emissions from Cumbre Vieja volcano, La Palma, Canary Islands*. Bull. Volcanol., 77:28.

Smith-Downey N.V., Randerson J.T., Eiler J.M., (2006). *Temperature and moisture dependence of soil H_2 uptake measured in the laboratory*. Geophys. Res. Lett., 33: L14813.

Thermal waters from the Apuseni mountains (western Romania) - a preliminary geochemical survey

Nicula A.M.[1], Ionescu A.[1,2,3], Pop C.I.[1], Roba C.[1], Orașeanu I.[4], Palcsu L.[5], Baciu C.[1]

[1]*Babeş-Bolyai University, Faculty of Environmental Science and Engineering, Cluj-Napoca, Romania*
[2]*Università di Perugia, Dipartimento di Fisica e Geologia, Perugia, Italy*
[3]*MTA-ELTE Volcanology Research Group Department of Petrology and Geochemistry, Budapest, Hungary*
[4]*Romanian Association of Hydrogeologists, Bucuresti, Romania*
[5]*Isotope Climatology and Environmental Research Centre (ICER), Hungarian Academy of Sciences (ATOMKI), Debrecen, Hungary*

Corresponding Author: *marius_alin92@yahoo.com*

The Apuseni Mountains, located in the western part of Romania, form an internal segment of the Carpathian range. The Apuseni Mountains belong to the Tisia lithospheric block, and roughly consist of two major structural units (Figure 1). The Northern Apuseni (Internal Dacides) are represented by complex sequences of nappes including metamorphites and Palaeo-Mesozoic sediments. Granitic bodies are an important part of this edifice. The Southern Apuseni (Transylvanides), representing the major Tethyan suture [Sandulescu, 1984], include ophiolitic complexes and their associated sedimentary cover, mainly Jurassic-Cretaceous in age. This pile of rocks is intersected by Neogene magmatic bodies that have generated important deposits of precious and base-metals (Metaliferi Mts.).

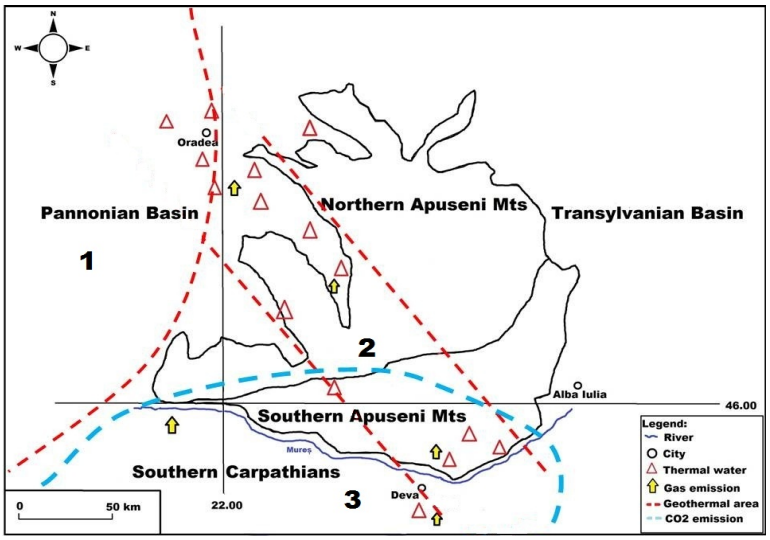

Figure 1 General features of the study region. 1. Geothermal area in the Pannonian Basin; 2. Geothermal area in the Apuseni Mts.; 3. Mophetic area of the Apuseni Mts.

The two adjacent Neogene sedimentary areas, the Pannonian Basin to the west, and the Transylvanian Basin to the east, show great contrast from a geothermal point of view. The Pannonian Basin is well-known as a large and important geothermal region, while the Transylvanian Basin is cold [e.g. Horvath et al., 2015; Tilita et al., 2018]. For the Apuseni Mts., the geothermal studies are still scarce [e.g. Oraseanu, 2016]. Data concern the hydrogeological features of the area, however few

interpretations of the water and gas geochemical are available, along with a deep understanding of the geothermalism at a regional scale that is still lacking. The thermal waters in the Apuseni Mts. mainly occur on a NW-SE lineament, crossing the two structural units, the Internal Dacides and the Transylvanides. Most of the thermal waters are related to karst formations, which are very well developed in the area. In spite of the extensive research performed during the last decades on the karst, relatively few interpretations of the hydrogeochemical data of the thermal waters are available. Considering the many unknowns of this area from a geochemical point of view, the present study aims to provide information on the genesis and distribution of the thermal waters in the Apuseni Mountains area. Another objective of the study is to establish whether similarities or relations exist between the Pannonian geothermal system and the Apuseni Mountains system.

A preliminary survey of the thermal water occurrences in the Apuseni area has been performed, and water samples have been collected from 37 sources. Gas samples have been collected from several points where the intensity of degassing allowed proper sampling. The pH varies between 6.00 and 8.72, the lowest values have been measured in the CO_2-rich waters in the south. Thermal water temperatures varied between 14.4°C and 78.7°C. The Ca-HCO_3 water type dominates in the southern and central part of the study area, while in the north-west the water type is generally $NaHCO_3$. The isotopic measurements show values between 0.9 and 2.18 for the $^3He/^4He$ ratio, and values fluctuating in the range 0.6229 and 40.8707 for the $^4He/^{20}Ne$ ratio. The intended research will continue with more detailed investigations of the thermal water geochemistry in the Apuseni Mts. area. We expect interesting conclusions from the minor, major and noble gases molecular and isotopic measurements.

References

Horvath F., Musitz B., Balazs A., Vegh A., Uhrin A., Nador A., Koroknai B., Pap N., Toth T., Worum G., (2015). *Evolution of the Pannonian basin and its geothermal resources*. Geothermics, 53, 328-352.

Orășeanu I., (2016). *Hidrogeologia Carstului din Munții Apuseni*. Editura Belvedere.

Săndulescu M., (1984). *Geotectonica României*. Editura Tehnică, Bucureşti.

Tiliță M., Lenkeyc L., Mațencoa L., Horváth F., Surányid G., Cloetingha S., (2018). *Heat flow modelling in the Transylvanian basin: Implications for the evolution of the intra-Carpathians area*. Global and Planetary Change, 171, 148-166.

Soil gas $^4He/CO_2$ ratio and volcanic activity

Padrón E.[1,2,3], Pérez N.M.[1,2,3], Hernández P.A.[1,2,3], Melián G.[1,2,3], Asensio-Ramos M.[1] and Alonso M.[1,2,4]

[1]*Instituto Volcanológico de Canarias (INVOLCAN), San Cristobal de La Laguna, Spain*
[2]*Instituto Tecnológico y de Energías Renovables (ITER), Granadilla de Abona, Spain*
[3]*Agencia Insular de la Energía de Tenerife (AIET), Granadilla de Abona, Spain*
[4]*Universidad Complutense de Madrid (UCM), Madrid, Spain*

Corresponding Author: *eleazar@iter.es*

Introduction

Magmatic gases are released not only through preferential degassing routes as fumaroles, but also percolate through the volcano's porous flanks and are released to the atmosphere in a non-visible (diffuse) way. This type of degassing represents an important mechanism to dissipate energy at volcanoes [Chiodini et al., 2005] and is a large contributor to the global volcanic degassing [Burton et al., 2013]. Some of the most studied gases is soil degassing studies are He and CO_2 because both species have similar low solubility in silicate melts at low pressures [Giggenbach, 1996] and are considered good geochemical tracers of magmatic activity [Hernández et al., 2001; Padrón et al., 2013]. However, once they are exsolved from the silicate melts, their movement through the crust towards the surface is very different. While CO_2, as reactive gas, is affected by the occurrence of interfering processes [Marini and Gambardella, 2005] (gas scrubbing by ground-waters and interaction with rocks, decarbonatation processes, biogenic production, etc.), He is chemically inert, radioactively stable, non-biogenic, highly mobile, and relatively insoluble in water [Padrón et al., 2013]. These properties minimize the interaction of this noble gas with the surrounding rocks or fluids during its ascent towards the surface. Their geochemical differences yield higher relative He/CO_2 ratio in the fumarole gases than is actually present in the magma, but it decreases when the magma reservoir reaches enough pressure to generate incipient fracture systems approaching the eruption, thus releasing considerably more of the magma volatiles [Thomas and Naughton, 1979]. Here we present some studies of soil He and CO_2 emission performed during recent volcanic unrest periods in the Canary Islands. The studies have been performed in a wide area of the volcanoes, thereby minimizing loss of information due to the inherent internal heterogeneity of the volcano.

Three case studies were used to test the hypothesis: El Hierro island, summit crater of Teide volcano and Cumbre Vieja volcano, all of them located in the Canary Islands. The recent submarine eruption at El Hierro Island in the Canaries started on October 12, 2011, has been an excellent opportunity to apply novel methodologies to monitor the volcanic activity. Among the geochemical methods applied to monitor the volcanic activity during the volcano-seismic unrest of El Hierro, special interest was addressed to diffuse degassing, because the island does not present any visible emanation of volcanic gases. Melián et al., [2014] estimated in a quasi-daily basis the CO_2 emission rate in the entire island and here we applied the same methodology to the He emission data already reported[4], allowing to estimate the quasi-daily diffusive He emission rate for the whole island. As can be observed in Figure 1, the increase of He/CO_2 emission ratio also preceded increases in the seismic activity during the volcanic unrest. Moreover, He/CO_2 emission ratio starts decreasing simultaneously with seismic activity, reaching a relative minimum at the eruption onset. The temporal analysis of the erupted volume

indicated an intense explosive activity during the early stages of the eruption, showing an important peak in 18 October, six days after eruption onset16. This observation coincides with a new increase in the He/CO_2 emission ratio which reached a relative maximum only one day after this date (Figure 1). We also observed a significant He/CO_2 emission peak (up to 5.5×10^{-4}) between 3 and 4 November some days before the period with the highest magma emission rate and hot hydrothermal fluids from the submarine vent (pink area in Figure 1).

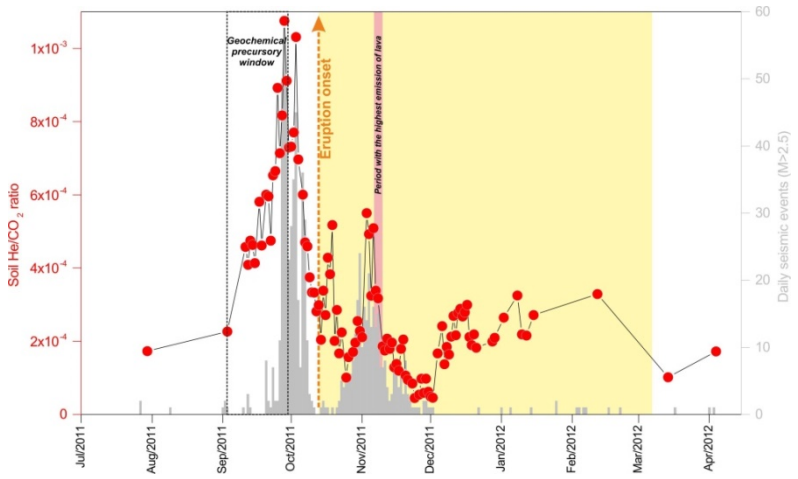

Figure 1 Temporal evolution of soil He/CO_2 emission ratio and number of seismic events with ML>2.5 (grey bars) recorded by the Spanish National Geographic Institute (http://www.ign.es) in the period 15 July 2011 - 15 April 2012 on El Hierro Island. The eruption onset is shown by a vertical orange arrow. The eruptive period is highlighted in yellow. Pink area highlights the period with the highest magna emission rates10. Black dashed lines indicate a geochemical precursory window (3-28 September 2011).

The He/CO_2 emission ratio has been monitored since 2006 at the summit crater of Teide volcano. The observed He/CO_2 emission ratio showed an average value of 5.6×10^{-4} between 2006 and mid-2016, and increased 4 times before the occurrence of a seismic swarm of long-period events on 2 October 2016. After recording this peak value, the He/CO_2 emission ratio has fluctuated greatly during a seismic unrest period observed in the island of Tenerife likely caused by the release of fluids due to the internal dynamic of the magmatic/hydrothermal system of Tenerife.

The last study case is Cumbre Vieja volcano, in La Palma island. Cumbre Vieja, the last stage in the geological evolution of the island, is the most active volcano of the Canaries, because 7 of the last 16 historical eruptions have occurred there. Seismic swarms beneath Cumbre Vieja have been recently recorded after 30 years of seismic quiescence. The Gutenberg Richter b-value reached values >1.9 for these seismic swarms. Furthermore, the high stress drop values retrieved for some of the strongest earthquakes, together with the depth of the hypocenters (15-25 km), seems to indicate that the seismicity was related to a magmatic intrusive episode. Monitoring of diffuse gas emission has been regularly performed at Cumbre Vieja over the last 17 years. In the period 2002-2017, the He/CO_2 emission ratio at Cumbre Vieja showed a pretty stable average value around 3.2×10^{-4}, and increased up to 2.7×10^{-3} immediately after the occurrence of the first seismic swarm on 7-9 October, 2017 (Figure 2). The consequent depressurization of a magma batch due to an upward magma migration from an ephemeral magmatic reservoir was the source of the volatiles observed at the surface, which matches the expected geochemical behavior of both gases.

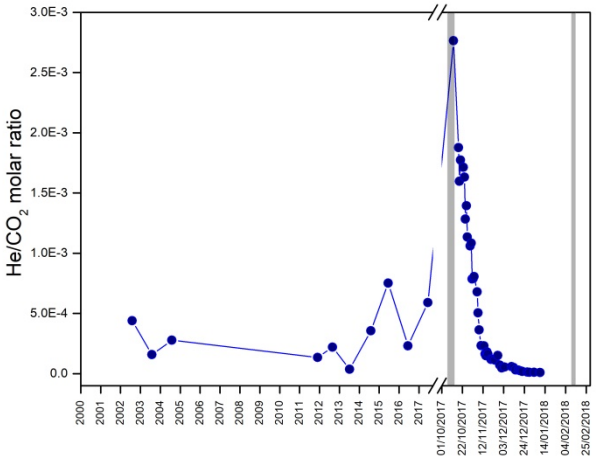

Figure 2 Temporal evolution of soil He/CO_2 emission ratio and number of seismic events with ML>2.5 (grey bars) recorded by the Spanish National Geographic Institute (http://www.ign.es) in the period 15 July 2011 - 15 April 2012 on El Hierro Island. The eruption onset is shown by a vertical orange arrow. The eruptive period is highlighted in yellow. Pink area highlights the period with the highest magna emission rates10. Black dashed lines indicate a geochemical precursory window (3-28 September 2011).

This new volcano monitoring method may contain information from a wide area of the volcano, thereby minimizing loss of information due to the inherent internal heterogeneity of the volcano. Our results highlight the importance of continuous monitoring of this ratio in active volcanic regions, mainly at those areas without visible manifestations of volcanic fluid discharges and the critical role that volcanic gases can play in the prediction of major volcanic events, even in the absence of visible manifestations of volcanic fluid discharges.

References

Burton M.R., Sawyer G.M. and Granieri D., (2013). *Deep carbon emissions from volcanoes*. Rev. Mineral. Geochem., 75:323-354.

Chiodini G., Granieri D., Avino R., Caliro S., Costa A. and Werner C., (2005). *Carbon dioxide diffuse degassing and estimation of heat release from volcanic and hydrothermal systems"*. J. Geophy. Res., 110(B08204).

Giggenbach W.F., (1996). *Chemical Composition of Volcanic Gases*. In Monitoring and mitigation of volcanic hazards, eds Scarpa R., Tilling R.I., Springer-Verlag Berlin Heidelberg, Germany, pp 221-256.

Hernández P.A., Notsu K., Salazar J.M., Mori T., Natale G., Okada H., Virgili G., Shimoike Y., Sato M. and Pérez N.M. (2001). *Carbon dioxide degassing by advective flow from Usu volcano, Japan*. Science, 292:83-86.

Marini L. and Gambardella B., (2005). *Geochemical modeling of magmatic gas scrubbing*. Ann. Geophys., 48:739-753.

Melián G., Hernández P.A., Padrón E., Pérez N.M., Barrancos J., Padilla G., Dionis S., Rodríguez F., Calvo D. and Nolasco D., (2014). *Spatial and temporal variations of diffuse CO_2 degassing at El Hierro volcanic system: relation to the 2011-2012 submarine eruption*. J. Geophys. Res., 119:6976-6991.

Padrón E., Pérez N.M., Hernández P.A., Sumino H., Melián G., Barrancos J., Nolasco D., Padilla G., Dionis S., Rodríguez F., Hernández I., Calvo D., Peraza M.D. and Nagao K., (2013). *Diffusive helium emissions as a precursory sign of volcanic unrest*. Geology, 41:539-542.

Thomas D.M. and Naughton J.J. (1979). *Helium/Carbon dioxide ratios as premonitors of volcanic activity*. Science, 204:1195-1196.

Etna eruption of 24-27 December 2018: inferences from geochemical parameters

Federico C., Bellomo S., Brusca L., Camarda M., Caracausi A., D'Alessandro W., De Gregorio S., Liuzzo M., Giuffrida G., Giudice G., Gurrieri S., Longo M., Paonita A., Rizzo A.

Istituto Nazionale di Geofisica e Vulcanologia, Sezione di Palermo, Italy

Corresponding Author: *antonio.paonita@ingv.it*

On the morning of 24 December 2018, following an earthquake swarm located mainly below the summit craters and south of these, an eruptive fissure opens up on the side of the New Southeast Crater (NCSE) at about 3100 m asl. The fracture spreads rapidly to the south-east, reaching an altitude of 2400 m asl and reaching a total length of about 2 km. The explosive activity sustained by the aforementioned crack, as well as by the Bocca Nuova and the Crater of N-E fueled an impressive plume of gas and ash. Finally, a series of mouths opened along the fissure fed an important lava effusion, which was however exhausted within a few days.
The geochemical monitoring carried out by the Palermo Section and by OE revealed some signals of certain interest, both prior to the eruptive activity and syn- and post-eruptive. The relative abundances of He-Ar-CO_2 in the gaseous emissions at the base of the volcano confirmed a dominant contribution deriving from the exsolution of magmatic gases from depths around 70-12 km bsl. The values of the $^3He/^4He$ isotope ratio in the same sites, after peaking in June 2018, showed stable values at medium-high levels until the beginning of the December eruption. This would indicate that the contribution of primitive magma in the deep system (7-12 km bsl) remained sustained for 5-6 months, although with rates lower than the pre-summer ones, determining conditions of considerable pressurization at the beginning of the eruptive activity of December.
The progressive deep pressurization would have been the cause of a sequence of impulsive events of ascent of magma bodies from the deep towards superficial portions of the feeding system (<3 km s.l.m). These events are clearly recognizable as different phases of marked increase from June to October of the flows of CO_2 diffused by soils, which correspond to increases in the CO_2/SO_2 ratio in the plume, which in fact indicate the contribution of less degassed magma. The phenomenologies observed at the summit craters from May 2018 (episodes of Strombolian activity and effusive) would be attributable to the same process. The marked decrease in CO_2 emissions from the soils of the volcano starting in November would indicate that the pre-eruptive transfer from the deep to the superficial system was probably limited by a high pressurization in the entire magma rising path, coherently also with low values of C/S at the beginning of the December 24 eruption. The significant drop in the $^3He/^4He$ sin- and post-eruptive isotopic ratio suggests that the system has certainly decompressed following the eruption.
The massive magmatic recharge processes that characterized 2018 and a large part of 2017 seem to have had an impact also on the structure of the volcano, at least on the systems of migration and disposal of magmatic fluids. The long trend of decreasing CO_2 in aquifers suggests a reduced interaction between magmatic fluids and underground water flow. The effect of the stress variations on this process would be evidenced by the minimum of dissolved CO_2 observed in October after the seismic event occurred at the beginning of the month, while the period immediately before the

intrusion of the dike and the seismic activity of December 26 is characterized by a narrow positive peak in the CO_2 contents of the aquifer. In the same context, we observed a significant increase in the CO_2 flow from soils of the Pernicana area, straddling the seismic event of 8 January 2019 occurred in the same area, probably linked to increases in permeability along the fault closely linked to the change in stress field.

Characterization of a hot "fumarolic mofette" at Caldeiras da Ribeira Grande/S. Miguel, Acores

Pfanz H.[1], Viveiros F.[2], Silva C.P.P.[2,3], Thomalla A.[1]

[1]*Institute of Applied Botany and Volcano Biology, University of Duisburg-Essen, Germany*
[2]*IVAR- Instituto de Investigação em Vulcanologia e Avaliação de Riscos, University of the Azores, Portugal*
[3]*CIVISA - Centro de Informação e Vigilância Sismovulcânica dos Açores, University of the Azores, Portugal*

Corresponding Author: *hardy.pfanz@uni-due.de*

A 10 x 10m subarea of a hot and heavily CO_2 emitting mofette on a hilly grassland at Caldeiras da Ribeira Grande, located on the north flank of Fogo Volcano, was studied. A 1 x 1m grid was laid on top of the area and at each intersection, soil gas measurements were performed at three different depths. CO_2, CO and O_2 were measured. In addition, soil CO_2 flux using the accumulation chamber method was measured and soil cores were taken at each grid intersection at a depth of 7-13cm as this depth was thought to reflect the main rooting horizon of grasses and herbaceous plants in that area. Soil water content, soil pH, conductivity and organic matter were determined. Quantitative vegetation analysis was carried out and total number of plant species as well as species total and individual coverage were estimated in each square.

Carbon dioxide was emitted in 4/5 of the total area and only 20m^2 showed no or a low CO_2 emission. Only the upper horizontal part of the mofette showed CO_2 background values in the upper soil horizon. The lower part of the area was strongly CO_2 emitting, with CO_2 concentrations reaching 90-100% at the left lower part of the area. Oxygen values inversely corresponded to the CO_2 concentrations. Oxygen was high when CO_2 was low and vice versa. Overall, CO_2 values increased with depth, whereas O_2 decreased. Soil CO_2 fluxes mirrored the CO_2 concentrations to a large extent.

In addition, soil temperature nicely mirrored CO_2 concentrations. Temperatures were close to ambient in the upper one-third of the area where CO_2 was low; temperature increased even in the upper soil horizon in the lower 2/3 of the area, where CO_2 emission was high. Also, temperature increased with soil depth but was 70°C even at only 20cm soil depth. Two dominant high temperature spots were found at the lower part of the mofette; a lower temperature "channel" divided the spots.

Total plant coverage showed a "Y" shape in the lower 5m of the area. Plant coverage was close to 100% all over the area except at those parts where soil temperature, soil CO and soil CO_2 concentrations were high (40-70°C). Interestingly, plant species number was lowest on low CO_2 emitting soils; between one and four species grew at these sites (2-12% CO_2). On higher emitting and warmer soils, species number slightly increased. Up to 13 different species were counted.

Two grasses, namely *Lolium perenne* (perennial ryegrass) and *Holcus lanatus* (meadow soft grass) grew only on cooler, low-CO_2-emitting sites; they thus reflect thermophobic and mofettophobic plant species [Pfanz et al. 2004; 2019]. *Cyperus esculentus* (earth almond), *Kyllingia brevifolia* (shortleaf spike sedge), and *Oxalis corniculata* (creeping wood sorrel) proved to be highly thermophilic [see also Delmer, 1974; Burns, 1997]. These species also proved to be mofettophilic as they also tolerate quite high CO_2 concentrations in their rooting horizon.

As in other mofettic places with CO_2 emissions at ambient temperatures [NW Czechia -

Saßmannshausen 2010; Thomalla, 2015; Laacher See Germany - Pfanz et al., 2019], also in hot and CO_2 emitting sites, plants can be found that indicate high CO_2 emission (mofettophiles) or high temperatures (thermophiles). In our case also thermo-mofettophiles were found.

References

Burns B., (1997). V*egetation change along a geothermal stress gradient at Te Kopia steamfield.* Journal of the Royal Society of New Zealand, 27: 279-294.

Delmer D.P., (1974). *Studies on the nature of adaptations of the monkey flower*, Mimulus gutattus, *to a thermophilic environment*. Canadian Journal of Botany, 52: 1509-1514.

Pfanz H., Vodnik D., Wittmann C., Aschan G., Raschi A., (2004). *Plants and geothermal CO_2 exhalations - survival in and adaptation to a high CO_2 environment*. In Esser K., Lüttge U., Kadereit J.W., Beyschlag W. (Hrsg.). Springer Verlag, Berlin, Heidelberg. Progress in Botany, 65, 499-538.

Pfanz H., Saßmannshausen F., Wittmann C., Pfanz B., Thomalla A., (2019). *Mofette vegetation as an indicator for geogenic CO_2 emission: A case study on the banks of the Laacher See Volcano, Vulkaneifel, Germany*. Geofluids, in press.

Saßmannshausen F., (2010). *Vegetationsökologische Charakterisierung terrestrischer Mofettenstandorte am Beispiel des west-tschechischen Plesná-Tals*. Dissertation, Universität Duisburg-Essen.

Thomalla A., (2015). *Boden - und vegetationskundliche Untersuchungen zur Charakterisierung der Ausgasungs - und Vegetationsdynamik zweier trockener Mofetten im west-tschechischen Plesnátal.* Dissertation, Universität Duisburg-Essen.

Post-eruptive development of an emerging subglacial/subaerial geothermal area on the caldera rim of Bárðarbunga volcano, Iceland

Pfeffer M.A.[1], Reynolds H.I.[2], Bergsson B.[1], Ófeigsson B.G.[1], Gudmundsson M.T.[2], Grassa F.[3], Giudice G.[4], Högnadóttir T.[2]

[1]*Icelandic Meteorological Office, Reykjavík, Iceland*
[2]*Nordic Volcanological Center, Institute of Earth Sciences, University of Iceland, Reykjavík, Iceland*
[3]*Istituto Nazionale di Geofisica e Vulcanologia, Sezione di Palermo, Italy*

Corresponding Author: *melissa@vedur.is*

Bárðarbunga is a subglacial volcano, situated beneath the Vatnajökull glacier, which underwent a large six-month long fissure eruption accompanied by a gradual caldera collapse in 2014-2015. About 1.5 km^3 of lava was erupted at the Holuhraun eruption site. Several ice cauldrons (depressions on the glacier surface) formed around the caldera rim due to geothermal melting at the glacier base. In July 2015, five months after the eruption ended, cauldrons were first observed on the southern caldera rim, where the ice is less than 150 m thick. These ice cauldrons continue to be active, four years after the eruption ended. The properties of the cauldrons have been observed to change during these four years, including their relative sizes, if melt water was visible, and if they were observably degassing. Subaerial geothermal gases coming from this geothermal area were first identified in June 2015. Monitoring this area is particularly challenging because the exposed geothermal areas are contained within glacial crevasses that form due to the changes in the ice induced by the geothermal heat. We measured the subaerial gases emitted by the geothermal area periodically from this difficult to access site by setting up secure snow anchors using glacial crevasse rescue techniques. We used MultiGAS, sometimes on the edge of the crevasse, sometimes lowered into the crevasse, and collected air samples with as high concentration of gases as possible by leaning over the edge of the crevasse for Carbon isotope of CO_2 analysis. Two distinct cauldrons within the geothermal area were measured to emit identical CO_2/H_2S ratios in June 2018 when both were degassing. The CO_2/H_2S ratio of the area had an initial peak in June 2015 (four months post-eruption) which decreased in July 2015 to its lowest values and has steadily increased until the most recent measurements in June 2019. The $\delta^{13}C_{CO2}$ values are quite scattered thus suggesting that fractionation processes may occur. The increasing CO_2/H_2S ratio can be attributed to declining emissions of H_2S as the magma intrusion cools. The combined volume of the two open cauldrons has not still not declined in the four years since their first appearance, indicating sustained and ongoing geothermal heat release following intrusion of the magma. Depending on the bedrock conditions (mostly permeability and temperature), there can be a delay between heat released from the cooling magma and a thermal signal at the surface. We will examine the different response times of the chemical and geophysical signals observable here. This geothermal area is located on the caldera rim, where the ice cover of Vatnajökull is thinnest over Bárðarbunga, giving the possibility for this area to become partially subaerial. The work described here give us insight into the monitoring of the far more numerous fully subglacial geothermal areas, which are more difficult to monitor due to the obscuring influence of the ice cover.

Assessing the state of Pico Basile volcano, Bioko island, Equatorial Guinea

Sealing C.[1], Tassi F.[2], Rizzo A.L.[3], Vanderkluysen L.[1]

[1]*Drexel University, Department of Biodiversity, Earth & Environmental Science, Philadelphia, USA*
[2]*Universitá di Firenze, Dipartimento di Scienze della Terra, Firenze, Italy*
[3]*Istituto Nazionale di Geofisica e Vulcanologia, Sezione di Palermo, Italy*

Corresponding Author: *crs358@drexel.edu*

Pico Basile is a 3007 m high, basaltic shield volcano located on Bioko Island (formerly Fernando Poo), Equatorial Guinea (Figure 1). The 700 km^2 island is located in the Gulf of Guinea, approximately 35 km from the coast of Cameroon. Straddling the edge of the continental shelf, it is geographically the first offshore expression of the intraplate Cameroon Volcanic Line (CVL). Bioko has a population of over 400,000 people, most of whom live in the capital city, Malabo, on the slopes of Pico Basile. The volcano is largely unmonitored, and no work has yet been done to elucidate the current activity state of the volcano.

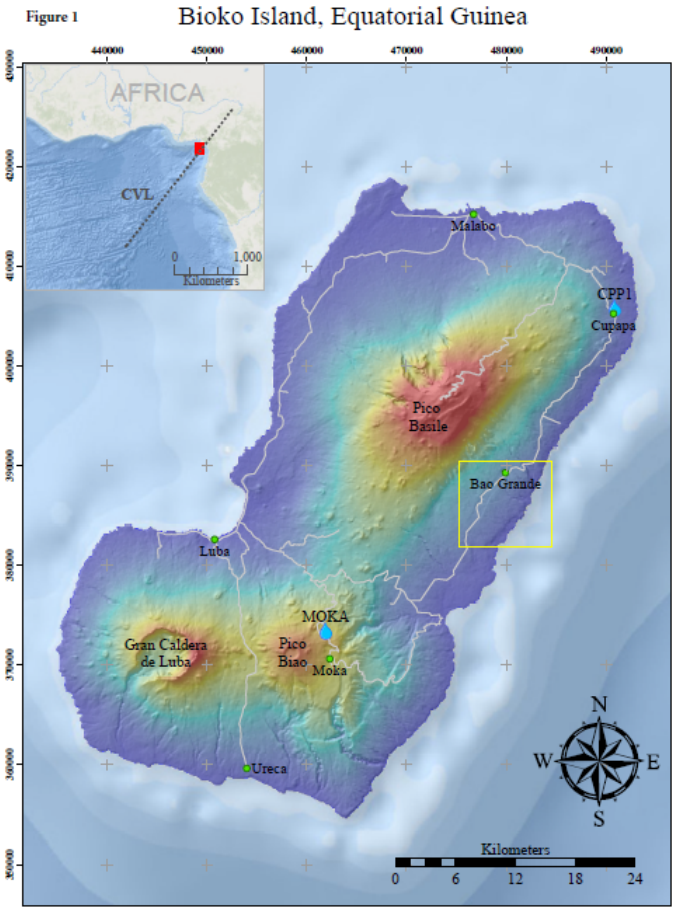

Figure 1 Bioko Island, Equatorial Guinea. Blue tear drops represent bubbling springs. Yellow rectangle surrounds the area of the last recorded magmatic eruption in 1923.

Activity and Hazards

Preliminary results from the broadband seismic study show significant seismicity surrounding the island [Amanda Lough, 2018, pers. comm.] A magmatic eruption in 1923 [Enciclopedia Universal Ilustrada, 1924] and steam events within the past decade demonstrate the vulnerability of the island if the volcano remains unstudied and unmonitored. Although there are no fumaroles known on the island, there are several vigorously bubbling springs on the lower flanks of Pico Basile volcano. Gas samples taken from one of these springs revealed them to be largely CO_2 of basaltic volcanic origin with a mantle carbon contribution of 87% [Aka et al., 2001].

Even in a state of outward quiescence, gas escape from roiling springs and the death of nearby animals indicate gas accumulation at potentially hazardous levels. The dense tropical forests and presence of highly stratified crater lakes present a real possibility for CO_2 related hazards on the island. Disasters have occurred previously along the CVL, when crater lakes at Nyos and Monoun overturned, releasing clouds of CO_2 that killed a cumulative total of over 1800 people and 3500 livestock. Although the eruptive history of Bioko Island is poorly understood, it is evident that volcanic hazards do exist and the potential for future unrest is not negligible. Therefore, it is important to assess the current state of the volcano and the potential for future activity to minimize risk for the people of the island and the capital of Equatorial Guinea.

The Study

To assess the current activity state of this volcano, we are undertaking several studies using gas geochemistry techniques. In 2018, we performed several soil degassing surveys using a LICOR-equipped CO_2 accumulation chamber to identify areas of high CO_2 flux. To determine the compositions of the bubbling springs, we have taken gas and water samples from springs on opposite sides of the volcano. Finally, we have obtained rock samples containing dunite and possibly lherzolite and harzburgite xenoliths from several locations and elevations on Pico Basile, from which we will analyze fluid inclusions for their volatile and noble gas content.

Results

Water Chemistry

Spring waters are cold with pH in the neutral range. Major ion chemistry indicates a meteoric composition with little-to-no water-rock interaction, suggesting the springs remain cold and percolate only at shallow depths. The difference in temperature between the springs at Cupapa and Moka most likely reflects a difference in air temperature at elevation, with the springs at 230 m and 1100 m, respectively.

SAMPLE	HCO_3^-	F^-	Cl^-	SO_4^{2-}	Ca^{2+}	Mg^{2+}	Na^+	K^+
	(mg/L)	(mg/L)	(mg/L)	(mg/L)	(mg/L)	(mg/L)	(mg/L)	(mg/L)
CPP02 1	116	0.065	2.4	2.2	9.31	16.7	3.1	1.6
CPP02 2	118.95	0.05	2.75	2.3	9.5	16.8	3.1	1.42
MOKA2	52.285714	0.02	2.6	1.8	7.7	4.2	2.6	1.33
LUBA1	103.7	0.07	2.3	2.12	13.1	9.9	6	1.9

Table 1 Spring water major ion chemistry. Samples labeled CPP are from the bubbling spring at Cupapa; MOKA2 is from the bubbling spring near Moka. The Luba sample represents a control spring at sea level with no gas bubbling. Samples were taken in March 2019.

Spring	T	pH	SPC	DO
	(°C)		µS/cm	%
Cupapa	25.6	6.48	83.2	33.8
Moka	19.2	-	68.2	33.7

Table 2 Water quality probe data from bubbling springs near Cupapa and Moka, taken in Feb 2018. No pH recorded at Moka due to instrument failure.

Gas Chemistry

Analyses of these samples confirm 65-79% CO_2 of predominately mantle origin. They also reveal ~20-30% CH_4 that is determined to be of thermogenic origin. Empirical evidence suggests that the CH_4 concentration at one of the springs may have changed significantly over the past year.

Sample	He ppm	O_2 %	N_2 %	CH_4 ppm	CO ppm	CO_2 %	C_2H_6 ppm
MKA01	20	4.1	15.16	4988	2.5	79.57	nd
CUP01A	41	0.11	0.8	280400	nd	69.7	2448
CUP02A	35	0.06	1.1	329100	4.1	65.9	3654
CUP02B	39	0.39	2.6	454500	3.6	51.5	3988

Sample	R/Ra c	He/Ne	[He] ppm	d13C-CO2 ‰ vs VPDB	d13C-CH4 ‰ vs VPDB	dD-CH4	CO2/3He
MKA01	6.70	6.18	21.96	-2.9	-34.4	-143	3.89E+09
CUP01A	4.49	33.68	44.50	-3	-34	-147	2.51E+09

Table 3 Chemistry of gas samples taken at bubbling springs near Moka (MKA) and Cupapa (CUP). Samples were taken in March 2019.

Soil CO_2 Flux

Multiple surveys found very little degassing from soils around the island. Profile surveys on Pico Basile and Pico Biao found no obvious CO_2 increases from base to summit. Instead, the CO_2 flux would remain at background levels until a few meters from the bubbling springs. Upon approaching the springs, the instrument would rapidly saturate, suggesting very high CO_2 flux only within the confines of the bubbling springs.

Discussion

Our results suggest that degassing from the island is mainly along structural pathways such as fractures on the lowest flanks of the volcano. The lavas appear young and soils are thin despite the tropical environment, presenting a relatively impermeable barrier to the rising gases. Fractures would present the path of least resistance for gas escape. Similarly, meteoric water would drain preferentially along these weaknesses in the shallow edifice. The geochemistry indicates that the CO_2 and CH_4 gases and spring waters are decoupled from one another. The lack of sulfur in the gas compositions suggests that the degassing magma sits well below the depth of sulfur exsolution. Given the island's tropical climate and position on the edge of the continental shelf, thermogenesis of CH_4 is likely occurring at base of the volcano within the carbonate sediments upon which it is built. Therefore, in our model of shallow fluid flow on Pico Basile, CO_2 rises from a deep magma reservoir, while thermogenic CH_4 is produced in sediments below the volcano. These rise to the surface independently through fractures in the volcanic edifice, eventually intersecting shallow meteoric

springs that are exploiting these same structural pathways. Little-to-no heat remains at the surfaces and residence time of the gases in the water is short enough that no mixing can occur.

Forthcoming Work

In September, we will analyze fluid inclusions in the rock samples collected from Pico Basile. Volatile and noble gas concentrations from the xenoliths will shed light on the composition and depth of the degassing magma body, as well as the dynamics of storage and ascent of magma to the surface. This information will help us understand the current state of the volcano and look for potential indicators of future unrest.

Acknowledgements

The accumulation chamber instrument was built at the Università degli Studi di Perugia. Many thanks to Carlo Cardellini for his hospitality and patient guidance throughout the building process. Logistics on Bioko Island were generously provided by the Bioko Biodiversity Protection Program in collaboration with the National University of Equatorial Guinea.

References

Aka F.T., Kusakabe M., Nagao K. & Tanyileke G., (2001). *Noble gas isotopic compositions and water/gas chemistry of soda springs from the islands of Bioko, São Tomé and Annobon, along with Cameroon Volcanic Line, West Africa*. Applied Geochemistry, Volume 16, pp. 323-338.

Enciclopedia Universal Ilustrada, (1924). *Fernando Poo*. Madrid, p. 833.

Fractional degassing of S, Cl and F on the rift-zone of Bárðarbunga volcanic system, Iceland

Sigmarsson O.[1,2], Moune S.[1,3], Gauthier P.J.[1]

[1]*Laboratoire Magmas et Volcans, Université Clermont Auvergne Aubière, France*
[2]*Institute of Earth Sciences, University of Iceland, Reykjavik, Iceland*
[3]*Observatoire Volcanologique et Sismologique de Guadeloupe, IPGP, France*

Corresponding Author: *olgeir.sigmarsson@uca.fr*

Gas composition emitted from volcanoes producing basalts may vary during an eruption and according to the volcano-tectonic configuration of the degassing vents. Post-eruptive filter-pack gas samples from the 2014-2015 crater Holuhraun on the Bárðarbunga rift-zone has lower ratios of S over halogens (Cl and F) and elevated F/Cl (~50 times lower S/Cl and ~5 times higher F/Cl; mass ratios) compared to samples of the syn-eruptive gas plume. The compositional changes are readily explained by Rayleigh distillation with decreasing sulfur and increasing halogens and F relative to Cl in the final gas phase. The gas-melt partition coefficients (D) decreased from at least 85 for Cl to 2.2 in residual degassing, whereas that of F remained uniform at approximately 1.8. High D for Cl may suggest an important role of sulfur on Cl solubility in basaltic melt. The primary gas during the Holuhraun eruption has similar ratios of S over Cl and F as observed at the Kilauea rift-zone that together with lower S/(Cl, F) in the residual gas in both cases suggest identical degassing mechanism. The gas composition, therefore, reflects the volcano-tectonic context on mantle-plume derived basaltic volcanoes. By inference, CO_2 degassing is likely to have occurred close to the Bárðarbunga central volcano before the 2014-2015 eruption on the rift-related fissure swarm.

Multi-level gas monitoring of a mofette to reveal mantel fluid movements

Woith H.[1], Daskalopoulou K.[1], Heeschen K.[1], Zimmer M.[1], Niedermann S.[1], Fischer T.[2], Vlček J.[2], Trubač J.[2], Barth J.A.C.[3]

[1]*GFZ, German Research Centre for Geosciences, Potsdam, Germany*
[2]*Charles University, Prague, Czech Republic*
[3]*Friedrich-Alexander-Universität Erlangen-Nürnberg, Germany*

Corresponding Author: *heiko.woith@gfz-potsdam.de*

Mofettes are gas emission sites where CO_2 ascends through conduits from as deep as the mantle. They provide natural windows to magmatic processes at depth. The primary objective of our research on mofettes is to clarify physical links between fluid properties, their pathways and the relation to swarm earthquakes. State-of-the-art fluid monitoring techniques allow for a high temporal resolution compared to the low-resolution discrete sampling approach used in the last decades. Gas and isotope compositions will be continuously analyzed *in-situ* at different depth levels (30 m, 100 m, 300 m) reached by a number of existing and planned drill holes. A unique approach will allow for ascending mantle fluids to be tracked vertically in a set of drillings from a depth of a few hundred metres to the surface. This setup can provide hints on the origin of temporal variations related to the opening of fault-valves, admixture of crustal fluids to a background mantle-flow or the release of hydrogen during fault rupturing. Gas migration velocities can thus be measured directly (from the arrival times of anomalies at different depth levels). In addition, potential admixtures of mantle fluids with crustal or meteoric fluids during the ascent to the Earth's surface can be quantified. In order to test the hypothesis that sites located on different faults react differently, we will repeatedly collect gas samples for noble gas isotope analyses from key sites in specific tectonic structures. These will be combined with stable isotope measurements of dissolved inorganic and organic carbon species to outline CO_2-H_2O interactions. The sampling will cover background and event-driven periods, with the latter triggered by earthquakes or fluid anomalies.

The Hartoušov mofette with a daily CO_2 flux of up to 97 t has been chosen as a key site in the frame of the ICDP project: "Drilling the Eger Rift: Magmatic fluids driving the earthquake swarms and the deep biosphere". It is located in the Cheb Basin, which terminates the Eger Rift to the West and is known for recurring earthquake swarms. Detailed fluid measurements before, during and after drilling of a 300 m deep well will be carried out to investigate possible influences of drilling activities on the local and regional fluid regime. Wells F1 (30 m) and F2 (108 m) already exist, F3 (target depth 300 m) will be drilled in August 2019.

ST02

GASES IN SEISMIC AND TECTONIC SETTINGS

REFERENCE: ANTONIO CARACAUSI

Deep fluids contribution to the freshwater of the San Vittorino plain (Central Italy): geochemical, isotopic and gas-geochemistry dataset with possible implication for crustal deformations studies

Barberio M.D.[1], Caracausi A.[2], Doglioni C.[1,3], Esposito G.[1], Italiano F[2] and Petitta M.[1]

[1]*Università degli Studi di Roma La Sapienza, Dipartimento di Scienze della Terra, Italy*
[2]*Istituto Nazionale di Geofisica e Vulcanologia, Sezione di Palermo, Italy*
[3]*Istituto Nazionale di Geofisica e Vulcanologia, Roma, Italy*

Corresponding Author: *marinodomenico.barberio@uniroma1.it*

Introduction

This study is included in a research program aimed at the identification of potential patterns of hydrogeological and geochemical changes in response to seismic activity, including possible variations of ion concentrations, gas compositions, and isotopic ratios in groundwater. Because of 1) the active degassing of deep volatiles and 2) the recognized link between fluids and seismicity in the area [Chiodini et al., 2011] in the San Vittorino Quaternary plain, in Central Italy, this area has been selected for this purpose. In this area 13 spring waters having with different hydrogeochemical facies, including typical calcium-bicarbonate and sulfate-calcium equilibrium with different deep gas contribution, have been selected. Two sampling campaigns were carried out in October 2018 and in January 2019. In each survey physical-chemical parameters including temperature, electrical conductivity and pH were measured in the field and samples were taken for the analysis of major and minor elements and for the isotopic analysis of H_2O ($\partial^{18}O$-D) and the chemical composition of the dissolved gases and the isotopic signature of He and Total Dissolved Inorganic carbon (TDIC). Some of these springs are also characterized by the presence of bubbling gases, so here we also sampled the free gases for determination of He, CO, CO_2, Ar, H_2, O_2 and N_2 concentration and isotope composition (He and carbon of CO_2).

Results show that all springs are CO_2-rich, and the water samples are aligned along a mixing line, whose end-members are Ca-HCO_3 and Ca-SO_4-HCO_3. The molar ratio between different chemical elements (e.g. B-Cs, Li-B, Li-Cs, Rb-Cs, Mg-Cl, Na-Cl and SO_4-Cl) allows to identify at least 3 different groups of springs with potential different groundwater flowpaths and mixing degree.

The results of the gas analysis allowed us to identify the possible sources and the mixing processes that occur between deep and shallow aquifers in the study area. The gas composition and concentration show a spatial distribution suggesting a mantle-derived origin and a tectonic control in the gas uplift. The He isotopic data highlighted traces of a of mantel-derived component that indicate a tectonic control in the fluid transfer.

Settings and Methods

The San Vittorino plain was chosen for this study due to the huge availability of groundwater and the intense deep degassing documented in the middle valley of the Velino River [Petitta et al., 2009; Giustini et al., 2013; Barbieri et al., 2017]. The San Vittorino plain is an intramountain depression located in the central Apennines (elevation of 400-412 m a.s.l.). The plain is the result of extensional and/or transtensive Quaternary tectonics, with displacements along major fault planes and regional

uplift. The hydrogeology of the San Vittorino plain is influenced by the overlap of different contributions of groundwater by shallow and deep circuits showing significant gaseous contributions. Many springs in the plain have particular hydrochemical characteristics (sulphurous water, ferruginous water with slightly hydrothermal characters, etc.), which depend on mixing with dominantly gaseous fluids rising along recent and/or active tectonic discontinuities. Temperature values vary between 7.3 and 19.4 °C, the electrical conductivity between 286 and 2780 µS/cm and pH between 6.022 and 8.165.

Results and discussions

Figure 1A shows the results of analyses of major ions. All springs have a calcium-bicarbonate equilibrium except for Acqua Puzza Antrodoco and Terme di Antrodoco, which show a sulphate-calcium equilibrium. The other springs instead show an enrichment in bicarbonates from right to left, with a slight increase in Na concentrations.

Figure 1B shows the results of stable isotopic analysis of water sampled in October 2018. The isotopic ratio of the groundwater agrees with previous study results, corresponding to the recharge area of the spring [Petitta, 2009]. In detail, it is possible to distinguish a different recharge area for the Cotilia and Paterno springs at lower altitude, due to the different recorded isotope values with respect to the other ones. The distribution along the meteoric line valid for the central Apennines, suggests that no further significant fractionation processes occur. In addition, the molar ratio between different chemical elements (e.g. B-Cs, Li-B, Li-Cs, Rb-Cs, Mg-Cl, Na-Cl and SO_4-Cl) allowed to identify different groups of spring with potential different groundwater flowpath and mixing degree as suggested by stable isotope results.

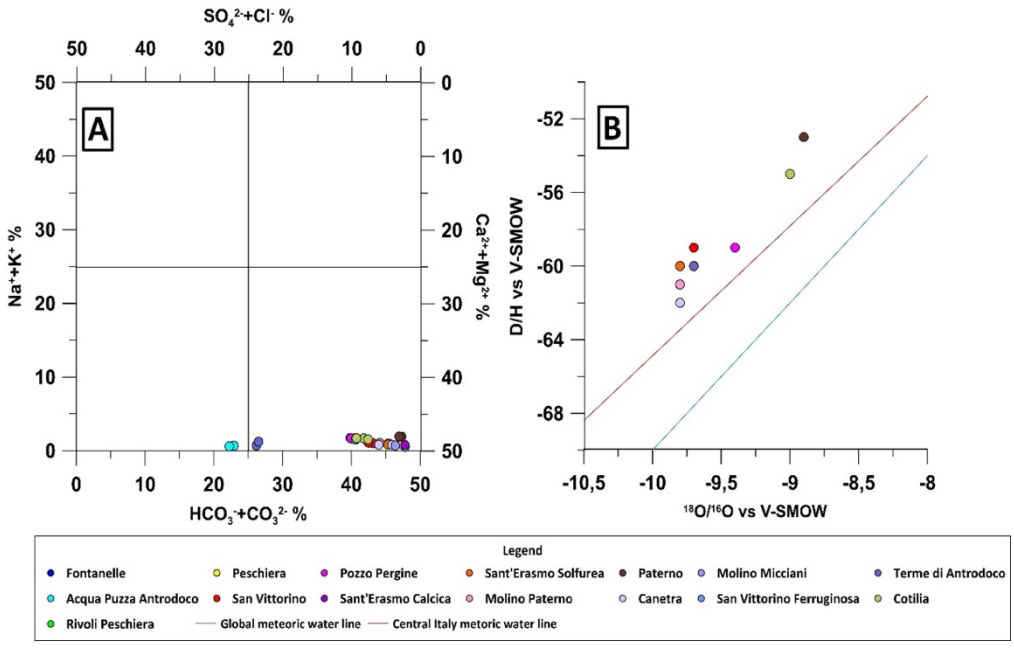

Figure 1 A) Chebotarev's classification diagram for groundwater. B) Isotope values samples plotted with the World Meteoric Line (WML) and the central Italy meteoric lines.

Figure 2 shows the results of $^3He/^4He$ (R/Ra) versus $^4He/^{20}Ne$ ratios for the 8 springs sampled in January 2019. The majority of these gases are characterized by $^4He/^{20}Ne$ ratios higher than 10 and their do not suvver of high air contamination. Assuming a Mid Oceanic Ridge Basalts reservoir for mantle (MORB, 8Ra), the typical He isotopic ratio due to the U andf Th decay into the crust (0.01Ra)

and the atmospheric He isotope signature (1Ra) it is possible to compute the percentages of each component (Sano et al., 1997). The samples from the San Vittorino plain have low but discernible contributions of the mantle-derived He and it is ~1-2% (Figure 2). However, the mantle below Italy results contaminated by subduction processes decreasing the pristine signature of the He isotopic ratio [e.g., Martelli et al., 2008]. Hence, if we assume an He isotopic signature lower that the typical MORB value (8±1Ra), the mantle contribution seems to be higher than the estimated values. In absence of active volcanoes, it is possible to argue that the tectonics discontinuities of the San Vittorino plain play a main role in the uprising of CO_2-dominated, mantle-type volatiles and in the release of ^4He probably trapped in buried crustal blocks. Such a mixing of a prevailing crustal component with mantle gases has been evidenced also by other studies [Giustini et al., 2013 and references].

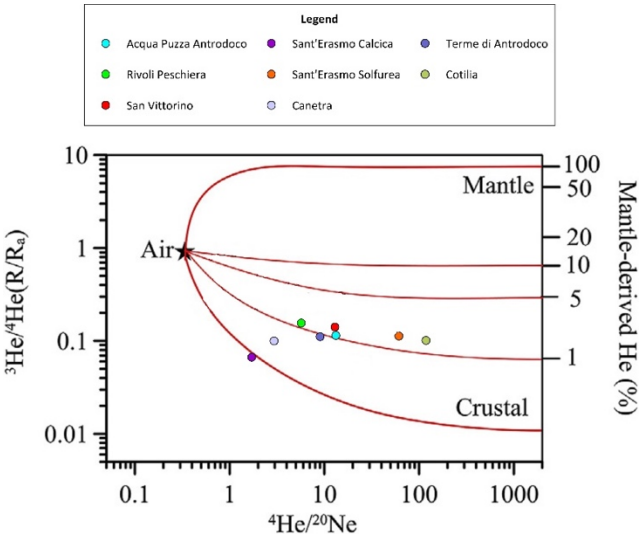

Figure 2 Diagram of $^3He/^4He$ (R/Ra) versus $^4He/^{20}Ne$ ratios. Mixing lines between the atmosphere and upper mantle and the atmosphere and crust were calculated using the end members: air ($^3He/^4He$ = 1.4 x 10^{-6}, $^4He/^{20}Ne$ = 0.318, [Ozima and Podosek, 2002]), upper mantle ($^3He/^4He$ = 12 x 10^{-6}, $^4He/^{20}Ne$ = 100,000, [Graham, 2002]), old continental crust ($^3He/^4He$ = 0.02 x 10^{-6}, $^4He/^{20}Ne$ = 100,000, [Ballentine et al., 2005]).

Conclusions

The multiparametric analysis performed on the analyzed springs made it possible to characterize the various contributions to groundwater flow in the San Vittorino Plain. In detail the results of chemical analysis allowed to identify different geochemical facies and different groups of spring with potential different groundwater flowpath. The results of the gas analysis help to identify the origin and the mixing processes that occur between deep and shallow aquifers in the study area. The He isotopic data highlighted a low component of mantle-derived volatiles that suggest a tectonic control in the fluid transfer. In this context, variation in the isotopic signature indicating different mixing contributions would be relevant to further studies on the effects of crustal deformations on groundwater composition related with the seismic cycle.

References

Ballentine C.J., Marty B., Sherwood L.B., Cassidy M., (2005). *Neon isotopes constrain convection and volatile origin in the Earth's mantle*. Nature, 433, 33 e 38.

Barbieri M., Nigro A. & Petitta M., (2017). *Groundwater mixing in the discharge area of San Vittorino Plain (Central Italy): geochemical characterization and implication for drinking use"*. Environmental Earth Sciences, 76(11), 393.

Chiodini G., Caliro S., Cardellini C., Frondini F., Inguaggiato S., Matteucci F., (2011). *Geochemical evidence for and characterization of CO_2 rich gas sources in the epicentral area of the Abruzzo 2009 earthquakes*. Earth and Planetary Science Letters, Volume 304, Issues 3-4, Pages 389-398, ISSN 0012-821X.

Giustini F., Blessing M., Brilli M., Lombardi S., Voltattorni N. & Widory D., (2013). *Determining the origin of carbon dioxide and methane in the gaseous emissions of the San Vittorino plain (Central Italy) by means of stable isotopes and noble gas analysis*. Applied Geochemistry, 34, 90-101.

Graham D.W., (2002). *Noble gas isotope geochemistry of mid-ocean ridge and ocean island basalts: characterization of mantle source reservoirs*. In: Porcelli et al., (Ed.), Noble Gases in Geochemistry and Cosmochemistry, Reviews in Mineralogy & Geochemistry, 47, pp. 247e317. Washington.

Martelli M., Nuccio P.M., Stuart F.M., Di Liberto V., Ellam R.M., (2008). *Constraints on mantle source and interactions from He-Sr isotope variation in Italian Plio Quaternary volcanism*. Geochemistry, Geophysics, Geosystems, 9, Q02001 http://dx.doi.org/10.1029/2007GC001730.

Ozima M., Podosek F.A., (2002). *Noble Gas Geochemistry*. Cambridge Univ. Press, Second ed., Cambridge, UK.

Petitta M., (2009). *Hydrogeology of the middle valley of the Velino River and of the S. Vittorino Plain (Rieti, Central Italy)*. Ital. J. Eng. Geol. Environ., 1, 157-181.

Sano Y., Tominaga T. & Williams S.N., (1997). *Secular variations of helium and carbon isotopes at Galeras volcano, Colombia*. Journal of Volcanology and Geothermal Research, 77(1-4), 255-265.

CO_2 degassing from the active fault zones in the capital area of China

Zhi Chen[1], Ying Li[2] and G. Martinelli[1]

[1]*CEA Key Laboratory of Earthquake Prediction, China Earthquake Administration, China*
[2]*ARPA Emilia-Romagna, Sezione di Reggio Emilia, Reggio Emilia, Italy*

Corresponding Author: *dugu_830822@163.com*

Abstract
Gas geochemistry and isotope investigation in 26 soil gas wells and 11 springs along the active fault zones in the capital area of China was carried out, to investigate the origin of CO_2 and mechanism for the spatial and temporal variations of CO_2. The geochemical and isotopic data analysis indicates that biogenic CO_2 is the main source for CO_2 from the soil gas wells in both basin and orogen regions, the crust-derived and mantle-derived CO_2 could have ascended through the deep-cut faults and got into the springs, with a few diffused into the soil gas wells, and minor air could have intruded into the soil gas wells in the orogen region through the faults cutting the surface, owing to the barometric pressure fluctuation. Much more higher He concentrations, CO_2 concentration and flux of soil gas from the wells were observed in the basin region than those in the orogen region, the more CO_2 produced during the procedure of the oxidation of organic matter during aerobic microbial respiration in the basin, where the organic matter accumulates in the thick clay cover strata, should take the major responsibility for it, assisted by the other two secondary factors: (1) the interactions between groundwater and carbonates widely distribute in strata of the basin region, (2) the intruded air into the soil gas wells in the orogen region, owing to the barometric pressure fluctuation. Larger temporal variations of CO_2 concentration and flux were observed in the soil gas wells in the basin region, where the seismic activity was stronger, compared to those in the orogen, indicating that the stronger seismic activity should be the main trigger for the jumpily temporal variations of CO_2 concentration and flux in gas from the soil gas wells in the basin region. The results suggest that observing the CO_2 concentration and flux in soil gas wells along the active fault zones could be a potential method for seismic activity monitoring in the capital area of China.

Introduction
Fault and fracture are preferential migration pathways for gases (CO_2, Rn, He etc.,) in the deep crust to migrate upward to surface with carrier gases, due to their enhanced permeability and porosity relative to the surrounding rocks, along which gases can buoyantly migrate upwards [Doăn et al., 2009; Fu et al., 2017; Chen et al., 2018]. Recent investigations of origin and output of soil CO_2 degassing from active faults have been performed in locations that include China, America, Turkey and California etc.[Kulongoski et al., 2013; Lewicki et al., 2013; Zhou et al., 2016; Yuce et al., 2017], and high soil CO_2 concentration and flux have been frequently observed at active fault zones worldwide [Chiodini et al., 2010; Han et al., 2014]. The results of these studies suggest that CO_2 output from active faults can be of great importance to the global carbon budget [Italiano et al., 2009; Zhao et al., 2018]. In addition, general overviews of the geochemical, structural, and seismic features in tectonically active areas have shown some evidence of correlation between soil gas CO_2 anormalies and tectonic activities, and CO_2 discharge through fault and fracture in the active fault zones can be enhanced by fault and earthquake activity [Wakita et al., 1980; Ciotoli et al., 1998; King et al., 1996; Italiano et al., 2009; Sciarra et al., 2017], and CO_2 concentration and flux surveys along active fault

zones have been widely undertaken for earthquake research and prediction [Caracausi et al., 2003; Fu et al., 2008; Sciarra et al., 2017].

Numerous active faults are distributed in the capital area of China [Xu, 2002]. Investigations of the soil CO_2 concentration and flux from the active faults in the capital area of China have been carried out, the highest CO_2 concentration and flux are 9.5% and 274.29 g m-2 d-1, respectively, the total output of CO_2 from nine faults in the west of the capital area of China is 2.0 Mt, which is twice as that from the rupture zones produced by Wenchuan Ms 8.0 earthquake in western Sichuan, China [Li et al., 2013; Li et al., 2018], and the CO_2 emission from the active faults in the capital area of China have been investigated, and there have been also sporadic reports of the relationship between the CO_2 degassing and tectonic activities [Sun et al., 2017; Wang et al., 2017; Yang et al., 2018]. Whereas, the origin of soil gas CO_2 and mechanism for the spatial and temporal variations of CO_2 from the active faults in the capital area of China are unknown. In the present study, we at first time investigate the origins of CO_2 collected from the soil wells along the active faults in the capital area of China, and analyze the mechanism for the temporal and spatial variations of the soil gas CO_2.

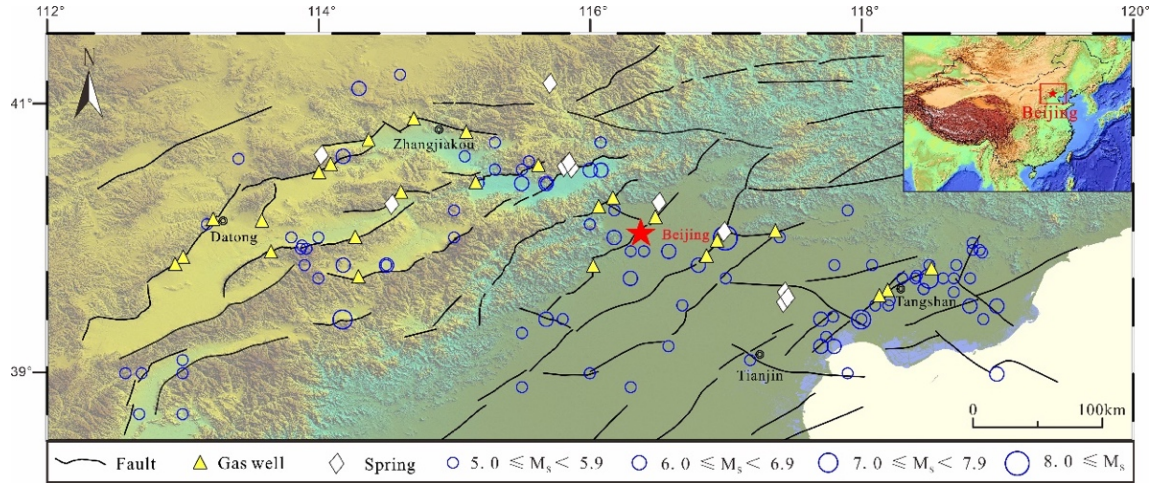

Figure 1 Schematic geologic map of the research area. Insert map shows location of the studied region in China.

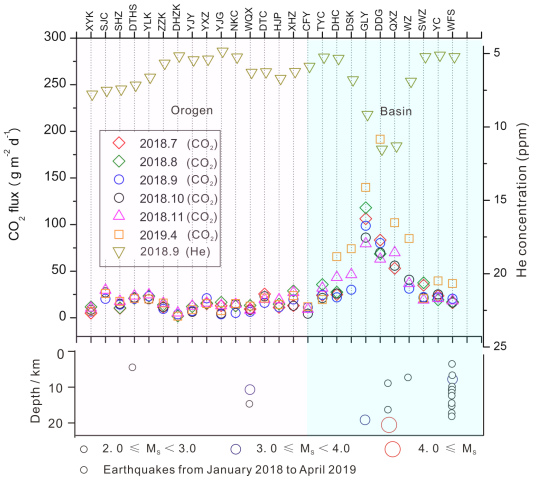

Figure 2 Relationship between earthquakes and variations of CO_2 fluxes and He concentrations in the soil gas wells.

Fault	Site	CO_2 flux (g m^{-2} d^{-1})						Standard deviation of CO_2 flux (g m^{-2} d^{-1})
		Jul-18	Aug-18	Sep-18	Oct-18	Nov-18	Apr-19	
TSF	WFS	16.26	17.07	20.48	16.40	18.19	36.75	7.25
	YC	23.66	19.29	21.92	25.12	20.82	39.52	6.73
	SWZ	34.91	37.59	22.27	21.24	19.12	20.82	7.35
JXF	WZ	-	-	31.17	40.90	36.79	84.92	21.34
XDF	QXZ	53.04	-	-	55.92	69.88	101.96	19.41
	DDG	83.38	68.63	80.11	69.91	63.05	191.45	44.67
GLYF	GLY	106.31	118.07	98.74	86.00	79.56	139.80	20.13
NKF	DSK	-	-	30.13	-	46.38	74.05	18.13
	TYC	24.98	27.47	21.96	25.97	43.42	65.59	15.36
BBSF	DHC	24.17	35.73	24.65	21.16	31.87	19.47	5.78
YFF	CFY	-	-	11.28	4.34	9.22	11.82	2.95
FZF	XHZ	13.16	28.89	19.65	12.85	27.21	23.75	6.30
	HJP	11.17	14.74	11.31	-	19.45	14.30	3.01
ZJKF	DTC	25.46	-	16.04	23.05	19.92	21.06	3.16
	WQX	9.42	13.31	6.42	8.42	8.28	12.50	2.43
YYF	NKC	12.85	12.68	5.17	15.05	14.53	15.32	3.47
HAF	YJG	12.93	16.72	3.73	4.58	13.07	7.65	4.78
YGF	YXZ	14.99	15.79	20.89	-	15.85	15.22	2.20
LLSF	YJY	-	12.06	7.37	6.30	12.60	8.66	2.51
	DHZK	-	1.95	3.68	-	5.31	1.67	1.47
YTF	ZZK	11.67	13.92	9.52	11.37	15.53	15.88	2.31
	YLK	-	23.33	23.10	19.85	24.72	20.11	1.91
DTVF	DTHS	20.93	20.89	20.31	21.71	23.44	20.70	1.03
KQF	SHZ	10.25	10.59	14.12	15.09	17.74	17.67	3.00
	SJC	-	-	20.33	27.29	29.60	26.03	3.42
	XYK	5.03	11.72	6.65	8.77	10.49	7.07	2.30

Table 1 CO_2 flux and its standard deviation of gas from the soil gas wells along the active fault zones in the Capital area of China.

Spring	CO_2 concentration (%)	$^{13}\delta_{CO2}$(‰)	He (ppm)	R/Ra	Rc/Ra	He_M(%)	$^4He/^{20}Ne$
TZQ	0.59	-15.6	2075.1	0.42	0.42	4.99	85.42
JYWQ	3.45	-12.3	2288.4	2.52	2.52	31.38	96.07
YYBG	1.30	-13.9	2853.0	0.10	0.10	0.99	185.52
SSSZ	1.43	-13.8	1835.2	1.02	1.02	12.53	149.34
SSY	0.53	-11.9	718.4	2.42	2.43	30.14	63.15
WLY	0.95	-13.3	669.6	2.03	2.04	25.29	28.83
DYWQ	1.11	-11.2	1437.5	0.16	0.16	1.72	82.53
WSJ	11.32	-8.9	4139.8	0.49	0.49	5.86	44.50
DJWQ	7.65	-11.1	616.9	0.48	0.48	5.75	85.63
ZGST	1.68	-9.8	574.0	0.47	0.46	5.55	17.80
HSW	1.48	-11.2	673.8	0.54	0.53	6.45	20.65

Table 2 Gas geochemical and isotopic data of gas from the springs along the active fault zones in the Capital area of China.

Equation

$$Rc/Ra = [(R/Ra \times X)-1]/(X-1),\ X=[(^4He/^{20}Ne)measured/(^4He/^{20}Ne)air] \times \beta_{Ne}/\beta_{He}. \quad (1)$$

References

Caracausi A., Favara R., Giammanco S., Italiano F., Paonita A., Pecoraino G., Rizzo A., and Nuccio P.M., (2003). *Mount Etna: Geochemical signals of magma ascent and unusually extensive plumbing system*. Geophysical Research Letters, 30(2):61-79.

Chen Z., Li Y., Liu Z.F., Wang J., Zhou X.C. and Du J.G., (2018). *Radon emission from soil gases in the active fault zones in the Capital of China and its environmental effects*. Scientific Reports, 8(1):16772.

Chiodini G., Granieri D., Avino R., Caliro S., Costa A., Minopoli C. and Vilardo G., (2010). *Non-volcanic CO_2 Earth degassing: Case of Mefite d'Ansanto (southern Apennines), Italy*. Geophysical Research Letters, 37(11):L11303.

Ciotoli G., Guerra M., Lombardi S. and Vittori E., (1998). *Soil gas survey for tracing seismogenic faults: A case study in the Fucino Basin, central Italy*. Journal of Geophysical Research, 103(B10):23781.

Dogăn T., Sumino H., Nagao K., Notsu K., Tuncer M. and Celik C., (2009). *Adjacent releases of mantle helium and soil CO_2 from active faults: observations from the Marmara region of the North Anatolian Fault zone, Turkey*. Geochemistry Geophysics Geosystems, 10(11):2009.

Fu C.C., Yang T.F., Chen C.H., Lee L.C., Wu Y., Liu T.K., Walia V., Kumar A. and Lai T.H., (2017). *Spatial and temporal anomalies of soil gas in northern Taiwan and its tectonic and seismic implications*. Journal of Asian Earth Sciences, 149:64-77.

Fu C.C., Yang T.F., Lee J., Walia V., Liu T.K., Lin S.J., Chen C.H. and Hou C.S., (2008). *Variations of soil gases on the active Chihshang Fault in a plate suture zone, eastern Taiwan*. Radiation Measurements, 44(9):940-944.

Han X., Li Y., Du J., Zhou X. and Zhang W., (2014). *Soil gas Rn and CO_2 geochemistry across the active fault zones in the capital area of China*. Natural Hazards and Earth System Sciences, 14:2803-2815.

Italiano F., Bonfanti P., Ditta M., Petrini R. and Slejko F., (2009). *Helium and carbon isotopes in the dissolved gases of Friuli Region (NE Italy): Geochemical evidence of CO_2 production and degassing over a seismically active area*. Chemical Geology, 266:76-85.

King C.Y., King B.S., Evans W.C. and Zhang W., (1996). *Spatial radon anomalies on active faults in California*. Applied Geochemistry, 11(4):497-510.

Kulongoski J.T., Hilton D.R., Barry P.H. and Esser B.K., (2013). *Volatile fluxes through the Big Bend section of the San Andreas Fault, California: Helium and carbon-dioxide systematics*. Chemical Geology, 339:92-102.

Lewicki J.L., Hilley G.E., Dobeck L., McLing T.L., Kennedy B.M., Bill M. and Marino B.D.V., (2013). *Geologic CO_2 input into groundwater and the atmosphere, Soda Springs, ID, USA*. Chemical Geology, 339:61-70.

Li J., Chen Z., Lu L.N., Zhou X.C. and Li Y., (2018). *Degassing of CO_2, Rn and Hg from the Xiadian active fault and their environmental significance*. Bulletin of Mineralogy, Petrology and Geochemistry, 37(4):629-638 (in Chinese).

Li Y., Du J., Wang X., Zhou X., Xie C. and Cui Y., (2013). *Spatial variations of soil gas geochemistry in the Tangshan area of Northern China*. Terrestrial, Atmospheric and Oceanic Sciences, 24(3):323.

Sciarra B.C. and Coltorti M., (2017). *Learning from soil gas change and isotopic signatures during 2012 Emilia seismic sequence*. Scientific Reports, 7(1): 14187.

Sun Y.T., Zhou X., Zheng G.D., Li J., Shi H., Guo Z.F. and Du J.G., (2017). *Carbon monoxide degassing from seismic fault zones in the Basin and Range province, west of Beijing, China*. Journal of Asian Earth Sciences, 149: 41-48.

Wakita H., Nakamura Y., Kita I., Fujii N. and Notsu K., (1980). *Hydrogen release: new Indicator of fault activity*. Science, 210(4466):188-190.

Wang X.L., Li Y., Du J.G., Chen Z., Zhou X.C., Li X.Y, Cui Y.J., Wang H.Y. and Zhang Z.H., (2017). *Geochemical characteristics of soil gases Rn, Hg and CO_2 and their genesis in the capital area of China*. Acta Seismologica Sinica, 39(1):85-101(in Chinese).

Xu X.W., (2002). *Latest crustal tectonic change and earthquakes in the capital area of China*. Science Press, Beijing (in Chinese).

Yang Y., Li Y., Guan Z.J. and Chen Z., (2018). *Correlations between the radon concentrations in soil gas and the activity of the Anninghe and the Zemuhe faults in Sichuan, southwestern of China*. Applied Geochemistry, 89:23-33.

Yuce G., Fu C.C., D'Alessandro W., Gulbay A.H., Lai C.W., Bellomo S., Yang T.F., Italiano F. and Walia V., (2017). *Geochemical characteristics of soil radon and carbon dioxide within the Dead Sea Fault and Karasu Fault in the Amik Basin (Hatay), Turkey*. Chemical Geology, 469:129-146.

Zhao J.M., Li Y., Chen Z., Liu Z.F., Zhao R.Q., Rong W.J., (2018). *Correlation between gas geochemical emission and fault activity of the Yuxian-Guangling and Kouquan faults.* Acta Seismologica Sinica, 40(6):1402-1416 (in Chinese).

Towards a national hydrogeochemical monitoring system: a further tool to investigate geological hazards

Comerci V.[1], Doglioni C.[2], Italiano F.[3], Baiocco F.[1], Barberio M. D.[4], Caracausi A.[3], Cuiuli E.[5], Guerra M.[1], Infantino V.[6], Insolvibile M.[1], Marcaccio M.[7], Martinelli G.[3], Menichetti S.[8], Onorati G.[9], Petitta M.[4], Palumbo V.[6], Peleggi M.[1], Richieri F.[10], Scaramella A.[1], Scotti E.[11], Testa M.[12]

[1]*ISPRA, Roma, Italy*
[2]*Istituto Nazionale di Geofisica e Vulcanologia, Roma, Italy*
[3]*Istituto Nazionale di Geofisica e Vulcanologia, Sezione di Palermo, Italy*
[4]*Università degli Studi di Roma La Sapienza, Dipartimento di Scienze della Terra, Italy*
[5]*ARPACal, Agenzia Regionale per la Protezione Ambientale, Calabria, Italy*
[6]*ARPA Sicilia, Agenzia Regionale per la Protezione Ambientale, Palermo, Italy*
[7]*ARPAE, Agenzia Regionale per la Protezione Ambientale, Emilia-Romagna, Italy*
[8]*ARPAT, Agenzia Regionale per la Protezione Ambientale, Firenze, Italy*
[9]*ARPAC, Agenzia Regionale per la Protezione Ambientale, Napoli, Italy*
[10]*ARPAP, Agenzia Regionale per la Protezione Ambientale, Torino, Italy*
[11]*ARPAL, Agenzia Regionale per la Protezione Ambientale, Genova, Italy*
[12]*ARPAS, Agenzia Regionale per la Protezione Ambientale, Cagliari Italy*

Corresponding Author: *valerio.comerci@isprambiente.it*

Last May 2019, SNPA (the National System for Environmental Protection composed of the Regional Environmental Protection Agencies - ARPA and ISPRA) and INGV (Istituto Nazionale di Geofisica e Vulcanologia) signed an operating agreement for the "Hydrogeochemical Monitoring and Geological Hazards" which aims to systematize, at national level, all the information, including physical and chemical parameters recorded in wells and springs, collected by the continuous monitoring systems managed by the ARPAs in their regional areas of competence. The ARPAs monitor both physical and chemical parameters of groundwater in order to describe the chemical and quantitative status of the groundwater bodies, according to the EU Directives 2000/60/EC and 2006/118/EC. Those data will be integrated with the continuous monitoring data that INGV records in different aquifers besides other chemical-physical parameters, allowing to build up a uniform database, useful to be correlated with the volcano-tectonic activity and for environmental studies over the Italian territory. The analysis of changes recorded in the monitored parameters will be aimed at identifying ongoing transient phenomena in the earth's crust, that may result particularly useful in volcanic and seismic prone areas. Fluids, in fact, are fast carriers of information about modifications in the physic-chemical conditions at any level in the crust and in the mantle. Groundwater, especially in confined aquifers, are mobilized by pressure gradients in the earth's crust, whose correlation with seismic activity is certainly interesting to investigate, as demonstrated by the recent literature on the subject [see Doglioni et al., 2014 and references therein]. Hydrogeochemical variations (e.g. piezometric levels in wells, changes in temperature, flow rate and geochemical features of natural springs), in addition to weather and seasonal fluctuations, can be induced by the stress field within the earth's crust. Aquifers, generally, show variations in response to the tectonic deformation to which they are subjected. Significant co-seismic and post-seismic hydrological changes occurred during and after the recent earthquakes of L'Aquila in 2009 [Amoruso et al., 2011], Emilia in 2012 [Marcaccio and Martinelli, 2012; Nespoli et al., 2015] and Central Italy in 2016 [e.g. Barberio et al., 2017; De Luca et

al., 2018; Petitta et al., 2018] as well as in coincidence of past strong earthquakes, as testified in coeval reports.
In several countries there is a long tradition of studies of hydrological variations and gas emissions aimed at environmental, seismic and volcanic monitoring. In Italy (in non-volcanic areas) a systematic long-term control of the hydrological and geochemical parameters has been performed only in coincidence of the 1997-1998 Umbria earthquake [Italiano et al., 2009]. Further specific projects [e.g. PRE-EARTHQUAKES - http://www.pre-earthquakes.org/] and studies have been carried out [e.g. Martinelli and Albarello, 1997; AA.VV. 2015; Martinelli and Dadomo, 2017; Martinelli and Tamburello, 2019] and are ongoing [e.g. TABOO project - http://taboo.rm.ingv.it/; *Rete geochimica in Toscana* - http://www.regione.toscana.it/-/rete-geochimica-in-toscana; Collaboration program between IMAA-CNR and GFZ-Potsdam - https://www.imaa.cnr.it/tutti-gli-eventi/64-programma-di-collaborazione-tra-imaa-cnr-e-gfz-potsdam-nel-settore-di-ricerca-terra-e-ambiente-progetti-in-corso-e-future-attivita-di-ricerca]. The importance of carrying out such monitoring in real or near-real time mode and with the greatest possible capillarity, homogeneity and systematicity is quite evident. In this regard, the automatic continuous monitoring networks represent one of the most effective existing tools and it is desirable that they spread further throughout the national territory.
In the framework of the SNPA Activity Plan 2018-2020, ISPRA with ARPACAL (Calabria), ARPAC (Campania), ARPAE (Emilia-Romagna), ARPAL (Liguria), ARPAP (Piemonte), ARPAS (Sardegna), ARPAT (Toscana) and ARPA Sicilia set up the "Hydrogeochemical Monitoring and Geological Hazards" Team, an operational structure aimed at implementing the aforementioned agreement with INGV. The Team is part of a structured Group of Experts composed of SNPA and INGV scientists and technicians; it can be expanded and it is open to scientific support and collaboration from Universities and Research Institutes. The involved ARPAs that already perform the automatic monitoring will provide to the SINAnet (National Environmental Information System Network based in ISPRA) the collected data that are significant for the project in near-real time and in a standardized format, for the organized storage and public data dissemination (open data). Further sites of interest on the national territory will be identified, in particular but not exclusively, among the wells and springs managed by the ARPAs. New automatic measurement devices will be installed in new sites or integrated in the already existing monitoring points. The instrumentation will be made available by INGV following the definition of specific agreements with the ARPAs, which will be in charge of maintenance of the equipment and the data management. The aforementioned Group of Experts, will define which data are useful to gather and it will evaluate the possibility of recording further data, in addition to those collected by the ARPAs. The collected data will be sent to the SINAnet node, according to a standardized format, and, successively, will be scientifically analyzed.
To date, the ARPAs involved in the project and available to provide data on Temperature, Piezometric Level and Electrical Conductivity in near real time are ARPAE (Emilia-Romagna), ARPAP (Piemonte) and ARPAT (Toscana).
In Emilia-Romagna the groundwater monitoring network started in 1976 and now includes 733 stations (wells and springs) in all type of aquifers located in the Region's territory [Mouton et al., 1982; Farina et al., 2014]. According to the law, the network is splitted into two: one is related to chemical (600 stations) and one to quantitative (633 station) data. This is due also to building characteristics of the stations that not always allow the two types of measurements. Six-monthly manual collection of quantitative and chemical data is performed in the wells. The 80 mountain springs are monitored every three years. The groundwater bodies in the Po plain are distinguished on several levels: lower confined aquifer, upper confined aquifer and phreatic aquifer. About 40 wells have been continuously monitored since 2007 at an hourly frequency by remote transmission of the Level, Temperature and Conductivity data.

The regional groundwater monitoring network in the Piemonte region consists of 592 points (wells and piezometers), which are distributed in the superficial and deep groundwater bodies identified in the plain areas of the regional territory. Of these points, 385 concern the shallow aquifer system and 207 the deep one. A subset of these points is made up of 117 piezometers of regional ownership, evenly distributed over the plain: they are instrumented for the automatic measurement of the piezometric level and are also equipped with the sensor for the continuous measurement of the temperature. 8 springs are also part of the monitoring network and are equipped with sensors for measuring water flow rate and temperature. The acquisition of the piezometric level and temperature data takes place continuously while the download every six months, with the two sampling campaigns for the determination of the chemical-physical parameters. All validated data are made available on the Arpa Piemonte geoportal (http://webgis.arpa.piemonte.it/geoportale/index.php/tematiche/acqua).
In Tuscany, semestral discrete sampling is performed at 400 points including wells and springs. Continuous monitoring is performed by the Hydrological Service from 2007-08 in selected wells. In a dozen points, generally springs, quantitative monitoring is performed. 138 stations are active with continuous reading (frequency of 15 minutes) of Level, Temperature and Conductivity. Generally, the wells are shallow, down to a maximum of 40-60 meters. In Val di Chiana and Valdarno they are deeper and in Amiata down to 250 m. Data are disseminated online (http://www.sir.toscana.it/idrometria-pub) without validation (they are validated at the end of the year).
ARPAV (Veneto) and ARPA Umbria manage automatic and continuous monitoring systems, but they are still not involved in the national project.
Also in Liguria and Sardegna control stations collect piezometric and temperature data continuously, but they are downloaded periodically, without a continuous transmission system. In Liguria 83 control stations are active and between them a dozen detect also conductivity, salinity, resistivity and TDS. Overall, in Liguria 200 wells in alluvial aquifers and 20 springs are monitored and 2-3 times a year field parameters are also taken. In Sardegna about 20 stations, since 2016, detect continuous data from alluvial aquifers. In general, the monitoring network consists of 638 stations between private wells, aqueduct wells, springs and piezometers in 114 water bodies belonging to 6 types of aquifers: Plio-Quaternary sedimentary, Plio-Quaternary volcanic, Tertiary sedimentary, Tertiary volcanic, Mesozoic and Paleozoic carbonate, Paleozoic granitoid. A further new network of about 40 piezometers with remote transmission of level and temperature data is planned.
Also in Campania and Calabria the structuring of new monitoring networks is planned both in flood plain and mountain areas. Within the project the possibility of instrumenting stations of interest with continuous measurement devices remotely connected will be verified.
In recent years, considerable progress has been made in geophysical prospecting of the earth's crust (just think, for example, of the increasingly sophisticated sensors on board of satellites launched for terrestrial monitoring, which make it possible to measure ground deformations or ground temperature changes). Therefore, the analysis of hydrogeochemical data deriving from a dense national network combined with geophysical data can certainly move forward the process of understanding the complex mechanisms that regulate the dynamics of the earth's crust and, hopefully, gain a better insight into the seismogenic process in order to detect possible precursory phenomena.

References

AA.VV., (2015). *DPC-INGV-S3 Project*. Bollettino di Geofisica Teorica Applicata, 56, 2, 71-356.

Amoruso A., Crescentini L., Petitta M., Rusi S., Tallini M., (2011). *Impact of the April 6, 2009 L'Aquila earthquake on groundwater flow in the Gran Sasso carbonate aquifer central Italy*. Hydrological Processes, 25(11), 1754-1764. https://doi.org/10.1002/hyp.7933.

Barberio M.D., Barbieri M., Billi A., Doglioni C., Petitta M., (2017). *Hydrogeochemical changes before and during the 2016 Amatrice-Norcia seismic sequence (central Italy)*. Scientific Reports, 7: 11735. doi: 10.1038/s41598-017-11990-8.

De Luca G., Di Carlo G., Tallini M., (2018). *A record of changes in the Gran Sasso groundwater before, during and after the 2016 Amatrice earthquake, central Italy*. Scientific Reports, 8:15982. doi: 10.1038/s41598-018-34444-1.

Doglioni C., Barba S., Carminati E., Riguzzi F., (2014). *Fault on-off versus coseismic fluids reaction*. Geoscience Frontiers, 5 (2014), 767-780. http://dx.doi.org/10.1016/j.gsf.2013.08.004.

Italiano F., Martinelli G., Bonfanti P., Caracausi A., (2009) *Long-term geochemical monitoring of gases from the seismic area of the Umbria region: 1997-2007*. Tectonophysics, 476 (2009), 282-296.

Farina M., Marcaccio M., Zavatti A., (2014). *Esperienze e prospettive nel monitoraggio delle acque sotterranee. Il contributo dell'Emilia-Romagna*. Pitagora Editrice, Bologna, 560 pp. (ISBN 88-371-1859-7).

Marcaccio M. and Martinelli G., (2012). *Effects on the groundwater levels of the May-June 2012 Emilia seismic sequence*. Annals of Geophysics, 55, 4, 2012; doi: 10.4401/ag-6139.

Martinelli G. and Albarello D., (1997). *Main constraints for siting monitoring networks devoted to the study of earthquake related hydrogeochemical phenomena in Italy*. Annali di Geofisica, Vol. XL, 6, 1997.

Martinelli G. and Dadomo A., (2017). *Factors constraining the geographic distribution of earthquake geochemical and fluid-related precursors*. Chemical Geology, 469, 176-184.

Martinelli G. and Tamburello G. (2019). *Geophysical and Geological factors constraining the occurrence of earthquake precursors in Geofluids*. ICGG, 15 Abstract.

Mouton J., Mangano F., Fried J.J., (1982). *Studio sulle risorse in acque sotteranee dell'Italia*. Commission of the European Communities, ECSC/EEC/EAEC, Brussels and Luxembourg. Schäfer GmbH, Hannover, 193 p. + annexes.

Nespoli M., Todesco M., Serpelloni E., Belardinelli M.E., Bonafede M., Marcaccio M., Rinaldi A.P., Anderlini L., Gualandi A., (2015). *Modeling earthquake effects on groundwater levels: evidences from the 2012 Emilia earthquake (Italy)*. Geofluids, doi: 10.1111/gfl.12165.

Petitta M., Mastrorillo L., Preziosi E., Banzato F., Barberio M.D., Billi A., Cambi C., De Luca G., Di Carlo G., Di Curzio D., Di Salvo C., Nanni T., Palpacelli S., Rusi S., Saroli M., Tallini M., Tazioli A., Valigi D., Vivalda P., Doglioni C., (2018). *Water table and discharge changes associated with the 2016-2017 seismic sequence in central Italy: hydrogeological data and conceptual model for fractured carbonate aquifers*. Hydrogeology Journal, 26(4), 1009-1026.

Images of ancient Calabrian-Sicilian earthquakes from a stereoscopic viewer of the early 20th century. The ethics of a natural disasters photo-gallery

Foresta Martin F.[1,3], Peppoloni S.[2], Tosi P.[4], De Rubeis V.[4], Sbarra P.[4], Topazio S.[4]

[1]*Istituto Nazionale di Geofisica e Vulcanologia, Sezione di Palermo, Italy*
[2]*Istituto Nazionale di Geofisica e Vulcanologia, Sezione di Geomagnetismo, Aeronomia e Geofisica Ambientale, Roma, Italy*
[3]*Laboratorio Museo di Scienze della Terra, Ustica, Palermo, Italy*
[4]*Istituto Nazionale di Geofisica e Vulcanologia, Sezione di Sismologia e Tettonofisica, Roma, Italy*
[5]*Istituto Nazionale di Geofisica e Vulcanologia, Amministrazione Centrale, Italy*

Corresponding Author: *sidereus@rocketmail.com*

This research was inspired by an old stereoscopic viewer from the early 1900s, containing forty-three glass slides depicting scenes from two ancient and almost forgotten Italian earthquakes. We refer to the earthquakes that struck Southern Calabria and Eastern Sicily in the years 1894 and 1905, causing extensive destruction and hundreds of deaths, but whose memory was blurred by the subsequent, great earthquake of the Sicilian Strait of December 28, 1908 (sometimes quoted as the Messina earthquake) which caused about 80,000 deaths.
The stereoscopic viewer, built on commission as a gift for two young spouses of the Agrarian Bourgeoisie in the Messina province, married in 1904, was placed on a small table in the living room in which they usually entertained friends. It was a *taxiphote* model, a handcrafted copy of the French Richard stereoscopic viewers, in vogue at the time of the Belle Époque. The instrument consisted of a wooden box equipped with two eyepieces that offered a three-dimensional view of the subjects depicted in the slides: a sort of augmented reality *ante litteram*.
The sequence of three-dimensional images shown by the viewer gave depth of field to scenes of collapses, debris, and victims, arousing feelings of dismay; nevertheless, the show had the hypnotic charm of the apocalypse and could be replicated at will with a few turns of the dial.
In this work, we describe the *taxiphote* apparatus; the places depicted in the stereoscopic plates and the seismic phenomena that caused the disasters exhibited. But above all, we investigate the social and cultural aims that pushed to show the effects of local earthquakes through this kind of primitive multimedia mechanism. We exclude that the *taxiphote*, with its photographic equipment, was merely an instrument of entertainment *pour épater les bourgeois*. We rather demonstrate that it carried out an educational task. The repetition of the sequence of tragic images of earthquakes through the stereoscopic viewer had the purpose of contributing to give awareness of the looming seismic risk and to accept rationally that nightmare.
The contemporary Middle European literature of the early twentieth century, through a page of Nobel Prize winner Elias Canetti (1905-1994), offers us the opportunity to prove how the representation of an earthquake in the form of scenic fiction had a pedagogical purpose. A geoethical approach to reducing the seismic risk needs also to rediscover cultural and technical traces in our history to better shape modern and more effective ways to change social risk perception and to improve mitigation actions.

High-resolution variations of gas and fluid geochemistry from the Taiwan Chelungpu-fault borehole during the 2013 Nantou earthquake

Ching-Chou Fu[1], Chun-Wei Lai[2], Tsanyao Frank Yang[2,†], Cheng-Hong Chen[2], Kuo-Fong Ma[3]

[1]*Institute of Earth Sciences, Academia Sinica, Taipei, Taiwan, Republic of China*
[2]*Department of Geosciences, National Taiwan University, Taipei, Taiwan, Republic of China*
[3]*Department of Earth Sciences & Institute of Geophysics, National Central University, Taiwan, Republic of China*
† Deceased

Corresponding Author: *ccfu@earth.sinica.edu.tw*

Monitoring of groundwater chemistry in seismically-active regions has been carried out since the 1980s in Taiwan. Change in groundwater chemistry has been observed before earthquakes and is proposed as a precursor signal. However, the biweekly/monthly sampling interval was commonly performed; some short-term precursory anomalies may not be caught due to the low sampling frequency. We designed an automatic sampling apparatus for the retrieval and temporal analysis of water geochemistry. The device was composed of the syringes connected to glass bottles with the septum for collecting fluids each day, which was installed at the Taiwan Chelungpu Fault Drilling Project (TCDP) *drilling well* in central Taiwan for observing the discharge of fluids (Figure 1). It was also equipped with a quadrupole mass spectrometer (QMS) for in-situ measurement of the dissolved gas composition. Variations of gases composition were transmitted to the laboratory through internet.

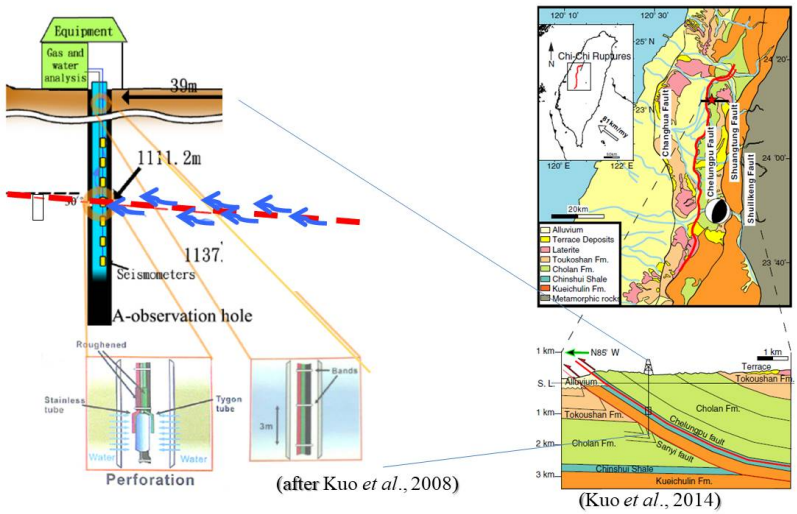

Figure 1 The regional map and principal tectonic structures around the Chelungpu Fault in Central Taiwan and a sketch of the monitoring station [after Kuo et al., 2008; Kuo et al., 2014].

The stable isotope ratios for oxygen and hydrogen anomalies of approximately +0.6‰ and +2.0‰, respectively, relative to the local background measured in groundwater were observed as the potential seismic precursor, one month before the Nantou earthquake (M6.2) in central Taiwan. The

findings could be explained by the mixture between the different chemical concentrations from groundwater and surrounding formations through water-rock interaction, which may be associated with pre-seismically induced changes of permeability or opening of preexisting micro-fractures along the fault zones due to high pressure fluid and/or gas. We infer that similar processes may be active at some suitable sites which provide the channel for fluids originated from deep crust to migrate upward to the surface, and that geochemical anomaly in groundwater may be useful for future researching on the earthquake precursor.

References

Kuo T.C., (2008). *Gas and Water Analyses during fluid injection into Chelungpu-fault zone, Taiwan (MS Thesis)*. Institute of Geophysics, National Central University, 82 pp. (in Chinese with English abstract).

Kuo L.W., Hsiao H.C., Song S.R., Sheu H.S. and Suppe J., (2014). *Coseismic thickness of principal slip zone from the Taiwan Chelungpu fault Drilling Project-A (TCDP-A) and correlated fracture energy*. Tectonophysics, 619-620.

Gas geochemistry and tectonics around the Sea of Marmara

Italiano F.[1], Woith H.[2], Seyis C.[3], Pizzino L.[4], Sciarra A.[4]

[1]*Istituto Nazionale di Geofisica e Vulcanologia, Sezione di Palermo, Italy*
[2]*GFZ, German Research Centre for Geosciences, Potsdam, Germany*
[3]*TÜBITAK-MAM, Gebze, Turkey*
[4]*Istituto Nazionale di Geofisica e Vulcanologia, Sezione di Sismologia e Tettonofisica, Roma, Italy*

Corresponding Authors: *francesco.italiano@ingv.it*

Introduction

Thermal, cold and mineral water springs/wells were jointly visited by INGV, TÜBITAK and GFZ scientists during two field trips carried out in 2013 and 2014 over the Marmara region (Figure 1), in the frame of MARsite Project [Italiano et al., 2014, 2015]. The study area includes segments of the northern and southern branches of the Northern Anatolian Fault Zone (NAFZ). One of the aims of the project was the collection and integration of seismological, geochemical, and geodetic data to detect and model the interactions between fluids, crustal deformation and ruptures of the active tectonic structures of the Marmara area and, thereby, to contribute to its seismic hazard assessment. Accordingly, our geochemical investigation was focused on the search for possible relationships between fluid geochemistry and the activity of NAFZ in its westernmost portion. This goal is also accomplished by the continuous monitoring of soil radon at 21 sites along with 17 thermal/mineral springs and wells. Geochemical time series, which contain data over several years, are analyzed for any possible changes related with seismic activity [i.e. Woith et al., 2006]. Positive or negative anomalies relative to normal variations could point to correlations with seismic activity.
A model of fluids circulation and interactions with the strike-slip NAFZ is proposed. The model accounts for the geochemical features of the fluids collected and analysed as well as for the information provided by the soil degassing and continuous monitoring activity.

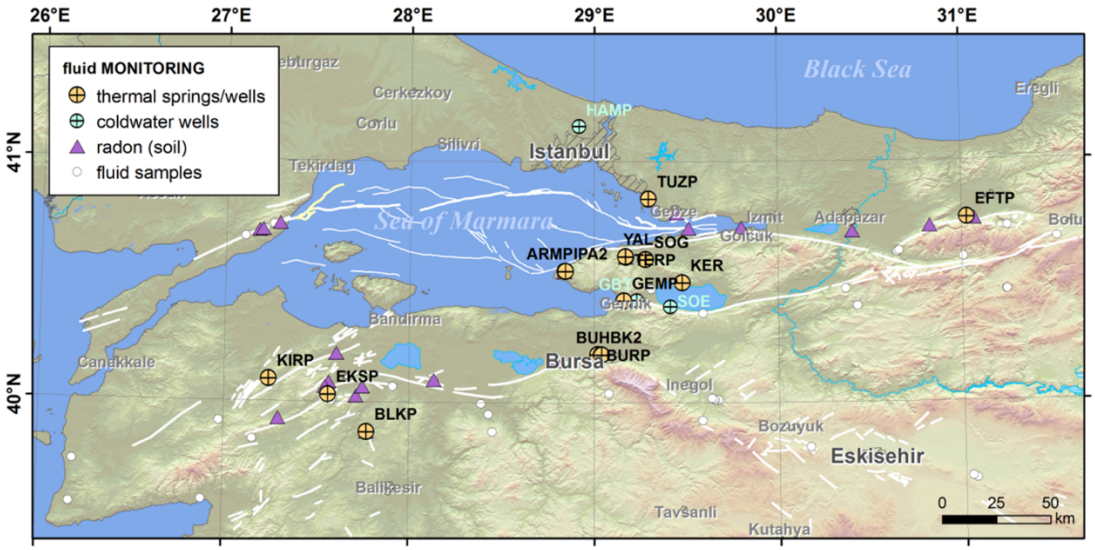

Figure 1 Location of: *i*) water sampling sites, *ii*) continuous monitoring water sites (springs and wells) and *iii*) continuous monitoring soil radon.

Work done

A suite of 120 fluid samples from 72 sites in the Marmara region have been collected from thermal and mineral waters marking the Northern and Southern branches of the NAFZ (Figure 1). Samples of free bubbling gases were taken whenever feasible; additionally, water samples with dissolved gases were collected. pCO_2 (in bar, as log) was computed for all waters by Phreeqc code, version 3 [Parkhurst and Appelo, 2013], using as input outlet temperature, pH, alkalinity and major elements. In addition, 52 CO_2 and CH_4 soil degassing measurements were also carried out at 9 locations in the vicinity of thermal/mineral springs.

Continuous monitoring includes water temperature and specific electrical conductivity at 9 sites, groundwater level/pressure and temperature at 8 sites in the Armutlu peninsula.

Results

Water chemistry

Chemical composition and salinity of groundwater revealed different water-rock interaction (WRI) processes promoted at various extents by variable amounts of dissolved CO_2. The following hydro-chemical *facies* were recognized: *i*) low to moderate-pCO_2, low saline Ca-Mg-HCO_3 waters, typical of the first stages of interaction between meteoric waters and rocks (including soils). These waters are in thermodynamic equilibrium with calcite; *ii*) high-pCO_2, high saline Na-HCO_3 waters. They acquire their composition through the dissolution of Na-bearing minerals from the silicic rocks in which waters circulate; extensive WRI is favoured by the presence of high amounts of dissolved CO_2, inducing the bicarbonate nature and the dis-equilibrium with respect to calcite; *iii*) low pCO_2, high saline Na-Cl, due to both seawater contribution and deep brine interactions; iv) Na-Ca-SO_4 waters, probably owing their nature to H_2S condensing into the liquid phase as well as from interaction with sulphate-bearing minerals.

CO_2-rich waters were mainly found in the Bursa and Bolu-Sakarya-Kocaeli areas. Spotty CO_2 enrichments occur in groundwater of Yalova and Eskisehir sectors.

Bubbling and dissolved gases

CO_2 is normally the main gas in most of the vented fluids, but GWI (gas-water interactions) decrease its concentration. A high CO_2 content indicates minor interactions, thus, the easier and faster is the path from the deep layers toward the earth's surface, the lower are the interactions and allow the volatiles to keep their pristine composition. GWI increases the relative contents of N_2 and other less soluble gases in ground waters. Consequently, the gases released at the monitoring sites result a mixture of two end-members: one dominated by N_2 and the other dominated by CO_2. All the gases collected at the monitoring stations, including dissolved and bubbling samples plot along a mixing line between the two gases at different extents. The map elaborated on the basis of the Normal Probability Plot (NPP) demonstrated how the spatial distribution of the gas emission at the surface is not homogeneous over the Marmara area. It is possible to infer that the gas flow rate variability is controlled by geological structures.

Regarding soil gas survey, a comparison between both CO_2 and CH_4 concentration and flux distribution maps highlighted an overlapping of the highest values in the Adapazari area [Italiano et al., 2015].

C and He isotopes

The higher is the CO_2 content, the more positive is the $\delta^{13}C$ showing that in the absence of fractionation processes the isotopic marker of most of the bubbling gases falls in the field of magmatic type volatiles.

The isotopic composition of helium, always used to discriminate the origin of a gas phase, displays values in the range from 0.1 to 4.8Ra (Ra is the isotopic ratio in air) showing a basically crustal origin with variable extents of mantle contribution at all the monitoring stations. This makes the monitored sites potentially useful to observe changes in the crust-mantle mixing ratios due to tectonic pulses. Since mantle degassing is not obvious in non-volcanic areas [e.g. Italiano et al., 2000], we argued that high helium isotopic ratios indicate mantle degassing through lithospheric faults. Deep lithospheric faults represent a preferential way for rising volatiles due to local high permeability.

Groundwater continuous monitoring

Within the main frame of MARSITE project, a monitoring strategy focused on the evaluation of potential indicators of the development of seismogenesis and its impact on the circulating fluids was followed. Seismically induced pressure transients were observed at geothermal reservoirs located on the Armutlu peninsula (Woith et al., 2014). The seismic activity recorded during the time interval of the project was mainly located on the different branches of the NAFZ. The events marked by M > 4 were extracted to carry out a preliminary check on the influence of ruptures on the fluids behaviour. Continuous monitoring provided information on how fluids behave over time. Changes in composition were found to be related either to periodical forces (e.g. tides) or to occasional events like human activities and seismogenesis.

A preliminary data analysis was performed on stations of geochemical continuous monitoring belonging to the TUBITAK and ARNET networks installed around the Marmara Sea Region. Whereas the cross correlation diagrams between temperature and conductivity and autocorrelation diagrams of the temperature data show periodical patterns for many stations, autocorrelation diagrams of the conductivity data do not show any periodical patterns.

Fluid circulation model

A possible circulation and interaction model is proposed following Doglioni et al., [2014], who indicates the Brittle-Ductile-Transition (BDT) zone as the area that ideally separates two layers with different strain rates, structural styles and geochemical features in circulating fluids (Figure 2).

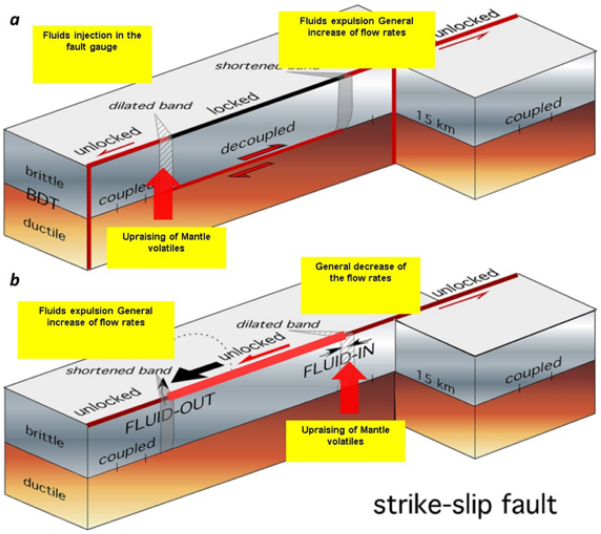

Figure 2 Fluid circulation model for the NAFZ. a) interseismic; b) coseismic. Modified after Doglioni et al., [2014].

On strike-slip faults (e.g. NAFZ) the deformation induces two opposite bands of dilation and shortening on the two sides of the fault. Mantle volatiles originate underneath the BDT and may rise towards the surface when dilatation occurs or through litospheric faults due to enhanced vertical permeability. The behaviour of the upper and lower layers divided by the BDT zone is totally different in case of the interseismic or coseismic stage. This behaviour determines a stress gradient that is eventually dissipated during the earthquake.
NAFZ-like strike-slip fault displays coexisting, locked and unlocked segments with opposite evolution (tension and shortening). During an interseismic period, they perform opposite evolutions inducing different behaviour in fluids circulation and changing both their geochemical features and flow rates. Before the rupture, the proportion of mantle fluids is expected to increase within the dilated band in contrast to an increased fluid expulsion over the shortened area. The contribution of mantle fluids over the same area might decrease during the coseismic period due to the enhancement of shallow fluids expulsion induced by the sudden compression of the dilated band due to the fault movement.
The crustal relaxation of the brittle crust will result in an increase of the mantle fluids upraise over the newly formed dilated band. Crustal deformation in dilating areas should be detectable by geodetic measurements.
The physical interpretation model proposed for the Marmara area firmly keeps together the fluids and the tectonic setting of a seismic-prone area. It has a general validity as it takes into account the origin, interactions and temporal behaviour of the fluids and the local tectonic structures. The application of the model gains new insights into the modelling of a seismogenic processes and may, in future, support actions taken to keep the seismic risk at the lowest possible levels.

Conclusions

The results of the investigations carried out on the fluids vented over the area of the Sea of Marmara show that crustal fluids are available along with mantle volatiles. The different geochemical features of the collected fluids (in terms of chemical and isotopic composition) associated to the evidence of an active natural degassing is a possible indication of different segments of the NAFZ cut crustal sections marked by variable geological and physical features (e.g. different rock types and permeability values). The composition of the circulating fluids was determined by the local geology (e.g. the hosting rocks where ground waters equilibrate or interact with gases). However, in the case of contributions of mantle fluids it is necessary that fractures or faults cut the whole crustal thickness allowing the volatiles of mantle origin to rise up and mix with crustal and other shallow fluids. In this case, the composition of the deep fluids is a matter of tectonics.
High helium isotopic ratios and CO_2 degassing indicate the presence of mantle volatiles through lithospheric faults. Evidence that fluids with a variable, although sometimes significant, mantle component are issued over the whole Marmara region implies a widespread lithospheric character of the various NAFZ branches. This feature highlights the possibility of detecting changes in the fault behaviour from temporal and spatial changes in the mixing proportion of the deep and shallow fluid components.

Acknowledgements

MARsite has received funding from the European Union's Seventh Programme for research, technological development and demonstration under grant agreement No 308417.

References

Doglioni C., Barba S., Carminati E. Riguzzi F., (2013). *Fault on-off versus coseismic fluids reaction*. Geoscience Frontiers, 1-14.

Italiano F., Martelli M., Martinelli G., Nuccio P.M., (2000). *Geochemical evidences of melt intrusions along lithospheric faults of Irpinian Apennines (Southern Italy): Geodynamic and seismogenetic implications*. Jour. Geoph. Res., 105, B6, 13569-13578.

Italiano F., Woith H., Seyis C., (2014). *Geothermal fluid inventory around the Sea of Marmara*. Geophysical Research Abstracts, Vol. 16, EGU2014-13830, EGU General Assembly 2014.

Italiano F., Woith H., Seyis C., Pizzino L., Sciarra A. and Favali P., (2015). *Gas geochemistry and tectonics around the Sea of Marmara*. Geophysical Research Abstracts, Vol. 17, EGU2015-5748, EGU General Assembly 2015.

Parkhurst D.L. and Appelo C.A.J., (2013). *Description of Input and Examples for PHREEQC Version 3-A Computer Program for Speciation, Batch-Reaction, One-Dimensional Transport, and Inverse Geochemical Calculations*. US Geological Survey Techniques and Methods, Book 6, Chapter A43, 497 pp.

Woith H., Venedikov A.P., Milkereit C., Parlaktuna M. and Pekdeger A., (2006). *Observation of crustal deformation by means of wellhead pressure monitoring*, Bulletin d'Information des Marees Terrestres, 141, 11277-11285.

Woith H., Wang R., Caka D., Irmak T.S., Tunc B., Luehr B.G. & Baris S., (2014). *Seismically induced pressure transients at geothermal reservoirs in the eastern Marmara region*. In: EGU 2014 European Geosciences Union General Assembly Vienna, Austria.

Exploring magmatic volatiles for understanding the volcano-tectonic structure of the Los Humeros geothermal field, Mexico

Jentsch A.[1,2], Jolie E.[1], Taylor-Curran H.[3] and Peiffer L.[4]

[1]*Helmholtz Centre Potsdam, GFZ, German Research Centre for Geosciences, Telegrafenberg, Germany*
[2]*Institute of Earth and Environmental Science, University of Potsdam, Germany*
[3]*Environmental Science Center, British Geological Survey, Nottingham, United Kingdom*
[4]*Departamento de Geología, Centro de Investigación Científica y de Educación Superior de Ensenada (CICESE), Ensenada, Baja California, Mexico,*

Corresponding Author: *ajentsch@gfz-potsdam.de*

Volcanic-hosted geothermal systems comprise a vast amount of thermal energy reaching supercritical conditions (T > 374 °C and P > 221 bar for pure water) near the brittle-ductile transition zone [Reinsch et al., 2017]. The assessment, characterization, and development of a so called super-hot geothermal resource is the focus of the Mexican-European research cooperation GEMex studying the Los Humeros Volcanic Complex (LHVC). The main control for fluid upflow in the reservoir is given by volcano-tectonic structures (e.g. faults and fractures) which cut through the low permeable pre-caldera Teziutlán formation [Gutiérrez-Negrín and Izquierdo-Montalvo, 2010]. In this study, we present the results of a systematic, large scale CO_2 efflux scouting survey in order to understand the spatial variability of CO_2 degassing and the relation to possible migration pathways of hydrothermal fluids reaching the surface. From all volcanic gases, CO_2 is the most abundant one and is a particularly useful parameter for soil gas measurements as it exsolves from magma at greater depth and has an elementary importance in geothermal-volcanic systems [Edmonds and Wallace, 2017]. CO_2 effluxes were measured by the accumulation chamber technique and complemented by the sampling of carbon and helium isotopes from selected sites. By means of carbon isotopic analysis the origin and different processes, affecting the migration of CO_2 can be identified. Helium isotopic ratios ($^3He/^4He$) are excellent tracer for deep derived fluids since ^3He is primordial released by the mantle [Karlstrom et al., 2013; Notsu et al., 2001]. Based on the CO_2 efflux results of the large scale scouting survey, four areas of increased CO_2 emissions were selected and grid spacing was refined to gain a higher resolution of the extent of increased degassing areas and relate them to the structural architecture of fault zones.

Geologic and structural setting

The Los Humeros Volcanic Complex is located at the eastern portion of the Trans-Mexican Volcanic Belt (TMVB) being the largest, active, silicic caldera complex and hosting a geothermal field with an installed capacity of 95 MW [Gutiérrez-Negrín, 2019]. The caldera has a complex geological and structural history and its evolution started around 164 ± 4.2 ka ago resulting in the 20 km wide Los Humeros collapse caldera. The activity continued with a series of plinian eruptions and was followed by a second caldera forming event at around 69 ± 16 ka ago leaving the semicircular Los Potreros caldera which hosts the active geothermal system. Norini et al., [2015] suggest that the NNW-SSE trending fault system (Los Humeros and Maztaloya Fault) as well as some sub-parallel smaller faults and fault splays (La Cuesta, Loma Blanca etc.) induce and preserve the permeability of the geothermal system. This is supported by the isotopic fingerprint of geothermal fluids, which show a mixing between

andesitic and meteoric waters concluding that geothermal fluids circulate in the Teziutlan Formation of the precaldera basement with a fault and fracture network cutting through the compact volcanic succession overlying the basement and allowing meteoric waters to infiltrate [Gutiérrez-Negrín and Izquierdo-Montalvo, 2010].

Methods and Results

Herein, all measurements of soil CO_2 efflux were performed with a portable LICOR LI-820 infrared gas analyzer from West Systems which is connected through a closed loop to an accumulation chamber (West Systems Ltd, 2019). A detailed description about the accumulation chamber method can be found in Chiodini et al., [1998]. Furthermore, soil temperatures were measured in 50 cm depth with a Greisinger GMH 285-BNC thermometer coupled to a Pt1000 sensor and a 620 mm long stainless steel probe (accuracy ±0.1 K). For the identification of the origin of CO_2, a total of 94 soil gas samples were collected from low, intermediate and high degassing areas for $\delta^{13}C_{CO2}$ isotopic ratios analysis. Isotopic determinations were performed with a Delta V Plus gas chromatograph coupled to an isotopic ratio mass spectrometer. To further constrain the origin of soil gases, six helium samples from weak to moderate steam vents were taken to determine the $^3He/^4He$ ratios. The samples were analyzed with a Helix SFT mass spectrometer and are normalized to the air ratio ($R/R_A = 1.386 \times 10^{-6}$).

CO_2 efflux values show a wide range and vary from 0 to 1,464.2 g m^{-2} d^{-1} (Figure 1).

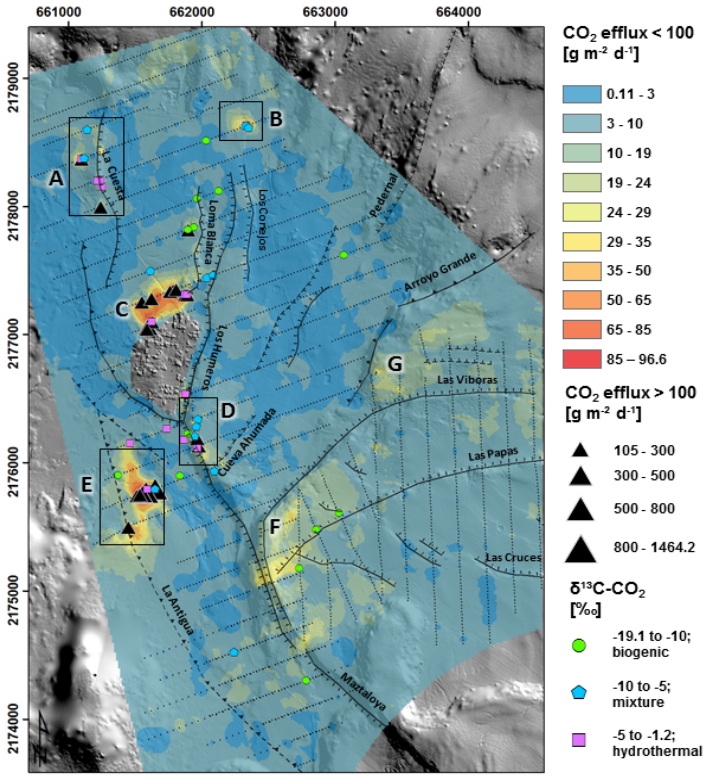

Figure 1 CO_2 efflux map from 2017 showing values until 100 g m^{-2} d^{-1}. Bold capital letters refer to areas explained in the chapters results and discussion. Black squares show the location and size of the small scale surveys performed in 2018. Graduated black triangles show CO_2 effluxes above 100 g m^{-2} d^{-1}. Small black dots represent CO_2 efflux sampling sites. Solid and dashed black lines refer to known and inferred faults. The grey cutout between Area C and D represents Los Humeros village.

By applying the graphical statistical analysis on the total dataset two inflection points where identified which divide the dataset into three populations. Population A corresponds to low 'background' effluxes (0.1 - 20. 7 g m^{-2} d^{-1}). Population B is a mixed population showing the widest range of values (20.7 - 640.8 g m^{-2} d^{-1}), and population C includes the highest measured values (670.8 - 1464.2 g m^{-2} d^{-1}). Zones exceeding the background thresholds (Area A to G) occur over the entire study area. However, Area A to E are located within a very pronounced N-S corridor (3 km x 1.5km) where the majority of production wells are located. Soil temperatures in 50 cm depth vary from 5.7 to 91.3 °C. Most thermal anomalies appear in areas of elevated degassing (Area A-E). Results for carbon isotopic analysis of CO_2 range from -23.2‰ to -1.2‰ ± 0.07‰ covering a broad spectrum of sources. The measured $^3He/^4He$ ratios range from 2.31 ± 0.58 to 4.88 ± 0.99 and deviate from the typical air helium isotopic ratio (R_A = 1.386 x 10-6) suggesting a mantle contribution.

Discussion

CO_2 efflux populations and origin of CO_2 based on $\delta^{13}C_{CO2}$ isotopic ratio analysis

The majority of measured CO_2 efflux values belongs to the background population (0 - 20 g m^{-2} d^{-1}). As shown for other active caldera complexes worldwide [Peiffer et al., 2014 & 2018; Werner et al., 2000], these low fluxes typically originate from biogenic degassing (i.e. soil respiration and organic decomposition). Additionally, most $\delta^{13}C$ analysis of soil CO_2 acquired in this study confirms this hypothesis ($\delta^{13}C$ < -10 ‰). However, 10 samples with an efflux value lower than 20 g m^{-2} d^{-1} have $\delta^{13}C_{CO2}$ isotopic compositions ranging from -3.9 to -10 ‰, indicating a clear contribution of hydrothermal CO_2. Peiffer et al. [2014] report that CO_2 of hydrothermal origin can be transported by advection at low rates, similar to biogenic degassing rates, due to a low-permeability of soil/rocks and/or low-pressure gradients. The relatively large range of effluxes in population B (20 - 669 g m^{-2} d^{-1}) results from combined CO_2 sources as well as transport mechanisms. Corresponding $\delta^{13}C_{CO2}$ values range from -18 ‰ up to -1.2 ‰. This constrains that CO_2 emissions are a result of biologic and volcanic degassing driven by diffusive and advective transport mechanisms. Population C (640 - 1468 g m^{-2} d^{-1}) is characterized by more heavy $\delta^{13}C_{CO2}$ values (-4 to -3 ‰), which typically indicate a magmatic source. Eventually we could show that the separation of CO_2 effluxes by only using the GSA method is not significant enough in order to distinguish between biogenic and hydrothermal soil degassing.

Soil degassing and its relationship to fault zone architecture

Our study areas show that CO_2 degassing is typically not limited to a single fault instead it is influenced by wide fault zones of anisotropic and heterogeneous characteristics. Faulds and Hinz, [2015] defined different structural settings in the Basin and Range Province which favor the development for geothermal systems. This general classification can be applied to other geothermal systems and is brought in to context with our results. We here discuss only two of the five settings. Area E is by far the largest degassing corridor (600 m E-W and 1000 m N-S extension) in Los Humeros with a strong magmatic contribution supported by both $^3He/^4He$ ratio and $\delta^{13}C_{CO2}$ values. Size and pattern of degassing is likely a result of a fault intersection or fault bend, which corresponds to long-term, critically stressed areas where fluid pathways tend to remain open. The degassing pattern follows the typical N-S orientation of faults in Los Humeros and gives further evidence to the existence of the inferred fault structure La Antigua. Area C is pronounced in a 550 m E-W corridor north of Los Humeros village and extends about 250 m in N-S direction. For our understanding, elevated emissions might be induced by a horsetail fault termination starting south of Los Humeros village. Thus, there is the possibility that another fault strand is running under Los Humeros village

and proceeds towards the north. Los Humeros is the range front fault with asymmetrically arranged faults spreading off and forming the horsetail. This configuration promotes the uprising of hot fluids as seen by hot surface temperatures (91.3°C), mantle derived helium and hydrothermal carbon in Area C.

Conclusion

We here present results of a comprehensive large-scale soil gas survey at Los Humeros geothermal field where we identified areas of increased permeability related to structural discontinuities in the subsurface of the main geothermal production zone. Our findings show that the majority of elevated CO_2 emissions at the surface is hydrothermally derived CO_2 suggesting a structural control on degassing from the reservoir. This is confirmed by the location of most of the production wells drilled along the NNW-SSE active fault system. Carbon and helium isotopic analysis provide crucial evidence for the relationship of elevated soil gases connected to the deep geothermal reservoir. Furthermore, results of carbon isotopic analyses showed that the application of determined $\delta^{13}C_{CO2}$ groups is an additional tool to delineate areas of deep derived CO_2 than solely using CO_2 effluxes. We encourage the application of soil gas studies for resource assessment in new and undeveloped geothermal sites and its use for the localization of potential drilling targets in combination with other scientific disciplines e.g. structural geology, 3D modelling, remote sensing.

References

Chiodini G., Cioni R., Guidi M., Raco B., Marini L., (1998). *Soil CO_2 flux measurements in volcanic and geothermal areas*. Appl. Geochemistry, 13, 543-552. https://doi.org/10.1016/S0883-2927(97)00076-0.

Edmonds M., Wallace P.J., (2017). *Volatiles and exsolved vapor in volcanic systems*. Elements, 13, 29-34. https://doi.org/10.2113/gselements.13.1.29.

Faulds J.E., Hinz N.H., (2015). *Favorable Tectonic and Structural Settings of Geothermal Systems in the Great Basin Region, Western USA: Proxies for Discovering Blind Geothermal Systems*. World Geotherm. Congr., 2015 1-6.

Gutiérrez-Negrín L.C.A., (2019). *Current status of geothermal-electric production in Mexico Current status of geothermal-electric production in Mexico*. In: IOP Conf. Series: Earth and Environmental Science, 249 (012017). https://doi.org/10.1088/1755-1315/249/1/012017.

Gutiérrez-Negrín L.C.A., Izquierdo-Montalvo G., (2010). *Review and Update of the Main Features of the Los Humeros Geothermal Field, Mexico*. In: World Geothermal Congress 2010.

Karlstrom K.E., Crossey L.J., Hilton D.R., Barry P.H., (2013). *Mantle ^3He and CO_2 degassing in carbonic and geothermal springs of Colorado and implications for neotectonics of the Rocky Mountains*. Geology, 41, 495-498. https://doi.org/10.1130/G34007.1.

Norini G., Groppelli G., Sulpizio R., Carrasco-Núñez G., Dávila-Harris P., Pellicioli C., Zucca F., De Franco R., (2015). *Structural analysis and thermal remote sensing of the Los Humeros Volcanic Complex: Implications for volcano structure and geothermal exploration*. J. Volcanol. Geotherm. Res., 301, 221-237. https://doi.org/10.1016/j.jvolgeores.2015.05.014.

Notsu K., Nakai S., Igarashi G., Ishibashi J., Mori T., Suzuki M., Wakita H., (2001). *Spatial distribution and temporal variation of ^3He / ^4He in hot spring gas released from Unzen volcanic area, Japan*. J. Volcanol. Geotherm. Res., 111, 89-98.

Peiffer L., Bernard-Romero R., Mazot A., Taran Y.A., Guevara M., Santoyo E., (2014). *Fluid geochemistry and soil gas fluxes (CO_2-CH_4-H_2S) at a promissory Hot Dry Rock Geothermal System: The Acoculco caldera, Mexico*. J. Volcanol. Geotherm. Res., 284, 122-137.

https://doi.org/10.1016/j.jvolgeores.2014.07.019.

Peiffer L., Carrasco-Núñez G., Mazot A., Villanueva-Estrada R.E., Inguaggiato C., Bernard Romero R., Rocha Miller R., Hernández Rojas J., (2018). *Soil degassing at the Los Humeros geothermal field (Mexico).* J. Volcanol. Geotherm. Res., 356, 163-174. https://doi.org/10.1016/j.jvolgeores.2018.03.001.

Reinsch T., Dobson P., Asanuma H., Huenges E., Poletto F., Sanjuan B., (2017). *Utilizing supercritical geothermal systems: a review of past ventures and ongoing research activities.* Geotherm. Energy, 5. https://doi.org/10.1186/s40517-017-0075-y.

Seismogeochemistry anomalies in the underground waters of Azerbaijan is indicator of the catastrophic earthquake in Italy (Amatrice city - 2016)

Keramova R.A.

Department "Complex geochemical researches" of Republican Seismic Survey Center of Azerbaijan National Academy of Sciences (RSSC at ANAS) Baku, Azerbaijan

Corresponding Author: *keramovar@mail.ru*

These researches present the analysis of results from the "Database…", which reflect the year-round monitoring of the seismogeodynamic (SFGD) regime of the fluids in Azerbaijan, before the catastrophic Earthquake in Italy (Amatrice c. - 24.08.2016). This "Database..." is unique, because it is the only one in the world that includes statistically huge and reliable factual material based on the results year-round SFGD monitoring during 1979-2019. Also it reflect changes of the fluid's regime during the preparation as both local, weak and strong earthquakes, as remote strong and catastrophic seismic events in the different regions of our planet. These researches include seismogeochemistry and seismohydrogeological monitoring of the fluid's regime, which are represented by underground waters and sea water of the Caspian Sea, dissolved gases and radioactive emanations in the waters and on the Earth's surface. The main purpose of the work at that period (1979-2000) was the retrospective identification of the informative, seismogeochemical criterias of earthquakes that were realized not only in the Caspian Sea and Azerbaijan, but and in another seismically active regions of our planet. For the first time, a retrospective comparison the data of the SFGD fields of Azerbaijan with seismicity was made in 1981, after a strong local Ismayilli earthquake, and then - a series of the Caspian seismic events (1986; 1989, 2000), more distant centers of catastrophic earthquakes in Armenia-Spitak (1988), Iran-Rudbar (1990) and etc.

As you know, the focus of Amatrice's catastrophic earthquake (24.08-26.08.2016 G.; M=6.2-6.6; h=4-10 km) were located in Central Italy. Physical and chemical processes that took place in the epicentral focal zone, caused a short-period changes in the environment at a great distance from it. They appeared not only as local tectonic faults, but also in the ion-salt composition of underground water of different genesis and migration conditions. This fact has been detected in another country, Azerbaijan, on the epicentral distance from the focus equal to 2690-2950 km. It is important to note that on the background seismic lull in the variations of the year-round of SFGD monitoring was discovered short-period (1÷3 days) anomalous as positive and as negative deviations of the concentration of the different parameters of the ion-salt composition rather background values. They reached 500-1200 % and was discovered at the many objects of observation almost synchronously, for 1-2 days before the realization this earthquake and another powerful (M=6.6) earthquake (Amatrice - 26.08.2016). They were represented by the ions: acid-base properties and redox potential of the environment, the bicarbonate, the amount of chlorine, bromine and iodine, sulfate, magnesium, calcium, sum of ions of sodium, potassium; mineralization.

As a result, it was confirmed our earlier (2001) made an important regularity: the acti-vation of seismicity is accompanied not only by stress-strain change of the environment on the Earth's surface, but also by short-period abnormal physical and chemical processes in its depths. They occur only at

the final stage, 1÷16 days before the realization of the earthquake. And for each earthquake is characterized specific, individual SFGD a “portrait” of a concrete focus of the natural earthquake.

Transregional, remote and operational forecast of the strong earthquakes in Italy and another regions according to the year-round monitoring of the seismogeodynamic re-gime of the fluids in Azerbaijan (2016-2019)

Keramova R.A.

Department "Complex geochemical researches" of Republican Seismic Survey Center of Azerbaijan National Academy of Sciences (RSSC at ANAS) Baku, Azerbaijan

Corresponding Author: *keramovar@mail.ru*

In the present research reflects the results obtained when were using two patented "Automated technologies №1 and №2 for the transregional, operational seismic forecast in any region of the world only on the basis of monitoring of seismogeodynamic regime of the fluids (SFGD) in Azerbaijan". Note, that this work is based on the daily interpretation of the factual material from "Database SFGD monitoring in Azerbaijan during time 1986-2019". When comparing these data with the seismological parameters from the published "Earthquakes Catalogs" and Internet sites (1979-2019), systematically studies comparing "retro" and "on-line" communication between seismic fields with the different magnitude (M≥3.0) and the seismogeochemical and seismohydrogeodynamics regime of the fluids in the preparation strong earthquakes in the different seismic regions of our planet, including Italy. The "Base SFGD Data of Azerbaijan..." is unique, because it is the only one in the world, which includes a statistically huge factual material for the 36 years of the 40 years of continuous observations (1979-2019).

Every day, on the basis of patented technologies, simultaneously for the different azimuth foci of predicted earthquakes, are determined the "intervals-ranges" of the main seismological parameters: coordinates; magnitude; time remaining before earthquakes realization. At the present time we are doing these works for the next areas of the world: 1. Caucasus-Caspian region; 2. Anatolian-Iranian region; 3. Countries of the seismogenic Tien Shan zone; 4. Countries of the seismogenic Hindu Kush zone of deep-focus earthquakes; 4. The centers of the planetary catastrophic earthquakes. This geography can be expanded if will be necessary. Now the reliability of the ours results reaches 80÷85 %, and in some cases higher.

For the purpose of performance a correct, transregional, operationa forecast of the earthquakes by SFGD method, to date, specifically for the territory of Italy, had been established the following regularities. In particular, these researches is efficient for the correct, transregional, operational forecast from Azerbaijan for Italy, if the lower threshold of the calculation of the main seismological parameters of the forecasting earthquake meets the next conditions: a) magnitude will be - mb≥5.5; b) the depth of the hypocenter will be equal h≥4.0; c) the forecasting period time to the realization of the earthquake will be equal to t forecasting=1÷10 days.

In the future, for the territory of Italy, if it is necessary to conduct more detailed researches for the purpose of identify seismogeochemical criteria for the transregional, operational seismic forecast, which based on SFGD technologies, obtained the actual material will be refined and corrected.

Different aspects of fluid migration (volatiles) in the NW-Bohemia region

Heinicke J.[1], Caracausi A.[2]

[1]*TU Bergakademie Freiberg, Institute of Geophysics and Geoinformatics, Germany*
[2]*Istituto Nazionale di Geofisica e Vulcanologia, Sezione di Palermo, Italy*

Corresponding Author: *Jens.heinicke@geophysik.tu-freiberg.de*

The occurrence and spatial-temporal variations of mantle derived fluids in the NW-Bohemian/ Vogtland region are under study since about 40 years. Relations to the tectonic as well as to the local seismicity were investigated [Heinicke et al., 2019]. Our presentation provides new aspects to the numerous open questions concerning the fluid migration pathways along deep reaching fault zones and their time scale. Different fluid-flow models in the upper crust in relation to variations of analysed volatiles, respectively $^{3}He/^{4}He$ ratios, will be used to discuss improved migration models.

References

Heinicke J., Stephan T., Alexandrakis C., Gaupp R., Buske S., (2019). *Alteration as possible cause for transition from brittle failure to aseismic slip: the case of the NW-Bohemia / Vogtland earthquake swarm region*. Journal of Geodynamics, 124, 79-92. 10.1016/j.jog.2019.01.010.

From Macro to Micro: Fluid emissions indicate tectonic features

Jens Heinicke[1], Hardy Pfanz[2]

[1]*TU Bergakademie Freiberg, Institute of Geophysics and Geoinformatics, Freiberg, Germany*
[2]*Lehrstuhl für Angewandte Botanik und VulkanbiologieUniversität, Duisburg-Essen Germany*

Corresponding Author: *Jens.Heinicke@geophysik.tu-freiberg.de*

The geodynamic activity of the NW-Bohemia/ Vogtland region with its earthquake swarm activities is mostly studied in relation to its local emission of juvenile fluids, in particular of CO_2. The migration and emission of these volatiles is bound to open fracture zones, partly of neo-tectonic activity.
Major tectonic fault zones are well documented on geological exposures and lithological boundaries. The orientation of a 70 km line of mantle originated CO_2 gas emission sites is bound to a NW-SE trending structure of numerous faults and fracture zones. This regional distribution of gas emission sites can be verified on traces of micro-structures that can be identified by lines of mofettic CO_2-emissions in the area of the Natural Park of Soos (Czech Republic). Investigations of these micro-structures by (i) gas sampling in the subsoil and (ii) aerial image analysis confirm the strike of the major tectonic structures. The preliminary results are given.

Observed changes of diffuse CO_2 degassing at Taal volcano (Philippines) in response to nearby large magnitude earthquake events

Hernández P.A.[1,2,3], Baldago M.CB.[5], Padilla G.D.[1,2], Padrón E.[1,2,3], Asensio-Ramos M.[1], Rodríguez F.[1], Alonso M.[1,2], Rodríguez-Pérez C.[1], Pérez N.M.[1,2,3], Arcilla C.[4,5,6], Mahar Lagmay A.[4,6] and Sumino H.[7]

[1]*Instituto Volcanológico de Canarias (INVOLCAN), San Cristobal de La Laguna, Spain*
[2]*Instituto Tecnológico y de Energías Renovables (ITER), Granadilla de Abona, Spain*
[3]*Agencia Insular de la Energía de Tenerife (AIET), Granadilla de Abona, Spain*
[4]*National Institute of Geological Sciences, University of the Philippines, Diliman, Quezon City, Philippines*
[5]*Philippine Nuclear Research Institute, Commonwealth Avenue, Diliman, Quezon City, Philippines*
[6]*University of the Philippines Resilience Institute, Diliman, Quezon City, Philippines*
[7]*Department of Basic Science, Graduate School of Arts and Sciences, The University of Tokyo, Japan*

Corresponding Author: *phdez@iter.es*

Monitoring the chemical composition and discharge rates of volcanic gases is one of the main tasks in volcano monitoring programs. Acid crater lakes are surface expressions of subaerial volcanoes and form when volcanic or hydrothermal fluids are trapped in a volcanic lake filled with meteoric water [Varekamp and Kreulen, 2000]. Volcanic lakes also represent an important degassing window to the atmosphere and one of the most extreme natural chemical environments at the Earth's surface [Sriwana et al., 2000; Pérez et al., 2011; Arpa et al., 2013]. On the other hand, volcanic crater lakes represent a unique hazard because of the danger posed by the storage of large volumes of water in proximity to near-surface magma bodies [Rowe et al., 1992]. Taal Volcano Island (Figure 1) is located in the center of the 30-km wide Taal Caldera, now filled by Taal Lake.

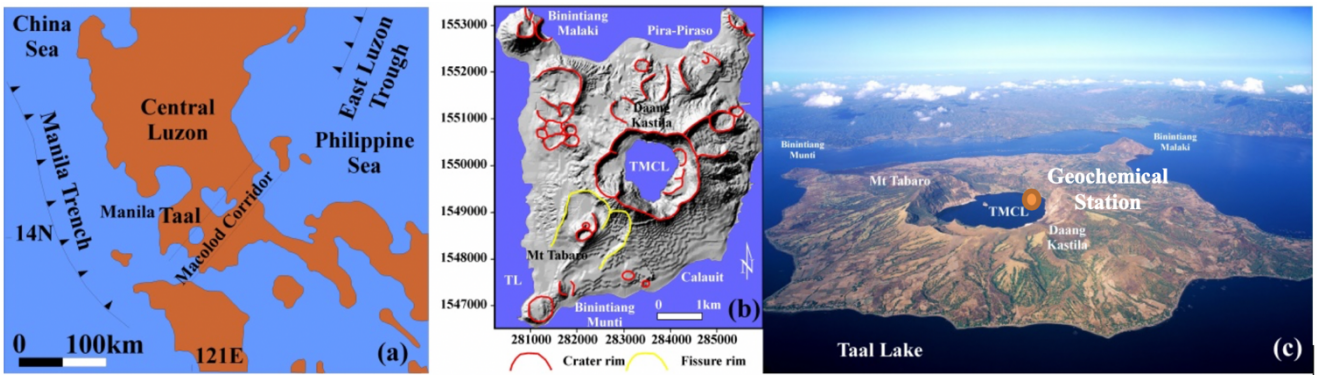

Figure 1 (a) Location of Taal Volcano, Philippines. (b) Shaded relief map and aerial view of Taal Volcano. MCL is the Main Crater Lake of the central island of the volcano. (c) Aerial picture of the volcano taken from the southeast showing the location of the geochemical station.

The Main Crater is now filled by a 1.2-km wide, 84-m deep acidic (~pH 2.8) lake (Taal Main Crater Lake; TMCL). Taal has erupted more than 30 times since 1572 [PHIVOLCS Volcano Catalog, 2009], and most of its eruptions have been hydromagmatic. Diffuse CO_2 emissions through both the MCL -

with the highest value of 4.670 t d^{-1} above a baseline of about 1000 t d^{-1} - and soils in September 2010 during a period of volcano-seismic unrest in April 2010-June 2011 were also documented [Arpa et al., 2013]. The increased CO_2 emission rate and changes in the fumarole gas compositions were mostly likely caused by magma rising from a deep to a shallow reservoir, giving rise to increased degassing. Hernández et al., 2017, reported changes in the chemical and isotopic composition of Taal MCL water and documented changes in the hydroacoustic features by echo-sounding surveys related to the same period of volcanic unrest.

Relatively high CO_2 fluxes also well correlate with both high heat flux areas (related to active and dormant volcanism) and areas with deep fractures/faults which transport CO_2 derived from magmatic and/or decarbonation processes [Hernández et al., 2001; Melián et al., 2012, 2014; Pérez et al., 2012, 2013; Toutain et al., 1999]. Irwin and Barnes, 1980, have shown that the global distribution of CO_2 degassing areas correlates with zones of seismicity and high tectonic stress. CO_2 degassing is also commonly related to active seismic faults characterized by high permeability and porosity and the occurrence of relatively high magnitude tectonic earthquakes [Salazar et al., 2002].

Between 2008 and 2014, ITER/INVOLCAN has collaborated with PHIVOLCS and from 2015 to the present with the University of the Philippines, also counting with the support of the Spanish Agency for International Development Cooperation (ACECID).

A continuous geochemical station (West Systems) was installed on January 2016, to monitor in a continuous mode the diffuse CO_2 emission at the northern portion of the main crater rim. The geochemical station measures in an hourly basis CO_2 efflux. To filter the possible influence of external parameters in the endogenous diffuse CO_2 emission, soil water content and temperature at a 40-cm depth and atmospheric parameters (wind speed and direction, air temperature and humidity, rainfall, and barometric pressure 1 m above the ground), are recorded simultaneously. Soil CO_2 diffuse values are estimated according to the accumulation chamber method [Parkinson, 1981]. Soil CO_2 efflux is measured by means of a LICOR LI-820, and data are stored on SD memory cards and sent later to INVOLCAN by e-mail. A time series of 19,975 hourly observations of diffuse CO_2 emission rate from January 2016 to April 2019 was recorded with about 8.000 missing data due to technical problems (29.7% of the total data). The observed diffuse CO_2 emission data ranged from negligible values up to 2.927 g m^{-2} d^{-1}. Figure 2 shows the time series of soil CO_2 efflux data with the moving average of 168 hours.

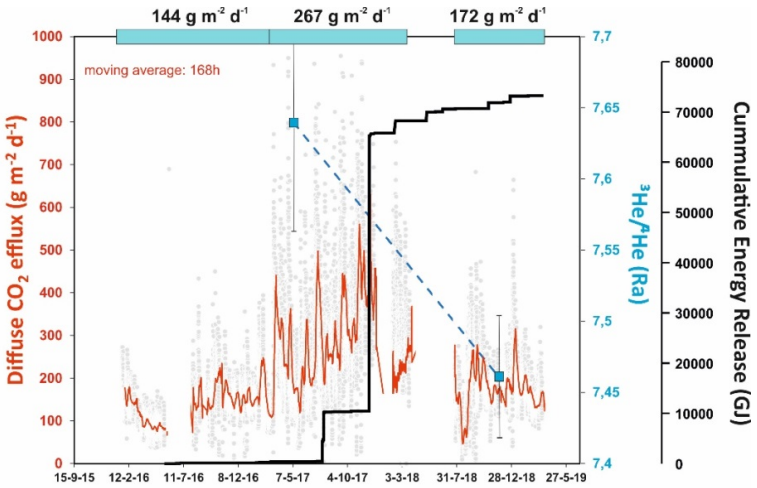

Figure 2 Time series of diffuse CO_2 emission from the geochemical station installed at Taal (red line) and $^3He/^4He$ ratios from Taal fumaroles (solid blue squares). Solid black line represents cumulative energy release.

Time series may be separated into three distinct set intervals: (i) from the beginning of the observation until February 2017, characterized by a quasi-stationary period and relatively lower diffuse CO_2 emission values with an average value of 144 g m^{-2} d^{-1}; (ii) sharp increasing in 14 March, 2017, when the station measured an increase of CO_2 emission from ~0.1 up to 1.1 kg m^{-2} d^{-1} in 9 hours and since that date, with the average value increasing from 144 to 267 g m^{-2} d^{-1} to March 2018; and (iii) a quasi-stationary period from April 2018 to April 2019, characterized by CO_2 efflux values similar to those observed within first period (172 g m^{-2} d^{-1}).

During 2017, two important seismic events occurred near Taal volcano; (a) an earthquake swarm, 13 of which had magnitudes 4.0 or greater, that originated around 30 km south of the volcano on April 4 to 11, 2017 and (b) a M 6.3 earthquake that occurred approximately 50 km east of Taal on August 10, 2017. Local seismic activity near Taal Volcano is described in terms of the accumulated released seismic energy ARSE (Figure 2) during the observation period, with a mean step related to the occurrence of the M 6.3 earthquake. A significant relationship between pre-seismic and co-seismic activity and temporal variations in CO_2 efflux is observed. Soil CO_2 efflux data recorded with the automatic geochemical monitoring station installed at Taal crater rim, showed an increase in CO_2 efflux together with an increase on the diffuse CO_2 emission from TMCL preceding both the earthquake swarm. When the M6.3 earthquake, the CO_2 emission rate from TMCL sharply rose until it peaked at 2.677 t d^{-1} on November 1, 2017, with the emission decreasing considerably after. The observed changes on the CO_2 efflux from the recorded time series of the geochemical station and from the surveys performed at the TMCL may be considered as precursory earthquake signals. These results suggest that fluid movement and release of CO_2 are related to the dynamics of stress accumulation and seismic swarm generation at Taal area. It has been widely accepted that fluids play an important role in faulting mechanisms and the triggering of earthquakes [Salazar et al., 2002]. Independent of the mechanism responsible for its generation, high pore pressure confined within the seimogenic zone will cause pore fluid to diffuse to surrounding areas, leading to fault slippage and seismicity [Shi and Wang, 1984-85]. Helium isotope signatures reveal a significant mantle component for the fluids discharged at Taal volcano (Figure 2). These findings suggest that the episodic release of deep magmatic fluids might be an additional source contributing to changes in the local stress field. Pore pressure changes induced by either changes in stress accumulation within the local faulting system and/or episodic injection of deeply sourced gases (mixing of mantle and metamorphic derived rich-CO_2 fluids) might account for our observations on the diffuse CO_2 soil efflux behavior.

References

Arpa M.C., Hernández P.A., Padrón E., Reniva P., Padilla G.D., Bariso E., Melián G., Barrancos J., Nolasco D., Calvo D., Pérez N.M. and Solidum Renato U. Jr., (2013). *Geochemical evidence of magma intrusion inferred from diffuse CO_2 emissions and fumarole plume chemistry: the 2010-11 volcanic unrest at Taal Volcano, Philippines.* Bulletin of Volcanology, 75, 1-13.

Hernández P.A., Notsu K., Salazar J.M., Mori T., Natale G., Okada H., Virgili G., Shimoike Y., Sato M., and Pérez N.M., (2001). *Carbon dioxide degassing by advective flow from Usu volcano, Japan*. Science, 292, 83-86.

Hernández P.A., Melián G., Somoza L., Arpa M.C., Pérez N.M., Bariso E., Sumino H., Padrón E., Varekamp J.C., Albert-Beltran J. and Solidum Renato U. Jr., (2017). *The acid crater lake of Taal Volcano, Philippines: hydrogeochemical and hydroacoustic data related to the 2010-11 volcanic unrest*. Geological Society, London, Special Publications, 437[1]:131.

Irwin W.P. and Barnes I., (1980). *Tectonic relations of carbon dioxide discharges and earthquakes*. Journal of Geophysical Research, 85, B6, P3115.

Melián G, Tassi F, Pérez N.M., Hernández P, Sortino F, Vaselli O, Padrón E, Nolasco D, Barrancos J, Padilla G, Rodriguez F, Dionis S, Calvo D, Notsu K, Sumino H., (2012). *A magmatic source for fumaroles and diffuse degassing from the summit crater of Teide volcano (Tenerife, Canary Islands): geochemical evidence for the 2004-05 seismic-volcanic crisis*. Bulletin of Volcanology, 74(6), 1465-1483. doi:10.1007/s00445-012-0613-1.

Melián G.V., Hernández P.A., Padrón E., Pérez N.M., Barrancos J., Padilla G., Dionis S., Rodríguez F., Calvo D., Nolasco D., (2014). *Spatial and temporal variations of diffuse CO_2 degassing at el Hierro volcanic system: relation to the 2011-2012 submarine eruption*. Journal of Geophysical Research, Solid Earth, 119(9):6979-6991. doi:10.1002/2014JB011013.

Parkinson K.J., (1981). *An improved method for measuring soil respiration in the field*. Journal of Applied Ecology, 18:221-228

Pérez N.M., Hernández P.A. Padilla G., Nolasco D., Barrancos J., Melían G., Padrón E., Dionis S., Calvo D., Rodríguez F., Notsu K., Mori T., Kusakabe M., Arpa M.C., Reniva P., Ibarra M., (2011). *Global CO_2 emission from volcanic lakes*. Geology, 39, 235- 38.

Pérez N.M., Padilla G., Padrón E., Hernández P.A., Melián G., Barrancos J., Dionis S., Nolasco D., Rodríguez F., Calvo D. and Hernández I., (2012). *Precursory diffuse CO_2 and H_2S emission signature of the 2011-12 El Hierro submarine eruption, Canary Islands*. Geophysical Research Letters, 39, L16311, doi:10.1029/2012GL052410.

Pérez N.M., Hernández P.A., Padrón E., Melián G., Nolasco D., Barrancos J., Padilla G., Calvo D., Rodríguez F., Dionis S. and Chiodini G., (2013). *An increasing trend of diffuse CO_2 emission from Teide volcano (Tenerife, Canary Islands): geochemical evidence of magma degassing episodes*. Journal of Geological Society of London, 170(4), 585-592, doi:10.1144/jgs2012-125.

Rowe G.L., Brantley S.L., Fernández M., Fernández J.F., Borgia A. and Barquero J., (1992). *Fluid volcano interaction in an active stratovolcano: the volcanic lake system of Poas Volcano, Costa Rica.* Journal of Volcanology and Geothermal Research, 49, 23-51.

Salazar J.M.L., Pérez N.M., Hernández P.A., Soriano T., Barahona F., Olmos R., Cartagena R., López D., Lima N., Melián, G., Galindo I., Padrón E., Sumino, H. and Notsu, K., (2002). *Precursory diffuse carbon dioxide degassing signature related A 5.1 magnitude earthquake in El Salvador, Central America.* Earth and Planetary Science Letters, 205, 81-89.

Sriwana T., Van Bergen M.J., Varekamp J.C., Sumarti S., Takano B., Van Os B.J.H. and Leng M.J., (2000). *Geochemistry of the acid Kawah Putih lake, Patuha Volcano, West Java, Indonesia*. Journal of Volcanology and Geothermal Research, 97, 77-104.

Toutain J.P. and Baubron J.C., (1999). *Gas geochemistry and seismotectonics: a review*. Tectonophysics, 301 1-27.

Varekamp J.C. and Kreulen R., (2000). *The stable isotope geochemistry of volcanic lakes with examples from Indonesia*. Journal of Volcanology and Geothermal Research, 97, 309-327.

Shi X.J. and Wang C.Y., (1984/85). *Instability on a weakening fault*. Pure and Applied Geophysics, 122, 478-491.

The spatial relationships between the distribution of geofluids and the location of seismogenic faults in peninsular Italy

Martinelli G.[1,2], Vannoli P.[3] and Valensise G.[3]

[1]*ARPAE, Agenzia Regionale per la Protezione Ambientale, Emilia-Romagna, Italy*
[2]*Istituto Nazionale di Geofisica e Vulcanologia, Sezione di Palermo, Italy*
[3]*Istituto Nazionale di Geofisica e Vulcanologia, Sezione di Sismologia e Tettonofisica, Roma, Italy*

Corresponding Author: *gianluca.valensise@ingv.it*

It is well established that any pressure gradients existing in the Earth's crust induces the expulsion of geofluids from deep geological formations toward the atmosphere. The intensity and duration of the expulsion processes depends mostly on crustal permeability [Gleeson and Ingebritsen, 2017] and to the driving forces that may induce pressure gradients. These forces include topographic relief, tectonic dilation and compression, diagenesis, heat, fluid sources [Bredehoeft et al., 1990].
For many years Earth scientists have attempted to explore and understand the relationships that exists between the location and the characteristics of anomalous or otherwise significant geofluids on the one hand, and the occurrence of significant earthquakes on the other hand [Irwin and Barnes, 1980; Gold and Soter, 1984; Manga et al., 2012].

How do geofluids relate to earthquakes and their causative faults?
Most of early investigators were mainly concerned with time-domain analyses, and particularly with the detection of possible changes in the chemico-physical characteristics of selected thermal springs or of gas emissions resulting from large earthquakes nearby.
Conventional studies tended to focus on a limited number of well-known springs or gas emissions with a limited earthquake dataset and on qualitative geodynamic and tectonic information. For instance, Barbier and Fanelli, [1976] used a point-to-point or point-to-line approach to correlate the presence of thermal springs with the epicentral location of Italian earthquakes and with "long lineations" derived from satellite imagery (ERTS-1).
In contrast, our approach is systematic and geographically extensive. We maintain that geofluids can be used to set firm constraints on the location and extent of major seismogenic sources by highlighting the existence of permanent lithospheric discontinuities, also providing valuable data for the assessment of seismic hazard in hard-to-investigate active regions.

Tackling an old question with newly organized data
Investigating the relationships between geofluids, earthquakes and their causative faults is now possible thanks to the availability of large, georeferenced geophysical and geochemical databases.
As for seismicity, we rely essentially on the *Catalogue of Strong Italian Earthquakes* [CFTI5Med: Guidoboni et al., 2019], a large database describing large Italian earthquakes of the past along with their effects on the natural and on the built environment.
As for seismogenic faults, we rely on the *Database of Individual Seismogenic Sources*, a national georeferenced repository of tectonic, seismological and paleoseismological information on Italy's faults that are capable of generating M 5.5+ earthquakes [DISS Working Group, 2018].

Finally, for the geofluids we rely on a number of recent, fully georeferenced, freely accessible compilations (Figure 1). These include:

a) Thermal springs - Information on the location of thermally anomalous springs in Italy is traditionally found in the wide literature devoted to hydrothermal/ thermomineral springs exploited for medical and industrial purposes since the end of the nineteenth century, but all the available evidence has been reorganized and classified between the 1980s and the most recent years. In our study we took advantage of the data supplied by Trumpy and Manzella, [2017] for the interval 30-150 °C and of some springs listed by Martinelli and Albarello, [1997] for the interval 25-30 °C.

b) CO_2 gas emissions - A data base of volcanic and non-volcanic CO_2 gas emissions in Italy was compiled by Chiodini et al., [2008] in the frame of a joint INGV-Italian Civil Protection project aimed atrecording all gaseous emissions of Italy (http://googas.ov.ingv.it). The database has been since updated by Cardellini et al., [2014] and is available at http://www.magadb.net.

c) CH_4 emissions and natural gas seeps - Available data about CH_4 gas emissions in Italy were published by Martinelli et al., [2012] after merging previous historical catalogues and scattered published observations. The dataset includes CH_4 emissions associated with mud volcanoes [Martinelli and Judd, 2004]. Etiope et al., [2013] set up a website devoted to Italian hydrocarbon seepages reported in the recent scientific literature.

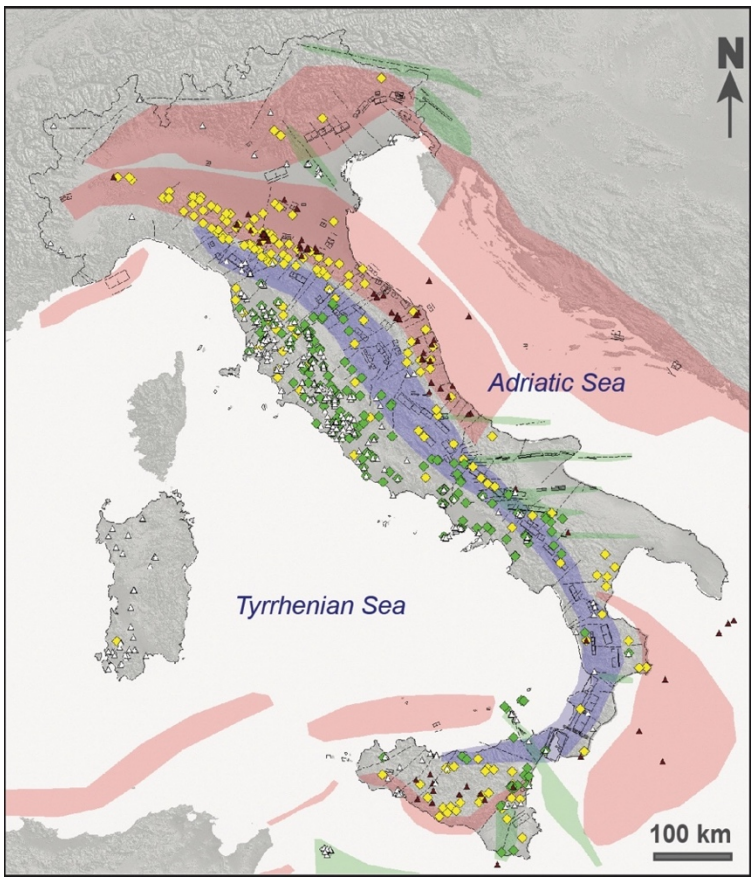

Figure 1 Study area and summary of data used for our study (see text for further details). Key to tectonic domains; blu: active extension; red: active compression; green: active strike-slip. Key to individual symbols; black boxes: surface projection of individual seismogenicsources (ISSs) from DISS 3.2.1 database; black dashed lines: transverse lineaments from various sources; white triangles: hot springs having T>25°C; green diamonds: natural CO_2 emissions; yellow diamonds: gas seeps; brown triangles: mud volcanoes.

Preliminary results

The results of our investigation can be summarized as follows:

1) On the one hand, most Italian thermal springs (white triangles in Figure 1) occurring in areas of low thermal gradient (i.e., always from areas that experienced recent magmatism) appear to fall on major lithospheric discontinuities, often referred to as "transverse lineaments" (black dashed lines); these discontinuity estend to act as segment boundaries for earthquake strain accumulation, allowing deep fluid circulation to reach the surface. On the other hand, thermal springs appear to be anticorrelated with the surface projection of major seismogenic sources (black empty boxes), implying that the relevant crustal volumes are less permeable than those crossed by the transverse lineaments.

2) Natural CO_2 emissions (green diamonds in Figure 1) are characteristic of areas undergoing extension, in agreement with the results by Tamburello et al., [2018], but their genetic and spatial relationships with seismogenic faulting are still largely obscure.

3) Most mud volcanoes (brown triangles in Figure 1) and natural gas seeps (yellow diamonds) occur in areas undergoing active compression. In particular, mud volcanoes often locate where the surface expression of active compressional structures (e.g. anticlines), comprising the engine for the formation of these peculiar landforms, intersect the already mentioned transverse lineaments.

References

Barbier E. and Fanelli M, (1976). *Main fractures of Italy from ERTS satellite images and correlations with thermal springs, volcanoes and earthquakes*. In: Aoki H. and S. Iizuka (Eds), Volcanoes and Tectonosphere, Tokai University Press, 321-331.

Bredehoeft J.D., Norton D., Engelder T., Nur A., Oliver J.E., Taylor H.P.Jr., Titley S.R., Vrolijk P.J., Walther J.V., Wickam S.M., (1990). *Overview and recommendations*. In: Bredehoeft J.D., Norton D., Engelder T., Nur A., Oliver J.E., Taylor H.P.Jr., Titley S.R., Vrolijk P.J., Walther J.V., Wickam S.M. (Eds), "The Role of Fluids in Crustal Processes", National Academic Press, 3-23.

DISS Working Group, (2018). *Database of Individual Seismogenic Sources (DISS), Version 3.2.1: A compilation of potential sources for earthquakes larger than M 5.5 in Italy and surrounding areas*. http://diss.rm.ingv.it/diss/, Istituto Nazionale di Geofisica e Vulcanologia, doi: 10.6092/INGV.IT- DISS3.2.1.

Gleeson T. and Ingebritsen S., (2017). *Crustal Permeability*. Wiley-Blackwell, Chichester, 472 p.

Gold T. and Soter S., (1984). *Fluid ascent through the solid lithosphere and its relation to earthquakes*. Pure Appl. Geophys., 122, 492-530.

Guidoboni E., Ferrari G., Tarabusi G., Sgattoni G., Comastri A., Mariotti D., Ciuccarelli C., Bianchi M.G., Valensise G., (2019). *CFTI5Med, the n release of the catalogue of strong earthquakes in italy and in the Mediterranean area*, Scientific Data 6, Article number: 80 (2019), doi: https://doi.org/10.1038/s41597-019- 0091-9.

Irwin W.P. and Barnes I., (1980). *Tectonic relations of carbon dioxide discharges and earthquakes*. J. Geophys. Res., 85, 3115.

Manga M., Beresnev I., Brodsky E.E., Elkhoury J.E., Elsworth D., Ingebritsen S.E., Mays D.C., Wang C-Y., (2012). *Changes in permeability caused by transient stresses: field observations, experiments, and mechanics*. Reviews of Geophysics, 50, RG2004/2012.

Martinelli G. and Albarello D., (1997). *Main constraints for siting monitoring networks devoted to the studies of earthquake related hydrogeochemical phenomena in Italy*. Annali di Geofisica, 40/6, 1,505-1,525. Database available from http:/www.ingv.it/.

Martinelli G., Judd A., (2004). *Mud volcanoes of Italy*. Geological Journal, 39, 49-61.

Martinelli G., Cremonini S., Samonati E., (2012). *Geological and geochemical setting of natural hydrocarbon emissions in Italy*. In: Al-MegrenH. (Ed.) Advances in Natural Gas Technology. INTECH Europe, Rijeka, 79-120.

Tamburello G., Pondrelli S., Chiodini G. and Rouwet D., (2018). *Global-scale control of extensional tectonics on CO_2 earth degassing*. Nature Communications, 9, Article number: 4608.

Trumpy E. and Manzella A., (2017). *Geothopica and the interactive analysis and visualization of the updated Italian National Geothermal Database*. International Journal of Applied Earth Observation and Geoinformation, 54, 28-37.

Tectonically induced signals recorded in Italy by geochemical and hydrogeological methods

Martinelli G.[1], Ciolini R.[2], Facca G.[3], Fazio F.[4], Gherardi F.[3] Heinicke J.[5] and Pierotti L.[3]

[1]*ARPAE Agenzia Regionale per la Protezione Ambientale Emilia Romagna, Italy*
[2]*Universitá di Pisa, Dipartimento di Ingegneria Civile e Industriale, Pisa, Italy*
[3]*Consiglio Nazionale delle Ricerche (CNR), Istituto di Geoscienze e Georisorse (IGG), Pisa, Italy*
[4]*GEODIXI, Catania, Italy*
[5]*Technische Universitat, Institute of Geophysics and Geoinformatics, Freiberg, Germany*

Corresponding Author: *faziogeo@tiscali.it*

Introduction

Crustal deformative processes are usually monitored by GPS or by satellite-based techniques. Significant signals have been recorded in many places of the world after strong earthquakes. Only in a few cases similar signals were detected before seismic events due to the relatively low sensitivity of equipments [Roeloffs, 2006; Cicerone et al., 2009]. Due to the about non compressible character of water and to deep origin of CO_2, deep originated fluid monitoring could be more sensitive in revealing weak signals related to crustal deformations and contribute to earthquake precursors researches [Martinelli and Albarello, 1997; Martinelli and Dadomo, 2017].

Methods

Dissolved and bubbling CO_2 and related gases [e.g. Pierotti et al., 2017] have been automatically monitored in thermal spring waters located in selected areas of Tuscany and Umbria regions (Central Italy). Water level has been automatically recorded in deep wells located in Eastern Sicily and in Southern Italy (Campania region).

Results

Recorded data do not show significant dependence to meteorological or artificial parameters. Part of the observed signals have been detected before mainshocks and could be related to aseismic slip (e.g. Johnston and Linde, [2002] or to seismic slip eventually induced by fluctuations in minor seismicity.

Conclusions

Earthquake forecasting researches could benefit by the joint utilization of different monitoring techniques applied to geofluids.

References

Cicerone R.D., Ebel J.E., Britton J., (2009). *A systematic compilation of earthquake precursors*. Tectonophysics, 476, 371-396.

Johnston M., Linde A., (2002). *Implications of crustal strain during conventional slow and silent earthquakes*. In: Lee W.H.K. et al., (Eds) International Handbook for Earthquake and Engineering Seismology, Part A. International Geophysical Services, 81, 589-605, Elsevier New York.

Martinelli G., Albarello D., (1997). *Main constraints for siting monitoring network devoted to the study of earthquake related hydrogeochemical phenomena in Italy*. Annals of Geophysics, 40, 1505-1525.

Martinelli G., Dadomo A., (2017). *Factors constraining the geographic distribution of earthquake geochemical and fluid-related precursors*. Chemical Geology, 469, 176-184.

Pierotti L., Gherardi F., Facca G., Piccardi L., Moratti G., (2017). *Detecting CO_2 anomalies in a spring on Mt. Amiata Volcano (Italy).* Physics and Chemistry of the Earth, Parts A/B/C, 98, 161-172.

Roeloffs E., (2006). *Evidence for Aseismic Deformation Rate changes Prior to Earthquakes*. Annual Review of Earth and Planetary Sciences, 34, 591-627.

Mantle degassing in continental collisional zone: new evidences from fluids in minerals along faults

Pantina M.[1], Censi P.[1], Caracausi A.[2], Gasparo M.[1,] Sulli A.[1], Coppola M.[3], Stagno V.[3], Romano C.[4], Billi A.[5]

[1]*Università degli Studi di Palermo, Dipartimento delle Scienze della Terra e del Mare, Palermo, Italy*
[2]*Istituto Nazionale di Geofisica e Vulcanologia, Sezione di Palermo, Italy*
[3]*Università degli Studi di Roma La Sapienza, Dipartimento di Scienze della Terra, Italy*
[4]*Università di Roma Tre, Dipartimento di Scienze, Roma, Italy*
[5]*Consiglio delle Nazionale Ricerche, IGAG, Rome, Italy*

Corresponding Author: *marco.pantina@you.unipa.it*

Introduction

The central Mediterranean is a very complex area constituted by a puzzle of different lithosphere segments, which geological evolution is due to the relation between the European and the African plate. In this geological domain the northern Sicily continental margin and adjacent coastal belt represent a link between the Sicilian chain and the Tyrrhenian extensional (back-arc) area in the north-south direction, whilst in the east-west direction a transition from a collisional (Sicilian-Maghrebian Chain) to a subduction system (Ionian-Tyrrhenian) is recognized.

The structure of lithosphere in this area is strongly matter of debate. Most of the uncertainties on the geologic evolution of the boundary between the European and African plate rise from the lack, up to now, of constraints and clear evidences of geometry of the lithosphere down to the crust-mantle interface. Along Northern Sicily (Central Mediterranean), deep seismic reflection data, gravimetric modeling and seismicity indicate the presence of mantle-wedging just below a thick-skinned deformed wedge cut by a dense system of faults down to the Mohorovicic discontinuity. In this collisional area mantle-volatiles outgas in different hydrothermal systems (Figure 1). Infact the He isotopic signatures in these fluids are from 0.4Ra to 1.3Ra (Ra is the He isotopic signature in air, 1.39×10^{-6}), whose heat-helium relationship highlights active degassing of melts [Caracausi and Sulli, 2019].

However large uncertainty is about: 1) the geographical extension of the release of mantle-derived volatiles; 2) the role of the tectonic discontinuities in the transfer of fluids and 3) the age of this this hydro-thermalism.

Analysis of the chemistry and noble gases released from fluid inclusions by in vacuo crushing promises to provide for palaeocrustal fluids the wealth of information currently being obtained from the analysis of noble gases in contemporary groundwaters.

In this paper, we report preliminary analyses and interpretation of the chemistry, noble-gas abundances and isotopes in fluid inclusion of fluorite to provide evidence on the source and interactions of the mineralising fluids.

Not surprisingly, these measurements indicate that many of the features of modern fluids in the hydrothermal system of the area are seen in the palaeo-fluids.

Geology and tectonics

In the study area the surfacing tectonic units consist of meso-cenozoic deep-water silico-carbonatic sedimentary succession. These tectonic units make up the main reliefs of the study area. The

southwest-ward staking of the tectonic units started in the middle Miocene. This tectonic event was followed by a transpressive deformation responsible for the activation of high-angle faults with a general NE-SW direction. The morphology of the area follows the trend of the faults produced by this last neotectonic deformation. In the study area we have recognized two main NE-SW left-lateral transpressive faults: M. San Calogero and San Leonardo respectively faults to east and west sector. The S. Calogero fault crops out for about 6 km, but which represents the extremity north of a larger fault. In particular, the fault of M. San Calogero dippig towards the south-eastern quadrants and appears to be responsible for the uplift of San Calogero Mount. Between these two faults, Meso-Cenozoic portions of the deep water carbonate succession outcrops in structural highs boundered by high-angle faults. In these structural highs there are abundant fluorite mineralizations, along fissures aligned to the fault structures, with a massive appearance or sometimes inside pockets, associated with barite mineralizations and filled with residual deposits. The occurrence, in the study area, of a preserved sequence of continental deposits of different ages, which have been attributed to "Unconformity Bounded Stratigraphic Units" (UBSU), with the rank of synthem or sub-synthem, allow to age-date the last fault system Late Pleistocene-Holocene. In this study the fluorites mineral rich in fluid inclusions are sampled in the outcrops of Cozzo Famo, Rocca Grande and at the foot of the NW slope of San Calogero in the relief of Poggio Balate (Figure 1).

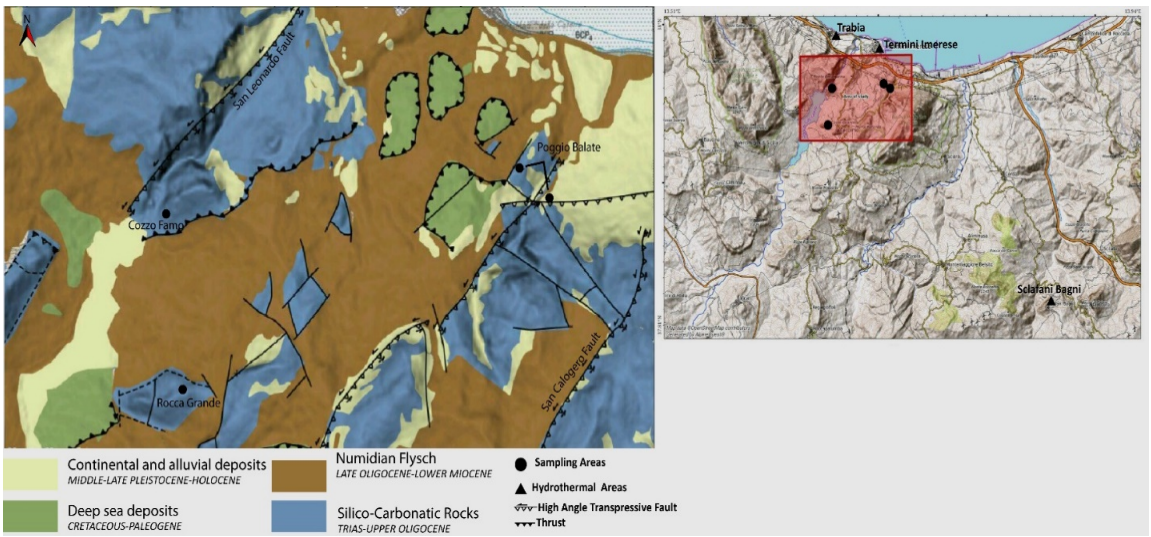

Figure 1 Geological map containing the locations of the sampling sites and the thermal springs.

Geochemistry of fluid inclusions: composition and noble gases

Crystals of fluorite labeled Poggio Balate AF (Figure 1) were crushed and few fragments embedded in epoxy resin and polished for preliminary observations conducted using an optical microscope with polarized light at the Department of Earth Sciences of Sapienza University of Rome (Italy). These revealed the presence of many inclusions of variable size generally oriented at least along two perpendicular directions (Figure 2a). Raman spectra were acquired with a Horiba LabRam HR 800 spectrometer at the Department of Science, Roma Tre University (Italy). Data were collected using a 600 grooves/mm spectrometer grating and CCD detector. A Neodimium-Yag laser at 532 nm (green laser) was used as the light source, with a confocal hole of 300 µm, slit of 200 µm and an exposure time of 30 s (2-3 times). A total of 8 measurements were performed to test the chemical homogeneity of the fluid inclusions. The backscattered Raman radiation was collected with a 50× objective and ~ 5 μm^2 spot size on a polished sample surface over a range from 200 to 1000 cm^{-1} on the crystalline matrix

and from 1000 to 4000 cm^{-1} on the fluid inclusion. The inclusions mostly consist of two phases, one fluid (possible brine) and one vapor identifiable as a bubble. Only occasionally, fluorites from Poggio Balate (PB) showed the presence of a tiny daughter minerals (Figure 2b). The fluid inclusions consist of Raman modes typical of CO_2 and amorphous carbon plus a small peak at higher frequency (~3445 cm^{-1}) that can be referred to water molecules. Interestingly, the gas phase represented by the bubble consists of CH_4 with typical vibrational modes of ~2910 cm^{-1}. Our results prove the presence of two-fluid inclusions in PB-AF consisting of C-O-H composition mainly as CO_2, CH_4, C-O-H and water as partly proposed by Bellanca et al., [1984; 1987] on petrographic and micro-thermometric basis.

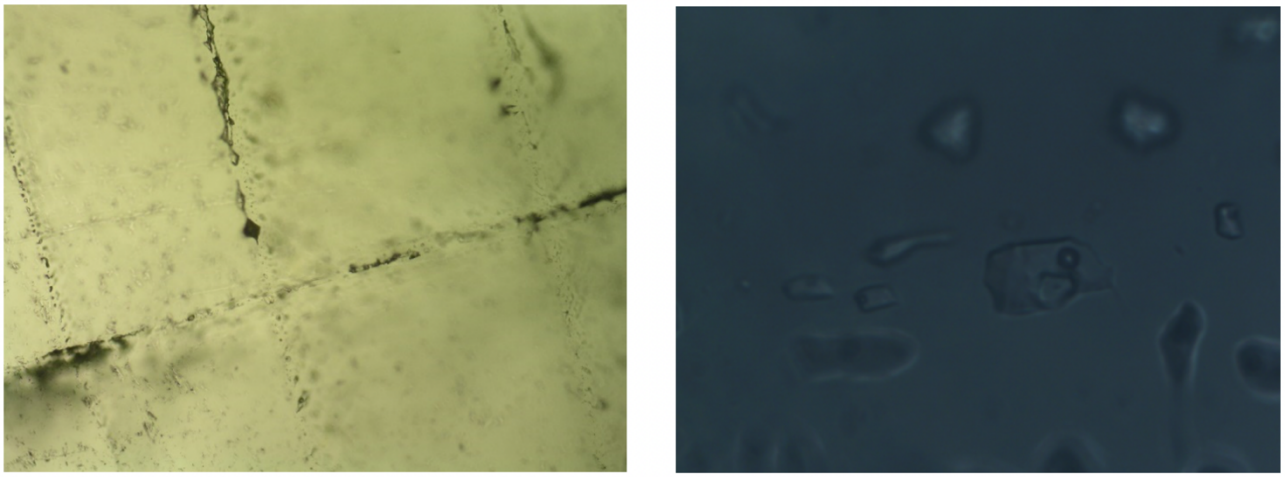

Figure 2 left) Fluid inclusions from Poggio Balate (PB) fluorites aligned along perpendicular planes; right) inclusion from PB showing the presence of a tiny crystal along with fluid and vapor.

Here we present the He isotopes ratio and the $^4He/^{20}Ne$ in fluorites collected in 4 different sites along faults (Figure 1). The noble gases analysis were carried out at the Istituto Nazionale di Geofisica e Vulcanologia, sezione di Palermo. All the samples are characterized by high $^4He/^{20}Ne$ ratios that are from 180 to 5600, orders of magnitude higher that the same ratio in atmosphere (0.318). So high $^4He/^{20}Ne$ ratios indicate that these volatiles suffer low air contamination notwithstanding H_2O is one of the main fluids trapped in the inclusions. The He isotopic ratios ranges from 0.1Ra to 0.5Ra and are in the range of the He isotopic signature (0.4-1.3Ra) in gases dissolved in the water circulating in the hydrothermal basins of the area suggesting that a mantle derived component is also trapped in the fluorites.

Conclusion

Fluorite crystallized along faults Late Pleistocene-Holocene in age and their origin is related to an active hydro-thermalism. Now there are not evidences of thermalism along these faults so fluorites are remnants of tectonic discontinuities that were able to transfer hot fluids. However, there are some thermal springs in10-20km (Figure 1) that testify the presence of active hydrothermal basins at regional scale. CO_2, CH_4 and H_2O are the main fluids trapped in the fluorites and these seems to be of meteoric and crustal origin [Bellanca et al., 1984 and 1987]. Helium is also trapped in fluid inclusions and its isotopic composition highlighted a mantle-derived component. In fact, the helium isotopic signature in the volatiles that are stored in the fluids inclusions of the fluorites ranges from 0.1Ra to 0.5Ra that overlap the He isotopic ratios in the gases dissolved in thermal waters. The outgassing of mantle-derived fluids in the region is related to the presents of melt at depth, which sustain the heat flow feeding the hydrothermal basins. The presence of melts at depth is due to

delamination processes that are subduction-related and the sucking of the mantle at regional scale [Caracausi and Sulli, 2019].

The presence of fluorite minerals in this area highlights that the release of hydrothermal fluids in the north central Sicily occurred in a region wider than now. Furthermore, the main tectonic discontinuities worked as a network of pathways for the transfer of volatiles through the crust. The next step will be to date the fluorites in order to obtain a minimum age of the hydrothermal systems, hence time of melts up-rise from the mantle that support that melts intrusion into the crust can also occur in compressional regime.

References

Bellanca A., Censi P., Di Salvo P., Neri R., (1984). *Textural, Chemical and Isotopic Variations Induced by Hydrothermal Fluids on Mesozoic Limestones in Northwestern Sicily*. Mineral Deposita, 19, 78-85.

Bellanca A., De Vivo B., Lattanzi P., Maiorani A. and Neri R., (1987). *Fluid inclusions in fluorite mineralization of northwestern Sicily, Italy*. Chem. Geol., 61, 209-216.

Caracausi A. and Sulli A., (2019). *Outgassing of mantle volatiles in compressional tectonic regime away from volcanism: the role of continental delamination*. Geochemistry, Geophysics, Geosystems, doi:10.1029/2018GC008046.

Shallow aquifer dynamics in a volcanic-hydrothermal environment: geochemical evidences from Bagnore spring, Mt. Amiata, Italy

Pierotti L., Facca G., Ferrari E. and Gherardi F.

Consiglio Nazionale delle Ricerche (CNR), Istituto di Geoscienze e Georisorse (IGG), Pisa, Italy

Corresponding Author: *l.pierotti@igg.cnr.it*

Introduction

Since 2004, the Bagnore spring is monitored with an automatic station for geochemical precursors of earthquakes [Pierotti et al., 2017]. The spring emerges at an altitude of 765 m a.s.l. on the southwestern slopes of the Mt. Amiata extinct volcano (Southern Tuscany, Italy). It drains a local, shallow, short-circuiting aquifer hosted in the volcanic rocks that mantle the upper part of the Mt. Amiata edifice [Pierotti et al., 2016], and is located above the structural high of the upper carbonate reservoir of the Bagnore geothermal field.

The Bagnore spring has flow rate of about 0.5 l/s, and an average temperature of 21.2°C, which is about 8 °C above mean ambient temperature in the area (13.4 °C; data from Hydrological Service of the Tuscan Region; http://www.sir.toscana.it/).

The current geochemical model of the aquifer drained by the Bagnore spring [Pierotti et al., 2016], considers that chemicals in solution are mainly acquired by leaching of primary solid constituents (volcanic glass and anorthite) and secondary carbonate cement, after absorption of hydrothermal gases. Hydrothermal gases are supposed to be prevalently conveyed to the surface in correspondence to the intersection of the Bagnore fault (one of the main faults of the volcano), and a NNW-SSE-trending fault/fracture system located SW of the volcano [Pierotti et al., 2017]. The presence of Tritium, the low dissolved salinity (< 250 mg/L) and Cl content (< 20 mg/L), along with their near-meteoric $\delta^{18}O$ signature, indicate that spring waters are not affected by mixing with geothermal waters hypothetically coming from the deep reservoir currently exploited for electricity generation.

Methods

The Bagnore automatic station is equipped with sensors for the simultaneous measurement of six parameters: temperature, pH, electrical conductivity, redox potential, and dissolved CO_2 and CH_4. Concentrations of dissolved CO_2 and CH_4 were measured with an IR spectrometer, upon gas extraction from the water by a cell specifically designed and built in the IGG-CNR-Pisa laboratories [Cioni et al., 2007]. The station works with flowing water (about 5 L per minute), and records a datum every 5 min, for all parameters. At the end of each day, data are transmitted by GPRS router to a server located in Pisa, at CNR-IGG. The station is regularly operative since 2004, and a huge data record of more than 1.5 million raw data has been produced since then.

Manual calibration procedures are done on a monthly basis, and/or in conjunction with anomalous variations of the signals [Pierotti et al., 2015]. At the same time of calibration operations, aliquots of water are collected for: (i) in situ analysis of temperature, electrical conductivity, pH, alkalinity; (ii) determination in laboratory of the main dissolved chemical constituents (Na, K, Ca, Mg, Cl, SO_4, SiO_2, F, B); (iii) determination in laboratory of the isotope composition of water $\delta^{18}O$, $\delta^{2}H$ on a regular basis, UT sporadically).

Results

The long data record acquired by the automatic station allow for an accurate description of the geochemical baseline of the natural manifestation, and for the identification of short- and/or medium-term temporal anomalies in the signals. Significant variations in all the monitored parameters were observed during the period June 2004 - July 2019.

In particular, Figure 1 shows temperature (box A), redox potential (box B) and dissolved CO_2 (box C) signals acquired by the Bagnore automatic monitoring station during this observation period. The blue dots delineate the trend of the values acquired every 5 minutes, while the red lines define the mobile average calculated on a single month basis.

The temperature (Figure 1A) show an average, minimum and maximum value of 21.2, 17.5 and 26.5°C, respectively. The signal shows seasonal variations with sudden decreases related to rainy events, but a significant increase in the maximum values has been registered since July 2011. In particular, a significantly large temperature increase up to 26.2°C was recorded on July 2017.

The redox potential (Figure 1B) was characterized by an average value of 230 mV, indicative of predominantly oxidized conditions in the shallow volcanic aquifer, until the beginning of 2016. Starting from March 2016, the signal started declining towards increasingly negative values down to a minimum of -248 mV, indicative of predominantly reductive conditions.

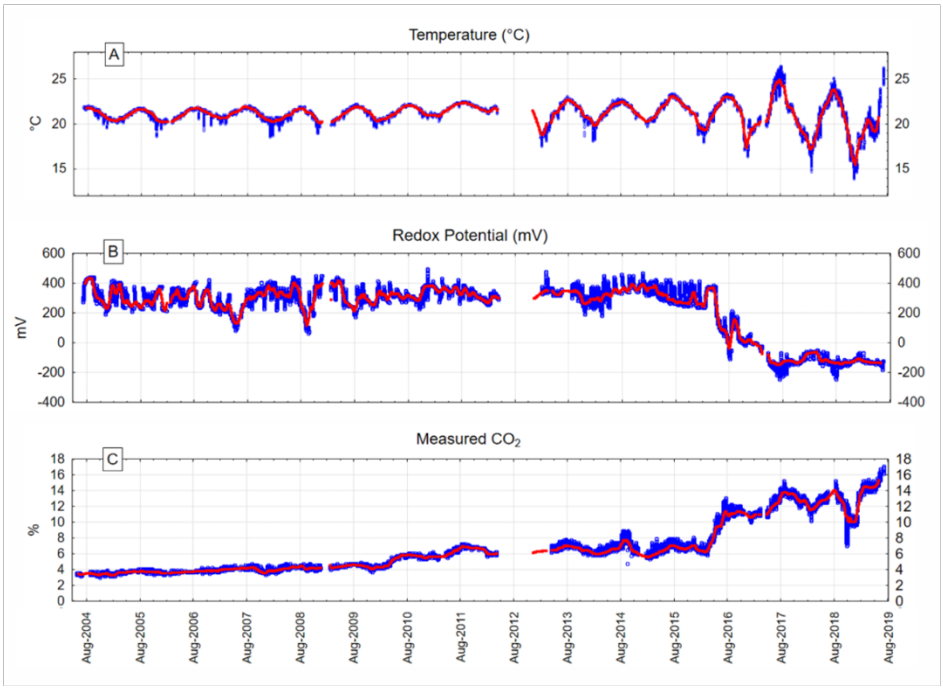

Figure 1 Continuous signals registered by the Bagnore automatic station over the period 2004-2017 (blue dots: parameters measured every five minutes; red lines: mobile average calculated on a single month basis). Box A: temperature (°C); box B: redox potential (mV); box C: dissolved CO_2 concentration (atm.%; gas concentration in the measuring chamber, after total stripping of the sampled water).

The concentration of CO_2 dissolved in the Bagnore waters (Figure 2C) steadily increased over the period 2004-2015, with an average reference value of 6.5 atm.% estimated for the period 2013-2015. Thus, the signal showed a first significant increase in April 2010, and a second one in August 2014. A very major increase was registered since the end of March 2016, which culminated with a relative maximum concentration of more than 13% in August 2016. Since then, additional peaks in CO_2 concentration were registered in 2017 and 2018, during the summer season, and in 2019, when

a trend of progressive increase was observed during the spring and summer seasons. All these episodes of CO_2 augmentation were mirrored by a concomitant decrease in pH. Since August 2016, the average concentration of CO_2 remained constantly above 10 atm.%.
All major variations observed since March 2016 were interpreted as an indication of mutated dynamic conditions within the aquifer. In fact, since that date, the aquifer appeared to respond more sensitively to external perturbations. In particular, the monitored geochemical parameters are consistent with both (i) a largely increased absorption of hydrothermal gases, and (ii) a more rapid and/or efficient entry of the meteoric recharge after major rainfall events. The first process is witnessed by the strongly correlated increase in CO_2 concentration and decrease in pH, and by the impressive switch of the redox potential from highly oxidized to reductive conditions, likely due to a larger inflow of H_2S into the aquifer. The second process is pointed out by the significantly lower values of the water temperature observed in concomitance with, or soon after the occurrence of, major rainfall events.

Conclusions

The automatic and discrete geochemical monitoring of the Bagnore spring allowed for gaining some understanding of the dynamics of the shallow aquifer hosted in the volcanic rocks of Mt. Amiata, and of the interactions occurring there between geothermal fluids and local groundwater. In particular, a significant increase in the inflow of hydrothermal gases has been observed since March 2016, as indicated by the increase in dissolved CO_2 concentration, and by the concomitant decrease in pH and redox conditions. Over the same period, water temperature showed a complex pattern, with alternated larger maximum values and lower minimum values, compared to the 2004-2015 period. Lower minima were observed concomitantly with high rainfall events. These features were interpreted as an effect of two someway competing processes: (i) the increase of maximum values was attributed to the augmented influx of hydrothermal gases from the underlying geothermal reservoir; (ii) the decrease of minimum values was put in relation with episodes of more efficient meteoric recharge during and/or at the end of rainy periods.

References

Cioni R., Guidi M., Pierotti L., Scozzari A., (2007). *An automatic monitoring network installed in Tuscany (Italy) for studying possible geochemical precursory phenomena*. Nat. Hazards Earth Syst. Sci., 7, 405-416.

Pierotti L., Botti F., D'Intinosante V., Facca G., Gherardi F., (2015). *Anomalous CO_2 content in the Gallicano thermo-mineral spring (Serchio Valley, Italy) before the 21 June 2013, Alpi Apuane earthquake (M = 5.2)*. Physics and Chemistry of the Earth, 85-86 (2015) 131-140.

Pierotti L., Cortecci G., Gherardi F., (2016). *Hydrothermal gases in a shallow aquifer at Mt. Amiata, Italy: insights from stable isotopes and geochemical modelling*. Isotopes in Environmental and Health Studies, 52, 414-426.

Pierotti L., Gherardi F., Facca G., Piccardi L. and Moratti G., (2017). *Detecting CO_2 anomalies in a spring on Mt. Amiata Volcano (Italy)*. Physics and Chemistry of the Earth, 98, 161-172.

Transfer of mantle derived fluids across the Calabrian-Peloritan arc: tectonic and geodynamic implications

Randazzo P.[1], Caracausi A.[2], Italiano F.[2], Aiuppa A.[1], Sulli A.[1]

[1]*Università degli Studi di Palermo, Dipartimento delle Scienze della Terra e del Mare (DiSTeM), Palermo, Italy*
[2]*Istituto Nazionale di Geofisica e Vulcanologia, Sezione di Palermo, Italy*

Corresponding Author: *paolo.randazzo@unipa.it*

Mantle degassing occurs principally through active volcanic systems and young oceanic lithosphere. Tectonically active regions on the continental crust may additionally contribute a (poorly quantified) fraction of the deep CO_2 budget.

We studied volatiles in thermal manifestations along the seismically active Nebrodi-Peloritani chains (NE Sicily), to investigate the origin of thermalism and the sources of the outgassing fluids. The geological evolution of the area has been controlled by the interaction between the European and African plates and links the African Maghreb with the European Apennines.
The collected samples exhibit ^3He excess, supporting active outgassing of mantle-derived volatiles. The computed mantle-derived He fluxes are up to 3 orders of magnitude higher than those in stable continental areas. These high fluxes support and advective transport of fluids through the regional tectonic discontinuities.

The investigated area, despite being a chain, is located between two of most active worldwide volcanic systems: Mt. Etna to south and the subduction-related Aeolian arc to north. Geophysical studies and experimental models [Piromallo et al., 2003] suggest the existence of toroidal flows in the mantle that, bypassing the subduction plate, produce mantle upraise in the area [Faccenna et al., 2011], eventually leading to magma accumulation at the mantle-crust interface, or in the crust. We propose deep fluids ascent occurs via deep regional tectonic discontinuities (the *Eolie-Tindari-Letojanni* fault system, figure 1), interpreted by either an offshoot of a regional lithospheric structure in the Ionian Sea [Polonia et al., 2016], or a slab tear or STEP type structure at the margin of subduction ionian plate [Doglioni et al., 2001]. Our study supports **a)** the possible presence of magmatic intrusions below this sector of the Maghrebian-Apenninic chain; **b**) the active role of the regional discontinuities in transferring mantle fluids towards the surface and **c**) the possible age of the magmatic intrusions.

Finally our results furnish new contributions to the crust-mantle tectonic in a region that is dominated by the interaction of two plates. Hence this study produces new contributions for a better knowledge of the geodynamic evolution of Mediterranean.

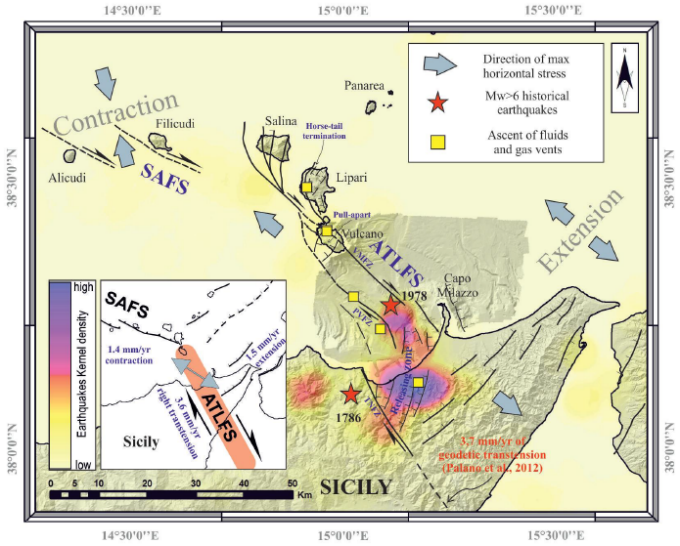

Figure 1 Kinematic and structural reconstruction of the northern sector of the Eolie-Tindari-Letojanni fault system (ATLFS); yellow squares = sites where there is a noticeable rise of fluids. [sites by Giammanco et al., 2008; Barreca et al., 2014; Cultrera F. et al., 2017].

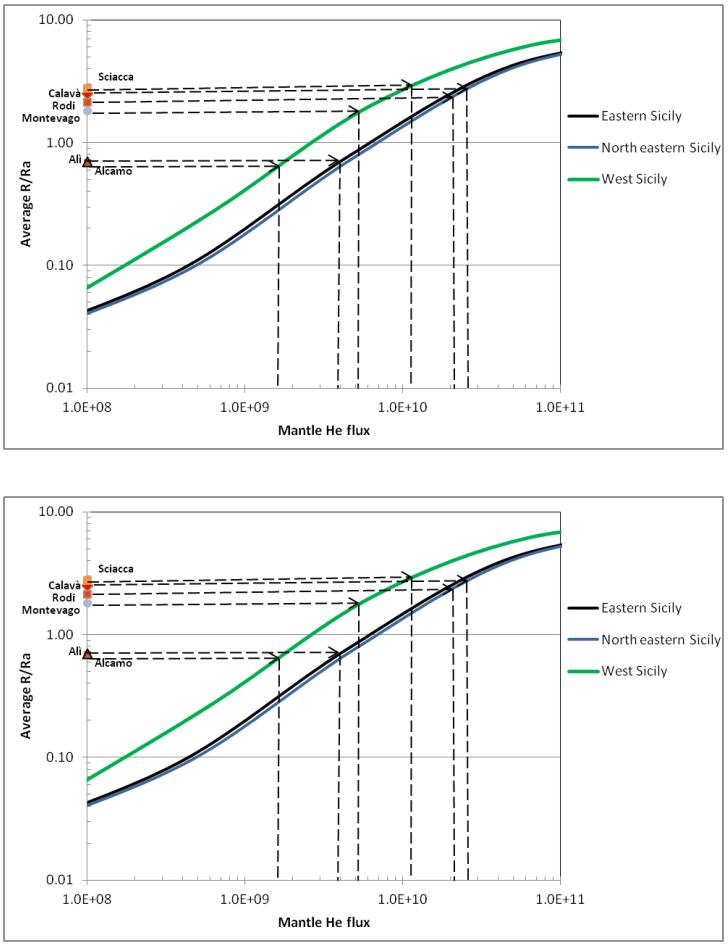

Figure 2 Relationship between helium-mantle flow and helium isotopic ratio, expressed as R/Ra, relative to the sites of North-eastern and western Sicily. Western Sicily data from Caracausi et al., [2005]. a) SCLM end member; b) MORB end member.

References

Barreca G., Bruno V., Cultrera F., Mattia M., Monaco C., Scarfì L., (2014). *New insights in the geodynamics of the Lipari-Vulcano area (Aeolian Archipelago, southern Italy) from geological, geodetic and seismological data*. Journal of Geodynamics, Vol 82, Pages 150-167.

Caracausi A., Favara R., Italiano F., Nuccio P.M., Paonita A. and Rizzo A., (2005). *Active geodynamics of the central Mediterranean Sea: Tensional tectonic evidences in western Sicily from mantle-derived helium.* Geophysical Research Letters, 32(4).

Cultrera F., Barreca G., Ferranti L., Monaco C., Pepe F., Passaro S., Barberi G., Bruno V., Burrato P., Mattia M., Musumeci C. & Scarfì L., (2017). *Structural architecture and active deformation pattern in the northern sector of the Aeolian-Tindari-Letojanni fault system (SE Tyrrhenian Sea-NE Sicily) from integrated analysis of field, marine geophysical, seismological and geodetic data*". Italian Journal of Geosciences, 136(3).

Doglioni C., Innocenti F. & Mariotti G., (2001). *Why Mt Etna?* Terranova https://doi.org/10.1046/j.1365-3121.2001.00301.x.

Faccenna C., Molin P., Orecchio B., Olivetti V., Bellier O., Funiciello F., Minelli L., Piromallo C., & Billi A. (2011). *Topography of the Calabria subduction zone (southern Italy): clues for the origin of Mt. Etna.* Tectonics, https://doi.org/10.1029/2010TC002694.

Giammanco S., Palano M., Scaltrito A., Scarfì L., Sortino F., (2008). *Possible role of fluid overpressure in the generation of earthquake swarms in active tectonic areas: The case of the Peloritani Mts. (Sicily, Italy).* Journal of Volcanology and Geothermal Research, Vol. 178, Issue 4, Pag. 795-806.

Piromallo C. & Morelli A., (2003). *P wave tomography of the mantle under the Alpine-Mediterranean area.* Journal of Geophysical Research, 108, Published Online. http://dx.doi.org/10.1029/2002JB001757.

Polonia A., Torelli L., Artoni A., Carlini M., Faccenna C., Ferranti L., Gasperini L., Govers R., Klaeschen D., Monaco C., Neri G., Nijholt N., Orecchio B. & Wortel R., (2016). *The Ionian and Alfeo-Etna fault zones: New segments of an evolving plate boundary in the central Mediterranean Sea?* Tectonophysics Vol. 675, Pages 69-90.

Fluid geochemistry and CO_2 output in the southern Apennine (Italy): Preliminary results from the study of cold and thermal waters

Randazzo P.[1], Caracausi A.[2], Apollaro C.[3], Cardellini C.[4], Chiodini G.[5], Paternoster M.[6], Rosiello A.[4], Aiuppa A.[1]

[1]*Università degli Studi di Palermo, Dipartimento delle Scienze della Terra e del Mare (DiSTeM), Palermo, Italy*
[2]*Istituto Nazionale di Geofisica e Vulcanologia, Sezione di Palermo, Italy*
[3]*DiBest, Università della Calabria, Italy*
[4]*Università degli Studi di Perugia, Dipartimento di Fisica e Geologia, Italy*
[5]*Istituto Nazionale di Geofisica e Vulcanologia, Sezione di Bologna, Italy*
[6]*Università degli Studi della Basilicata, Dipartimento di Scienze, Italy*

Corresponding Author: *paolo.randazzo@unipa.it*

Although central to our understanding of planetary evolution over geological time, past and present natural CO_2 fluxes are poorly quantified [Berner e Lasaga, 1989]. This limited knowledge is caused by CO_2 being emitted from the Earth's interior in different geodynamical contexts, in different modes and at different rates.

CO_2 Earth degassing is mainly concentrated in volcanic regions and in young oceanic lithosphere setting [e.g., Foley and Fisher, 2018 and references therein]. However, active CO_2 degassing also occurs in seismically/tectonically active regions [e.g., Chiodini et al 1999 and 2004; Caracausi and Sulli, 2018], which are punctuated by CO_2-rich manifestations, including cold gas vents, degassing soils and CO_2-rich springs. These manifestations are clear hints for anomalous transport of deep CO_2 toward the surface through faults systems that are zones of enhanced permeability in the crust. Regional aquifers, in particular, can dissolve large amounts of CO_2 providing geochemical evidences for deep degassing processes at regional scale [Chiodini et al., 2000]. Studying regional aquifers and their main springs is thus key to establishing regional CO_2 budgets [e.g., Chiodini et al., 2000; Burton et al., 2013 and references therein]. Unfortunately, relatively few studies have targeted CO_2 degassing from worldwide non-volcanic areas. Furthermore, a link has been identified between CO_2 output and seismicity [Chiodini et al., 2004], so that the study of CO_2 degassing in active tectonic region can furnish new tool to investigate the seismogenetic processes.

Here we present preliminary results of a geochemical study on CO_2 degassing in the southern Italy (Basilicata-Calabria area). The investigated area is a tectonically active region, where historical and recent earthquakes have been recorded (magnitude up to 5.2) [Presti et al., 2013 and reference therein].
We collected and analysed 45 samples, both cold and thermal groundwaters, with the aim of defining the origin of the dissolved gases, quantifying the CO_2 output at regional scale and understanding the origin for regional thermalism. In this contest, helium has been used as the key tracer for recognizing the contributions of crustal and mantle components and possibly the associated heat [Mamyrin and Tolstikhin, 1984].
The collected waters fall into 3 groups on the basis of their major element chemistry: Ca(Mg)-HCO_3, Mg(Ca)-HCO_3 and Ca(Na)-SO_4. The δ^8O and δD isotopic signature of groundwaters falls close the

Eastern Mediterranean Meteoric Water Line [EMMWL, Gat and Carmi, 1970; Rindsberger et al., 1983; Apollaro et al., 2012; Vespasiano et al.,2015] indicating their meteoric origin.
The dissolved gases are CO_2- and N_2-dominated with some samples that fall on the mixing line between an ASW (Air Saturated Water) and CO_2-rich end member. Helium and neon isotopes indicate our samples fall in the field of ASW, with the exception of the thermal waters, where the source of He is mainly the decay of U and Th in the crust. Coupling Total Dissolved Inorganic Carbon (TDIC) and $\delta^{13}C$ compositions we identified 2 groups of waters (i) infiltrating waters, with low $\delta^{13}C_{TDIC}$, and (ii) a group of samples with more positives $\delta^{13}C_{TDIC}$ and higher TDIC, indicative of outgassing of deeply sourced CO_2.

By applying the carbon mass balance approach proposed by *Chiodini et al.* [2000] and considering the hydrogeological parameters of the studied springs, a first estimate of the deep CO_2 flux has been attempted. The preliminary results indicate that the deep carbon flux for the studied area is in the range of 10^5-10^7 mol y^{-1}. These values refer, for some aquifers, only to a part (sampled) of their entire discharge and is compatible with deeply derived CO_2 flux extrapolated by Chiodini et al., [2004] for central Italy (1-3x10^{11} mol y^{-1}) (Apennine aquifers), considering that this refers to an area much larger than the one we studied. For comparison the estimated flux for the studied area is comparable with the amount of CO_2 discharged by Mt. Etna (Italy) [Burton et al., 2013 and reference therein]. Our results therefore support the hypothesis that a high deep CO_2 contribution also extends in the southern Apennines.

References

Apollaro C., Dotsika E., Marini L., Barca D., Bloise A., De Rosa R., Doveri M., Lelli M., Muto F., (2012). *Chemical and isotopic characterization of the thermomineral water of Terme Sibarite springs (Northern Calabria, Italy)*. Geochemical Journal, GJ 46(2):117-129.

Berner R.A., Lasaga A.C., (1989). *Modeling the geochemical carbon cycle*. Sci. Am., 260, 74-81.

Burton R.M., Sawyer M.G., Granieri D., (2013). *Deep Carbon Emissions from Volcanoes*. Reviews in Mineralogy & Geochemistry, Vol. 75 pp. 323-354.

Caracausi A., Sulli A, (2018). *Outgassing of Mantle Volatiles in Compressional Tectonic Regime Away from Volcanism: The Role of Continental Delamination*. Geochemistry, Geophysics, Geosystems, vol.4, issue 2, 2007-2020.

Caracausi A., Paternoster M., (2015). *Radiogenic helium degassing and rock fracturing: A case study of the southern Apennines active tectonic region*. Journal of Geophysical Research, Solid Earth, 120(4).

Chiodini G., Frondini F., Kerrick D.M., Rogie J., Parello F., Peruzzi L., Zanzari A.R., (1999). *Quantification of deep CO2 fluxes from Central Italy. Examples of carbon balance for regional aquifers and of soil diffuse degassing*. Chem. Geol., 205-222.

Chiodini G., Frondini F., Cardellini C., Parello F., Peruzzi L., (2000). *Rate of diffuse carbon dioxide Earth degassing estimated from carbon balance of regional aquifers: The case of central Apennine, Italy*. J. Geophys. Res., Vol. 105, NO. B4, pages 8423-843.

Chiodini G., Cardellini C., Amato A., Boschi E., Caliro S., Frondini F., Ventura G., (2004). *Carbon dioxide Earth degassing and seismogenesis in central and southern Italy*. Geophys. Res. Lett., vol. 31, L07615, doi: 10.1029/2004GL019480;

Chiodini G., Caliro S., Cardellini C., Frondini F., Inguaggiato S., Matteucci F., (2011). *Geochemical evidence for and characterization of CO_2 rich gas sources in the epicentral area of the Abruzzo 2009 earthquakes*. Earth Plan. Sci. Lett., 304; 389-398.

Mamyrin B.A., Tolstikhin I.N., (1984). *Helium isotopes in nature*. Elsevier, Amsterdam.

Presti D., Billi A., Orecchio B., Totaro C. Faccenna C., Neri G., (2013). *Earthquake focal mechanisms, seismogenic stress, and seismotectonics of the Calabrian Arc, Italy*. Tectonophysics, vol.602, pp 153-175.

Vespasiano G., Apollaro C., De Rosa R., Muto F., Larosa S., Fiebig J., Mulch A., Marini L., (2015). *The Small Spring Method (SSM) for the definition of stable isotope elevation relationships in Northern Calabria (Southern Italy)*. Applied Geochemistry, 63, 333-346.

Groundwater Oxygen Anomaly Related to Earthquakes in Japan

Yuji Sano[1,2], Satoki Onda[1], Takanori Kagoshima[1], Naoto Takahata[1], Tomo Shibata[3], Chika Nakagawa[4], Tetsuji Onoue[4,5] and D.L. Pinti[6]

[1]*Atmosphere and Ocean Research Institute, University of Tokyo, Kashiwa, Japan*
[2]*Institute of Surface-Earth System Science, Tianjin University, Tianjin, China*
[3]*Institute for Geothermal Sciences, Kyoto University, Beppu, Japan*
[4]*Department of Earth and Environmental Sciences, Kumamoto University, Kumamoto, Japan*
[5]*Deparment of Earth and Planetary Science, Kyushu University, Nishiku, Japan*
[6]*GEOTOP, Research Center on Earth System Dynamics, Université du Québec à Montréal, Canada*

Corresponding Author: *ysano@aori.u-tokyo.ac.jp*

Introduction

Geochemical precursors of seismic activity have attracted the attention of researchers worldwide, because they are not entirely unexpected [King et al., 1995; Ingebristen and Manga, 2014]. Monitoring groundwater has been carried out for earthquake prediction in USA, Japan, China and Italy since 1970s [Roeloff, 1988; Barberio et al., 2017]. Even though noble gas anomalies such as radon and helium were well documented [Sugisaki and Sugiura, 1985; Igarashi et al., 1995], there is a lack of knowledge on their geochemical behavior to produce those changes [Sano et al., 2016]. As major components of groundwater, possible variations of hydrogen and oxygen isotopes were discussed in seismically active regions [O'Neil and King, 1981]. Hydrogeochemical changes including stable isotopes were reported before and after a major earthquake in Iceland [Claesson et al., 2004]. Oxygen isotopes changes were detected contemporarily to the occurrence of earthquake in India and a model of aquifer breaching and mixing of different groundwater were proposed [Reddy et al., 2011]. Complicated variations of oxygen and hydrogen isotopes were observed before and after two consecutive earthquakes in Iceland [Skelton et al. 2014]. Even though these anomalies are promising in future seismic hazard mitigation, more data are required to confirm the predictability. We present here data of oxygen and hydrogen isotope variations in groundwater related to earthquakes recently occurred in Japan.

Experiment

We have collected commercial bottled mineral water samples covering a couple of years of seismic events. This method is based on a study of groundwater chemical changes prior and after the M7.2 Kobe earthquake in 1995 [Tsunogai and Wakita, 1995]. There are two series of mineral water samples, those related to the M6.6 Tottori earthquake (October 2016) and those to the M7.3 Kumamoto earthquake (April 2016). Both groundwater samples were filtered and sealed in polyethylene terephthalate bottles and distributed on the market. Hydrogen (D/H) and oxygen ($^{18}O/^{16}O$) isotopes of water samples were measured by a cavity ring-down spectroscopy (L2120-I Analyzer, PICARRO Co. Ltd) without any chemical preprocessing. Observed hydrogen and oxygen isotopic ratios were calibrated against our in-house standard and converted into the conventional V-SMOW unit, expressed as per mil (‰). Instrumental error of $\delta^{18}O$ and δD values were less than 0.05‰ and 0.3‰ at 2σ.

Results and Discussion

At the Tottori earthquake, significant oxygen isotopic anomaly - +0.24‰ relative to the local groundwater background - was observed a few months before the M6.6 event. Small but substantial increase of 0.07‰ was also observed soon after the earthquake [Onda et al., 2018]. On the other hand, there is no anomalous change of the δD values. The most probable mechanism to cause $\delta^{18}O$ enrichment without δD change is a ^{18}O-shft caused by water-rock interaction [Craig, 1963]. We have measured $\delta^{18}O$ values of aquifer rocks in the Tottori region, ranging +8.2‰ to +8.6‰. Since the mineral water samples show $\delta^{18}O$ values of approximately -8.2‰, much lower than those of aquifer rocks, a progressive isotopic equilibration of oxygen would make the groundwater $\delta^{18}O$ values increase. On the other hand, the δD values of groundwater remain unchanged because the hydrogen content of aquifer rocks is significantly lower compared with that of water. During the M7.3 Kumamoto event, similar $\delta^{18}O$ anomaly - up to +0.4‰ relative to the local groundwater background - was observed a few months before the earthquake. In addition, a large $\delta^{18}O$ anomaly of +0.5‰ was observed one month after the earthquake. Again, there is no anomalous change of the δD values during the time interval when the M7.3 earthquake occurred. These observations, consistent with the Tottori earthquake, suggest that water-rock interactions may be the main mechanism of groundwater anomaly before the earthquake in Japan [Onda et al., 2018]. In the case of Iceland, both δD and $\delta^{18}O$ values of groundwater were changed before and after earthquakes [Claesson et al., 2004; Skelton et al., 2014]. The difference may be attributable to location specific or geological conditions and will be resolved in future research.

References

Barberio M.D., Barbieri M., Billi A., Doglioni C. and Petitta M., (2017). *Hydrogeochemical changes before and during the 2016 Amatrice-Norcia seismic sequence (central Italy)*. Scientific Reports, 7, 11735.

Claesson L., Skelton A., Graham C., Dietl C., Morth M., Torssander P. and Kockum I., (2004). *Hydrogeochemical changes before and after a major earthquake*. Geology, 32, 641-644.

Craig, H. (1963) *The isotopic geochemistry of water and carbon in geothermal areas*. In: Nuclear geology on geothermal areas. Pisa, 17-53.

Igarashi G., Saeki S., Takahata N., Sumikawa K., Tasaka S., Sasaki Y., Takahashi M. and Sano Y., (1995). *Ground-water radon anomaly before Kobe earthquake in Japan*. Science, 269, 60-61.

Ingebritsen S.E. and Manga M., (2014). *Hydrogeochemical precursors*. Nature, Geoscience 7, 697-6983.

King C., Koizumi N. and Kitagawa Y., (1995). *Hydrogeochemical anomalies and the 1995 Kobe earthquake*. Science, 269, 38-39.

Onda S., Sano Y., Takahata N., Kagoshima T., Miyajima T., Shibata T., Pinti D.L., Lan T., Kim N.K., Kusakabe M. and Nishio Y., (2018). *Groundwater oxygen isotope anomaly before the M6.6 Tottori earthquake in Southwest Japan*. Scientific Reports, 8, 4800.

O'Neil J.R. and King C., (1981). *Variations in stable-isotope ratios of ground waters in seismically active regions of California*. Geophys. Res. Lett., 8, 429-432.

Reddy D.V., Nagabhushanam P. and Sukhija B.S., (2011). *Earthquake (M5.1) induced hydrogeochemical and $\delta^{18}O$ changes: validation of aquifer breaching-mixing model in Koyna, India*. Geophys. J. Int., 184, 359-370.

Roeloff E., (1988). *Hydrologic precursors to earthquakes: A review*. Pageoph, 126, 177-209.

Sano Y., Takahata N., Kagoshima T., Shibata T., Onoue T. and Zhao D., (2016). *Groundwater helium anomaly reflects strain change during the 2016 Kumamoto earthquake in southwest Japan*. Scientific Reports, 6, 37939.

Skeleton A., Andren M., Kristmannsdottir H., Stockmann G., Morth C.-M., Sveinbjornsdottir A., Jonsson S., Sturkell E., Gudrunardottir H.R., Hjartarson H., Siegmund H. and Kochum I., (2014). *Changes in groundwater chemistry before two consecutive earthquakes in Iceland*. Nature, Geoscience, 7, 752-756.

Sugisaki R. and Sugiura T., (1985). *Geochemical indicator of tectonic stress resulting in an Earthquake in central Japan*. Science, 229, 1261-1262.

Tsunogai U. and Wakita H., (1995). *Precursory chemical changes in ground water: Kobe earthquake, Japan*. Science, 269, 61-63.

The application of Multi-Gas instrument for the in-situ analysis of the gas-emissions of the Eastern Carpathians (Romania)

Szalay R.[1], Kis Boglárka-Mercédesz[1,2], Harangi Szabolcs[2], Palcsu László[3], Ionescu A.[2,4], Calabrese S.[5], Daskalopoulou K.[5], Baciu C.[4], Pop C.[4], Bitetto M.[5] & Aiuppa A.[5]

[1]*Institute of Geology, Babes-Bolyai University, Cluj-Napoca, Romania*
[2]*MTA-ELTE Volcanology Research Group, Eötvös University, Budapest, Hungary*
[3]*Isotope Climatology and Environmental Research Centre (ICER), Hungarian Academy of Sciences (ATOMKI), Debrecen, Hungary*
[4]*Faculty of Environmental Science and Engineering, Babes-Bolyai University, Cluj-Napoca, Romania*
[5]*Università degli Studi di Palermo, Dipartimento delle Scienze della Terra e del Mare (DiSTeM), Palermo, Italy*

Corresponding Author: *szalay.j.roland@gmail.com*

The Carpathian-Pannonian region, was dominated by diverse volcanic activity for the last 20 million years, and even 1 million years ago there was precedent for active zones. Although volcanic eruptions are very uncommon in the region today, but the frequent earthquakes in the Carpathian-bend, the numerous and intense gas-emissions in the southeastern areas of the regions, as well many petrochemical and geochemical volcanologic studies, indicate that the area is not completely inactive. The gas emissions investigated by us, may be directly related to these geodynamic processes [Kis et al., 2019; Laumonier et al., 2019].

In Romania, the Eastern Carpathian Neogene-Quaternary volcanic chain and it's neighboring zones contain most of the carbon dioxide rich gas emissions, which also occur in the form of natural mofetes, bubbling pools and springs. They also appear in frequently populated settlements and cellars, which put the inhabitants there in direct danger. The motivation of our work is to gather information from the composition of the gas-emissions in the above mentioned area. Furthermore, we would like to clarify if there is any relation between the tectonic characteristics of the area and the manifestation, concentration of gas-emissions.

The Multi-Gas instrument was developed at the University of Palermo and the INGV, under the supervision of Alessandro Aiuppa and Hiroshi Shinohara [Aiuppa et al., 2005; Shinohara et al., 2005]. The Multi-Gas instrument is an important tool for the investigations and monitoring of volcanic systems worldwide, because it can be easily placed on a volcano and can provide real-time data on the compositional changes of the fluids that are released [Aiuppa et al., 2005, Shinohara et al., 2005]. We used a specially designed Multi-Gas to gather in situ compositional information about low-temperature, CO_2-rich gases, emerging from different manifestations like dry gas emissions (mofettes), bubbling pools and springs.The instrument is equipped with two IR sensors for CO_2 (0-100%) and CH_4 (0-7%) and one electrochemical sensor for H_2S (0-200 ppm). The Multi-Gas was used during several field surveys between September 2018 and June 2019 across the Eastern Carpathians area, where a total of 135 gas emissions were investigated for their CO_2, CH_4 and H_2S concentrations. Concentrations of the different gas-species varied according to the geological context. The CO_2 concentrations varied between 0.96 and 98.08 %. The highest values were measured in the the volcanic area of Ciomadul, the youngest volcano of the Eastern Carpathians 32 kyr, characterized by high CO_2 gas output up to 8700 t/year [Kis et al., 2017]. High values were measured also in the thrusted and folded area of the Carpathian Flysch and, suggesting the tectonic control over the

appearance of the gas emissions. The CH_4 concentrations ranged between 0.21 and 6.76% and were higher at hydrocarbon-prone areas, such as the sedimentary deposits of the Transylvanian Basin and Carpathian Flysch. In these cases the CO_2 concentrations were low (up to 4.6%). The concentrations of H_2S were higher at the volcanic area of Ciomadul, reaching values above the detection limit (~200 ppm).

In conclusion the Multi-Gas proved to be useful tool in the in-situ investigation of cold gas emissions of the Eastern Carpathians, being efficient especially for the measurement of the H_2S concentrations that are very sensitive for oxidation processes.

References

Aiuppa A., Federico C., Giudice G., Gurrieri S. (2005). *Chemical mapping of fumarolic field: La Fossa Crater, Vulcano Island (Aeolian Islands, Italy)*. Geophysical Research Letters, Vol. 32, LI3309.

Kis B.M., Ionescu A., Cardellini C., Harangi Sz., Baciu C., Caracausi C. & Viveiros F., (2017). *Quantification of carbon dioxide emissions of Ciomadul, the youngest volcano of the Carpathian-Pannonian Region (Eastern-Central Europe, Romania)*. Journal of Volcanology and Geothermal Research, 341, 119-130.

Kis B.M., Caracusi A., Palcsu L., Baciu C., Ionescu A., Futó I., Sciarra A., Harangi Sz., (2019). *Noble Gas and Carbon Isotope Systematics at the Seemingly Inactive Ciomadul Volcano (Eastern-Central Europe, Romania): Evidence for Volcanic Degassing*. Geochemistry, Geophysics, Geosystems, vol.20, issue 6, 3019-3043.

Laumonier M., Karakas O., Bachmann O., Gaillard F., Lukács R., Seghedi I., Menand T., Harangi Sz., (2019). *Evidence for a persistent magma reservoir with large melt content beneath an apparently extinct volcano*. Earth and Planetary Science Letters, 521, 79-90.

Shinohara H., (2005). *A new technique to estimate volcanic gas composition: plume measurements with a portable multi-sensor system*. Journal of Volcanology and Geothermal Research, 143, 319- 333.

Geophysical and Geological factors constraining the occurrence of earthquake precursors in Geofluids

Martinelli G.[1,2], G. Tamburello[3]

[1]*ARPAE, Agenzia Regionale per la Protezione Ambientale Emilia-Romagna, Reggio Emilia, Italy*
[2]*Istituto Nazionale di Geofisica e Vulcanologia, sezione di Bologna, Italy*

Corresponding Author: *giancarlo.tamburello@ingv.it*

Introduction

Earthquake precursors are those anomalous phenomena that precede an earthquake sequence. The detection of such events is one of the premises of earthquake forecasting. In the last decades the number of likely earthquake precursors reported in literature increased as a response of not only the technological development of the monitoring networks and the increment of their spatial coverage, but also of the increasing interest of the scientific community in this topic. A relevant part of these precursors are related to under-ground fluids such as aquifers or gases: given the incompressibility of the water, confined aquifers act as natural strainmeters; accumulated deep gases, instead, can be released during rock fracturing and rise to the surface. Fluid accumulation in the crust can also be indirectly detected by measuring temporal variations of the local b-value. This increasing number of case studies is showing the important role fluids play in the earthquake precursor processes.

An updated catalogue of earthquake precursors

In this work we update the catalogue compiled by Cicerone et al., [2009] focusing more on the geochemical and fluid-related earthquake precursors and providing additional information on precursor type, distance from the earthquake and timescales. The catalogue includes ~400 precursors recorded in ~40 different countries since 1960 (Figure 1). The precursor times display a bimodal log-normal distribution with modes centred at ~1 (~10 days) and ~3 (~ 1000 days). Precursor-earthquake distances ranges from few kilometres up to ~ 2000 km. This wide range of values poses serious doubts on the past validations of the earthquake precursor and suggests caution in future studies.

Where earthquake precursors can be observed

The global distribution of the majority of the recorded precursor displays a clustered distribution along the seismically active areas. This feature suggests that in certain areas there is a suitable monitoring network and more sensitivity for the detection of earthquake precursors, but it also suggests that the areas where most of the precursors occur satisfy certain conditions, contrary to the areas with few or no recorded precursors. Thus we analyse the spatial distribution of the precursors at a global scale and compare with data regarding volcanic locations, heat flow [Goutorbe et al., 2011], earth degassing areas [Tamburello et al., 2018], crustal deformation patterns and the depth of seismic events. Relations among the considered geophysical and geological parameters and the fluid-related earthquake precursors are discussed. We conclude that the occurrence of fluid-related earthquake precursory phenomena is apparently possible in specific geodynamic contexts that we attempt to identify [Manga et al., 2012]. Thus geophysical models utilized to explain the occurrence of earthquake precursors should be updated. Only some areas of the world can be considered suitable for earthquake fluid-related precursor monitoring [e.g. Martinelli and Dadomo, 2017].

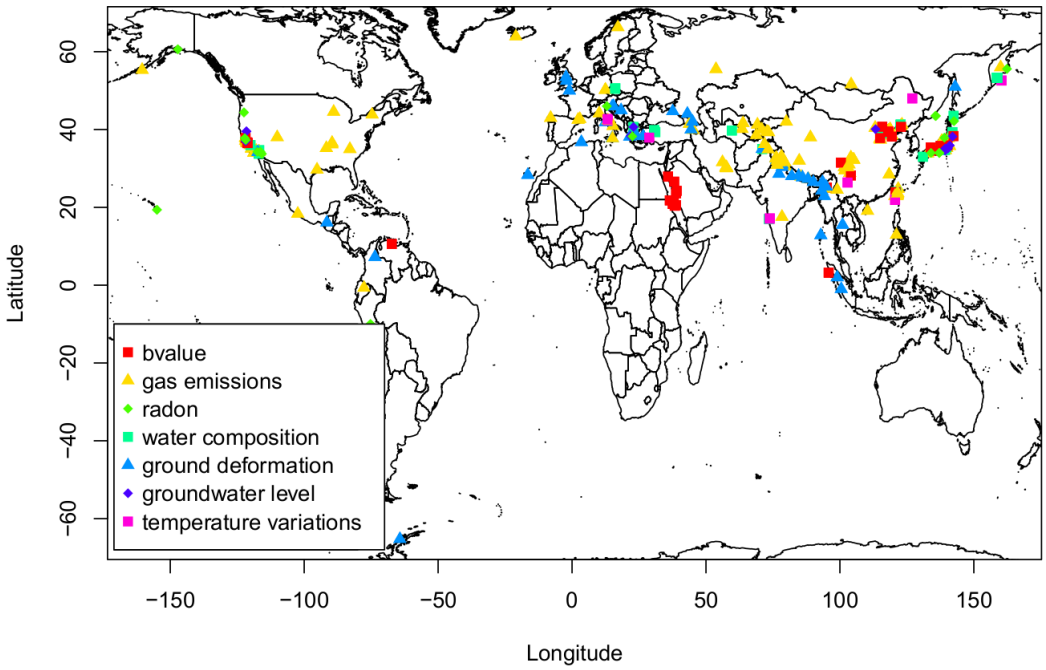

Figure 1 Map of the earthquake precursors listed in our catalogue.

The role of fluids in earthquake precursors

Fluids may play an important role in earthquake precursors origin [Martinelli and Dadomo, 2017]. Here we take advantage of global indicators of under-ground fluids (carbon dioxide-rich springs, from Irwin and Barnes, [1980] and Tamburello et al., [2018]; heat flow from Goutorbe et al., [2011]) in order to delineate the areas where earthquake precursors may be triggered by fluids. We identify three main scenarios: (i) areas with precursors but little or no evidence of fluids, (ii) areas with spatial correspondence between fluids and precursors and (iii) areas where precursors cluster at the edge of the under-ground fluid dominated areas. In this work, we attempt to provide an explanation of this complex spatial relation between fluids and earthquake precursors taking under consideration multiple geophysical parameters such as the hypocentral depths of the earthquakes.

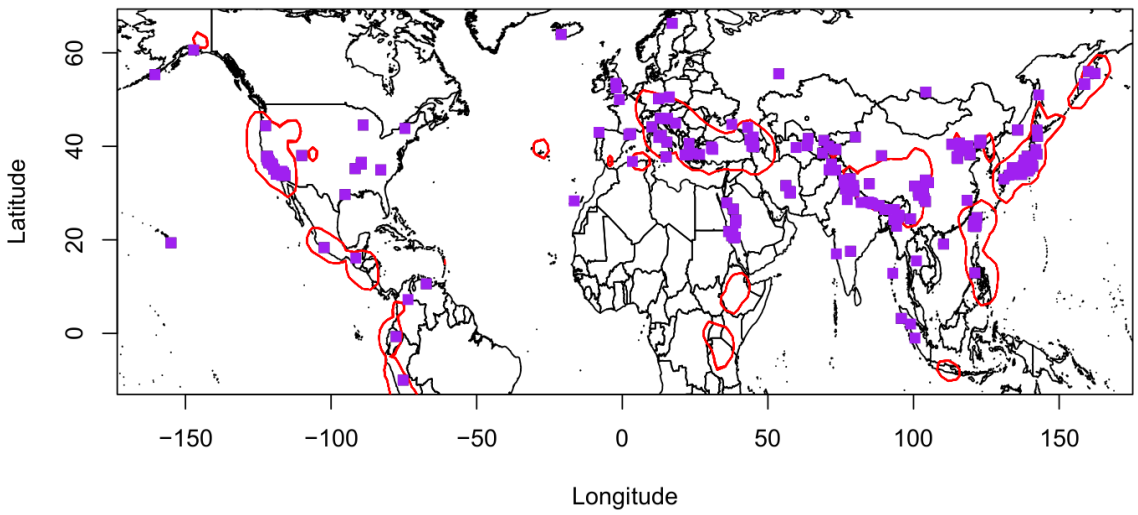

Figure 2 Distribution of fluid-related precursors (purple squares) occorred in areas characterized by anomalous heat flow (> 70 mW/m^2). Potential under-ground fluid-rich areas are also indicated by red contour.

References

Cicerone R.D., Ebel J.E. & Britton J., (2009). *A systematic compilation of earthquake precursors*. Tectonophysics, 476(3-4), 371-396. https://doi.org/10.1016/j.tecto.2009.06.008

Irwin W.P. and Barnes I., (1980). *Tectonic relations of carbon dioxide discharges and earthquakes*. J. Geophys. Res., 85, 3115.

Manga M., Beresnev I., Brodsky E.E., Elkhoury J.E., Elsworth D., Ingebritsen S.E., Mays D.C., Wang C-Y., (2012). *Changes in permeability caused by transient stresses: field observations, experiments, and mechanics*. Reviews of Geophysics, 50, RG2004/2012.

Goutorbe B., Poort J., Lucazeau F. & Raillard S., (2011). *Global heat flow trends resolved from multiple geological and geophysical proxies*. Geophysical Journal International, 187(3), 1405-1419. https://doi.org/10.1111/j.1365-246X.2011.05228.x.

Martinelli G. & Dadomo A., (2017). *Factors constraining the geographic distribution of earthquake geochemical and fluid-related precursors*. Chemical Geology, 469, 176-184. https://doi.org/10.1016/j.chemgeo.2017.01.006.

Tamburello G., Pondrelli S., Chiodini G. & Rouwet D., (2018). *Global-scale control of extensional tectonics on CO_2 earth degassing*. Nature Communications, 9(1), 4608. https://doi.org/10.1038/s41467-018-07087-z.

Spatial variation of soil gas Rn, Tn and CO_2 in the Liupan Shan fault, central-north China and its tectonic implications

Ying Li[1], Jiang Yang[1], Xiaokun Han[2], Anhui Sun[1], Xiaocheng Zhou[1], Zhi Chen[1]

[1]*Key Laboratory of Earthquake Prediction (Institute of Earthquake Forecasting, China Earthquake Admin., China*
[2]*Institute of Surface-Earth System Science, Tianjin University, China*

Corresponding Author: *liying@cea-ies.ac.cn*

Soil gas components such as Rn, Hg and CO_2 have been identified to be good tracers of fault activity, and have been widely used as earthquake or volcano monitoring [Li et al., 2013; Yang et al., 2018]. The geochemical characteristics of soil gases and their correlations to fault activity at the segments of Liupan Shan fault, located at the northeastern margin of the Tibetan Plateau are studied in this work. Soil gas Rn, Tn and CO_2 were measured at 773 sampling sites along 8 profiles across the Liupan Shan fault in 2013 (Figure 1).

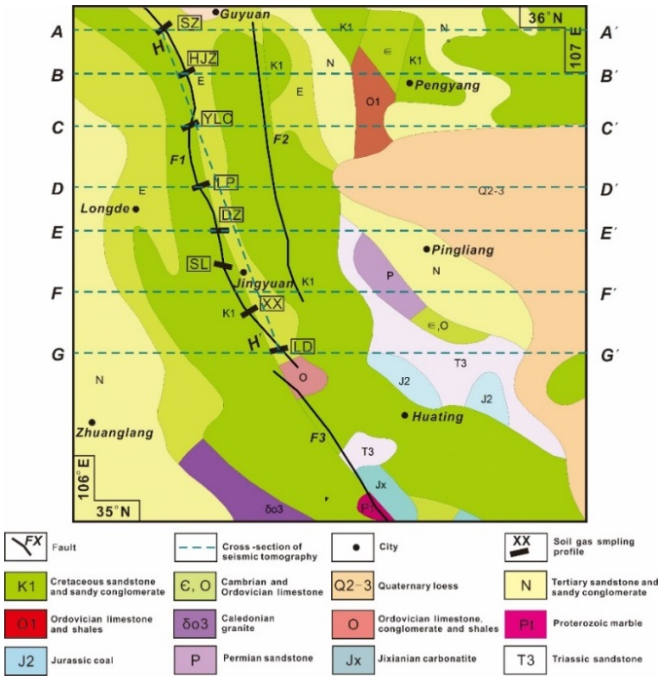

Figure 1 Geological map of the study area. The short black line represents the soil gas sampling section. The blue dashed line represents the location of the seismic wave sections from A-A' to H-H'. F1=Liupan Shan fault, F2= Xiaoguan Shan fault, F3=Guguan-XianGong fault.

The average values of Rn, Tn and CO_2 concentrations at the 8 profiles that represent the degassing intensity of the fault, present an decreasing trend spatially along the Liupan Shan fault from north to south (Figure 2), which could be correlated to the larger horizontal dislocations and younger active age in the north and central segment identified by earlier seismic geology study. In addition, the relative coefficient K_Q of Rn activity ranges from 2.55 to 8.13 and is also higher in north and central segments (Tab. 1), indicating a more intensive tectonic activity in the north and central segment of

Liupanshan fault. Seismic wave tomography research is carried out across and along the Liupanshan fault in this study, which shows that the upper crust in north and central segments is fluid enriched and more materials from western area identified to be with lower CO_2 concentration are thrust down to the erodes block in the south segment, which indicates that the soil gases attained near the surface could be originated from the crust and migrate up through the faults and cracks. It can be concluded according to the soil gas and seismic tomography results that the soil gas emission is highly correlated to fault activity and the material source in the Liupanshan fault. The central-north segment of the Liupan Shan fault with highly degassing intensity is more tectonically active.

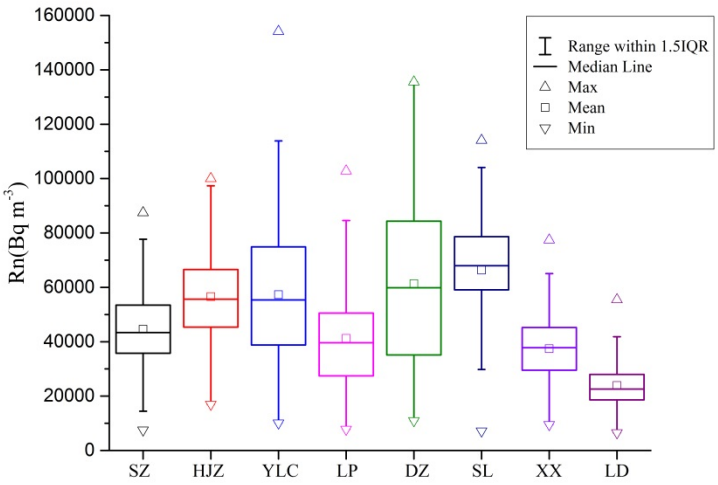

Figure 2 Variation of the Rn concentrations in the Liupanshan fault.

Location	SZ	HJZ	YLC	LP	DZ	SL	XX	LD
K_Q of Rn	8.11	2.55	8.13	7.02	7.21	4.8	4.77	3.62

Table 1 K_Q values of Rn in the measuring sections.

References

Li Y., Du J.G., Wang X., Zhou X.C., Xie C., Cui Y. J., (2013). *Spatial Variations of Soil Gas Geochemistry in the Tangshan Area of Northern China.* Terrestrial Atmospheric & Oceanic Sciences, 24, 323-332.

Yang Y., Li Y., Guan Z., Chen Z., Zhang L., Lv, C.J., (2018). *Correlations between the radon concentrations in soil gas and the activity of the Anninghe and the Zemuhe faults in Sichuan, southwestern of China.* Applied Geochemistry, 89, 23-33.

Background model of fluid circulation and gas-water interaction in the seismically-active area along The Alto Tiberina Near-Fault Observatory (Umbria Apennines, Central Italy)

Ventura Bordenca C.[1], Caracausi A.[2], Camarda M.[2], Chiaraluce L.[3], De Gregorio S.[2], Favara R.[2], Aiuppa A.[1] and Pik R.[4]

[1]*Università degli Studi di Palermo, Dipartimento delle Scienze della Terra e del Mare (DiSTeM), Palermo, Italy*
[2]*Istituto Nazionale di Geofisica e Vulcanologia, Sezione di Palermo, Italy*
[3]*Istituto Nazionale di Geofisica e Vulcanologia, Sezione di Sismologia e Tettonofisica, Roma, Italy*
[4]*CRPG – Université de Lorraine, 15 Rue Notre Dame des Pauvres, France*

Corresponding Author: claudio.venturabordenca@unipa.it

The occurrence of natural degassing far from volcanic systems, such as the Earth's regions affected by continental rifting and active tectonics, has been called to particular attention over the past few decades [e.g., Chiodini et al., 2000; Mörner and Etiope, 2002; Bräuer et al., 2018]. Large emissions of deep CO_2-rich fluids are commonly reported worldwide in seismically- and tectonically-active regions [e.g., Chiodini et al., 2004; Italiano et al., 2009; Tamburello et al., 2018; Caracausi and Sulli, 2019] as they can substantially contribute to the present-day global carbon output.
However, the primary composition of uprising volatiles can be modified upon migration to the surface as a result of secondary chemical processes at shallow levels (e.g., mixing processes, fractionation mechanisms due to gas-water interaction, mineral precipitation, etc.) that mask the pristine composition of the fluids creating misunderstanding in the evaluation of the contributions due to the different sources.
In this respect, the long-term geochemical monitoring allows to the identification of such processes and is of crucial importance to constrain any potential seismicity-induced anomalies of the emitted fluids. Therefore, the acquisition of the background level in seismic areas during quiescent periods is a fundamental requirement to investigate the behavior of geochemical anomalies as a consequence of the development of seismogenic processes. Here we report the investigation of the chemical and isotopic signature of gaseous manifestations discharged in the highly monitored, earthquake-prone area of the Umbria region (central Apennines, Italy). This region is strongly affected by widespread surface degassing (mainly CO_2) and characterized by fluid over-pressure at depth [Chiodini et al., 2004].
The gas emissions are distributed across the whole Umbria region (Figure 1) and fall along the Tiber river Valley within the framework of the interdisciplinary research network of TABOO (The AltotiBerina near fault ObservatOry; [Chiaraluce et al. 2014a-b]). The observatory consists of a dense geophysical network equipped with multi-sensor stations (seismometers, GPS, geochemical and electromagnetic sensors) located in the central-northern Apennines, with the aim of investigating the seismogenic potential of the Alto Tiberina Fault, an active extensional NW-trending low-angle normal fault (dip 15°-25°).
Carbon dioxide is overall the main component in all of the collected manifestations (78-97 CO_2 vol.%), except for the CH_4-dominated gas emission of Nogna. Helium and nitrogen concentrations are significantly variable. The highest He and N_2 contents are associated to the lowest CO_2 abundances. The measured 3He/4He ratios of the gas emissions vary from 0.01 to 0.69 Ra with corresponding

$^{4}He/^{20}Ne$ ratios in the range of 102-4130. A progressive decrease in terms of $^{3}He/^{4}He$ values is observed from south to north in the Umbria region. These data confirm a regional variation of the He isotopic signature in the outgassing volatiles. The isotope signature of carbon ranges from -14.3 to -0.6‰ for $\delta^{13}C\text{-}CO_2$ vs. V-PDB. We observe that the $\delta_{13}CCO_2$ of the sampled gases tends to be more negative from south to north along with a gradual enrichment of the less soluble volatiles (He and N_2) with respect to CO_2 abundance.

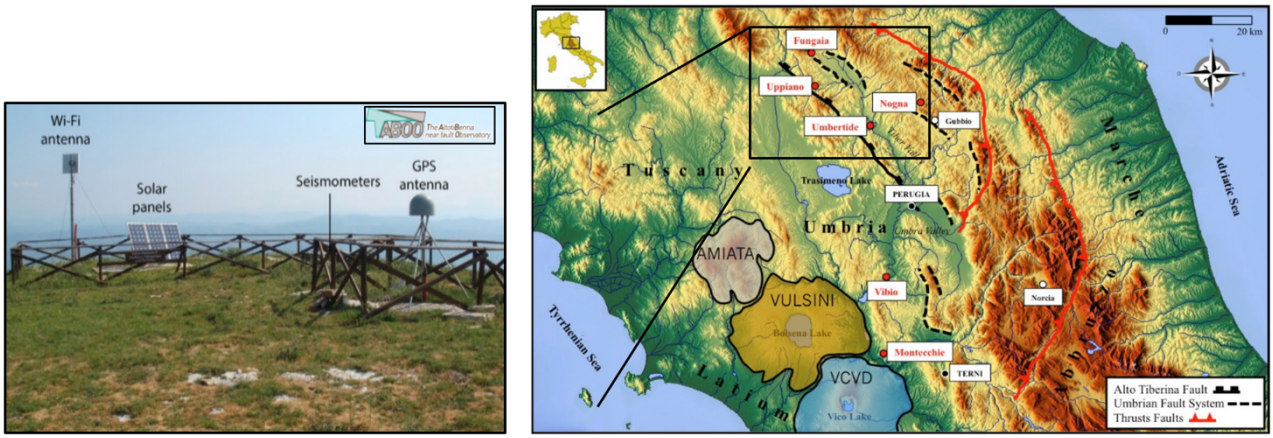

Figure 1 Topographical map of central Italy showing the location of the sampled gaseous manifestations (red filled circles) with the main tectonic features. Zoom: example of a standard on-field installation of the TABOO research network [from Chiaraluce et al., 2014b]. The volcanic district of Mt. Amiata, Vulsini and Vicano-Cimino (VCVD), located in close proximity of the Umbria region, are also reported.

We show that either mixing processes involving two or more gas sources or solubility-controlled Rayleigh fractionation mechanisms due to water-gas interaction can be invoked in order to explain the observed variability of the chemistry of the collected gases. The identification of chemical processes able to affect the gas geochemistry of the studied gas emissions can be achieved by coupling the elemental abundances of the main components (i.e., He, N_2) to carbon stable isotopes ($\delta^{13}C\text{-}CO_2$). Partial dissolution of uprising CO_2 in circulating groundwaters can affect the primary $\delta^{13}C\text{-}CO_2$ of the gas phase leading to an increase of the He/CO_2 and N_2/CO_2vs. $\delta^{13}C\text{-}CO_2$ ratios in the residual gas phase. The main goal of this investigation is to emphasize the physicochemical processes governing the concentrations and isotope signature of natural emissions in seismic regions. Moreover, this study is also aimed at the development of a hydrogeological model necessary to shed light on the possible relationship between crustal degassing, fluid flow-induced seismicity, tectonics and water-gas interaction at regional scale. We propose a model of fluid circulation and secondary chemical processes (i.e., mixing and gas-water interaction) acting under quiescence condition of seismic activity that could serve as background for future geochemical monitoring and seismic surveillance of a vulnerable and high-risk area as the central Apennines in Italy.

References

Bräuer K., Kämpf H., Niedermann S., and Strauch G., (2018). *Monitoring of helium and carbon isotopes in the western Eger Rift area (Czech Republic): Relationships with the 2014 seismic activity and indications for recent (2000-2016) magmatic unrest*. Chem. Geol., 482, pp.131-145.

Caracausi A. and Sulli A., (2019). *Outgassing of mantle volatiles in compressional tectonic regime away from volcanism: the role of continental delamination*. Geoch., Geophy., Geosys., 20, pp. 2007-2020.

Chiodini G., Frondini F., Cardellini C., Parello F., and Peruzzi L., (2000). *Rate of diffuse carbon dioxide Earth degassing estimated from carbon balance of regional aquifers: The case of central Apennines, Italy*. J. of Geoph. Res., vol.105, NO. B4, pp.8423-8434.

Chiodini G., Cardellini C., Amato A., Boschi E., Caliro S., Frondini F. and Ventura G., (2004). *Carbon dioxide Earth degassing and seismogenesis in central and southern Italy*. Geoph. Res. Lett., vol. 31.

Chiaraluce L., Collettini C., Cattaneo M. and Monachesi G., (2014a). *The shallow boreholes at The AltotiBerina near fault Observatory (TABOO; northern Apennines of Italy)*. Scientific Drilling, 17,31-35.

Chiaraluce L. and other 17 authors (2014b). *The Alto Tiberina Near Fault Observatory (northern Apennines, Italy)*. Annals of Geophysics, 57, 3, S0327.

Italiano F., Martinelli G., Bonfanti P., and Caracausi A., (2009). *Long-term (1997-2007) geochemical monitoring of gases from the Umbria-Marche region*. Tectonophysics, 476, pp.282-296.

Mörner N. and Etiope G., (2002). *Carbon degassing from the lithosphere*. Global and Planetary Changes, 33, pp. 185-203.

Tamburello G., Pondrelli S., Chiodini G. & Rouwet D., (2018). *Global-scale control of extensional tectonics on CO_2 earth degassing*. Nature, Comm. 9.

Rn and CO_2 in depth, as a proxy for pre-seismic research

Hovav Zafrir[1,4], Uri Malik[1], Elad Levintal[2], Noam Weisbrod[2], Yochai Ben Horin[3], Zeev Zalevsky[4], Nimrod Inbar[5]

[1]*Geological Survey of Israel, Jerusalem, Israel*
[2]*The Zuckerberg Institute for Water Research, Ben-Gurion University, Israel*
[3]*Soreq Nuclear Research Center, Israel*
[4]*Faculty of Engineering, Bar Ilan University, Israel*
[5]*Ariel University, Israel*

Corresponding Author: *hzafrir@gmail.com*

Over view

A multi-detector monitoring station of radon, CO_2, relative humidity and climatic parameters probes were installed in deep drilling (100-m deep and 0.9-m wide) at Sde Eliezer site closed to the Hula valley western border fault (HWBF), one of the Dead Sea Fault Zone (DSFZ) segments in Northern Israel.

The aim was to determine whether there is a link between radon and other gases anomalies at depth, and the pre-seismic process as accumulation and relaxation of lithospheric stress and strain.

The long-term monitoring in deep borehole method assumes that the climatic influence on physicochemical parameters is limited since its energy decreases with the increase in thickness of the geological cover. Hence, the natural gases monitoring of radon, CO_2 and other parameters above and below the water table in deep boreholes, enables to eliminate the climatic-induced periodic contributions, from the residual portion of the signals that are associated with the regional geodynamic processes, as have been proved by us recently.

Introduction

Radon monitoring is carrying out at the Sde-Eliezer site during the first course of two and a half years (848 days) from February 2015 to May 2017. The radon monitoring setup was based on three gamma detectors (at depth of 10, 60 and 88m), one alpha detector (at 40m), and few probes for the recording of the environmental conditions above and inside the borehole.

The measured parameters during the first curse are presented in Figure 1, including: barometric pressure (in dark red), ambient temperature (in green), borehole temperature at 10m depth (in pink), radon within the surrounding rocks at 10 m depth as measured by gamma rays (in red), radon within the borehole air space at 40 m depth as measured by alpha particles (in dark yellow), radon within the surrounding rock at 60 m depth as measured by gamma rays (in blue), radon within the groundwater at 88 m depth (Since November 2015, in cyan) and more than 200 earthquakes greater than magnitude M=2, recorded by the Israel Seismic Network of The Geophysical Institute of Israel [http://seis.gii.co.il].

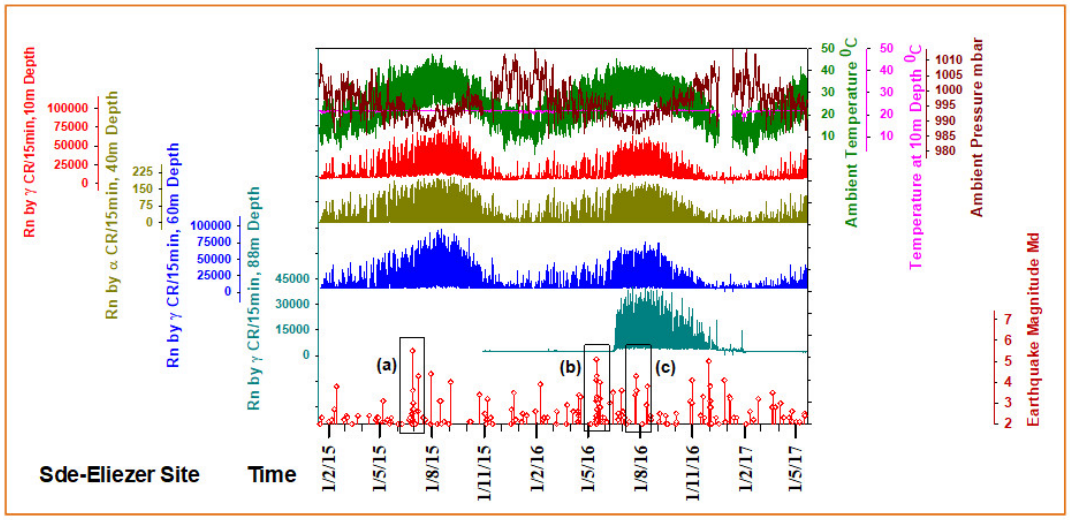

Figure 1 Continuous time series of the measured parameters at the Sde Eliezer site (15-min temporal resolution) collected during the first course of two and a half years (844 days) since February 2015. An interesting feature is the change in the signature of the radon detector at 88m depth, caused by the decreasing of the water table below 88m, as result of over pumping in the Hula Valley (also happened year after in the same month).

The periodical effect of the climatic variables on the radon temporal variation

Monitoring the temporal variability of radon concentration recovers the intermixing effect between the different contributions of the temperature and pressure, even at depth. The everyday appearance of each type of such radon signals that are induced by pressure in the early morning and those that are induced by temperature in the afternoon are easily identified (see Figure 2).

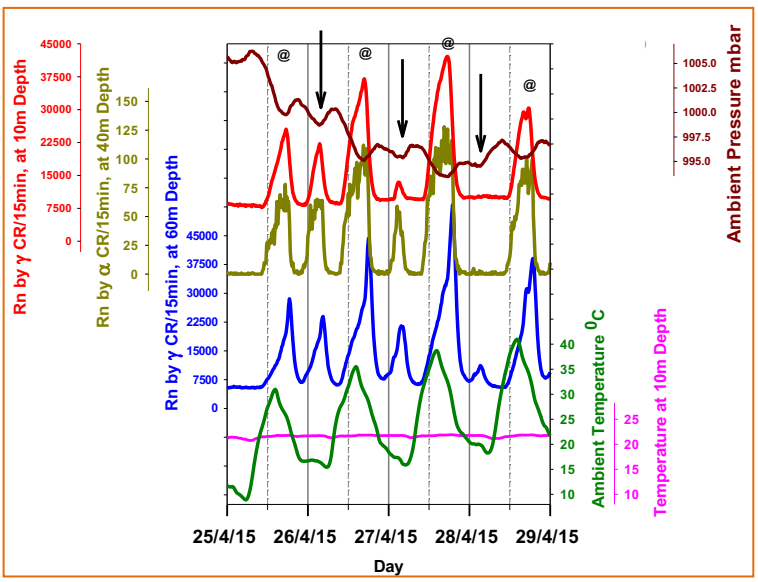

Figure 2 Radon exhibits early morning semi-diurnal signals by the three Rn detectors with anti-correlations to the pressure (see arrows) in addition to its response to the daily temperature periodicity after noon (@ symbols).

The lag time of about 2 hours between the maximum values of the two gamma detectors (10 and 60 m depth) separated vertically by 50 m, define the radon vertical velocity as 25m per hour in the local subsurface porous media.
Since the borehole casing is not perforated down to the water table, therefore the radon can enter the casing only from the groundwater. According to this assumption the values of the radon measurements, as was measured by alpha detector within the airspace inside the well pipe (40 m depth), return almost to zero since the semi daily increase in pressure prevents the migration of radon from the groundwater into the air space.

Radon time series versus earthquake events

In order to understand the capability of the radon monitoring system to isolate and characterize the impact of tectonic driving forces on radon behavior, the recorded list of earthquakes that occurred during the 848 days of 2015 to mid-2017 in the DSFZ region, was added to the acquired data from the Sde-Eliezer site (Figure 1).
Very pronounced signals that became different in shape appeared during three disparate events, that occurred during the above-mentioned time interval of two and a half years, and are marked with a, b and c, in Figure 1, and in Figure 3, a1, a2, b, and c, respectively. These radon anomalous signals were characterized according to their expansion in time. They are wider than the expected width of the separate periodic radon diurnal and semidiurnal signals.

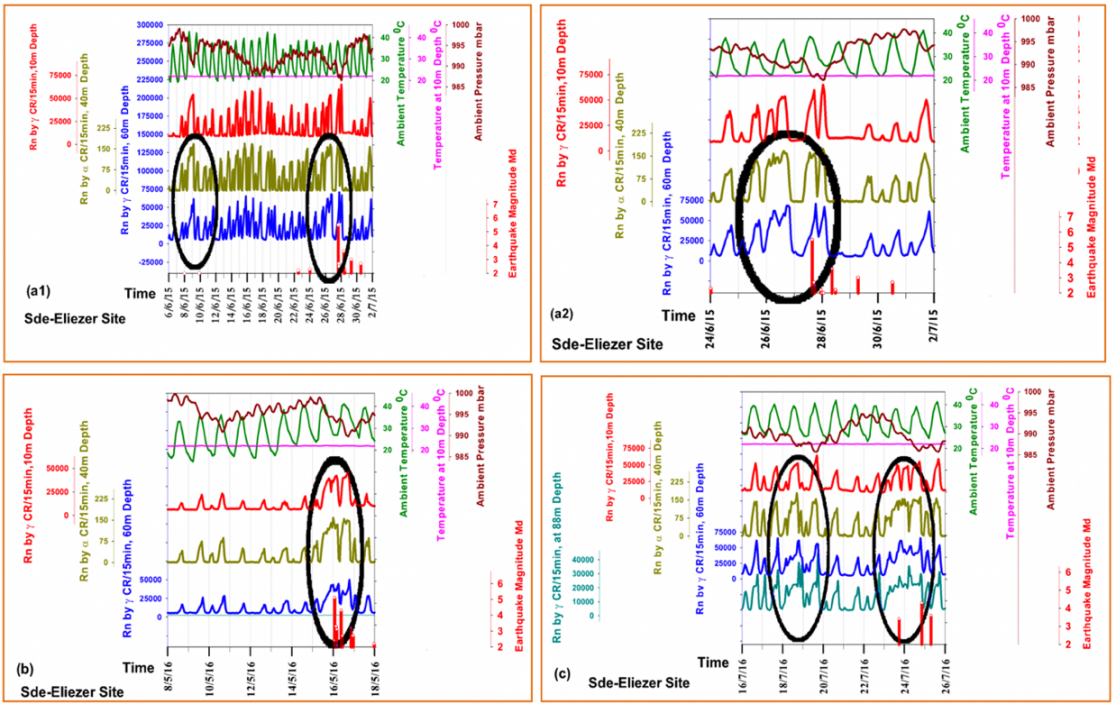

Figure 3 (a1) & (a2) The 26 June broadened radon anomalous signal preceding by one day the Nuweiba (in the Gulf of Eilat) M 5.5 earthquake occurred on 27 June 2015. It was different from the radon periodic signals appearing usually once or twice a day. (b) The broadened radon signal appeared 14 hours before the next Nuweiba M5.1 earthquake on 16 May 2016, (c) On 17 and 23 July 2016, two broadened radon anomalous signal appeared 7 and 2 days before new Palmyra Syria M 4.4 earthquake on 25 July 01:30 AM. The deepest detector at 88m depth became the most pronounced radon detector after the water level decreasing below 100m on 25 June 2016.

Preliminary calculations for isolating the components belonging to the periodic signals produced by the climatic parameters in the measured time series, and also utilizing spectrogram extraction method that relies on the Modulation Spectral Analysis, were carried out in order to differentiate between the periodic radon signals and the anomalies that are expected to be discrete and wider than the regular width of the separated diurnal and semidiurnal signals [Zafrir et al., 2016].

Radon and CO_2 in depth, as a proxy for investigating tectonic pre-seismic processes

On 2017 the setup at Sde Eliezer site expended to investigate the effect of atmospheric conditions on air transport inside the deep dry borehole at Sde-Eliezer site using together: radon, CO_2, absolute humidity and atmospheric temperature and pressure [Levintal et al., 2018]. Since then, to present, all borehole data were logged at high 30-sec temporal resolution.

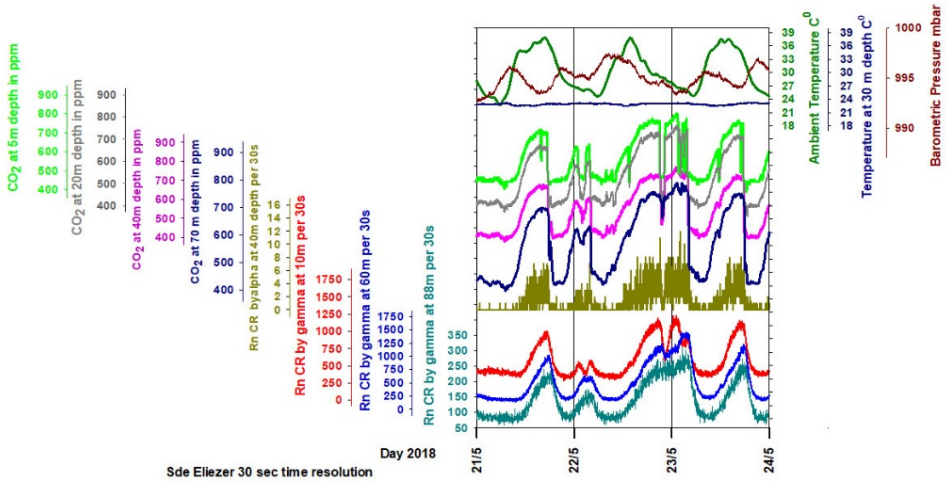

Figure 4 The improvement of the measurement time intervals to 30-second segments, allowed to discover that the rate of changes in the width of the radon and CO_2 signals in depth, occur simultaneously at the same time.

Implementing four CO_2 detectors in different depths, allowed to measure the CO_2 velocity at Sde Eliezer borehole, under the influence of barometric pressure that are seems to be more effective than temperature, within the air space inside the open well. The air velocities inside the borehole and CO_2 emissions to the atmosphere were quantified, fluctuating from 0 and up to ~6 m/min and ~5 g-CO2/min, respectively [Levintal et al., 2018; 2019].

The main achievements can be summarized as follow:

(a) Radon in a **rock porous media** is driven by the surface temperature gradient ΔT, and moves down to a proven depth of 100 m, with the same daily cycle and a specific time lag. Radon within the **open borehole air space** is driven by the pressure variation ΔP. Therefore, radon may have daily and semidaily pressure periodicity.

(b) The high-resolution time interval (30 sec to 15 min) enables to distinguish between the diurnal periodical effect of the ambient temperature and the semidiurnal effect of the ambient pressure, on the radon temporal spectrum, and determination, for the first time, the radon movement velocity within rock layers at depths of several tens of meters, namely, 25 m/h on average [Zafrir et al., 2016].

(c) A very pronounced signal that became different in shape appeared **during a day** before the Nuweiba (in the Gulf of Eilat) M 5.5 earthquake of 27 June of 2015 - wider than the expected width of the periodic signals appearing usually once or twice a day.

(d) This phenomenon repeats itself twice: on 16 May 2016, preceding **by 12 hours** the Nuweiba M 5.1 earthquake, and on 17 and 23 July 2016, two broadened radon anomalous signal appeared **7 and 2 days** before new Palmyra Syria M 4.4 earthquake on 25 July of 2016 at 01:30 AM.

(e) Radon and the CO_2 that emerge from the groundwater to the borehole airtight casing, reveal the same daily & semi daily periodicity, under the same influence of the climatic driving forces and simultaneously parallel non-periodic broadening in time under the influence of tectonic driving forces.

Hence, the deep gas monitoring technology especially heavy gases monitoring, can become a useful tool as proxy for pre-seismic precursory before earthquakes. The large amount of collected data can assist in the future to train and then to apply deep learning and artificial intelligence algorithms for more efficient prediction of earthquakes.

References

Zafrir H., Ben Horin Y., Malik U., Chemo C. and Zalevsky Z., (2016). *Novel determination of radon-222 velocity in deep subsurface rocks and the feasibility to using radon as an earthquake precursor*. J. Geophys. Res. Solid Earth, 121, 6346-6364, doi: 10.1002/2016JB013033.

Levintal E., Zafrir H., Dragila M.I., Weisbrod N., (2018). *The role of atmospheric conditions in driving air movement along a deep borehole using radon and CO_2 mutual relation*. Geophysical Research Abstracts, Vol. 20, EGU2018-6075, 2018, EGU General Assembly 2019.

Levintal E., Zafrir H., Dragila M.I., Weisbrod N., (2019) *The role of atmospheric conditions in CO_2 and radon emissions from an abandoned water well*. Geophysical Research Abstracts, Vol. 21, EGU 2019-6593-1, 2019, EGU General Assembly 2019. http://seis.gii.co.il/heb/earthquake/feltEarthquakes.php.

ST03

GASES IN SEDIMENTARY BASINS

REFERENCE: FAUSTO GRASSA

Geogenic emissions of methane in Romania - general features

Baciu C., Ionescu A., Pop C.

Babes-Bolyai University Faculty of Environmental Science and Engineering, Romania

Corresponding Author: *calin.baciu@ubbcluj.ro*

Romania is among the countries with the longest tradition in oil and gas extraction in the world. Several total petroleum systems (TPS) have been identified on the Romanian territory, which yielded important amounts of oil and gas over the last 150 years. The Carpathian - Balkanian Basin Province [Pawlewicz, 2007], overlapping southern Romania and northern Bulgaria, includes the Moesian Platform Composite TPS and the Dysodile SchisteTertiary TPS. The Transylvanian Composite TPS is entirely confined to Romania, while the eastern side of the Pannonian Basin covers western Romania. Approximately 470 oil and gas seeps were inventoried over these petroleum-prone areas, and an online database (HYSED-RO) has been setup [Ionescu et al., 2017]. Part of the inventory is based on literature data, as not all the seeps can be currently identified in the field. Numerous Romanian seeps have been investigated in detail during the last two decades, mostly as part of the collaboration between Babes-Bolyai University and INGV Rome and Palermo [*e.g.* Etiope et al., 2004; Baciu et al., 2008; Baciu et al., 2018]. The research was focused mainly on the gas seeps from the Eastern Carpathians Foredeep and from the Transylvanian Basin. The biggest mud volcanoes are located in the Foredeep (*e.g.* Paclele Mari, Paclele Mici) and everlasting fires (*e.g.* Andreiasu). Everlasting fires may also occur in the flysch zone (*e.g.* Lopatari, Lepsa). In the Moldavian Platform, the seeps are smaller, they generally occur as flattened mud volcanoes. In Transylvania, the seeps are also small, with the exception of Sarmasel everlasting fire.
The geochemical investigations have shown the thermogenic origin of the gases in the Carpathian Foredeep and Moldavian Platform. Biodegradation processes have been documented in some of the investigated seeps. In the Transylvanian Basin, the gas is mainly microbial, however a thermogenic component cannot be excluded in the deeper reservoirs and in the eastern part of the basin, as suggested by the presence of the C_2-C_4 alkanes. The total output of gas from macroseepage has been approximated at about 3000 t CH_4 y^{-1}. A similar amount is inferred to be released by the microseepage in the hydrocarbon-prone areas [Baciu et al., 2018].

Acknowledgments
The authors acknowledge support from the Deep Energy Community of the Deep Carbon Observatory, and from UEFISCDI, project PN-III-P1-1.2-PCCDI-2017-0721.

References

Baciu C., Etiope G., Cuna S., Spulber L., (2008). *Methane seepage in an urban development area (Bacau, Romania): origin, extent, and hazard*. Geofluids, 8/4, 311-320.

Baciu C., Ionescu A., Etiope G., (2018). *Hydrocarbon seeps in Romania: Gas origin and release to the atmosphere*, Marine and Petroleum Geology, 89, 1, 130-143.

Etiope G., Baciu C, Caracausi A., Italiano F., Cosma C., (2004). *Gas flux to the atmosphere from mud volcanoes in eastern Romania*. Terra Nova, 16:179-184.

Ionescu A., Burrato P., Baciu C., Etiope G., Kis B.-M., (2017). *Inventory of Onshore Hydrocarbon Seeps in Romania (HYSED-RO Database)*. Geosciences, 7(2), 39.

Chemical and isotopic characteristic of Paleozoic natural gases in the southern Ordos Basin, China: fractionation in highly mature coal-derived gases

Dan Liu[1], Jiaqi Liu[1], And Jian Li[2]

[1]*Institute of Geology and Geophysics, Chinese Academy of Science, China*
[2]*PetroChina Research Institute of Petroleum Exploration and Development, China*

Corresponding Author: *liudan@mail.iggcas.ac.cn*

As exploration of Paleozoic gas in Ordos Basin expanded into the south Basin, more and more gases were found to show carbon and hydrogen isotopic reversals. Most previous studies discussed about origin of the partial carbon isotope ($\delta^{13}C\text{-}CH_4 < \delta^{13}C\text{-}C_2H_6 > \delta^{13}C\text{-}C_3H_8$) of Ordos gases and attributed it to the mixing of gases generated from different source rocks [Dai et al., 2014a; Zhao et al., 2014]. In recent year, a small number of studies have reported the complete carbon isotope reversals ($\delta^{13}C\text{-}CH_4 > \delta^{13}C\text{-}C_2H_6 > \delta^{13}C\text{-}C_3H_8$) in Ordos gases [Xia et al., 2013; Dai et al., 2016; Feng et al., 2016; Liu et al., 2016] and they all agreed that the complete carbon isotopic reversals were caused by high temperature (>200°C), which also attributed to the carbon isotopic reversals in over mature shale gases. As a result, most previous studies explained the complete carbon isotopic reversal of Ordos gas and that of shale gas with the same mechanism. However, there are some problems in such kind of explanations: (1) The shale gas belongs to oil-type gas, which was generated from type I kerogen, while the Ordos gas is mainly coal-derived gas, which generated from type III kerogen. Reactions take place in the gas generation process of these two types of source are different; (2) complete carbon isotopic reversal is universal in over mature shale gases [Burruss et al., 2010; Zumberge et al., 2012], while not all over mature coal-derived gas show complete carbon isotopic reversals as the gas in south Ordos Basin [Dai et al., 2014b]. (3) Beside the similar complete carbon isotopic reversal, the gases in south Ordos Basin show some unique characteristics different from the over mature shale gas, one is the evolution trend of the hydrogen isotope.

In this paper, by comparing the geochemical character of south Ordos gas and shale gas, we discussed the isotopic fractionation of over mature coal-derived gas separately from shale gas. We also combined the geochemical data for gases from other fields with different maturities in the Ordos Basin to discuss how the isotope evolve with increment of maturity. Moreover, we discussed the origin of hydrogen isotopic reversal in south Ordos Basin for the first time.

Results indicate that carbon isotopic series are related to maturity (Figure 1). Complete isotopic reversal mostly occurs in regions with vitrinite reflectance (R_o) > 2.4 %. Where 2.4 % > R_o > 2.0 %, almost all gases display partial isotopic reversal, with $\delta^{13}C\text{-}CH_4 > \delta^{13}C\text{-}C_2H_6$ or $\delta^{13}C\text{-}C_2H_6 > \delta^{13}C\text{-}C_3H_8$. Reversal carbon isotope in coal-derived gases is not caused by an abiogenic origin, mixing of gases from different types of source rock, abiogenic polymerization, wet gas cracking, or other mechanisms that contribute to reversal in shale gases. Based on the unique structure of coaly source rock and the geology of the Ordos Basin, closed-system aromatization-polycondensation reactions are considered the most likely explanation for carbon isotopic reversal. During the reactions isotopic light gases were generated by recombination of previously formed hydrocarbons and residual kerogen-coal. Hydrogen isotopic reversal in southern Ordos Basin may also be caused by aromatization-polycondensation reactions.

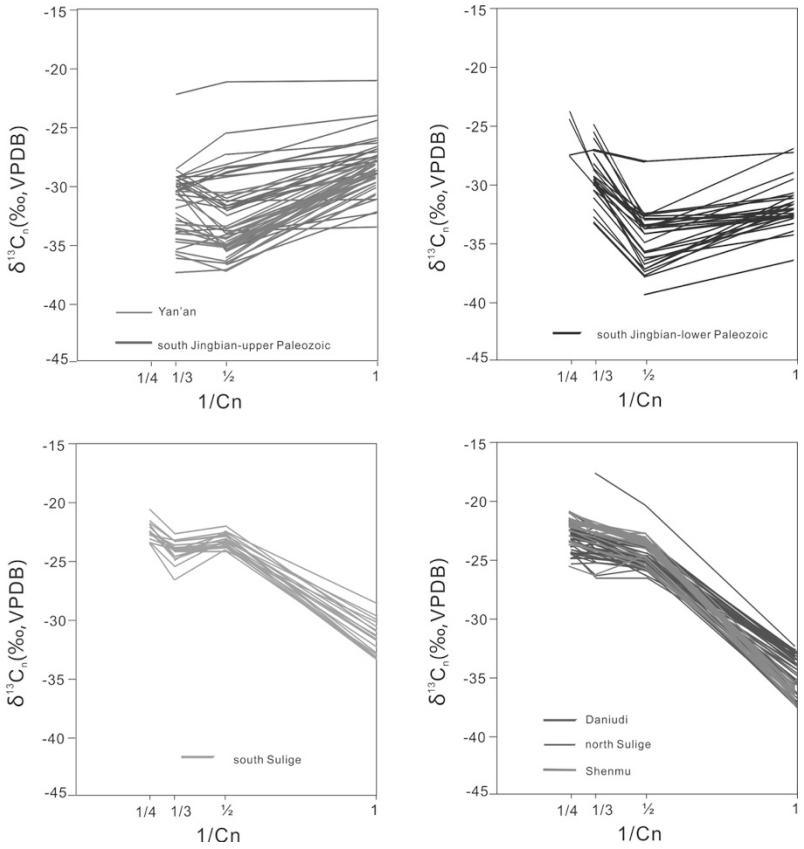

Figure 1 Carbon isotopic series of alkane gases in (a) Yan'an and upper Paleozoic South Jingbian gas fields; (b) lower Paleozoic South Jingbian field; (c) southern Sulige field; (d) Daniudi, northern Sulige, and Shenmu gas fields.

References

Burruss R.C., Laughrey C.D., (2010). *Carbon and hydrogen isotopic reversals in deep basin gas: Evidence for limits to the stability of hydrocarbons*. Organic Geochemistry, 42,1285-1296.

Dai J.X., Ni Y.Y., Yu C. et al., (2014a). *Genetic types of alkane gases in giant gas fields with proven reserves over 1000×10^{8}m^3 in China*". Energy Exploration & Exploitation, 32, 1-13.

Dai J.X., Zou C.N., Li W., (2014b). *Large coal-derived gas fields in China and their sources*. Science Press, Beijing.

Dai J.X., Ni Y.Y., Huang S.P. et al., (2016). *Origins of secondary negative carbon isotopic series in natural gas*. Natural Gas Geoscience, 27(1), 1-7.

Feng Z.Q., Liu D., Huang S.P. et al., (2016). *Geochemical characteristics and genesis of natural gas in the Yan'an gas field, Ordos Basin, China*. Organic Geochemistry, 102, 67-76.

Liu D., Zhang W.Z., Kong Q.F. et al., (2016). *Lower Paleozoic source rocks and natural gas origins in Ordos Basin, NW China*. Petroleum Exploration and Development, 43(4), 591-601.

Xia X., Chen J., Braun R., (2013). *Isotopic reversals with respect to maturity trends due to mixing of primary and secondary products in source rocks*. Chemical Geology, 339, 205-212.

Zumberge J., Ferworn K., Brown S., (2012). *Isotopic reversal ('rollover') in shale gases produced from the Mississippian Barnett and Fayetteville formations*. Marine and Petroleum Geology, 31, 43-52.

Defining Baseline Conditions of Methane and Ethane in Thick Cretaceous Shales of the Williston Basin, Canada

Hendry M.J.[1], Barbour S.L.[2], Schmeling E.[1], Mundle S.O.C.[3] and Huang M.[2]

[1]*Department of Geological Sciences, University of Saskatchewan, S7N 5E2 Canada*
[2]*Department of Civil and Geological Engineering, University of Saskatchewan, S7N 5A2 Canada*
[3]*Great Lakes Institute for Environmental Research, University of Windsor, N9B 3P4 Canada*

Corresponding Author: *jim.hendry@usask.ca*

Natural gas extraction from unconventional shale gas reservoirs is the subject of considerable environmental debate. A key concern is the impact of leaking fugitive natural gases on shallow potable groundwater resources. Baseline data on the natural distribution, fate, and transport of these gases and their isotopes through undisturbed geological formations prior to development are lacking. Here we defined baseline characteristics of methane (CH_4) and ethane (C_2H_6) in thick Cretaceous shales and overlying Quaternary tills at four sites in the Williston Basin (WB), Canada using high-resolution vertical profiling. Strong positive correlations with the conservative natural tracer Cl^- suggest a lack of measurable production or consumption of gases in the shale to the depths investigated while the CH_4 and C_2H_6 concentrations at the upper boundary are controlled by release, consumption, lateral migration and/or dilution in permeable zones. Curvilinear increasing concentrations with depth in the shale at all sites coupled with 1-D solute transport modelling suggest long-term (over millions of years) upward diffusion of CH_4 and C_2H_6 from deeper WB sources, likely the Second White Speckled Shale Formation (SWSS; ~790 m below ground surface). In contrast to ^{13}C-enriched thermogenic isotopic signatures of CH_4 and C_2H_6 in deeper oil-producing WB intervals, carbon isotope values from the till suggest the CH_4 is likely of biogenic origin. $\delta^{13}C$-CH_4 profiles in the shale are consistent with upward diffusional fractionation of isotopes from the SWSS. We show that the diffusive fractionation of $\delta^{13}C$-CH_4 (following glaciation) can complicate fugitive gas interpretations. The sensitivity of the $\delta^{13}C$-CH_4 profile development to glacial timing suggests it may also be a valuable tracer to characterize the timing of geologic events that exert controls on the transport of CH_4 and C_2H_6 enabling the CH_4 that rapidly migrates upward through a well annulus or other conduit to be distinguished from CH_4 that diffuses upwards naturally.

The accumulation of natural gas and potential exploration regions in the Southern Margin, Junggar Basin

Jianping Chen[1], Xulong Wang[2], Yunyan Ni[1], Baoli Xiang[2], Fengrong Liao[1]

[1]*PetroChina Research Institute of Petroleum Exploration and Development, Beijing, China*
[2]*PetroChina Xinjiang Oilfield Company, Karamay, China*

Corresponding Author: *chenjp@petrochina.com.cn*

The Southern Margin of the Junggar Basin has the similar history of sediment and tectonic evolution with the Kuqa Depression of the Tarim Basin, but has never made a great breakthrough in natural gas exploration. Based on the results of genetic type and origin of the natural gas, this paper discusses the conditions for natural gas generation and accumulation compared with the Kuqa Depression, and the favorable exploration regions and potential target in the region. The results show that the natural gases in the Southern Margin are dominated by thermogenic wet gas, which are divided into three types, coal-derived gas, mixed gas and oil-associated gas, and are dominated by former two types. The Jurassic coal measures is the main natural gas source rocks in the Southern Margin, and its main period of gas generation matches the formation epoch of the anticline structures, which constitutes the best source-trap combination for gas accumulation. The Permian lacustrine and the Upper Triassic lacustrine-limnetic facies source rocks may also be important natural gas source rocks, whose main period of gas generation is earlier than the formation epoch of most anticline structures in the central region, but coincides with the epoch of anticline formation in the western region.

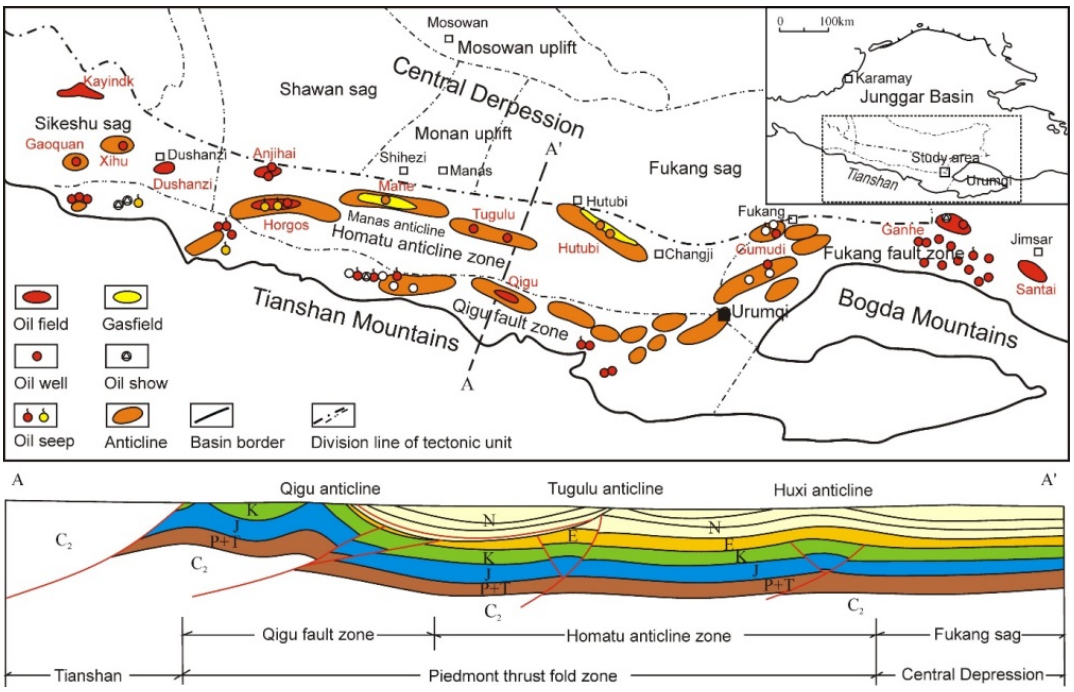

Figure 1 Distribution of the anticline traps, oil and gas fields in the Southern Margin, Junggar Basin.

Compared with the Kuqa Depression, the Southern Margin has batter material base of hydrocarbon generation than the Kuqa depression, but the maturity of the source rocks of the Jurassic coal measures is slightly lower than that of the Kuqa depression, the capping of the caprock and the scale of reservoir rock are slightly inferior to those of the Kuqa depression. The Southern Margin still has the conditions for forming large-scale oil and gas fields. The combination of the Permian-Jurassic-Cretaceous in the deep is the most favorable system for natural gas exploration, where the western part is a favorable target area for finding and discovering Jurassic coal-derived oil and gas reservoirs, and the middle part is a favorable target area for finding and discovering Jurassic coal-derived gas reservoirs. The combination of the Cretaceous-Neogene in the shallow is a secondary system for natural gas exploration, with the potential to find and discover a certain-scale of natural gas reservoirs.

Microseepage of methane and its emission mechanism in the Dawanqi Oil-gas field

Junhong Tang[1], Yue Xu [1], Zhenzhen Zhu[1], Guojian Wang[2]

[1]*College of Materials and Environmental Engineering, Hangzhou Dianzi University, Hangzhou 310018, China*
[2]*Wuxi Research Institute of Petroleum Geology, Research Institute of Petroleum Exploration and Production, SINOPEC, Wuxi Jiangsu 214151, China*

Corresponding Author: *tang_jhjh@163.com*

Introduction

Methane (CH_4) is a radiatively active gas, and it is one of the most important greenhouse gases in the atmosphere. CH_4 has a global warming potential that is 28 times higher than that of CO_2 on a 100-year time horizon, and its concentration has risen from ~0.7 ppmv to ~1.9 ppmv now [es. Etiope et al., 2019]. Therefore, the assessments of the natural and anthropogenic sources and sinks of CH_4 are central to studies of climate change.

In the recent years, geologic CH_4 emission could play an important role in the atmospheric CH_4 budget, numerous studies have shown that the CH_4 in the reservoirs of the sedimentary basin can seepage to the surface through faults, fissures and permeable rocks, mud volcanism, marine seeps and geothermal manifestations [es. Etiope et al., 2006; Lassey et al., 2007]. CH_4 which failed to be oxidized and degraded may finally be released into the atmosphere. The CH_4 fluxes in sedimentary basins normally are a few units or tens of mg m^{-2} day^{-1}, and may be at the hundreds level in active tectonic and faulted regions [es. Tang et al., 2017]. According to Asia, Europe, the United States and other pooled methane flux and hydrocarbon basins data, global methane emissions from hydrocarbon basins is about 10-28 Tg y^{-1}, which cannot be ignored in the atmospheric CH_4 budget [Abrams, 2005].

Experimental

The field work was performed in the August of 2014. According to the geological structure and surface geochemical database, the fault block 105 and 109 area were chosen as the studied area, which were the main oil and gas resource development region in Dawanqi oilfield. The samples were collected at 51 points with a distance of 100m along three lines (Figure 1).

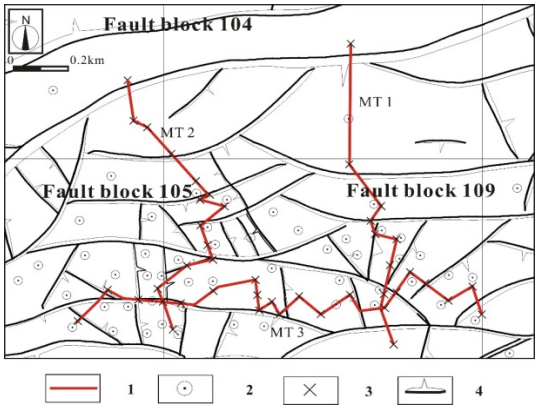

Figure 1 Sampling point map of Dawanqi Oilfield. 1. The measurement transect (MT). 2. Oil wells. 3. The measurement site. 4. Faults.

The north-south lines 1 and 2 went through fault block 109 and 105 respectively, and the east-west line 3 went through fault block 105 and 109. Background samples were obtained outside the oilfield.

Results and Discussion

The CH_4 and CO_2 fluxes

CH_4 fluxes monitoring sites in the Dawanqi oilfield show that methane emission is widespread (Table 1). Table 2 shows the descriptive statistical variables for the CH_4 and CO_2 fluxes in the Dawanqi area. According to Table 2, CH_4 fluxes ranged from -1.4 to 329.9 mg m^{-2} d^{-1}, and the average CH_4 flux was 17.4 mg m^{-2} d^{-1}. CO_2 fluxes ranged from 0.03 to 76.8 g m^{-2} d^{-1}, and the average CO_2 flux was 5 g m^{-2} d^{-1}, which were in the normal range for soil respiration fluxes. Of the 51 individual chamber measurements, 40 resulted.

Fund project: National Natural Science Foundation of China (Grant No.41373121 and 41872126).

In positive flux values and 11 resulted in negative fluxes. Negative fluxes are typical and normal in dry soil as a consequence of methanotrophic activity. For this reason, soil is a net sink for atmospheric CH_4 on a global scale. At the two sampling points in the background area, the average flux of methane was -1.43 and -1.35 mg m^{-2} d^{-1}, respectively, which is a typical area affected by methane oxidizing bacteria in the arid region.

Table 1 Flux and Isotopic Data of CH_4 and CO_2 on the surface (na: not analyzed).

	Sites	CH_4 (mg $m^{-2}d^{-1}$)	CO_2 (g $m^{-2}d^{-1}$)	$\delta^{13}C_{CH4}$ ‰ VPDB	$\delta^{13}C_{CO2}$ ‰ VPDB
Faulted zones	18-7	41.6	76.8	-36.2	-12.5
	19-4	-0.4	2.8	-44.5	-8.3
	541-14	0.8	12.8	-42.1	-9.1
	542-13	-0.4	15.6	na	na
	545-12	69.2	14.6	-34.8	-13.2
	546-12	131.5	4.4	-32.7	-12.8
	547-11	-1.4	1.6	-46.3	-7.1
	556-10	0.5	3.8	na	na
	559-8	0.8	3.6	na	na
	554-15	0.8	1.5	na	na
	554-14	2.8	0.3	na	na
	554-11	75.2	7.3	-30.7	-14.9
	544-23	-0.2	4.8	na	na
	546-20	1.5	3.2	-41.3	-12.5
	544-16	-0.6	1.3	na	na
	543-28-1	-0.1	4.7	na	na
	543-28-2	0.2	3.3	na	na
	543-28-3	222.5	8.6	na	na
	543-28-4	0.3	0.5	na	na
	543-28-5	0.1	0.5	na	na

Unfaulted zones	17-5	-1.2	9.6	-45.1	-8
	543-13	-1.2	4.7	-45.1	-8.7
	545-13-1	0.1	2.1	na	na
	545-13-2	3.1	4.2	-39.7	-11.7
	549-11	-1.3	2.6	na	na
	550-10	0.4	0.8	na	na
	551-10	0.2	1.4	na	na
	552-10	1.1	0.2	na	na
	553-9	2.9	0.6	-42.7	-8.9
	554-9	1.0	0.4	na	na
	557-9	1.1	14.7	na	na
	558-8	-0.6	1.0	na	na
	559-7	0.4	1.2	na	na
	546-13	-0.5	6.7	na	na
	555-20	0.9	0.3	-43.4	-9.2
	555-18	0.2	0.4	na	na
	555-16	329.9	5.0	na	na
	555-13	0.9	1.5	na	na
	553-10	0.1	1.3	na	na
	553-7	0.6	0.03	na	na
	542-26	0.7	0.8	-43.8	-10.7
	543-25	0.9	2.6	na	na
	545-21	0.3	0.5	na	na
	545-20	0.4	1.3	na	na
	546-19	0.2	2.2	-40	-13.3
	544-18	0.2	0.7	na	na
	544-17	0.4	0.1	na	na
	543-16	1.1	2.5	na	na
	541-15	3.0	8.5	-40.2	-10.3
	542-12	-0.1	1.3	-41	-9.9
	542-26-2	0.4	2.7	na	na

Table 2 Descriptive Statistical Variables of CH_4 (mg m^{-2} d^{-1}) and CO_2 (g m^{-2} d^{-1}) Flux.

	Average fluxes	Median	Standard Deviation	Range
CH_4	17.4	0.4	58.7	-1.4—329.9
CO_2	5	3	1	0.03—76.8

The method of CH_4 microseepage emission

In the on-line monitoring of methane flux, portable greenhouse gas analyzers show two ways of methane emission, one is continuous emission, the concentration continues to rise (Figure 2); the other is intermittent emission, methane emission is presented discontinuity (Figure 3). The former occurs mostly at sampling points with higher methane concentrations (554-11, 545-12), while the latter occurs more at lower concentration sampling points (543-28-1, 543-28-5). The reason for the emergence of these two modes of emission may be related to the vertical microseepage migration of methane.

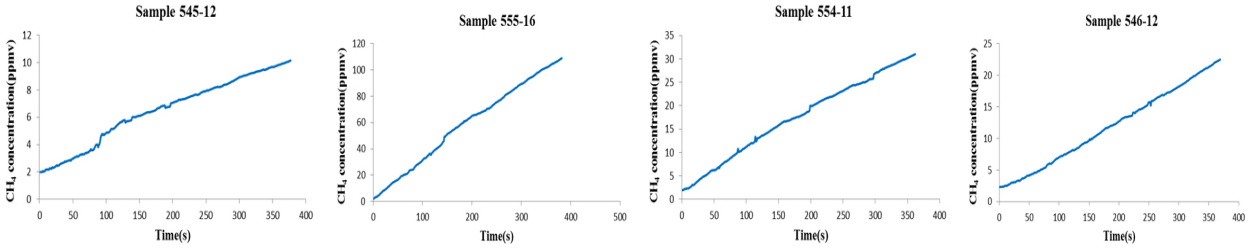

Figure 2 Continuous emission of methane microseepage

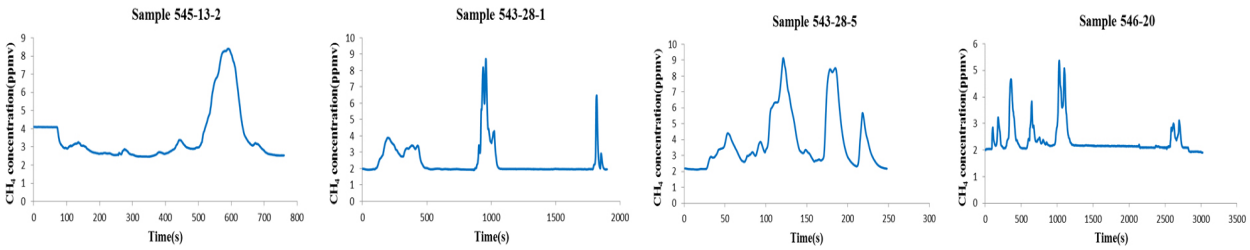

Figure 3 Intermittent emission of methane microseepage.

Conclusions

At present, the Dawanqi oil-gas field is about 30km^2, and the emission factor of the Dawanqi oil-gas field is consistent with the global emission factor distribution. Most of the areas are low-seepage grades (0-5 mg m^{-2} d^{-1}). However, because the Dawanqi oil-gas field is located in the fault-developing area, its high-seepage area accounts for 10% of the flux measurement area, which is much higher than the global average. The average methane flux of Dawanqi oil-gas field is 17.5mg m^{-2} d^{-1}, which is very similar to the CH_4 flux of oil-gas fields in the global geological tectonic active area. According to the microseepage database, in the petroliferous basin, these three grades account for 3%, 12% and 34% respectively, so multiplying the actual emission factor by the corresponding area can estimate the flux in the Dawanqi oil-gas field to be 112.2 t/y.

References

Abrams M.A., (2005). *Significance of hydrocarbon seepage relative to petroleum generation and entrapment*. Marine and Petroleum Geology, Volume 22, Issue 4, Pages 457-477.

Etiope G., Papatheodorou G., Christodoulou P. et al., (2006). *Methane and hydrogen sulfide seepage in the NW Peloponnesus petroliferous basin (Greece): Origin and geohazard*. Amer. Assoc. Petrol. Geol. Bull., v. 90, no. 5 (May 2006), pp. 701-713.

Etiope G., Ciotoli G., Schwietzke S., Martin S., (2019). *Gridded maps of geological methane emissions and their isotopic signature*. Earth Syst. Sci. Data, 11, 1-22, 2019, https://doi.org/10.5194/essd-11-1-2019 Copernicus Publications.

Lassey K.R., Lowe D.C., Smith A.M., (2007). *The atmospheric cycling of radio methane and the "fossil fraction" of the methane source*. Atmos. Chem. Phys., 7(8)·May 2007.

Tang J.H., Xu Y., Wang G.J. et al., (2017). *Microseepage of methane to the atmosphere from the Dawanqi oil-gas field, Tarim Basin, China*. Journal of Geophysical Research: Atmospheres. doi: https://doi.org/10.1002/2016JD026385.

Migration of the miocene microbial gas to mesozoic basement reservoirs and mesozoic thermogenic hydrocarbons to miocene reservoirs of the Polish Carpathian foredeep: isotopic and geological approach

Kotarba M.J.

AGH University of Science and Technology, Faculty of Geology, Geophysics and Environmental Protection, Kraków, Poland

Corresponding Author: *kotarba@agh.edu.pl*

The Carpathian Foredeep is a tectonic depression and the largest gas basin among all foredeep basins of the Alpine orogenic system in Europe. It extends along the front of the Carpathian Overthrust, and partly underlies the Carpathian nappes, ranging from the Vienna Forest in the west, through the Czech Republic, Slovakia, Poland and Ukraine up to the Iron Gate in Romania in the southeast. In the Polish sector it is filled with the autochthonous Miocene strata. The Miocene mollase strata rest unconformable Palaeozoic-Mesozoic complex. More than 100 gas fields and about 20 oil and fields have been discovered in eastern part between Kraków and Przemyśl since the middle 1960s in the Upper Badenian and Lower Sarmatian strata and their Palaeozoic-Mesozoic basement (Mississipian, Upper Jurassic and Upper Cretaceous reservoirs), respectively. Methane concentrations in natural gas accumulated in Miocene strata exceed 95 vol%. Methane is mainly isotopically light ($\delta^{13}C$ from -71.4 to -64.0‰) [Kotarba, 2001]. Isotopic studies reveal that methane and partly ethane and even propane accumulated within the autochthonous Miocene strata were generated by microbial reduction of carbon dioxide in marine depositional environments, mainly during sedimentation of the Miocene clays and muds (Kotarba, 2001; Kotarba et al., 2011). The natural gas accumulated in Mesozoic reservoirs include microbial, thermogenic (low-temperature) types associated with oil and condensate, and thermogenic (high-temperature) non assosiated types [Kotarba and Jawor, 1993; Kotarba, 2012].

Methane dominates in the molecular composition of natural gas accumulated in the Cenomanian sandstone reservoir of the Brzezowiec field and one Upper Jurassic carbonate block of the Lubaczów field dominates methane with $\delta^{13}C(CH_4)$ equal to -67.3‰ and -64.7‰, respectively. This indicates that the natural gas is of microbial origin and migrated from the autochthonous Miocene strata.

In the lower part of the Miocene molasse sequence of the Tarnów field oil and isotopically hydrocarbon gases [$\delta^{13}C(CH_4)$ -36.2‰, $\delta^{13}C(C_2H_6)$ -27.9‰ and $\delta^{13}C(C_3H_8)$ -25.8‰] occur. Oil and natural gas migrated from the Upper Jurassic reservoir [$\delta^{13}C(CH_4)$ -35.6‰, $\delta^{13}C(C_2H_6)$ -27.2‰ and $\delta^{13}C(C_3H_8)$ -26.3‰].

In the Miocene reservoir of the Góra Ropczycka field isotopically heavy hydrocarbon gases occur [$\delta^{13}C(CH_4)$ -48.1‰, $\delta^{13}C(C_2H_6)$ -27.6‰ and $\delta^{13}C(C_3H_8)$ -26.7‰] evidencing that these gases migrated from the Upper Jurassic reservoir [$\delta^{13}C(CH_4)$ -36.0‰, $\delta^{13}C(C_2H_6)$ -28.4‰ and $\delta^{13}C(C_3H_8)$ -26.0‰].

Acknowledgements

The research was financially supported from the National Science Centre research grant UMO-2016/22/M/ST10/00589.

References

Kotarba M.J., (2011). *Origin of natural gases in the autochthonous Miocene strata of the Polish Carpathian Foredeep*. Annales Societatis Geologorum Poloniae, 81, 409-424.

Kotarba M.J., (2012). *Origin of natural gases in the Paleozoic-Mesozoic basement of the Polish Carpathian Foredeep*. Geologica Carpathica, 63 (4), 307-318.

Kotarba M.J. and Koltun Y.V., (2006). *The origin and habitat of hydrocarbons of the Polish and Ukrainian Parts of the Carpathian Province. In: Golonka J and Picha F.J (eds.) The Carpathians and their foreland: geology and hydrocarbon resources*. American Association of Petroleum Geologists, Memoir 84: 395-442.

Kotarba M.J., Peryt T.M. and Koltun Y.V., (2011). *Microbial gas system and prospectives of hydrocarbon exploration in Miocene strata of the Polish and Ukrainian Carpathian Foredeep*. Annales Societatis Geologorum Poloniae, 81, 523-548.

Influence of pressure on the generation and expulsion of liquid hydrocarbons and its implications for gas generation in the hogh maturity stage of the Tarim Basin, Northwest China

Long Su[1], Dongwei Zhang[1,2], Jihui Lin[1,2]

[1]*Key Laboratory of Petroleum Resources, Gansu Province / Key Laboratory of Petroleum Resources Research, Institute of Geology and Geophysics, Chinese Academy of Sciences, China*
[2]*University of Chinese Academy of Sciences, China*

Corresponding Author: *longsu@lzb.ac.cn*

Abstract
In this study, simulation experiments were conducted to investigate the influence of pressure, including lithostatic stress (LS) and fluid pressure (FP) on yield and process of hydrocarbon generation (Table 1).

Table 1 The experiment conditions in two series of the pressured experiments (P-T-t) and the non-pressured experiments (T-t) based on the model in the Tarim basin.

HR[a] (°C/h)	t[b] (h)	T[c] (°C)	Depth (m)	P-T-t (MPa)				T-t (MPa)		
				LP[d] (MPa)	FP[e] (MPa)			LP[d]	FP (MPa)	
					Mid.[f]	Min.[g]	Max.[h]		Min.	Max.
	5.0	200	1200	27.6	12.0	12.0	16.8	6.0	2.0	5.0
5.0	15.0	250	1600	36.8	18.0	16.0	22.4	6.0	2.0	5.0
5.0	25.0	300	2400	55.2	27.0	24.0	33.6	6.0	2.0	5.0
5.0	30.4	327	3000	69.0	32.0	30.0	42.0	6.0	2.0	5.0
5.0	33.0	314	2500	57.5	25.0	25.0	27.0	6.0	2.0	5.0
2.19	40.3	330	3600	82.8	41.0	36.0	50.4	6.0	2.0	5.0
2.19	41.7	327	3200	73.6	32.0	32.0	34.0	6.0	2.0	5.0
3.37	44.6	337	4000	92.0	48.0	40.0	56.0	6.0	2.0	5.0
7.5	51.7	390	6400	147.2	76.0	64.0	89.6	6.0	2.0	5.0
7.5	59.7	450	7000	161.0	83.0	70.0	98.0	6.0	2.0	5.0
7.5	66.4	500	7400	170.2	89.0	74.0	103.6	6.0	2.0	5.0
7.5	73.0	550	7800	179.4	94.0	78.0	109.2	6.0	2.0	5.0

[a]HR: Heating rate; [b]t: Heating time; [c]T: Temperature; [d]LP: Lithostatic pressure; [e]FP: Fluid pressure; [f]Mid.: The middle value of the LP; [g] Min.: The minimum value of the LP; [h] Max.: The maximum value of the LP.

Two systematic comparative pyrolysis experiments, including pressured experiments and non-pressured experiments were conducted in hydrous experimental condition. The results show that the following parameters, including Ro, ratio of the expelled oil to eluted oil, the accumulated yield of the expelled oil and liquid hydrocarbons, are lower in pressured experiments than that of non-pressured experiments. However, the accumulated yields of eluted oil and residual oil are higher in pressured experiments than that of non-pressured experiments. Additionally, the expulsion efficiencies of the oil range from 20% to 25%, which are lower in pressured experiments than that of non-pressured experiments near the oil generation-window. However, the yields of hydrocarbon gas in pressured

experiments are greater compared with the yields in non-pressured experiments at the high maturity stage. Based on the characteristics of hydrocarbon generation in the experimental results, hydrocarbon generation process can be divided into three stages. Generally, existence of LS and FP could retard the process of mudstone maturation as well as the generation and expulsion processes of the liquid hydrocarbons. Therefore, the residual liquid hydrocarbons in high-pressure condition can act as another source of deep gas generation in the high maturity stage. The results could help us to properly evaluate hydrocarbon generation potentials of sources rocks in petroleum-producing sedimentary basin in China and elsewhere.

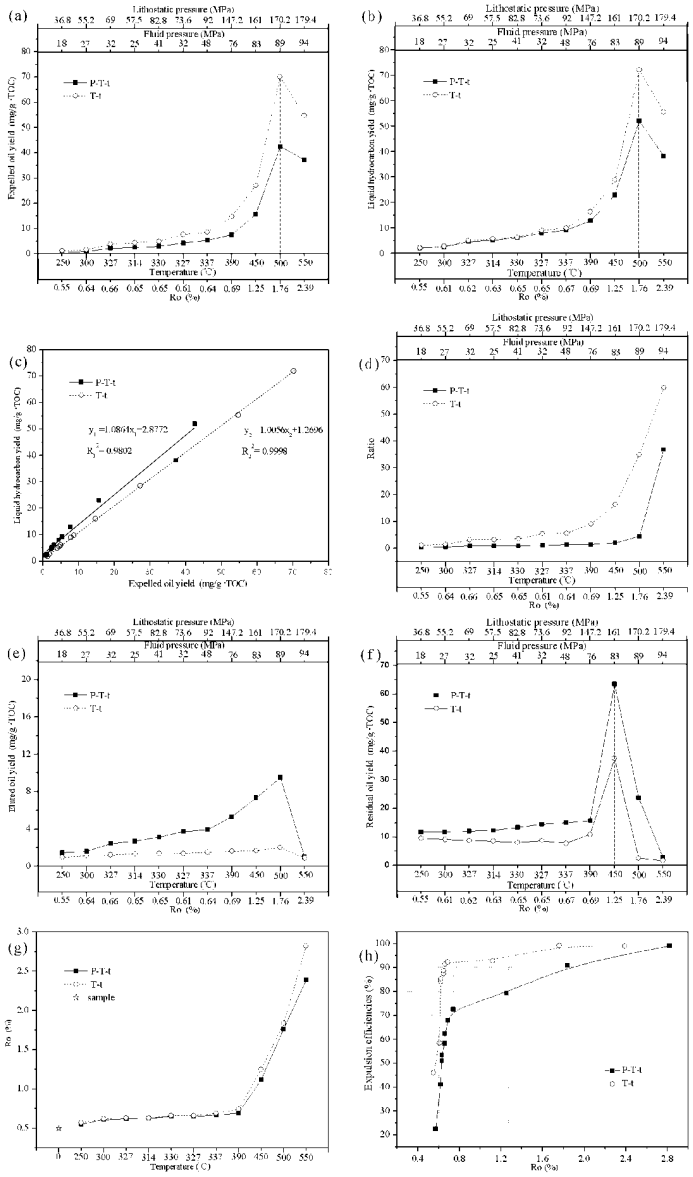

Figure 1 The accumulated yields of the expelled oil (a); the liquid hydrocarbons (b); (c) the positive correlation of the expelled oil and the liquid hydrocarbons for P-T-t (R_1^2= 0.9802) and for T-t (R_2^2= 0.9998); (d) the ratio of the expelled oil and the eluted oil; the eluted oil (e); the residual oil yield (f), and Ro (g) and the expulsion efficiencies of the liquid hydrocarbons (h) derived from organic rich mudstone in two series of the pressured experiments (P-T-t, square) and the non-pressured experiments (T-t, circle). The X axis is divided equally in order to figure the beauty. The Ro value at X axis measurements is from the solid residual kerogen of the sample after the pressured experiments (P-T-t, square). In fact, the Ro is Rc of the asphalt reflectivity in the abstract.

Distribution and Geochemical Characteristics of Hydrogen in Natural Gas, Jiyang Depression, Eastern China

Qingqiang Meng[1,2], Quanyou Liu[1,2], Dongya Zhu[1,2], Weilong Peng[1,2], Jiayi Liu[1,2]

[1]*State Key Laboratory of Shale Oil and Gas Enrichment Mechanisms and Effective Development, SINOPEC, China*
[2]*Petroleum Exploration & Production Research Institute, SINOPEC, China*

Corresponding Author: *mengqq.syky@sinopec.com*

Hydrogen gas has been regarded as a promoter for hydrocarbon generation in source rocks. The lack of knowledge of hydrogen distribution and its origin in natural gas, however, becomes one of the main obstacles to further exploration. In this paper, to get a better understanding of the distribution and origin of hydrogen gas in Jiyang Depression, eastern China, geochemical analysis and trace gas compound-specific carbon and hydrogen isotope analysis were conducted. The hydrogen gas in this region is widespread and its content typically ranges from 0.01% to 0.1%. The ratio of $H_2/^3He$ suggests that hydrogen of mantle origin is dominant. Even in tectonically relatively stable areas which are far away from deep fluid activities, the occurrence of hydrogen of mixed sources suggests the effects of mantle-derived deep fluid, hydrogenation to source rocks in particular, are not limited in deep fluid regions only. The isotopic composition of hydrogen is mostly light and in the range of -798~-628 ‰ (SMOW). In areas where deep fluid activities are estimated to be dominant, deep source hydrogen gas has similar isotopic compositions. In relatively stable areas, the isotopic composition of hydrogen gas becomes heavier. Therefore, hydrogen isotopic composition analysis is necessary to fully understand the origins of hydrogen gas.

References

Lewan M.D., (1997). *Experiments on the role of water in petroleum formation*. Geochimica et Cosmochimica Acta, 61, 3691-3723.

Dai J., Zou C., Zhang S., Li J., Ni Y., Hu G., Luo X., Tao S., Zhu G., Mi J., Li Z., Hu A., Yang C., Zhou Q., Shuai Y., Zhang Y., Ma H., (2008). *On the identification of organic- and inorganic-originated hydrocarbon gas*. Science in China-Series D, 38(11), 1329-1341.

Zhang C., Duan Z., (2009). *A model for C-O-H fluid in the Earth's mantle*. Geochimica et Cosmochimica Acta, 73, 2089-2102.

Sherwood L., Onstott C., Lacrampe-Couloume G., Ballentine C., (2014). *The contribution of the Precambrian continental lithosphere to global H_2 production*. Nature, 516, 379-382.

Carbon and hydrogen isotope fractionation of alkanes gases during abiogenic oxidation: insight from the closed system pyrolysis

Quanyou Liu[1,2], Weilong Peng[1,2], Qingqiang Meng[1,2], Dongya Zhu[1,2], Zhijun Jin[1,2], Xiaoqi Wu[1,2], Jinzhong Liu[3]

[1]*State Key Laboratory of Shale Oil and Gas Enrichment Mechanisms and Effective Development, SINOPEC, China*
[2]*Petroleum Exploration & Production Research Institute, SINOPEC, China*
[3]*State Key Laboratory of Organic Geochemistry, Guangzhou Institute of Geochemistry, Chinese Academy of Sciences, Guangzhou, China*

Corresponding Author: qyouliu@sohu.com

Thermochemical sulfate reduction (TSR) in marine carbonate gas reservoirs can produce different carbon and hydrogen isotopic compositions from those of conventional thermogenic gas reservoirs [Hao et al., 2008; Liu et al., 2014; 2019]. This study aims to better understand how TSR can affect geochemical and isotopic compositions of gas reservoirs. Laboratory simulation of TSR was conducted with crude oil in the presence of $MgSO_4$ at temperatures of 350°C, 360°C, and 370°C for different durations of 4~219 h in a closed system. Results show that the amount of CH_4, CO_2 and H_2S produced during thermal cracking of crude oil at the temperature of 360°C is significantly lower than those formed in the presence of $MgSO_4$ under the same conditions, which suggests that TSR can oxidize hydrocarbons and produce CO_2 and H_2S. In addition, carbon and hydrogen isotope compositions of alkane gas resulted from the TSR became heavier with increasing carbon number, i.e., $\delta^{13}C_1<\delta^{13}C_2<\delta^{13}C_3$ and $\delta^2H\text{-}C_1<\delta^2H\text{-}C_2<\delta^2H\text{-}C_3$. However, at the same temperature, $\delta^{13}C_1$ decreased at first and then became larger with increasing heating time within a certain range. Compared with the $\delta^{13}C_3$, $\delta^{13}C_2$ and $\delta^{13}C_3$ increased in a much wider range as heating continued. Specifically, the $\delta^{13}C_2$ varied in a range slightly smaller than the $\delta^{13}C_3$. The narrower variation range of $\delta^{13}C_1$ was because of rapid oxidation of hydrocarbons by TSR which produced methane with similar carbon and hydrogen isotope compositions to the source material. In addition, carbon and hydrogen isotopes of alkane gas from TSR became larger with increasing gas souring index (GSI), i.e., $H_2S/(H_2S+\sum C_{1\text{-}5})$, and the CH_4 had a smaller variation range than the C_2H_6. $\delta^{13}C_1-\delta^{13}C_2$ and $\delta^2H\text{-}C_1-\delta^2H\text{-}C_2$ normally decreased as organic matter underwent thermal cracking. However, they may show an increasing trend because TSR can reduce the variation range of carbon and hydrogen isotopes of CH_4. The carbon and hydrogen isotope compositions of C_2H_6 were more heavily affected by thermal cracking before oxidization by TSR, which resulted in their short variation range. Comparative simulation experiments of C_9 in the presence of $MgSO_4$ produced partially reversed carbon and hydrogen isotope series, which confirmed the ability of TSR to alter the isotopic composition of alkanes in natural gas. The rapid oxidation of hydrocarbons by TSR resulted in the series of $\delta^{13}C_1>\delta^{13}C_2$, which is similar to the isotopic composition of source materials. ^{13}C was gradually enriched in the residual heavy alkanes during the TSR process, which increased the $\delta^{13}C_2$ value and changed the partially reversed isotope sequence to positive.

References

Hao F., Guo T.L., Zhu Y.M., Cai X.Y., Zhou H.Y., Li P.P., (2008). *Evidence for multiple stages of oil cracking and thermochemical sulfate reduction in the Puguang gas field, Sichuan Basin, China*. AAPG Bulletin, 92(5), 611-637.

Liu Q.Y., Worden R.H., Jin Z., Liu W., Li J., Gao B., Zhang D., Hu A., Yang C., (2013). *TSR versus non-TSR processes and their impact on gas geochemistry and carbon stable isotopes in Carboniferous, Permian nad Lower Triassic marine carbonate gas reservoirs in the Eastern Sichuan Basin, China*. Geochimica et Cosmochimica Acta, 100, 96-115.

Liu Q., Wu X., Wang X., Jin Z., Zhu D., Meng Q., Huang S., Liu J., Fu Q., (2019). *Carbon and hydrogen isotopes of methane, ethane, and propane: A review of genetic identification of natural gas*. Earth-Science Reviews, 190, 247–272.

Genetic type, distribution and enrichment mechanism of helium in China's Petroliferous basins

Shengfei Qin[1], Feng Li[2], Changyi Zhao[1], Xiowan Tao[1], Zheng Zhou[3]

[1]*Research Institute of Petroleum Exploration & Development (RIPED), PetroChina, P. R. China*
[2]*Science and Technology Management Department of PetroChina, P. R. China*
[3]*Lancaster Environment Centre, Lancaster University, Lancaster, United Kingdom*

Corresponding Author: *qsf@petrochina.com.cn*

Helium has the lowest melting point and boiling point found in nature, and is widely used in aerospace, nuclear industry, deep sea diving, scientific research and high technology. However, global helium resources are very limited, and helium resources are mainly from natural gas. Although China has discovered potential helium resources in both superimposed petroliferous basins in Midwestern China and the rift basins in Eastern China. However, the distribution law and enrichment mechanism of helium have been weakly studied. These affect the evaluation and exploration of helium resources in China.

The helium in the superimposed basins is mainly originated by the radioactive origin of uranium and thorium in the crust. Due to the existence of deep and large faults in the eastern rift basins, helium is once considered to be mainly from the deep mantle, but according to the $^{3}He/^{4}He$ ratio, the helium in most samples is still mainly from the radioactive decay.
The content of uranium and thorium in the earth's crust is very low, and the half-life is very long. The helium produced by radioactive decay is widely dispersed in the earth's crust and the content of helium is extremely low. The helium cannot accumulate individually to form a separate helium gas pool. It needs to be transported by using other fluids as carriers to enrich. This carrier is often formation water, not other gases.

Through the research on the large-scale helium-rich gas fields discovered in China, it is found that the helium is mainly from the decay of uranium and thorium in granite or metamorphic rock base, not from the source rocks, nor from the formation water or reservoir. The base such as granite contains relatively abundant uranium and thorium, which decays to produce helium. The helium is transported and enriched by formation water. The helium dissolved in the water then experienced depressurization and exsolution due to the late Himalayan uplifting movement, and integrated with the natural gas in the trap to form a helium-rich natural gas field. Along the groundwater flow direction, the content of helium in natural gas is gradually increasing (Figure 1). Vertically, in the same gas field, the content of helium gradually increases from top to bottom (Figure 2). Although helium is highly penetrating in the formation and is highly prone to diffuse, the preservation of helium in natural gas reservoirs has no special requirements for the cap rocks.

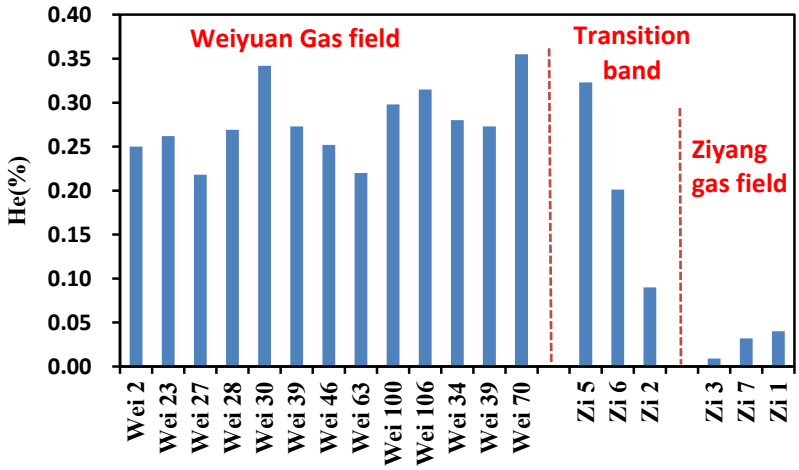

Figure 1 Helium content in Sinian gas reservoirs of Weiyuan and Ziyang gas fields.

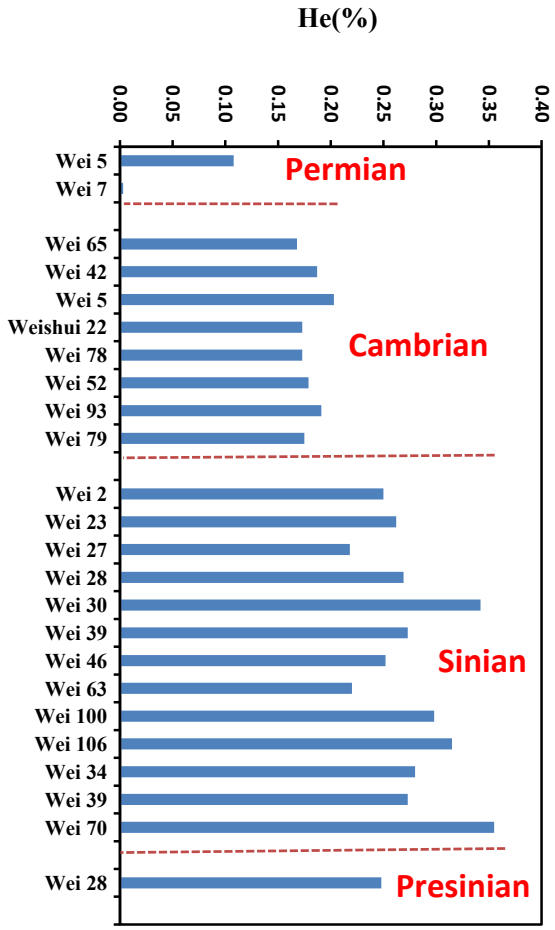

Figure 2 Helium content in different layers of Weiyuan gas field.

Geochemistry Characteristics of tight sandstone Gas in Xujiahe Formation of the Upper Triassic in Sichuan Basin, China

Shizhen Tao[1], Jingkui Mi[1], Shengfei Qin[1], Weibo Zhao[2], Zhenglian Pang[1]

[1]*Research Institute of Petroleum Exploration & Development (RIPED), PetroChina, P. R. China*
[2]*Research Institute of Petroleum Exploration & Development of Changqing Oilfield Company, PetroChina, P. R. China*

Corresponding Author: *tsz@petrochina.com.cn*

Terrestrial tight sandstone gas is abundant Xujiahe (XJH) Formation in Sichuan Basin, China (Figure 1). Its reserve is over $0.6\times10^{12}m^3$. Though has such a huge reserve, origin and evolution of this tight sandstone gas haven't been studied thoroughly.

This study is to clarify geochemical characteristics of gas formation and evolution in XJH Formation based on the comparative geochemical analysis of gas samples from fluid inclusions and gas fields. Experiments showed the great differences between gas in inclusions and from fields. There are low-medium maturity coal-derived tight sandstone gases in XJH Formation. Source rocks are mainly kerogen type-II_2 and III, but coal series are type-III. The Ro is 0.8-1.4%. They are presently at post-mature to early high-mature stage, but the gas/oil ratio in present gas reservoirs is high. XJH reservoir rocks have large amount of gaseous hydrocarbon inclusions, few liquid hydrocarbon inclusions, indicating coal series type generates mainly gas [Dai et al., 1997; 2012]. XJH natural gas is dominated by methane, with higher concentration of heavier C_{2+} hydrocarbons, belonging to kerogen-degraded gas. The gas dryness ratios are normally less than 0.95, mainly wet gas. The content of methane in the inclusions is low, rather lower for those of C_{2+} hydrocarbons, while that of non-hydrocarbons (CO_2) is higher.

Isotopic features show that tight sandstone gas of XJH Formation is typical coal-derived gas. The gas $\delta^{13}C_1$ ranges from -45.5‰ to -36.5‰ and $\delta^{13}C_2$ from -30‰ to -25‰. The $\delta^{13}C_1$ and $\delta^{13}C_2$ in fluid inclusions are similar, but mostly slightly heavier, with a $\delta^{13}C_1$ of -36‰~-45‰ and $\delta^{13}C_2$ of -24.8‰~-28.1‰ (Figure 2), characterized as coal-type gas. The $\delta^{13}C_{CO2}$ of gas from fields ranges from -15.6‰ to -5.6‰, and that of inclusions is lighter, ranging from -16.6‰ to -9‰, which is organic origin. The CO_2 captured in the inclusions in a relatively closed system, characterizing as heavier carbon isotopic composition for alkane gas and lighter for that of CO_2, was derived from source rocks, and biogenic CO_2 was mixed less. The gases in inclusions reflect primitive state when source rocks were generating gas, and rather weak isotopic filtration for gases in a closed system, thus it is characterized as heavier carbon isotopes for alkane gas and lighter for non-hydrocarbon CO_2.

In short, the causes of the difference between gases from inclusions and reservoirs are the maturity of source rock, migration fractionation effect and contamination of water soluble gas.

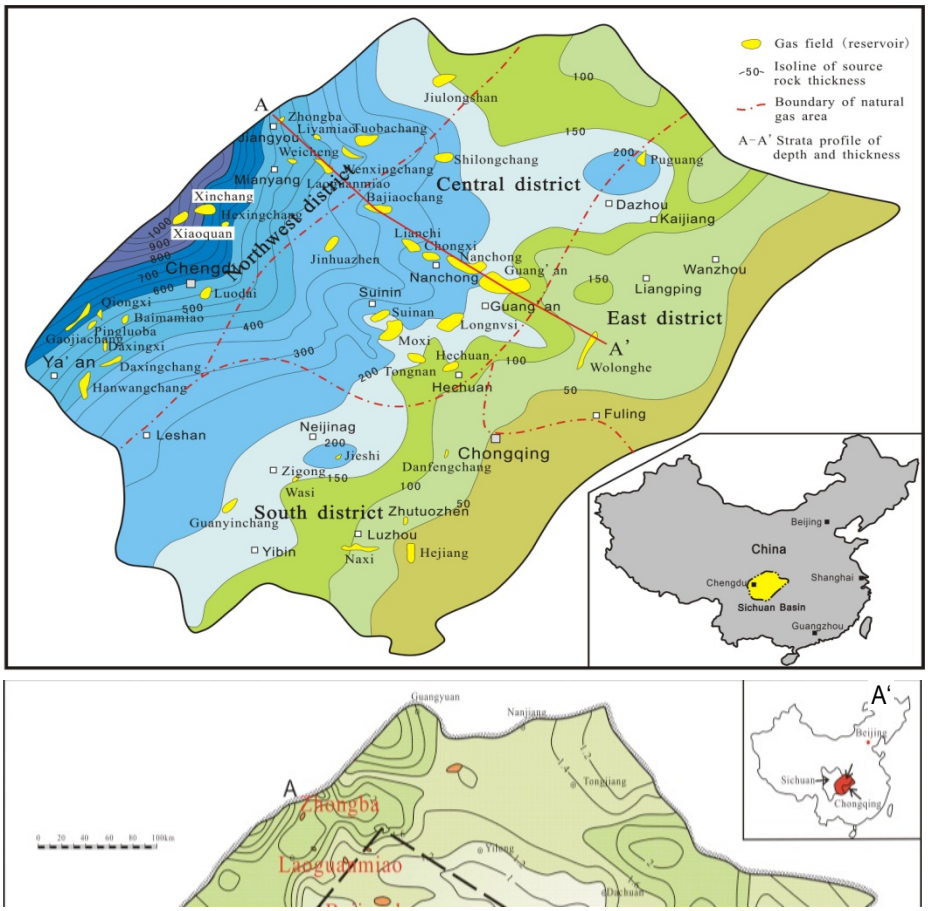

Figure 1 The distribution of the Xujiahe Formation source rock and gas fields in the Sichuan Basin.

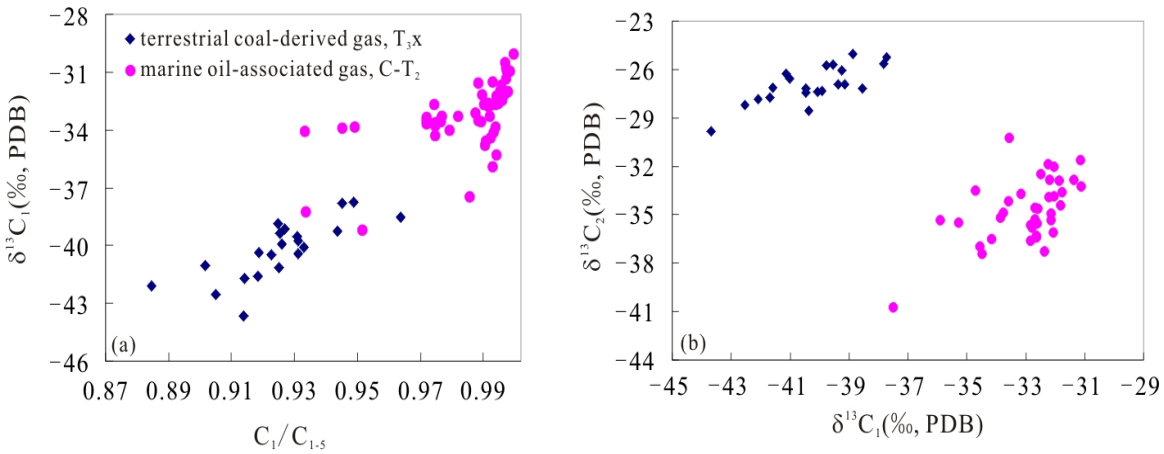

Figure 2 $\delta^{13}C_1$-C_1-5(left) and $\delta^{13}C_2$-$\delta^{13}C_1$(right) diagrams of Xujiahe Formation-reservoired natural gas in central Sichuan Basin.

Aromatic Hydrocarbon Demethylation--A Possible Mechanism Causing the Carbon Isotope Series Reversal in High-Over Mature Coal-derived Gas

Weilong Peng[1,2], Quanyou Liu[2], Qingqiang Meng[2], Dongya Zhu[2]

[1]*State Key Laboratory of Shale Oil and Gas Enrichment Mechanisms and Effective Development, SINOPEC, China*
[2]*Petroleum Exploration & Production Research Institute, SINOPEC, China*

Corresponding Author: *pengwl26@yeah.net*

Natural gas has the plurality of gas parent material and the diversity of gas-generation mechanism, which attracts a large number of scholars to investigate the formation mechanism of natural gas. After years of studies, the theory of natural gas formation has made great progress, but with the exploration target gradually turning to deep and unconventional gas, new problems are encountered [Liu et al., 2019]. For example, geochemical anomalies often occur in coal-derived gas at high over-mature stage, including reversal of carbon isotope series of alkane gas, rollover of carbon isotope and even negative carbon isotope series. Scholars have made useful explorations on the abnormal geochemical phenomena of natural gas. While a series of achievements have been made, there are still disputes among different viewpoints [Dai et al., 2004]. The long-standing controversy of multiple viewpoints reflects the complexity of the problem and the limitations of current understanding. In view of the fact that the gas reservoirs discovered are mainly formed by the thermal maturation of organic matter, and that the simulation experiment can dynamically study the whole process of gas generation, thermal simulation experiment is considered to be one of the most effective ways to study the formation of natural gas [Peng et al., 2018]. In order to further understand the formation mechanism of natural gas and provide theoretical basis for natural gas exploration, the thermal simulation experiments of coal and high-purity toluene are used to study the mechanism of carbon isotope fractionation during the formation of coal-derived gas, mainly based on the analysis of geochemical parameters of natural gas and previous studies.

By calculating the geochemical parameters such as the relative content of components and the abundance of organic matter, the productivity of thermal simulated gases can be obtained, and the gas generating potential of coal can be studied. The maximum CH_4 yields of the selected Ordos Basin (China) sample were 229.41 ml/g TOC and 302.26 ml/g TOC in the rapid heating (20°C/h) and slow heating (2°C/h) experiments, respectively. The maximum yields of alkane gas with rapid and slow heating were 230.16 ml/g TOC and 320.74 ml/g TOC, respectively. The relative content of CH_4 in both rapid and slow heating experiments is increasing with the temperatures, and at the same temperature point, the relative content of CH_4 in rapid heating is lower than that in slow heating method. The distribution ranges of $\delta^{13}C_1$ values of products from rapid and slow heating products were −34.8‰~−23.6‰ and −35.5‰~−24.0‰, respectively. The distribution ranges of $\delta^{13}C_2$ values of products from rapid and slow heating products were −28.0‰~−9.0‰ and −28.9‰~−8.3‰, respectively. The distribution ranges of $\delta^{13}C_3$ values of products from rapid and slow heating products were −25.8‰~−14.7‰ and −26.4‰~−13.2‰, respectively. It is noteworthy that the rollover phenomena of the values of $\delta^{13}C_2$ and$\delta^{13}C_3$ found in this experiment at high temperature (the isotope values of $\delta^{13}C_2$ and $\delta^{13}C_3$ become more negative after the maximum values of $\delta^{13}C_2$ and $\delta^{13}C_3$ at high temperature stage) (Figure 1).

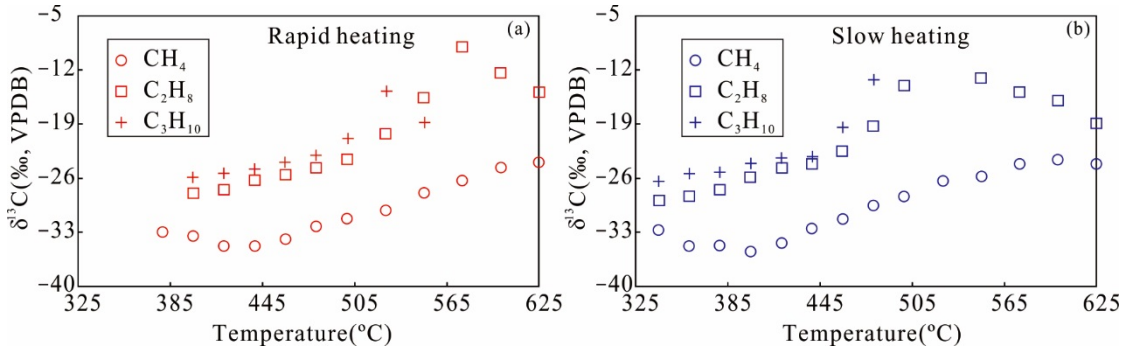

Figure 1 Law mature coal of the Ordos Basin: (a) $\delta^{13}C$ characteristics of rapid heating; (b) $\delta^{13}C$ characteristics of slow heating.

In this thermal simulation experiment of gold tube of coal, only one temperature point carbon isotope reversal occurred, but in the high temperature stage, carbon isotope rollover of $\delta^{13}C_2$ and $\delta^{13}C_3$ occurred (Figure 1). It is noteworthy that carbon isotope series reversal and negative carbon isotope series have been confirmed by scholars in many gas reservoirs, and previous research show that isotope reversal can occur in coal-derived gas in the high-over mature stage. This indicates that the natural gas in the high-over mature stage may be the key factor causing the anomalous geochemical characteristics, and further illustrates the complexity of the formation mechanism of the high-over mature natural gas [Hill et al., 2003]. We believe that the reversal of carbon isotope values of heavy hydrocarbon gas in the over mature stage may indicate that the source of heavy hydrocarbon gas has changed in the over mature stage. We speculate that there is a new source of heavy hydrocarbon gas in the over mature stage. In order to further analyze this phenomenon, we consider it necessary to start with the thermal maturation structure of organic matter. With the thermal maturation of source rock, both sapropelic and humic organic matter will continuously enrich carbon and dehydrogenate, aromatize or graphitize organic matter. In the over mature stage, the source rocks contain a large number of aromatic ring structures, and aromatic ring demethylation should be the main mode of gas generation (Figure 2). Starting from the thermal simulation experiment of aromatic hydrocarbons should be a good point for studying the formation mechanism of natural gas at high-over mature stages. Because humic organic matter contains more aromatic ring structures, aromatic ring demethylation of humic organic matter is intense in the over mature stage. Whether humic or sapropelic organic matter is in over mature stage, CH_4 should be the gas generated when methyl side chain is removed from the structure of organic matter in theory. However, the exploration results and thermal simulation experiments confirm that both simulated gas and coal-derived gas at high-over mature stages contain a certain amount of heavy hydrocarbon gas, which may contain heavy hydrocarbon gas formed by the early stage of organic matter, but the carbon isotope reversal of heavy hydrocarbon gas indicates that heavy hydrocarbon gas with more negative carbon isotope value must be formed. Although only one temperature point in this coal thermal simulation experiment has obvious carbon isotope reversal, many discovered natural gas does have carbon isotope reversal characteristics at high-over mature stage.

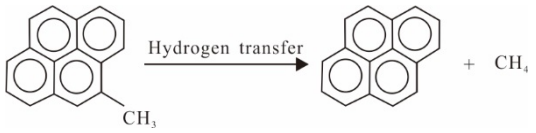

Figure 2 Demethylation of aromatic hydrocarbons to form CH_4.

In order to further explore the formation mechanism of natural gas at high-over mature stage, we take toluene as an example to study the characteristics of aromatic hydrocarbon pyrolysis products, so as to compare and study the geochemical characteristics of products in high-over mature stage of source rocks. The thermal simulation gas generation experiments of toluene in gold tubes at different temperatures were carried out. Because of the high stability of aromatic compounds, the temperature of aromatic compounds increased rapidly to the target temperature at 20°C/h, and then kept constant for 72 hours. It was found that not only CH_4 but also a small amount of heavy hydrocarbon gas were formed in the toluene thermal simulation experiment, and the carbon isotope reversal of alkane gas was formed in the toluene thermal simulation products. Gas products were detected after 450°C in toluene thermal simulation experiment. We believe that in the high mature stage, on the one hand, the droped methyl can be hydrogenated to form CH_4; on the other hand, the link between methyl and methyl can form a small amount of C_2H_6. Carbon isotope rollover was also found in C_3H_8 pyrolysis at 550°C, and carbon isotope reversal did occur in the pyrolysis products of toluene (450°C). With the increase of simulated temperature, the carbon isotopes of toluene pyrolysis products also exhibit fractionation effect. It is suggested that the formation of CH_4 is due to the demethylation of aromatic rings in kerogen and the formation of heavy hydrocarbon gas is due to the polymerization of methyl groups at the later stage. Because of the stability of aromatic compounds, the short side chains of aromatic structures in kerogen fall off later. The isotope fractionation effect of aromatic compounds lags behind that of kerogen cracking gas and retained hydrocarbons cracking gas in the early stage. The formation and cracking of heavy hydrocarbon gas is also in a dynamic state at high temperature. There are heavy hydrocarbon gases cracked under high temperature, but also a small amount of heavy hydrocarbon gases formed by aromatic ring demethylation at high temperatures. There is inconsistency between the isotope fractionation effect of early formed natural gas and that of late formed natural gas, that is, the carbon isotope fractionation of late formed natural gas lags behind. When organic matter evolves into its structure, mainly aromatic methyl side chains, the methyl carbon isotopes falling off at this time are usually heavier than those falling off at relatively low evolution stages. When organic matter evolves to the side chain mainly being aromatic methyl, the methyl carbon isotopes that fall off are usually heavier than those that fall off at relatively low matured stages. However, it does not mean that all the methyl groups falling off the coal structure at this time are $-^{13}CH_3$, and there are also a lot of $-^{12}CH_3$, but there are more $-^{13}CH_3$ in the methyl groups falling off the coal structure at lower maturity. That is to say, the methyl groups falling off from coal structure both have$-^{12}CH_3$ and $-^{13}CH_3$. In the process of forming C_2H_6 and C_3H_8 by further joining methyl from coal structure, because the mass of $-^{12}CH_3$ is lighter than that of $-^{13}CH_3$ and its energy and chemical activity are stronger, the probability of $-^{12}CH_3$ and $-^{12}CH_3$ joining is higher than that of $-^{12}CH_3$ and $-^{13}CH_3$ joining, which leads to more ^{12}C in C_2H_6 and C_3H_8 formed by methyl joining. Therefore, it is possible that $\delta^{13}C_2$ is more negative than $\delta^{13}C_1$ and $\delta^{13}C_3$ is more negative than $\delta^{13}C_2$. A very small amount of C_2H_6 and C_3H_8 formed at this stage of high-over mature may cause isotope anomalies, such as carbon isotope rollover. If the rollover results in $\delta^{13}C_2 > \delta^{13}C_3$ to a certain extent, partial reversal of C_2H_6 and C_3H_8 carbon isotopes will be formed. If $\delta^{13}C_1 > \delta^{13}C_2$, partial reversal of CH_4 and C_2H_6 carbon isotopes is formed. Therefore, the carbon isotope fractionation effect of organic matter in the process of aromatic ring demethylation and methyl bonding to form heavy hydrocarbon gas at high maturity stage may be an important reason for the formation of anomalous geochemical phenomena such as carbon isotope series inversion or reversal of coal-derived gas at high matured stage.

References

Dai J., Xia X., Qin S., Zhao J., (2004). *Origins of partially reversed alkane $\delta^{13}C$ values for biogenic gases in China*. Organic Geochemistry, 35(4): 405-411.

Peng W., Hu G., Liu Q., Jia N., Fang C., Gong D., Yu C., Lyu Y., Wang P., Feng Z., (2018). *Research status on thermal simulation experiment and several issues of*. Journal of Natural Gas Geoscience, 3, 283-293.

Hill RJ, Tang Y, Kaplan I., (2003). *Insight into cracking based on laboratory experiments*. Organic Geochemistry, 34(12), 1651-1672.

Liu Q., Wu X., Wang X., Jin Z., Zhu D., Meng Q., Huang S., Liu J., Fu Q., (2019). *Carbon and hydrogen isotopes of methane, ethane, and propane: A review of genetic identification of natural gas*. Earth-Science Reviews, 190, 247-272.

Discussion on Genesis and Origins of Natural Gases in Middle Assemblages from Jingbian Gas Field in the Ordos Basin, China

Xiaobo Wang[1,2,3], Caineng Zou[2,3], Jian Li[1,2,3], Guoqi Wei[2,3], Zengye Xie[1,2,3], ChunLin Zhang[1,2,3], Jianying Guo[1,2,3], Zhisheng Li[1,2,3], Yifeng Wang[1,2,3], Sonqi Pan[1,2,3], Chunlong Yang[1,2,3]

[1]*Gas Geology Research Center of PetroChina Research Institute of Petroleum Exploration & Development, China*
[2]*PetroChina Research Institute of Petroleum Exploration & Development, China*
[3]*Key Laboratory of Gas Reservoir Formation and Development, CNPC, China*

Corresponding Author: *Wangxb69@petrochina.com.cn*

The Jingbian gas field, Which is a large-scale lithologic-paleogeomorphic weathering crust gas reservoir of marine carbonate rocks with the largest gas reserves in single layer in China, has been discovered in the upper assemblages (Mawu1-Mawu4) of the Majiagou Formation of the Ordovician [Dai et al., 2005].In recent years, with the deepening of gas exploration and researches on Jingbian gas field, great breakthroughs have been made in the dolomite type of the Middle assemblages (Mawu5-Mawu10) of the Majiagou Formation of the Ordovician in the new formation[Yang et al., 2009; 2011], showing a good gas exploration prospects. The genesis and origins of natural gases in Middle assemblages of the Jingbian Gas Field in the Ordos Basin are systematically discussed by means of geochemistry and geological researches.

The main research results are followed as: The natural gases in middle assemblages of Jingbian Gas Filed have the characteristics of high methane content, low heavy hydrocarbon content, non-hydrocarbon gas nitrogen and carbon dioxide, high drying coefficient. The carbon isotopic values of methane, ethane and propane in the middle assemblages are generally slightly lighter than the upper Paleozoic gases with some samples are partial reversed. The natural gas in middle assemblages in Jingxi area is mainly coal-formed gas, while in the center and eastern of Jingbian area it is mainly oil-derived gas. The coal-formed gases in middle assemblages are mainly from the Upper Paleozoic Carbonate-Permian coal-series source rocks, while the oil-derived gas in in middle assemblages are mainly from the lower Paleozoic Ordovician marine source rocks.

References

Dai J.X., Li J., Luo X. et al., (2005). *Alkane carbon isotopic composition and gas source in giant gas fields of Ordos Basin*. Acta Petrolei Sinica, 26(1), 18-26.

Yang H., Zhang W.Z., Zan C.L. et al., (2009). *Geochemical Characteristics of Ordovician Subsalt Gas Reservoir and Their Significance for Re understanding the Gas Source of Jingbian Gas field, East Ordos Basin*. Natural Gas Geoscience, 20(1), 8-14.

Yang H., Bao H.P., (2011). *Characteristics of hydrocarbon accumulation in the Middle Ordovician assemblages and their significances for gas exploration in the Ordos Basin*. Natural Gas Industry, 31(12), 11-20.

Genetic types and source of H_2S-bearing gas in the Middle Triassic Leikoupo Formation in the Western Sichuan Depression, China

Xiaoqi Wu[1], Quanyou Liu[2], Yingbin Chen[1], Changbo Zhai[1], Yanqing Wang[1]

[1]*Exploration and Development Center in the Sichuan area, Petroleum Exploration and Production Research Institute, SINOPEC, China*
[2]*Petroleum Exploration and Production Research Institute, SINOPEC, China*

Corresponding Authors: *xqwu@163.com*

Natural gas exploration in the Middle Triassic Leikoupo Formation (T_2l) in the Western Sichuan Depression has achieved great breakthrough continuously in recent years [Li et al., 2016]. The genetic identification of natural gas is notably important for assessment of its sources [Liu et al., 2019]. There is no consensus on the genetic types and source of H_2S-bearing gas in the T_2l, which results from the complicated geochemical characteristics of natural gas and existence of multiple sets of potential source rocks.

The study on gas geochemistry indicates that the T_2l gas is extremely dry (C_1/C_{1-4}>0.99) and contains H_2S. Several gas samples have high CO_2 contents due to the acid fracturing on the reservoirs, and the other gas samples display positive correlation between H_2S and CO_2 contents, suggesting the alteration of thermochemical sulfate reduction (TSR). The $\delta^{13}C_1$ and $\delta^{13}C_2$ values range from -34.0‰ to -30.3‰ and from -34.8‰ to -29.6‰, respectively. The δ^2H_{CH4} values range from -157‰ to -136‰ and are positively correlated with the $\delta^{13}C_1$ values, which suggest the maturity trend. The high $\delta^{13}C_{CO2}$ values (-7.3‰ to +3.3‰) suggest inorganic origin. The geochemical difference of gases results from the maturity difference rather the large-scale lateral migration. The T_2l gas is identified as secondary oil-cracking gas.

The comparison of $\delta^{13}C$ values between ethane and kerogen indicates that, the T_2l gas has a good affinity with the Upper Permian Longtan Formation (P_3l) argillaceous source rocks and T_2l carbonate source rocks. However, the T_2l source rocks have TOC contents mainly lower than 0.4%, and only a few rock samples with TOC>0.4% have certain hydrocarbon potentials. The biomarkers indicate that the solid bitumen in the reservoirs are mainly derived from the T_2l carbonate source rocks. However, the solid bitumen are in a very limited scale, which suggests that the reservoirs have experienced direct filling of natural gas rather than the accumulation and subsequent cracking of large-scale oil pools. According to the gas accumulation models [Galimov, 2006], the T_2l gas follows the instantaneous accumulation model of the P_3l source rocks in the over-mature stage, rather than the cumulative model of the T_2l source rocks. Therefore, the T_2l gas is mainly derived from the P_3l argillaceous source rocks, and the gas reservoirs are accumulated by direct filling of secondary oil-cracking gas, with only a few contribution by the T_2l carbonate source rocks.

References

Galimov E.M., (2006). *Isotope organic geochemistry*. Organic Geochemistry, 37(10): 1200-1262.

Li S., Xu G., Song X., (2016). *Forming conditions of Pengzhou large gas field of Leikoupo Formation in Longmenshan piedmont tectonic belt, western Sichuan Basin*. China Petroleum Exploration, 21(3): 74-82.

Liu Q., Wu X., Wang X., Jin Z., Zhu D., Meng Q., Huang S., Liu J., Fu Q., (2019). *Carbon and hydrogen isotopes of methane, ethane, and propane: A review of genetic identification of natural gas*. Earth-Science Reviews, 190: 247-272.

Long-term variations of acid gas trapping in different mechanisms in carbonate formations of Tarim basin, China

Xiaoyan Zhang[1,2], Qi Li[1,2], Liange Zheng[3], Xiaying Li[1,2], Liang Xu[1,2]

[1]*State Key Laboratory of Geomechanics and Geotechnical Engineering, Institute of Rock and Soil Mechanics, Chinese Academy of Sciences, China*
[2]*University of Chinese Academy of Sciences, China*
[3]*Energy Geoscience Division, Lawrence Berkeley National Laboratory, Berkeley, USA*

Corresponding Author: *zhangxiaoyan_92@163.com*

An enormous amount of acid gas, containing carbon dioxide (CO_2) and hydrogen sulphide (H_2S), is generated in the exploitation of oil and gas reservoirs in Tarim basin, China, and appropriate engineering management is required. Injection of acid gas into deep formation is one of viable strategies - it mitigates the emission of greenhouse gases and reduces the cost of the desulfurization. Key issues including the potential physical and geochemical impacts and trapping evolution should be fully investigated. Reactive transport simulation based on the mineralogical composition and hydrochemical characteristics of carbonate formation in Tarim basin, was conducted to identify the physical and geochemical interactions of acid gas with mineral matrix and formation water. Acid gas (59% CO_2 and 41% H_2S) was injected at a constant rate of 19200 Nm^3/d for 25 years, and the simulation was run for a period of 10000 years by the TMVR_EOSG module of TOUGHREACT code. The results indicate that the maximum gas saturation is 0.27, and the pressure buildup region extends in the whole domain though the effect is not obvious. Due to the preferential dissolution of H_2S, the maximum mass fraction of CO_2 in gas phase is almost 1, then decreases to 59% when the mass fraction of H_2S increases to 41%. With the addition of weaker acidity of H_2S, pH decreases sharply and subsequently increases slightly. Small changes of calcite and quartz occur, thus porosity nearly remain constant. The dissolution trapping of H_2S is higher than that of CO_2 after acid gas injection. In terms of the acid gas mixture, 54% is trapped by dissolution trapping at the end of injection. The results improve the understanding of the acid gas injection and provide insight for the in-site engineering practice in Tarim basin, China.

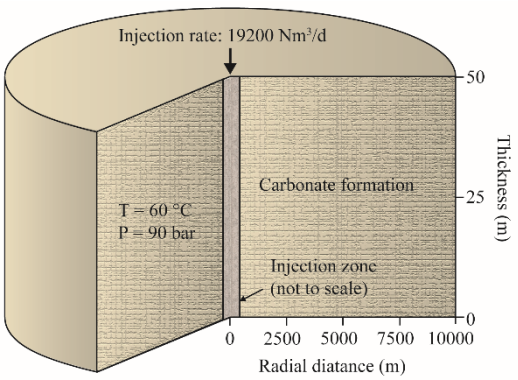

Figure 1 Schematic diagram of the 1D radial model.

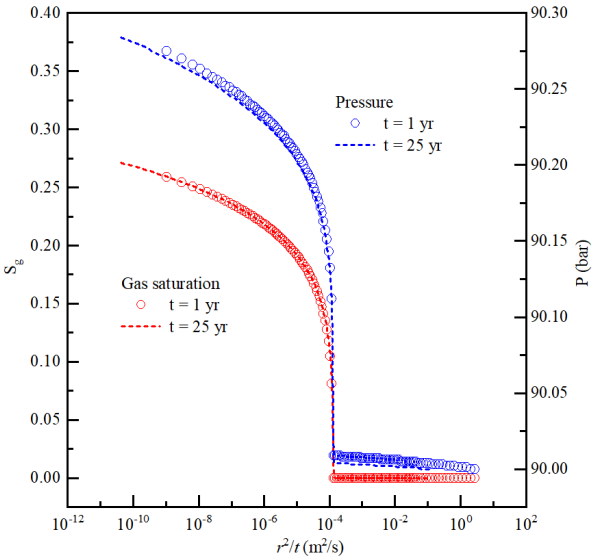

Figure 2 Simulated gas saturation and pressure as a function of the similarity variable.

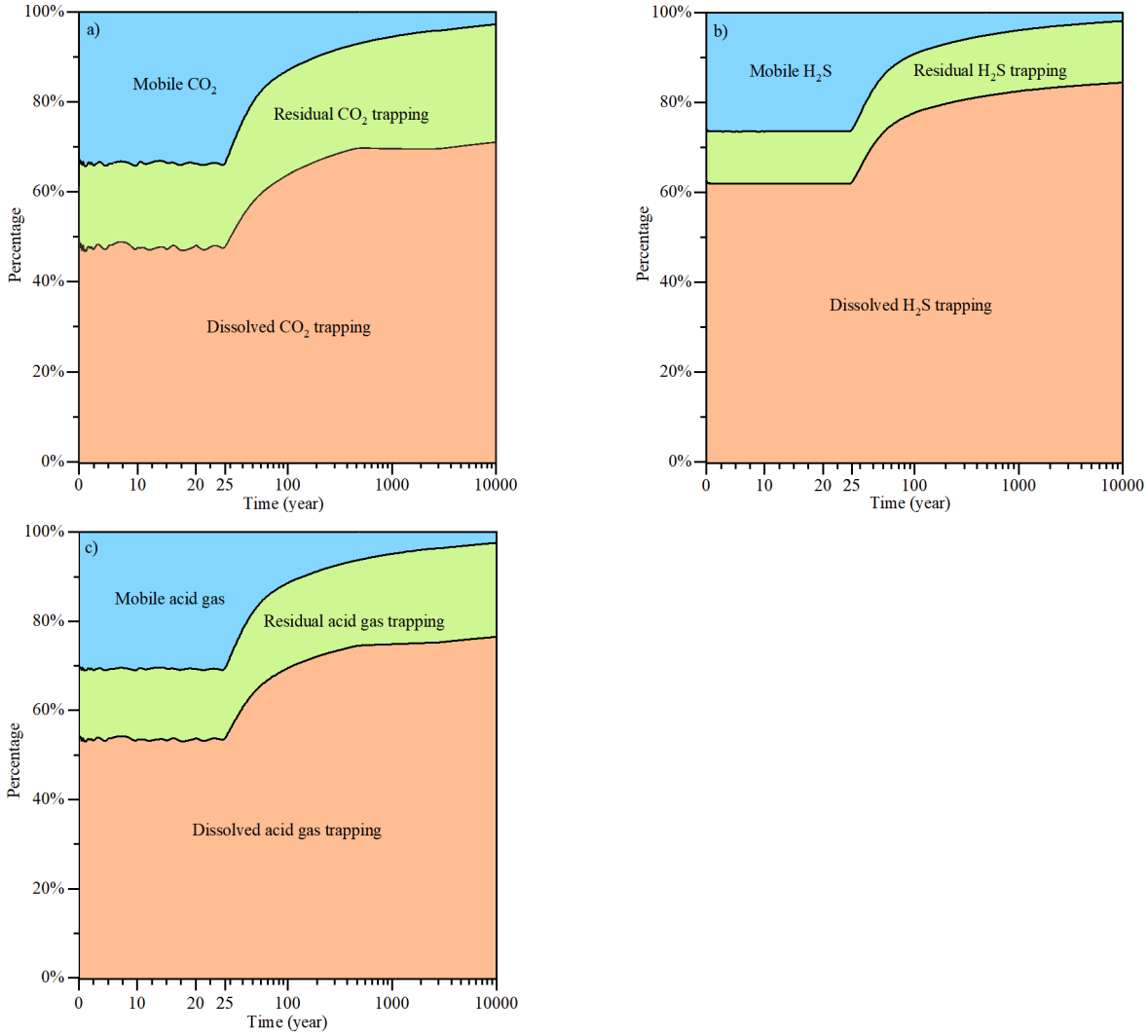

Figure 3 Evolution of a) CO_2, b) H_2S, c) acid gas trapping at different times.

References

Bacon D.H. et al., (2014). *Simulating geologic co-sequestration of carbon dioxide and hydrogen sulfide in a basalt formation*. International Journal of Greenhouse Gas Control, 21: 165-176.

De Silva G.P.D., Ranjith P.G. and Perera M.S.A., (2015). *Geochemical aspects of CO_2 sequestration in deep saline aquifers: A review*. Fuel, 155: 128-143.

Talman S., (2015). *Subsurface geochemical fate and effects of impurities contained in a CO_2 stream injected into a deep saline aquifer: What is known*. International Journal of Greenhouse Gas Control, 40: 267-291.

Xu T.F. et al., (2007). *Numerical modeling of injection and mineral trapping of CO_2 with H_2S and SO_2 in a sandstone formation*. Chemical Geology, 242: 319-346.

Zhang W., Xu T.F., Li Y.L., (2011). *Modeling of fate and transport of coinjection of H_2S with CO_2 in deep saline formations*. Journal of Geophysical Research Solid Earth, 116: B02202.

Zheng L.G. et al., (2013). *On modeling the potential impacts of CO_2 sequestration on shallow groundwater: Transport of organics and co-injected H_2S by supercritical CO_2 to shallow aquifers*. International Journal of Greenhouse Gas Control, 14: 113-127.

Influence of biodegradation on the gas generation behaviour of crude oils

Yuhong Liao[1,2], Weimin Liu[1,2], Yinhua Pan[1], Xiaofeng Wang[3], Yunpeng Wang[1], Ping'An Peng[1]

[1]*State Key Laboratory of Organic Geochemistry, Guangzhou Institute of Geochemistry, Chinese Academy of Sciences, PR China*
[2]*University of Chinese Academy of Sciences, Yuquan Road, PR China*
[3]*State Key Laboratory of Continental Dynamics, Department of Geology, Northwest University, China*

Corresponding author: *liaoyh@gig.ac.cn.*

Due to multi-stage tectonic movements, quite a few paleo-oil reservoirs in typical superimposed basins of China suffered huge variations in burial depth, such as the Central Sichuan Uplift of the Sichuan Basin (Figure 1) [Zou et al., 2014] and the Tarim Basin [Zhang et al., 2004]. Such burial depth variations can result in complicated secondary alterations. Typically, due to low burial depth or severe denudation, the oil reservoirs in superimposed basins used to experience biodegradation at the early stage, and succeeded by thermal alteration at the late stage. Here, we call them superimposed secondary alteration. Biodegradation could significantly alter the chemical compositions and molecular structures of in-reservoir oils, including both hydrocarbon and non-hydrocarbon fractions [Liao et al., 2009; Pan et al., 2015]. Thus biodegradation of crude oils may affect their gas generation behavior, gas generation potentials and pyrobitumen yields. A lack of knowledge about such influence may cause deviations in hydrocarbon gas generation potential/resource evaluation and hydrocarbon gas generation stage judgment. In this work, a sequence of crude oil and bitumen sand that are of identical origin but at different biodegradation stages (from non-biodegraded to severely biodegraded) were collected from the Liaohe Basin of China (Table 1). The non-biodegraded oil and the biodegraded bitumens were heated in a closed system to evaluate the impacts of biodegradation on the gas generation of residual oils.

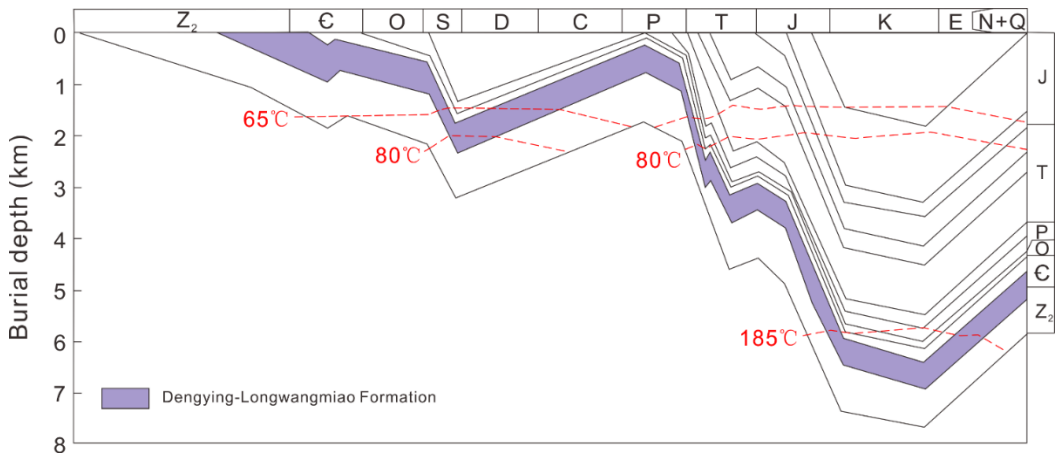

Figure 1 The reconstructed thermal history of Moxi-Gaoshiti area in the Sichuan Basin, modified from Zou et al., [2014].

Table 1 Properties of Liaohe crude oil and extracted bitumen.

Samp. ID	$\delta^{13}C$ (‰)	Biodegradation scale (PM level)	SARA (wt%)				Biomarker parameters			
			Sat.	Aro.	Res.	Asph.	H_{30}/TT_{23}	$C_{27}RS/S_{22}$	$C_{28}RS/S_{22}$	$C_{29}RS/S_{22}$
L-0	-29.2	0	60.9	14.4	20.2	4.5	50.2	17.8	32.3	35.4
L-2	-29.4	2-3	41.5	13.3	33.8	11.3	42.3	16.7	26.4	33.2
L-5	-30.2	5-6	26.6	14.6	42.4	16.5	34.8	5.9	7.8	11.2
L-8	-30.0	8	18.8	11.8	40.3	29.0	11.1	0.4	1.3	3.4

Our results show that the hydrocarbon gas generation potentials are significantly reduced at the slight to moderate biodegradation stage, as with the removal of normal and branched alkanes. Besides, hydrocarbon gases generated from the more severely biodegraded oils are also drier, attributable to the decreasing yields of C_2-C_5 gases and the increasing yields of methane. At low thermal maturity levels, the methane generated from more severely biodegraded oils is relatively enriched in ^{13}C. Furthermore, the kinetic modeling results suggest that the moderately and severely biodegraded oils are thermally less stable than the non-biodegraded and slightly biodegraded oils. The bulk hydrocarbon gas yields from the non-biodegraded oil do not exceed those from the moderately biodegraded oils until EasyRo > 1.6%. In EasyRo% range of 1.6~2.5, pyro-bitumens yielded by heavily-severely biodegraded oils were about 2~4 times that of non-biodegraded oil. In other word, the gas yields normalized by the weight of pyro-bitumen from heavily-severely biodegraded oil is only 1/4~1/2 of the gas yield of non-biodegraded oil. Therefore, hydrocarbon gas generation resource evaluation based on pyrobitumen content should be very careful if superimposed alteration used to occur in the oil reservoir.

References

Liao Y., Geng A., Huang H., (2009). *The influence of biodegradation on resins and asphaltenes in the Liaohe Basin [J]*. Organic Geochemistry, 40(3), 312-320.

Pan Y., Liao Y., Zheng Y., (2015). *Effect of biodegradation on the molecular composition and structure of asphaltenes: Clues from quantitative Py-GC and THM-GC*. Organic Geochemistry, 86, 32-44.

Zhang S., Wang Z., Wang F., Liang D., (2004). *Oil accumulation history in Tadong 2 oil reservoir in Tarim Basin, NW China - A case study of oil stability and cracking*. Petroleum Exploration and Development, 31, 25-30.

Zou C., Du J., Xu C., Wang Z., Zhang B., Wei G., Wang T., Yao G., Deng S., Liu J., Zhou H., Xu A., Yang Z., Jiang H., Gu Z., (2014). *Formation, distribution, resource potential, and discovery of Sinian-Cambrian giant gas field, Sichuan Basin, SW China*. Petroleum Exploration and Development, 41, 306-325 (In Chinese with English Abstract).

Stable carbon and hydrogen isotopes of the natural gases from Central Sichuan Basin, China and its implications

Yunyan Ni, Jianping Chen, Fengrong Liao, Limiao Yao, Jinliang Gao

Research Institute of Petroleum Exploration and Development, PetroChina, China

Corresponding Author: *niyy@petrochina.com.cn*

Carbon and hydrogen are fundamental elements for natural gas and the research of their isotope ratio is an important method to understand gas generation, migration and gas-source correlation. Compared with the carbon isotope, hydrogen isotope has the ability to better reflect the changes of geochemical environments due to the fact that hydrogen has the largest range of stable isotope ratios because of the largest mass difference between H and D. Sichuan Basin is one of the most important gas enriched basins in China and the Upper Triassic Xujiahe Formation has been a set of significant source rocks for the coal-derived gases. However, disagreements exist about the depositional environment of this formation. Bases on the analysis of the components and carbon and hydrogen isotopes of gases from the Triassic Xujiahe and other formations in the Sichuan, this study investigated the gas origin, gas source correlation and depositional environment of source rocks for the gases from Xujiahe Formation in the Central Sichuan Basin, China.

The results show that gas from the Xujiahe Formation is mainly coal-derived gas and dominated by methane. The content of methane is 67.89% ~ 98.05%, and the content of heavy hydrocarbon (C_{2+}) is 0.42% ~ 16.62%. Except the dry gas (dryness coefficient: 0.991) in the Yuanba area, gases from the Xujiahe Formation in other areas in the Central Sichuan Basin have dryness coefficient less than 0.95, indicative of wet gas. The $\delta^{13}C_1$ value varies from −43.8‰ to −29.2‰, $\delta^{13}C_2$ value ranges from −33.5‰ to -20.7‰, $\delta^{13}C_3$ value is −33.6‰~−19.3‰ and $\delta^{13}C_4$ value is −27.2‰~−22.2‰. The $\delta^{2}H_1$ value is −191‰~-148‰, $\delta^{2}H_2$ value is −165‰~-115‰ and $\delta^{2}H_3$ value is−153‰~-107‰. Methane and its homologues (C_{2-4}) become more enriched in ^{13}C and D with increasing carbon number ($\delta^{13}C_1<\delta^{13}C_2<\delta^{13}C_3<\delta^{13}C_4$, $\delta^{2}H_1<\delta^{2}H_2<\delta^{2}H_3$), which are consistent with the carbon and hydrogen isotopic characteristics of thermogenic gases.

The thermal maturity R_o of natural gas from Xujiahe Formation in Yuanba is 1.09% ~ 1.78%, and the R_o value of the natural gas from Xujiahe Formation in other areas of Central Sichuan Basin is 0.64% ~ 0.92%. Natural gas from the Xujiahe Formation in the Central Sichuan Basin is mainly from the coal measure source rocks of the Xujiahe Formation. Natural gas from the second Member of Xujiahe Formation in Yuanba is mixed gas, i.e., a mixture of the high-mature coal-derived gas from the coal measure source rock of Xujiahe Formation and the Lower Cambrian (Lower Silurian) oil-cracked gas. The $\delta^{2}H$ value of methane from the Xujiahe Formation in the Sichuan Basin is relatively high, >−200‰. Compared to the coal-derived gas from the source rocks formed in limnetic facies with freshwater in the Taibei sag, Turpan-Hami Basin, though at similar thermal maturity, the difference of the $\delta^{2}H$ values of methane can be as high as 90‰, indicating that the source rock of Xujiahe Formation is formed in an environment with water salinization.

Carbon-isotope anomalies of the Lower Silurian shale gas, Sichuan Basin, China Insight from the Rayleigh-type fractionation model

Ziqi Feng[1,2], Fang Hao[1,2], Dazhong Dong[3], Wei Wu[4] And Chen Xie[4]

[1]*School of Geosciences, China University of Petroleum, Qingdao, 266580, China*
[2]*Key Laboratory of Deep Oil and Gas (China University of Petroleum (East China), P. R. China*
[3]*Research Institute of Petroleum Exploration & Development, (PetroChina), China*
[4]*Research institute of Petroleum Exploration and Development, Southwest Oil & Gas Company, PetroChina, China*

Corresponding Author: *ziqi0314@163.com*

Unraveling the geological processes creating the geochemical anomalies of the shale gas in the Sichuan Basin has great significance for understanding the mechanism of gas generation in the late stage. Through the first supplement of gas samples in the southwestern part of the Fuling block and the expanded exploration areas in Changning-Zhaotong and Weiyuan, a systematic comparison study including gas composition, stable carbon, hydrogen and nitrogen isotopic composition, and noble gas component was carried out from the perspective of the Rayleigh-type fractionation model and geological distribution.

The results reveal that the Lower Silurian shale gas is characterized by extraordinarily high methane (>96.11%) and low C_{2+} hydrocarbon (<0.51%). The rest non-hydrocarbon gas is consist of a small amount of N_2 and a mixed source of CO_2. The $\delta^{15}N_{N_2}$ values of the LM shale gases range from -5.2 ‰ to -1.1‰, suggesting the nitrogen is produced from the thermal ammoniation of organic matter at high temperature. Helium component is typical crustal genesis as its concentration range from 144.8 ppm to 237.5 ppm and its R/R_a range from 0.01 to 0.05. Full reversal ($\delta^{13}C_3 < \delta^{13}C_2 < \delta^{13}C_1$) phenomenon and abnormally positive $\delta^{13}C_1$ value constitute the carbon-isotope anomalies of the Lower Silurian shale gas.

Geological distribution of the carbon-isotope composition is controlled by thermal evolution, fault development and shale sealing conditions. This paper first supplements gas samples in the southwestern part of the FL block to comprehensively analyze the isotopic distribution in the Sichuan Basin.

The $\delta^{13}C_1$ and $\delta^{13}C_2$ values in the Fuling block near the fault zone are more positive compared to the values away from the faults, indicating the cumulative effects of diffusion after long-term geological process.

References

Dai J., Zou C., Dong D., Ni Y., Wu W., Gong D., Wang Y., Huang S., Huang J., Fang C. and Liu D., (2016). *Geochemical characteristics of marine and terrestrial shale gas in China*. Marine and Petroleum Geology, v.76, p.44-463.

Guo T. and Zeng P., (2017). *Geological characteristics, resource potential, and key factors for shale gas in the tectonically complex region (in Chinese)*. Beijing, Science Press, 496p.

Hao F.and Zou H., (2013). *Cause of shale gas geochemical anomalies and mechanisms for gas enrichment and depletion in high-maturity shale*. Marine and Petroleum Geology, v. 44, n. 3, p.1-12.

Oil-Gas-Water-Rock Interactions in Mud Volcanoes in Xinjiang, China

Guodong Zheng[1], Wang Xu[1,2], Xiangxian Ma[1], Zhi Chen[3], Zhengfu Guo[4], Wenbin Zhao[4]

[1]*Key Laboratory of Petroleum Resources,Gansu Province / Lanzhou Center for Oil and Gas Rescources, Institute of Geolgy and Geophysics, CAS, P.R. China*
[2]*State Key Laboratory of Oil and Gas Reservoir Geology and Exploitation, Chengdu University of Technology, P.R. China*
[3]*CEA Key Laboratory, Institute of Earthwauake Forcasting, China Earthquake Admintration, P.R. China*
[4]*Key Laboratory of Cenozoic Geology and Environment, Institute of Geolgy and Geophysics, CAS, P.R. China*

Corresponding Author: *gdzhbj@mail.iggcas.ac.cn*

Petroleum-related mud volcanoes are one kind of geofluids emission system with significance to petroleum resources, environmental impacts, natural hazards, and also the tourism resources. A series of samples including emitted gases, formation water, mud, and also their host rocks were collected from the Dushanzi mud volcano system along with one argillite sample distal from the crater for comparison in south margin of the Junggar Basin, NW China. Their mineral and chemical compositions and also iron species were determined using XRD, XRF, and Mössbauer spectroscopy, respectively. The results indicated a series of marked oil-gas-water-rock interactions in the mud volcano systems with the following main changes: 1) chemical and isotopic variations for emitted gases compared with their correlated natural gases from the reservoir nearby; 2) some conversion of clay minerals from smectite into chlorite and illite, and also the precipitation of newly formed calcite and siderite; 3) silicon depletion and significant elemental enrichment of Fe, Mg, Mn, Ca and P; 4) transformation of Fe from ferric species in hematite and smectite into ferrous species in siderite, chlorite, illite and even pyrite. These geochemical reactions likely induced the color change of the original reddish Neogene argillite to the mud breccia in gray or black, resulted of elemental reduction and/or mieneral alteration along with hydrocarbons oxidation, which is so-called bleeaching effect. Such a complex process might be positively contributive to the reduction of greenhouse effort of erupted gases from mud volcanic systems compared to direct emission natural gas from the corrrespoding petroleum reservoirs, and also eventually significant to a better understanding of physical properties such as porosity and permeability of reservoir rocks and also the migration pathways, and even implicable to the evolution of long-term stability of geologically sequenced carbon dioxide.

References

Xu et al. (2017). *Acta Geol. Sinica* 92, 2201-2213.

Chen et al., (2018). *Carbon isotope variations in inorganic carbon materials: Implications for mud volcanic carbon cycling in the northern Tianshan fold zone, Xinjiang, China.* Appl. Geochem. 97, 32-39.

Ji et al., (2018). *Characteristics of mixed sporopollen assemblage from sediments of Dushanzi mud volcano in southern Junggar Basin and indication to the source of mud and debris ejecta*. Mar. Petro. Geol., 89, 194-201.

Zheng et al., (2017). *Gas geochemistry and methane emission from Dushanzi mud volcanoes in the southern Junggar Basin. NW China.* J. Asia Earth Sci. 149, 184-190.

Zheng et al., (2010). *Chemical speciation of redox sensitive elements during hydrocarbon leaching in the Junggar Basin, Northwest China*. J. Asia Earth Sci., 39, 713-723.

Nakada et al., (2011). *A geochemical study on mud volcanoes in the Junggar Basin, China*. Appl. Geochem., 26, 1065-1076.

ST04

GASES IN MARINE ENVIRONMENT

REFERENCE: MANFREDI LONGO

Water column monitoring at CO_2 leaking sites near Panarea Island

Beaubien S.E.[1], De Vittor C.[2], Bigi S.[1], Celussi M.[2], Comici C.[2], Graziani S.[1], Kralj M.[2], Lombardi S.[1], Pacciaroni M.[2] & Viezzoli D.[2]

[1]*Università degli Studi di Roma La Sapienza, Dipartimento di Scienze della Terra, Italy*
[2]*Istituto Nazionale di Oceanografia e di Geofisica Sperimentale-OGS, Trieste, Italy*

Corresponding Author: *stanley.beaubien@uniroma1.it*

Abstract
The fate and transport of geologically produced CO_2 that leaks from the sea floor into the overlying water column has numerous important implications related to large scale carbon cycling and potential impact on marine organisms, and is of interest for the development of improved monitoring techniques and strategies for offshore Carbon Capture and Storage (CCS) sites. The CO_2 leakage areas off the east coast of Panarea Island, Italy provides an excellent environment to study these processes given the wide range of different flux rates in relatively shallow water. The water column at this site was monitored using two completely different but complementary approaches, continuous monitoring along short 2D transects using GasPro pCO_2 sensors and discrete seasonal sampling along a 700 m transect crossing multiple leakage areas. Results are discussed in terms of the movement of CO_2, and associated tracers, in the water column.

Introduction
The release of large volumes of magmatic, mantle and/or thermometamorphic CO_2 from the seafloor into the overlying marine water column is relatively common in volcanic and tectonically active regions world-wide. While direct sampling and analysis of the gas at the release points gives critical information regarding the geological processes in the subsurface, related to genesis and subsequent changes along the flow path, issues related to the fate of the CO_2 once it dissolved and enters the water column is less well studied due to the significant logistical problems associated with monitoring in a harsh and poorly accessible environment.
Instead, the degassing area near Panarea Island, Italy, presents conditions that facilitate this type of study, given that the CO_2 leaks tend to occur in shallow, accessible waters. This area is located 3 km to the east of Panarea on a submerged volcanic platform in 5-30 m deep water. Gas leaks from two main gas-permeable fracture systems (NE-SW and NW-SE) [Esposito et al., 2006], with flux styles and rates ranging from diffuse, gentle bubbling to intense point vents. Most fluid release points are gas only, although some points also release mixed geothermal water / seawater [Tassi et al., 2009]. Aside from occasional gas burst events linked to deep magma activity, the overall flux is relatively stable in both gas chemistry (e.g. 98% CO_2, 1.7% H_2S plus other trace gases) and rates (7-9 x 10^6 L/d) [Caliro et al., 2004]. In addition to the extensive volcanic, tectonic, and geochemical research conducted at Panarea, this site has also been used as a natural laboratory to understand potential risks and improve safety of offshore Carbon Capture and Storage (CCS) sites. This included work conducted within two projects funded by the European Community, RISCS and ECO_2. In the following we present results from both projects, including small-scale continuous and large-scale discrete monitoring of the water column in gas leakage areas.

Small-Scale Temporal Monitoring

Temporal Monitoring Methods

Small, low-power-consuming, and low-cost pCO_2 gas probes ("GasPro") developed by the authors were used for continuous monitoring of the water column [Graziani et al., 2014]. Each GasPro unit is housed in a 200 mm long, 78 mm diameter Plexiglas cylinder. Measurement is based on equilibration of a small-volume headspace, containing a miniature NDIR detector, with the surrounding water via diffusion through a gas permeable membrane. A second, isolated chamber contains control electronics, memory, and batteries. All probes are equipped with a water temperature sensor, while a pressure sensor was mounted on one probe to monitor tidal fluctuations. All probes were programmed to make measurements every 10 minutes. Two experiments were conducted via the deployment of 20 sensors along cross-sections through the Panarea water column. At the first site the units were placed across a 20 m long and 4 m high, vertical water-column transect in 7 m deep water for 5 days. The transect was perpendicular to the main current and to the long-axis of a near-by CO_2-leaking pockmark. At the second site the same units were deployed for 2.5 days along an 8 m long and 6 m high, vertical water-column transect in 20 m deep water. The transect was positioned parallel to the main current direction with the central vertical line located within a strong single bubble flare.

Temporal Monitoring Results

The first monitoring site was chosen due to its vicinity to a well-known pockmark near Bottaro Island, which at present has constant, diffuse degassing from its base but which was originally formed during a strong blow-out event in 2002. The goal of this deployment was to try to image the movement of the dissolved CO_2 plume associated with this pockmark, which, for spatial reference, is located "behind" the plot shown in Figure 1a.

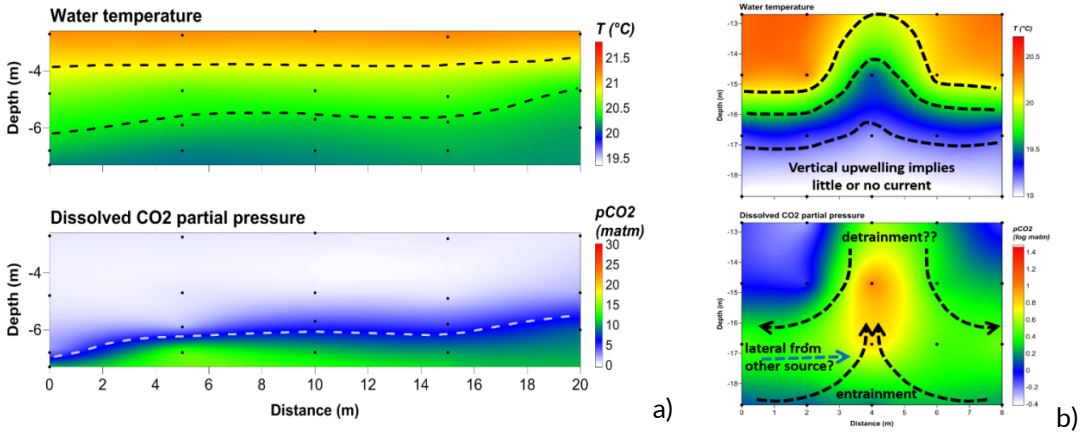

Figure 1 Results from the first (a) and second (b) GasPro grid deployments, with water temperature on the top and CO_2 partial pressure on the bottom. Note the log scale used for the pCO_2 values in (b).

During the observation period there were occasions where a circular or oval anomaly was observed to move into, across, and out of the monitored plane, however the lack of current data makes it difficult to determine the actual origin of these anomalies. Perhaps more interesting, instead, was the strong influence that temperature stratification and storm mixing had on the observed behaviour of dissolved CO_2. The initial period was characterised by calm conditions and strong stratification, with significant basal CO_2 anomalies often entering the plane from the right-hand side (Figure 1a) where waters are

deeper. This behaviour implies upwelling of colder, CO_2 charged waters onto the shallower platform, with vertical mixing limited due to the stable stratification. This behaviour changed suddenly when a storm passed through the area, resulting in efficient water column mixing. During this event, and for the 2-day duration of the monitoring period, CO_2 anomalies were smaller in magnitude and moved more irregularly throughout the entire water column, sometimes even arriving from the top and moving downwards.

The second site was focused on a single bubble flare, with the central line and its four GasPro sensors located directly within the rising bubbles themselves. During this deployment, the weather conditions were much calmer and it is assumed that the main currents at this depth (20 m) were relatively gentle and primarily controlled by tidal processes. One of the most common behaviors observed was the occurrence of a relatively discrete vertical oblong halo around the central bubble flare combined with its impact on the horizontal temperature stratification. An example is shown in Figure 1b, where temperature doming in the center of the transect implies entrainment of deeper colder waters into the bubble stream, potentially also transporting basal waters with higher CO_2 concentrations into the flare core. This observation has implications for CO_2 behavior and efforts to model it, as this will impact on gradients and thus dissolution rates. It is also possible that the higher basal values in this figure may be, in part, a function of the process of detrainment of lateral waters from the rising flare, although this would be difficult to demonstrate. In contrast to that seen in this figure in other cases only the central flare is observed, with surrounding waters, and even the lowest point on the central column, having much lower dissolved values than what occur in the body of the flare. This shows how a single flare may be totally isolated or may, instead, interact with other, near-by flares. Other observed behaviors include the clear deflection of the flare to one side or another of the section, as horizontal currents shift the dissolved phase away from the source bubble flare, and the complete disappearance of the flare as currents force the flare completely out of the measurement plane.

Large-Scale Discrete Monitoring

Discrete Monitoring Methods

Sampling from an 8 m long Zodiac boat was performed during four seasonal campaigns along a 700 m long transect (7 points, 3 depths each) which crossed both venting and non-venting areas. Sample point precision was likely on the order of 10-15 m. A SeaBird 19 CTD equipped with sensors for temperature, conductivity, pressure, fluorescence, pH, and dissolved oxygen was lowered by hand at each transect point. A 5L Niskin water sampling bottle was hand-lowered at each point and triggered with a lead messenger. Once on board the Niskin was immediately sub-sampled for various analyses in the following order: dissolved O2, dissolved gases, pH, alkalinity, DIC, DOC, inorganic nutrients, major elements, viral and prokaryotic abundance, and bacterial community structure. All samples were placed in coolers with ice packs on the boat, then transferred to refrigerators or freezers on shore at the end of the day. Analytical procedures are reported elsewhere [Karuza et al. 2012; Ingrosso et al. 2016]. Two Acoustic Doppler Current Profilers (ADCP) were also deployed during the sampling periods.

Discrete Monitoring Results

The repeat measurements performed along the 700 m long transect showed the challenges of working from a small boat. First, sample location uncertainty was high due to limited GPS accuracy and boat movement caused by variable wind and currents. Second, sampling and associated sample preparation is time consuming and affected by meteorological conditions (e.g. rough seas) and

daylight hours available. As such, the entire transect was sampled in one day only during one campaign, on two consecutive days during two campaigns and on two days separated by a day of rough weather during one campaign. Sampling on different days was often accompanied by a change in stratification and current conditions, which had a significant impact on the observed results. For this reason the integration of continuous ADCP current monitoring and the transect profiling was critical for a proper interpretation of chemical and biological data.

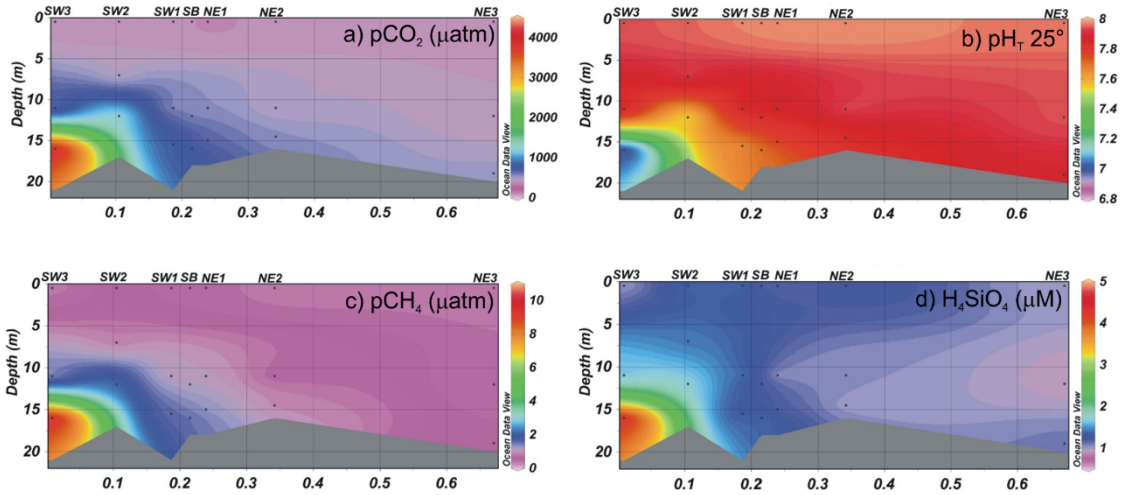

Figure 2 Select chemical data from the March 2012 sampling campaign along the long profile, with different parameters showing similar behaviour. Data plotted using ODV [Schlitzer, 2018].

Of the many results obtained during the transect work, perhaps the most important were related to the limited nature of observed anomalies and impacts despite the large volume of CO_2 being released at the site. The strongest chemical anomalies associated with leakage were observed during the one campaign conducted in a single day when the water column was stable and density stratified, with carbonate parameter anomalies (pCO_2, pH, DIC) located in the deepest part of the transect (Figure 2a, b). This transect also showed the clearest anomalies with associated parameters, such as CH_4 and H_4SiO_4 (Figure 2c, d). These results indicate how other, co-leaking species, if bio-chemically stable, can be used as tracers of the CO_2 leakage and water column migration processes. Whereas other campaigns did show some water column anomalies, these tended to be smaller in magnitude and spatial extent, again demonstrating the effectiveness of current mixing in diluting the leaked CO_2. In general, very little biological impact was observed, even in the well-stratified transect with the most significant anomalies.

Summary and Conclusions

Two different approaches were used to study CO_2 behavior in the Panarea water column. In the first, 20 GasPro pCO_2 sensors were deployed along 2D vertical transects around or near CO_2 leakage sites to monitor small scale, near field dissolved CO_2 behavior and migration. These probes, deployed for a few days each time and programmed to make measurements every 10 minutes, show the effects of temperature stratification, tidal currents, storm mixing, and bubble column entrainment on the behavior, distribution and concentration of dissolved CO_2 in the water column at the small scale over short time periods. In contrast, the second approach involved manual sampling during four seasonal campaigns of a 700 m long transect that crossed multiple leakage areas, together with current monitoring during the sampling periods. A total of three depths at seven points along the transect

were sampled for dissolved gases, pH, and nutrients to assess large-scale process and seasonal effects. These results highlight the difficulty of discrete sampling of the water column, considering the dynamic nature of the currents that control CO_2 movement. That said, this work highlighted similar behavior of other parameters associated with the CO_2 leakage, such as silica, pH and CH4, as the spring field campaign provided the most consistent results and strongest anomalies due to gentler currents and strong temperature stratification.
The spatial-temporal monitoring at the Panarea site has highlighted the extreme temporal and spatial variability in pCO_2 values and distributions in the natural environment, an observation that is important for understanding the fate of leaked CO_2, its potential impact on the local ecosystem, and in the design of sampling and monitoring programs.

Acknowledgements
This work was part of the RISCS and ECO_2 projects. RISCS (Research into Impacts and Safety in CO_2 Storage) was funded by the EC 7th Framework Programme (grant agreement 240837) and industry partners ENEL I&I, Statoil, Vattenfall AB, E.ON and RWE. ECO_2 (Sub-seabed CO_2 storage: Impact on Marine Ecosystems) received support from the EC 7th Framework Programme under grant agreement [265847].

References

Caliro S., Caracausi A., Chiodini G., Ditta M., Italiano F., Longo M., Minopoli C., Nuccio P.M., Paonita A., and Rizzo A., (2004). *Evidence of a recent input of magmatic gases into the quiescent volcanic edifice of Panarea, Aeolian Islands, Italy*. Geophysical Research Letters, 31, L07619.

Esposito A., Giordano G., and Anzidei M., (2006). *The 2002-2003 submarine gas eruption at Panarea volcano (Aeolian Islands, Italy): Volcanology of the seafloor and implications for the hazard scenario*. Marine Geology, 227, 119-134.

Graziani S., Beaubien S.E., Bigi S., and Lombardi S., (2014). *Spatial and Temporal pCO_2 Marine Monitoring Near Panarea Island (Italy) Using Multiple Low-Cost GasPro Sensors*. Environmental Science & Technology, 48, 12126-12133.

Ingrosso G., Giani G., Comici C., Kralj M., Piacentino S., De Vittor C., Del Negro P., (2016). *Drivers of the carbonate system seasonal variation in a Mediterranean gulf*. Estuarine Coastal Shelf Science, 168, 58-70.

Karuza A., Celussi M., Cibic T., Del Negro P., De Vittor C., (2012). *Virioplankton and bacterioplankton in a shallow CO_2-dominated hydrothermal vent (Panarea island, Tyrrhenian sea)*. Estuarine, Coastal and Shelf Science, 97, 10-18.

Schlitzer, R., (2018). *Ocean Data View*, odv.awi.de.

Tassi F. et al., (2009). *Low-pH waters discharging from submarine vents at Panarea Island (Aeolian Islands, southern Italy) after the 2002 gas blast: Origin of hydrothermal fluids and implications for volcanic surveillance*. Applied Geochemistry, 24, 246-254.

Investigating gas flow rate variations at Panarea hydrothermal system by mean of passive hydro-acoustics: evidences of a linkage with Stromboli volcano

Longo M.[1], Caruso C.[1], Corbo A.[1], Gattuso A.[1], Lazzaro G.[1], Romano D.[1], Scirè S.[1], Italiano F.[1,2]

[1]*Istituto Nazionale di Geofisica e Vulcanologia, Sezione di Palermo, Italy*
[2]*EMSO Interim Office, c/o INGV, Roma, Italy*

Corresponding Author: *cinzia.caruso@ingv.it*

Passive acoustics in submarine environment, using hydrophones, gives back to us relevant information concerning biological or geological issues. Several arrays of hydrophones have been used to follow magma batches, along with their fluids, ascending to the seafloor, mostly along mid-ocean ridges (MOR). Seismic and hydro-acoustic signals, generated by intrusion of magma, and consequent faulting of brittle oceanic crust, could be recorded by using Hydrophones. Moreover, "tremor-like" signals, produced by magmatic and hydrothermal fluids, flowing through cracks in the oceanic crust could be detected.

On 2002, a big gas explosion occurred in the seafloor 2 miles E offshore Panarea Island. The explosion was caused by a release of magmatic gases that suddenly reached the surface and interacted with hydrothermal fluids. Fluxes of fluids discharged from the sea bottom increased by two orders of magnitude with respect to the normal degassing. These anomalous conditions turned back to pre-crisis conditions only on July 2003. Monitoring the gas outflow over time was crucial to understand the evolution of the event. Hydro-acoustics detection methods represent the best instrument to track fluids dynamics. Base concept consists in earing the noise generated by bubbling gases in well-defined ranges of frequencies. We thus can consider noise variation generated by bubbling gases as a surrogate of the gases flux variation.

A multidisciplinary submarine observatory was set-up and deployed on the sea-bottom, 23-meter depth, in the middle of the islets area, E offshore Panarea. The sea bottom area is characterized by gas bubbling, discharged along local tectonic fractures and springs of hot and acid hydrothermal waters. The submarine observatory is equipped by an hydrophone and thus, it is able to detect noise generated by bubbling gases. Here we analyze data from the submarine observatory spanning from June 2016 to December 2017. Acoustics records in selected range of frequency within 280 and 395 Hz, show seasonal behaviour due to natural forces such as tides, atmospheric pressure, hydrostatic pressure and temperature. Even though seasonal trend, they show anomalies that depart from the normal behaviour, suggesting an endogenous input that makes gases flux increase starting from November 2016 and lasting until April 2017, and once again on October - November 2017.

Searching for possible sources of a deep input, we analysed volcanic activity in the entire area and the reliable relationship with the Panarea hydrothermal system.

At Stromboli volcano, twelve miles far NE from Panarea, due to a newer pressurization of the shallow plumbing system, CO_2 emission rate started to increase to higher values just on November 2016, when the mean degassing style set up around 10000 g m-2 d-1 for several months. Moreover, a new abrupt change of CO_2 fluxes was recorded on October 2017 when mean values suddenly jumped up and stabilized around 15000 g m-2 d-1 until December 2017. November 2016 therefore represents

the opening of the unrest of Stromboli and exactly corresponds with the beginning of the anomalous acoustics records, related to gases flux, coming from the Panarea hydrothermal system. Furthermore, during the entire analysed period, hydrophone recorded also a continuous 'tremor-like' signal, in very low acoustic frequency, within the range 2-25 Hz. Astonishingly variations over time of 'acoustic-tremor', recorded at Panarea sea bottom, precisely shadowed (R2>0.7) CO_2 fluxes variations recorded on Stromboli craters, 12 miles far.
Those acoustic observations, paired with the comparable behaviour of the He isotope marker in the fluids coming from both volcanoes, suggesting a possible "Panarea-Stromboli linkage" that could concern the deep roots of the two volcanoes. In this frame, N 40 °E tectonic structure represents the common way of escapes for magmas, along with their fluids, that feed Stromboli-Panarea volcanic system.

References

Dziak R.P., Bohnenstiehl D.R., Matsumoto H., Fowler M.J., Haxel J.H., Tolstoy M. and Waldhauser F., (2009). *January 2006 Seafloor-spreading event at 9_500N, East Pacific Rise: Ridge dike intrusion and transform fault interactions from regional hydroacoustic data*. Geochem. Geophys. Geosyst., 10, Q06T06, doi: 10.1029/2009GC002388.

Heinicke J., Italiano F., Maugeri R., Merkel B., Pohl T., Schipek M. and Braun T. (2009). *Evidence of tectonic control on active arc volcanism: The Panarea-Stromboli tectonic link inferred by submarine hydrothermal vents monitoring (Aeolian arc, Italy)* Geophysical Research Letters, vol. 36, L04301, doi:10.1029/2008GL036664.

Inguaggiato S., Vita F., Cangemi M. and Calderone L., (2019). *Increasing Summit Degassing at the Stromboli Volcano and Relationships with Volcanic Activity (2016-2018)* Geosciences, 9, 176; doi: 10.3390/geosciences9040176.

Sgroi T., Montuori C., Agrusta R., and Favali P. (2009). *Low-frequency seismic signals recorded by OBS at Stromboli volcano (Southern Tyrrhenian Sea)* Geophysical Research Letters, vol. 36, L04305, doi:10.1029/2008GL036477.

Tolstoy M., Cowen J.P., Baker E.T., Fornari D.J., Rubin K.H., Shank T.M., Waldhauser F., Bohnenstiehl D.R., Forsyth D.W., Holmes R.C., Love B., Perfit M.R., Weekly R.T., Soule S.A., Glazer B., (2006). *A Sea-Floor Spreading Event Captured by Seismometers*. Science, vol 314, www.sciencemag.org.

Gases and seabed fluid fluxes at the Panarea shallow hydrothermal vents (Aeolian Islands)

De Vittor C.[1], Beaubien S. E.[2], Kralj M.[1], Relitti F.[1], Comici C.[1], Bigi S.[2], Lombardi S.[2], Graziani S.[2]

[1]*OGS (Istituto Nazionale di Oceanografia e Geofisica Sperimentale di Trieste), Trieste, Italy*
[2]*Università degli Studi di Roma La Sapienza, Dipartimento di Scienze della Terra, Italy*

Corresponding author: *cdevittor@inog.it*

Introduction

CO_2 leaking into the shallow sediments and overlying seawater is partitioned in different forms, each migrating at its own rate and having potentially different impacts. To begin with the CO_2 gas will migrate through the shallow subsurface either alone as a free gas or together with associated deep fluids (e.g. brines), with the free-phase CO_2 equilibrating with the surrounding pore waters/associated brines. Migrating upward these fluids will enter the base of the water column, with the release of gas bubbles (and possibly associated waters) from the sediments into the overlying seawater. The bubbles will rise in the water column creating what is known as a bubble "flare" with the CO_2 in the bubbles dissolving in the surrounding surface water as they rise. Depending on the depth and the chemical/physical characteristics of the water column, these bubbles may or may not reach the water surface. Any co-migrating water/brine will also be released into the water column, creating a plume having a chemical composition that is distinct from the surrounding seawater, consisting of dissolved gases (mainly CO_2), elements in the original brine, and elements liberated via CO_2-induced water-rock interaction. The height that this dissolved plume will reach in the water column will depend on the original flow rate across the sediment-water interface and the density contrast between the plume and surrounding seawater. Both the gas-induced and water plumes will then migrate laterally and vertically as a result of the local currents, water column stratification, and density effects, meaning that there is the potential for impact both in the near and far field for pelagic organisms, both in terms of a lower pH and the possibility of elevated concentrations of toxic elements. This study was carried out in the framework of two EC funded projects, RISCS and ECO2 related to research on sub-seabed CO_2 storage as climate change mitigation strategy, and potential impact on marine ecosystems. Here, we investigated how CO_2-leakage, a risk associated with subseafloor CO_2-storage, can affect physical and chemical characteristics of the surrounding ecosystem. We studied the Panarea natural laboratory site (Aeolian Islands), where natural CO_2 is leaking from the seafloor into the overlying water column, as an analogue for a leakage scenario.

Study Area

Panarea (Figure 1a) is the smallest of the islands of the Aeolian archipelago (Tyrrhenian Sea, Italy) a 200 km long volcanic arc composed of 7 islands and 10 seamounts. It represents the emergent part of a wide stratovolcano that has been volcanically active over the last 400 ka. Deep origin magmatic CO_2 (and other trace gases) is released in large volumes to the east of Panarea Island into the overlying shallow marine environment near three small islets. This gas leaks along, or at the intersection between, two main gas-permeable fracture systems (NE-SW and NW-SE). Aside from occasional gas burst events linked to magma activity at great depth, the leaking gas is relatively stable in terms of both chemistry (e.g. 98% CO_2, 1.7% H_2S plus other trace gases) and flux rates (7-9 x 10^6

L d^{-1}) [Caliro et al., 2004]. The majority of emissions are of gas only, although at some points a mixture of geothermal water and seawater in different proportions is released.

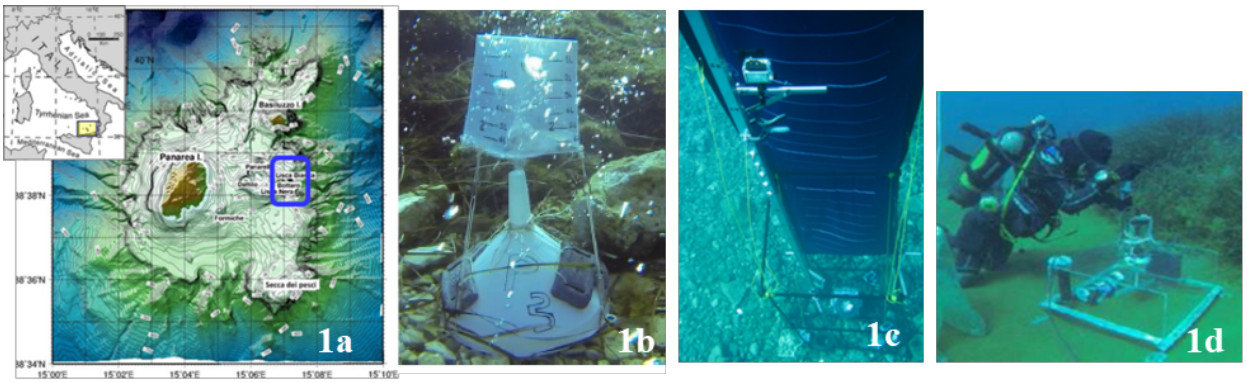

Figure 1 Study area (a), gas flux measurement (b), discrete bubble dynamics experiment (c), benthic flux measurement (d).

Experimental

Different series of experiments were performed close to the Bottaro Islet (Figure 1a) where, on the 3rd of November 2002, an impressive "gas burst" (consisting of emissions of a mixture of gas mainly composed of CO_2, fine-grained suspended sediments and colloidal S released from the sea floor at a depth of 10-15 m) led to the formation of a crater-like depression about 20 x 14 m wide and 10 m deep [Tassi et al., 2009]. The aim was to measure gas fluxes and benthic fluxes and to model discrete bubbles dynamics in order to better understand the fate of CO_2 in the water column after it has migrated out of the sediments (Figure 1a-d).

Gas Bubble Fluxes

Gas fluxes from the sea floor to the overlying water column at the Bottaro Crater were measured in July 2014. Fluxes were calculated by measuring the time required to capture a given volume of gas (from 0.1 to 6 L) using a funnel of known surface area (0.17 m^2) and a graduated, inverted container (Figure 1b). Results were converted to STP (1 bar and 298.5 K) conditions to allow for a comparison of the volume flows at sites having different water depths, as well as a mass flux. The area of the Bottaro crater is in 8-10 m deep water, with the base of the crater itself at a depth of about 11-12 m. The crater was subdivided into three different zones (Figure 2) based on the different leakage styles present: Zone 1 is a semi-circular area of uniform diffuse degassing; Zone 2 has isolated points of weak leakage; and Zone 3 has isolated points of moderate to stronger leakage that form bubble flares.

Measurements in Zones 1 and 2 were conducted along linear, regularly spaced profiles, which were placed irrespective of leakage points to obtain a representative statistical estimate of the average leakage rate. Sample spacing was 1 m and 2 m, respectively, and the average flux for each profile was multiplied by that zone's surface area to estimate total flow for that zone. In contrast, all major leakage points were measured in Zone 3 and all measured values were summed to calculate the total flux of this zone.

The zone and total flows estimated using the above described approach are summarized in the Table of Figure 2, which shows how most of the CO_2 leaking from the crater originates from the diffuse area of Zone 1 (c. 80%). It must be highlighted, however, that the assumptions made in extrapolating the individual point measurement results over the chosen surface area for that zone can influence the final calculated value. It is interesting to note, that whereas the diffuse degassing

from Zone 1 is volumetrically the most important, the bubble flare from this feature does not rise as high in the water column as that observed for the individual points of Zone 3, some of which reached the water surface. This is due to the smaller average Zone 1 bubble size spread over a wider area, which allows for a more rapid dissolution. In contrast, the focussed flow from the moderate to strong individual vents results in larger bubbles that break-up and dissolve more slowly, which may allow for equilibration with O_2 and N_2 in the water column thus stabilizing and prolonging the "life" of the rising bubbles. This could have important consequences for hydroacoustic monitoring, and the use of this technique to estimate leakage rates for highly soluble gases like CO_2 (as opposed to less soluble ones like CH_4).

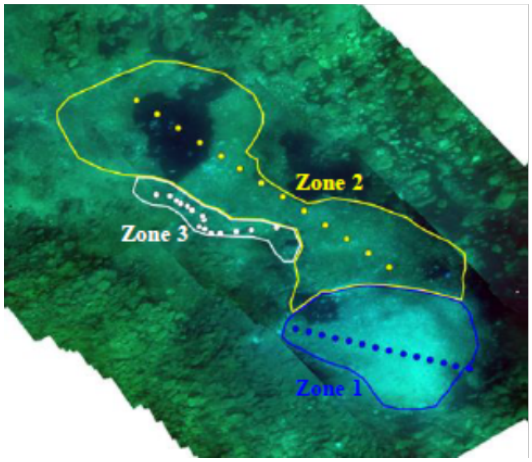

	L_{STP} CO2/minute	T CO2/year	% total
Zone 1	336	323	82
Zone 2	3.9	3.7	1
Zone 3	70	68	17
Total	410	395	

Figure 2 Montage of video stills taken from the water surface showing the Bottaro crater and the mapped zones with the associated table of estimates of CO_2 leakage rates given as both volume and mass flows.

Discrete Bubbles dynamics

As a CO_2 bubble rises it will exchange gases, such that CO_2 dissolves into the water and N_2 and O_2 are stripped out of the water into the bubble. These processes, combined with such factors as bubble diameter, depth (i.e. confining pressure), temperature, and salinity, will control the life of the bubble and how it evolves in size and composition during its ascent. Once dissolved in the water, the CO_2 can then be transported via currents, react chemically or biologically, or can eventually be released to the atmosphere.

The bubble dynamic experiments were conducted primarily during a campaign in October 2012 and then repeated on May 2014, using a 3x1x1 m, hollow-tube frame, mounted on the floor of the Bottaro crater (12 m depth) in which natural CO_2 leakage is occurring. The structure had a 10 m tall guide mounted on the front face along which an HD video camera and other equipment can slide or be fixed and a dark blue cloth mounted on the back face (10 m tall) for contrast and distance from bottom measurements (Figure 1c). Bubbles were made using the gas released from the seafloor, but using a system which allowed for control of both bubble size and bubble numbers. The use of the *in situ* gas, within a leakage area that affects the surrounding water column, allowed us to conduct the experiment in real-world leakage scenario but with control on bubble characteristics. Measurements and sampling performed during the various experiments included: bubble rise velocity, bubble size at different heights, bubble composition at different heights, water column chemistry at different heights (carbonate system parameters and dissolved gases), and a CTD cast near the structure to obtain salinity, temperature, and DO profiles. In addition, two GasPro-pCO_2 sensors were deployed at different heights on the structure to continuously monitor dissolved CO_2 and temperature.

Bubble size decreased in an almost linear manner before disappearing at about 2 m above the release point. Bubble rise velocity averaged around 30 cm/s; the similar velocity despite changing bubble size implies the importance of the vertical current regime in influencing rise velocity in a natural system.
During the experiment, which lasted more than 3 hours, pCO_2 ranged from a minimum of 350 µatm to a maximum of 820 µatm. In collaboration with D. McGinnis (IGBB Berlin) these data have been modelled using the Discrete Bubble Model (DBM) [McGinnis et al., 2011]. Based on an input gas concentration equal to that of the first bubble measured, the model was able to predict very well the subsequent gas bubble concentrations measured higher in the water column. In contrast, a higher concentration was needed to match the bubble diameter values, perhaps indicating that the field technique for this measurement requires refinement.

Benthic fluxes
Benthic chambers (Fig 1d) were used to measure the flux of various chemical and biochemical components across the sediment water interface in October 2010, July 2011, January 2012 and March 2012. Two sites were measured in the Bottaro Crater, one near a point of gas leakage (referred to here as the "vent site") and a background site located about 100 m away where no leakage was observed (referred to here as the "control site"). Two different chambers were deployed at each site, one dark and one transparent. This was done to determine *in situ* benthic flux due to benthic metabolism (production and respiration) and diffusive fluxes from or into the sediments, as well as to assess the spatial variability of pore-water flux associated with the venting phenomena. Because the goal of these measurements was to study the flux of the aqueous phase and not the bubbles, the chambers deployed at the vent site were located near, but not on, the points of bubble emission. Sub-samples, collected from the benthic chambers by SCUBA divers with a plastic syringe approximately once every hour over a total deployment period of about 7 hours, were analysed for a wide range of parameters.
Of all the parameters measured during this study, only six show significant trends (in some or all chamber measurements) that are likely directly linked with a significant flux: dissolved inorganic carbon, pH, pCO_2, silica, hydrogen sulphide, and ammonium. At the control site, values are almost always low and stable throughout the measurement period. At the vent site, the first three campaigns show the most interesting results, illustrating slightly different behaviours. For example, examining the carbonate parameters, both in the transparent chamber of campaign 1 and in the opaque chamber of campaigns 3 a small increase in DIC (Dissolved Inorganic Carbon) was observed, however in the latter very large anomalies for both pH and pCO_2 where present, whereas in the former the anomalies are relatively small. In contrast, in both the opaque chambers of campaigns 2 and 3 large pH and pCO_2 anomalies were observed, but the DIC values of the latter are much smaller than those of the former.
Regarding benthic fluxes, most major elements showed relatively constant concentrations over the measurement period for both chambers at both sites, indicating little movement of these species out of the sediments into the overlying water column. Increased fluxes of the reduced gas H_2S were often observed at the vent site reaching the higher values during the second and third campaign (279992 and 263531 µmol $m^{-2}d^{-1}$, respectively). Among nutrients, a large flux of silica (18461 µmol $m^{-2}d^{-1}$) was measured at the vent site during the second campaign due to the co-migration of this nutrient with CO_2, as suggested by the significant correlation ($p<0.05$) between these two species; instead, all other deployments generally showed relatively low fluxes suggesting the overlapping of several processes such as microbial and chemical dissolution of opal, dependence on redox conditions, assimilation by benthic diatoms and flocculation and co-precipitation of silicon polymers and clay minerals with Fe(III).

Such differences can be attributed to spatial and / or temporal variability of pore water leakage, to diffusive versus advective flux modes, or to interference caused by the lateral ingress of denser, CO_2-charged bottom waters at the chamber base.

Conclusions

Work performed at the Panarea test site highlights the usefulness of studying natural leaking systems to obtain a more complete (and realistic) understanding of the possible consequences of a seabed leak of anthropogenic stored CO_2. Such large-scale, complex sites allow for a more assessment of the potential spatial and temporal impact of the leaking gas on marine chemistry, biology, and physics, as well as the testing of various parameters and new technologies for their sensitivity for leakage monitoring.

Acknowledgements

This work was part of the RISCS and ECO_2 projects. RISCS (Research into Impacts and Safety in CO_2 Storage was funded by the EC 7th Framework Programme (grant agreement 240837 and industry partners ENEL I&I, Statoil, Vattenfall AB, E. ON and RWE. ECO_2 (Sub-seabed CO_2 storage: Impact on Marine Ecosystems received support from the EC 7th Framework Programme under grant agreement [265847].

References

Caliro S., Caracausi A., Chiodini G., Ditta M., Italiano F., Longo M., Minopoli C., Nuccio P.M., Paonita A., and Rizzo A., (2004). *Evidence of a recent input of magmatic gases into the quiescent volcanic edifice of Panarea, Aeolian Islands, Italy*. Geophys. Res. Lett., 31, L07619.

McGinnis D.F., Schmidt M., DelSontro T., Themann S., Rovelli L., Reitz A., Linke P., (2011). *Discovery of a natural CO_2 seep in the German North Sea: Implications for shallow dissolved gas and seep detection*. J. Geophys. Res.: Oceans, 116, C03013.

Tassi F., Capaccioni B., Caramanna G., Cinti D., Montegrossi G., Pizzino L., Quattrocchi F., Vaselli O., (2009). *Low-pH waters discharging from submarine vents at Panarea Island (Aeolian Islands, southern Italy after the 2002 gas blast: origin of hydrothermal fluids and implications for volcanic surveillance*. Appl. Geochem., 24, 246-254.

Hydrothermalism at Panarea island (Aeolian arc, italy): the last significant discoveries from earth to Mars

Di Bella M.[1], Andaloro F.[2], Esposito V.[3], Romeo T.[2,6], Sabatino G.[4], Canese S.[2,5], Scotti G.[6], Battaglia P.[2] & Italiano F.[1]

[1]*Istituto Nazionale di Geofisica e Vulcanologia, Sezione di Palermo, Italy*
[2]*Stazione Zoologica Anton Dohrn (SZN), Napoli, Italy*
[3]*Istituto Nazionale di Oceanografia e di Geofisica Sperimentale (OGS), Trieste, Italy*
[4]*Università di Messina, Dipartimento di Scienze Matematiche e Informatiche, Scienze Fisiche e Scienze della Terra (MIFT), Italy*
[5]*Istituto Superiore per la Protezione e la Ricerca Ambientale (ISPRA), Roma, Italy*
[6]*Istituto Superiore per la Protezione e la Ricerca Ambientale (ISPRA), Italy*

Corresponding Author: *mdibella@unime.it*

Recent multidisciplinary researches carried out on two peculiar hydrothermal sites, discovered in the shallow-water hydrothermal area off Panarea Island, in the Aeolian Volcanic Arc (South Tyrrhenian Sea) significantly improve the knowledge about the Mediterranean hydrothermalism and the past hydrothermal activity of Early Earth and Mars. The two exceptional sites were mapped and explored during two research cruises carried out respectively, in 2010 and 2015, conducted by ISPRA (Italian Institute for Environmental Protection and Research) in collaboration with INGV on board of the research vessel Astrea, with the aim to characterize the Panarea hydrothermal area on the geological, biological and geochemical point of views.

At Panarea, thermal fluids and CO_2-dominated gases, that currently seep from the sea bottom, originated typical hydrothermal low temperature Fe oxyhydroxide precipitates from 80 to 120 m depth. The first discovered site is located at 70±80 m depth off the South-westerncoast of the islet of Basiluzzo, and is called “Smoking Land” for the exceptional presence of a large number of wide and high active chimneys [Esposito et al., 2018]. The second important site was discovered at 80 m depth in the NE platform of Basiluzzo islet (38°40,429;15°07,651E) where an unlithified, soft sediment, now known as “ooid sand deposit” was observed [Di Bella et al., 2019].

In general, the Panarea Volcanic Complex represents the emergent part of a submarine composite volcano, belonging to the Aeolian Arc in the southern Tyrrhenian Sea, largely dismantled by erosion and neo-tectonic regime. Remnantsof the primary volcanic structures, such as eruptive centers and lava domes, are traceable e.g.at Secca dei Pesci, to the S and SW area of Panarea and to the NW and NE of Basiluzzo [Gamberi et al., 1998]. The most remarkable active tectonic structure of the area is a NNE-SSW, NE-SW trending graben, located North-East of Panarea. Gas venting is frequent at the base and at thetop of these faults. In the sedimented areas close to the faults, hydrothermalis witnessed by the presence of white patches of sulphide mineralization and accumulations of Fe-rich ochre and red-colored sediments containing fragments of consolidated Fe-oxide crusts [Gamberi et al., 1998].In the investigated area, the presence of hydrothermal activity had already been revealed byseveral authors [Italiano and Nuccio, 1991; Price et al., 2015].

Specifically, the undertaken researches evidenced that:
1) The "Smoking land" includes a total of more than 200 chimneys, different in size and shape, 39 of which were described by means of ROV video images. On the whole, these complex structures were characterized by a wide biotic colonization and the presence of yellow to red precipitates, probably composed of iron oxyhydroxides (see below), distributed along the body of the chimneys or close to the upper and lateral mouths. Among all the observed chimneys, 14 showed clear effusive activity as revealed by the emission of bubble plumes or hydrothermal fluids, having visibly different density in comparison to the surrounding marine water. The pCO_2 concentration in the water column close to the chimney spills recorded values from ~601 to ~1800 ppm and off scale values (2,000 ppm).
The discovery of this vent field supplies new and important information on the minero-geochemical and biological features of the shallow-water hydrothermal systems of the Mediterranean Sea. Morevoer, these first findings evidence a submarine dynamic habitat where geological, chemical and biological processes are intimately connected, making the Smoking Land an important site in terms of marine heritage that should be safeguarded and protected.
2) The "ooid sand deposit" consists of coarse-grained, unconsolidated sand with a whitish biogenic component and dark brown rust ooidal grains. The iron grains are known in literature as "ooids" and are considered as sedimentary particles widely documented in the fossil record, extremely rarein modern settings. The origin and genesis of fossil iron ooids and oolitic ironstones, and their extensive distribution, have long been a matter of debateand controversy, invoking both abiotic processes [see Di Bella et al., 2019] and biologically induced mechanisms. The results of the study show that Panarea iron ooids perfectly match their fossil counterparts. They were formed by the deposition of iron oxyhydroxides (mainly goethite) in concentric laminae around nuclei represented by pyroclastic particles and, more rarely, by sponge spicules or other skeletal components. The spherical laminated structure resulted from the constant agitation by degassing of CO_2-dominated fluids through the seafloor sediments. Any sound evidences of microbial–mediated micro-texture (such as cell remain or induced structures, as biofilm, already reported from other hydrothermal environments including the Panarea area [Bortoluzzi et al., 2017; Esposito et al., 2018], were found. Moreover, implications are important also for the observed analogies between ooids from Panarea and hematite spherules recently detected on the Mars surface by the NASA rovers [Di Bella et al., 2019].

References

Esposito V. et al., (2018). *Exceptional discovery of a shallow-water hydrothermal site in the SW area of Basiluzzo islet (Aeolian Archipelago, South Tyrrhenian Sea): An environment to preserve*. PLoS ONE 13(1): e0190710.

Di Bella M. et al., (2019). *Modern Iron Ooids of Hydrothermal Origin as a Proxy for Ancient Deposits*. Scientific Reports, 9, 7107.

Gamberi F. et al., (1998). *Contesto morfo-tettonico e depositi idrotermali di solfuri ed ossidi di ferro in una porzione sommersa dell'Arco Eoliano (in base ad indagini ad alta definizione).* Boll. Soc. Geol. Ital., 117, 55-71.

Italiano F. and Nuccio F., (1991). *Geochemical investigations of submarine volcanic exhalations to the east of Panarea, Aeolian Islands, Italy*. J. Volcanol. Geotherm., 46, 125-141

Price R. et al., (2015). *Subsurface hydrothermal processes and the bioenergetics of chemolithoautotrophy at the shallow-sea vents off Panarea Island (Italy).* Chemical Geology, 407, 21-45.

Effect of hydrothermal gas seeps on fate and mobility of trace metals and REY in a shallow marine environment: a case study in the Levante bay of Vulcano Island (Aeolian Islands, Italy)

Falcone E.E., Federico C., Boudoire G.

Istituto Nazionale di Geofisica e Vulcanologia, Sezione di Palermo, Italy

Corresponding Author: *eddaelisa.falcone@gmail.com*

Effects of submarine hydrothermal venting on the balance of chemicals in seawater are known since the mid-1970s [German et al., 2002 and references therein]. The present study provides insights upon geochemical processes involving trace metals and REEs discharged by submarine hydrothermal vents in the Levante Bay of Vulcano (Aeolian Islands). Samples were collected on July 2012 and October 2013 from several submarine vents, small natural pools and one thermal well, and analyzed for Fe, Mn, Cr, Ti, V, Se, Zn, Cs, Sr, Ba, As, and REY, besides major ions. The REY concentrations were measured by ICP-MS after co-precipitation onto newly-forming $Fe(OH)_3$ [Raso et al., 2013]. Analytical data were elaborated and compared with the results of equilibrium and reaction path modeling.

The very reactive volcanic fluids undergo chemical modification during ascent, upon cooling and extensive water-rock interaction. When these fluids are emitted in submarine environment, dissolved metals undergo oxidative scavenging onto suspended particulate matter (SPM). Competitive equilibria between the aqueous complexes and SPM drive the fate of chemicals and affect their concentrations as result of fractionation mechanisms. The contamination of ambient seawater by hydrothermal fluids can be recognized by the pattern of normalized REYs and some major and trace metals. Where acidic vapour is emitted from submarine vents, it likely remobilizes metals and REY from local sediments, thus increasing their mobility. Manganese, Cs, Ba, Rb, Fe and REY are typically enriched in submarine samples contaminated by hydrothermal fluids (Figure 1 and 2). Other elements, namely Ti, As U, V, Cr, Co, Sr have concentrations similar to ambient seawater or lower (Figure 1). We suggest that the formation of Fe-oxyhydroxides and clay minerals, where the seawater affected by H_2S-rich hydrothermal vapour is further oxidated near the seeps, can scavenge many chemicals. The Y/Ho ratio is widely used to ascertain the competitive role of complexation and the precipitation of secondary minerals in controlling the fate of chemicals in seawater. The highest REY contents were measured in the bubbling pools and show near- or sub-chondritic Y/Ho ratios ($43 < Y/Ho < 51$), due to the isochemical leaching of local volcanic rock, driven by the H_2S-rich hydrothermal vapour. The higher than chondritic Y/Ho ratio in seawater has been attributed to the differential scavenging of Y and Ho in the SPM, having Ho a larger affinity for Fe-oxyhydroxides.

The results of the equilibrium and reaction-path modeling show that the contents of chemicals are controlled by both the contamination of deep fluids and the processes of oxidation and co-precipitation in seawater. The model shows that, when acidic and reducing fluids interact with seawater, trace metals, metalloids and REY are scavenged by the newly forming solid carbonates, fluorite, Fe-oxyhydroxides or clay minerals, while they are also increasingly complexed in solution, and the interplay between these two processes differs from an element to another.

This study provides some clues on the fate of some trace elements discharged by hydrothermal vents directly into the photic zone, the most interested by the biogeochemical cycle of metals. The

understanding of the processes controlling the mobility of iron and other trace metals, following the same fate, improves the prediction of the role of such elements in buffering ocean productivity and carbon cycling.

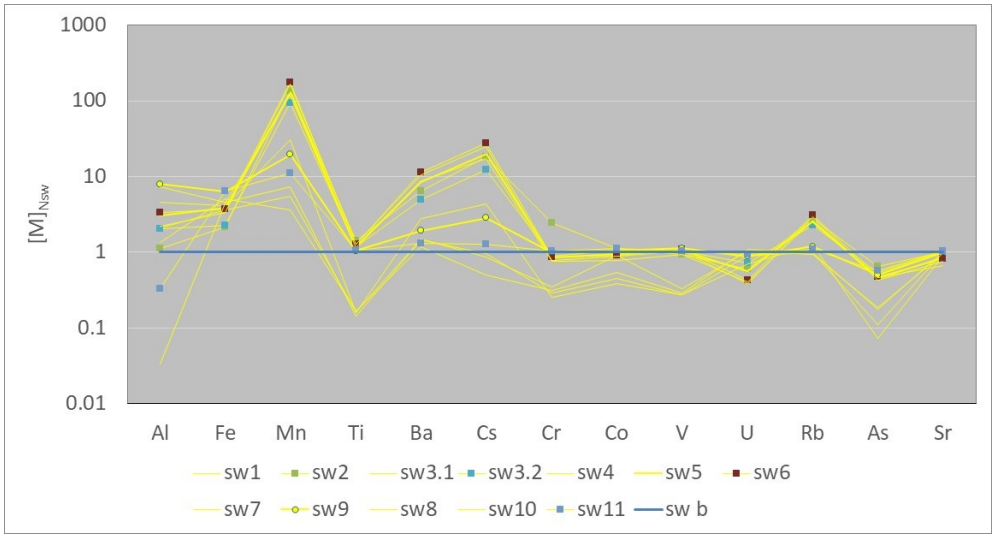

Figure 1 Concentrations of analyzed trace elements in submarine samples (sw1 to sw11) normalized to the ambient seawater (sample sw b, blue line).

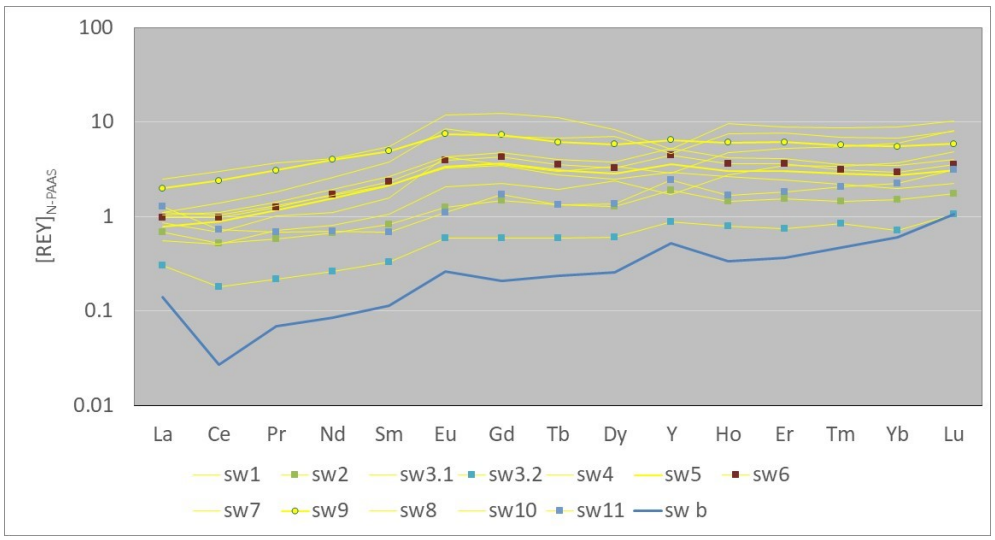

Figure 2 Concentrations of analyzed REE and Y in submarine samples normalized to PAAS.

References

German C.R., Colley S., Palmer M.R., Khripounoff A. and Klinkhammer G.P., (2002). *Hydrothermal plume-particle fluxes at 13 N on the East Pacific Rise*. Deep Sea Research Part I: Oceanographic Research Papers, 49(11), 1921-1940.

Raso M., Censi P. and Saiano F., (2013). *Simultaneous determinations of zirconium, hafnium, yttrium and lanthanides in seawater according to a co-precipitation technique onto iron-hydroxide*. Talanta, 116, 1085-1090.

Diffuse CO_2 emission from Port Foster bay at Deception Island, Antarctica

Hernández P.A.[1,2,3], Padrón E.[1,2,3], Melián G.[1,2,3], Barrancos J.[1,2], Rodríguez F.[1,2], Pérez N. M.[1,2,3] and Sumino H.[5]

[1]*Instituto Volcanológico de Canarias (INVOLCAN), San Cristobal de La Laguna, Spain*
[2]*Instituto Tecnológico y de Energías Renovables (ITER), Granadilla de Abona, Spain*
[3]*Agencia Insular de la Energía de Tenerife (AIET), Granadilla de Abona, Spain*
[4]*Department of Basic Science, Graduate School of Arts and Sciences, The University of Tokyo, Japan*

Corresponding Author: *phdez@iter.es*

Monitoring the chemical composition and discharge rates of volcanic gases is one of the main tasks in volcano monitoring programs. Highly mobile volcanic gases are released to the atmosphere owing to progressive depressurization of magma during ascent and can reach the surface well before their parental magma [Arpa et al., 2013; Hernández et al., 2001; Granieri et al., 2006; Melián et al., 2012; 2014; Pérez et al., 2011; 2012; 2013]. Among volcanic gases, CO_2 is widely used in volcano studies and monitoring because it is one of the earliest released gas species from ascending magma, and it is considered conservative [Gerlach, 1985].

Deception Island is a volcanic island located at 62°59´S and 60°41´W in the South Shetland archipelago. It constitutes a back-arc stratovolcano with a basal diameter of ~ 30 Km, rising ~ 1400 m from the seafloor to a height of 540 m above sea level [Smellie, 2001]. The island has a horse-shoe shape with a large flooded caldera with a diameter of about 6x10 km and a maximum depth of 190m. This caldera also known as Deception Bay is open to the sea through a narrow channel of 500m at Neptune Bellows. The caldera was formed during a massive emptying of a shallow magma chamber that caused the collapse of a ~ 640m high volcano [Torrecillas et al., 2013]. The rocks of the island are dominated by basalts and basaltic andesites but there is a minor proportion of evolved rocks [Smellie, 2001]. Deception Island has suffered several historical eruptions since the late 18th century, and well documented eruptions occurred in 1967, 1969 and 1970. Faults that have originated from regional tectonics have controlled highly explosive and hydrovolcanic post-caldera eruptions at low elevations and less explosive eruptions at higher elevations [Smellie 2001]. Kusakabe et al., [2009] reported that magma emplaced beneath Deception was derived from a wedge mantle geochemically similar to mid-ocean ridge basalt (MORB) that is contaminated by a slab that is subducting beneath the Bransfield back-arc basin. The most obvious hydrothermal discharges in Deception are low temperature (~ 100°C) fumaroles present in the Fumarole Bay area, with a CO_2/H_2O ratio of ~ 0.16 and H_2S as the main sulphur species (~ 0.18 mol.%) [Caselli et al., 2007]. Intense seismic swarms occasionally occur at Deception Island [Carmona et al., 2012]. The seismic activity of Deception volcano includes long-period (LP) events, volcanic tremor episodes and volcano-tectonic earthquakes. Several periods of intense LP activity have been registered in summer field surveys at Deception volcano [Carmona et al. 2012]. The LP events are generally low-amplitude signals linked to alterations in the shallow hydrothermal system [Carmona et al., 2012]. Padrón et al., [2015], reported an excellent temporal agreement between diffuse CO_2 emissions measured by an automatic geochemical station between 7 December 2009 and 13 February 2010 and the LP seismicity recorded during December 2009. Therefore, to investigate CO_2 emission at Deception volcano is

very important since it is an active volcanic system and it is significantly affected by local faults, seismicity and tectonic structures [Padrón et al., 2015].
To provide a complementary geochemical approach to the volcanic monitoring program at Deception, we have carried out three diffuse CO_2 emission surveys at the surface environment of Deception bay covering an area of approximately 37,8 km^2. The surveys were performed at Deception bay in November-December, 2009, in November 2011 and in January 2012. About 377, 434 and 414 surface water CO_2 efflux measurements were carried out at each survey along the flooded caldera. Measurements of CO_2 efflux were performed at the water surface of the bay by means of a modification of the accumulation chamber method [Parkinson, 1981] consisting on a floating device equipped with a LI820 CO_2 gas analyzer. Sea water temperatures were measured using a K-type thermocouple probe and dual data logger thermometer at 0.5 m depth. Figure 1 shows the spatial distribution of measurement sites and diffuse CO_2 emision values on the water surface at each survey. Spatial distribution maps were constructed using sequential Gaussian simulation (sGs) algorithms provided by GSLIB software [Deutsch and Journel, 1998]. Diffuse CO_2 efflux was measured according to the accumulation chamber method.

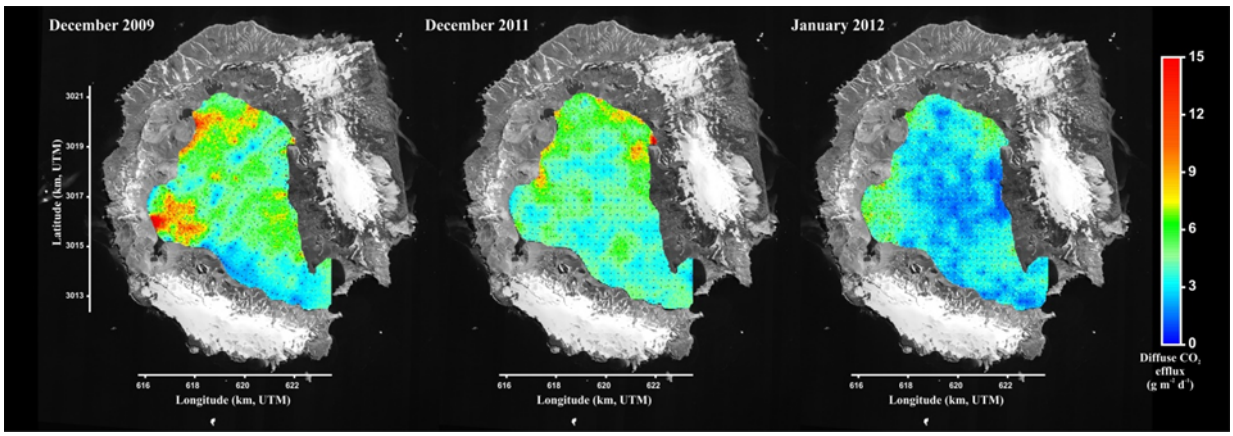

Figure 1 Average spatial distribution map of CO_2 efflux values measured at the water surface of the MCL of Taal Volcano from 100 sequential Gaussian simulations for December 2009, December 2011 and January 2012.

For December 2009, December 2011 and January 2012 surveys, sea water CO_2 efflux values ranged from non-detectable up to 120 g m^{-2} d^{-1}, 92.3 g m^{-2} d^{-1}, and 127.5 g m^{-2} d^{-1}, respectively. Most of the studied area showed background levels values of (⍰3 g m^{-2} d^{-1}), while peak levels values (>20 g m^{-2} d^{-1}) were mainly identified inside the Fumarole Bay, Telefon Bay and Pendulum Cove areas (Figure 1), showing a close spatial correlation with the location of the seismic swarms produced by the volcanic activity of Deception [Ibáñez et al., 2003]. The diffuse CO_2 emission from Deception Bay estimated for December 2009, December 2011 and January 2012 surveys were 191 td^{-1} ± 9 td^{-1}, 182 td^{-1} ± 5 td^{-1} and 98 td^{-1} ± 5 td^{-1}, respectively.
During the study periods, seismic arrays were deployed in Fumarole Bay as part of a long-term seismo-volcanic monitoring project at Deception Island operated by University of Granada, Spain [Carmona et al. 2012, Carmona et al. 2014]. Two types of seismicity are generally detected. Tectonic and volcano-tectonic (VT) earthquakes are characterized by wide-band signals related to the occurrence of fractures in the medium. Long-period (LP) seismicity is characterized by narrow-band signals that include both isolated events and volcanic tremor, and are often interpreted as a consequence of interactions between solids and hot fluids in volcano environments

[https://volcano.si.edu/showreport.cfm?doi=10.5479/si.GVP.BGVN201506-390030]. Between the 1999 VT earthquake series [Ibáñez et al., 2003] and 2011, the seismic activity was relatively quiet, with occasional peaks of activity.

Figure 2 shows the temporal evolution of the diffuse CO_2 emission from Deception bay together with the number of LP events recorded by the University of Granada and the time series of the diffuse CO_2 emission recorded by the automatic geochemical station installed by INVOLCAN at Deception Island between 7 December 2009 and 13 February 2010. Padrón et al., [2015], identified two different periods in the diffuse CO_2 emission time series. In the first period, from the beginning of the observation time to the end of December 2009, soil CO_2 efflux was characterized by high variance (15.274 g m^{-2} d^{-1}) and showed a median of 69.6 g m^{-2} d^{-1}. The second period, which corresponded to the remaining study period, was characterized by a much lower variance (53.8 g m^{-2} d^{-1}) and a median of 10.3 g m^{-2} d^{-1}. Carmona et al., [2012] reported significant LP dominant seismicity between December 2009 and February 2010 indicating the activation of a new source of seismicity with smaller dimensions or different fluid properties. The first event showed an excellent temporal agreement with the diffuse CO_2 emissions time series recorded in the geochemical station. They addressed the absence of such a temporal correlation with the second LP seismicity cluster recorded in January 2010 to a different source for seismicity. During the first LP cluster this anomalous hot fluid leakage occurred mainly from the hydrothermal system that feeds the Fumarole Bay fumaroles. The second source of LP seismicity probably had the same origin and affected a second hydrothermal system distant from Fumarole Bay in the direction of Stonethrow Ridge.

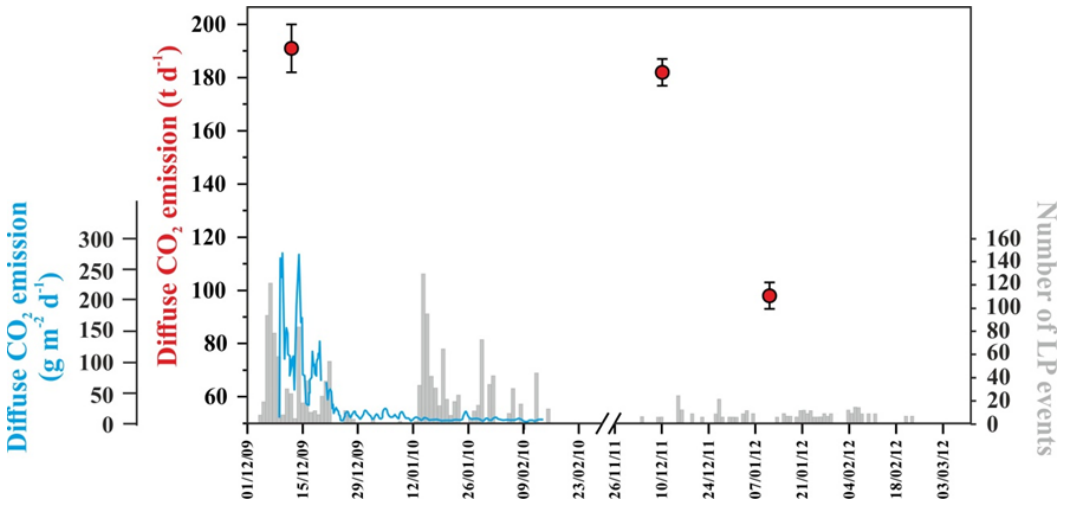

Figure 2 Time series of diffuse CO_2 emission released from the surface environment of Deception bay (res dots) together with the number of LP seismic events recorded during the Antarctic summers of 2009-2010 and 2001-2012) [source: https://volcano.si.edu/showreport.cfm?doi=10.5479/si.GVP.BGVN201506-390030] (grey bars) and time series of diffuse CO_2 emission from the automatic geochemical station installed at Deception Island [Padrón et al., 2015].

The relatively high diffuse CO_2 emission rate measured during December 2009 survey (191 td^{-1} ± 9 td^{-1}) was related to pressure fluctuations in the volcano-hydrothermal systems beneath Deception volcano that were probably caused by a deep injection of undegassed magma before

December 2009 [Padrón et al., 2015]. The similar emission rate value estimated for December 2011 survey (182 td^{-1} ± 5 td^{-1}), could be related to a same process. This is supported by similar $^3He/^4He$ ratios measured at Fumarole Bay fumaroles in December 2009 (7.48 ± 0.11 R_A; [Padrón et al., 2015]) and December 2011 (7.74 ± 0.23 R_A). However, between November 2011 and March 2012, LP seismicity was much lower compared to the period between November 2009 and March 2010. The Decrease on the diffuse CO_2 emission rate observed for January 2012 survey (98 td^{-1} ± 5 td^{-1}) could be related to a decrease in the volcanic gas pressure in the volcano-hydrothermal systems beneath Deception volcano. Since not detailed information about the source of the seismicity recorded during the period November 2011-March 2012 is available at the moment, we cannot conclude about the process responsible of the observed changes in the diffuse CO_2 emission rate from Deception bay. More diffuse CO_2 surveys are needed to understand the degassing dynamics and its relation to the volcanic activity at Deception volcano.

References

Arpa M.C., Hernández P.A., Padrón E., Reniva P., Padilla G., Bariso E., Melián G., Barrancos J., Nolasco D., Calvo D., Pérez N.M. and Solidum R.U., (2013). *Geochemical evidence of magma intrusion inferred from diffuse CO_2 emissions and fumarole plume chemistry: the 2010-2011 volcanic unrest at Taal Volcano, Philippines*. Bulletin of Volcanology, 75(747). doi:10.1007/s00445-013-0747-9.

Carmona E., Almendros J., Serrano I., Stich D. and Ibáñez J.M., (2012). *Results of seismic monitoring surveys of Deception Island volcano, Antarctica, from 1999-2011*. Antarctic Science, 24, doi:10.1017/S0954102012000314.

Carmona E., Almendros J., Martín R., Cortés G., Alguacil G., Moreno J., Martín B., Martos A., Serrano I., Stich D., Ibáñez J.M., (2014). *Advances in seismic monitoring at Deception Island volcano (Antarctica) since the International Polar Year*. Annals of Geophysics, 57(3), SS0321, doi:10.4401/ag-6378.

Caselli A., Badi G., Bonatto A.L., Bengoa C.L., Agusto M.R., Bidone A. and Ibáñez J., (2007). *Actividad sísmica y composición química fumarólica anómala debido a posible efecto sello en el sistema volcánico, Isla Decepción (Antártida)*. Revista Asociación Geológica Argentina, 62, 545-552.

Deutsch C. and Journel A., (1998). *GSLIB: Geostatistical Software Library 740 and Users Guide*. 2nd ed., Oxford Univ. Press, New York.

Gerlach T.M. and Graeber E.J., (1985). *Volatile budget of Kilauea volcano*. Nature, 313(6000), 273-277.

Granieri D., Carapezza M.L., Chiodini G., Avino R., Caliro S., Ranaldi M., Ricci T. and Tarchini L., (2006). *Correlated increase in CO_2 fumarolic content and diffuse emission from La Fossa crater (Vulcano, Italy): Evidence of volcanic unrest or increasing gas release from a stationary deep magma body?* Geophysical Research Letters, 33, L13316, doi:10.1029/2006GL026460.

Hernández P.A., Notsu K., Salazar J.M., Mori T., Natale G., Okada H., Virgili G., Shimoike Y., Sato M. and Pérez N.M., (2001). *Carbon dioxide degassing by advective flow from Usu volcano, Japan*. Science, 292, 83-86.

Ibañez J. M., Carmona E., Almendros J., Saccorotti G., Del Pezzo E., Abril M., Ortiz R. [2003]. *"The 1998-1999 seismic series at Deception Island volcano, Antarctica"*. Journal of Volcanology and Geothermal Research. 128, 65-88.

Kusakabe M., Nagao K., Ohba T., Seo J.H., Park S.-H., Lee J.I. and Park B.-K., (2009). *Noble gas and stable isotope geochemistry of thermal fluids from Deception Island, Antarctica*. Antarctic Science, 21, doi:10.1017/S0954102009001783.

Melián G., Tassi F., Pérez N.M., Hernández P., Sortino F., Vaselli O., Padrón E., Nolasco D., Barrancos J., Padilla G., Rodriguez F., Dionis S., Calvo D., Notsu K., Sumino H., (2012). *A magmatic source for fumaroles and diffuse degassing from the summit crater of Teide volcano (Tenerife, Canary Islands): geochemical evidence for the 2004-05 seismic-volcanic crisis*. Bulletin of Volcanology, 74(6), 1465-1483. doi:10.1007/s00445-012-0613-1.

Melián G.V., Hernández P.A., Padrón E., Pérez N.M., Barrancos J., Padilla G., Dionis S., Rodríguez F., Calvo D., Nolasco D., (2014). *Spatial and temporal variations of diffuse CO_2 degassing at el Hierro volcanic system: relation to the 2011-2012 submarine eruption*. Journal of Geophysical Research, Solid Earth, 119(9):6979-6991. doi:10.1002/2014JB011013.

Padrón E., Hernández P., Carmona E., Pérez N., Melián G., Sumino H., Almendros J., Kusakabe M., Wakita H. and Padilla G., (2015). *Geochemical evidence of different sources of long-period seismic events at Deception volcano, South Shetland Islands, Antarctica.* Antarctic Science, 27(6), 557-565. doi:10.1017/S0954102015000346.

Parkinson K.J., (1981). *An improved method for measuring soil respiration in the field*. Journal of Applied Ecology, 18, 221-228.

Pérez N.M., Hernández P.A., Padilla G., Nolasco D., Barrancos J., Melían G., Padrón E., Dionis S., Calvo D., Rodríguez F., Notsu K., Mori T., Kusakabe M., Arpa M.C., Reniva P. and Ibarra M., (2011). *Global CO_2 emission from volcanic lakes*. Geology, 39 (3), 235-238. doi:10.1130/G31586.

Pérez N.M., Padilla G., Padrón E., Hernández P.A., Melián G., Barrancos J., Dionis S., Nolasco D., Rodríguez F., Calvo D. and Hernández I., (2012). *Precursory diffuse CO_2 and H_2S emission signature of the 2011-12 El Hierro submarine eruption, Canary Islands*. Geophysical Research Letters, 39, L16311, doi:10.1029/2012GL052410.

Pérez N.M., Hernández P.A., Padrón E., Melián G., Nolasco D., Barrancos J., Padilla G., Calvo D., Rodríguez F., Dionis S. and Chiodini G., (2013). *An increasing trend of diffuse CO_2 emission from Teide volcano (Tenerife, Canary Islands): geochemical evidence of magma degassing episodes*. Journal of Geological Society of London, 170(4), 585-592, doi:10.1144/jgs2012-125.

Smellie J.L., (2001). *Lithostratigraphy and volcanic evolution of Deception Island, South Shetland Islands*. Antarctic Science, 13, 188-209.

Torrecillas C., Berrocoso M., Felpeto A., Torrecillas M.D. and García A., (2013). *Reconstructing palaeo-volcanic geometries using a Geodynamic Regression Model (GRM): application to Deception Island volcano (South Shetland Islands, Antarctica)*. Geomorphology, 182, 79-88.

Black sea methane flares from the seafloor: tracking outgassing by using acoustics

Longo M.[1], Caruso C.[1], Lazzaro G.[1], Radulescu V.[2], Romano D.[1], Scirè Scappuzzo S.[1], S. Balan[2], D. Birot[3], Italiano F.[1]

[1]*Istituto Nazionale di Geofisica e Vulcanologia, Sezione di Palermo, Italy*
[2]*Institutul National de Cercetare - Dezvoltare pentru Geologie si Geoecologie Marina - GeoEcoMar - Romania*
[3]*IFREMER, Département Ressources physiques et Ecosystèmes de fond de Mer (REM), Unité des Géosciences Marines, France*

Corresponding Author: *manfredi.longo@ingv.it*

In the Black Sea, significant volumes of both deep thermogenic and shallow biogenic cold seeps are continuously escaping to the seafloor and into the water column.
Methane transfer from the seafloor to the atmosphere may become an important issue affecting global climate change in the very next future. Since methane flares are widespread recognized from the continental shelf to the deepest part of Black sea basin, during 2019, in the framework of the ENVRI Plus project and the activities related to the EMSO ERIC, two oceanographic campaigns were performed on the Romanian sector of the Black Sea.
The main target was to detect and track methane flares from the seafloor in order to better constrain the possible mechanisms responsible for the injection of methane from the marine sediments, through the water column into the atmosphere. By the cooperation of three European Research Institutions (INGV, GeoEcoMar, IFREMER), a multidisciplinary submarine observatory (EMSO-MedIT 001) was deployed at the depth of 110 meter, for a 5 days-long period (D1) (Figure 1).

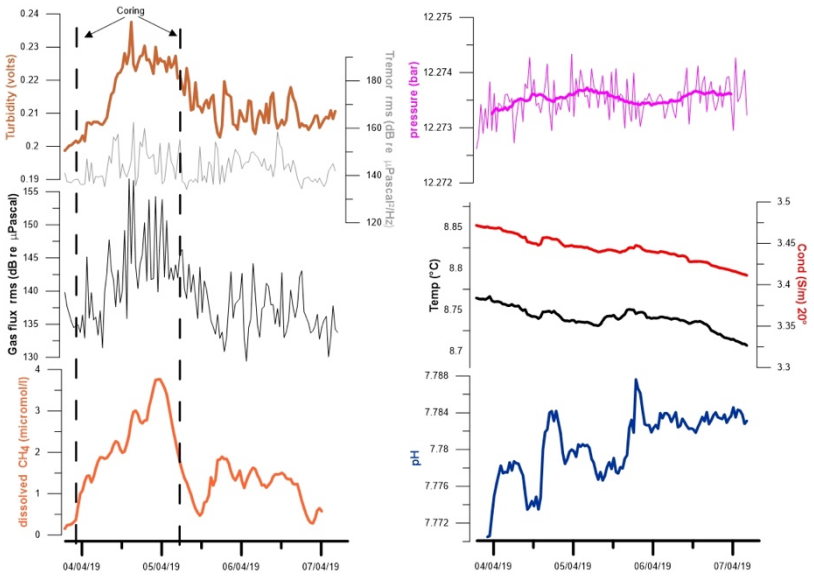

Figure 1 Picture shows data acquired during D1. In the left side, from the top to the bottom, graphics show variation over time of: Turbidity, Tremor, Gas flux, Dissolved methane. In the right side: Hydrostatic Pressure, Conductivity, Temperature, pH.

The Observatory was recovered, the data downloaded and re-deployed a few hundred meters away from the first site, for two months-long acquisition period (D2) (Figure 2).

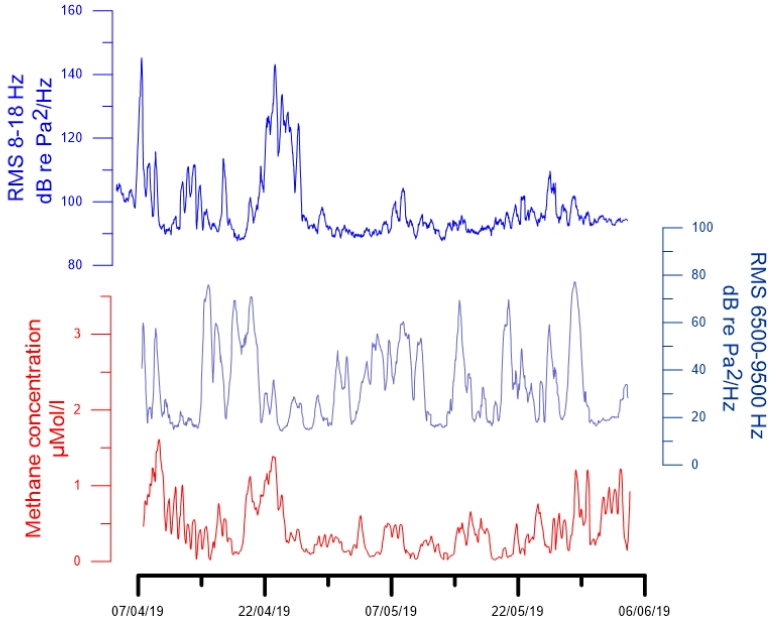

Figure 2 Picture shows data acquired during D2. From the top to the bottom, graphics show variation over time, Tremor, Gas flux, Dissolved methane.

The multidisciplinary sea floor observatory is able to operate in extreme submarine environment up to the depth of 4000 meters. It has been equipped with probes for acoustic signals, dissolved CH_4, Temperature, Pressure, Conductivity, pH and Turbidity.
Chemical-physical data (Temperature, Conductivity, pH, Hydrostatic pressure), recorded during both D1 and D2 deployments, showed the typical features of the seawater layers close to the seafloor without any significant variation over the time. Only pH values (about 7.8) were lower with respect the normal seawater due to the high concentration of H_2S close to the seafloor.
The first dataset, coming from D1, has shown a strong correlation between changes in the passive acoustics signals, and dissolved CH_4 concentration in seawater, increased up to 4 micromol/l. Passive acoustic data allowed to reveal changes in the bubbling activity intensity (noise generated from clusters of methane bubbles), as a proxy of the submarine gas outflow. The increasing of dissolved methane values matched the turbidity trend. The latter provides information on the presence in the water column of both sediments and bubbles. The acoustics values in terms of sound intensity followed the trends of turbidity as well. All the changes recorded during the D1 time period, were induce by the coring operations performed during the campaign, showing how methane emissions can be efficiently enhanced stripping the gas dissolved in the sea floor sediments due to anthropogenic perturbations as well as from natural events such as local or regional earthquakes.
Data acquired during the second, two-months long deployment showing variations of dissolved methane ranging between 200 nanomol/l and 1.5 micromol/l. Passive acoustics in the range 6500-9500 Hz, accounting for gas outflow changes, show variations in the noise generated by methane flares. RMS (very low acoustics frequency in the range of 8-18 Hz), accounting for “tremor” generated by gas dynamics along cracks emitting methane, shows high correlation with the dissolved methane recorded by the electrochemical probe.

References

Dziaka R.P., Matsumoto H., Embley R.W., Merle S.G., Lau T.-K., Baumbergera T., Hammondc S.R., Raineaultd N., (2018). *Passive acoustic records of seafloor methane bubble streams on the Oregoncontinental margin*. Deep-Sea Research, Part II 150 (2018) 210-217 https://doi.org/10.1016/j.dsr2.2018.04.001.

Hovland M., Judd A.G. and Burke R.A., (1993). *The global flux of methane from shallow submarine sediments*. Chemosphere, v. 26, no. 1-4, p. 559-578.

Schmale O., Greinert J. and Rehder G., (2005). *Methane emission from high-intensity marine gas seeps in the Black Sea into the atmosphere*. Geophysical Research Letters, v. 32, no. 7.

Tracking methane from the geosphere to the atmosphere: First results and first lessons learnt from the Envri Methane cruise

Ruffine L.[1], Paris J. D.[2], Grilli R.[3], Italiano F.[4], Schumacher M.[5], Leau H.[1], Bălan S.[6], Blouzon C.[3], Birot D.[1], Donval J. P.[1], Giunta T.[1], Greinert J.[5], Guyader V.[1], Lazzaro G.[4], Longo M.[4], Rinnert E.[1], Scalabrin C.[1], Scirè S.[4]

[1]*IFREMER, Département Ressources physiques et Ecosystèmes de fond de Mer (REM), Unité des Géosciences Marines, France*
[2] *Laboratoire des Sciences du Climat et de l'Environnement, CEA-CNRS-UVSQ, France*
[3] *CNRS, Univ. Grenoble Alpes, IRD, Grenoble INP, IGE, France*
[4] *Istituto Nazionale di Geofisica e Vulcanologia, Sezione di Palermo, Italy*
[5] *GEOMAR Helmholtz Centre For Ocean Research, Kiel, Germany*

Corresponding Author: *livio.ruffine@ifremer.fr*

Methane is a powerful greenhouse gas, and accordingly it is important to decipher the different sources that can provide input to the atmosphere [Saunois et al., 2016]. Over the last decades, the discovery of cold seeps on continental margins has shed the light on large sources of marine (microbial) methane [Hovland et al., 1993; Suess, 2014]. Indeed, due to the important accumulation of organic matter on continental margins, large amounts of methane are generated within the sediment and a fraction of it is discharged in the water column. The ocean is a powerful machine capable of mitigating marine methane input to the atmosphere. Indeed, most of the methane is oxidized within the sediment [Knittel and Boetius, 2009], and the ascent in the water column. Therefore, only a small fraction of the produced microbial methane can potentially reach the atmosphere and contributing to global warming [McGinnis et al., 2006; Rehder et al., 2009].

The injection into the atmosphere occurs under certain conditions. Previous studies have shown that methane transfer from the sediment to the atmosphere dependent on site and depth [Greinert et al., 2010; Romer et al., 2017; Shakhova et al., 2010]. Therefore, it is important to know when these conditions are met and to quantify the release in order to better understand the dynamics of marine methane.

Closed or semi-closed seas like the Black Sea, the Caspian Sea and the Sea of Marmara are characterized by intense methane emissions [*e.g.* Bezrodnykh et al., 2013; 2012; Ruffine et al., 2018; Schmale et al., 2005], from shallow to deep depths. They are consequently good candidates for investigating and better constraining the fate of marine methane and its potential input into the atmosphere to derive complete and consistent methane budget for a specific region.

In April 2019, in the frame of the H2020 ENVRI Plus program[1], the scientific cruise *Envri Methane* has been undertaken in the Romanian sector of Black Sea coupling different methodologies for quantifying marine methane transfer from the sediment to the atmosphere. The scientific motivation behind this cruise is to achieve a holistic understanding of the transfer processes involved. Thus,

[1] H2020 INFRADEV ENVRI Plus «ENVironnemental Research Infrastructures» GA n°654182

operations combined multiple expertise for measuring concentrations and fluxes of methane in the different spheres, from the geosphere to the atmosphere. Twenty scientists from four different research infrastructures (RI) in Europe (European Multidisciplinary Seafloor and water-column Observatory- EMSO, Integrated Carbon Observation System- ICOS, European Aerosol, Clouds, and Trace gases Research Infrastructure- ACTRIS, and an alliance of European research fleets- EuroFleets) combined their forces for this expedition. They developed a joint monitoring strategy for methane quantification. Both *in situ* measurements and onshore analyses from collected samples were carried out.

First, acoustic surveys of the water column over two methane-seep clusters were performed to map their extent and evaluate the release of free methane. Two sites, characterized by multiple gas flares detected during echosounder surveys, were investigated.

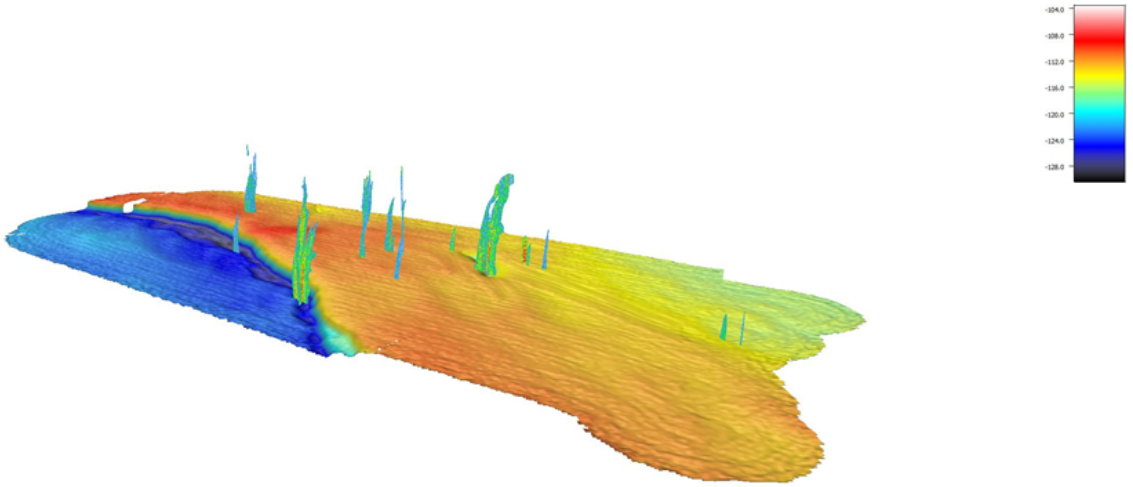

Figure 1 3D mapping of the gas flares identified during the campaign from the echosounder EK80.

A seafloor observatory has been deployed close to a selected seep for a five days monitoring period, and left on the seafloor for long term monitoring after the campaign. Gas-charged sediment as well as seawater over the entire water column have been sampled for laboratory measurements of methane content and isotopic composition. In addition, real-time *in situ* gas measurements were carried out through the investigated water mass using three different instruments: two *in situ* spectrometers- the membrane inlet laser spectrometer (MILS) SubOcean [Grilli et al., 2018] and the in situ mass spectrometer (ISMS)-, and the commercial METS sensor from Franatec. Prior to the cruise, the two Franatec sensors were tested at variable pressures and methane concentrations using a novel high-pressure gas-calibration bench purposely developed for this work within the ENVRI Plus program. Simultaneously, continuous measurements of methane and its main isotopes in the atmosphere were carried out with Picarro analyzers. For the monitoring of the methane emissions in the water column, a seafloor observatory was deployed close to a selected seep for five days.

Overall, there was a good agreement between the *in situ* measurements of methane using the SubOcean probe and the Franatec sensor. There was also a good agreement between the results obtained from onshore methane concentration measurement at two different laboratories. The major discrepancy was observed from water samples collected near the seafloor where methanotrophy is expected to be more important. Oxygen concentration measured *in situ* with the ISMS was in agreement with those measured by the CTD-connected optode.

It appears from this experience that the combination of the four RIs is an appropriate cluster to study the dynamics of marine methane from the lithosphere to the atmosphere.
The main outcomes from the cruise can be summarized as follows:

- Methane concentration drastically decreases from the lithosphere to the atmosphere, highlighting its degradation and dispersion along the pathway to the atmosphere.
- The seafloor observatory effectively detect changes in methane concentration over time. In this case, the change was induced by the coring operation, highlighting how sensitive methane emissions are regarding environmental or anthropogenic perturbations.
- The atmospheric measurements show a more important contribution of marine methane to the atmosphere at shallow water depth.
- An in-depth calibration of the *in situ* methane sensors is required as function of pressure, temperature and competing dissolved gases which may affecting the output signal.

References

Bezrodnykh Y.P., Deliya S.V., Lavrushin V.Y., Yunin E.A., Poshibaev V.V. and Pokrovskii B G., (2013). *Gas seeps in the North Caspian water area*. Lithology and Mineral Resources, v. 48, no. 5, p. 373-383.

Greinert J., McGinnis D.F., Naudts L., Linke P. and De Batist M., (2010). *Atmospheric methane flux from bubbling seeps: Spatially extrapolated quantification from a Black Sea shelf area*. Journal of Geophysical Research, Oceans, v. 115.

Grilli R., Triest J., Chappellaz J., Calzas M., Desbois T., Jansson P., Guillerm C., Ferré B., Lechevallier L., Ledoux V. and Romanini D. (2018). *Sub-Ocean: subsea dissolved methane measurements using an embedded laser spectrometer technology*. Environ. Sci. Technol., 52, 10543-10551, doi: 10.1021/acs.est.7b06171.

Hovland M., Judd A.G. and Burke R.A., (1993). *The global flux of methane from shallow submarine sediments*. Chemosphere, v. 26, no. 1-4, p. 559-578.

Knittel K. and Boetius A., (2009). *Anaerobic oxidation of methane: progress with an unknown process*: Annual review of microbiology, v. 63, p. 311-334.

McGinnis D.F., Greinert J., Artemov Y., Beaubien S.E., Wüest A., (2006). *Fate of rising methane bubbles in stratified waters: How much methane reaches the atmosphere?* J. Geophys. Res. Oceans 111, C09007. doi: 10.1029/2005JC003183.

Rehder G., Leifer I., Brewer P.G., Friederich G., Peltzer E.T., (2009). *Controls on methane bubble dissolution inside and outside the hydrate stability field from open ocean field experiments and numerical modeling*. Mar. Chem., 114, 19-30. doi: 10.1016/j.marchem.2009.03.004.

Romer M., Wenau S., Mau S., Veloso M., Greinert J., Schluter M., and Bohrmann G., (2017). *Assessing marine gas emission activity and contribution to the atmospheric methane inventory: A multidisciplinary approach from the Dutch Dogger Bank seep area (North Sea)*. Geochemistry Geophysics Geosystems, v. 18, no. 7, p. 2617-2633.

Ruffine L., Ondreas H., Blanc-Valleron M.-M., Teichert B.M.A., Scalabrin C., Rinnert E., Birot D., Croguennec C., Ponzevera E., Pierre C., Donval J.-P., Alix A.-S., Germain Y., Bignon L., Etoubleau J., Caprais J.-C., Knoery J., Lesongeur F., Thomas B., Roubi A., Legoix L.N., Burnard P., Chevalier N., Lu H., Dupré S., Fontanier C., Dissard D., Olgun N., Yang H., Strauss H., Özaksoy V., Perchoc J., Podeur C., Tarditi C., Özbeki E., Guyader V., Marty B., Madre D., Pitel-Roudaut M., Grall C., Embriaco D., Polonia A., Gasperini L., Çağatay M.N., Henry P. and Géli L., (2018). *Multidisciplinary investigation on cold seeps with vigorous gas emissions in the Sea of Marmara (MarsiteCruise): Strategy for site detection and sampling and first scientific outcome*. Deep Sea Research, Part II: Topical Studies in Oceanography.

Saunois M., Bousquet P., Poulter B., Peregon A., Ciais P., Canadell J.G., Dlugokencky E.J., Etiope G., Bastviken D., Houweling S., Janssens-Maenhout G., Tubiello F.N., Castaldi S., Jackson R.B., Alexe M., Arora V.K., Beerling D.J., Bergamaschi P., Blake D.R., Brailsford G., Brovkin V., Bruhwiler L., Crevoisier C., Crill P., Covey K., Curry C., Frankenberg C., Gedney N., Hoeglund-Isaksson L., Ishizawa M., Ito A., Joos F., Kim H.-S., Kleinen T., Krummel P., Lamarque J.-F., Langenfelds R., Locatelli R., Machida T., Maksyutov S., McDonald K.C., Marshall J., Melton J.R., Morino I., Naik V., O'Doherty S., Parmentier F.-J.W., Patra P.K., Peng C., Peng S., Peters G.P., Pison I., Prigent C., Prinn R., Ramonet M., Riley W.J., Saito M., Santini M., Schroeder R., Simpson I.J., Spahni R., Steele P., Takizawa A., Thornton B.F., Tian H., Tohjima Y., Viovy N., Voulgarakis A., van Weele M., van der Werf G.R., Weiss R., Wiedinmyer C., Wilton D.J., Wiltshire A., Worthy D., Wunch D., Xu X., Yoshida Y., Zhang B., Zhang Z., and Zhu Q., (2016). *The global methane budget 2000-2012*. Earth System Science Data, v. 8, no. 2, p. 697-751.

Schmale O., Greinert J. and Rehder G., (2005). *Methane emission from high-intensity marine gas seeps in the Black Sea into the atmosphere*. Geophysical Research Letters, v. 32, no. 7.

Shakhova N., Semiletov I., Salyuk A., Yusupov V., Kosmach D. and Gustafsson O., (2010). *Extensive Methane Venting to the Atmosphere from Sediments of the East Siberian Arctic Shelf*. Science, v. 327, no. 5970, p. 1246-1250.

Suess E., (2014). *Marine cold seeps and their manifestations: geological control, biogeochemical criteria and environmental conditions*. International Journal of Earth Sciences, v. 103, no. 7, p. 1889-1916.

REE and trace elements fractionation in a wide range pH and Eh in shallow hydrothermal vents at Panarea island (Italy)

Sposito F.[1,2], Longo M.[1] and Brusca L.[1]

[1]*Istituto Nazionale di Geofisica e Vulcanologia, Sezione diPalermo, Italy*
[2]*Università degli Studi di Palermo, Dipartimento delle Scienze della Terra e del Mare (DiSTeM), Palermo, Italy*

Corresponding Author: *fabio.sposito@unipa.it*

The Rare Earth Elements (REE; lanthanides and yttrium) are important tracers of natural and anthropic geochemical processes. In this paper we show some recent progresses concerning the study of REE and trace elements geochemistry in natural system.
Trace Elements and REE geochemical behaviour have been investigated in SHVs (shallow sea-water hydrothermal vents) in the sourranding area of Panarea Island (Eolian Island, Italy) [Italiano et al., 1991]. Samples were collected on June and November 2015 and June 2018 from several several submerged vents at different depth (5-40m) and analyzed for Al, V, Cr, Mn, Fe, Co, Ni, Zn, As, Cd, Sb, Ba, Pb, Th, U and REE; all concentrations were measured by ICP-MS after triethylamine-assisted $Mg(OH)_2$ preconcentration-coprecipitation method [Arslan et al., 2018].
Discharged volcanic fluids are responsible of chemical modification in terms of physical-chemcal parameters, inducing a wide range of pH (4.1 - 8.2) and Eh (-235 - 186 mV) values. The variability of pH and Eh conditions is responsible of the chemical composition and fractionation of REE, having a wide range of concentration values, spanning from 55.9 to 23594.4 ng l^{-1}. ΣREE (total REE concentration) is higher than ΣREE reference seawater value [Censi et al., 2007] up to three order of magnitude and are inversely correlated relative to pH values. Furthermor minor Ce anomaly (Ce/Ce^* >0.6) have been calculated respect the well documented Ce anomaly in seawater (Ce/Ce^* =0.2) [4]. Probably the redox condition (Eh <0 mV) do not allow the oxidation of Ce(III) to Ce(IV), as a result the preferential scavenging activity over REE(III)s is inhibited.
The pH and Eh conditions play a key role on water composition in terms of minor and trace elements, controling the precipitation of Fe and Al-bearing minerals inducing changes both in Mn, As and V concentrations both in REE fractionation [Inguaggiato et al., 2015].
As a result, REE Patterns normalized to PAAS show two different trends: type-1, increasing trend from La to Lu, due to carbonate complexation of REE as usual in seawater; Type-2, caracterised by Light REE depletion (LREE: La-Sm), probably due to adsorption to Al and Fe-oxyhydroxides. In particular LREE depletions (Ce_N/Lu_n <1.0) are observed respect MREE (Middle REE: Eu-Dy) and HREE (Heavy REE: Ho-Lu). Plotting Ce_N/Lu_N vs ΣREE, an hyperbolic array is displayed (Figure 2) formed by two end-members: EM1 (green dot in figure 2) characterised by higher Ce/Lu and Low Al and Fe concentrations (REE Pattern type-1); EM2 (red dot in figure 2) with Lower Ce/le and high Al and Fe concentrations (REE Pattern Type-2). Since a positive correlation among REE-Al-Fe is observed (figure 3), the simultaneous variation of these elements indicates the involvement of Al and Fe controlling REE abundance.
The same hyperbolic trends also are observed for trace element as Mn-V *vs* Al and As *vs* Fe, suggesting that the formation of Al and Fe-oxyhydroxides is also responsible for fractionation of Mn, V and As [Sherman et al., 2003], while the fractionation for the other analysed elements is controlled by carbonate complexation process occurring in seawater. All these evidences demonstrate that the contamination of discharging fluids and consequent formation of Fe and Al-bearing minerals controls

the fractionation of REE and trace elements. As a result, the fate of trace metals and REE is mainly conveyed by both processes of scavenging onto newly forming Al and Fe-oxyhydroxides and carbonate complexation.

The suggested model provides important details on the fate of trace metals and REE discharged by shallow hydrothermal vents showing the interactions between hydrothermal fluids and seawater, demonstrating the chemical composition is controlled by contamination of discharging fluids and the typical process of oxidation and co-precipitation occurring in seawater.

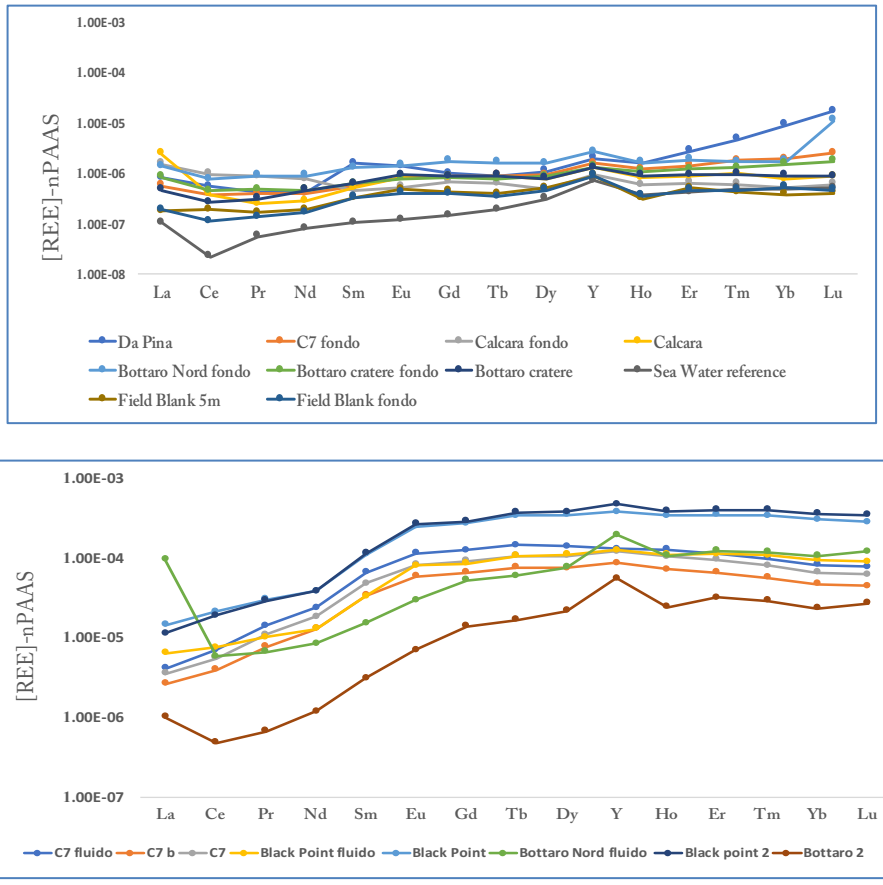

Figure 1 PAAS-Normalised REE Patterns: a) Pattern type-1; b) Pattern type-2.

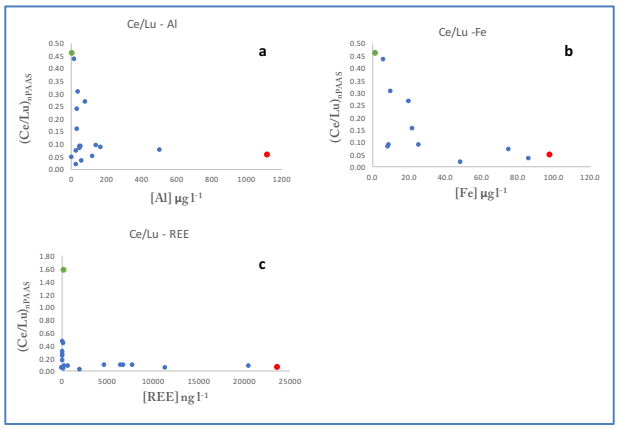

Figure 2 Correlation between Al-Fe-REE concentrations and Ce_n/Lu_n ratio.

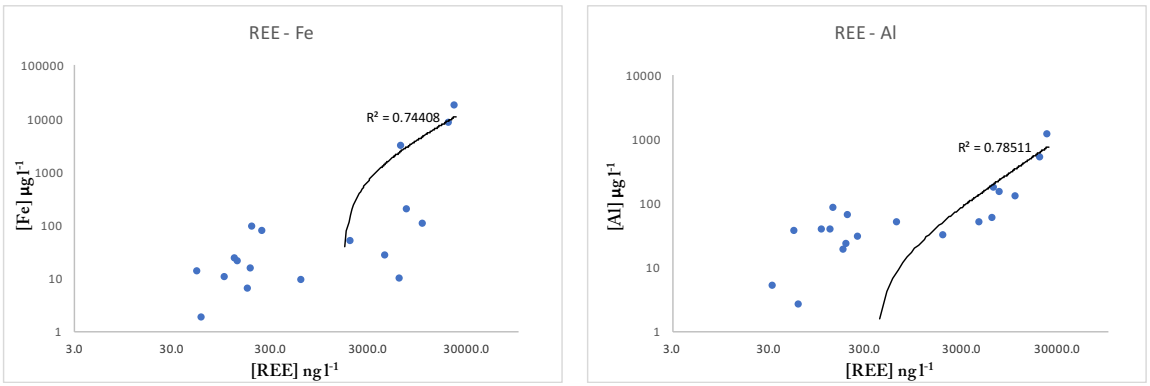

Figure 3 Correlation between Total REE concentrations with Fe and Al.

References

Italiano F. and Nuccio P.M., (1991). *Geochemical investigations of submarine volcanic exhalations to the east of Panarea, Aeolian Islands, Italy*. In: Journal of Volcanology and Geothermal Research, 46, 125-141.

Arslan Z., Oymak T., ans White L., (2018). *Triethylamine-assisted $Mg(OH)_2$ coprecipitation/ preconcentration for determination of trace metals and rare earth elements in seawater by inductively coupled plasma mass spectrometry (ICP-MS)*. Analytica Chimica Acta, 1008, 18-28.

Censi P., Sprovieri M., Larocca D., Aricò P., Faiano F., Mazzola S. and Ferla P. (2007). *Alteration effects of volcanic ash in seawater: Anomalous Y/Ho ratios in coastal waters of the Central Mediterranean Sea*. Geochimica et Cosmochimica Acta, 71 (22), 5405-5422.

Alibo, D.S., and Nozaki, Y., 1999. *Rare earth elements in seawater: particle association, shale normalization, and Ce oxidation*. Geochim Cosmochim Acta 63, 363-372.

Inguaggiato C., Censi P., Zuddas P., Londono J.M., Chacòn Z., Alzate D., Brusca L. and D'Alessandro W. (2015). *Geochemistry of REE, Zr and Hf in a wide range of pH and water composition: The Nevado del Ruiz volcano-hydrothermal system (Colombia)*. Chemical Geology, 417, 125-133.

Sherman D.M. and Randall S.R., (2003). *Surface complexation of arsenie(V) to iron(III) (hydr)oxides: Structural mechanism from ab initio molecular geometries and EXAFS spectroscopy*. Geochimica et Cosmochimica Acta, 67(22) 4223-4230.

Evidence of fluids emission in the Northern Sicily continental margin

Sulli A.[1], Grassa F.[2], Caracausi A.[2], Italiano F.[2], Zizzo E.[1], Spatola D.[3], Pennino V.[4], Interbartolo F.[4]

[1]*Università degli Studi di Palermo, Dipartimento delle Scienze della Terra e del Mare (DiSTeM), Palermo, Italy*
[2]*Istituto Nazionale di Geofisica e Vulcanologia, Sezione di Palermo, Italy*
[3]*Marine Geology and Seafloor Surveying, Department of Geosciences, University of Malta, Malta*
[4]*ARPA, Agenzia Regionale per la Protezione Ambientale Sicilia, Italy*

Corresponding Author: *fausto.grassa@ingv.it*

The presence of morphological submarine structures linked with escaping fluids alongside the northern Sicily continental margin has been documented, through high resolution and multichannel seismic profiles coupled with multibeam echosounder (seafloor relief) data.
The northern Sicily continental margin is located in the southern Tyrrhenian Sea, from the north Sicily coastal belt to the Marsili Abyssal Plain, in the transitional area between the Sicilian-Maghrebian chain to the south and the Tyrrhenian Basin to the north. It originated as a consequence of a complex interaction of compressional events, crustal thinning and strike-slip faulting that produced a very complex morphostructural setting. Along the margin, morphology of the high-gradient continental slope is irregular due to the presence of structural highs, slope failures and canyons, and is interrupted by flat areas at a mean depth of 1500 m. In this context, the occurrence of different types of structures with highly contrasting seismic and morphologic signatures, both dome-type and concave-upward structures was recognized.
Seismostratigraphic analysis tools and methods were used to identify fluid escape structures and to work out a classification on the basis of their morpho-acoustic characteristics.
The concave-upward structures have a typical circular shape and are better known as pockmarks. These depressions have a mean axis of 400 m, mean depth of 20m and wall slope gradient of 2-4°. Some of them appear contiguous with other depressions, forming elongated channels in a uniform direction, instead at places they are organised in clusters or are isolated.
Morphobathymetric, seimo-stratigraphic and structural data show in the subseafloor of these structures continuous reflectors with concave upward geometry up to the seafloor often accompanied by acoustic anomalies. In most cases they occur along fault planes, mainly associated with diagenetic carbonates and fluid venting activity. Therefore, pockmarks could be the result of both fault and landslide structures, as they appear aligned along a straight direction and occur in proximity of the slope and are associated with slope instabilities.
In the Palermo and Termini Imerese bays we identified small mounds more than 10 m high, 5 km long and 200 m wide, arranged predominantly along the NNW-SSE trend and ENE-WSW trend respectively.
In the Termini Imerese area we identified also seismic anomalies, such as reflection-free seismic units, associated with diffraction hyperbolas, local bottom-simulating reflectors, vertical blanked areas, which could be associated with the presence of gas in the sedimentary succession.
Taking into account the directions of alignment of both pockmarks and mounds, which fit the deformational pattern produced by the present-day stress field in the Northern Sicily continental margin, we suppose that the structural features are possibly associated with the recent tectonics mapped on-land as well as the widespread seismicity of the margin.

Faults associated with pockmarks could be a preferential escape route for fluids. In order to evaluate the nature of these fluids, a 2.3 m long sediment core was collected in correspondence of a pockmark at a depth of 414 m. Extracted pore waters were sampled every 10 cm and analysed in relation to their conductivity (EC), major and minor chemical composition and stable isotopes (δD and $\delta^{18}O$).
The main geochemical features reveal that pore water has a salinity slightly lower than modern Mediterranean Seawater. The stable isotope composition of pore water and the distribution profiles of EC, ion/Chloride ratios seem to indicate the existence of an external source of fluids and the occurrence of sediment-fluids interaction processes. The destabilisation of gas hydrates has been inferred as a possible mechanism causing pore water freshening.

ST05

ENVIRONMENTAL IMPACT OF GASEOUS EMISSIONS (AIR POLLUTION AND MONITORING, RN AND ENVIRONMENTAL RADIOACTIVITY)

REFERENCE: MARCELLO LIOTTA

α-radiation from home building materials likely affecting human health in Northern Vietnam

Dương Nguyễn-Thùy[1], Hướng Nguyễn-Văn[1], Thomas Streil[2], Nguyệt Thị Ánh Nguyễn[1], Minh Ngọc Schimmelmann[3], and Arndt Schimmelmann[3]

[1]*Falculty of Geology, VNU University of Science, Vietnam National University Hanoi, Việt Nam*
[2]*SARAD GmbH, Dresden, Germany*
[3]*Indiana University, Department of Earth and Atmospheric Sciences, USA*

Corresponding Author: *duongnt_minerals@vnu.edu.vn*

Radon is a radioactive gas that is widely generated in rocks, soils, and building materials. It has been recognized as the second most important factor triggering lung cancer, after smoking as the leading cause. This survey (i) quantifies the nuclide-specific α-radiation of ^{222}Rn (radon) and ^{220}Rn (thoron) in common types northern Vietnamese houses constructed with different materials, and (ii) evaluates the total annual effective dose rate of indoor α-radiation for inhabitants. Surveyed homes were built with traditional local materials such as clay, soil, stone and crushed limestone. Measurements of both radon and thoron were performed with a SARAD® RTM 2200 in different types of houses in the center of rooms and near walls.

The average total ^{222}Rn abundance in indoor air of all types of homes was < 100 Bq m^{-3}, but ^{220}Rn concentrations were far higher than ^{222}Rn and expressed a trend of increasing values from the center of rooms to locations closer to interior walls. Thoron concentrations peaked close to walls built from compacted and dried soil, unfired-clay bricks and bricks made from crushed limestone. A maximum thoron concentration of up to 1052 Bq m^{-3} was measured in air close to a wall of unfired-soil bricks. The thoron levels in the center of rooms without wall coverings (i.e. exposing the raw building materials) exceeded 150 Bq m^{-3}, 15 times higher than the average environmental level of 10 Bq m^{-3} for thoron [UNSCEAR, 2000]. In contrast, thoron in the center of rooms was below the detection limit when walls were constructed with fired-clay bricks or concrete, and was 86 Bq m^{-3} when compacted soil walls had been covered with a layer of plaster.

The total annual effective dose rates from radon and thoron and their progenies to inhabitants who spend about 13 hours per day in the various types of houses in northern Vietnam are estimated to be higher than 10 mSv a^{-1} in houses where raw building materials are exposed on walls, especially up to 37 mSv a^{-1} for houses built with compacted soil. A range from 6.5 to 9.5 mSv a^{-1} is estimated for houses constructed with fired-clay bricks or where walls are covered with plaster. The total excess lifetime cancer risks from indoor α-radiation in affected northern Vietnamese homes range from about 20×10^{-3} to 130×10^{-3}, which is much higher than the world average of 1.45×10^{-3} [ICRP, 1991; Shausha and Ahmad, 2016]. Practical mitigation strategies are needed to reduce indoor α-radiation from thoron in many traditional homes in northern Vietnam.

Funding Statement
The content of this manuscript is based upon work supported by the Vietnam National Foundation for Science and Technology Development (NAFOSTED) grant number 105.99-2016.16. Measurements with the SARAD® RTM 2200 were supported by the U.S. Department of Energy, Office of Science, Office of Basic Energy Sciences, Chemical Sciences, Geosciences, and Biosciences

Division under Award Number DE-SC0006978.

References

ICRP, (1991). *Recommendations of the International Commission on Radiological Protection*. ICRP Publication, 60, Ann. ICRP 21 (1-3).

Shousha H.A. and Ahmad F., (2016). *Lifetime cancer risk of gamma radioactivity results from smoking*. Radiat. Cancers Review., 3, 1-9.

UNSCEAR, (2000). *The United Nations Scientific Committee on the Effects of Atomic Radiation*. In: Sources, vol. I. United Nations, New York.

Geochemical characteristics of natural gases related to Late Paleozoic coal measures in China

Gong Deyu, Dai Jinxing, Wei Yanzhao

Research Institute of Petroleum Exploration and Development, PetroChina, China

Corresponding Author: *deyugong@petrochina.com.cn*

By 2013, more than 20 gas fields related to the Late Paleozoic coal measures had been discovered in China. The total proven reserves of these gas fields is more than 3200×10^9 m^3, accounting for 30% of the proven gas reserves in China. After analyzing the molecular compositions, stable carbon isotopes, and helium isotopes of 375 gas samples, genetic types and origins of the natural gas, as well as the secondary alterations it experienced, are discussed. Most of the gases are coal-type gas, with some of the gases from the Sichuan Basin and the Jingbian gas field in the Ordos Basin being oil-type gases generated from marine mudstones. The Ro values of natural gas vary from 0.8% to 2.5%, indicating the mature-over mature stage. Because the carbon isotopes of the C_{2-4} gases are only slightly affected by thermal maturity, they can be used as an effective criterion to distinguish coal-type and oil-type gases. Positive carbon isotopic series are observed in most gas samples, and carbon isotopic reversals occur in the forms of $\delta^{13}C_1 > \delta^{13}C_2$ and $\delta^{13}C_1 < \delta^{13}C_2 > \delta^{13}C_3$. The former resulted from the admixture of oil-type and coal-type gases, while the latter resulted from the admixture of coal-type gases of different maturities. High concentrations of H_2S in natural gas from the Sichuan Basin and the Chenghai gas field in the Bohai Bay Basin resulted from thermochemical sulfate reduction (TSR), which causes, to some extent, the fractionation of ethane carbon isotopes. By contrast, the fractionation of methane carbon isotopes resulting from the TSR effect is not clear. CO_2 from the Bohai Bay and Junggar Basins is primarily biogenic, generated via the thermal decomposition of organic matter, while that from the Ordos Basin, Sichuan Basin, and Chenghai gas field is generated via the thermal decomposition of carbonates. CO_2 related to the TSR effect has also contributed to the Sichuan Basin and Chenghai gas field.

CO_2 and radon distribution in groundwater of the urban area of Rome (central Italy): geo-structural control and Gas Hazard assessment in a highly populated area

Pizzino L.[1], Sciarra A.[1], Gallo F.[2] and Di Renzo D.[2]

[1]*Istituto Nazionale di Geofisica e Vulcanologia, Sezione di Sismologia e Tettonofisica, Roma, Italy*
[2]*Geologist, Rome, Italy*

Corresponding Author: *luca.pizzino@ingv.it*

Introduction

The city of Rome is located in the Roman Magmatic Province (RMP onward, central Italy, Washington, 1906), where large sectors experience a huge degassing both from soils and aquifers [Pizzino et al., 2002; Annunziatellis et al., 2003; Carapezza et al., 2019; Chiodini et al., 2004; Barberi et al., 2007; Mariucci et al., 2008; Frondini et al., 2008; Cinti et al, 2011; 2013; 2014; 2019; Pizzino, 2015; Pizzino et al., 2015]; gas composition is dominated by CO_2, that can act as a carrier for other minor components such as N_2, CH_4, H_2S and radon. Large amounts of carbon dioxide are produced at depth; in general, CO_2 is considered to be a mixture of mantle degassing sources and the by-product of decarbonation of crustal carbonates, present in variable proportions [e.g. Chiodini & Frondini, 2001]. During its ascent, CO_2 is trapped in buried structural highs, made up of Mesozoic permeable limestones, as evidenced by positive gravity anomalies [Cesi et al., 2008]. These horsts, covered by impermeable terrains, become sources of a high CO_2 flux toward the surface. CO_2 moves upward through crustal weaknesses, dissolves in shallow aquifers, creating wide areas with high pCO_2 in groundwater [i.e. Diffuse Degassing Structures, Pizzino et al., 2002; Chiodini et al., 2004, Minissale et al., 2019]. Aquifers can result in an over-saturation state with respect to CO_2, allowing the free phase to escape towards surface, permeating soils. Moreover, local volcanic outcrops are characterized by high concentrations of natural radionuclides (uranium, thorium and potassium), becoming an important source of radon both in soils and groundwater. Geochemical features of volcanic products substantially enhance the regional radiation background [e.g. Ciotoli et al., 2017].

Where hydrogeological, hydrochemical, structural and lithological conditions are favourable, both CO_2 and radon exhaled from soils and aquifers can enter houses (mainly their depressed parts such as cellars, and basements) in highly urbanized areas, potentially reaching harmful indoor levels. Indeed, CO_2 can have a short-term toxicity if it overcomes fixed indoor thresholds, while radon can cause lung cancer at prolonged exposures. Therefore, an evaluation of the level of Gas Hazard (from now on GH) to which these areas are exposed, must be done.

By now, detailed information on CO_2 and radon distribution in ground waters was assessed both for the Sabatini [e.g. Cinti et al., 2011; 2013; 2019] and Colli Albani [e.g. Chiodini & Frondini, 2001; Pizzino et al., 2002] volcanic complexes (located N and S of Rome, respectively). These researches allowed to discriminate sectors where analysis of indoor-gas levels has to be carried out and deepened, in order to lessen their impact on human health. Such an investigation (i.e. an evaluation of the possible GH in highly populated areas) was still lacking for the urban territory of the Italian capital, where about 2800000 people habitually live; accordingly, an extensive study of CO_2 and radon distribution in the groundwater circulating in the urban area of Rome is ongoing since 2011.

Work done

A detailed geochemical study in ground waters (a sort of micro-zonation, following the approach used by Pizzino et al., [2002] in two municipalities of the Colli Albani volcano) started in 2011 and is currently going on in the urban area of Rome. Around 240 sampling sites (wells and springs) were investigated for both chemical and carbon (TDIC) isotopic compositions. pCO_2 [in bar] was computed for all waters by Phreeqc code, version 3 [Parkhurst and Appelo, 2013], using as input outlet temperature, pH, alkalinity and major elements. Dissolved radon sample was collected, where possible, measured by stripping on Active Charcoal Collectors (ACCs) through a portable degassing unit, and successively analysing in the laboratory with γ-spectrometry [e.g. Mancini et al., 2000].

Results: CO_2 and Radon distribution in ground waters

The CO_2 distribution allowed us to recognise and mark off areas characterised by CO_2-rich waters (figure 1). Different classes were determined by a statistical analysis [Sechman & Dzieniewicz, 2011]. High pCO_2 values (ranging between -0,30 and -1,28 bar) emphasised the presence of five sectors actively degassing in Rome: *Cassia*, *Salaria*, *Tor di Quinto-Flaminio-Saxa Rubra* in the north and *Eur-Torrino-Laurentino and Appio-Tuscolano-Capannelle* in the south. Isotopic composition of dissolved carbon highlighted a prevalent inorganic (i.e. deep-derived) origin for dissolved CO_2 [Pizzino, 2015]. In the remnant territory of Rome low-pCO_2 waters (spanning from -1,28 and -3,45 bar) circulate; in these samples, soil-derived CO_2 is dominant [Pizzino, 2015].

High-pCO_2 sectors represent Diffuse Degassing Structures in the urban area. Therefore, these sectors can be considered as potential GH-prone areas, potentially exposed to hazardous CO_2 emissions from soils.

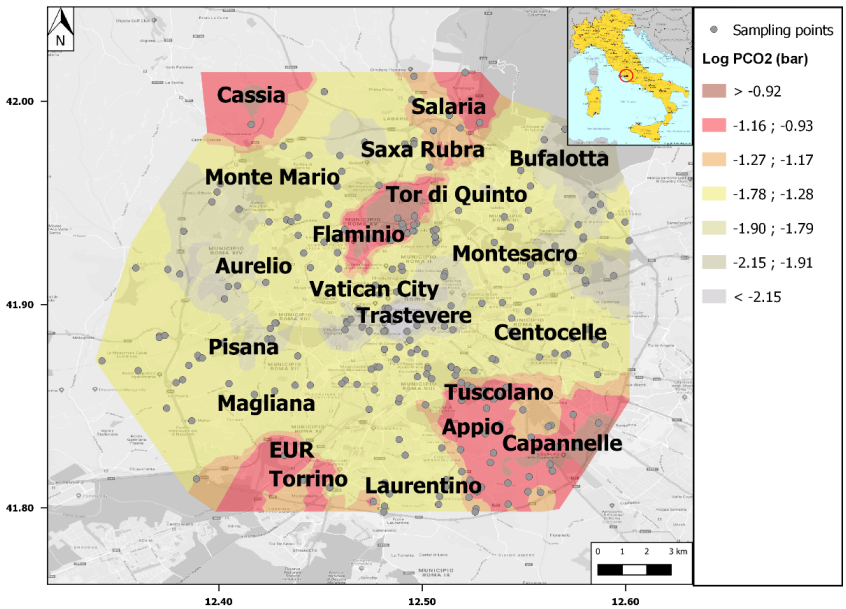

Figure 1 pCO_2 distribution in ground waters of the urban area of Rome. Different classes were determined using a statistical approach.

Radon-rich waters roughly mimic the CO_2 distributions and circulate diffusely in the southern and eastern sectors of Rome (Figure 2). They represent potential GH-prone areas, potentially exposed to hazardous radon emissions from soils. Spotty, high radon activity was found in CO_2-rich waters of central and northern sectors.

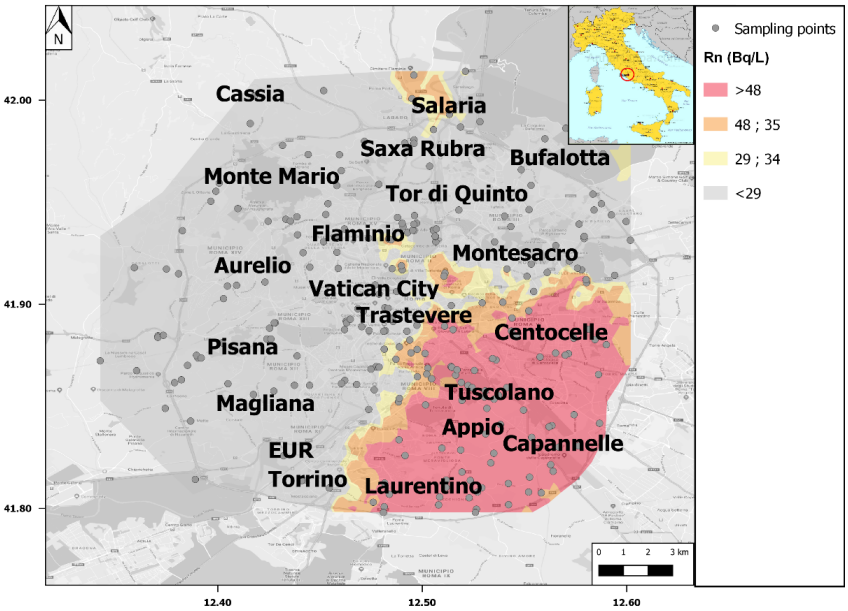

Figure 2 Radon distribution in ground waters of the urban area of Rome. Different classes were determined using a statistical approach.

Conclusions

The detailed study of CO_2 and radon distribution in groundwater of the urban area of Rome allowed to:

- Identify five sectors actively degassing, characterized by high pCO_2 levels, similar to those found in both Sabatini and Colli Albani volcanoes. CO_2 distribution is tectonic-controlled and marks the carbonate structural highs at depth (named *Tor di Quinto*, *Eur-Torrino-Spinaceto*, *Appio-Tuscolano*), through which a continuous degassing from their tops or flanks occurs. *Cassia* and *Salaria* are located very close to the southern edge of the most degassing sector of the Sabatini volcano [Cinti et al., 2011], while *Saxa Rubra* hosts an eccentric crater linked to the Sabatini volcano activity. Moreover, in this last site a significant contribute of mantle-derived He was found in groundwater [Pizzino, 2015], testifying the existence of deep-rooted faults.
  Fluid geochemistry demonstrated a very powerful and low-cost method to define and delimit the areal extension of these highly degassing deep tectonic structures. In this regard, the study of groundwater was particularly effective in the area of Rome, where evidence of ongoing degassing at surface (i.e. gas vents, bubbling pools) is absent or has been obliterated over time due to the huge urban expansion of the last decades;
- Discriminate the different sources of dissolved CO_2, ranging from organic (i.e. shallow, characteristic of low pCO_2 values) to deep-derived, marking the CO_2-rich waters;
- Identify the eastern and south-eastern sectors as characterised by radon-rich groundwater, due to their interaction with the cropping out Colli Albani volcanic products. Therefore, radon distribution is chiefly lithological-controlled; however, in other sectors of Rome (e.g. Salaria), radon activity can be locally enhanced through the CO_2 transportation.

CO_2 and radon water-rich sectors can be considered as prone to GH. Accordingly, a detailed soil-gas survey is highly recommended in these areas in order to quantify how much gas permeate soils, where houses and dwellings are built. Furthermore, quick exploratory surveys to determine the CO_2 and radon indoor levels in the individuated GH-prone areas must be promoted by local authorities, mainly in the most populated sectors, where the presence of gas in soils and/or indoor could represent a very big concern.

References

Annunziatellis A., Ciotoli G., Lombardi S., Nolasco F., (2003). *Short and longterm gas hazard: the release of toxic gases in the Alban Hills volcanic area (central Italy)*. J. Geochem. Explor., 77, 93-108.

Barberi F., Carapezza M.L., Ranaldi M., Tarchini L., (2007). *Gas blowout from shallow boreholes at Fiumicino [Rome]: induced hazard and evidence of deep CO_2 degassing on the Tyrrhenian margin of Central Italy*. J. Volcanol. Geotherm. Res., 165, 17-31.

Carapezza M.L., Barberi F., Ranaldi M., Tarchini L. & Pagliuca N.M., (2019). *Faulting and gas discharge in the Rome area (Central Italy) and associated hazards*. Tectonics, 38, 941-959.

Cesi C., Eulilli V., Ferri F., (2008/. *Analisi ed interpretazione dei valori delle anomalie di gravità del territorio dell'area romana: correlazione con gli elementi geologici di superficie e la struttura profonda*. In: Funiciello R., Praturlon A., & Giordano G. (ed.) "La Geologia di Roma", Memorie descrittive della Carta Geologica d'Italia, LXXX, 97-113.

Chiodini G., Cardellini C., Amato A., Boschi E., Caliro S., Frondini F., (2004). *Carbon dioxide Earth degassing and seismogenesis in Central and southern Italy*. Geophys. Res. Lett., 31, L07615.

Cinti D., Procesi M., Tassi F., Montegrossi G., Sciarra A., Vaselli O., Quattrocchi F., (2011). *Fluid geochemistry and geothermometry in the western sector of the Sabatini Volcanic District and the Tolfa Mountains (Central Italy)*. Chem. Geol., 284 (1-2), 160-181.

Cinti D., Poncia P.P, Procesi M., Galli G., Quattrocchi F., (2013). *Geostatistical techniques application to dissolved radon hazard mapping: An example from the western sector of the Sabatini Volcanic District and the Tolfa Mountains (central Italy)*. Applied Geochemistry, 35, 312-324.

Cinti D., Tassi F., Procesi M., Bonini M., Capecchiacci F., Voltattorni N., Vaselli O., Quattrocchi F., (2014). *Fluid Geochemistry and Geothermometry In The Unexploited Geothermal Field Of The Vicano-Cimino Volcanic District (Central Italy)*. Chemical Geology, 371, 96-114.

Cinti D., Vaselli O., Poncia P.P, Brusca L., Grassa F., Procesi M, Tassi F., (2019). *Anomalous concentrations of arsenic, fluoride and radon in volcanic-sedimentary aquifers from central Italy: Quality indexes for management of the water resource*. Environmental Pollution, 253, 525-537.

Frondini F., Caliro S., Cardellini C., Chiodini G., Morgantini N., Parello F., (2008). *Carbon dioxide degassing from Tuscany and Northern Latium (Italy)*, Global and Planetary Change, 16, 89-102.

Mancini C., Quattrocchi F., Guadoni C., Pizzino L., Porfidia B., (2000). *^{222}Rn study during the geochemical surveillance of some seismogenic areas: comparison between different techniques for discrete monitoring*. Annali di Geofisica, 43, (1), 31-60.

Mariucci M.T., Pierdominici S., Pizzino L., Marra F., Montone P., (2008). *Looking into a volcanic area: an overview on the 350 m scientific drilling at Colli Albani (Rome, Italy)*. J. Volcanol. Geotherm. Res., 176, 225-240.

Minissale A., Donato A., Procesi M., Pizzino L., Giammanco S., (2019). *Systematic review of geochemical data from thermal springs, gas vents and fumaroles of southern Italy for geothermal favourability mapping*. Earth-Science Reviews, 188, 514-535.

Parkhurst D.L. and Appelo C.A.J., (2013). *Description of Input and Examples for PHREEQC Version 3-A Computer Program for Speciation, Batch-Reaction, One-Dimensional Transport, and Inverse Geochemical Calculations*. US Geological Survey Techniques and Methods, Book 6, Chapter A43, 497 pp.

Pizzino L., Galli G., Mancini C., Quattrocchi F., Scarlato P., (2002). *Natural gas hazard (CO_2, ^{222}Rn) within a quiescent volcanic region and its relations with tectonics: the case of the Ciampino-Marino area, Alban Hills volcano, Italy*. Natural Hazards, 27, 257-287.

Pizzino L., (2015). *Fluid geochemistry and Natural Gas Hazard in the urban area of Rome*. Tesi di dottorato, in italian, Università degli Studi Roma 3, 152 pp.

Pizzino L., Cinti D., Procesi M., Sciarra A., (2015). *Caratterizzazione chimica preliminare delle acque sotterranee di Roma Capitale; Preliminary chemical characterization of groundwater in the Rome Municipality*. Acque Sotterranee, - Italian Journal of Groundwater - AS15072: 047 - 057, 47-57.

Sechman H. & Dzieniewicz M., (2011). *The example of background determination and mathematical processing of data from surface geochemical survey for the purposes of petroleum exploration*. Journal of Petroleum Science and Engineering, 78 (2), 396-406.

Washington H.S., (1906). *The Roman Comagmatic Region*. Carnegie Institute vol. 57., Washington, 1-199.

Geogenic radon potential map as tool to evaluate indoor radon

Sciarra A.[1,2], Giustini F.[2], Ruggiero L.[3,2], Ciotoli G.[2,1], Bigi S.[3], Lucchetti C.[3], Pizzino L.[1], Tartarello M.C.[3], Siriani P.[2], Voltaggio M.[2], Galli G.[1]

[1]*Istituto Nazionale di Geofisica e Vulcanologia, Sezione di Sismologia e Tettonofisica, Roma, Italy*
[2]*Consiglio delle Nazionale Ricerche, IGAG, CNR, Istituto di Geologia Ambientale e Geoingegneria, Roma, Italy*
[3] *Università degli Studi di Roma La Sapienza, Dipartimento di Scienze della Terra, DST-Sapienza, Roma, Italy*

Corresponding Author: *alessandra.sciarra@ingv.it*

This work was conducted in the framework of the LIFE-Respire project. The aim of this study was to investigate the relationships among indoor radon concentrations (IRC) and some proxy variables, as Geogenic Radon Potential (GRP), terrestrial and indoor gamma radiation (TGR and IGR) in the Caprarola municipality. For the purposes of the LIFE-Respire project, three municipalities with different GRP (i.e., high, medium and low) were selected in Italy. In particular, the Caprarola municipality occurs in the area of highest GRP as highlighted by the GRP map of Lazio Region. In this work, the estimated GRP map of Caprarola was compared with TGR map. The maps show similar patterns of the anomalies, whereas the main urbanized area is characterized by low GRP and high TGR, probably because of the contribution of the buildings material (mainly tuff). We also compared IRC and IGR that show a poor correlation with GRP; IGR instead, shows a slightly positive correlation with indoor radon, also in this case specifically induced by the use of volcanic buildings material. The comparison of all indoor measurements collected in the selected municipalities highlights consistent results with the GRP, thus confirming the initial ranking and that Caprarola municipality is characterized by high radon potential. These results confirm the usefulness and the robustness of the Geogenic Radon Potential maps at regional scale from the local authorities, for land use planning and to plan further focused and more detailed indoor surveys.

Introduction

Radon is a naturally occurring radioactive noble gas, invisible, odourless and tasteless, produced via the decay chain of primordial radionuclides. Being inert, radon itself does not possess any hazard, but it is considered an indoor air pollutant because its short-life progeny, emitting alpha, beta and gamma particles, may cause serious health risks to population. Inhaling relatively high levels of radon and its decay products, which can attach to fine and ultrafine particles present in indoor environment, can expose lung tissue to significant doses of ionizing radiations, which may in turn cause lung cancer [WHO, 2009]. Assessing the indoor exposure of people to radon and its progeny is therefore very important. The indoor radon concentrations (IRC) are primary controlled by the geology, such as the soil and rock contents of its parent radionuclides, the permeability and porosity of the bedrock, and also the fault activity. Further factors controlling the indoor radon levels are meteorological factors (e.g., wind, humidity, temperature and atmospheric pressure) which affect the rate of Rn entry into the buildings. Finally, building characteristics (e.g., presence of a foundation, quality of building fabric, construction materials) and ventilation habits of the individual occupants influence the radon indoor concentrations. Because the indoor radon concentration is a tangle function of many different parameters and factors, the prediction of its amount into houses is a difficult task. Recently, the concept of the 'geogenic radon potential' (GRP) has been introduced, where GRP is the parameter

that quantify the amount of radon transported from nearby geological formation to the atmosphere [Ciotoli et al., 2017]. It can be, in principle, inferred using solely geological information. A relationship between GRP and indoor radon concentration was demonstrated in several studies [Kemski et al., 2009; Cinelli et al., 2011].
This work was conducted in the framework of the LIFE-Respire project in three municipalities of Lazio Region (Ciampino, Celleno and Caprarola) with different GRP (i.e., high, medium and low). We present the results of the Caprarola municipality, which occurs in the area of the highest GRP as highlighted by the GRP map of Lazio Region [Ciotoli et al., 2017]. We developed a GRP map of Caprarola using Empirical Bayesian Kriging Regression (EBKR), a method which provide accurate predictions of data on a local scale. We also investigated the relationships among indoor radon concentrations and some proxy variables, as GRP, terrestrial and indoor gamma radiation (TGR and IGR) in the Caprarola municipality.

Material and Methods

The study area

Caprarola municipality is located about 50 km north of Rome, in central Italy; it extends on a surface of about 60 km^2. The geology of the area is dominated by the volcanic products of the Vico apparatus, which belong to the volcanic complex of Mts. Cimini (~0.90-1.30 Ma) [Nicoletti et al. 1969]. Volcanic products (tuff and freatomagmatic facies) mainly outcrop in the south-eastern sector of the study area; they are particularly enriched on natural radionuclides, and were traditionally used as building materials in the old centre of the Caprarola village. Around the Vico lake and in the north-western sector of the municipality, instead, outcrop the recent alluvial deposits.

Field survey and laboratory analyses

The field work and laboratory analyses of the samples collected at Caprarola municipality consisted of the following activities: soil gas survey, soil permeability measurements, high-resolution gamma spectrometry, terrestrial and indoor gamma dose rate measurements, indoor radon concentration measurements.

Soil gas survey

In October 2017, 180 soil gas samples (^{222}Rn, CO_2) were collected in order to define spatial distributions, baseline populations, and anomaly thresholds of the measured parameters. Soil gas sampling was conducted according a consolidated procedures reported in Beaubien et al. [2015]. Gases were analyzed in the field by using portable gas analyzers (Draeger X-am 7000 for CO_2 and alpha detector RAD7 Durridge for ^{222}Rn). Permeability measurements were also collected at soil gas sampling sites. Measurements were performed using a permeameter developed by University of Roma Tre [Castelluccio et al., 2015]. Moreover, terrestrial gamma dose rate measurements were carried out in 187 locations (1 m above the ground level), whereas indoor measurements were carried out in 115 rooms (center of the room and 1 m above the floor). The gamma survey was carried out by means of a portable gamma spectrometer, the “Exploranium GR-135 Plus -The identifier”, equipped with a NaI crystal. Data were later converted from nSv·h-1 to $\mu Sv \cdot h^{-1}$.

High-resolution gamma spectrometry

Soil and rock samples, representative of the main lithological units present in the study area, were collected and analyzed by high-resolution gamma spectrometer equipped with a low-background HPGe coaxial detector (GEM - EG&G ORTEC) to determine the activity concentrations of

radionuclides ^{238}U, ^{226}Ra, ^{232}Th and ^{40}K. Radon emanation coefficient and radon flux are additionally calculated according to the equations in [Giustini et al., 2019].

Indoor radon measurements

Indoor radon concentration (IRC) were measured in selected private and public dwellings and cellars (114 samples), by using passive nuclear track detectors (CR-39, RADOSYS). Exposure time of detectors was 3 months (November 2018-February 2019). The track detectors were placed for each site, generally in the main rooms (living room or bedroom) at a height of 1.0-1.5 m from the floor, and at a distance of ~30 cm from the wall. The tracks leaved by the alpha particles on the CR-39 were analyzed by using RADOSYS automatic electronic microscope system. Indoor gamma dose rate measurements were carried out in 115 rooms (at the center of the room and at 1 m above the floor) by the same portable gamma spectrometer used for terrestrial gamma radiation measurements.

Mapping technique

Empirical Bayesian Kriging Regression (EBKR) was applied to develop a local spatial model of the GRP of the municipality Caprarola combining several proxy variables. EBRK is a geostatistical interpolation method that combines Ordinary Least Square regression and simple kriging, providing accurate predictions of moderately non-stationary data at a local scale [Krivoruchko, 2012]. In addition, EBRK constructs a regression model by using the principal components of the explanatory variables, and thus it is able to solve the problem of multicollinearity. The spatial regression model developed by EBRK considers soil-gas radon concentrations as the response (i.e., dependent) variable and several proxy variables, derived from geological, topographic and geochemical data as predictors (i.e., independent). On the basis of the available and collected data, the regression model includes the following predictors: soil-gas CO_2 concentration, natural content of radium, uranium, thorium and potassium, radon emanation coefficient, calculated radon flux, terrestrial gamma dose rate, soil permeability measurements, Digital Terrain Model (DTM).

Results and Discussions

Mapping geogenic radon potential of Caprarola

Empirical Bayesian Kriging Regression model was built to produce a map of the geogenic radon potential, i.e., the quantity of radon directly related to the local geology. The GRP map highlights areas with high values in the south-east sector of the municipality and areas with low GRP values in the north-western sector (Figure 1a). This pattern is in accordance with the spatial distribution of outcropping lithologies, mainly volcanic rocks with high content of Rn parent nuclides, in the south-east, and sedimentary rocks (with low content of Rn parent nuclides) in the north-west. The map of terrestrial gamma radiation shows distribution similar to the GRP map, but highlights an area of particularly high values in correspondence of the urbanized area of the Caprarola village (Figure 1b). This pattern could be explained considering that the gamma radiation values measured in the urban environment are probably affected by the building materials (mainly tuff).

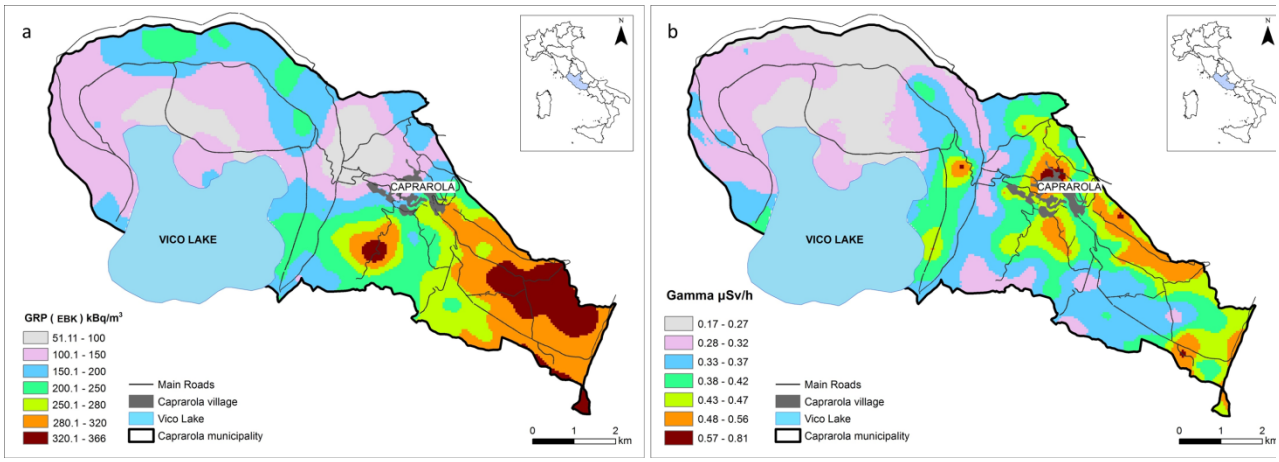

Figure 1 (a) Geogenic Radon Potential map of Caprarola municipality; (b) Terrestrial gamma dose rate map.

Geogenic Radon Potential maps at regional scale

Considering the three municipalities selected in Italy for the LIFE-Respire project, namely Caprarola, Celleno and Ciampino, the relationship between IRC and GRP at regional scale can be evaluated. The box-plots of figure 2 show that the values of indoor Rn and indoor gamma radiation are high in Caprarola and low at Ciampino, while Celleno shows intermediate values. This behaviour confirms the robustness of the Geogenic Radon Potential map of Lazio [Ciotoli et al., 2017] from which the three Respire municipalities were selected based on the following relationships: Caprarola, high GRP values, Celleno, average GRP values, Ciampino, low GRP values. Although there is no direct correlation between indoor Radon and GRP at the local level, at regional scale this correlation seems evident.

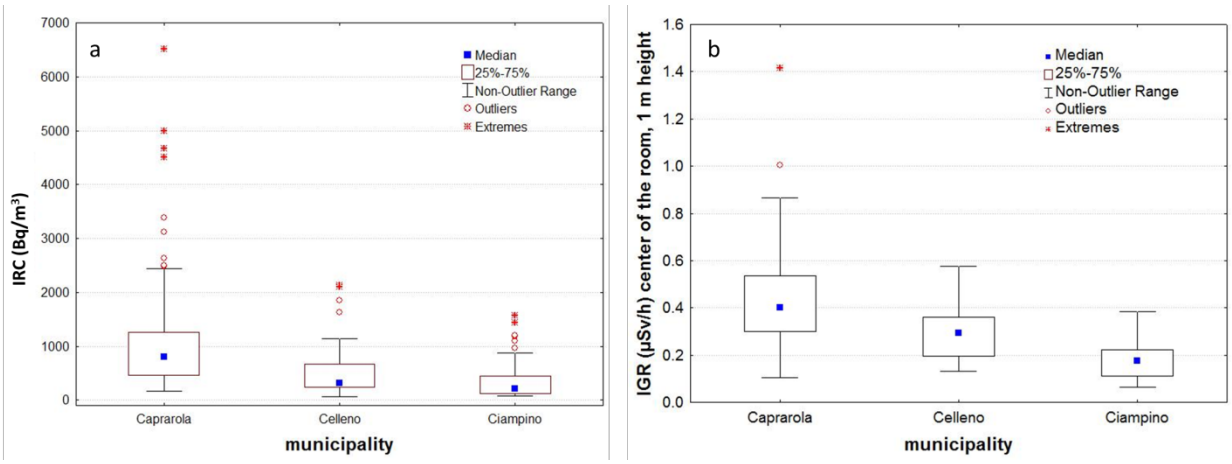

Figure 2 (a) Box-plot of IRC for the three municipalities, (b) Box-plot of IGR for the three municipalities of the Life-Respire project.

Conclusions

In this work we investigated the capability of regression kriging to construct the GRP map of the municipality of Caprarola by using radon concentrations in soil gas and some proxy variables. Then, we evaluate the relationships among indoor radon concentrations and gamma radiation with the geogenic radon in order to verify the usefulness of the GRP map as tool evaluate the indoor radon risk. This study highlights that, at local scale, the geogenic radon contribution is probably masked by several external factors (i.e., anthropic and meteorological parameters); the indoor gamma radiation

seems to be affected by the use of volcanic rocks as building materials. At regional scale, however, the comparison of all indoor measurements (radon and gamma radiation) in the three sites selected in Italy (Caprarola, Celleno and Ciampino municipalities) for the LIFE-Respire project, highlights consistent results with the GRP map of the Lazio region, thus confirming the usefulness and the robustness of the Geogenic Radon Potential map at regional scale for land use planning and for planning further focused and detailed indoor surveys.

References

Beaubien S.E., Ruggiero L., Annunziatellis A., Bigi S., Ciotoli G., Deiana P., Graziani S., Lombardi S. & Tartarello M.C., (2015). *The importance of baseline surveys of near-surface gas geochemistry for CCS monitoring, as shown from onshore case studies in Northern and Southern Europe.* Oil & Gas Science and Technology, Rev. IFP Energies nouvelles, 70(4), pp. 615-633.

Castelluccio M., de Simone G., Lucchetti C., Moroni M., Salvati F. & Tuccimei P., (2015). *A new technique to measure in situ soil gas permeability.* Journal of Geochemical Exploration, 148, pp. 56-59.

Cinelli G., Tondeur F. & Dehandschutter B., (2011). *Development of an indoor risk map of the Wallon region of Belgium, integrating geological information.* Environmental Earth Science, 62, pp. 809-819.

Ciotoli G., Voltaggio M., Tuccimei P., Soligo M., Pasculli A., Beaubien S.E. & Bigi S., (2017). *Geographically weighted regression and geostatistical techniques to construct the geogenic radon potential map of the Lazio region: A methodological proposal for the European Atlas of Natural Radiation.* Journal of Environmental Radioactivity, 166, pp. 355-375.

Giustini F., Ciotoli G., Rinaldini A., Ruggiero L. & Voltaggio M., (2019). *Mapping the geogenic radon potential and radon risk by using Empirical Bayesian Kriging regression: a case study from a volcanic area of central Italy.* Science of the Total Environment, 661, pp. 449-464.

Kemski J., Klingel R., Siehl A. & Valdivia-Manchego M.R., (2009). *From radon hazard to risk prediction-based on geological maps, soil-gas and indoor radon measurements in Germany.* Environmental Geology, 56, pp. 1269-1279.

Krivoruchko K., (2012). *Empirical Bayesian Kriging.* ArcUser Fall, 2012.

Nicoletti M., (1969). *Datazioni argon-potassio di alcune vulcaniti delle regioni vulcaniche Cimina e Vicana.* Periodico di Mineralogia, 38, pp. 1-20.

World Health Organization (WHO), (2009). *Sets radon action level of 2.7 - less lung cancer risk than EPA 4.0. Global Press Release Distribution.* The website: www.PRLog.org, 2009.

Multiple seasonality in soil radon concentration: insights from continous wavelet analysis

Siino M., Scudero S.[2], Cannelli V.[1], Piersanti A.[1], D'Alessandro A.[2]

[1]*Istituto Nazionale di Geofisica e Vulcanologia, Sezione di Sismologia e Tettonofisica, Roma, Italy*
[2]*Istituto Nazionale di Geofisica e Vulcanologia, Osservatorio Nazionale Terremoti, Italy*

Corresponding Author: *salvatore.scudero@ingv.it*

Introduction

Radon (^{222}Rn) is a radioactive gas with a relative short half-life ($T_{1/2}$ = 3.8 days) which originates in rocks through a process of natural decay of other radioactive elements. Since it is carcinogenic nature, the monitoring of soil radon emission is of crucial importance, but it can be also useful to address a multitude of geological and environmental issues. Among the geological processes, radon is studied as a tracer of volcanic and tectonic activity, and earthquake precursor [Barbosa et al., 2015; Woith, 2015; Baskaran, 2016]. The latter is largely debated nowadays worldwide because several clues of tectonic-induced anomalies in radon signals have been reported in the literature [Hartman & Levy, 2005; Riggio and Santulin, 2015]. Such anomalies likely arise from the preparatory crust fracturing processes leading to an earthquake: the release of stress within the crust eases the migration of radon from deeper sources. The main difficulty of the use of radon as earthquake precursor is that the earthquake-related anomaly cannot be easily and univocally discriminated from other anomalies of different origin. In fact, radon variations are directly and indirectly influenced by several factors such as flux of carrier gases, environmental and climatic variables, characteristics of the ground soil, tide, solar effect, etc [see Siino et al., 2019 and reference therein]. The radon monitoring is usually carried out for punctual and short period experiments, but recently proper networks were established since the long-tem monitoring over extended areas, and with homogeneous instrumentation is the only way to characterize the soil radon emission, weeding out the local effects [Cannelli et al., 2018]. The identification of the periodic variations, both in the long-term and short-term, which are usually related to the environmental and climatic variables, allow to filter the radon signals and enhance the anomalies related to the geological processes. In this work we use descriptive statistics and a power spectral analysis in time-frequency domains to characterize the soil radon concentration time series and their relationship with the temperature.

Data and Method

IRON, Italian Radon mOnitoring, Network, is a network of about 50 permanent monitoring station for soil radon concentration, installed since 2009 and extending over large part of Italy [Cannelli et al., 2018]. We select the nine stations with the longer available data records. All the sites are equipped with the same type of sensor (Lucas cell) and they are coupled with temperature measures taken with co-located sensors. We investigated both high frequency (2-hourly) and low frequency (24-hourly) radon time series.

The time series have been analyzed in the frequency domain by means of the continuous wavelet transformation (CWT). This technique has been recently employed for the detection of long-range memory in radon time series [Yan et al. 2017; Siino et al. 2019]. By means of this methodology, we identify and quantify the presence of long-range memory analyzing a single time series and we deal

with the time-frequency dependencies between two time series (i.e. radon versus the climatic variables). The description of the CWT methodology is out of the purposes of this work, therefore we address the reader to the specific literature [Daubechies 1992, Conraria and Soares 2011]. The longer the series, the more robust are the results of the CWT, and it is appropriate to use sequence with high number of complete cycles of the longer investigated period. Nevertheless, if the sequence is not so long and truncated, this methodology still allows to detect the presence of persistence periodicity. Moreover, in order to examine the relationships between radon time series and temperature, the global cross-wavelet power and the phase difference have been computed. The global cross-wavelet power spectrum can be interpreted as the covariance between two time series; it is computed from 16 to 512 days based on the daily time series. Because the radon concentration is highly correlated with the temperature in the annual cycle, the phases and phase-differences are computed in the period ranging between 360 and 370 days.

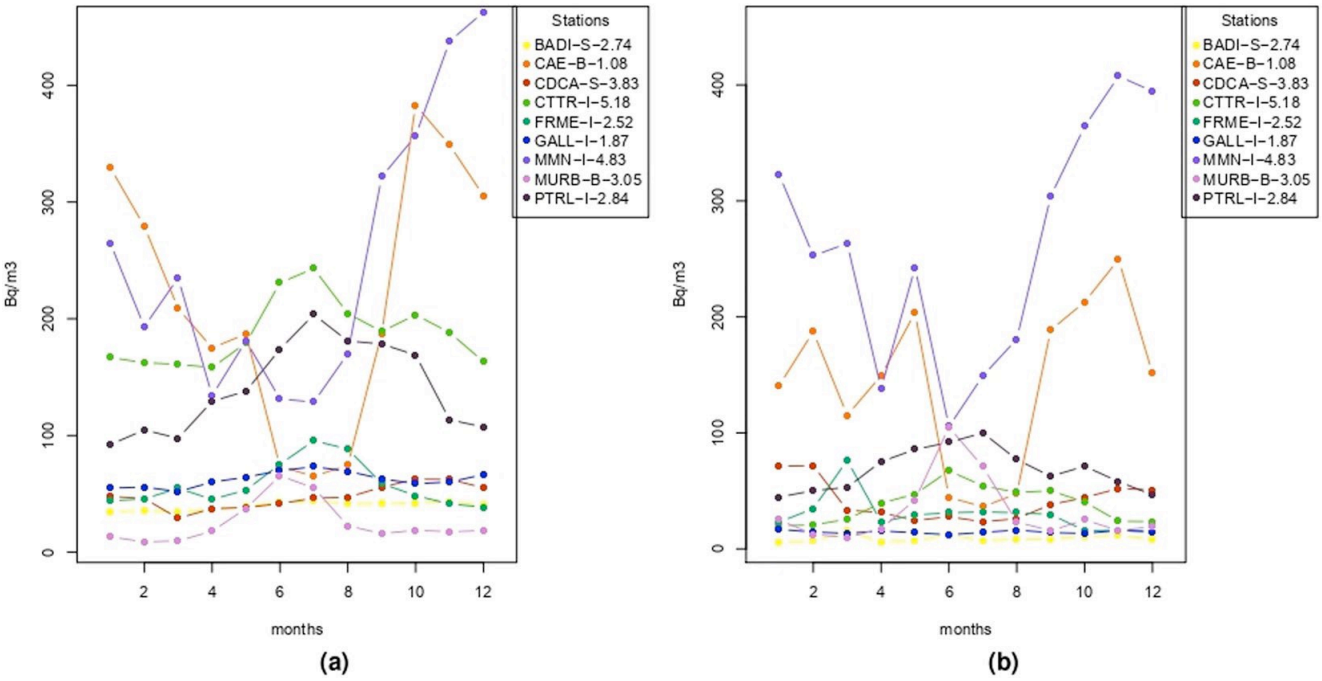

Figure 1 Left: for each station, the colored line joins the soil radon monthly average concentrations. Right: soil radon monthly standard deviation. The type of installation ("B" is borehole, "I" is indoor and "S" indicates shelter installation) and the time series length in years are also indicated.

Results

To investigate the seasonal behavior, for each site, the monthly means are computed (Figure 2). The stations located in shelter (BADI and CDCA) show a less evident seasonal variations if compared with the other stations. Indoor stations are characterized by a marked seasonality over the annual cycle, except for GALL, which trend is comparable to the shelter type. CAE and MMN are the sites characterized by the higher variation in the monthly means; also the MURB borehole station shows a seasonal variation.

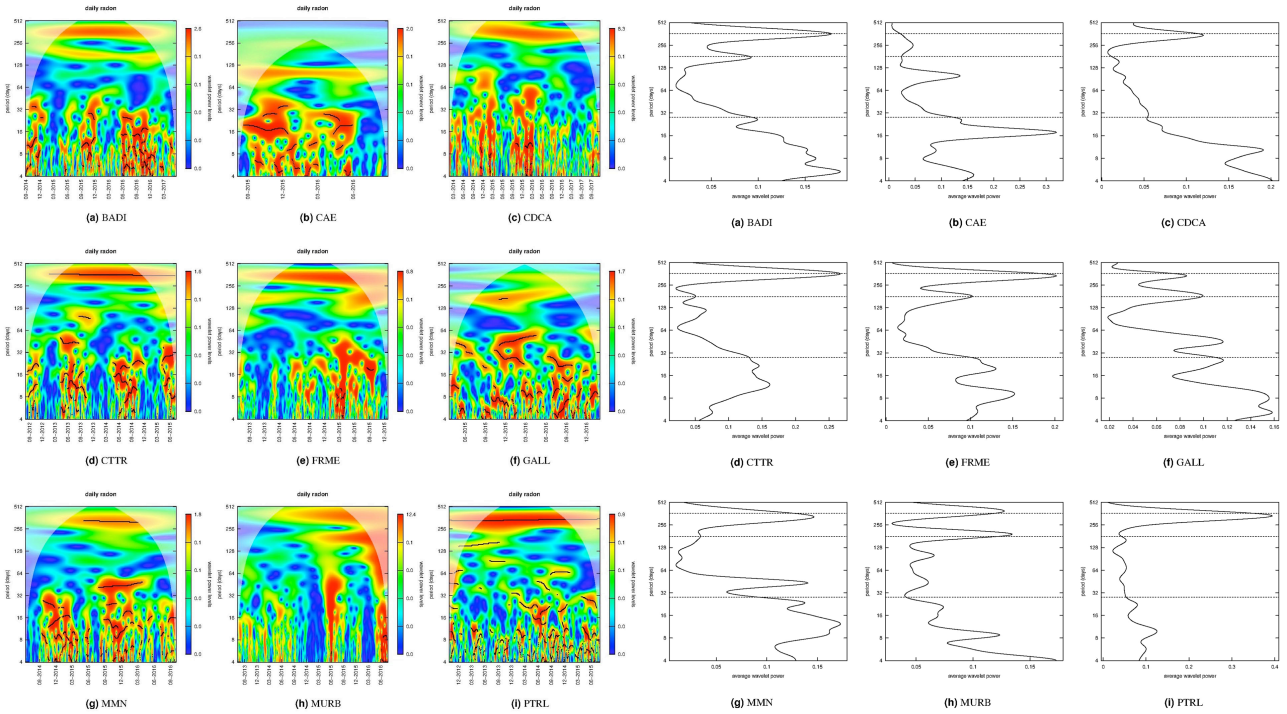

Figure 2 Left: Wavelet power spectrum of daily radon series; The black contour indicates the significant period with 90% confidence level. The lighter shade is the regions influenced by edge effects. Right: Global power spectrum density for mean daily radon time series. The horizontal lines are for the 28-day, 180-day and 365-day periods.

The power spectral density calculated from the 2-hourly series for the period from 4 hours to 16 days. the global wavelet power spectrum, obtained averaging over time, shows a main peak indicating a marked period at 1 day for all the nine selected sites and a secondary one at 12 hours (Figure not shown). These periodicities are consolidated and recognizable in the most of the radon time series worldwide, and it is due to the effect of the diurnal pressure and temperature cycle [Kumar et al., 2015; Barberio et al., 2018]. Intuitively radon sensor deployed in shelter and specially in boreholes should be less sensitive to climatic effects, but such rule is not unequivocal in the analysed time series. No other peaks in power spectrum density for the 2-hourly radon measurements are shared among all the sites.

For the daily radon data, the wavelet power spectrum (WPS) is shown Figure.2; the period ranges from 4 to 512 days. The thick black contour indicates the 90% confidence level and the lighter shade indicates regions inside the cone of influence due to the border effect. The Figure 3 shows the global wavelet power spectrum; the horizontal lines provide reference at 28, 180, and 365 days. All the series (except CAE) show a clear 1-year periodicity that, differently from 1-day periodicity, is persistent along time. A subordinate periodicity at about 180 days results in all the stations apart CDCA, MMN, and PTRL. Other periodicities characterize each single site but none of those correspond exactly to the 29-days period ascribable to tides; however, the periods in the range between 8 and 32 days could be related to tidal effects. The annual and semi-annual cycles on radon signals have been correlated to the annual variation of the climatic variables (mainly the temperature) in relation to the solar annual and solar semiannual cycles [Udovičić, et al., 2011; Inan et al., 2012; Piersanti et al., 2015].

The relationship between radon concentration and temperature was explored with the cross-wavelet power spectrum and phase differences in the band between 360 and 370 days (Figure 3). The results

show different values of phase difference at the various stations, but the series synchronisation at the selected frequencies is almost constant over time. The occurrence of a 1-year cycle in the radon concentration, as well in the temperature, suggests that both the observations could be somehow related to a common causative factor. The phase shift (black dashed lines in Figure 3) is peculiar at each site and almost constant over time; and also the overall in-phase/out-of-phase relationships is site-dependent. This complex behavior could likely result from the interactions of the shift between temperature and rainfall cycles and their reflections on the convective dynamics near the surface. Therefore, we can reasonably affirm that climatic-environmental variables can account for all the observed oscillations of the investigated radon concentration time series.

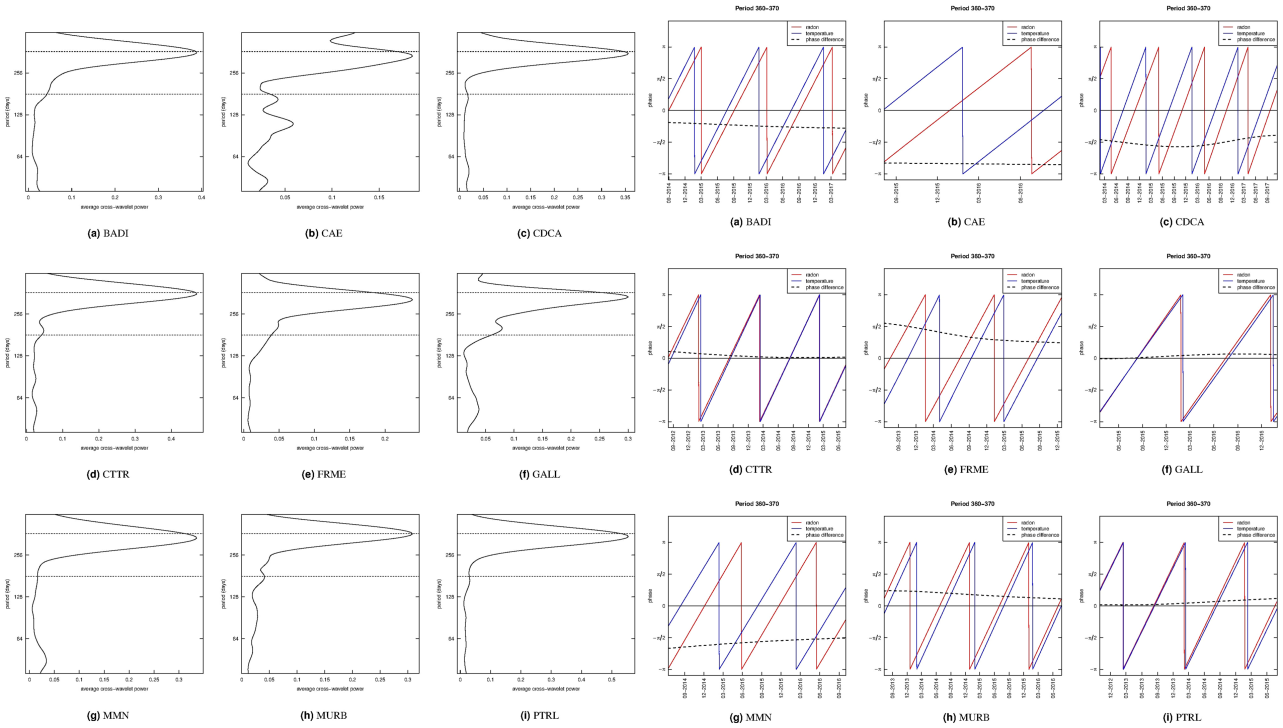

Figure 3 Left: Global cross-wavelet power spectrum of mean daily radon and temperature time series. The horizontal lines are for the 180-day and 365-day periods. Right: Phases and phase differences between radon and local temperature time series at the period between 360 and 370 days.

Conclusions

Radon signals are very complex time series and require the application of advanced analysis techniques to be described thoroughly. At nine different sites belonging to IRON, we observed: i) shared daily cycles, ii) local multi-hours and multi-day signals, iii) shared periodic annual and semi-annual signals. We suggested explanation for the observed patterns, in relation with the climatic variables: variations of atmospheric pressure and temperature would be responsible for short-term periods while for long term-ones also seasonal rainfall cycles are likely to play an important role [Canelli et al., 2018; Siino et al., 2019].

However, in the end, the conditions resulting from local geological and environmental settings and installation types of instrument at station are what really matter in the final recorded signal. With respect to the results in the time-frequency domain the power spectral density presents some regularities over time that seem to be dependent on the seasons. This indicates that the magnitude and variability of radon measurements change over time with a specific pattern. However to further investigate this aspect, it would be important to analyze even longer time series. For future analysis,

well identified cycles, both in the short-term and in the long-term, can certainly help the comprehension of variation in radon time series and the characterization of site-depended radon behavior.
The approach followed in this study is not focused to immediately detect earthquake-related anomaly, however it would turn useful because the de-noising of the series removing the identified cycles, would enhance the anomalies related to geological processes.

References

Barberio M., Gori F., Barbieri M., Billi A., Devoti R., Doglioni C., Petitta M., Riguzzi, F. and Rusi, S., (2018). *Diurnal and semidiurnal cyclicity of radon (222rn) in groundwater, Giardino spring, central Apennines, Italy*. Water, 10, 1276.

Barbosa S., Donner R. and Steinitz G., (2015). *Radon applications in geosciences - progress & perspectives*. The European Physical Journal Special Topics, 224, 597-603.

Baskaran M., (2016). *Radon: A tracer for geological, geophysical and geochemical studies*. Springer.

Cannelli V., Piersanti A., Galli G. and Melini D., (2018). *Italian radon monitoring network (iron): A permanent network for near real-time monitoring of soil radon emission in Italy*. Annals of Geophysics, 61, 444.

Conraria L.A. and Soares M.J., (2011). *The continuous wavelet transform: A primer*. NIPE Working Paper, 16, 1-43.

Daubechies I. (1992). *Ten lectures on wavelets*. Siam, vol. 61.

Hartmann J. and Levy J.K., (2005). *Hydrogeological and gasgeochemical earthquake precursors-a review for application*. Natural Hazards, 34, 279-304.

İnan S., Kop A., Çetin H., Kulak F., Pabuçcu Z., Seyis C., Ergintav S., Saatcilar R. and Nuri Bodur M., (2012). *Seasonal variations in soil radon emanation: long-term continuous monitoring in light of seismicity*. Natural Hazards, 62, 575-591 (2012).

Kumar A., Walia V., Arora B.R., Yan T.F., Lin S.J., Fu C.C., Chen C.H. and Wen K.L., (2015). *Identifications and removal of diurnal and semidiurnal variations in radon time series data of Hsinhua monitoring station in SW Taiwan using singular spectrum analysis*. Natural Hazards, 79, 317-330.

Piersanti A., Cannelli V. and Galli G., (2015). *Long term continuous radon monitoring in a seismically active area*. Annals of Geophysics, 58, 0437

Riggio A. and Santulin M., (2015). *Earthquake forecasting: a review of radon as seismic precursor*. Bollettino di Geofisica Teorica ed Applicata, 56.

Siino M., Scudero S., Cannelli V., Piersanti A. and D'Alessandro A., (2019). *Multiple seasonality in soil radon time series*. Scientific Reports, 9, 8610.

Udovičić V. Aničin I., Joković D., Dragić A., Banjanac R., Grabež B. and Veselinović, N., (2011). *Radon time-series analysis in the underground low-level laboratory in Belgrade, Serbia*. Radiation Protection Dosimetry, 145, 155-158.

Woith H., (2015). *Radon earthquake precursor: A short review*. The European Physical Journal Special Topics, 224, 611-627.

Yan R., Woith H., Wang R. and Wang G., (2017). *Decadal radon cycles in a hot spring*. Scientific reports, 7, 12120.

Analysis of Thermal Anomaly in Association with Radon Concentration for Pre-Post China Earthquakes

Suryanshu C. and Sudarshan C.

Centre for Earth & Space Science, Rabindranath Tagore University, India

Corresponding Author: *csuryansh@gmail.com*

Thermal anomaly was well associated for radon concentration over the seismic region. Land Surface Temperature (LST) had been observed by using meteorological stations in the China region during the preparation period of May 12, earthquake with magnitude 7.9. Present study demonstrates the process of energy transformation under stress stimulated rocks by means of LST changes. Radon concentration ionized the upper boundary layer of atmosphere and registered thermal infrared signals over the main epicenter. Quality-Centered (QC) filter technique was also proved earthquake associated thermal anomalies in the prone earthquake region.

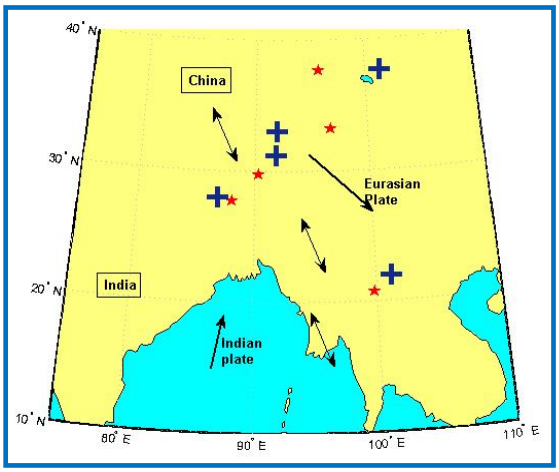

Figure 1 Location Map.

S. No	Earthquake	Date	Location	Magnitude	Depth
1	Eastern Xiang (China)	6/10/08	18°N, 88°E	6·4	12 km
2	Northern Qinghai (China)	28/8/09	37.7°N, 95.6°E	6·2	13 km
3	Southern Qinghai (China)	13/4/10	33.2°N, 96.6°E	6·9	17 km
4	Myanmar region	24/3/11	20.6°N, 99.8°E	6·9	8 km
5	India-Nepal region	18/9/11	27.7°N, 88°E	7.2	19.7 km

Sources and sinks of greenhouse gases in Florence (Italy) as determined by carbon isotopic ratios

Tassi F.[1,2], Venturi S.[1,2], Cabassi J.[1,2], Gioli B.[3], Baronti S.[3], Vaselli O.[1,2], Caponi C.[1], Vagnoli C.[3], Picchi G.[1], Zaldei A.[3], Magi F.[1], Miglietta F.[3], Capecchiacci F.[4]

[1]*Universitá di Firenze, Dipartimento di Scienze della Terra, Firenze, Italy*
[2] *Istituto di Geoscienze e Georisorse (IGG), Consiglio Nazionale delle Ricerche (CNR), Firenze, Italy*
[3]*Instituto di Biometeorologia (IBIMET), Consiglio Nazionale delle Ricerche (CNR), Firenze, Italy*
[4]*Istituto di Geofisica e Vulcanologia, Sezione di Napoli - Osservatorio Vesuviano, Italy*

Corresponding Author: *franco.tassi@unifi.it*

Introduction

According to the Paris Agreement, 195 countries worldwide set a target for an 80 % reduction below 1990 levels of global greenhouse gas (GHG) emissions by 2050. For this goal, plans and policies for renewable energy deployment have to be urgently activated. Urban policies can play a major role in both climate change mitigation and adaptation, since 70 % of energy related GHG emissions can be attributed to urban and suburban activities, where housing and transport sectors account for more than 50 % of direct household emissions of urban citizens. The Municipality of Florence (Tuscany, central Italy) recently adopted a series of initiatives aimed to lowering GHG emissions (e.g. partial pedestrianization of the city center, expansion of the bycicle lanes and construction of a tramway network). With a population of more than 350,000 inhabitants and more than 10 million of tourists per year, Florence urban area is responsible for more than 1.2×10^6 Mg CO_2 annually emitted into the atmosphere, mainly due to vehicular traffic and domestic heating. These anthropogenic sources partially contribute also to urban CH_4 emissions, although most of the CH_4 flux from the city was attributed to the distribution of fossil fuels. In this study, CO_2 fluxes, CO_2 and CH_4 concentrations and $\delta^{13}C$-CO_2 and $\delta^{13}C$-CH_4 values, monitored during summer and fall from the roof of a building sited in the city center, are presented. The aim was to investigate the temporal patterns of these GHGs to identify, on a geochemical (isotopic) basis, the local emitting sources and the seasonal variations in their relative contributions.

Materials and Methods

The roof of the Ximenes Observatory (a couple hundred meters from the Santa Maria del Fiore Cathedral), hosted the instrumentation used to carry out nearly continuous measurements of turbulent fluxes of CO_2 at half-hourly intervals by Eddy Covariance method, and the concentrations and $\delta^{13}C$ values of CO_2 and CH_4 using a CRDS (Cavity Ring Down Spectroscopy) analyzer (Picarro G2201-i).
The observation periods were from the 7th to the 21st of July, 2017 and from the 10th of October to the 15th of December 15, 2017.

Results and Discussion

The CO_2 flux was characterized by a regular diurnal cycle during the whole monitoring period (Figure 1a), with minimum values during nighttime and a sharp increase in the morning. Differently, CO_2 concentrations showed distinct diurnal patterns in summer and fall seasons (Figure 1b). The $\delta^{13}C$

values were inversely correlated to the CO_2 concentrations (Figure 1c), with peak values being recorded during low CO_2 concentration phases (in the afternoon in July and at nighttime and early morning during fall) and minimum $\delta^{13}C$ values during CO_2 concentration maxima (at 07:00 in July, and around noon during fall).

The emitting sources contributing to the atmospheric CO_2 concentrations measured in Florence were investigated on the basis of the Keeling approach [Keeling, 1961]. Considering both (i) nighttime data, when atmospheric stability contributed to the accumulation of airborne pollutants emitted during the day and potential sinks (i.e. photosynthesis) were not active, and (ii) early morning data, when anthropogenic sources were active contributing to the sharp increase in CO_2 emissions from the city (Figure 1a) and photosynthetic uptake was negligible, the estimated $\delta^{13}C$ values of the CO_2 non-atmospheric source ranged from -28 to -23 ‰ vs. V-PDB in July, from -37 to -26 ‰ vs. V-PDB in October, from -41 to -29 ‰ vs. V-PDB in November and from -41 to -32 ‰ vs. V-PDB in December, indicating that gasoline and natural gas combustion accounted for about 32 and 68 % of non-background atmospheric CO_2, respectively, with an increasing contribution from natural gas combustion (i.e. domestic heating) during fall.

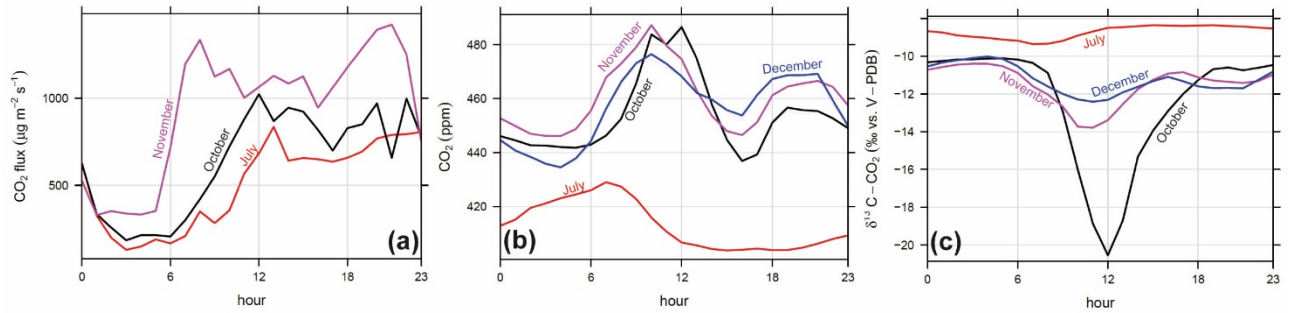

Figure 1 Average temporal pattern (daily) of (a) CO_2 fluxes, (b) CO_2 concentrations, and (c) $\delta^{13}C$-CO_2 values for each sampling month.

The diurnal variations in CH_4 concentrations (Figure 2a) resembled the CO_2 concentration pattern. In July, the highest CH_4 concentrations were recorded at night, whereas $\delta^{13}C$-CH_4 values showed no relevant diurnal variations (Figure 2b). During fall, CH_4 concentrations showed two maxima, i.e. at 9:00-10:00 and at 21:00 (Figure 2a). The $\delta^{13}C$-CH_4 diurnal pattern recorded in November and December showed lowest values at night followed by an increase until 21:00. Differently, in October a large peak in $\delta^{13}C$-CH_4 values was observed at 17:00, followed by an sharp decrease down to a minimum value at 20:00 (Figure 2c).

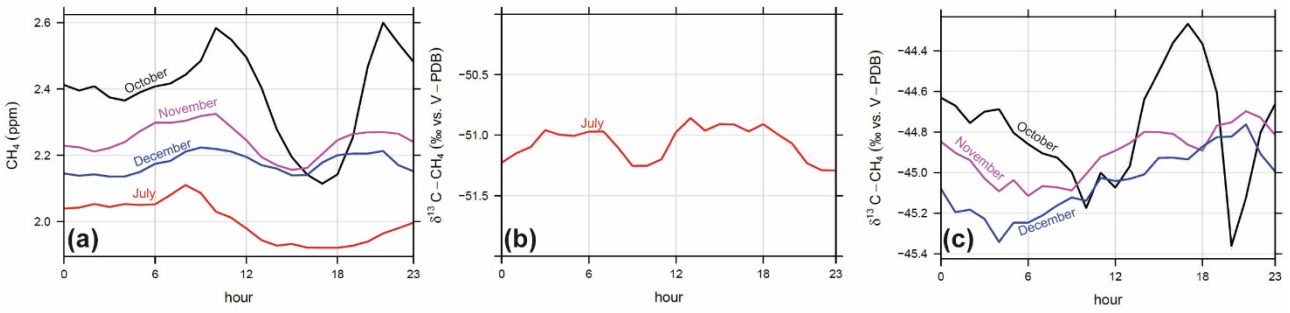

Figure 2 Average temporal pattern (daily) of (a) CH_4 concentrations, and (b) $\delta^{13}C$-CH_4 values in July and (c) $\delta^{13}C$-CH_4 values in October, November and December.

The isotopic composition of the CH_4 emitting sources, calculated with the Keeling method on nighttime data, ranged from -51 to -47 ‰ vs. V-PDB in October, from -56 to -47 ‰ vs. V-PDB in November and from -52 to -40 ‰ vs. V-PDB in December. These values approached the isotopic signature of natural gas (around -44 ‰ vs. V-PDB). No relevant differences were observed in the $\delta^{13}C$-CH_4 values prior and after the beginning of the domestic heating season, suggesting that the CH_4 emission in the metropolitan area during the fall season was mostly related to leakage from the natural gas pipeline network.

Conclusions

Vehicular traffic and domestic heating were recognized as the main emitting sources of CO_2 in the urban area of Florence, the latter being particularly relevant during the fall season. Local emitting sources of CH_4 were mainly related to natural gas distribution and combustion. In particular, our data suggested that fugitive emissions from the urban natural gas pipeline network represent a relevant source of CH_4 in Florence.

References

Hoornweg D., Sugar L., Lorena C., Gómez T., (2011). *Cities and greenhouse gas emissions: moving forward*. Environment & Urbanization, 23(1), 207-227.

Keeling C.D., (1961). *The concentration and isotopic abundances of carbon dioxide in rural and marine air*. Geochimica et Cosmochimica Acta, 24, 277-298.

Synoptic Analysis of a Decade of Daily Measurements of SO_2 Emission in the Troposphere from Volcanoes of the Global Ground-Based Network for Observation of Volcanic and Atmospheric Change

Arellano S.[1], Galle B.[1], Apaza F.[2], Bobrowski N.[3], Bornas M.A.[4], Burton M.[6], Chacón Z.[5], Chigna G.[7], Costa F.[8], De Moor M.[9], Delgado-Granados H.[10], Di Muro A.[11], Duarte E.[9], Garzón G.[5], Hidalgo S.[12], Inguaggiato S.[13], Kern C.[14], Kunrat S.[15], López C.M.[5], Mapendano M.Y.[16], Masias P.[2], Montalvo F.[17], Newhall C.[8], Platt U.[3], Rivera C.[10], Saballos A.[18], Salerno G.[6], Vásconez F.[12], Velázquez G.[19], Vita F.[13]

[1]*Department of Space, Earth and Environment, Chalmers University of Technology, Sweden*
[2]*Instituto Geológico, Minero y Metalúrgico (INGEMMET), Peru*
[3]*Institute of Environmental Physics, Heidelberg University, Germany*
[4]*Centre for Volcanology and Geological Hazard Mitigation (CVGHM), Indonesia*
[5]*Servicio Geológico Colombiano (SGC), Colombia*
[6]*Istituto Nazionale di Geofisica e Vulcanologia, Sezione di Catania - Osservatorio Etneo, Italy*
[7]*Instituto Nacional de Sismología, Vulcanología, Meteorología e Hidrología, Guatemala*
[8]*Earth Observatory of Singapore, Nanyang Technological University (EOS), Singapore*
[9]*Observatorio Vulcanológico y Sismológico de Costa Rica (OVSICORI), Costa Rica*
[10]*Instituto de Geofísica, Universidad Nacional Autónoma de México (UNAM), Mexico*
[11]*Institut de Physique du Globe de Paris (IPGP), France*
[12]*Instituto Geofísico, Escuela Politécnica Nacional (IGEPN), Ecuador*
[13]*Istituto Nazionale di Geofisica e Vulcanologia, Sezione di Palermo, Italy*
[14]*Volcano Disaster Assistance Program, United States Geological Survey, United States*
[15]*Philippine Institute of Volcanology and Seismology (PHIVOLCS), Philippines*
[16] *Observatoire Volcanologique de Goma (OVG), DR Congo*
[17]*Servicio Nacional de Estudios Territoriales (SNET), El Salvador*
[18]*Instituto Nicaragüense de Estudios Territoriales (INETER), Nicaragua*
[19]*Servicio Nacional de Geología y Minería (SERNAGEOMIN), Chile*

Corresponding author: *fabio.vita@ingv.it*

Volcanic plumes are common and far-reaching manifestations of volcanic activity during and between eruptions. Observations of the rate of emission and composition of volcanic plumes are essential to recognize, and in some cases predict, the state of volcanic activity. Measurements of the size and location of the plumes are import to assess the impact of the emission from sporadic or localized eventsto persistent or widespread processes of climatic importance. These observations provide clues on volatile budgets on Earth, chemical evolution of magmas, and atmospheric circulation and dynamics. Space-based observations during the last decades have given us a global view of Earth's volcanic emission, particularly of sulphur dioxide (SO_2). These consistent measurement programmes have produced time-averaged global emission budgets and revealed that tropospheric plumes, produced from persistent degassing of weak sources, dominate the total emission of volcanic SO_2. Since lower atmosphere emissions have historically been less accessible from space, knowledge of their magnitude and short-term variability remain largely uncertain. Operational monitoring of volcanic plumes, at scales relevant for adequate surveillance, has been facilitated through the use of ground-based scanning differential optical absorption spectrometers (scanDOAS) since the beginning of this century, largely due to the coordinated effort of the Network for Observation of Volcanic and

Atmospheric Change (NOVAC). In this study, we present a compilation of results of homogenized post-analysis of measurements of SO_2 flux and plume parameters obtained during the period March 2005 to January 2017 on 32 volcanoes of NOVAC. This inventory opens a window into the short-term emission patterns of a diverse set of volcanoes in terms of magma composition, geographical location, magnitude of emission, and style of eruptive activity. The use of a standard method allows intercomparison between different volcanoes and between ground- and space-based measurements of the same volcanoes. An open-access data repository will enable further exploitation of this unique dataset, with a focus on volcanological research, risk assessment, satellite-sensors validation, and improved quantification of the prevalent tropospheric component of global volcanic emission.

References

Andres R.J., and Kasgnoc A.D., (1998). *A time-averaged inventory of subaerial volcanic sulfur emissions*. Journal of Geophysical Research, 103, 25, 251-261, doi: 10.1029/98JD02091.

Arellano S.R., Hall M., Samaniego P., Le Pennec J.-L., Ruiz A., Molina I., Yepes H., (2008). *Degassing patterns of Tungurahua volcano (Ecuador) during the 1999-2006 eruptive period, inferred from remote spectroscopic measurements of SO_2 emissions*. Journal of Volcanology and Geothermal Research, Volume 176, 1, 151-162, ISSN 0377-0273, doi: 10.1016/j.jvolgeores.2008.07.007.

Arellano S., (2014). *Studies of Volcanic Plumes with Remote Spectroscopic Sensing Techniques*. PhD thesis, Chalmers University of Technology, Gothenburg, 96 pp.

Bluth G.J.S., Shannon J.M., Watson I.M., Prata A.J. and Realmuto V.J., (2007). *Development of an ultra-violet digital camera for volcanic SO_2 imaging*. Journal of Volcanology and Geothermal Research, 161(1-2): 47-56, doi: 10.1016/j.jvolgeores.2006.11.004.

Brantley S. and Koepenick K., (1995). *Measured carbon dioxide emissions from Oldoinyo Lengai and the skewed distribution of passive volcanic fluxes*. Geology, 23, 933-936, doi:10.1130/0091 7613(1995)023<0933:MCDEFO>2.3.CO;2.

Burton M.R., Caltabiano T., Murè F., Salerno G., and Randazzo D., (2008). *SO_2 flux from Stromboli during the 2007 eruption: Results from the FLAME network and traverse measurements*. Journal of Volcanology and Geothermal Research, 18, 214-220. doi: 10.1016/j.jvolgeores.2008.11.025.

Carn S., Krotkov N., Yang K. and Krueger A.J., (2013). *Measuring global volcanic degassing with the Ozone Monitoring Instrument (OMI)*. Geological Society, London, Special Publications, 380, doi: 10.1144/SP380.12.

Carn S., Fioletov V., McLinden C., Li C., Krotkov N., (2017). *A decade of global volcanic SO_2 emissions measured from space*. Scientific Reports, 7, 44095, doi:10.1038/srep44095.

Chance K., and Kurucz R.L., (2010). *An improved high-resolution solar reference spectrum for earth's atmosphere measurements in the ultraviolet, visible, and near infrared*. Journal of Quantitative Spectroscopy and Radiative Transfer, 111, 9, 1289-1295, doi: 10.1016/j.jqsrt.2010.01.036.

Dee D.P., Uppala S.M., Simmons A.J., Berrisford P., Poli P., Kobayashi S., Andrae U., Balmaseda M.A., Balsamo G., Bauer P., Bechtold P., Beljaars A.C., van de Berg L., Bidlot J., Bormann N., Delsol C., Dragani R., Fuentes M., Geer A.J., Haimberger L., Healy S.B., Hersbach H., Hólm E.V., Isaksen L., Kållberg P., Köhler M., Matricardi M., McNally A.P., Monge-Sanz B.M., Morcrette J., Park B., Peubey C., de Rosnay P., Tavolato C., Thépaut J. and Vitart F., (2011). *The ERA-Interim reanalysis: configuration and performance of the data assimilation system*. Quaterly Journal of the Royal Meteorological Society, 137: 553-597. doi: 10.1002/qj.828.

Dinger F., Bobrowski N., Warnach S., Bredemeyer S., Hidalgo S., Arellano S., Galle B., Platt U. and Wagner T., (2018). *Periodicity in the BrO/SO_2 molar ratios in the volcanic gas plume of Cotopaxi and its correlation with the Earth tides during the eruption in 2015*. Solid Earth, 9, 247-266, 654

doi: 10.5194/se-9-247-2018, 2018.

Edmonds M., Herd H., Galle B. and Oppenheimer C., (2003). *Automated, high time-resolution measurements of SO_2 flux at Soufrière Hills Volcano, Montserrat, West Indies*. Bulletin of Volcanology, 65, 578-586, doi: 10.1007/s00445-003-0286-x.

Fioletov V.E., McLinden C.A., Krotkov N., Li C., Joiner J., Theys N., Carn S. and Moran M.D., (2016). *A global catalogue of large SO_2 sources and emissions derived from the Ozone Monitoring Instrument*. Atmospheric Chemistry and Physics, 16, 11497-11519, doi: 10.5194/acp-16-11497-2016.

Galle B., Oppenheimer C., Geyer A., McGonigle A., Edmonds M., Horrocks L., (2003). *A miniaturised ultraviolet spectrometer for remote sensing of SO_2 fluxes: a new tool for volcano surveillance*. Journal of Volcanology and Geothermal Research, 119(1-4): 241-254, doi: 10.1016/S0377-0273(02)00356-6.

Galle B., Johansson M., Rivera C., Zhang Y., Kihlman M., Kern C., Lehmann T., Platt U., Arellano S. and Hidalgo S., (2010). *Network for Observation of Volcanic and Atmospheric Change (NOVAC): A global network for volcanic gas monitoring -Network layout and instrument description*. Journal of Geophysical Research, 115(D5): D05304 doi: 10.1029/2009JD011823.

Galle B., Delgado H., Garzon G., Vogel L., Platt U., (Eds.), (2011). *NOVAC project Final Report. EU-FP6, 100 pp., Chalmers University of Technology, Gothenburg, Sweden. Global Volcanism Program, 2013. Volcanoes of the World, v. 4.3.4. Venzke, E. (ed.). Smithsonian Institution. Halmer, M.M. and Schmincke, H.U., Graf, H.F., 2002. The annual volcanic gas input into the atmosphere, in particular into the stratosphere: a global data set for the past 100 years*. Journal of Volcanology and Geothermal Research, 115, 3-4, 511-528, doi: 10.1016/S0377-0273(01)00318-3.

Granieri D., Vita F., Inguaggiato S., (2017). *Volcanogenic SO_2, a natural pollutant: Measurements, modeling and hazard assessment at Vulcano Island (Aeolian Archipelago, Italy)*. In Environmental Pollution, Volume 231, Part 1, 2017, Pages 219-228, ISSN 0269-7491, doi.org/10.1016/j.envpol.2017.07.101.

Horton K.A., Williams-Jones G., Garbeil H., Elias T., Sutton A.J., Mouginnis-Mark P., Porter J.N., Clegg S., (2006). *Real-time measurement of volcanic SO_2 emissions: Validation of a new UV correlation spectrometer (FLYSPEC)*. Bulletin of Volcanology, 68: 4, 323-327, 2006a, doi: 10.1007/s00445-005-0014-9.

Inguaggiato S., Vita F., Rouwet D., Bobrowski N., Morici S., Sollami A., (2011). *Geochemical evidence of the renewal of volcanic activity inferred from CO_2 soil and SO_2 plume fluxes: the 2007 Stromboli eruption (Italy)*. Bullettin of Volcanology, doi.org/10.1007/s00445-010-0442-z.

Johansson M., Galle B., Zhang Y. and Rivera C., (2009a). *The dual-beam mini-DOAS technique-measurements of volcanic gas emission, plume height and plume speed with a single instrument*. Bulletin of Volcanology, 71(7): 747-751, doi: 10.1007/s00445-008-0260-8.

Johansson M., (2009b). *Application of Passive DOAS for Studies of Megacity Air Pollution and Volcanic Gas Emissions*. PhD thesis, Chalmers University of Technology, Gothenburg, 64 pp.

Kern C., (2009). *Spectroscopic Measurements of Volcanic Gas Emissions in the Ultra-Violet Wavelength Region*. PhD thesis, University of Heidelberg, Heidelberg, 318 pp.

Kern C., Deutschmann T., Vogel L., Wöhrbach M., Wagner T., Platt U. (2010a). *Radiative transfer corrections for accurate spectroscopic measurements of volcanic gas emissions*. Bulletin of Volcanology, 72, 2, 233-247, 10.1007/s00445-009-0313-7.

Kern C., Kick F., Lübcke P., Vogel L., Wöhrbach M., Platt U., (2010b). *Theoretical description of functionality, applications, and limitations of SO2 cameras for the remote sensing of volcanic plumes*. Atmospheric Measurement Techniques 3:733-749, doi: 10.5194/amt-3-733-2010.

Khokhar M., Frankenberg C., Van Roozendael M., Beirle S., Kühl S., Richter A., Platt U., Wagner T., (2005). *Satellite observations of atmospheric SO_2 from volcanic eruptions during the time-period of 1996-2002*, Advances in Space Research, 36, 5, 879-887, doi: 10.1016/j.asr.2005.04.114.

Krueger A.J. et al., (1995). *Volcanic sulfur dioxide measurements from the total ozone mapping spectrometer instrument*. Journal of Geophysical Research, 100(D7): 14057-14076, doi: 10.1029/95JD01222.

Kuhn J., Bobrowski N., Lübcke P., Vogel L., Platt U., (2014). *A Fabry-Pérot interferometer-based camera for two-dimensional mapping of SO_2 distributions*. Atmospheric Measurement Techniques, 2014, 7, 3705-3715, doi: 10.5194/amt-7-3705-2014.

Langmann B., (2014). *On the role of climate forcing by volcanic sulphate and volcanic ash*. Advances in Meteorology, 2014, 340123, 17 pp. doi: 10.1155/2014/340123.

Louban I., Bobrowski N., Rouwet D., Inguaggiato S., Platt U., (2009). *Imaging DOAS for volcanological applications*. Bulletin of Volcanology, 71, 7, 753-765, doi: 10.1007/s00445-008-0262-6.

Lübcke P., Bobrowski N., Arellano S., Galle B., Garzón G., Vogel L. and Platt U., (2014). *BrO/SO_2 molar ratios from scanning DOAS measurements in the NOVAC network*. Solid Earth, 5, 409-424, doi: 10.5194/se-5-409-2014.

McGonigle A., Pering T., Wilkes T., Tamburello G., D'Aleo R., Bitetto M., Aiuppa A., Wilmott J., (2017). *Ultraviolet imaging of volcanic plumes: a new paradigm in volcanology*. Geosciences, (3), 68, doi: 10.3390/geosciences7030068.

Moffat A.J. and Millan M.M., (1971). *The applications of optical correlation techniques to the remote sensing of SO_2 plumes using sky light*. Atmospheric Environment, 5(8): 677-690, doi: 10.1016/0004-6981(71)90125-9.

Mori T., and Burton M., (2006). *The SO_2 camera: A simple, fast and cheap method for ground-based imaging of SO_2 in volcanic plumes*. Geophysical Research Letters, 33, L24804, doi: 10.1029/2006GL027916.

Mori T., Hirabayashi J., Kazahaya K., Mori T., Ohwada M., Miyashita M. and Iino H., (2007). *A compact ultraviolet spectrometer system (COMPUSS) for monitoring volcanic SO_2 emission: Validation and preliminary observation*. Bulletin of the Volcanological Society of Japan, 52, 105-112, doi: 10.18940/kazan.52.2_105.

Mori T., Shinohara H., Kazahaya K., Hirabayashi J.-i., Matsushima T., Mori T., Ohwada M., Odai M., Iino H. and Miyashita M., (2013). *Time-averaged SO_2 fluxes of subduction-zone volcanoes: Example of a 32-year exhaustive survey for Japanese volcanoes*. Journal of Geophysical Research Atmospheres, 118, 8662-8674, doi: 10.1002/jgrd.50591.

Myhre G., Shindell D., Bréon F.-M., Collins W., Fuglestvedt J., Huang J., Koch D., Lamarque J.-F., Lee D., Mendoza B., Nakajima T., Robock A., Stephens G., Takemura T. and Zhang H., (2013). *Anthropogenic and Natural Radiative Forcing*. In: IPCC, 2013: Climate Change 2013: The Physical Science Basis. Contribution of Working Group I to the Fifth Assessment Report of the Intergovernmental Panel on Climate Change. Stocker T.F., Qin D., Plattner G.-K., Tignor M., Allen S.K., Doschung J., Nauels A., Xia Y., Bex V. and Midgley P.M., Eds. Cambridge University Press, pp. 659-740.

Oppenheimer C., (2010). *Sulfur: Ultraviolet Sensing of Volcanic Sulfur Emissions*. Elements, 6, (2), 87-92.

Platt U. and Stutz J., (2008). *Differential Optical Absorption Spectroscopy Principles and Applications*. Physics of Earth and Space Environments, Springer, 597 pp, ISBN 978-3-540-75776-4.

Platt U., Lübcke P., Kuhn J., Bobrowski N., Prata F., Burton M., Kern C., (2015). *Quantitative imaging of volcanic plumes - Results, needs, and future trends*. Journal of Volcanology and Geothermal Research, 300, 7-21, doi: 10.1016/j.jvolgeores.2014.10.006.

Prata A.J., Bernardo C., (2014). *Retrieval of sulphur dioxide from a ground-based thermal infrared imaging camera*. Atmospheric Measurement Techniques, 7, 2807-2828, doi:10.5194/amt-7-2807-742, 2014.

Queier M., Burton M., Theys N., Pardini F., Salerno G., Caltabiano T., Varnam M., Esse B., Kazahaya R., (2019). *TROPOMI enables high resolution of SO_2 flux observations from Mt. Etna, Italy, and beyond*. Scientific Reports, 9(1):957, doi: 10.1038/s41598-018-37807-w.

Retscher C., De Mazière M., Meijer Y., Vik A., Boyd I., Niemeijer S., Koopman R., Bojkov B., (2011). *The Generic Earth Observation Metadata Standard (GEOMS), Version 1.0*. https://avdc.gsfc.nasa.gov/index.php?site=1178067684, accessed on 2019-07-08.

Robock A., (2000). *Volcanic eruptions and climate*. Reviews of Geophysics, 38, 2, 191-219, doi: 10.1029/1998RG000054.

Ryan W.B.F., Carbotte S.M., Coplan J.O., O'Hara S., Melkonian A., Arko R., Weissel R.A., Ferrini V., Goodwillie A., Nitsche F., Bonczkowski J., Zemsky R., (2009). *Global Multi-Resolution Topography synthesis*. Geochemistry Geophysics Geosystems, 10, Q03014, doi: 10.1029/2008GC002332.

Salerno G.G., Burton M.R., Oppenheimer C., Caltabiano T., Randazzo D., Bruno N., Longo V., (2009). *Three-years of SO_2 flux measurements of Mt. Etna using an automated UV scanner array: Comparison with conventional traverses and uncertainties in flux retrieval*. Journal of Volcanology and Geothermal Research, 183, 1-2, 76-83, doi: 10.1016/j.jvolgeores.2009.02.013.

Schmidt A., Mills M.J., Ghan S., Gregory J.M., Allan R.P., Andrews T., Bardeen C., Conley A., Forster P., Gettelman A., Portmann R., Solomon S., Toon O.B., 2018. *Volcanic radiative forcing from 1979 to 2015*. Journal of Geophysical Research: Atmospheres, 123, 12491- 12508. doi: 10.1029/2018JD028776.

Schnetzler C.C., Bluth G.J.S., Krueger A.J. and Walter L.S., (1997). *A proposed volcanic sulfur dioxide index (VSI)*. Journal of Geophysical Research, 102(B9), 20087-20091, doi: 10.1029/97JB01142.

Sparks R.S.J., (2003). *Dynamics of magma degassing*. Geological Society, London, Special Publications, 213, 5-22, doi: 10.1144/GSL.SP.2003.213.01.02.

Sparks R.S.J., Biggs J., Neuberg J.W., (2012). *Monitoring volcanoes*. Science 335, 6074, 1310-1311. doi: 10.1126/science.1219485.

Smekens J.F. and Gouhier M., (2018). *Observation of SO_2 degassing at Stromboli volcano using a hyperspectral thermal infrared imager*. Journal of Volcanology and Geothermal Research, 356, 75-89, doi: 10.1016/j.jvolgeores.2018.02.018.

Stoiber R.E. and Jepsen A., (1973). *Sulfur dioxide contributions to the atmosphere by volcanoes*. Science, 182(4112): 577-578, doi:10.1126/science.182.4112.577.

Stremme W., Krueger A., Harig R. and Grutter M., (2012). *Volcanic SO_2 and SiF_4 visualization using 2-D thermal emission spectroscopy - Part 1: Slant-columns and their ratios*. Atmospheric Measurement Techniques, 5, 275-288, doi: 10.5194/amt-5-275-2012.

Theys N., Campion R., Clarisse L., Brenot H., van Gent J., Dils B., Corradini S., Merucci L., Coheur P.-F., Van Roozendael M., Hurtmans D., Clerbaux C., Tait S. and Ferrucci F., (2013). *Volcanic SO_2 fluxes derived from satellite data: a survey using OMI, GOME-2, IASI and MODIS*. Atmospheric Chemistry and Physics, 13, 5945-5968, doi: 10.5194/acp-13-5945-2013.

Theys N., Hedelt P., De Smedt I., Lerot C., Yu H., Vlietinck J., Pedergnana M., Arellano S., Galle B., Fernandez D., Carlito C., Barrington C., Taisne B., Delgado-Granados H., Loyola D., Van Roozendael M., (2019). *Global monitoring of volcanic SO_2 degassing with unprecedented resolution from TROPOMI onboard Sentinel-5 Precursor*. Scientific Reports 9, 2643, doi: 10.1038/s41598-019-39279-y.

Vita F., Inguaggiato S., Bobrowski N, Calderone L., Galle B., Parello F. (2012). *Continuous SO_2 flux measurements for Vulcano Island, Italy*. Annals of Geophysics, 55, 2, 2012; doi: 10.4401/ag-5759.

Vita F., Kern C., Inguaggiato S., (2014). *Development of a portable active long-path differential optical absorption spectroscopy system for volcanic gas measurements*. Journal of Sensor and Sensor Systems, 3, 355-367, (2014) doi: 10.5194 jsss-3-355-2014.

Warnach S., Bobrowski N., Hidalgo S., Arellano S., Sihler H., Dinger F, Lübcke P., Battaglia J., Steele A., Galle B., Platt U., Wagner T., (2019). *Variation of the BrO/SO_2 Molar Ratio in the Plume of Tungurahua Volcano Between 2007 and 2017 and Its Relationship to Volcanic Activity*. Frontiers in Earth Science, 7, 132, doi:10.3389/feart.2019.00132.

ST06

GASES IN MINERALS AND ROCKS

REFERENCE: ANDREA RIZZO

Petrology and volatile content of mantle xenoliths from Eifel Rift

Rizzo A.L.[1,2], Coltorti M.[2], Faccini B.[2], Casetta F.[2], Ntaflos T.[3] and Italiano F.[1]

[1]*Istituto Nazionale di Geofisica e Vulcanologia, Sezione di Palermo, Italy,*
[2]*Università degli Studi di Ferrara, Dipartimento di Fisica e Scienze della Terra, Ferrara, Italy*
[3]*Department of Lithospheric Research, Universität Wien, Wien, Austria*

Corresponding Author: *clt@unife.it*

Eifel Volcanic Field (Germany) is a key locality for the investigation of the European Sub-Continental Lithospheric Mantle (SCLM), since huge amounts of ultramafic xenoliths are brought to the surface by the Neogenic to Quaternary volcanic products both on the western and eastern side of the rift system.
This work focuses on the geochemical characterization of a large collection of mantle xenoliths sampled within lava, sills and/or necks (eastern part of the rift system), as well as within scoria cone and/or pyroclastic deposits (western part of the rift system). A detailed textural and petrological study of the bulk xenoliths and the primary mineral phases was complemented by the determination of the concentration of volatiles (He, Ne, Ar, CO_2) in mineral-hosted Fluid Inclusions (FI) after single-step crushing.
The xenoliths are generally lherzolitic, harzburgitic and wehrlitic in composition, with the occasional modal presence of both amphibole and phlogopite documented only in samples from the western localities. Few ol-clinopyroxenites and one ol-websterite are also present. Texture varies from protogranular, porphyroclastic and equigranular in most of the xenoliths, to cumulitic in some samples.
Olivine is typified by Mg# [MgO/(MgO+FeO_{tot}) mol%] varying from 83 to 92; similarly, orthopyroxene has Mg# of 84-92, whereas clinopyroxene has Mg# between 84 and 94. Al_2O_3 content of orthopyroxene and clinopyroxene ranges from 0.5 to 6.5 wt% and from 0.7 to 8.2 wt%, respectively. Spinel is characterized by Cr# [Cr_2O_3/(Cr_2O_3+Al_2O_3) mol%] ranging between 10 and 82, and by Mg# varying from 40 to 78.
A remarkable difference exists between the xenoliths sampled in the eastern and western localities. The formers are in fact characterized by the highest Mg# for clinopyroxene and Cr# for spinel, together with the lowest Al_2O_3 contents for both pyroxenes.
Volatiles analyses suggest that clinopyroxenes and most of the orthopyroxenes have the highest CO_2 and noble gas concentration, while olivines are gas-poor. This variability in FI concentration seems not related to the variations observed in the He, Ne, and Ar isotopic compositions.
$^3He/^4He$ values range between 5.5 and 6.9 Ra, where Ra is the $^3He/^4He$ ratio of air (1.39×10^{-6}), lying within the range proposed for the European SCLM (6.3±0.4 Ra), and slightly below that of MORB (Mid-Ocean Ridge Basalts; 8±1Ra), being also comparable to previous measurements performed in western Eifel.
The Ne and Ar isotope ratios fall along a binary mixing trend between air and MORB-like mantle. He/Ar* ratios in FI and Mg# vs. Al_2O_3 trends of the main mineral phases indicate that variable extents of partial melting, followed by metasomatic processes, affected the local mantle domains.
The ongoing carbon isotopic measurements in the most CO_2-rich xenoliths, complemented by the noble gases measurements in FI and by mineral chemical analyses will provide new insights on: i) the

volatile content and recycling processes occurring within the European SCLM; ii) the composition of fluids rising through the crust, intimately related to the monitored emissions in volcanic/seismic active contexts.

Noble gases composition of mantle xenoliths from west Antarctic rift system

Correale A.[1], Pelorosso B.[2], Rizzo A.L.[1], Coltorti M.[2], Italiano F.[1], Bonadiman C.[2], Giacomoni P.P.[2]

[1]*Istituto Nazionale di Geofisica e Vulcanologia, Sezione di Palermo, Italy*
[2]*Università degli Studi di Ferrara, Dipartimento di Fisica e Scienze della Terra, Ferrara, Italy*

Corresponding Author: *alessandra.correale@ingv.it*

Anhydrous and hydrous spinel-bearing lherzolite and harzburgite samples from three localities in Northern Victoria Land (Baker Rocks, Greene Point and Handler Ridge) were investigated about the noble gas composition (He, Ne, Ar) with the aim to study the characteristics of the lithospheric mantle beneath this area. The coupled He-Ar geochemistry highlighted that melting processes variably interested this mantle portion, being the $^4He/^{40}Ar$ ratios (0.004-0.39) measured in olivines, pyroxenes and amphiboles, much lower than those typical of fertile mantle (1-5). The $^3He/^4He$ ratios range from 2.30 to 19.79 Ra (Figure 1) with the highest variability of isotopic helium systematically corresponding with the lowest He concentrations at each of the investigated localities. The highest and lowest $^3He/^4He$ ratios of data set result from the addition of cosmogenic ^3He and radiogenic ^4He to FI and are responsible to modify the primary helium signature.

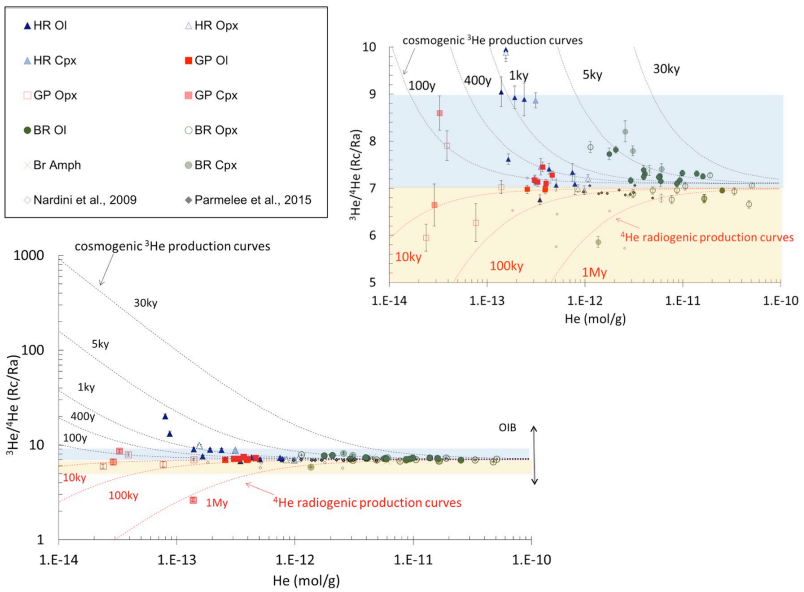

Figure 1 He content versus $^3He/^4He$ ratio (Rc/Ra) for HR, GP and BR xenoliths. Dotted black and red curves indicate the cosmogenic and radiogenic He-isotope variations, respectively, for fixed starting He concentrations and variable times.

By filtering the data for these secondary effects, we constrain the $^3He/^4He$ signature of the subcontinental lithospheric mantle below this area to 7.1±0.4 Ra (mean±standard deviation) that is in according with previous measurements in mantle xenoliths and lavas from other localities of the WARS, evidencing a homogeneous He-isotope composition beneath the entire rift. These isotopic

helium signature, as evidenced by the simultaneous presence of MORB- and SCLM-type He, highlights that the SCLM experienced the influence of ascending asthenospheric melts with a MORB-type signature.
In according to these results and differently from typical plume signatures, Ne isotopes mostly fall along or slightly below the air-MORB mixing line, at $^{21}Ne/^{22}Ne$=0.06 and $^{20}Ne/^{22}Ne$=12.5 (Figure 2).

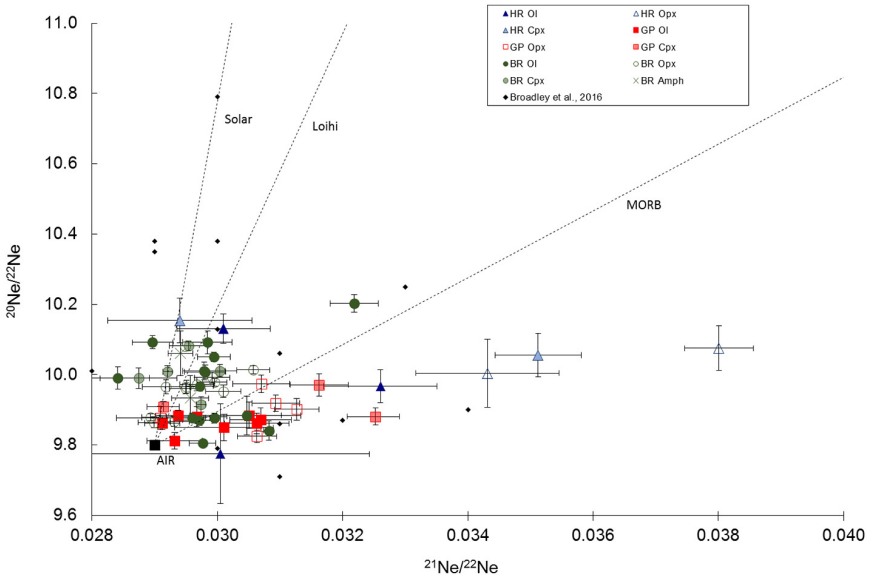

Figure 2 Ne-isotope plot for Antarctic xenoliths. The MORB-air, solar-air [Sarda et al., 1988] and Loihi-air mixing lines [Honda et al., 1993] are also reported for comparison.

These evidences lead us to consider more likely that the mantle beneath WARS was refertilized by a MORB component and the relative magmatism was triggered by alternative processes, such as decompression melting or tectonic-related lithosphere extension rather than to support the hypothesis of a WARS origin related to a plume.

References

Honda M., McDougall I., Patterson D.B., Doulgeris A., Clague D.A., (1993). *Noble gases in submarine pillow basalt glasses from Loihi and Kilauea, Hawaii: a solar component in the Earth*. Geochimica and Cosmochimica Acta, 57, 859-874.

Sarda P., Staudacher T., Allegre C.J., (1988). *Neon isotopes in submarine basalts*. Earth and Planetary Science Letters, 91, 73-88.

Geochemistry of noble gases and CO_2 of mantle xenoliths in the Joya Honda Maar (Central Mexico)

Sandoval Velasquez A.L[1]., Rizzo A.L.[2], Aiuppa A.[1], Frezzotti M.L.[3]

[1]*Università degli Studi di Palermo, Dipartimento delle Scienze della Terra e del Mare (DiSTeM), Palermo, Italy*
[2]*Istituto Nazionale di Geofisica e Vulcanologia, Sezione di Palermo, Italy*
[3]*Università di Milano Bicocca, Dipartimento di Scienze dell'Ambiente e della Terra, Milano, Italy*

Corresponding Author: *andreslibardo.sandovalvelasquez@unipa.it*

Introduction

The Joya Honda maar (JHm) is located approximately 35 km NE of the city of San Luis Potosí (central Mexico) and is part of the Ventura Espiritu Santo Volcanic Field (VESVF) in the south of the extensional province Basin and Range [Luhr et al., 1989; Aranda -Gómez and Luhr, 1996, Saucedo et al., 2017]. The JHm is an elliptical crater with vertical walls and a depth that varies between 150 - 300 m; it was formed by cutting calcareous mudstones, chert lenses and shales which are part of the Cuesta del Cura (Albian-Cenomanian) and Tamaulipas (Aptian) Formations [Aranda-Gómez and Luhr, 1996]. This volcano was formed by the eruption of alkaline magmas of mafic composition that when cooling favored the emplacement of olivine-nepheline basanites and olivine basalts, it is also characterized by the presence of mantle xenoliths described as spinel lherzolites and pyroxenites [Luhr et al., 1989; Aranda-Gómez et al., 2005]. The eruption that formed the maar was dated at 311+ 19 ka and its stratigraphic sequence is divided into five volcanic units [Saucedo et al., 2017]; each unit denotes the presence of this type of xenoliths. Although petrological studies have been carried out on these rocks, it is the first time that data on noble gases and CO_2 have been reported in fluid inclusions. Therefore, the objective of this study is the evaluation of the mexican lithospheric mantle features and related processes (e.g., metasomatism, partial melting) integrating the petrography, chemistry and isotope signature of noble gases and CO_2 in fluid inclusions (FI) from selected mantle xenoliths found in the Joya Honda maar (JHm).

Preliminary Results

1. For the analysis, twelve fresh xenolites with diameters between 5 and 10 cm were selected; these were extracted from the youngest deposits of the maar. The rocks were cut in such a way that one part was used for the generation of thin sections and the other was crushed for the separation of individual crystals of olivine (Ol), orthopyroxene (Opx) and clinopyroxene (Cpx); this for the study of noble gases and CO_2 in fluid inclusions. From the petrographic study, it was determined that the set of xenoliths are formed by the same paragenesis: Ol> Opx> Cpx >> Spinel. All samples are plagioclase-free and are classified as Spinel Lherzolites and Harzburgites (Figure 1). All have a protogranular to porphyroclastic texture in which two generations of Ol and Opx are observed: the first type corresponds to large and elongated crystals of sizes greater than 3 mm (porfiroclasts), generally deformed; and the second type corresponds to small crystals with polygonal shapes (neoblasts), usually without deformation and occur in the rock as a consequence of an intense recrystallization process. All xenoliths are affected by veins; both the boundaries and the fractures of the crystals develop veins composed of yellowish glass and tiny crystals of carbonates. The veins have variable thickness between 0.1 - 0.3 mm and generally do not react with the Ol crystals, but they do with the Opx and especially with Cpx. These veins can be associated with deep

metasomatism events as they tend to react with crystals, however, in some samples these veins show signs of alteration.

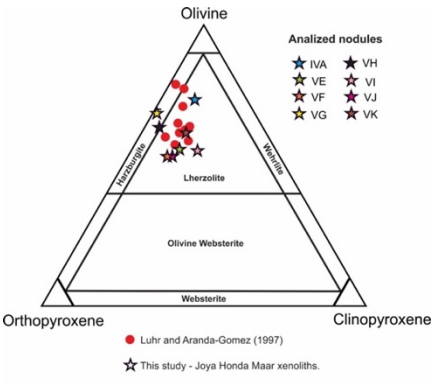

Figure 1 The ternary classification for ultramafic and mafic rocks [Streckeisen, 1976].

2. As preliminary results of noble gases, the xenoliths present Rc/Ra ($^3He/^4He$ corrected for air contamination) as follows: Ol has 7.13 - 7.68 Ra, Opx 6.94 - 7.54 Ra, and Cpx 7.06 - 7.59 Ra. These $^3He/^4He$ values are representative of local lithospheric mantle and compatible with a MORB-like source [Graham, 2002; Figure 2A]. The highest concentrations of CO_2 are reported in Opx and Cpx. The He/Ar* ratios vary between 0.14 and 3.11, which is in part within the typical production ratio of the mantle (1-5). This variability can respond to variable degrees of partial melting in the local mantle (Figure 2B).
3. The isotope composition of carbon of CO_2 expressed as $\delta^{13}C$ values vs V-PDB varies between -1.6 and -2.3%, whose values tend to pose over the mixing line MORB-Limestone (Figure 2C). This suggests the possible occurrence of carbonate recycling during the neighboring subduction process.

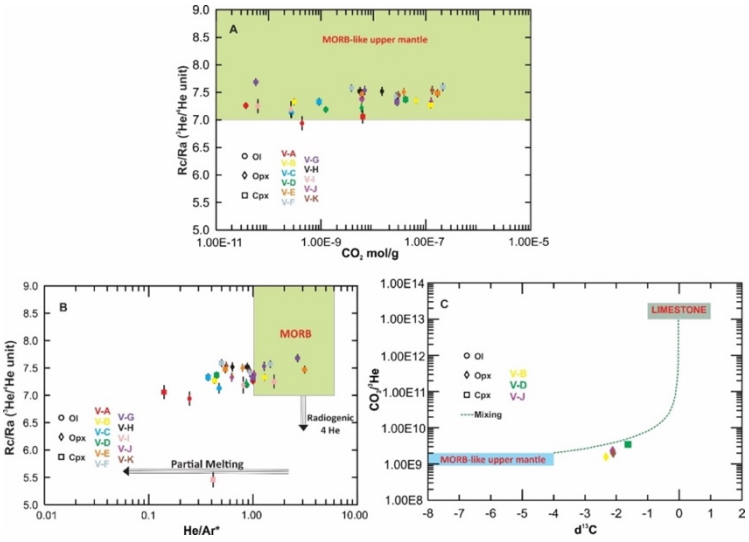

Figure 2 A) Concentration of CO_2 vs. $^3He/^4He$ corrected for air contamination (Rc/Ra). The green bar indicates the range of $^3He/^4He$ ratios for a MORB-like mantle [8 ± 1 Ra; Graham, 2002]. B) Ratio He/Ar* vs. $^3He/^4He$ corrected for air contamination (Rc/Ra). C) C-isotope composition ($\delta^{13}C$) vs. $CO_2/^3He$. The blue bar indicates the range of $\delta^{13}C$ values for a MORB-like mantle ($-8‰ < d^{13}C < -4‰$; [Sano and Marty, 1995]), while the gray bar is for limestone ($-1‰ < \delta^{13}C < +1‰$; [Sano and Marty, 1995]).

References

Aranda-Gómez J.J. and Luhr J.F., (1996). *Origin of the Joya Honda maar, San Luis Potosí, Mexico*. Journal of Volcanology and Geothermal Research, v. 74, pp. 1-18.

Aranda-Gómez J.J., Luhr J.F., Housh T.B., Valdez-Moreno G. and Chávez-Cabello G., (2005). *El vulcanismo tipo intraplaca del Cenozoico tardío en el centro y norte de México.* Boletín de la Sociedad Geológica Mexicana, v. 57, pp. 187-225.

Graham D.W., (2002). *Noble gas isotope geochemistry ofmid-ocean ridge and ocean island basalts: characterization of mantle source reservoir*. In: Porcelli D.P., Ballentine C.J. and Wieler R., (Eds.), Noble gases in geochemistry and cosmochemistry. Rev. Mineral. Geochem, v. 47, pp. 247-317.

Luhr J.F., Aranda-Gómez J.J. and Pier J.G., (1989). *Spinel lherzolite bearing, Quaternary volcanic centers in San Luis Potosí, México. I. Geology, mineralogy and petrology*. Journal of Geophysical Research, v. 94, pp. 7916-7940.

Luhr J.F. and Aranda-Gómez J.J., (1997). *Mexican Peridotite Xenoliths and Tectonic Terranes: Correlations among Vent Location, Texture, Temperature, Pressure, and Oxygen Fugacity*. Journal of Petrology, v. 38, pp. 1075-1112.

Sano Y. and Marty B., (1995). *Origin of carbon in fumarolic gas from island arcs*. Chem. Geol, v. 119, pp. 265-274.

Saucedo R., Macías J.L., Ocampo-Díaz Y.Z.E., Gómez-Villa W., Rivera-Olguín E., Castro-Govea R., Sánchez-Núñez J.M., Layer P.W., Torres-Hernández J.R. and Carrasco-Núñez G., (2017). *Mixed magmatic-phreatomagmatic explosions during the formation of the Joya Honda maar, San Luis Potosí, Mexico*. Geological Society, Special Publications, v. 446, pp. 255-280.

ST07

ADVANCES IN GAS MEASUREMENTS AND TECHNIQUES

REFERENCE: MARCO LIUZZO

Evaluation of the transfer of pollutants from a groundwater body to associated lake water bodies and estimate of related impacts on their environmental quality status in Castelvetrano-Campobello di Mazara Plain (TP)

Abita A., Palumbo V., Nicolosi M., Pellerito S., Costa N.

ARPA, Agenzia Regionale per la Protezione Ambientale Sicilia, Palermo, Italy

Corresponding Author: *vpalumbo@arpa.sicilia.it*

ARPA Sicilia carried out a study on the hydrogeological system of "Castelvetrano-Campobello di Mazara Plain" (TP) aimed at evaluating the interactions between the homonymous groundwater body, characterized by punctual exceedances of quality standards and threshold values reported in Legislative Decree n.30/2009, and the surface water bodies connected to it, represented by lakes of karstic origin "Preola, Murana and Gorghi Tondi", characterized by a poor chemical status and an ecological status from bad to sufficient, as well as sites of Natura 2000 network and wetlands of international importance under the "Ramsar Convention". The study, conducted in order to verify the fulfillment of the conditions concerning the good chemical status of the groundwater body foreseen by the D. lgs. 30/2009 (article 4, paragraph 2, letter c, point 2 and Annex 5, points 4.b, 4.c), consisted of an initial investigation, aimed at the preliminary characterisation, the conceptual modeling of the hydrogeological system and the execution of new field surveys, and in a subsequent evaluation phase of the groundwater flow and contaminant transport processes, focused on the western sector of aquifer where Preola, Murana and Gorghi Tondi lakes are located, based on numerical simulation models implemented in the study area.
The study carried out allowed for:

- to elaborate a preliminary pressure-impact conceptual model of the western sector of groundwater body (relations between punctual and diffuse sources of pressure and relative potential impacts on groundwater body and the interconnected surface water bodies);
- to assess the extent of the transfer to Preola, Murana and Gorghi Tondi lakes of dissolved arsenic and nitrate pollutants detected in groundwater body and coming mainly from disused municipal solid waste landfills and from areas subjected to agricultural and livestock activities that are located in the western sector of the groundwater body;
- to estimate the possible impacts of the transfer of dissolved arsenic and nitrate pollutants on the environmental quality status of Preola, Murana and Gorghi Tondi lakes.

On the basis of the results obtained from the study, the conditions concerning the good chemical status of groundwater body of "Castelvetrano-Campobello di Mazara Plain" foreseen by the D. lgs. 30/2009 (article 4, paragraph 2, letter c, point 2) are considered not satisfied, since the quantity and the concentrations of pollutants transferred by it to the interconnected surface water bodies (Preola, Murana and Gorghi Tondi lakes), estimated on the basis of the implemented transport models, determine, with a reliability within the degree of approximation of the models, a possible impact on their ecological status.

Keywords: Directive 2000/60/CE, Directive 2006/118/CE, interaction between groundwater body and associated lake water bodies, implementation of dissolved arsenic and nitrate transport simulation model, impact of pollutants transfer on environmental quality status of lakes.

References

Bonanno A., Ciabatti P., Liguori V., Provenzano M.C. & Sortino G., (2000). *Studio idrogeologico ed idrogeochimico dell'acquifero multifalda della Piana di Castelvetrano e Campobello di Mazara (Sicilia occidentale)*. Quaderni di Geologia Applicata, 7, 4, 45-59.

Cassa per il Mezzogiorno - Ripartizione progetti idrici divisione V - Schemi idrici della Sicilia, (1982). *Indagini idrogeologiche per l'approvvigionamento idrico del Sistema II Nordoccidentale della Sicilia (Acquiferi principali)*. Arlab S.r.l.

Cusimano G., Hauser S., Vassallo M., (2006). *Hydrogeochemistry of a wetland area of southwestern Sicily (Italy)*. EWA (European Water Association).

European Commission, (2009). *Guidance on Groundwater Status and Trend Assessment*. Guidance Document No. 18 - 2009. ISBN 978-92-79-11374-1. European Communities, 2009 Luxembourg.

European Commission, (2015). *Technical Report on Groundwater Associated Aquatic Ecosystems*. Technical Report, N. 9 - 2015. ISBN 978-92-79-53895-7. European Communities, 2015 Luxembourg.

Jayasumana C., Fonseka S., Fernando A., Jayalath K., Amarasinghe M., Siribaddana S., Gunatilake S., Paranagama P., (2015). *Phosphate fertilizer is a main source of arsenic in areas affected with chronic kidney disease of unknown etiology in Sri Lanka*. Springerplus, 2015 Feb 24; 4:90. doi: 10.1186/s40064-015-0868-z. eCollection 2015.

First measurements with the Picam uv camera in northern Chile volcanoes

Aguilera F.[1,2], Layana S.[1,3], Rojas F.[2], Arratia P.[2], Wilkes T.[4], McGonigle A.[4], Pering T.[4]

[1]*Núcleo de Investigación en Riesgo Volcánico - Ckelar Volcanes, Universidad Católica del Norte, Chile*
[2]*Departamento de Ciencias Geológicas, Universidad Católica del Norte, Chile*
[3]*Programa de Doctorado en Ciencias mención Geología, Universidad Católica del Norte, Chile*
[4]*Departament of Geography, The University of Sheffield, UK*

Corresponding Author: *feaguilera@ucn.cl*

Introduction

The SO_2 is a toxic gas that comes from different anthropogenic sources, but is also emitted from persistently degassing and eruptive volcanoes, having an impact in environment and economics [Gliß et al., 2018]. SO_2 emission rates and its fluctuations have been measured because indicate possible changes in the magma flux [Smekens et al., 2015], and is considered as a proxy for eruptions [Rodriguez and Nadeau, 2015]. SO_2 has been measured/monitored using several techniques including satellite-based remote sensing as Total Ozone Mapping Spectrometer-TOMS, Ozone Monitoring Instrument-OMI, aerosols in gas plumes, MultiGas in plumes, direct sampling of fumarolic gases, and ground-based remote techniques as Correlation Spectrometer-COSPEC, Differential Optical Absorption Spectrometer-DOAS, Fourier Transformation Infrared Spectrometer-FTIR, Infrared-IR and Ultraviolet-UV cameras.

The UV camera technique has been used for volcanological purposes since 2005 [Mori and Burton, 2006], being characterized by its high temporal resolution and its capability to determine plume speed, solving two error sources in other SO_2 flux methodologies [Smekens et al., 2015]. UV cameras have been used to understand the flow dynamics in volcanic conduits [e.g. Moussalam et al., 2016], to determine mass flow rates models [e.g. Delle Donne et al., 2016], to evaluate eruptive periods of a single volcano [e.g. Kasahaya et al., 2011], to determine the global fluxes along volcanic zones [e.g. Moussalam et al., 2017], to correlate degassing and seismological data [e.g. Burton et al., 2015], among others.

Despite several gas measurements have been performed in northern Chile volcanoes, including direct sampling techniques, aerosols in plumes, COSPEC and DOAS, only few works have been carried out using UV cameras, including only six of the thirteen permanently degassing volcanoes [Geoffroy, 2014; Tamburello et al., 2014; Stebel et al., 2015; Gliß et al., 2018; Lopez et al., 2018].

In this work we present the first results obtained using the new low-cost PiCam UV camera in nine persistently degassing volcanoes from northern Chile in order to compare our results with previous data from other ground-based remote techniques and to determine the several factors that can influence positively and/or negatively the data quality of the new camera.

Northern Chile Volcanoes

The Central Andean Volcanic Zone (CAVZ) is located between at ca. 14° to 27° S, covering the southern Peru, western Bolivia, northwestern Argentina and northern Chile. CAVZ presents more than 40 volcanic centers that have registered eruptive activity in the last ca. 10 ka [e.g. de Silva and Francis, 1991]. About northern Chile volcanoes, activity has been reported in some detail from the

19th century, which include intense fumarolic activity without historical eruptions recorded (Tacora, Guallatiri, Olca, Ollagüe, Apacheta, Putana, Alitar, Lastarria and Ojos del Salado volcanoes), phreatic to phreatomagmatic events with VEI 2 (Isluga, Irruputuncu and San Pedro volcanoes), and a subplinian eruption in Lascar volcano with VEI 4 during April 19-20, 1993 [Gonzalez-Ferrán, 1995]. Nine of thirteen persistently degassing volcanoes from northern Chile develop permanent gas plumes, which vary widely in intensity and gas concentration, being from north to south to Guallatiri, Isluga, Irruputuncu, Olca, Ollagüe, San Pedro, Putana, Lascar and Lastarria volcanoes.

Methodologies

PiCam UV camera and Post Processing

The PiCam is a low-cost SO_2 UV camera, based on modified Raspberry Pi camera modules. The camera sensor (Omnivision OV5647) was modified following Wilkes et al., [2016] by chemical removal of the sensor's Bayer filter. The optical system was built [following Wilkes et al., 2016; 2017] around this detector using a 3D printed lens holder and an off-the-shelf plano-convex lens (9 mm focal length, 6 mm diameter; Edmund Optics Inc.). The resulting camera has a field-of-view of 23.1˚ × 17.3˚ (width × height). Filters (Edmund Optics Inc.) were mounted to the fore of the lens, using typical on- (310 nm) and off- (330 nm) bands for SO_2 detection [e.g. Mori and Burton, 2006]. The cameras were connected to Raspberry Pi 3 Model B computers for interfacing, all housed within a PeliCase along with a battery and GPS for timestamping acquisitions. A Windows laptop was used to communicate with the Raspberry Pis wirelessly, controlling data capture via custom Python 3 code.
Image calibration was performed using gas cells containing column densities of 100, 467 and 1989 (all ±10%) ppm·m. In all field cases the calculated apparent absorbances and column densities displayed a good linear fit.
Image processing was performed post-acquisition, not in real-time. Again, this used custom Python 3 code; a detailed description of processing techniques for SO_2 cameras is provided by Gliß et al., [2017]. Image registration was performed via one of two methods: automated registration using the findTransformECC function of the OpenCV library; manual control point selection and subsequent warping using the warp function of the scikit-image module. Other typical processing techniques were performed. All images were dark image corrected. Image vignetting was corrected for using a clear-sky mask acquired in the field. Clear-sky background intensity was determined by averaging intensity of a region of sky close to the plume. Plume speed was calculated using the cross-correlation technique [e.g. Mori and Burton, 2006]. No light dilution correction was done in the totally of the measurements presented in this work.

Fieldwork

In this work we present data from several field campaigns carried out in the period November 2017-January 2019, where 9 of the 13 persistently degassing volcanoes in the northern Chile that produce gas plumes were measured. All measuring points were located in an altitude between 3,965 and 5,300 m a.s.l. and distances between 0,6 and 10.8 km from active craters and/or fumarolic fields. Measurements were carried out between 9:48 and 18:47 hrs local time (UTC -3), with time span ranging 30-55 minutes. Shutter speed for filters A and B varies from 55 to 700, and 10 to 100, respectively, whereas image capture frequency was set up in 0.2 and 0.25, which correspond to one image every 4 and 5 seconds, respectively.

Results

The totally of the sequences in the nine volcanoes measured were post processed using Open CV

library and control point methods. Data from Guallatiri volcano include seven measurement sequences performed during 3 days, with plume speed calculated from 1.0 to 10.3 ms^{-1}. Averages of the SO_2 emission rate varies from 19.1±4.5 and 50.5±12.3 td^{-1}, with a maximum rate reaching up to 101.1 td^{-1}. The overall SO_2 output for the 3 days was 29.1±22.6 td^{-1}. All the processing was done for the gas plume related to the summit fumarolic field, due processing for southern flank fumarolic field released no reliable data.

5 sequences were obtained during 1 day of measurements from Isluga volcano, obtaining plume speeds between 7.0 and 13.1 ms^{-1}. SO_2 emission rates vary from 129.4±28.3 and 282.1±93.6 td^{-1}, and with a peak of 569.4 td^{-1}. In the case of Irruputuncu volcano, 6 sequences were carried out in two days of measurements. The range of plume speed varies from 2.6 and 5.9 ms^{-1}, and SO_2 emission rates averages for all sequences vary from 16.5±5.4 to 56±10 td^{-1}, being the highest SO_2 emission rate of 80.4 td^{-1}. The overall SO_2 output for both days was 32.3±15.6 td^{-1}. Isluga and Irruputuncu volcanoes are characterized by the emission of a plume coming from a single "small size" crater (~100 m diameter).

Putana and Lastarria volcanoes correspond to multiple fumarolic fields systems, which produce single bulk plume, as a result of the combination of several plumes emitted from those fumarolic fields. Putana volcano was measured during two days, whereas Lastarria during 6 days along several seasons (May 2018, November and January 2019). Plume speeds had variations from 1.8 and 16.7 ms^{-1}. In the case of Putana volcano, average SO_2 emission rates ranged between and 3.92±1.33 and 31.92±9.80 td^{-1}, with a maximum of 66.83 td^{-1}, and an overall SO_2 output of 15.55±14.84 td^{-1}. Lastarria volcano is the system with the highest SO_2 emission rates between all measured systems, varying from 806 and 1,000 td^{-1} as average rates for bulk plume. Considering single fumarolic fields an overall SO_2 output measured is 243.5±164 td^{-1}.

Lascar volcano is characterized by a single central active crater, which produces an extended gas plume, and was measured during 8 days during summer, winter and spring seasons. Plume speeds measured ranging 1.9 and 9.1 ms^{-1}, with an overall SO_2 output of 49±23 td^{-1} and maximum SO_2 emission rates of 88.9 td^{-1}.

Discussions

Several effects were observed during the data acquisition and data processing, which depends of the external factors and PiCam software properties. Wind effect is one of the most important external factors that can affect PiCam UV camera measurements, affecting during the data acquisition and post processing. Lateral movement of the camera in the field produced by wind blows, generates displacement and unfocussing of the acquired images. We observed that if a complete sequence partially affected by wind movement is processed, SO_2 emission rates are underestimated. Processing of not wind-affected images allow improving the plume speed estimation and consequently the emission rates, due separation of displaced/unfocussed images avoids errors related to the movement of Integrated Column Amount (ICA) respect to the integration line. After of the correction by wind effects in the PiCam, we have estimated that the maximum improvement of the SO_2 emission rates reach up to ~50%.

Campion et al., [2015] showed that other external factor is the atmospheric effect in the measurements carried out using UV cameras, which are related to the atmospheric conditions as pressure, humidity and aerosol concentration, SO_2 concentration and distance from the plume, producing an underestimation of the SO_2 emission rates. In the case of northern Chile volcanoes, located in altitudes over 5,000 m a.s.l., the zone is characterized by a thin atmosphere and a very dry environment, where the dilution effect is more reduced. We performed measurements in Guallatiri and Putana volcanoes at several distances from the gas plume sources, which despite where done in

different periods of time, were carried out in the same atmospheric conditions (cloud free sky). Assuming that degassing in both volcanic systems has been constant in the last century (absence of eruptive activity in the same period) and comparing measurements with similar plume speeds (differences of ±0.5 ms^{-1}), we have calculated that dilution effect in the northern Chile area produce an underestimation of SO_2 emission rates between 7 and 40%. Additionally, measurements carried out at long distances (9.5 and 10.8 km from the gas source in Putana and Guallatiri volcanoes respectively) demonstrate the high-quality performance of PiCam UV camera for measure SO_2 emission rates.

Overestimation of wind speed and SO_2 emission rates has been occasionally detected in our measurements due to differences between images alignment, which is consequence of the alignment methods incorporated in the PiCam post processing software. Open CV method can produce errors in the alignment of the images, creating a double plume, which is observed as a shadow of the original recorded plume. This error is related to the occasional inability of the method to align automatically the borders of the volcanic edifice, generating an overestimation of the SO_2 emission rates. The overestimation can be corrected using the Control Points (CP) method, which allows aligning manually the images from the two lenses, by use of control points in both images. Our data demonstrate that CP method can reduce the overestimation of the SO_2 emission rates in ~30%.

Several authors have reported SO_2 emission rates in 6 of our studied volcanoes, corresponding mostly to discrete field campaigns carried out by DOAS, and more restricted using UV camera [Clavero et al., 2006; Geoffroy, 2014; Tamburello et al., 2014; Stebel et al., 2015; Gliß et al., 2018; Lopez et al., 2018]. In mostly of the cases, higher SO_2 emission rates were reported, being only in Irruputuncu and Lastarria volcanos measured similar rates. We have attributed the differences between our and other authors measurements mainly to i) potential errors while measurements were carried out, including measuring position respect to gas plume direction (affecting the geometry of the measured plume), weather conditions, calibration process, among others; ii) accuracy of the determination of plume speed, which depends in the case of mobile and permanent DOAS of the method used to estimate wind speed (e.g atmospheric model); iii) light dilution effect related with the distance of the measuring point from the crater and/or fumarolic field; iv) seasonal effects related with the period of the year when measurements were carried out. The last can be clearly observed in Isluga volcano, which is continuously measured since December 2014 by OVDAS-SERNAGEOMIN using a permanent DOAS station (from NOVAC system). Higher SO_2 emission rates are measured during winter season, characterized by faster wind speeds, whereas during the dry summer season, when slower winds speeds are recorded, SO_2 emission rates decrease, producing an oscillatory pattern along a single year.

References

Burton M.R., Prata F., Platt U., (2015). *Volcanological applications of SO_2 cameras*. Journal of Volcanology and Geothermal Research, 300, 2-6.

Campion R., Delgado-Granados H. and Mori T., (2014). *Image-based correction of the light dilution effect for SO_2 camera measurements*. Journal of Volcanology and Geothermal Research, 300, 48-57.

Clavero J., Soler V., Amigo A., (2006). *Caracterización preliminar de la actividad sísmica y de desgasificación pasiva de volcanes activos de los Andes Centrales del norte de Chile*. Congreso Geologico Chileno, 11, 443-446.

Delle Donne D., Ripepe M., Lacanna G., Tamburello G., Bitetto M. and Aiuppa, A., (2016). *Gas mass derived by infrasound and UV cameras: Implications for mass flow rate*. Journal of Volcanology and Geothermal Research, 325, 169-178.

de Silva S. and Francis P., (1991). *Volcanoes of Central Andes*. Springer-Verlag, Heidelberg.

Geoffroy C., (2014). *Estimación de la emisión de dióxido de azufre en penachos volcánicos mediante una cámara ultravioleta*. Undergraduate thesis, Universidad de Chile.

Gliß J., Stebel K., Kylling A., Dinger A. S., Sihler H., and Sudbø A., (2017). *Pyplis-A Python Software Toolbox for the Analysis of SO_2 Camera Data*. Implications in Geosciences, 7, 134.

Gonzalez-Ferrán O., (1995). *Volcanes de Chile*. Instituto Geografico Militar, Santiago.

Kasahaya R., Mori T., Takeo M., Ohminato T., Urabe T., Maeda Y., (2011). *Relation between single very-long-period pulses and olvanic gas emissions at Mt. Asama, Japan*. Geophysical Research Letters, 38.

Lopez T., Aguilera F., Tassi F., Maarten de Moor J., Bobrowski N., Aiuppa A., Tamburello G., Rizzo A., Liuzzo M., Viveiros F., Cardellini C., Silva C., Fischer T., Jean-Baptiste P., Kazayaha R., Hidalgo S., Malowany K., Lucic G., Bagnato E., Bergsson B., Reath K., Liotta M., Carn S., Chiodini G. (2018). *New constraints on the magmatic-hydrothermal system and volatile budget of Lastarria Volcano, Chile: Integrated results from the 2014 IAVCEI CCVG 12th Volcanic Gas Workshop*. Geosphere 14, 983-1007.

Mori T. and Burton M.R., (2006). *The SO_2 camera: a simple, fast and cheap method for ground based imaging of SO_2 in volcanic plumes*. Geophysical Research Letters, 161, 47-56.

Moussallam Y., Bani P., Curtis A., Barnie T., Moussallam M., Peters N., Schipper C.I., Aiuppa A., Giudice G. and Amigo A., (2016). *Sustaining persistent lava lakes: Observations from high-resolution gas measurements at Villarrica volcano, Chile*. Earth and Planetary Science Letters, 454, 237-247.

Moussallam Y., Tamburello G., Peters N., Apaza F., Schipper C.I., Curtis A., Aiuppa A., Masias P., Boichu M., Bauduin S., Barnie T., Bani P., Giudice G., Moussallam M., (2017). *Volcanic gas emissions and degassing dynamics at Ubinas and Sabancaya volcanoes; implications for the volatile budget of the central volcanic zone*. Journal of Volcanology and Geothermal Research, 343, 181-191.

Rodríguez L. and Nadeau P., (2015). *Resumen de las principales técnicas de percepción remota usadas en volcanes para monitorear las emisiones de gas en tierra*. Revista Geológica de América Central, 52, 67-105.

Smekens J.F., Burton M.R., Clarke A.B., (2015). *Validation of the SO_2 camera for high temporal and spatial resolution monitoring of SO_2 emissions*. Journal of Volcanology and Geothermal Research, 300, 37-47.

Stebel K., Amigo A., Thomas H. and Prata A.J., (2015). *First estimates of fumarolic SO_2 fluxes from Putana volcano, Chile, using an ultraviolet imaging camera*. Journal of Volcanology and Geothermal Research, 300, 112-120.

Tamburello G., Hansteen T. H., Bredemeyer S., Aiuppa A. and Tassi F., (2014). *Gas emissions from five volcanoes in northern Chile and implications for the volatiles budget of the Central Volcanic Zone*. Geophysical Research Letters, 41, 4961-4969.

Wilkes T.C., McGonigle A.J.S., Pering T.D., Taggart A.J., White B.S., Bryant R.G. and Willmott J.R., (2016). *Ultraviolet Imaging with Low Cost Smartphone Sensors: Development and Application of a Raspberry Pi-Based UV Camera*. Sensors, 16, 1649.

Wilkes T.C., Pering T.D., McGonigle A.J.S., Tamburello G. and Willmott J.R., (2017). *A lowcost smartphone sensor-based UV camera for volcanic SO_2 emission measurements*. Remote Sensing, 9, 27.

The Ground CO_2 Mapper - An innovative tool for the rapid and precise mapping of CO_2 leakage distribution

Beaubien S.E., Graziani S., Tartarello M.C., Ruggiero L., Bigi S.

Università degli Studi di Roma La Sapienza, Dipartimento di Scienze della Terra, Italy

Corresponding Author: *stanley.beaubien@uniroma1.it*

The recently developed Ground CO_2 Mapper ("Mapper" for short) is an inexpensive, light, robust, and low power consuming tool for determining the distribution of CO_2 at the soil-atmosphere contact as an indicator of CO_2 leakage. The basic premise behind the Mapper is that the contact between the ground surface and the atmosphere represents an interval where CO_2 leaking from the subsurface can accumulate in anomalous concentrations due to two mechanisms, the higher density of CO_2 with respect to air and the tendency of wind speed (and thus mixing) to approach zero near the ground surface due to frictional drag. Because of its measurement target and the tool's very rapid response time, Mapper surveys can be conducted very quickly at a high sampling density, yielding accurate maps of CO_2 spot anomalies. The unit can be used by anyone and deployed within only 5-10 minutes after sensor and GPS signal warm-up. Here we describe the Mapper and present results from a site of natural diffuse CO_2 degassing in central Italy.

Introduction

The flux of biogenic CO_2 from the ground surface to the atmosphere is ubiquitous due to microbial and root respiration in the soil. This flux is controlled by numerous geological (soil type, permeability, organic matter content, etc.) and environmental (temperature, water content, etc.) conditions, resulting in relatively smooth spatial distributions that are influenced by higher-order variables (topography, land-use, etc.) and temporal variations that are closely linked with diurnal and seasonal variations. In some settings the leakage of a second source can be superimposed on this background distribution due to the upward migration of deep-origin geologically produced CO_2 along faults and discontinuities in geothermal or volcanic settings. This flux, commonly referred to as diffuse degassing, can range from levels similar to those of biogenic up to 3-4 orders of magnitude higher, tends to be more stable in time, and is distributed both as low-level leaks controlled by diffusion and as high-level, smaller "vents" controlled by advection. A second potential deep source could be the leakage of man-made CO_2 stored in deep geological reservoirs (i.e., Carbon Capture and Storage, CCS), although to date this has not been observed [e.g., Beaubien et al., 2013].

The goals of measuring CO_2 flux for either geogenic- or CCS-related studies are typically one of the following: i) to map its distribution to understand the underlying migration pathway (e.g., fault distribution); ii) to quantify the total amount being released to determine, for example, heat flow in geothermal areas, carbon loading to the atmosphere, or CCS storage integrity / carbon credit auditing; or iii) to assess any potential leakage-related risks to human health or the local ecosystem. These goals are usually accomplished by making many point flux measurements over the study area, using the accumulation chamber technique, followed by statistical/geostatistical analysis and spatial interpolation [e.g., Cardellini et al., 2003]. However, point sampling of a spatially variable parameter, especially one that can exhibit small sized anomalies with values significantly higher that background (i.e., "hot spots") risks to completely miss anomalies if sample spacing is too large, which could in turn

lead to errors in data interpolation. Because the number of flux measurements (and thus sample density) is limited by logistics and costs, a rapid, reconnaissance tool to focus flux surveying on areas of interest, or even act as a proxy, could potentially be very helpful.
The Ground CO_2 Mapper ("Mapper" hereafter) was recently developed with this goal in mind, extending and greatly improving upon a proof-of-concept prototype that was previously created by the present authors [Annunziatellis et al., 2008; Jones et al., 2009]. Here we describe the characteristics and capabilities of this new low-cost, robust, low power consuming, precise and sensitive tool and illustrate its potential using field test results from a natural diffuse degassing site in central Italy.

Methods

The Mapper is premised on the fact that CO_2 released from the soil tends to accumulate at the contact between the ground surface and atmosphere due to the higher density of this gas relative to air as well as near-zero wind speeds in this interval (known as the roughness height) due to frictional drag [Garratt, 1994]. The Mapper is mounted on a small hand cart and pushed around the area of interest at a normal walking speed. While moving, air is constantly pumped from a 6 mm diameter tube (whose inlet is dragged along the ground surface) into a fast-response, low-cost miniature NDIR CO_2 sensor (Alphasense IRC-A1) and the resultant CO_2 concentration is paired with coordinates from an integrated differential Global Navigation Satellite System (D-GNSS) (UBlox C94-M8) for precise spatial mapping. Operation is via a touch screen, data are saved to an internal flash memory, and data is downloaded via WiFi using a cellular phone or computer. Measurements are made at 4Hz, resulting in a sample spacing of 20-40 cm along line while lateral line-to-line spacing is chosen by the operator based on the area to cover and expected anomaly size; typical line spacing would be on the order of 2-5 m.
Point flux measurements were performed using an accumulation chamber system built by the authors, and whose response has been verified by comparison with commercial instruments.

Results and Discussion

Laboratory tests

Sensitivity of a mobile system is based not only on sensor stability but also on response time, as the faster the response the closer the instrument will come to measuring the true value before moving into an area with a different value. These two instrument characteristics can be in conflict, however, because the increased flow rate necessary to decrease response time tends to increase sensor noise. Extensive development work on the Mapper focused on finding a compromise between these two parameters, with the resultant values presented below.
The background noise level was assessed by running the Mapper in acquisition mode and drawing outdoor atmospheric air from a third-floor window, where concentrations were expected to remain essentially constant for the 10-minute monitoring period (Figure 1a). The measurements yielded 2σ = 20 ppm, meaning that values greater than the average background value plus 20 ppm can be considered anomalous at the 95% confidence level (given the Gaussian distribution of the data). In addition, it should also be noted that sensor background noise is high frequency, whereas a true anomaly encountered during motion across a leakage area will result in a lower frequency anomaly, opening the possibility for time domain filtering. This is simply illustrated by calculating a two-point running average of the same data, which yields 2σ = 16 ppm.

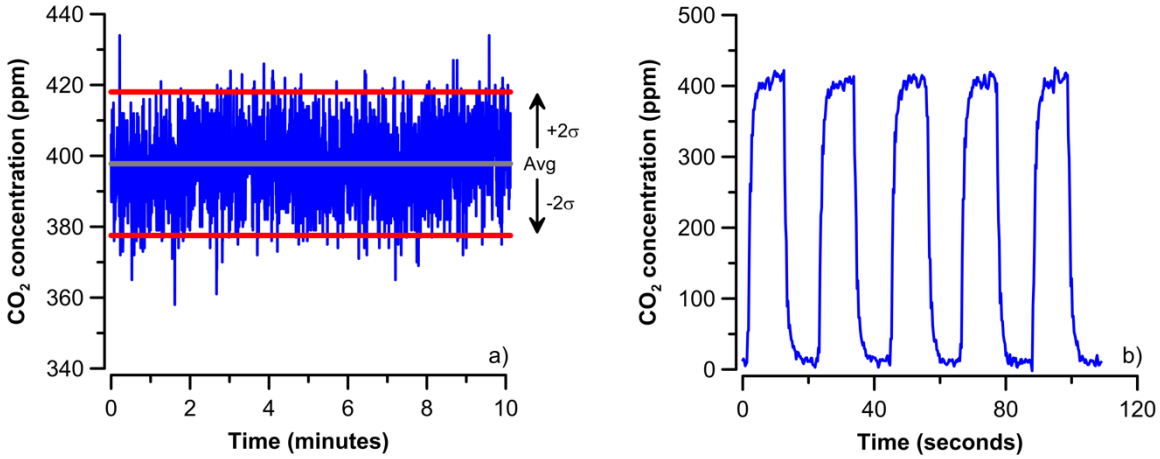

Figure 1 Results showing the level of background noise (a) and the response time (b) of the Mapper. Data are collected at 4 Hz; raw data are presented in (a) while a 2-point running average is given in (b) to remove the strong signal oscillations that occur during very rapid, large concentration changes.

The response time of the Mapper was assessed by attaching the system's inlet tube to a two-way valve that gave alternating access to 1L Tedlar bags filled with i) pure nitrogen and ii) a CO_2 standard of 395 ppm. The valve was actuated manually every 10 seconds and at the same time a text character was inserted into the data stream to mark the time zero of each switch. Results of the 11 valve switches performed over a two-minute period show highly reproducible behavior (Figure 1b), defining a T_{70} (i.e., time required to reach 70% of the new value) of about 1.75 seconds. It should be remembered, however, that in actual field conditions changes will tend to be along a gradient and not via instantaneous, drastic changes like those tested here. The response time could affect field data in two ways. If the leakage area is sufficiently large relative to the surveying speed, the resultant anomaly will simply be shifted slightly but measured concentrations will not be strongly affected. Instead with a small anomaly there is also the potential that the measured concentration anomaly will be smaller because there is insufficient exposure to the sampled gas. These relations must be taken into consideration when deciding the survey walking speed.

Field tests

Field testing of the Mapper was conducted in October 2018, near the town of Ailano, Italy, in an area known for extensive diffuse CO_2 degassing [Ascione et al., 2018]. A total of four fields were measured, each being unique in terms of the strength and size of the leaks and the height of the vegetation (which impacts on the roughness height). Surveys were performed over a 5-day period, during which the light wind conditions varied only slightly. Duplicate surveys were conducted in different directions in all measured fields. Results from the "Ailano-2" field are presented here, which are representative of the collected data.

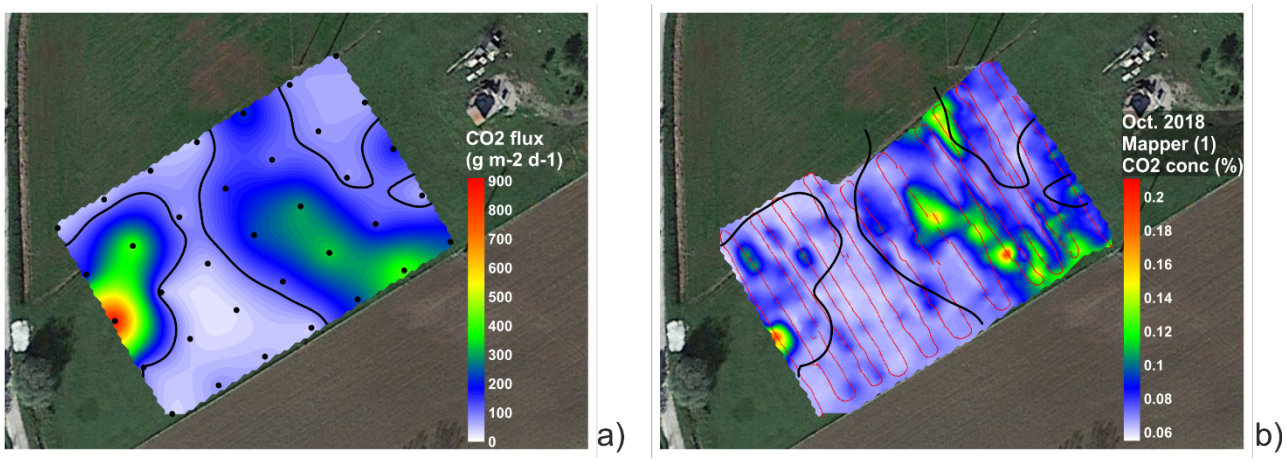

Figure 2 Mapper field test: a) contoured CO_2 flux based on point flux measurements performed on a 10 m spaced grid; and b) contoured Mapper CO_2 concentration results, with the 100 g m^{-2} d^{-1} flux contour (black line) plotted for reference and red dots showing the Mapper sample points.

The Ailano-2 field is flat, generally not cultivated, and covers a total area of about 4500 m^2; measurements were performed on a central area covering 2400 m^2. In an aerial photograph there are no obvious signs of CO_2 leakage, although visual inspection during the survey period did show some areas of thin vegetation. At the time of the campaign the field was filled with grasses and weeds ranging in height from 3 to 30 cm. Point flux measurements were made on a regular 40 x 60 m grid having 10 m sample spacings (Figure 2a). Results highlight two primary areas of enhanced leakage, one elongated feature trending generally NW-SE on the eastern side of the grid and a more oval feature located on the western edge. Values range from 30 to 900 g m^{-2} d^{-1}, although only one sample point (in the middle of the grid's western boundary) exceeds 400 g m^{-2} d^{-1}.
A Mapper survey was conducted over the same area, performed at a walking speed that resulted in c. 25 cm sample spacing along lines and a chosen 2 m spacing between lines. Measured CO_2 concentrations ranged from 550 to 2000 ppm, with Mapper anomaly distribution (Figure 2b) matching closely that defined by the point flux measurements (Figure 2a). The much closer sample spacing of the Mapper permitted a more detailed definition of the leakage points, highlighting a series of nearby, semi-amalgamated, concentrated leakage areas rather than the smoother, more homogeneous image resulting from interpolation of the more widely spaced CO_2 flux results. A second Mapper survey conducted in an orthogonal direction in the same field (data not shown) yielded very similar results. It is important to note that while measurement of the flux grid of 35 samples required approximately 2 hours the Mapper survey was completed in about 15 minutes. Similar results were obtained in the other three fields, despite the fact that some had been recently cut leaving vegetation that was only 2-3 cm high.

Summary and Conclusions

A new tool, the "Mapper", has been developed for the rapid reconnaissance mapping of CO_2 spot leakage areas, to quickly cover large areas and to focus more detailed and time-consuming point flux measurements. Laboratory tests show that anomalies can be defined as 20 ppm above CO_2 average baseline values and that the response time (T_{70}) of the present configuration is about 1.75 seconds. Field surveys at a site of natural defuse degassing in central Italy illustrate excellent correlation with CO_2 flux distribution defined using point measurements and show good instrument reproducibility and sensitivity under real-world conditions of different leakage rates, different vegetation lengths, and slightly variable wind conditions.

Highly detailed tests under controlled leakage conditions are now being conducted to better define the sensitivity of the tool, both in terms of absolute sensor response as well as its response as a mobile platform that is moved across spatially discrete anomalies. These experiments, being conducted on a constructed test site, will address such issues as anomaly size, flux rate, walking speed, vegetation height, and wind conditions, and how they may impact on the tool's capabilities. The goal of this work is to determine the minimum CO_2 flux level that can be recognized by the Mapper, under both ideal and less-than-ideal conditions. Experiments are also being conducted to improve sensor response time and signal to noise ratio, with progress having been made since the version used during the October 2018 campaign reported here.

Acknowledgements

This research was conducted within the ENOS project, which received funding from the European Union's Horizon 2020 research and innovation programme under grant agreement No 653718.

References

Annunziatellis A., Beaubien S.E., Ciotoli G., Coltella M. and Lombardi S., (2008). *Development of a rapid, low-cost technique for sensitive CO_2 leakage mapping*. Vol. 10, EGU2008-A-10641, EGU General Assembly 2008, Vienna, Austria.

Ascione A., Ciotoli G., Bigi S., Buscher J., Mazzoli S., Ruggiero L., Sciarra A., Tartarello M.C., and Valente E., (2018). *Assessing mantle versus crustal sources for non-volcanic degassing along fault zones in the actively extending southern Apennines mountain belt (Italy)*. GSA Bulletin, v. 130, p. 1697-1722.

Beaubien S.E., Jones D.G., Gal F., Barkwith A.K.A.P., Braibant G., Baubron J.C., Ciotoli G., Graziani S., Lister T.R., Lombardi S., Michel K., Quattrocchi F. and Strutt M.H., (2013). *Monitoring of near-surface gas geochemistry at the Weyburn, Canada, CO_2-EOR site, 2001-2011*. International Journal of Greenhouse Gas Control, v. 16, Supplement 1, p. S236-S262.

Cardellini C., Chiodini G. & Frondini F., (2003). *Application of stochastic simulation to CO_2 flux from soil: mapping and quantification of gas release*. Journal of Geophysical Research, v. 108, 2425, https://doi.org/10.1029/2002JB002165.

Garratt J.R., (1994). *Review: the atmospheric boundary layer*. Earth-Science Reviews, v. 37, p. 89-134.

Jones D.G., Barlow T., Beaubien S.E., Ciotoli G., Lister T.R., Lombardi S., May F., Moller I., Pearce J.M. and Shaw R.A., (2009). *New and established techniques for surface gas monitoring at onshore CO_2 storage sites*. Energy Procedia, v. 1, p. 2127-2134.

Development of a test bench for characterization of dissolved methane sensors in marine operating conditions

Birot D., Verberckt S., Podeur C., Ruffine L., Tuon A., Bertin M., Peyronnet C., Leost P.Y., Bigourdan B., Donval J P., Brandily C.

Ifremer Brest, Department of Physical Resources and Deep-Sea Ecosystems, Plouzané, France

Corresponding Author: *Dominique.Birot@ifremer.fr*

Methane is an important greenhouse gas that contributes to global warming. As part of the European ENVRIplus project, one of the objectives of which is the quantitative contribution study of ocean methane to the atmospheric budget in a small area of the Black Sea, a test bench has been developed at IFREMER for evaluation of dissolved methane sensors. This poster presents this test equipment and the results of the first characterizations performed on a metal oxide gas sensor from the company Franatech. This sensor was tested at concentrations, hydrostatic pressure and temperature ranges corresponding to those applied during sea campaigns. These experiments show that the signal measured by the sensor is influenced by pressure and temperature and also by the absence of oxygen. Finally, work on sensor response modelling has been initiated based on results obtained by the previous experiments. Even though the resulting model still needs to be improved, it already demonstrated the interest of taking pressure into account in the calibration equation.

Isotope determination of carbon and oxygen of CO_2 in natural and atmospheric gases using laser-based analyzer

Capasso G., Di Martino R M.R., Caracausi A., Favara R.

Istituto Nazionale di Geofisica e Vulcanologia, Sezione di Palermo, Italy

Corresponding Author: *giorgio.capasso@ingv.it*

Introduction

The isotopic signature of CO_2 provides constraints on the carbon sources as well as on the exchanges between the carbon reservoirs and sinks. Carbon isotope composition of the CO_2 ($\delta^{13}C_{(CO2)}$) has been largely used to discriminate and characterize the gas source (e.g. biogenic, atmospheric, magmatic). The development of a new optical class of isotope analyzer has allowed the *in situ* determination of the isotopic composition of CO_2, when the concentrations are on the order of part per million by volume to several percents by volume. At the same time, the relatively fast measurement procedures result in significant increases in temporal resolution without specific pre-treatments of the sample. In addition, the technical development of compact instruments has enabled measurements to be conducted directly in the field with accuracies comparable to laboratory instruments.
This work focuses on the development of a set of fast methods for the determination of stable isotope composition of carbon dioxide (carbon and oxygen) directly on the field using a laser based analyzer DeltaRay™ with the aim to investigate the sources of CO_2 in different environmental scenarios.

Methods

The Delta Ray is a laser-based instrument which can be deployed in the field for measurements of stable isotopic compositions. The analyzer is based on the direct absorption spectroscopy of the laser light at 4.3 µm, which is generated by two tunable laser diodes in the near-infrared range and combined in a nonlinear crystal. The concentration range allowed for Delta Ray prevents direct isotope determination in the soil gases because there the expected amounts of carbon dioxide exceeds the 3500 ppm vol frequently. In order to overcome these technical limitations, the Thermo Scientific Instrument equips users with a dilutor kit (with CO_2-free synthetic air) which allows the measurements provided that the CO_2 concentration in the gas sample is known.

Case Studies

Hereafter we will present three case studies based on the use of fast methods for the determination of isotope composition of CO_2 directly on the field, performed at Vulcano Island, Palermo and Migianella (Central Appennine) cold vent.

Vulcano Island

The determination of the isotope composition of CO_2 in the soil gases was performed at Vulcano Island (Aeolian Islands - Italy) on a sampling grid consisting in 50 measurement points over an area of 2.2 km^2 around the north and northwestern sides of the La Fossa cone. Since the end of the last eruption (1888-1890), the activity of Vulcano has been featured mainly by fumarole gas discharges from the “La Fossa” crater cone and “Levante” beach. However, large amounts of CO_2 are released from the inner part of the “La Fossa” caldera, and from the area between “Porto di Ponente” and “Faraglione”.

The quantification of the amount of deep-origin CO_2 (endogenous) was targeted during the field survey at Vulcano coupling onsite measurements of $\delta^{13}C_{(CO2)}$ in the soil gases with the CO_2 flux and concentration [Di Martino et al., 2016]. These measurements compose a consistent dataset for estimating the budget of CO_2 discharged from the soils of Vulcano.
The anomalous degassing zones were identified at Faraglione, in the north-eastern side of the island, and Palizzi in the southwest side of the volcanic cone of La Fossa volcano (Figure 1a).
The values of CO_2 concentrations and $\delta^{13}C$ of the CO_2 in the ground gases are consistent with the three components mixing process, in which the endmembers of the CO_2 are: i) Hydrothermal; ii) Biogenic; iii) Air. The three components mixing model can be managed easily in the $\delta^{13}C_{(CO2)}$ vs concentration plot (Figure 1a). Three mixing lines are designed among the points representative of the CO_2 sources in this plot, and each line defines a binary mixing process between two endmembers. The position of each gas sample in the plot results from a mixing process between a binary mixture with the third endmember. Thanks to the huge availability of isotope analysis, it has been possible to quantify these fractions and use them as a multiplier for the CO_2 flux values for the accurate evaluation of the full amount of deep-origin CO_2.

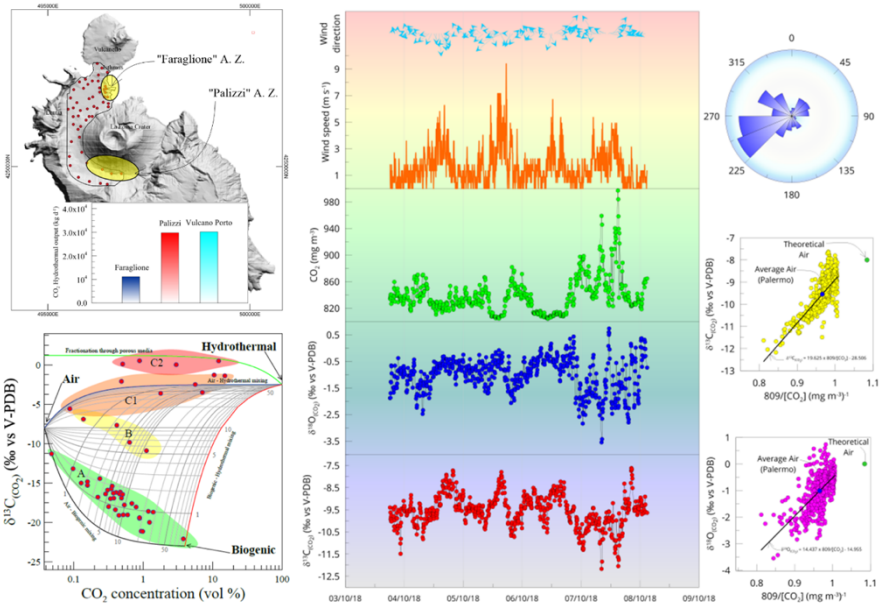

Figure 1 Vulcano island. The red spots indicate the sampling grid, while the yellow ellipses indicate the anomalous zone (A. Z.) of Faraglione and Palizzi. The amount of CO_2 (kg d^{-1}) from the deep origin is reported in the histogram. The $\delta^{13}C_{(CO2)}$vs concentration plot after Di Martino et al., [2016] (see text and reference for the details). Palermo case study. Timeseries of $\delta^{13}C_{(CO2)}$, $\delta^{18}O_{(CO2)}$, CO_2 concentration, wind speed and direction at the measurement site (INGV-Palermo research area). The Keeling plots for $\delta^{13}C_{(CO2)}$ and $\delta^{18}O_{(CO2)}$ are shown in the right side.

Palermo

Palermo is the fifth city of Italy for the number of inhabitants and is situated in the NW part of the island of Sicily. In this area, the major sources of CO_2 are connected to anthropogenic activity such as industrial, agricultural, and urban mobility by vehicles.
In order to study the evolution of both the amount and stable isotope composition of urban CO_2, systematic monitoring has been launched in Palermo (Figure 1b).
The results of the monitoring activity in this urban area indicate that the amount of CO_2, the critical greenhouse gas, was 838 mg/m^3 (427 ppm vol). That value overcomes the current weakly average

CO_2 concentration measured at Mauna Loa Observatory for the same period (809 mg/m^3). The data indicates that the average isotope compositions are $\delta^{13}C_{(CO2)}$ = - 9.5 ‰ and $\delta^{18}O_{(CO2)}$ = - 1‰ (vs V-PDB), suggesting that the carbon dioxide of the air is depleted in ^{13}C. The carbon isotope composition changes over time in the range of ^{13}C-depleted values -12‰ ÷ -7.5‰ vs V-PDB, while the most depleted oxygen have $\delta^{18}O_{(CO2)}$ = -3.5 vs V-PDB. In agreement with the regression lines computed in the keeling plots, the data are consistent with a binary mixing process between the theoretical unpolluted air and the CO_2 source whose stable isotope composition is in the range of CO_2 produced by combustion of fossil fuels (Figure 1b).

Umbertide - Near Faults Observatory - Taboo

An important motivation to develop an high frequency geochemical monitoring in the NFO TABOO is the recognized relationship between seismicity and fluids in this sector of the Apennine. Several investigations [Miller et al., 2004; Chiodini et al., 2000] highlighted that the prolonged aftershock seismic sequences can be explained in terms of subsequence failures promoted by fluid circulation. The existence of a regional active degassing of fluids is supported by the existence of several localized high flux emissions of CO_2 [Burton et al., 2013] characterized by CO_2 overpressure at about 85% of the lithospheric load. This site was selected as the first attempt to obtain a high frequency continuous monitoring of CO_2 isotope composition with the aim to investigate the relationship between geochemical and geophysical parameter in a seismic area.

The Migianella vent is one of these emissions, located near Umbertide village (Umbria region), along the Alto Tiberina valley. It is a vigorous gas vent (10-13°C) situated in a little elliptical depression bubbling trough a small water pool. The dominant gas component is CO_2 (>94 vol. %) with minor contents of N_2 and CH_4 [Italiano et al., 2009; Chiodini et al., 2004; Caracausi and Petrnoster, 2015]. The estimation of total gas flux was around 16 t*d^{-1}. The sampling system consists of an inverted funnel immersed in the spring to obtain a hydraulic closure for atmospheric air. A 15 m silicone tube is connected to the funnel which carries the gas to the instrument inside a little wooden hut (Figure 2).

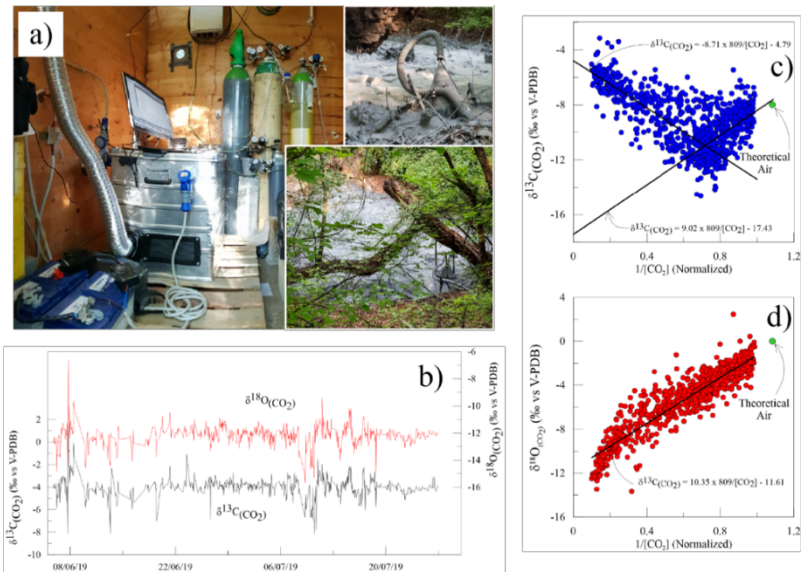

Figure 2 Migianella case study. a) The DeltaRay installed in the field at Migianella. The reversed funnel inserted in the pull allows collecting the cold vent gases. b) Timeseries of $\delta^{13}C_{(CO2)}$ and $\delta^{18}O_{(CO2)}$. c) Keeling plot for $\delta^{13}C_{(CO2)}$. The mixing lines are reported for two data clusters statistically identified. d) Keeling plot for $\delta^{18}O_{(CO2)}$. The data distribution of the oxygen isotopes can be modeled by a binary mixing line.

The DeltaRay performs the isotope determinations of the cold vent gases and the air CO_2 on hourly basis using an external valve allowing to switch between the different analytical gas samples. The initial data-processing of these data consists of the calculation of the hourly measurements which are the average of fifteen minutes of analysis over the vent and forty minutes over the air's CO_2, respectively.

The database analysis indicates that the isotope composition of the vent gases is $\delta^{13}C_{(CO2)}$ = -4.0 ± 0.25 ‰ and $\delta^{18}O_{(CO2)}$ = -12.17 ± 0.25 ‰ (vs V-PDB), which are consistent with the average values recorded by the discontinuous survey for carbon isotope composition. However, the time-series of the measurements collected on hourly basis indicates that the isotope composition of the cold vent gases changes daily over a fairly broad range (Table 1), which is an unprecedented observation obtained through the onsite continuous monitoring of the stable isotope composition. Furthermore, some tests performed at a higher frequency of measurement acquisition (two hours of minutes-averaged acquisition) demonstrate that a sinewave hourly-based variability is not an instrumental bias, but reveal the multiscale temporal variability of the isotope composition in the cold vent gases. Despite the average value of the carbon isotope composition of the air CO_2 is analogous to the air measured at Palermo, the average oxygen isotope composition ($\delta^{18}O_{(CO2)}$ = -5.08 ± 0.25 ‰ vs V-PDB) and CO_2 concentration (857 ppm vol) demonstrates that the CO_2 in the air close to the cold vent is greatly affected by the emission itself. Indeed, the carbon isotope composition of the air's CO_2 changes over ten delta units (Table 1) and the ^{13}C-enriched data ($\delta^{13}C_{(CO2)}$ = -3.2 ‰ vs V-PDB) identify the endogenous origin of the gases. The keeling plot allows estimating the isotope composition of the endmember of gases through the computation of the dataset's regression lines (Figure 2). The data distribution can be modeled by a three-sources mixing model where the unpolluted theoretical air ($\delta^{13}C_{(CO2)}$ = -8.0 ‰ vs V-PDB; $\delta^{18}O_{(CO2)}$ = 0 ‰ vs V-PDB) mixes with the cold vent gases, which is featured by highest concentration of CO_2 (up to 98% vol), ^{13}C-enriched and ^{18}O-depleted values. The third endmember affecting the air close to the cold vent emission is ^{13}C-depleted and has the same oxygen isotope composition of the vent gases (Figure 2), which is compatible with the homegrown biogenic gas source.

	Min $\delta^{13}C_{(CO2)}$	Average $\delta^{13}C_{(CO2)}$	Max $\delta^{13}C_{(CO2)}$	Min $\delta^{18}O_{(CO2)}$	Average $\delta^{18}O_{(CO2)}$	Max $\delta^{18}O_{(CO2)}$
Cold vent CO_2	-6.0	-4.0	+1.5	-15.7	-12.2	-6.1
Air CO_2	-14.6	-9.2	-3.2	-13.7	-5.1	+2.5

Table 1 Statistical parameters of the isotope composition of the cold vent gases and the air CO_2 at the Migianella monitoring site. The isotopic values are expressed in δ-notation ‰ vs V-PDB.

Conclusions

The results reported in this paper highlight how the new available technologies can be effective in the identification of the sources of CO_2 in various environmental scenarios, allowing the investigation of a natural system with unexampled time-detail and providing a new tool to the understanding of unexplored so far scenarios.

At Vulcano Island the obtained results demonstrate that the extensive measurements of CO_2 fluxes and $\delta^{13}C_{(CO2)}$ provides a more detailed estimation of the different sources of CO_2 discharged through the soils in volcanic areas, while the measurements made in Palermo's atmosphere confirm that the current amount of CO_2 in increases over time due to the fossil fuel burning dependent on human activities (home heating and/or fuel for vehicles).

In the framework of the NFO TABOO program, the continuous monitoring of the stable isotope composition of the cold vent emission gases from Migianella has been performed with the aim to recognize the relationship between seismicity and fluids in the Apennine zone. The preliminary data collected in the field indicate the multiscale variability of the isotope composition of carbon dioxide up to seven delta units. These variations should be modeled through a mixing process between multiple sources of carbon dioxide. The next challenging step will allow comparing these variations with seismicity in the area for investigating the relationship between fluids, rock deformation, faulting, and seismicity.

References

Burton M.R., Sawyer G.M., Granieri D., (2013). *Deep carbon emissions from volcanoes*. Rev. Mineral. Geochem., 75, 323-354.

Caracausi A. & Paternoster M., (2015). *Radiogenic helium degassing and rock fracturing: a case study of the southern Apennines active tectonic region*. Journal of Geophysical Research - Solid Earth, doi: 10.1002/2014JB011462.

Chiodini G., Frondini F., Cardellini C., Parello F. & Peruzzi L. (2000). *Rate of diffuse carbon dioxide Earth degassing estimated from carbon balance of regional aquifers: The case of central Apennines, Italy*. Journal of Geophysical Research, vol.105, NO. B4, 8423-8434.

Chiodini G., Cardellini C., Amato A., Boschi E., Caliro S., Frondini F. and Ventura G., (2004). *Carbon dioxide Earth degassing and seismogenesis in central and southern Italy*. Geophysical Research Letters, vol. 31, L07615.

Di Martino R.M.R., Capasso G. & Camarda M. (2016). *Spatial domain analysis of carbon dioxide from soils on Vulcano Island: Implications for CO_2 output evaluation*. Chemical Geology, 444, 59-70.

Italiano F., Martinelli G., Bonfanti P., and Caracausi A. (2009). *Long-term (1997-2007) geochemical monitoring of gases from the Umbria-Marche region*. Tectonophysics, 476, 282-296.

Miller S.A., Collettini C., Chiaraluce L., Cocco M., Barchi M. and Kaus B.J.P., (2004). *Aftershocks driven by a high pressure CO_2 source at depth*. Nature, 427, 724-727.

The INGV geochemical monitoring network at Stromboli volcano. The 3rd July 2019 Paroxysm

Liuzzo M[1]., Paonita A[1]., Caltabiano, T[2]., Gattuso A[1]., Giudice G[1]., Giuffrida G[1]., Inguaggiato S[1]., Murè F[2]., Rizzo A[1]., Salerno G[2]., Vita F[1]., Francofonte V[1]., Calderone L.[1]

[1]*Istituto Nazionale di Geofisica e Vulcanologia, Sezione di Palermo, Italy*
[2]*Istituto Nazionale di Geofisica e Vulcanologia, Sezione di Catania – Osservatorio Etneo*

Corresponding Author: *alessandro.gattuso@ingv.it*

On July 3rd of 2019 at 3:45 pm GMT a paroxysmal explosion suddenly occurred at the Stromboli volcano (Aeolian Archipelago, off the northern coast of Sicily). Stromboli is one of the most active and monitored volcanoes on earth and at the same time it's a famous tourist destination. It was well known in archaeological times as the "Lighthouse of Mediterranean" because of its persistent explosive activity. The volcanic activity mainly consist of low-energy explosions producing scoria, lapilli, ash and bombs falling inside the crater terrace. This classic activity is sometimes interrupted by explosions characterized by medium-to-high energy called as 'Major', which erupted products are commonly spread in the area where tourists normally stop to watch the explosions. A third kind of events know as paroxysmal events and are featured by a very high explosive energy due to the gas content in the magma and their occurrence are unpredictable. The paroxysmal products could generate an eruptive column up to ~ 5km and pyroclastic flows over the flank and the Sciara del Fuoco, a depression located in the NW flank of the island. Lava flows are also common from eruptive fissure in the Sciara del Fuoco or as overflow from the summit craters reaching the sea. A potential collapse of a sector of the Sciara del Fuoco could generate a tsunami as occurred in December 2002. On 3rd of July 2019 a paroxysm events occurred after the 2002-2003 and 2007 episodes with largest magnitude and explosive energy and magma volumes erupted by a single blast.

Figure 1 The summit craters of Stromboli after the paroxysm event of 3th July.

Stromboli is well monitored by geophysical, geochemical and thermal/visible camera monitor networks by the Istituto Nazionale di Geofisica e Vulcanologia (INGV). Seismic stations, inclinometers, acoustic sensors and soil deformation stations are located at the top and on the volcano slopes. The diffuse carbon dioxide fluxes from the soil are recorded at Pizzo Sopra La Fossa and at Scari areas by two automatic accumulation chambers. In addition, the emissions rate of SO_2 and CO_2 in the volcanic plume are monitored as well.

Figure 2 The C/S geochemical station installed on 20th July after paroxysm.

The geochemical monitor network at Stromboli volcano is in chief of INGV Palermo and Catania. The Palermo monitoring network consists of a near real time continuous monitoring of the diffuse CO_2 soil fluxes at the foot of the Stromboli volcano, in the Scari sector and at the crater area; two automatic MultiGas stations for CO_2/SO_2 ratio at Pizzo Sopra la Fossa and Fortini areas. All data are transmitted continuously to the COA (Advanced Operative Centre of Civil Protection) at Stromboli and to the monitoring room at Palermo INGV by wi-fi and radio system respectively. Monthly, during the ordinary strombolian activity, the sampling of five thermal wells, at the foot of the volcano, for chemical and isotopic laboratory analysis occur. In case of an anomalous/crisis period of the volcano, the frequency and the number of sampling increase. From the beginning of 2016 to march 2018 we recorded an increasing of diffuse soil CO_2 flux at Pizzo sopra la Fossa, from a daily average around 4000 g m^2 day up to 22500 g m^2 day. In 2017, seven major explosions and an overflow inside the terrace crater occurred. A general increase occurred from October 2018 to the end of June 2019 where a daily average of soil CO_2 flux reached 10000 g m^2 day.
The INGV Catania monitoring system consists of a network of scanner DOAS spectrometers, which automatically measure, and in real time bulk SO_2 flux from the plume. Data showed an increase since the end of June 2019 reaching an average daily value of 400 t/day exceeding the threshold limit attention of 300 t/day for Stromboli volcano. After the paroxysm of 3rd of July, SO_2 emission rate recorded a maximum value of ~600 t/day, twice the standard value of SO_2 in the plume for Stromboli volcano (250-300 t/day).
The CO_2/SO_2 ratio showed a fluctuating trend from January 2019 to the end of June with values comprised between 1 and 35.7.
Complete temporal series of the $^3He/^4He$ isotopic ratios of five thermal wells in the period 2017-2019, highlighted two recharge trends of a new deep magma at the end of 2017 and at the beginning

of 2019. Similar magnitude values have been recorded in 2014 during the eruptive activity.
According to geochemical parameters recorded at Stromboli volcano, the geochemical data could explain the deep dynamics of the volcano plumbing system and it could recognize the anomalous events that could happen in a future due to the variation of the physical-chemical and isotopic composition of the volcanic fluids.

Test of Argon Isotope Composition in Air at Different Altitudes

Liwu Li, Chunhui Cao, Yuhui Wang, Zihan Gao, Jian He

Key Laboratory of Petroleum Resources, Gansu Province and Key Laboratory of Petroleum Resources Research, Northwest Institute of Eco-Environment and Resources, Chinese Academy of Sciences, Gansu, China

Corresponding Author: llwu@lzb.ac.cn

Argon has three stable isotopes, ^{36}Ar, ^{38}Ar and ^{40}Ar. Air is generally used as a reference in the analysis of argon isotope composition. It is very important to determine the isotopic composition of argon in air accurately. With the improvement of the accuracy of argon isotope composition measurement, some areas that were previously difficult to carry out research work will be developed, such as degassing of the earth, ancient atmospheric argon isotope composition, the relationship between argon isotope composition and temperature, etc. [Mark et al., 2011]. Nier, [1950] proposed argon isotope ratios in air of $^{40}Ar/^{36}Ar$ = 295.5 and $^{38}Ar/^{36}Ar$ = 0.1880, which are widely used in gas geochemistry research. Lee et al., [2006] re-analyzed the modern air argon isotope ratios and acquired new ratios of $^{40}Ar/^{36}Ar$ = 298.56 and $^{38}Ar/^{36}Ar$ = 0.1885, with a precision of 0.1%. Valkiers et al. [2010] also acquired similar data (298.709 and 0.18977 respectively). Their $^{40}Ar/^{36}Ar$ ratios are about 1% higher than that of Nier, [1950]. The air argon isotope ratio ($^{40}Ar/^{36}Ar$) of 298.6 [Lee et al., 2006] has been referred to recently [e.g. Byrne et al., 2018].

It is not clear whether altitude affects argon isotope composition of air. From the usual relationship between atmospheric pressure P and altitude h:

$$P = P_0 \exp(-Mgh/RT) \quad (1)$$

For argon isotopes, assuming,

$$C_0 = P_0(^{40}Ar)/P_0(^{36}Ar) \quad (2)$$

then,

$$C = P(^{40}Ar)/P(^{36}Ar) = C_0 \, Exp[(40-36)/1000*(-gh/RT)] \quad (3)$$

with g = 9.8 m/s^2, R = 8.314 J/mol/K, T = 293 K, h = 5000 m, we get C = 0.922, So altitude difference may cause about $(C_0-C)/C_0$ = 7.8% difference of $^{40}Ar/^{36}Ar$ in air. In order to solve this problem, the work of this paper has been carried out.

In this paper, air samples at different altitudes in China were collected. Pressure cylinders (about 750 cm^3) each equipped with two shut-off valves were used to collect the air samples. Each cylinder was previously vacuumed, and about 0.3MPa air was pressed into during sampling. Each time, about 0.18 mm^3 STP air sample was introduced by a gas pipette into a Zr-Al getter at room temperature and then waiting for 10 minutes to remove active gases. The purified noble gases were separated using a cryogenic trap filled with activated charcoal. The He+Ne and Ar gases were released at the cryogenic trap temperature of 70 K and 250 K, respectively. A Noblesse SFT mass spectrometer (MS) produced by Nu Instruments Ltd. was used to analyze the argon isotope composition of these samples. A single Faraday cup was used as the receiver for ^{36}Ar, ^{38}Ar and ^{40}Ar isotopes using peak-jump mode, the MS intensity of *m/e* = 40 is between 20.5 V to 21.7 V for all samples. The data show that the relative standard deviation of $^{40}Ar/^{36}Ar$ is 0.63% and there is no significant difference among these samples

with different altitudes (Figure 1). Formula (1) may not be suitable for calculating the variation of argon isotope composition with altitude.

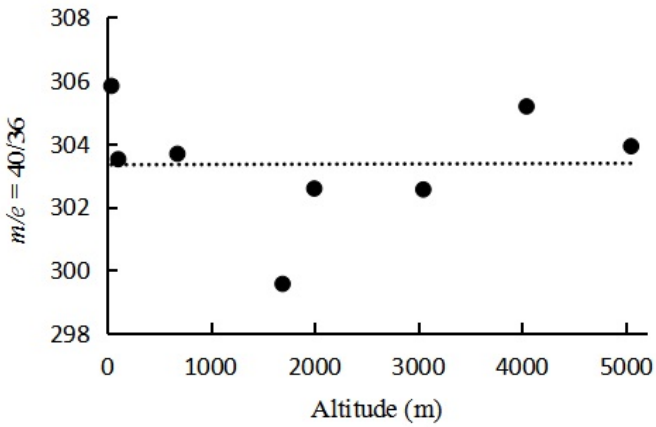

Figure 1 The mass spectrometer peak intensity ratios of *m/e* = 40/36 in the air of different altitudes.

Each air sample could also be analyzed repeatedly to acquire more accurate data. In 2016, a reference air sample has been analyzed five or more times to acquire the average. Nine such averages were acquired. For *m/e* = 40/36 and *m/e* = 38/36, the averages of the nine averages are 300.0 and 0.1880 respectively, and the relative standard deviations of the nine averages are 0.08% and 0.3% respectively. No reference air sample was inserted in Figure 1, so there was a systematic error. This systematic error may be caused by mass discrimination [refer to Zhang and Honda, 2017]. The repeated analyses for *m/e* = 40/36 and *m/e* = 38/36 of air samples at different altitudes are still in progress.

In recent years, mass spectrometers for high precision measurement of argon isotope ratios have been produced, such as the noble gas mass spectrometer with multiple receivers [Mark et al., 2011], the $^{40}Ar/^{36}Ar$ measurement precision is better than ±1‰, and the $^{38}Ar/^{36}Ar$ measurement precision can be better than ±2‰. Noble gas mass spectrometers with multiple receivers may be able to detect the variation of altitude on argon isotope composition more effectively.

Acknowledgments

This work was supported financially by NSF of China (No.41473062) and the Science and Technology Innovation Fund for the 13th Five-Year Plan of Lanzhou oil and gas resources research center (No. 135CCJ20160518)

References

Byrne D.J., Barry P.H., Lawson M. and Ballentine C.J., (2018). *Determining gas expulsion vs retention during hydrocarbon generation in the Eagle Ford Shale using noble gases*. Geochimica et Cosmochimica Acta, 241: 240-254.

Lee J.Y., Marti K., Severinghaus J.P., Kawamura K., Yoo H.S., Lee J.B. and Kim J.S., (2006). *A redetermination of the isotopic abundances of atmospheric Ar"*. Geochimica et Cosmochimica Acta, 70: 4507-4512.

Mark D.F., Stuart F.M. and de Podesta M., (2011). *New high-precision measurements of the isotopic composition of atmospheric argon*. Geochimica et Cosmochimica Acta, 75: 7494-7501.

Nier A.O., (1950). *A redetermination of the relative abundances of the isotopes of carbon, nitrogen, oxygen, argon and potassium*. Phys. Rev., 77: 789-793.

Valkiers S., Vendelbo D., Berglund M. and de Podesta M., (2010). *Preparation of argon primary measurement standards for the calibration of ion current ratios measured in argon*. International Journal of Mass Spectrometry, 291: 41-47.

Zhang, X.D. and Honda M, (2017). *Minimisation of pressure dependent mass discrimination in the ion source of the Helix MC Plus noble gas mass spectrometer*. Chemical Geology, 473: 50-54.

Etna International Training School of Geochemistry. Science meets Practice

Pecoraino G.[1], Bitetto M.[2], Bobrowski N.[3,4], Brugnone F.[2], Cabassi J.[5], Calabrese S.[1,2], Cantarero M.[6], Consoli S.[6], Capecchiacci F.[7], Daskalopoulou K.[8], Giammanco S.[6], Giuffrida G.B.[1], Fuchs C.[3], Ionescu A.[9,10], Kuhn J.[3,4], Li Vigni L.[1], Randazzo L.[11], Tamburello G.[12], Tassi F.[5], Venturi S.[5], Italiano F.[1], Privitera E.[6]

[1]*Istituto Nazionale di Geofisica e Vulcanologia, Sezione di Palermo, Italy*
[2]*Università degli Studi di Palermo, Dipartimento delle Scienze della Terra e del Mare (DiSTeM), Palermo, Italy*
[3]*Institut für Umweltphysik, Universität Heidelberg, Heidelberg, Germany*
[4]*Max Planck Institut für Chemistry, Mainz, Germany*
[5]*Dipartimento di Scienze della Terra, Università degli Studi di Firenze, Florence, Italy*
[6]*Istituto Nazionale di Geofisica e Vulcanologia, Sezione di Catania - Osservatorio Etneo, Italy*
[7]*Istituto Nazionale di Geofisica e Vulcanologia, Sezione di Napoli - Osservatorio Vesuviano, Italy*
[8]*GFZ, German Research Centre for Geosciences, Potsdam, Germany*
[9]*Faculty of Environmental Science and Engineering, Babes - Bolyai University, Romania*
[10]*Università degli Studi di Perugia, Dipartimento di Fisica e Geologia, Perugia, Italy*
[11]*Università della Calabria, Dipartimento di Biologia, Ecologia e Scienze della Terra, Cosenza, Italy*
[12]*Istituto Nazionale di Geofisica e Vulcanologia, Sezione di Bologna, Italy*

Corresponding Author: *giovanella.pecoraino@ingv.it*

Also this year, the "*Etna International Training School of Geochemistry. Science meets practice*" took place at Mt. Etna, now in its fourth edition. The school was hosted in the historical Volcanological Observatory "Pizzi Deneri", one of the most important sites of the INGV - Osservatorio Etneo for geochemical and geophysical monitoring.

Mount Etna, located in eastern Sicily, is the largest active volcano in Europe and one of the most intensely degassing volcanoes of the world [Allard et al., 1991; Gerlach, 1991]. Mt Etna emits about 1.6 % of global H_2O fluxes from arc volcanism [Aiuppa et al., 2008] and 10 % of global average volcanic emission of CO_2 and SO_2 [D'Alessandro et al., 1997; Caltabiano et al., 2004; Aiuppa et al., 2008; Carn et al., 2017]. Furthermore, Gauthier and Le Cloarec, [1998] underscored that Mt. Etna is an important source of volcanic particles, having a mass flux of particle passively released from the volcano during non-eruptive period estimated between 7 to 23 tons/day [Martin et al., 2008; Calabrese et al., 2011]. In general, Etna is considered to be still under evolution and rather 'friendly', which, along with the above, makes it a favorable natural laboratory to study volcanic geochemistry.

The Observatory Pizzi Deneri was sponsored by Haroun Tazieff, and it was built in 1978 by the CNR - International Institute of Volcanology under the direction of Prof. Letterio Villari. It is located at the base of the North-East crater (2,850 m a.s.l.), near the Valle del Leone and it was built on the rim of the Ellittico caldera. A picturesque building, consisting of two characteristics domes in front of the breath-taking panorama of the summit craters. Even though it is quite spartan as an accommodation facility, the dormitories, kitchen, seminar room and laboratory are well equipped. In other words, the Pizzi Deneri observatory is a unique place close to the top of the most active volcano of Europe. The observatory lies in a strategic location making it one of the most important sites for monitoring, research and dissemination of the scientific culture.

After six field multidisciplinary campaigns (2010-2015) organized by a group of researchers of several institutions (INGV of Palermo, Catania, Naples, Bologna; Universities of Palermo, Florence, Mainz, Heidelberg), the idea of sharing and passing on the experience to the new generation of students has materialized, and the "*Etna International Training School of Geochemistry. Science meets practice*" was born in 2016. The four editions of the school were partially funded by INGV of Palermo and Catania, European Geoscience Union (EGU), Società Geochimica Italiana (SoGeI) and Associazione Naturalistica Geode.

Figure 1 Group photos of the four editions of the "*Etna International Training School of Geochemistry. Science meets Practice*".

The conceptual idea of the school is to share scientific knowledge and experiences in the geochemical community, using local resources with a low-cost organization in order to allow as many students as possible access to the school. The "*Etna International Training School of Geochemistry. Science meets practice*" is addressed to senior graduate students, postdoctoral researchers, fellows, and newly appointed assistant professors, aiming to bring together the next generation of researchers active in studies concerning the geochemistry and the budget of volcanic gases. Introduce the participants with innovative direct sampling and remote sensing techniques. Furthermore, it gives young scientists an opportunity to experiment and evaluate new protocols and techniques to be used on volcanic fluid emissions covering a broad variety of methods. The teaching approach includes theoretical sessions (lectures), practical demonstrations and field applications, conducted by international recognized geochemists. We thank all the teachers who helped to make the school possible, among these: Tobias Fischer (University of New Mexico Albuquerque), Jens Fiebig (Institut für Geowissenschaften Goethe-Universität Frankfurt am Main), Andri Stefansson (University of Iceland, Institute of Earth Sciences), Mike Burton (University of Manchester), Nicole Bobrowski (Universität Heidelberg

Institute of Environmental Physics and Max Planck Institute for Chemistry), Alessandro Aiuppa (Università di Palermo), Franco Tassi (Università di Firenze), Walter D'Alessandro (INGV of Palermo), Fatima Viveiros (University of the Azores). Direct sampling of high-to-low temperature fumaroles, plume measurement techniques (using CO_2/SO_2 sensors such as Multi-GAS instruments, MAX-DOAS instruments and UV SO_2 cameras, alkaline traps and particle filters), measurement of diffuse soil gas fluxes of endogenous gases (CO_2, Hg^0, CH_4 and light hydrocarbons), sampling of mud volcanoes, groundwaters and bubbling gases. Sampling sites include the active summit craters, eruptive fractures and peripheral areas.

The students have shown an active participation both to the lessons and the fieldworks. Most of them describe the school as formative and useful experience for their future researches. Their enthusiasm is the real engine of this school.

Figure 2 Field activities.

References

Aiuppa A., Giudice G., Gurrieri G., Liuzzo M., Burton M., Caltabiano T., McGonigle A.J.S., Salerno G., Shinohara H., Valenza M., (2008). *Total volatile flux from Mount Etna*. Geophysical Research Letters, Vol. 35, L24302.

Allard P., Carbonnelle J., Dajlevic D., Le Bronec J., Morel P., Robe M.C., Maurenas J.M., Faivre-Pierret R., Martin D., Sabroux J. C., Zettwoog P., (1991). *Eruptive and diffuse emissions of CO_2 from Mount Etna*. Nature, vol. 351, pp. 387-391.

Burton M.R., Sawyer G.M., Granieri D., (2013). *Deep Carbon Emissions from Volcanoes*. Reviews in Mineralogy & Geochemistry, 75, 323-354. doi: 10.2138/rmg.2013.75.11.

Calabrese S., Aiuppa A., Allard P., Bagnato E., Bellomo S., Brusca L., D'Alessandro W., Parello F., (2011). *Atmospheric sources and sinks of volcanogenic elements in a basaltic volcano (Etna, Italy)*. Geochimica et Cosmochimica Acta, vol. 75 (23), pp. 7401-7425.

Caltabiano T., Burton M., Giammanco S., Allard P., Bruno N., Murè F., Romano R., (2004). *Volcanic Gas Emissions fron the Summit Craters and Flanks of Mt. Etna, 1987 - 2000*. In Mt. Etna: Volcano Laboratory; Bonaccorso A., Calvari S., Coltelli M., Del Negro C., Falsaperla S., Eds.; Geophysical Monograph Series; American Geophysical Union: Washington, DC, USA; vol. 143, pp. 111-128.

Carn S.A., Fioletov V.E., McLinden C.A., Krotkov N.A. (2017). *A decade of global volcanic SO_2 emissions measured from space*. Sci. Rep. 7, 44095; doi: 10.1038/srep44095.

D'Alessandro W., Giammanco S., Parello F., Valenza M., (1997). *CO_2 output and $\delta^{13}C(CO_2)$ from Mount Etna as indicators of degassing of shallow asthenosphere*. Bulletin of Volcanology, vol. 58 (6), pp. 455 - 458.

Gauthierab P.J., Le Cloarec M.F., (1998). *Variability of alkali and heavy metal fluxes released by Mt. Etna volcano, Sicily, between 1991 and 1995*. Journal of Volcanology and Geothermal Research, vol.81 (3 - 4), pp. 311-326.

Gerlach T., (1991). *Etna's greenhouse pump*. Nature, vol. 351, pp. 352-353.

Martin R.S., Mather T.A., Pyle D.M., Power M., Allen G., Aiuppa A., Horwell C.J., Ward E.P.W., (2008). *Composition-resolved size distributions of volcanic aerosols in the Mt. Etna plumes*. Journal of Geophysical Research, vol. 113, D17211.

Measurement of very short-lived radon daughters in volcanic plumes

Terray L.[1,2], Breton V.[2], Gauthier P.J.[1], Falvard A.[2], Bonnefoy R.[2], Achard C.[2] and Magaud G.[2]

[1]*Laboratoire Magmas et Volcans, Campus des Cézeaux, France*
[2]*Laboratoire de Physique de Clermont, Campus des Cézeaux, France*

Corresponding Author: *luca.terray@uca.fr*

Radioactive disequilibria between the three last ^{222}Rn daughters (namely ^{210}Pb, ^{210}Bi and ^{210}Po) in magmatic gases are recognized to provide unique information about the kinetics of magma degassing at depth, such as the residence time of the magma in the degassing reservoir or the gas transfer time from this reservoir to the surface [Lambert et al., 1985; Gauthier et al., 2000]. A recent theoretical study has suggested that important ^{222}Rn degassing in the magma could modify the activity of ^{210}Pb in magmatic gases and substantially change the values of degassing parameters inferred from ^{210}Pb-^{210}Bi-^{210}Po radioactive disequilibria [Terray et al., 2018]. It is therefore needed to measure ^{222}Rn in magmatic gases along with its daughters. In this contribution, we present a new device developed at University Clermont Auvergne that is dedicated to the measurement of ^{222}Rn in acidic dilute volcanic plumes, based on the detection of the ionizing particles emitted by its daughters previously collected on a filter. Named RAVIOLI for Radon Analysis on Volcanoes with In-situ Observations of short-Lived Isotopes, it has been successfully tested on Etna, providing direct measurements of very short-lived daughters (^{218}Po, ^{214}Pb, ^{214}Bi and ^{214}Po) in the plume.

Advantages of radon daughters measurement compared to direct ^{222}rn measurement in a volcanic plume
Because of the noble gas nature of Rn, direct measurement of ^{222}Rn implies to draw the air or plume sample inside a finite volume where the detection of ^{222}Rn and its short-lived daughters is performed. Therefore, the sensitivity of such instruments is proportional to the detector volume. As can be seen from figure 1, the sensitivity of common ^{222}Rn commercial devices is not sufficient to measure precisely (< 5% relative uncertainty) and in a short time (1h) a ^{222}Rn activity of the order of 10 Bq/m^3, as expected in a dilute volcanic plume. A solution could be to increase the volume of detection but large instruments are very complex to handle in the field. Moreover, operating detection volumes in humid and acidic environments pose several problems that require a proper treatment (humidity and acidity traps for instance).

An alternative consists in measuring the first very short-lived ^{222}Rn daughters in the plume (see table 1). Because of their very short half-lifes (at most 26.9 min), the activity of these daughters in the plume reflects the activity of ^{222}Rn itself, provided the *equilibrium factor* is known. Moreover, because of their metallic elemental nature they are mostly attached to aerosol particles and can therefore be sampled by filtration of the plume. The filter radioactivity is then analysed to determine radon daughters activities in the plume. The advantages of this approach are threefold:

(i) The sensitivity can be easily increased by increasing the volume of filtrated plume.
(ii) Only the filtration system needs to be placed inside the acidic plume, the filter can be analysed afterwards out of the plume.
(iii) Because ^{222}Rn daughters activity measurement is non-destructive, the same filter can be later used to measure ^{210}Pb-^{210}Bi-^{210}Po radioactive disequilibria.

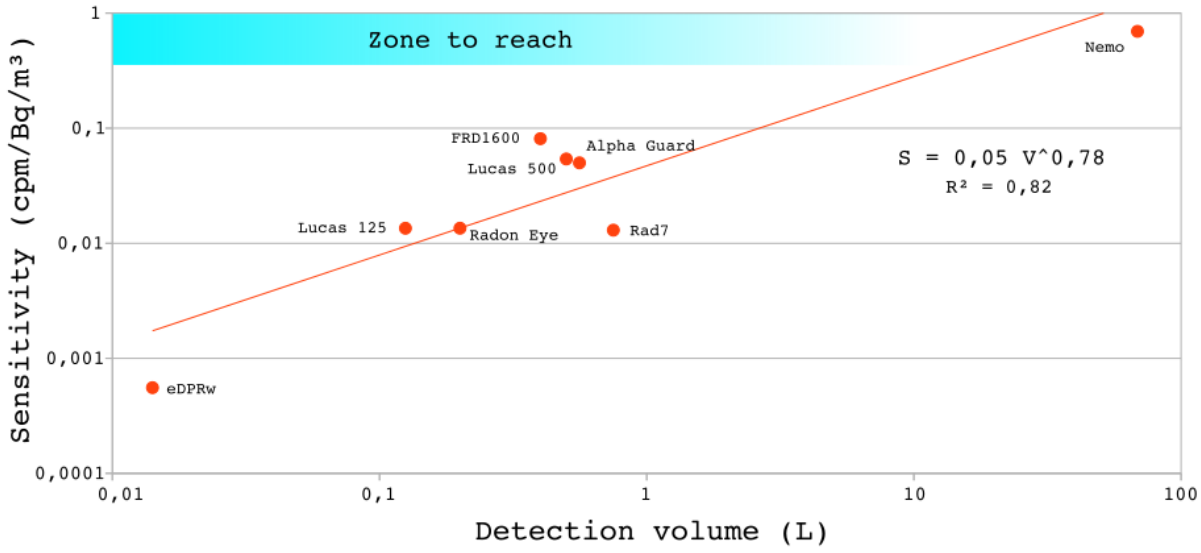

Figure 1 Sensitivity versus volume of common ^{222}Rn measurement devices. The *zone to reach* defines the specifications that an instrument dedicated to measure ^{222}Rn in a volcanic plume has to reach: small (< 10L for a volume device) and sensitive enough to measure low level of ^{222}Rn (10 Bq/m^3) with accurate precision (<5%) in a short time (<1h).

Nevertheless, measuring very-short-lived ^{222}Rn daughters involves some constraints: (i) the need to measure activity in the filter very quickly after plume filtration is finished, before ^{222}Rn daughters have completely decayed and (ii) the need to know the *equilibrium factor* between ^{222}Rn and its daughters.

Name	Half-life	Main nuclear emission
^{218}Po	3.07 min	α (6002.35 keV)
^{214}Pb	26.916 min	β^- (e^- + γ)
^{214}Bi	19.8 min	β^- (e^- + γ)
^{214}Po	162.3 µs	α (7686.82 keV)

Table 1. Half-lifes and nuclear emissions of ^{222}Rn daughters.

RAVIOLI: a new device to measure ^{222}rn daughters in a volcanic plume

We recently developed an instrument dedicated to measure very short-lived ^{222}Rn daughters in volcanic plume filters (see figure 2). This instrument is called RAVIOLI for Radon Analysis on Volcanoes with In-situ Observations of short-Lived Isotopes. It has been designed to be portable to active volcanic craters, which implies that the instrument has to be robust and light (<5 kg). RAVIOLI detection system is composed of a NaI scintillator and a Si photodiode for γ and α/e^- nuclear spectrometry respectively. The filter impregnated with plume aerosols is placed between the two detectors at the closest distance in order to optimize solid angle. Detector signals are amplified and read by a single electronic board equipped with a 100 MHz-14 bits ADC with 4 time-synchronized channels and a FPGA micro-processor providing trigger and pulse height analysis. The system returns a time-ordered list of α/e^- particles and γ photons detected together with their energy. All the system is powered with two 12V Li-ION batteries of 50 Ah offering a 10-hour autonomy.

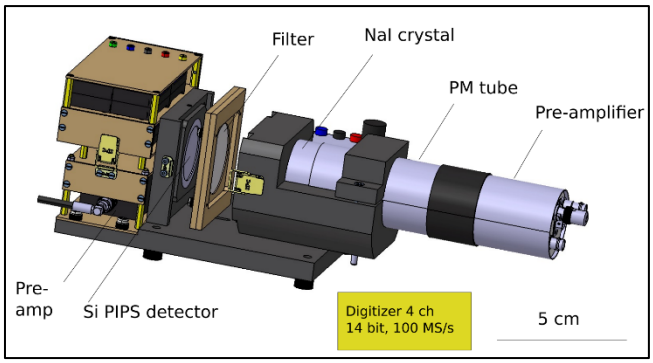

Figure 2 Representation of RAVIOLI instrument with its main components.

The approach followed to measure ^{222}Rn daughters in a volcanic plume using RAVIOLI requires three steps:

1- The plume is filtrated for 30 min to 1h at a typical flow rate of about 2 m^3/h. We use PTFE membranes as filters since the aerosol particles are collected at the surface of the membrane and are not burried inside the filter which would produce a significant attenuation of α particles energy.
2- At the end of filtration, the filter is transferred in a few minutes to the RAVIOLI device located in the vicinity of the plume filtration spot, but out of the influence of the plume acid gasses.
3- The filter is analysed on the field for one hour in order to observe the complete decay of ^{218}Po and a significant portion of the ^{214}Pb/^{214}Bi decay.

RAVIOLI data

The figure 3a represents an α/e$^-$ energy spectrum obtained using RAVIOLI on a filter collected at Mount Etna Central Crater in june 2019. The spectrum displays a first peak at low energy mixing electrons emitted during β$^-$ decay of ^{214}Bi and ^{214}Pb together with electronic noise and background cosmic radiations, and three α-particle peaks corresponding to three different α emitters present in the filter: ^{210}Po, ^{214}Po, and ^{212}Po from the ^{220}Rn decay chain. Very good spectral separation of these three different peaks demonstrates that α particles attenuation is very small within the air layer between the membrane surface and the detector. The α-particles from ^{218}Po can not be disentangled from those emitted by ^{210}Po and ^{214}Po. However, because of its very short half life (3.1 minutes), its contribution becomes negligible after 15 minutes. From such a spectrum ^{210}Po activity in the plume can be directly inferred due to its long half-life. ^{214}Bi activity in the filter is equal to ^{214}Po activity due to the very short half-life of ^{214}Po (162.3 µs). However, because of ^{214}Bi production inside the filter due to ^{214}Pb decay, a correction has to applied to obtain ^{214}Bi activity in the plume. This correction is done by fitting the temporal variation of the activity of ^{214}Po (green spectrum) during the measurement with the decay law of ^{214}Pb-^{214}Bi pair. This fit also allows the determination of ^{214}Pb that is not directly detectable. Nevertheless, in Radon rich environnments such as caves, γ rays from ^{214}Pb are directly observed in the NaI detector (figure 3b) and enable a direct measurement of ^{214}Pb. The instrument was calibrated using a numerical-experimental coupled approach. The detector was simulated with GEANT4-GATE Monte Carlo simulation toolkit in order to obtain the efficacity of the detector for various types of geometries and nuclear particles. The simulation was finally validated by checking that it could reproduce precisely an experimental measurement of a radioactive source.

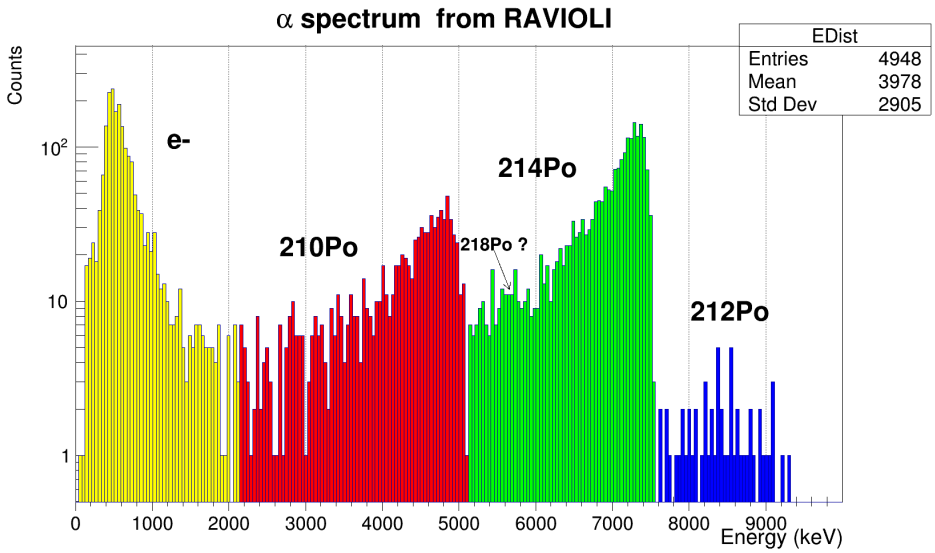

(a)

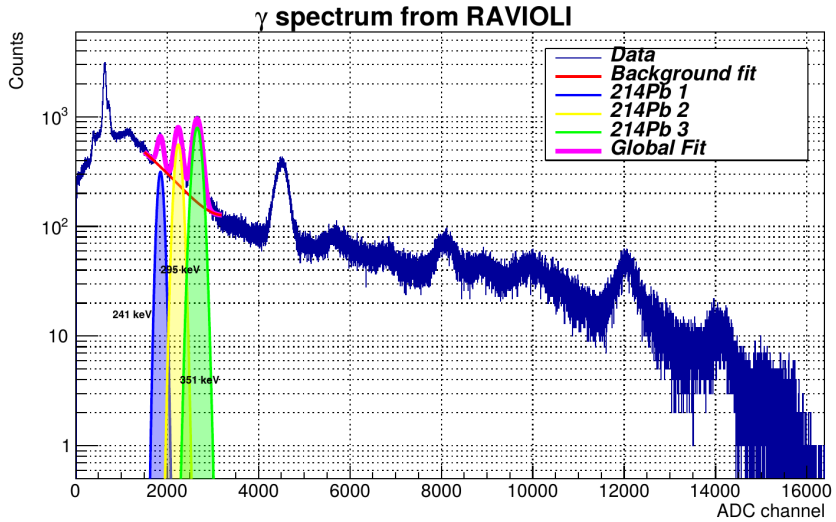

(b)

Figure 3 (a) Example of an α/e⁻ spectrum obtained with RAVIOLI on a plume sample from Mount Etna. (b) Example of a γ spectrum obtained with RAVIOLI on an air sample from a ^{222}Rn rich environnment in Auvergne, France. Three γ peaks of ^{214}Pb are clearly observed.

References

Lambert G., Le Cloarec M.F., Ardouin B. and Le Roulley J.C., (1985). *Volcanic emission of radionuclides and magma dynamics*. Earth and Planetary Science Letters, Volume 76, 1-2, December 1985, Pages 185-192.

Gauthier P.J., Le Cloarec M.F. and Condomines M., (2000). *Degassing processes at Stromboli inferred from short-lived disequilibria (^{210}Pb-^{210}Bi-^{210}Po) in volcanic gases*". Journal of Volcanology and Geothermal Research, Volume 102, Issue 1-2, p. 1-19.

Terray L., Gauthier P.J., Salerno G., Caltabiano T., La Spina A., Sellitto P., and Briole P., (2018). *A New Degassing Model to Infer Magma Dynamics from Radioactive Disequilibria in Volcanic Plumes*". Geosciences, *8*(1), 27.

Assessment of gas and water chemistry of Kizildag and Erzin ophiolites (Hatay/Turkey) for geothermal potential

Yüce G.[1], D'Alessandro W.[2], Italiano F.[2], Bellomo S.[2], Gulbay A.H.[3], Yasin D.[3]

[1]*Hacettepe University, Department of Geological Engineering, Hydrogeology, Ankara, Turkey*
[2]*Istituto Nazionale di Geofisica e Vulcanologia, Sezione di Palermo, Italy*
[3]*Eskisehir Osmangazi University, Department of Geological Engineering, Meselik, Turkey*

Corresponding Author: *galipyuce@gmail.com*

The Kizildag and Erzin (Hatay) ophiolite bodies, as a remnants of the peri-Arabian ophiolite belt, is nearby the Dead Sea Transform Fault and the triple-junction zone of Anatolian, Arabian and African plates, respectively. To better understand geothermal potential of Kizildag and Erzin Province, water and dissolved gas samples were collected and analyses. Also, hydrochemical processes and facies were examined by different diagrams. Kizildag ophiolite body has typically hyperalkaline waters due to serpentinisation processes with high pH values. To estimate and compare reservoir temperature of these two areas, silica and chalcedony geothermometries were used. As a result, both areas have low enthalpy geothermal province by 50 °C at Kizildag and 130 °C at Erzin, based on chalcedony geothermometers. The mantle He contribution in the waters from Erzin ophiolite is relatively much higher than those of Kizildag ophiolite due to seismogenic faults therein.

This research was supported by TUBITAK project No. 111Y090.

Chemical and isotopic characteristics of seepage gases from mud volcanoes in the southern margin of the Junggar Basin, NW China

Wang Xu[1,2,3], Guodong Zheng[2,3], Xiangxian Ma[2,3], Qi Li[4], Danielle Fortin[5], Mingliang Liang[6], Yanqing Xia[2,3]

[1]*College of Energy, Chengdu University of Technology, China*
[2]*Northwest Institute of Eco-Environment and Resources, Chinese Academy of Sciences, China*
[3]*Key Laboratory of Petroleum Resources, Gansu Province, China*
[4]*State Key Laboratory of Geomechanics and Geotechnical Engineering, Institute of Rock and Soil Mechanics (IRSM), Chinese Academy of Sciences, China*
[5]*Department of Earth and Environmental Sciences, University of Ottawa, 25 Templeton St., Ottawa, Canada*
[6]*Institute of Geomechanics, Key Lab of Shale Oil and Gas Geological Survey, Chinese Academy of Geological Sciences, China*

Corresponding Author: *gdzhbj@mail.iggcas.ac.cn*

The chemical and carbon isotopic composition of seepage gases from three mud volcanoes were analyzed and compared with their corresponding reservoir gases from three nearby reservoirs in the southern margin of the Junggar Basin. The results showed a clear change of both the chemical and isotopic composition of the seepage gases. The seepage gases released from the vents/craters were relatively enriched in methane and depleted in ethane and propane when compared to their corresponding reservoir gases. Advection during the gas ascent to the surface and diffusion during the gas migration through sandy rocks or liquid horizons, as well as gas-water-rock-microbe interactions are potentially the main factors inducing such molecular fractionation. However, high gas fluxes and eruption triggered by earthquakes limited the fractionation. Moreover, the seepage gases had relatively lighter carbon isotopes in CH_4, similar carbon isotopes in C_2H_6 and heavier carbon isotopes in C_3H_8 when compared to their corresponding reservoir gases. Diffusive processes led to the lighter carbon isotopes of the seepage gases whereas gas-water-rock-microbe interactions might have contributed to the heavier ones. Such molecular and isotopic fractionations caused by geochemical processes provide unique information towards a better understanding of the vertical migration characteristics of hydrocarbons from reservoirs to the ground surface.

ST08

GAS-BIOTA INTERACTION

REFERENCE: WALTER D'ALESSANDRO

Microbial impact on the isotope composition of methane in both thermal and hyperalkaline waters of central Greece

D'Alessandro W.[1], Gagliano A.L.[1], Daskalopoulou K.[2], Calabrese S.[1,3], Li Vigni L.[1]

[1]*Istituto Nazionale di Geofisica e Vulcanologia, Sezione di Palermo, Italy*
[2]*GFZ, German Research Centre for Geosciences, Potsdam, Germany*
[3]*Università degli Studi di Palermo, Dipartimento delle Scienze della Terra e del Mare (DiSTeM), Palermo, Italy*

Corresponding Author *walter.dalessandro@ingv.it*

Introduction

The different origins of methane can be subdivided in biogenic (either directly produced by microbial activity or deriving by decay of organic matter at T > 150°C) and abiogenic (from pure inorganic reactions). Among the latter, one of the most debated origins comes from serpentinization processes of ultramafic rocks in ophiolitic sequences at low temperatures (T < 80 °C). Moreover, further secondary processes (diffusion, inorganic or microbial oxidation, etc.) may also contribute and thus mask the original chemical and/or isotope composition. Primary and secondary processes acting on CH_4 can be recognised mainly through its isotope ($\delta^{13}C$ and $\delta^{2}H$) composition and the ratio between CH_4 and C_2+C_3 light hydrocarbons [Bernard et al. 1978; Schoell 1980].

Microorganisms may be involved in the methane cycle not only as active producers but also as consumers. Methane oxidizing bacteria (or methanotrophs) are microorganisms with the ability to use methane as the only source of carbon for energy and biomass production. Methanotrophs are ubiquitous and play an important role in the global carbon cycle, acting as a natural filter between the subsoil and the atmosphere. They were isolated from several environments such as soils, wetlands, freshwater, marine sediments, water columns, groundwater, rice paddies, and peat bogs [Murrell and Jetten, 2009]. Some species were adapted also at extreme environments characterized by high temperature (up to 81.6 °C), extremely low or high pHs (1.5-11) or even anaerobic conditions. Due to the fact that methanotrophs metabolize preferentially light isotopes, biologic methane oxidation brings sometimes to extremely positive $\delta^{13}C$ and $\delta^{2}H$ values [Cadieux et al., 2016].

The Greek territory belongs to the geodynamically active Alpine-Himalayan orogenic belt. As such, it shows intense seismic activity, active volcanic systems and areas of enhanced geothermal fluxes. One of these areas is the Sperchios Basin and the northern part of Euboea Island in central Greece, where thermal manifestations are widespread [D'Alessandro et al., 2014]. The complex geology of Greece includes also two important parallel running ophiolitic belts, with the Othrys Massif (central Greece) belonging to the westernmost of them. In and around this wide ophiolite outcrop, some cold hyperalkaline and some hypothermal (T < 30°C) alkaline waters are present.

In the present paper we discuss data about chemistry and methane isotope composition of bubbling or dissolved gases in both thermal springs and hyperalkaline springs of Central Greece.

Sampling and Analytical Methods

Free bubbling gas samples were taken using an inverted funnel. All free gas samples were stored in Pyrex bottles with two vacuum stopcocks. Samples for dissolved gas analyses were collected in glass vials sealed underwater. In the laboratory, the chemical analyses were carried out by gas-chromatography (Agilent 7890B GC System) using Ar as the carrier gas. Dissolved gases were

extracted after equilibrium was reached at constant temperature with a host-gas (high-purity argon) injected in the sample bottle. The measurement precision was better than ±5% for common gases and ±10% for trace gases such as the alkanes. The chemical composition of the dissolved gas phase was obtained from the gas-chromatographic analyses taking into account the solubility coefficients (Bunsen coefficient "β", cc_{gas}/ml_{water} STP) of each gas specie, the volume of gas extracted and the volume of the water sample (details in Capasso and Inguaggiato, [1998] and Liotta and Martelli, [2012]). Starting from the total amount of dissolved gases (ccSTP/L) we calculated the relative abundances for every single gas species in equilibrium with the dissolved gas phase and expressed the analytical results in μmol/mol of gas at atmospheric pressure, allowing the comparison of dissolved gases with free gases.
Carbon and hydrogen isotope compositions of CH_4 were measured using a Thermo TRACE GC and a Thermo GC/C III interfaced to a Delta Plus XP gas source mass spectrometer. $^{13}C/^{12}C$ ratios are reported here as $\delta^{13}C$ values (±0.1 ‰) with respect to the V-PDB standard. $^{1}H/^{2}H$ ratios are reported here as $\delta^{2}H$ values (±2 ‰) with respect to the V-SMOW standard.
The oxygen and hydrogen isotopic compositions of water were analysed on unfiltered samples with the use of Analytical Precision AP 2003 and FinniganMAT Delta Plus IRMS devices, respectively. The isotope ratios are expressed as the deviation per mil (δ‰) from the reference V-SMOW. The uncertainties (±1‰ were ±0.1% for $\delta^{18}O$ and ±1% for $\delta^{2}H$.

Results

Five thermal springs, with temperatures from 33 to 80°C, were sampled in the study area. All show elevated fluxes of bubbling gases whose prevailing species are either CO_2 or N_2. Methane concentrations range from 27 to 4000 μmol/mol, whilst the isotope composition of CH_4 covers a wide range with $\delta^{13}C$ values ranging from -21.7 to +16.9‰ and $\delta^{2}H$ values ranging from -124 to +370‰.
Seven alkaline hypothermal waters were collected in five areas (Amplas, Platystomo, Kaitsa, Smokovo and Soulanta) while 10 hyperalkaline waters in two areas (Archani and Ekkara); all samples were collected from different springs and wells and some of the sites presented bubbling. All samples present low concentrations of H_2 (from <2 to 2500 μmol/mol), CO_2 (up to 26,000 but generally below 1000 μmol/mol) and O_2 (up to 16,000 but generally below 3000 μmol/mol). Gases in alkaline waters (pH <10) are in their majority dominated by CH_4 (from 128,000 to 915,000 μmol/mol). Hyperalkaline (pH > 11) waters are N_2 dominated (from 727,000 to 977,000 μmol/mol) and have CH_4 concentrations from 11,500 to 279,000 μmol/mol. Also all these samples display a wide range of isotope compositions of CH_4 ($\delta^{13}C$ from -74.5 to -14.5 ‰ and $\delta^{2}H$ from -343 to -62 ‰).

Discussion

Thermal springs

Methane in most of the bubbling gases found in the thermal waters of Greece display a small range in isotope composition close to -21‰ for carbon and to -130‰ for hydrogen [Daskalopoulou et al., 2018] and plot in the middle of the field of volcanic and geothermal systems (Figure 1). In the study area, only the hottest (Edipsos) of the thermal manifestations displays similar values. All the remaining samples fit a methane oxidation trend reaching extremely positive values (Figure 1).

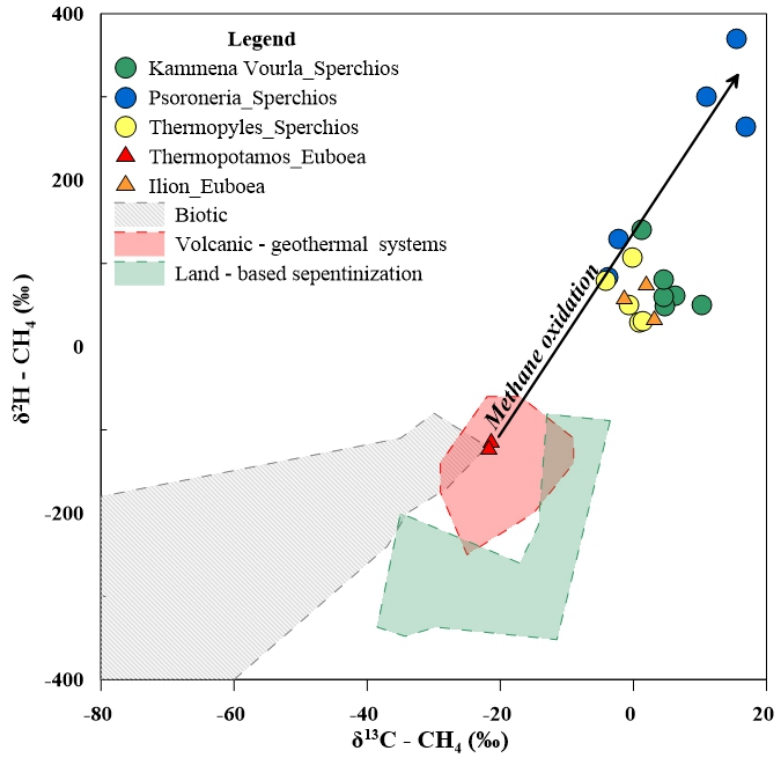

Figure 1 $\delta^{13}C$ vs. $\delta^{2}H$ of methane in the gases collected in the thermal springs of Sperchios Basin and northern Euboea.

If we consider the lowest values as the deep hydrothermal marker the obtained $\Delta H/\Delta C$ values range between 5 and 13 which are close to those typical of microbially driven oxidation [Coleman et al., 1981].

Although the outlet temperature of the hottest manifestations is at the upper limit for methanotrophic microrganisms [Sharp et al., 2014], we can hypothesize that environmental conditions are not favourable for their survival at this site. On the contrary, methanotrophs can thrive in the sites characterized by lower temperatures (33-65 °C), strongly consuming methane. The most positive values were measured at Psoroneria and indicate a very high consumption fraction. Considering again the values of Edipsos as the deep hydrothermal marker, a Rayleigh fractionation modelling in a closed system and kinetic fractionation factors for microbial oxidation [Coleman et al., 1981] we estimate a consumption of more than the 75% of the initial CH_4.

Alkaline and hyperalkaline waters

Alkaline waters present mostly isotope values for CH_4 compatible with a biogenic origin ($\delta^{13}C$ from -62.0 to -37.5 ‰ and $\delta^{2}H$ from -247 to -154 ‰). Only the sample of Kaitsa falls above the biogenic field, indicating possible fractionation due to CH_4 oxidation (Figure 2). Most of the hyperalkaline waters have CH_4 isotope values compatible with an abiogenic origin through serpentinization processes (Figure 2). But some of the CH_4 collected in the hyperalkaline waters show values falling in the biogenic field, with at points, very negative $\delta^{13}C$ values (< -70‰). Methanogens were found also in other hyperalkaline waters taking advantage of the presence of sometimes very high hydrogen concentrations [Woycheese et al., 2015; Miller et al., 2018]. Also methanotrophs were rarely found in hyperalkaline waters [Woycheese et al., 2015; Miller et al., 2018] and their presence may justify the most positive values found in the study area (Figure 2).

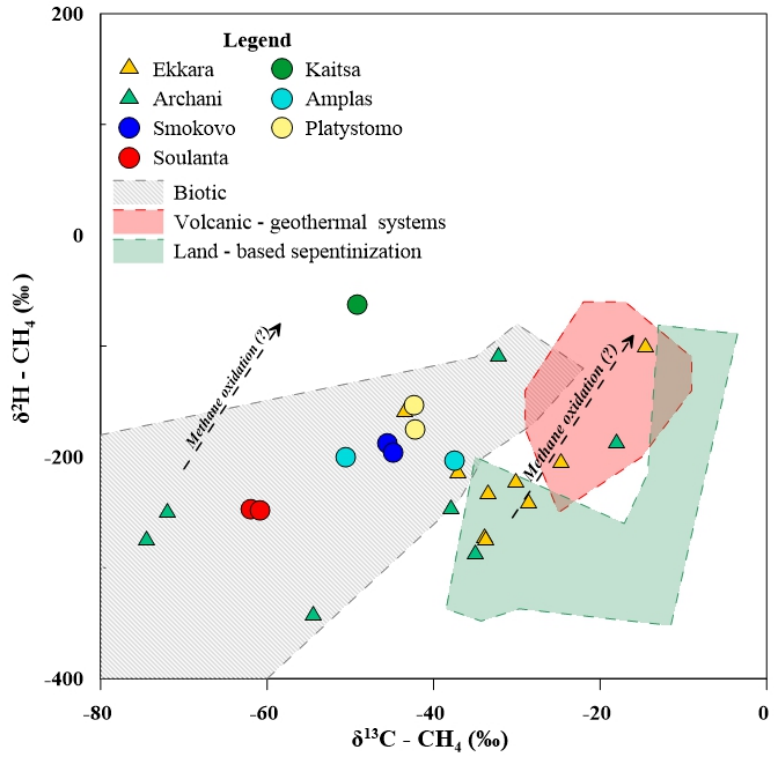

Figure 2 $\delta^{13}C$ vs. $\delta^{2}H$ of methane in the gases collected in alkaline and hyperalkaline waters of the Othys massive.

References

Bernard B.B., Brooks J.M., Sackett W.M., (1978). *A Geochemical Model for Characterization of Hydrocarbon Gas Sources in Marine Sediments*. Offshore Technol. Conf., Houston, USA, pp. 435-438.

Cadieux S.B., White J.R., Sauer P.E., Peng Y., Goldman A.E., Pratt L.M., (2016). *Large fractionations of C and H isotopes related to methane oxidation in Arctic lakes*. Geochim. Cosmochim. Acta, 187, 141-155.

Capasso G., Inguaggiato S., (1998). *A simple method for the determination of dissolved gases in natural waters. An application to thermal waters from Vulcano Island*. Appl. Geochem., 13, 631-642.

Coleman D.D., Risatti J.B., Schoell M., (1981). *Fractionation of carbon and hydrogen isotopes by methane-oxidizing bacteria*. Geochim. Cosmochim. Acta, 45, 1033-1037.

D'Alessandro W., Brusca L., Kyriakopoulos K., Bellomo S., Calabrese S. (2014). *A geochemical traverse along the "Sperchios Basin - Evoikos Gulf" Graben (Central Greece): origin and evolution of the emitted fluids*. Mar. Petrol. Geol., 55, 295-308.

Daskalopoulou K., Calabrese S., Grassa F., Kyriakopoulos K., Parello F., Tassi F., D'Alessandro W., (2018). *Origin of methane and light hydrocarbons in natural fluid emissions: a key study from Greece*. Chem. Geol., 479, 286-301.

Kinnaman F.S., Valentine D.L., Tyler P.A. (2007). *Carbon and hydrogen isotope fractionation associated with the aerobic microbial oxidation of methane, ethane, propane and butane*. Geochim. Cosmochim. Acta, 71, 271-283.

Liotta M., Martelli M., (2012). *Dissolved gases in brackish thermal waters: an improved analytical method*. Geofluids, 12, 236-244.

Miller H.M., Chaudhry N., Conrad M.E., Bill M., Kopf S.H., Templeton A.S., (2018). *Large carbon isotope variability during methanogenesis under alkaline conditions*. Geochim. Cosmochim. Acta, 237, 18-31.

Murrell C.J., Jetten M.S.M., (2009). *The microbial methane cycle*. Environ. Microbiol., Rep. 1, 279-284

Schoell M., (1980). *The hydrogen and carbon isotopic composition of methane from natural gases of various origins*. Geochim. Cosmochim. Acta, 44, 649-661.

Sharp Smirnova A.V., Graham J.M., Stott M.B., Khadka R., Moore T.R., Grasby S.E., Strack M., Dunfield P.F. (2014). *Distribution and diversity of Verrucomicrobia methanotrophs in geothermal and acidic environments*. Environ. Microbiol., 16, 1867-1878.

Woycheese K.M., Meyer-Dombard D.R., Cardace D., Argayosa A.M. and Arcilla C.A., (2015) *Out of the dark: transitional subsurface-to-surface microbial diversity in a terrestrial serpentinizing seep (Manleluag, Pangasinan, the Philippines)*. Front. Microbiol., 6, 44.

An overview of the benthic habitat of the Bottaro crater hydrothermal vent system at Panarea (Aeolian Islands, Italy)

Auriemma R.[2], De Vittor C.[2], Gaglioti M.[1], Esposito V.[2], Teixido N.[1], Gambi M.C.[1]

[1]*Stazione Zoologica Anton Dohrn, Napoli, Italy*
[2]*Istituto Nazionale di Oceanografia e Geofisica Sperimentale, Trieste, Italy*

Corresponding Author: *vesposito@ogs.it*

Introduction

Acconding to recent forecast models, a dramatic increase of partial pressure of CO_2 at the ocean surface is expected within the end of this century, if carbon dioxide emissions in the atmosphere will continue at the current rate. This led to a resulting increase in ocean acidification (OA), a complex chemical process implying a lowering of the pH and an alteration of the carbonate chemistry. Studies on OA effects on the marine biota have seen an important increase in these last years, with an increasing use of naturally acidified systems, such as CO_2 vents, as a proxy to simulate future scenarios of pH and carbonate alteration [see for recents reviews Foo et al., 2018; Gonzalez-Delgado and Hernandez, 2018; Rastrick et al., 2018]. The island of Panarea, and its many nearby small islets, represents the largest hydrothermal system of the whole Mediterranean Sea, and one of the most suitable natural laboratory to assess the effects of water acidification and hot fluids on benthic organisms [Vizzini et al., 2010; Goffredo et al., 2014; Rogelja et al., 2016; Auriemma et al., 2019; Gaglioti et al., 2019]. An overview of the benthic habitat around the crater of Bottaro, one of the many hydrothermal vent systems off the island of Panarea (Aeolian Islands, Italy), is here provided integrating various kind of data derived from surveys conducted as part of the activities of the Scientific Diving Summer School at Panarea (2016-2018) [Gambi et al., 2018; Bigi, 2018]. The School is hosted at the ECCSEL NatLab-Italy laboratory, funded by the Italian Ministry of University and Research and managed by the OGS. The laboratory belongs to the Italian components of the European Carbon Dioxide Capture and Storage Laboratory Infrastructure (ECCSEL).

Study sites material and methods

The waters facing the islets of Lisca Bianca and Bottaro, off Panarea, were upset by a submarine explosion of low energy and degassing between 2nd and 3rd November 2002 (with emissions mainly of CO_2, with traces of H_2S and other gaseous species) that formed a submarine crater (about 20-25 m wide, over 60 m long and about 8 m deep (38° 38'13.58'' N; 15° 6'33.95'' E) [Esposito et al., 2006; Italiano, 2009]. The explosion was followed by a long-lasting degassing activity (over a time span of about a year and a half) from the main crater in which the system remained highly energetic for months, CO_2 release rate vented in the seawater several million liters per day until the mid-2003. Nowadays, most of the venting activity from the original crater has exhausted (although the "main crater" depression still exists) and the "bubbles emissions" are both diffusive and aligned along fractures and faults. The area of the main crater of Bottaro; is now characterized by a main depression at 11 m depth, 14 m wide and 20 m long. During the past three editions of the Panarea summer school of scientific diving (2016-2018) we concentrated in this area various observation by visual census (25x25 cm quadrats), photographic transects and collection of benthic samples (20x20 cm surface) along a transect of 3 stations, at a depth between 8 and 10 meters. The stations were located

at the rim of the crater (station B3) were the lowest pH values were recorded, at 7 m from the rim (station B2, intermediate pH), and at 30-35 m from the rim (station B1, control area with normal pH value [see Goffredo et al., 2014; Auriemma et al., 2019]. Along this transect, at each stations various observation and sampling collections have been performed during the scientific dive and in addition water samples were collected by Niskin bottles for the carbonate system chemical analyses system and continuous recording pCO_2 sensors (CO_2GasPro, by the University La Sapienza; Beaubien et al., [2014]) were placed to measure CO_2 concentration. Here we synthesize a general overview of the habitat features along the transect integrating data from visual census quadrats (25x25 cm quadrats: 8 replicates in B1 and B3; 10 replicates in B2); and benthic samples (20x20cm scrapings on plot colonized by *Cystoseira brachycarpa*, 4 replicates in B1 and B2, 3 replicates in B3) performed both in late September 2016 [Auriemma et al., 2019].

Results and Discussion

The seawater temperature at the bottom was similar along the transect varying from 23.1 °C (B3 station) to 22.9 °C (stations B1 and B2), while a decreasing pH gradient was detected towards the more impacted stations with pH_T values of 8.020, 7.887 and 7.811 at B1, B2 and B3, respectively. Except a few invertebrates, such as the cnidarians *Maasella edwardsi* and *Balanophyllia europaea*, the mollusks *Vermetus triqueter* and *Pinna nobilis*, the crustacean Paguridae (inside shells of the gastropod *Exaplex trunculus*), and the sponge *Crambe crambe*, the megabenthic community is dominated by macrophytes (macroalgae and the seagrass *Posidonia oceanica*) (Figure 1).

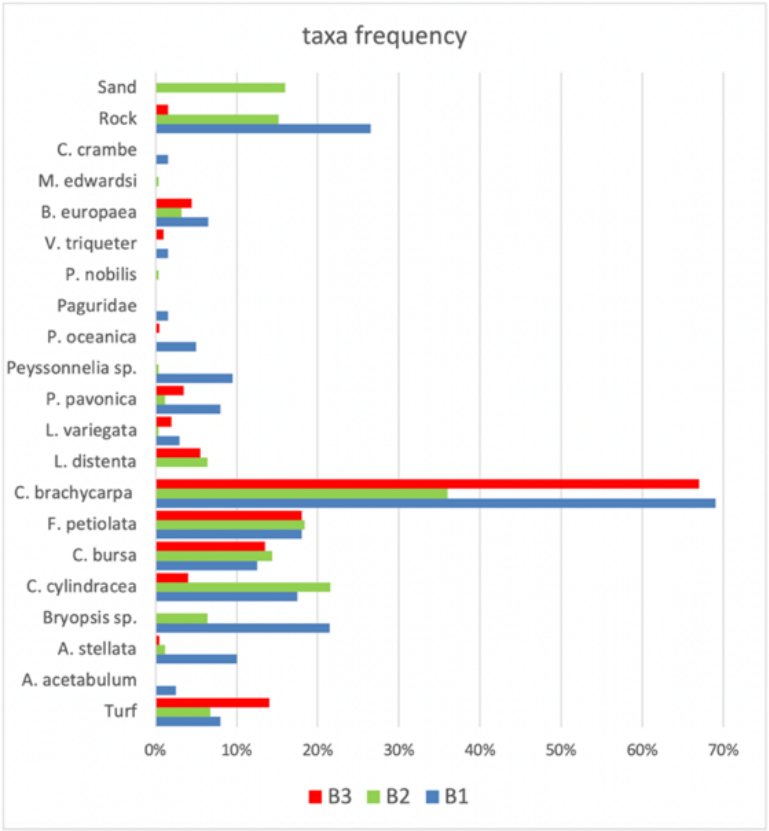

Figure 1 Frequency (% of occurrence in 25x25 cm quadrats: 8 replicates in B1 and B3, 10 replicates in B2) of the main mega-taxa along the Bottaro crater stations during the visual census survey in September 2016.

While the benthic samples, associated to *Cystoseira brachycarpa* host a more diversified invertebrate motile fauna (89 taxa were recorded as a whole in all stations and replicates), mainly composed by small peracarids crustaceans (amphipods, tanaids and isopods) and polychaetes [Auriemma et al., 2019].
The rim of the crater, were st. B3 is located at 8 m depth, is characterized by large boulders and stones irregularly placed, which are colonized by turf and macroalgae, manly by a dense population of the habitat-former brown alga *Cystoseira brachycarpa*, that represent the most frequent macroalga being present on more than 65% of the surveyed surface of the visual census quadrats in stations B1 and B3, and 38% in B2 (Figure 1), and common also on the surrounding areas [Bellissimo et al. 2014]. However, analysing the quantitative benthis samples, *Cystoseira* here showed the lowest cover and biomass (Table 1). Other abundant taxa were Turf, *Flabellia petiolata*, *Codium bursa*, the alien green alga *Caulerpa cylindracea* [already reported in the area, Andaloro et al. 2011; Gaglioti and Gambi, 2018], and the scleractinia *B. europaea* [already reported by Goffredo et al., 2014].

Here we register the lowest diversity (in term of number of species and the Shannon-diversity H' index) (Table 1) of the small invertebrates associated to *Cystoseira*; however the fewer species occur with relatively high abundances, such as the polychaete *Amphiglena mediterranea*, the amphipods *Erichtonius brasiliensis* and *Apherusa* spp., and the tanaid *Condrochelia savignyi* [Auriemma et al., 2019]. The station B2 (7 m far from the crater rim) is characterized by the dominance of *C. brachycarpa*, present in approx. 40% of the surveyed area (Figure 1), but with higher cover and biomass respect to station B3 (Table 1). Other abundant taxa were *F. petiolata*, *C. cylindracea*, Turf, *Bryopsis* sp., *Liagora distenta* and *B. europaea*, while also the bare substrates, represented by rock and sand, were relatively frequent (Figure 1), indicating a high patchiness of the habitat and community. In this area, the rocky bottom all around the crater is also colonized by small patches of *Posidonia oceanica*. The invertebrate fauna associate to *Cystoseira* show here the highest abundances and a number of species comparable to that of the control station B1 (Table 1).

Stations	**B1**	**B2**	**B3**
Number of invertebrate species (S)	35.7 (3.7)	37.5 (4.4)	27.3 (0.5)
Abundance (number of individuals) (N)	244.7 (109.5)	528.7 (192.7)	370 (169)
Diversity (H' index)	4.34 (0.13)	3.58 (0.59)	2.82 (0.43)
Cystoseira biomass (g.d.w.)	15.17 (4.30)	17.77 (4.39)	6.14 (1.56)
Cystoseira cover (%)	166.9 (79.2)	135.8 (35.1)	73.1 (14.2)

Table 1 Values (means and standard deviations in brackets) of the main features of the invertebrate fauna associated to *Cystoseira brachycarpa* (20x20 cm scrapings, 4 replicates in B1 and B2; 3 replicates in B3) along the Bottaro crater stations (September 2016; from Auriemma et al., [2019], modified).

The control station B1 (located approx. 30 m far from the rim of the crater) show a complex mosaic of boulders and rocks interspersed with large patches of *Posidonia oceanica* settled on the rocky substrate. On the hard bottoms, *C. brachycarpa* is still the dominant macroalga (with frequency over 65% of the surveyed surface on the 25x25 cm quadrats; Figure 1) and with relatively high cover and biomass (Table 1), followed by various taxa, such as the macroalgae *Bryopsis* sp., *Anadyomene stellata*, *Peyssonnelia* sp., *Codium bursa*, *C. cylindracea*, *Padina pavonica*, *Acetabularia acetabulum*, and the scleractinia *B. europaea*, some of which with calcified tissue (es., *P. pavonica*, *A. acetabulum*, *Pyssonnelia*

sp., *B. europaea*), indicating a reduced effect of the ocean acidification. The invertebrate motile fauna associated to *Cystoseira* in this area showed the highest diversity and a better structured community, where also most of the calcified species, such as mollusks and echinoderms, are relatively abundant [Auriemma et al., 2019]. In general, it worth to note the absence of sea urchins in all the stations surveyed, including the control station B1, and although the dominance of the macroalgae.

Conclusions

The Bottaro crater benthic habitat shows in general a relatively low benthic biodiversity, especially of the sessile/sedentary organisms. The habitat shows a high patchiness and an irregular mosaic of hard substrates and interspersed Posidonia patches, starting a few meters from the rim of the crater, and is dominated by a few species of macroalgae. This macrophyte-dominated habitat show a few invertebrates both sessile (es., *B. europaea*, *V. triqueter*) and motile (es., peracarid crustaceans and polychaetes), these latter mainly associated to the dominant brown alga *C. brachycarpa*. In particular, the *Cystoseira* invertebrate assemblage, although very simplified, respect to that occurring on *Cystoseira* in different ecological setting and areas [Piazzi et al., 2018], showed more relevant changes in the structure and composition between stations B1 and B2, and station B3; this could be mainly related to the ocean acidification gradient, somehow modulated by the indirect effects of the habitat complexity provided by the habitat-former algal species. In the B3 station, all the considered variables (see Table 1) result strongly reduced and affected by both the more severe conditions of lower pH level and its higher variability, coupled with the reduction of habitat complexity, in fact, although *C. brachycarpa* is frequent, its overall cover and biomass are lower than in the other stations. In addition to the possible effect of OA, we should consider that the studied area has been affected by the 2002 gas blast episode and therefore has been recolonized since a relatively short period, this imply that the local community may still need time to recover to a more mature and complex condition (climax stage) also in the B1 station control zone.

Acknowledgements

We wish to thank Andrea Fogliuzzi (Amphibia diving) for support at sea during field work, and all the students and participants of the editions of the Panarea Summer School of Scientific Diving.

References

Andaloro F., Romeo T., Ancora S. and Italiano F., (2011). *La biodiversita marina in aree vulcaniche. Effetti dell'idrotermalismo sulle specie ittiche dell'area eoliana.* In: Coiro P., Russo G.F. (eds), Il fuoco dal mare. Vulcanismo e ambienti sottomarini. I Quaderni di uomo e natura 3. Giannini, Napoli: 69-78.

Auriemma R., De Vittor C., Esposito V., Gaglioti M. and Gambi M.C., (2019). *Motile Fauna associated to Cystoseira brachycarpa along a gradient of Ocean Acidification at a vent system off Panarea (Aeolian Islands, Italy).* Biol. Mar. Mediter. 50° Congress, Livorno 4-10 June 2019 Preprints (www.sibm.it): 180-183.

Beaubien S.E., Graziani S., Annunziatellis A., Bigi S., Ruggiero L., Tartarello M.C. and Lombardi S., (2014). *Spatial -temporal water column monitoring using multiple, low -cost GasPro -pCO_2 sensors: implications for monitoring, modelling, and potential impact*. Energy Procedia, 63: 3840-3847.

Bellissimo R., Rull Lluch J., Tomasello A. and Calvo S., (2014). *The community of Cystoseira brachycarpa J. Agardh emend. Giaccone (Fucales, Phaeophyceae) in a shallow hydrothermal vent area of the Aeolian Islands.* Plant Biosyst., 148(1): 21-26.

Bigi S., (2018). *Scientific diving training for underwater monitoring. CO_2GeoNet Highlights*. The Newsletter of the European Network of Excellence on the Geological Storage of CO_2, N. 15, October 2018.

Esposito A., Giordano G. and Anzidei M., (2006). *The 2002-2003 submarine gas eruption at Panarea volcano (Aeolian Islands, Italy): Volcanology of the seafloor and implications for the hazard scenario*. Mar. Geol., 227(1-2): 119-134.

Foo S.A., Byrne M., Ricevuto E. and Gambi M.C., (2018). *The carbon dioxide vents of Ischia, Italy, a natural laboratory to assess impacts of ocean acidification on marine ecosystems: an overview of research and comparisons with other vent systems*. Oceanogr. Mar. Biol. Ann. Rev., 56: 236-310.

Gaglioti M. and Gambi M.C., (2018). *The natural laboratory of the CO_2 vents off Panarea (Aeolian Archipelago): a special ecological setting and a further stepping stone for some alien macrophytes*. Notiziario SIBM, 74: 111-117.

Gaglioti M., Auriemma R., De Vittor C., Esposito V., Teixido N. and Gambi M.C., (2019). *A pilot study on Posidonia oceanica features of a hydrothermal system at Panarea (Aeolian Islands, Italy)*. Biol. Mar. Mediterr., 50° Congress, Livorno 4-10 June 2019 Preprints (www.sibm.it): 236-237.

Gambi M.C., De Vittor C., Bigi S. and Italiano F., (2018). *Third School of Scientific Diving at Panarea (Aeolian Islands, Tyrrhenian Sea, Italy): the first international edition*. Notiziario SIBM, 74: 104-110.

Goffredo S., Prada F., Caroselli E., Capaccioni B., Zaccanti F., Fantazzini P., Fermani S., Reggi M., Levy O., Fabricius K.E., Dubinsky Z., and Falini G., (2014). *Biomineralization control related to population density under ocean acidification*. Nature Clim. Ch., 4: 293-297.

Gonzalez-Delgado S. and Hernandez J.C., (2018). *The importance of natural acidified systems in the study of Ocean Acidification: What have we learned?* Adv. Mar. Biol., doi: 10.1016/bs.amb.2018.08.001

Italiano F., (2009). *Hydrothermal fluids vented at shallow depths at the Aeolian Islands: relationships with volcanic and geothermal systems*. FOG - Freiberg Online Geoscience, 22: 1-8.

Piazzi L., Bonaviri C., Castelli A., Ceccherelli G., Costa G., Curini-Galletti M., Langeneck J., Manconi R., Montefalcone M., Pipitone C., Rosso A. and Pinna S., (2018). *Biodiversity in canopy-forming algae: Structure and spatial variability of the Mediterranean Cystoseira assemblages. Estuar*. Coast. Shelf Scie., 207: 132-141.

Rastrick S., Graham H., Azetsu-Scott K., Calosi P., Chierici M., Fransson A., Hop H., Hall-Spencer, J.M. Milazzo M., Thor P. and Kutti T., (2018). *Using natural analogues to investigate the effects of climate change and ocean acidification on Northern ecosystems*. ICES J. Mar. Scie., 75(7): 2299-2311.

Rogelja M., Cibic T., Pennesi C. and De Vittor C., (2016). *Microphytobenthic community composition and primary production at gas and thermal vents in the Aeolian Islands (Tyrrhenian Sea, Italy)*. Mar. Environ. Res., 118: 31-44.

Vizzini S., Tomasello A., Di Maida G., Pirrotta M., Mazzola A. and Calvo S., (2010). *Effect of explosive shallow hydrothermal vents on $\delta^{13}C$ and growth performance in the seagrass* Posidonia oceanica. J. Ecol., 98(6): 1284-1291.

Soil gases interaction with biota at geothermal/volcanic areas

Gagliano A.L.[1], Tagliavia M.[2] and D'Alessandro W.[1]

[1]*Istituto Nazionale di Geofisica e Vulcanologia, Sezione di Palermo, Italy*
[2]*IRIB - CNR, via Ugo La Malfa 153, 90146 Palermo, Italy*

Corresponding Author: *lisagagliano86@gmail.com*

Soils are multicomponent biogeochemical systems reflecting the influences of weathering and living organisms on the parent material; they contain a large population of macro-, meso-, and microscale organisms, and are characterized by solid inorganic and organic compounds, ions and molecules, and a gaseous phase containing N_2, O_2, CO_2, water vapor, Ar and CH_4 plus other trace gases.
Soils represent the interface between geosphere and atmosphere and most life supporting components derive, either directly or indirectly, from them. The generally neutral pH values make soils hospitable for life. Acid rain, consequence of anthropogenic input of acidifying components to the atmosphere, led sometimes to severe soil acidification with a strong impact on the capacity of soils to sustain life. In geothermal areas, chemistry and pH of the soil are influenced by the composition of fumarolic gases (water vapor, CO_2, H_2S, etc.). Although H_2S, like CO_2, is a weak acid, it represents the main contributor to acidification of these soils. When it reaches the surface, it is oxidized to sulphuric acid, which is a strong acid (pK_2 = 1.92), hence lowering the pH of soil to very low values. These are also accompanied by high temperatures due to fumarolic water vapor condensation. Soil pH and temperature are, therefore, the main limiting factors for microoganisms and vegetation in geothermal soils [Brock, 1978].
Gases emitted from volcanic/geothermal soils represent the result of several processes occurring in the deeper layer or the lithosphere. Apart from the above-mentioned main components, also other gases (CO, CH_4, H_2, NH_3, N_2) successfully reach the subsurface and even if at low amounts they play an important role in term of interaction with the biota. Soil microorganisms consuming these trace gases may act as filters in the final step that lead the gases from the lithosphere up to the atmosphere. All the gaseous species shape the soil microbial ecosystems that, in turn, interact with the fluids, changing their final composition.
Here we report on the results of several field campaigns conducted in Sicily (Italy) and Greece aiming to ascertain the role of the biota in the removal of GHG (in particular methane) escaping from the subsurface and the main interaction of biota and the hydrothermal gas species.

Sampling sites and analytical methods
The sampling sites were selected at geothermal/volcanic field located at Pantelleria Island, Nisyros Island and Vulcano Island.
Soil gas samples from the three sites were taken through a sampling device with 2 mm ID tubes tapping soil gases at 50 cm depth, using a gastight plastic syringe and stored in 12ml Exetainer® vials. The vials were analysed in the laboratory for CH_4, CO_2, N_2, O_2 and H_2 by using a Perkin Elmer Clarus 500 GC equipped with Carboxen 1000 columns, two detectors (HWD and FID), and argon as the carrier gas. Analytical precision (± 1σ) was always better than ± 3 %. The detection limits were about 0.1 µmol mol^{-1} for CH_4, 2 µmol mol^{-1} for H_2, 10 µmol mol^{-1} for CO_2 and 200 µmol mol^{-1} for O_2 and N_2.

Methane flux measurements were made by accumulation chamber method [Livingston and Hutchinson, 1995; D'Alessandro et al., 2009]. The chamber was made of plastic material and had cross section area of 0.07 m^2 and height of 10 cm. Three gas samples were drawn from the chamber at fixed intervals after the deployment (5, 10 and 15 min). The samples, stored in 12 ml Exetainer® vials, were analyzed in the same way as the soil gas samples.

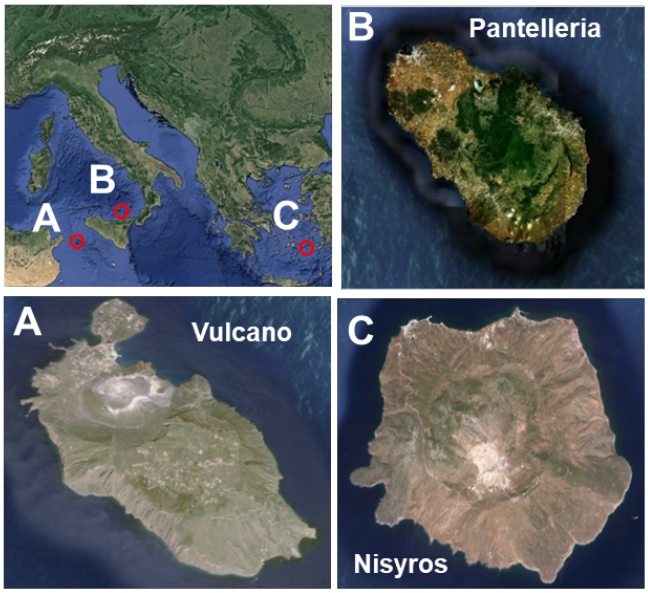

Figure 1 Sampling sites - A) Pantelleria Island, B) Vulcano Island - Italy; C) Nisyros Island – Greece.

Soils were sampled using a sterile hand shovel and stored in sterile plastic bags, and used for bacterial cultivation and incubation experiments, for DNA extraction and genetics analysis.
In order to enrich for methanotrophic bacteria, 15 gr of soil were placed in 125-ml sealed serum bottles in atmosphere supplemented with methane (25%) and incubated at 37° for 2 weeks. Two g of enriched soil crumbles were transferred in 125-ml serum bottles containing 20 ml of low salt mineral medium M3 adjusted to pH 6 under the same conditions [Islam et al., 2008]. After 2 weeks incubation aliquots of M3 enrichment cultures were inoculated on M3 agar-slunts in 125-ml sealed serum bottles under methane enriched atmosphere and incubated as described above for 2 weeks. As soon as colonies appeared, they were transferred to obtain pure cultures that were checked for methane consumption by GC analysis.
A similar procedure was employed to enrich for sulphate-reducing bacteria, using PYE (containing $Na_2S_2O_3$ as S source) as culture medium, and incubating at 65°C.
Genomic DNA was extracted from 10 ml M3-CH_4 broth culture of each isolate grown in the conditions described above by the method described by Sambrook et al. [1989] and used as template for the amplification of the 16S rRNA gene with universal primers [Gagliano, 2014] and *pmoA*.
Methane oxidation potential of the soils was analyzed by transferring 15 gr of each air-dried soil sample in a 160-ml glass serum bottle, that was capped with a rubber stopper and sealed with aluminum crimps, after wetting with about 1 ml sterile distilled water. After sealing the bottle atmosphere was enriched in CH_4 to reach about 1000-2000 µmol mol^{-1}. Bottles were maintained at room temperature (23- 25°C) and the CH_4 concentration was measured at the beginning of the experiment and at about 24h intervals for 5 days. To better constrain the methane consumption in samples that after 24h consumed more than 30% of the initial CH_4 the experiments were repeated measuring the concentrations at about 2h interval. Methane concentration in the headspace of the

bottles was measured by GC. Incubation experiments were made in duplicate and the results expressed as average value in ng CH_4 per g of soil (dry weight) per h (ng g^{-1} h^{-1}).

Results and discussion

The three areas showed several differences in chemical-physical parameter and in methane flux from soils. Higher values of temperature were measured at Pantelleria Island (up to 112 °C), lower pH values were recorded at Nisyros Island (as low as 1.81).

Soil gases sampled at Pantelleria Island were richer in CH_4 than the other two sites, and some of the sampled sites were also rich in N_2 and O_2. Most of the soils showed a pH > 6 and molecular analysis indicated the prevalence of methane oxidant bacteria in the whole microbial community. Incubation experiment allowed to isolate some methanotrophs from these sites (e.g. *Methylocistis s.p.*) and to evaluate the methane oxidation potential rate up to 950 ng/g/h. At the same area, one of the sampling site was characterized by lower pH (~3), high value of CH_4, CO_2, and H_2. Here the microbial community seems to be based on substrates as NH_3, H_2 and CO [Hedrich and Johnson, 2013]. H_2 sustains the acidophilic Fe(II) oxidizers of the genera *Acidithiobacillus*. High concentrations of NH_4^+, measured at this site sustain ammonia-oxidizing bacteria (AOB) and archaea (AOA) such as *Nitrosococcus*. CO oxidizers *Ktedonobacter* coxL sequences were found at Pantelleria island soils, it was proposed that this species might represent a novel CO-oxidizing lineage with a chemolithotrophic/mixotrophic metabolism [Weber and King, 2010; Chang et al., 2011; Gagliano et al., 2015].

Soils from Pantelleria were used for enrichment cultures to isolate sulphate-reducing bacteria, whose presence was evidenced by the formation of insoluble, black precipitate (FeS). Such enriched communities of sulphate-reducing bacteria still need further characterization, including isolation and identification.

Figure 2 Enrichment cultures to isolate Sulphur-reducing bacteria.

At Vulcano island, due to the high alteration of the soils, the molecular analysis was performed with difficulties. The cultural approach and the incubation experiments gave indirect evidence of methanotrophy. Soils from Vulcano island had very low pH (up to 1.91), not very high temperatures (up to 60 °C), high H_2S flux [Capaccioni et al., 2001], methane flux even if significant is lower with respect to other geothermal/volcanic areas; all these conditions make the nearly absence of methanotrophs not unexpected, although some low CH_4 consumption was recorded. Negative results from *pmoA* gene detection in samples from Vulcano Island were presumably due to low quality of the extracted DNA (due to the altered and maybe salt and/or humic acid-rich nature of that soil, which tend to copurify with DNA, making it unsuitable), as even the 16S gene, a universal bacterial target, failed to amplify.

Methane flux values measured at Nisyros Island were up to 1420 mg m^{-2} d^{-1}, negative values indicating CH_4 oxidation was also measured in some of the sampling sites. Soil gases were rich in H_2S, CO_2 and showed low values of O_2 and N_2. The obtained potential CH_4 consumption in the range of 4 - 40 ng/g/h was an indirect evidence of methanotrophy. Molecular analysis on DNA extracted from the enrichment cultures and *pmoA* confirmed the indirect evidences.

Geothermal System	CO_2/CH_4	H_2S ppm	Methane consumption up to (ng g^{-1} h^{-1})
Pantelleria	25 - 30	< 100[a]	950
Vulcano	~50	~ 20,000[b]	57
Nisyros	30 - 300	60,000 - 250,000	39

Table 1 Comparison between the studied geothermal systems. a) D'Alessandro et al., [2009]; b) Capaccioni et al., [2001].

Conclusion

Interest in the study of CH_4 output to the atmosphere is increasing every day to reach a correct estimation of the geologic, and the volcanic/geothermal contribution in the total CH_4 budget in the atmosphere. The discovery of new species of methanotrophs belonging to Verrucomicrobia brought to reconsider the balance between CH_4 emissions and sinks in the soils. For geothermal sites, sinks were before considered inefficient due to the extreme environmental conditions. We studied 3 geothermal systems differing in temperature, pH, CH_4 and H_2S flux. At all the investigated sites CH_4 emissions are naturally limited by microbial oxidation, as demonstrated by soil CH_4 consumption and for Pantelleria the identification of methanotrophs. The recorded methane oxidation rate was different in the three areas; Principal Component Analysis were applied to compare data from different sites using temperature, pH, H_2S content as factors. According with the analyzed components, the highest consumption values were measured in soils with higher pH, lower in H_2S contents and lower CO_2/CH_4 ratios.

Methane oxidation potential strictly depends on CH_4 availability. Laboratory experiments and correlation between CH_4 flux indicate a high CH_4 oxidation rate when CH_4 availability is higher. Moreover, high CH_4 consumption were recorded in the areas with high CH_4 flux such as Pantelleria, the lowest at Vulcano Island, were emission are lower. The major difference between Pantelleria and the others sites is in the H_2S emissions that at Pantelleria island are lower. Hydrothermal conditions within the geothermal system of Pantelleria are such that little H_2S is produced. This means that even if the hydrothermal gas flux is sustained, the soil pH generally does not reach very low values. At Nisyros the CO_2/CH_4 flux ratio indicate low CH_4 values in comparison to Pantelleria (even if still very significant), H_2S in this sites reach really high values being a major component the soil gases. Even with these extreme conditions methanotrophs are active. On the contrary, high temperature does not seem a main limiting factor for CH_4 consumption in the investigated soils, at least up to 60 °C. In the end, we can disregard that only extremophile methanotrophs live in geothermal soils because Pantelleria island hosts a wide number of Proteobacterial methanotrophs. Indeed thermo-tollerant species could found their niches in the geothermal soils where the temperatures are not so high, pH not so low, thriving on the abundant upraising hydrothermal CH_4.

References

Brook T.D., (1978). *Thermophilic Microorganisms and Life at High Temperatures*. Springer.

Chang Y.J., Land M., Hauser L. et al., (2011). *Non-contiguous finished genome sequence and contextual data of the filamentous soil bacterium Ktedonobacter racemifer type strain (SOSP1-21)*. Standards in Genomic Sciences, 5, 97-111.

Gagliano A.L., D'Alessandro W., Tagliavia M., Parello F. and Quatrini P., (2014). *Methanotrophic activity and diversity of methanotrophs in volcanic geothermal soils at Pantelleria (Italy)*. Biogeosci., 11, 5865-5875.

Gagliano A.L., Tagliavia M., D'Alessandro W., Franzetti A., Parello F. and Quatrini P., (2015). *So close, so different: geothermal flux shapes divergent soil microbial communities at neighbouring sites*. Geobiology, 14, 150-162.

Hedrich S. and Johnson D.B., (2013). *Acidithiobacillus ferridurans sp. nov., an acidophilic iron-, sulfur- and hydrogen-metabolizing chemolithotrophic gammaproteobacterium*. Int J Syst Evol Microbiol., 63 11 4018-2.

Islam T., Jensen S.., Reigstad L.J., Larsen Ø. and Birkeland N.K., (2008). *Methane oxidation at 55oC and pH 2 by a thermoacidophilic bacterium belonging to the Verrucomicrobia phylum*. Microbiology, January 8, vol. 105, no. 1, 301.

Livingston G.P., Hutchinson G.L., (1995). *Enclosure-based measurement of trace gas exchange: applications and sources of error*. In: Biogenic Trace Gases: Measuring Emissions from Soil and Water. Methods in Ecology (Matson, P.A. and Harriss, R.C. eds.), pp. 14-51. Blackwell Science Cambridge University Press, London.

Sambrook J., Fritsch E.F. and Maniatis T.A., (1989). *Molecular Cloning: A Laboratory Manual*," 2nd ed. Cold Spring Harbor, USA: Cold Spring Harbor Laboratory Press.

Weber C.F., King G.M., (2010). *Distribution and diversity of carbon monoxide-oxidizing bacteria and bulk bacterial communities across a succession gradient on a Hawaiian volcanic deposit*. Environmental Microbiology, 12, 1855-1867.

Microclimatic changes within a dry CO_2 gas lake and its weather induced variations

Kies A.[1], Pfanz H.[2]

[1]*University of Luxembourg, L-1511 Luxembourg*
[2]*Applied Botany and Volcano Biology, University Duisburg-Essen, Germany*

Corresponding Author: *antoine.kies@uni.lu*

CO_2 seeping from the ground is usually dispersed by mixing with the surrounding air, However, at some locations, there is an area surrounding the source where the emerging CO_2 is less easily dispersed by the wind, accumulates and stays close to the source area. These sites commonly have the form of depressions around the emission points, on the scale of meters to tens of meters and more in diameter [Holloway et al., 2007]. As a result of CO_2 accumulation a CO_2 gas lake may develop [Pfanz, 2008; Kies et al., 2015] and even a CO_2 gas river [Chiodini et al., 2010]. Within these dry gas lakes, most organisms die due to a lack of oxygen or due to hypercapnia. On the other side, these CO_2 lakes are natural experimental sites where microclimatic changes can be determined. Our experimental site is the Bossoleto, a bow-like depression, located near Rappolano in Tuscany (Italy), with a diameter of 100 m, a depth of 5 meters and surrounded by trees (Figure 4). In the Bossoleto extensive dioxide degassing from a non-volcanic source happens at the bottom and lower flanks. In order to investigare the dynamics of CO_2 fluctuations within the gas lake, a measuring tower was erected in the center of the Bossoleto. Temperature and CO_2 were recorded each 40 cm starting from 40 cm at the bottom (Figure 4). A weather station on top allowed information on atmospheric conditions.

Every day, a transient CO_2 gas lake forms and vanishes. Due to the irregular heating of the air within the depression and the absorption of near infrared radiation by carbon dioxide, thermal changes occur within the gas lake. A pattern of changing CO_2 concentrations were already published [Kies et al., 2015]. Daily temperature variations induce changes in the vertical temperature gradient allowing the accumulation of the dense CO_2 gas or its reject into the atmosphere.

A normal, sunny Mediterranean day induces three phases within the gas lake: (1) very low CO_2 concentrations starting from 11.00 a.m. to late afternoon hours (18.00), (2) the formation of a stratified gas lake starting late afternoon, reaching its highest extend in early morning hours (08.00). (3) Homogenization of CO_2 concentrations within the lower strata, followed by the total disintegration of the gas lake (10.00 -11.00). After a strong overheating of the homogeneous gas lake, the whole gas system empties completely from the valley during tenth of minutes (Figure 1 and Figure 2).

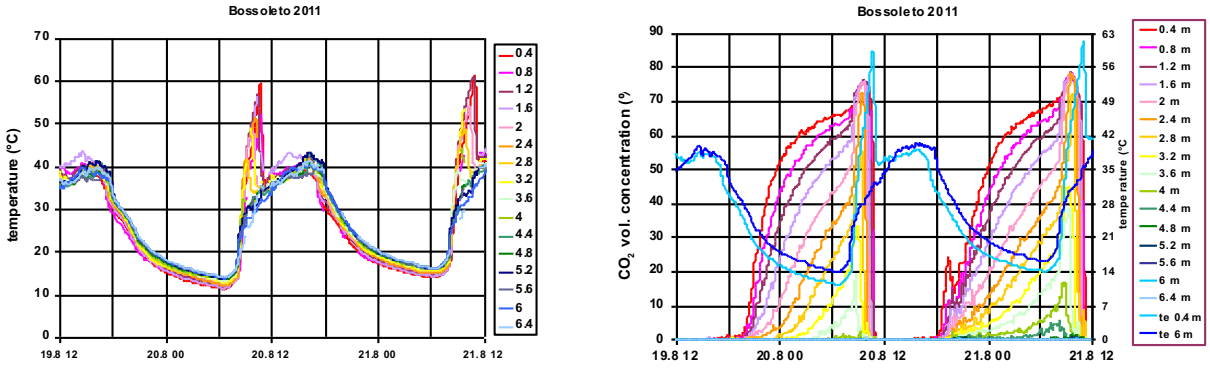

Figure 1 Example of the repetitive temperature and CO_2 profiles measured on the observation tower situated in the center of the Bossoleto. A stable positive temperature gradient at night retains CO_2 in the Bossoleto (phase 2). A sharp gradient change in the morning induces phase 3.

The climatic processes within lake formation and lake disintegration are astonishing. Especially the formation of a homogeneous gas lake at the bottom of the Bossoleto (phase 3), with a duration of up to 2 hours, is unusual. Figure 2 shows the gradual CO_2 accumulation in the gas lake, the short evolution into homogenization at the lower strata and its abrupt dissolution. Now it is safe to enter the Bossoleto.

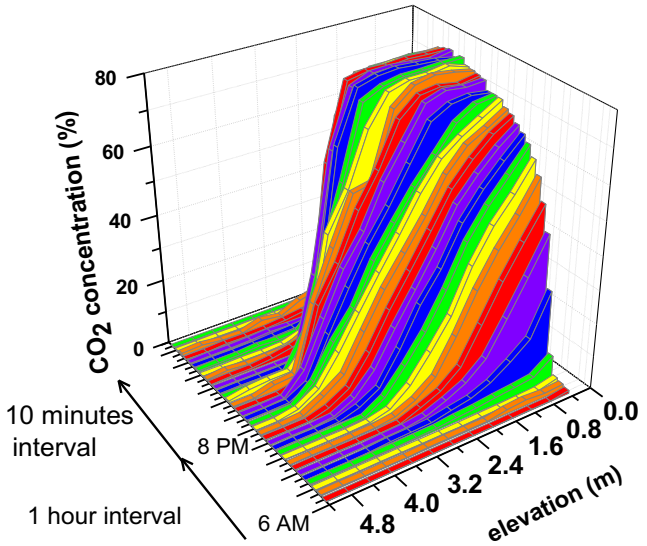

Figure 2 Filling of the CO_2 lake, its homogenization for the lower strata and the breakup.

Stable weather conditions during summer guarantee a repetitive pattern of the described diurnal cycles within the CO_2-lake. Yet, heavy wind gusts, rain events, or just cloudy skies strongly disturb the normal gas lake pattern. This happened frequently during the spring campaign, end of March to early May. Gas lake formation may be hindered or lake disintegration may be prolonged. The influences of the disturbing weather parameters on the CO_2 dynamics of the Bossoleto gas lake were studied and analyzed.

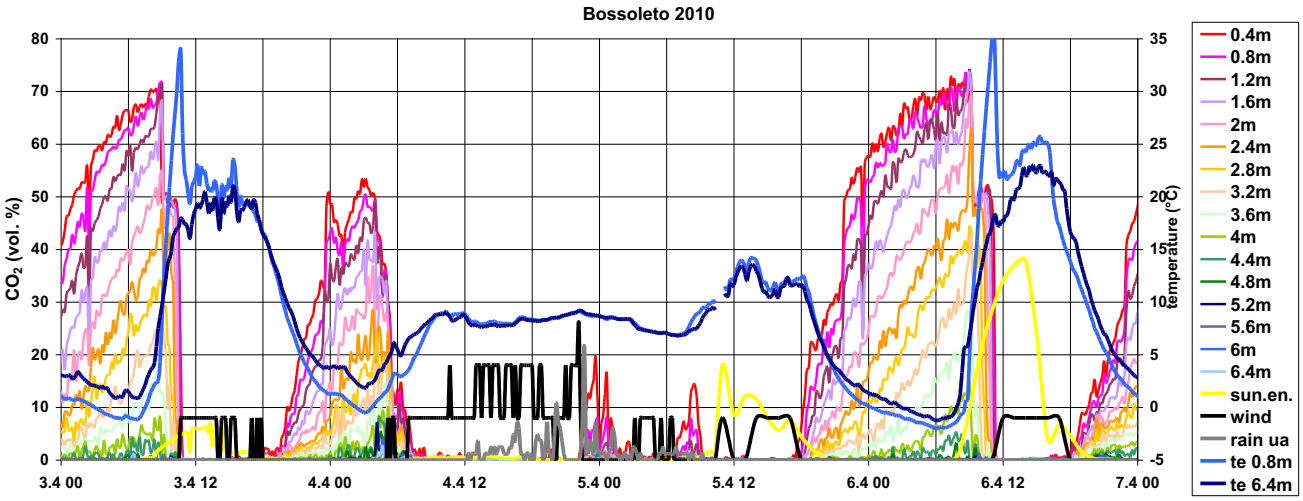

Figure 3 documents the disturbed temperature- CO_2 Cycles measured in spring, with low temperatures and changing atmospheric conditions.

A stable positive temperature gradient is mandatory but not sufficient for the CO_2 accumulation process. Especially strong wind removes CO_2 from the Bossoleto, even under strong positive temperature gradient conditions. Instabilities in air movements showed frequent irregularities in the accumulation process for lower strata. If not too important, the positive restoring force of buoyancy restores the usual stratification and CO_2 escape of the lake is limited. For cloudy days with rain, in the middle of the day CO_2 can accumulate at the bottom to dangerous levels. On overcast spring days visitors should relay on a CO_2 alert inspector.

Figure 4 Inside the Bossolet with the observation tower. The photo was done late summer morning before the desintegration of the homogeneous gas lake (75 % CO_2) at the bottom, below a haze that marks the upper extend of the gas lake. The autor was positioned slightly above the haze.

References

Chiodini G., Granieri D., Avino R., Caliro S., Costa A., Minopoli C., (2010). *Non-volcanic CO_2 Earh degassing: Case of Mefite d'Ansanto (southern Apenines), Italy*. Geophysical Research Letters, 32, L11303, 1-4.

Holloway S., Pearce J.M., Hards V.L., Ohsumi T., Gale J., (2007). *Natural emissions of CO_2 from the geosphere and their bearing on the geological storage of carbon dioxide*. Energy. 32, 1194-1201.

Kies A., Hengesch O., Tosheva Z., Raschi A., Pfanz H., (2015). *Diurnal CO_2-cycles and temperature regimes in a natural CO_2 gas lake*. International Journal of Greenhouse Gas Control, 37, 142-145.

Pfanz H., (2008). *Mofetten - Kalter Atem schlafender Vulkane*. RVDL Verlag, Köln.

Botanical and pedological characterization of a meadow mofette system at South-Hartousov/Czechia

Pfanz H. and Thomalla A.

Institute of Applied Botany and Volcano Biology, University of Duisburg-Essen, Germany

Corresponding Author: *hardy.pfanz@uni-due.de*

A 9 x 9 m subarea of a CO_2 emitting mofette system in a meadow South of Hartousov/Czechia was chosen to study the effects of geogenic CO_2 emission on the prevailing vegetation. The mofette emits CO_2 at ambient temperature. The whole area is relatively undisturbed but the meadow is mowed once a year. A 1 x 1m grid was laid on top of the area and at each intersection, soil gas measurements were performed at four different depths (10, 20, 40, 60cm); the soil gases CO_2 and O_2 were measured. In addition, soil CO_2 flux was measured and soil cores were taken at each grid intersection at a depth of 7-13cm as this depth was thought to reflect the main rooting horizon of grasses and herbaceous plants in that area. Soil water content, soil pH, buffering capacities, soil conductivity and organic matter were determined. Additionally, quantitative vegetation analysis was carried out and total number of plant species as well as species total and individual coverage were estimated in each square.

Carbon dioxide was emitted in the whole area with a centre at the upper right part of the area. Only the lowest left section showed no gas emission. Oxygen values inversely corresponded to the CO_2 concentrations. Oxygen was high when CO_2 was low and vice versa. Overall, CO_2 values increased with depth, whereas O_2 concentrations decreased. Soil CO_2 fluxes nicely mirrored the CO_2 concentrations in deeper soil horizons.

Two smaller plots differed from the rest of the site. They showed very high CO_2 fluxes and were void of vegetation. A vegetation ring composed of *Carex nigra* (meadow sedge) framed the bare soil.

Interestingly, the soil pH within the barren plots showed the lowest values (down to pH 2.7) of the area and the highest soil conductivities; up to 1400 µS cm^{-1} were measured. At plots, where the CO_2 flux was much lower but CO_2 concentrations were still high, pH values between 3.9 - 4.3 were determined. Total plant coverage was low where CO_2 concentrations were high and zero where additionally the CO_2 flux was high. Plant coverage increased with decreasing CO_2 emission [cf Saßmannshausen, 2010; Thomalla, 2015]. Similar results were obtained with the number of plant species within the different plots. At sites with high CO_2 fluxes, no plants existed. The species number was low at sites with higher CO_2 concentrations (2-4 species m^{-2}) and increased up to 20 species m^{-2} at sites with low or background CO_2-emission. Positive mofette indicating plants [mofettophiles; Pfanz, 2008; Pfanz et al., 2019] only grew at plots of high to medium CO_2, whereas negative indicators (mofettophobes) were reduced to low or zero emission sites. *Carex nigra* (meadow sedge) and *Nardus stricta* (moor matgrass) proved to be the only eu-mofettophilic plant species in the area. They grew exclusively on high CO_2 emitting soils. On the other hand, *Achillea ptarmica* (sneezewort), *Agrostis capillaris* (common bent), *Alopecurus pratensis* (meadow foxtail), and *Holcus lanatus* (meadow soft grass) clearly avoided CO_2 degassing soil and exclusively grew on plots with background CO_2 concentration. They proofed to be mofettophobic.

References

Pfanz H., Vodnik D., Wittmann C., Aschan G., Raschi A., (2004). *Plants and geothermal CO_2 exhalations - survival in and adaptation to a high CO_2 environment*. In Esser K., Lüttge U., Kadereit J.W., Beyschlag W., (Hrsg.). Springer Verlag, Berlin, Heidelberg. Progress in Botany, 65, 499-538.

Pfanz H., Saßmannshausen F., Wittmann C., Pfanz B., Thomalla A., (2019). *Mofette vegetation as an indicator for geogenic CO_2 emission: A case study on the banks of the Laacher See Volcano, Vulkaneifel, Germany*. Geofluids, in press.

Saßmannshausen F., (2010). *Vegetationsökologische Charakterisierung terrestrischer Mofettenstandorte am Beispiel des west.tschechischen Plesná-Tals*. Dissertation, Universität Duisburg-Essen.

Thomalla A., (2015). *Boden- und vegetationskundliche Untersuchungen zur Charakterisierung der Ausgasungs- und Vegetationsdynamik zweier trockener Mofetten im west-tschechischen Plesnátal*. Dissertation, Universität Duisburg-Essen.

ICGG15

EXHIBITIONS

The distributed multidisciplinary laboratory for the research in marine environment

Cuttone G.[1], Bonanno A.[2], Caruso C.[3], Corsale F.[3], Italiano F.[3], Lazzaro G.[3], Papaleo R.[1], Piattelli P.[1], Riccobene G[1], Sapienza P.[1], Sorelli D. [1], Scirè Scappuzzo S.[3]

[1] *Istituto Nazionale di Fisica Nucleare (INFN) - Laboratori Nazionali del Sud, Catania, Italy*
[2]*CNR - IAS - Unità Operativa di Capo Granitola, Trapani, Italy*
[3]*Istituto Nazionale di Geofisica e Vulcanologia, Sezione di Palermo, Italy*

Corresponding Author: *papaleo@lns.infn.it*

IDMAR is a research infrastructure funded by Regione Siciliana within the ERDF 2014-2020. IDMAR is one of the 3 RIs defined by Regione Siciliana as strategic for the economic and technological development of the Island.
The main goal of the project if the development of a distributed (on-shore and off-shore) multidisciplinary laboratory for the research in marine environment. The main sites where the RI will be developed are Portopalo, Catania, Milazzo, Palermo and Capo Granitola.
Each site will have its own specific expertise, depending on the existing infrastructure on site, of the investments carried out over the years by the research institutes participating in the funding project through ordinary funds and (European, national and regional).
The project strength is the possibility to create a network of infrastructure and facilities for research, testing and development in marine environment. This will be a unique in the European and perhaps world landscape.
At the end of project, the Sicilian Region will effectively become a world-class hub in the research, development and testing of systems and equipment for monitoring and sustainable development of the marine environment.
IDMAR infrastructures will be used to host some of the most important European deep-sea research infrastructure such as EMSO and KM3NeT. They will be connected to the underwater technological backbone realized within the project.
A new deep-sea real time network (main electro optical cable plus junction boxes) will be realized in Portopalo, to connect the underwater site at 3.500 m depth (100km away from the SE Sicilian coast) with the onshore lab, located in the Capo Passero Laboratories.
In Palermo INGV will build the new building to host the management and operative branch focused on research in marine environment. The building will host laboratories, testing facilities and the most of the marine infrastructures to be deployed as a component of the distributed multidisciplinary laboratory.
The INGV operative office located in Milazzo will be the site that will host a stand alone fleet of multidisciplinary underwater research modules.
Capo Granitola will host a new pool for testing and qualification of acoustic and multidisciplinary underwater sensors and equipment.
IDMAR will be a funding attractor for new potential investment in underwater and deep sea environment for both Italian and foreign companies.

The 1906 Ustica earthquake sworm: a case study of civil protection of the last century

Foresta Martin F.[1,2]

[1]*Istituto Nazionale di Geofisica e Vulcanologia, Sezione di Palermo, Italy*
[2]*Laboratorio Museo di Scienze della Terra, Ustica, Palermo, Italy*

Corresponding Author: sidereus@rocketmail.com

In the spring of 1906, from March 18 to April 6, the volcanic island of Ustica (60 km from Palermo), was hit by a sequence of small and medium-intensity earthquakes. The seismic sworm consisted of about 50 shocks, with maximum intensity of VI degree on the Mercalli Scale [Martinelli, 1910; Foresta Martin et al., 2011]. According to the Parametric Catalog of Italian Earthquakes [Rovida et al., 2016] the energy released by the main shock of the sequence corresponds to a Richter magnitude of 4.72 ± 0.34. Despite the light magnitude of the earthquakes, officials of Palermo Civil Engineering Office reported extensive damage to the village of Ustica, concentrated in the eastern part of the island, where they recorded slumps and injuries to the buildings [Foresta Martin et al., 2011]. All the earthquakes were recorded only by a small seismoscope placed in the island's meteorological station (Semaforo of Monte Guardia Grande), while no other instruments in nearby Palermo or in other parts of Italy were able to detect these events, due to the fact that the hypocenters were very superficial [Alfani, 1906]. A scientific mission formed by professors T. Zona, G. Di Stefano and M. Gemmellaro, from the University of Palermo, made a careful survey of the Island, without detecting dislocations of land or faults [Foresta Martin et al., 2011].
At that time, was still alive the dismay caused by an earthquake in Calabria that a few months before (September 8, 1905) had caused more than 500 deaths and destroyed some small towns. Moreover, some volcanologists feared the reactivation of the old and dormant Ustica's volcanoes [Alfani, 1906]. Fearing the arrival of a strong and destructive shock also at Ustica, the Prefect of Palermo ordered the evacuation of about 1,000 people and 600 prisoners confined in the island. All that people was transported to Palermo on board civil and military ships. This was the first case of evacuation of a town of the young Italian State. The event was widely reported by media, with comments sometimes exaggerated.
When the emergency ended, while the displaced inhabitants were returning in the island impoverished and deprived of food and other basic necessities, the King of Italy Vittorio Emanuele III and Queen Elena, who were on an official visit to Palermo, unexpectedly landed on the tiny island to encourage the inhabitans and to offer economic support [Foresta Martin et al., 2011].

References

Alfani G., (1906). *Sul terremoto di Ustica*. In: La Nazione, 31 marzo - 1 aprile 1906, Firenze, p.1.
Foresta Martin F., Calcara G., Ailara V., (2011). *Ustica s'inabisserà? Cronistoria della sequenza sismica del 1906 che causò l'abbandono dell'isola*. Centro Studi e Documentazione Isola di Ustica, pp. 196.
Martinelli G., (1910). *La sismicità all'isola di Ustica, il periodo marzo-aprile 1906*. Estratto dagli Annali dell'Ufficio Centrale Meteorologico e Geodinamico, Vol. XXX, I, Roma, 1910.

Rovida A.N., Locati M., Camassi R.D., Lolli B., Gasperini P., (2016). *CPTI15, the 2015 version of the Parametric Catalogue of Italian Earthquakes*. https://emidius.mi.ingv.it/CPTI15-DBMI15/index_en.htm.

The geochemical features of fluids vented over the Calabro-Peloritani area: an area destroyed by several strong earthquakes of the past

P. Bonfanti[1], A. Caracausi[2], F. Italiano[2], P. Randazzo[3]

[1]*Istituto Nazionale di Geofisica e Vulcanologia, Sezione di Catania - Osservatorio Etneo, Italy*
[2]*Istituto Nazionale di Geofisica e Vulcanologia, Sezione di Palermo, Italy*
[3]*Università degli Studi di Palermo, Dipartimento delle Scienze della Terra e del Mare (DiSTeM), Palermo, Italy*

Corresponding Author: *pietro.bonfanti@ingv.it*

The Southern portion of the Apennines, the Calabro-Peloritan Arc (CPA), develops over an area struck by some of the most destructive seismic events ever seen in Europe (e.g. Calabria 1783, 1894, 1905; Messina 1908). The Nebrodi and Peloritani (N-P) mountains are the southern CPA extension stretching E-W along the northern Ionian and Tyrrhenian coast for about 100km. Indeed, its complicated tectonic setting has been satisfactory constrained only in recent times although it is still under investigation.

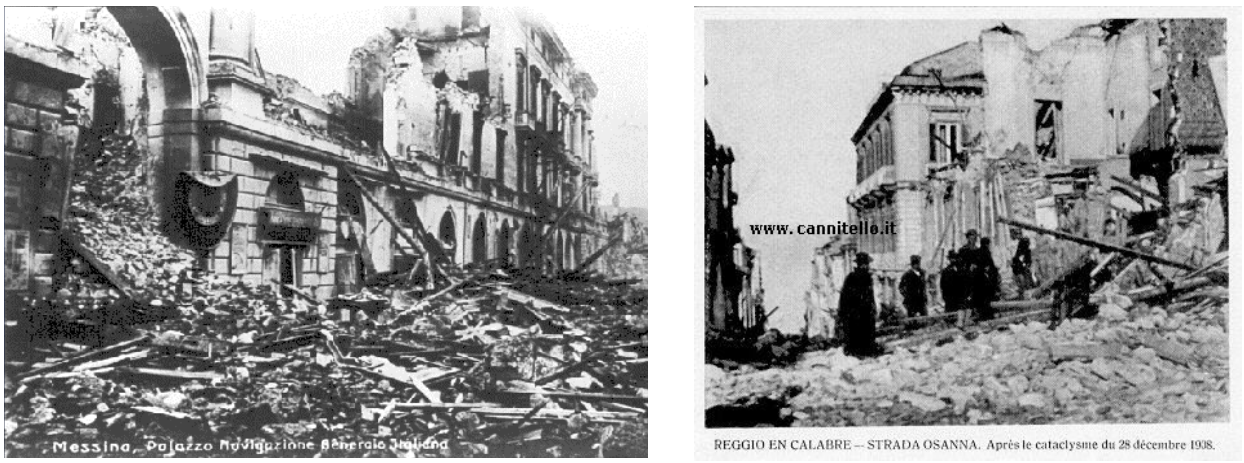

Figure 1 Pictures of the destructions caused by the 1908 M 7.4 earthquake in Messina (Sicily) and Calabria (Reggio Calabria) regions.

It is well known that the occurrence of earthquakes provoke modifications in the natural setting of a seismic area and may induce modifications in the fluid phases, such as decrease/increase of water level in wells, changes in temperature and/or chemical composition of groundwaters, variations in the flow-rate of both water springs and gas discharges, as well as in their chemical and isotopic composition.

A way to approach the wide problem of the fluids geochemistry and the seismogenesis over the areas affected by active tectonics was to collect all the geochemical data having local significance and to evaluate them in a geochemical interpretative model. The presence of thermal springs as well as the degassing occurring the Calabro-Peloritan Arc (CPA) shown by the widespread presence of gases bubbling in thermal waters and in shallow sea waters, is a clue of the close connection of the fluids'

circulation pattern with local tectonic structures [Italiano et al., 2006; 2008ab; 2010; 2019; Bonfanti et al., 2006; 2007].

The venting of geothermal fluids occurs over both the Tyrrhenian and Ionian coast of the CPA, with geothermal anomalies and gas emissions located either over Sicily and Calabria regions.
The geodynamic context of the area deeply influences the composition and the behavior of the fluids in terms of both chemical and isotopic composition. Shallow-originated fluids may mix with fluids coming from different depths of the crust and/or from the upper mantle. The mixings ratios may change with the time due both to seasonal variations and/or to the development of a seismogenic process (stress accumulation, deformation, strain release etc.).

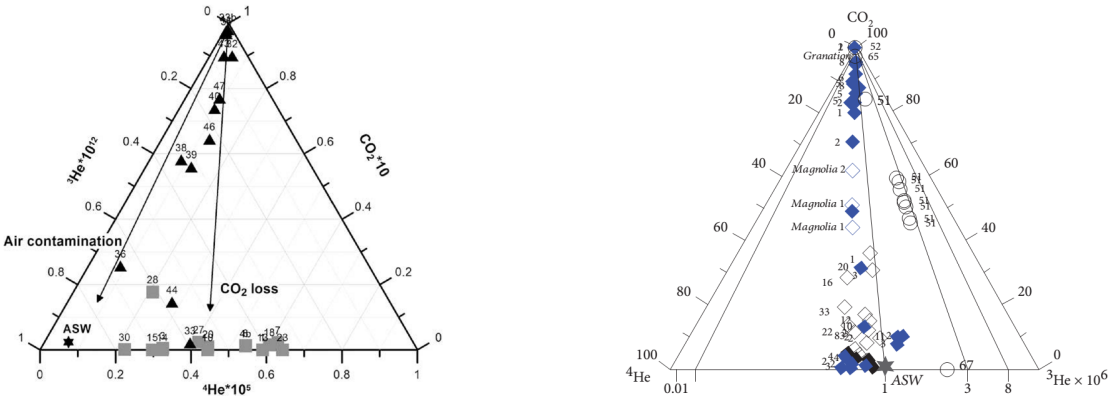

Figure 2 Isotopic composition of helium in fluids vented over the Calabrian (left) and Sicilian (right) sectors of the CPA.

As the fluids have high mobility migrating through fractures and faults, are fast carriers of information on the physico-chemical conditions and to quickly reveal changes in the equilibrium conditions, are able to develop high pore pressures at depth that may reduce the effective frictional strength of rocks, we carried out several geochemical prospections with the aim of collecting the fluids vented over the CPA across the Sicily and Calabria regions besides the evaluation of the natural soil degassing in terms of CO_2 and Rn.

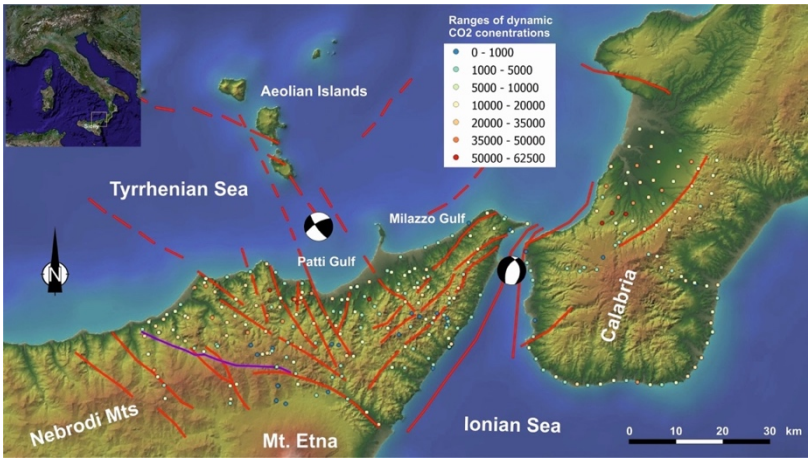

Figure 3 Distribution of the CO_2 dynamic concentration through the soils of the area. The values ranged from 200 to 220000 ppm.

References

Italiano F., Bonfanti P., Maugeri S.R., (2019). *Evidence of Tectonic Control on the Geochemical Features of the Volatiles Vented along the Nebrodi-Peloritani Mts (Southern Apennine Chain, Italy)*. Geofluids, 6250393, doi: https://doi.org/10.1155/2019/6250393.

Italiano F., Bonfanti P., Pizzino L., Quattrocchi F., (2010). *Geochemistry of fluids discharged over the seismic area of Southern Apennine (Calabria region, Southern Italy): implications for Fluids-Faults relationships*. Applied Geochemistry, vol. 25, p. 540-554, doi: 10.1016/j.apgeochem.2010.01.011.

Italiano F., Bonfanti P., Caracausi A., Ditta M., Favara R., Gagliano Candela E., Maugeri R., Nigro F., Renda P., Scaletta C., (2006). *Attività di emissione di fluidi lungo strutture tettoniche: risultati nell'area della Sicilia nord-orientale*. In: 25° Convegno Nazionale del Gruppo Nazionale di Geofisica della Terra Solida, p. 302-305, ISBN: 88-902-101-1-7.

Italiano F., Bonfanti P., Ciaccio C., Gesù M., Piazza G., Romano C., Schiavone S., (2008a). *Degassamento di radon e modifiche del dna della popolazione siciliana: possibili relazioni con il terremoto del 1908*. Miscellanea INGV, 3, 72-73.

Italiano F., Bonfanti P., Maugeri R., (2008b). *Relazioni tra fluidi circolanti e tettonica attiva nel settore meridionale dell'Arco Calabro: uno strumento per la valutazione dei processi sismogenetici*. In: 1908 - 2008 Scienza e Società a 100 anni dal grande Terremoto. Miscellanea INGV, 3, 70-71, Bonfanti P., Caratozzolo C., Caruso C., Ditta M., Italiano F., Maugeri R., Pizzullo S., (2007). *Understanding the relationships between tectonics and circulating fluids: the southern sector of the Calabrian arc*. In: 26° Convegno Nazionale GNGTS.

Bonfanti P., Ditta M., Italiano F., Maugeri S. (2008). *Circulating fluids and tectonics: new data along the Southern Apennine chain*. Geophysical Research Abstracts, vol. 10.

CISAS "International centre of advanced study in environment, ecosystem and human health"

The CISAS working group, Maria Bonsignore, IAS-CNR

Corresponding Author: *maria.bonsignore@ias.cnr.it*

The CISAS project "aims at elucidating the complex phenomena of environmental pollution in highly contaminated industrial, the effects on ecosystem and health of populations living in the surrounding areas.
The project is carried out in areas recognized as "sites of national interest for remediation (Augusta-Priolo, Milazzo-Pace del Mela, Crotone-Cassano-Cerchiara), where a wide spectrum of pollutants and different patterns of contamination of the environment can be found. The link between environment and ecosystem was evaluated through the understanding of the mechanisms modulating the dynamics of contaminants in the environment, starting from the source of emission to the transfer into various environmental matrixes (air, water, soil, sea, sediments, food chain). The use of modern and innovative conceptual tools and the support of geospatial models helped to identify the main pathways of reaction and diffusion of contaminants, the chemical-physical processes regulating their distribution in the environmental as well as their transfer to the ecosystem and the human body. The Project also investigates the molecular mechanisms responsible for the onset of diseases associated with exposure to pollutants using model animal organisms performing in vivo and in vitro experiments. A better understanding of the association among pollutants and selected diseases, specific for each study area, was identified on the basis of available epidemiological knowledge.

In particular, the investigations are focused on: the association between the exposure to organic contaminants and an increased risk for liver diseases (in particular hepatocellular carcinoma) in the Augusta/Priolo area; the association between the exposure to heavy metals and organic compounds and an increased risk of thyroid diseases (in particular malignancies) in Milazzo; the association between exposure to heavy metals and an increased risk of cardiovascular and renal diseases in Crotone.

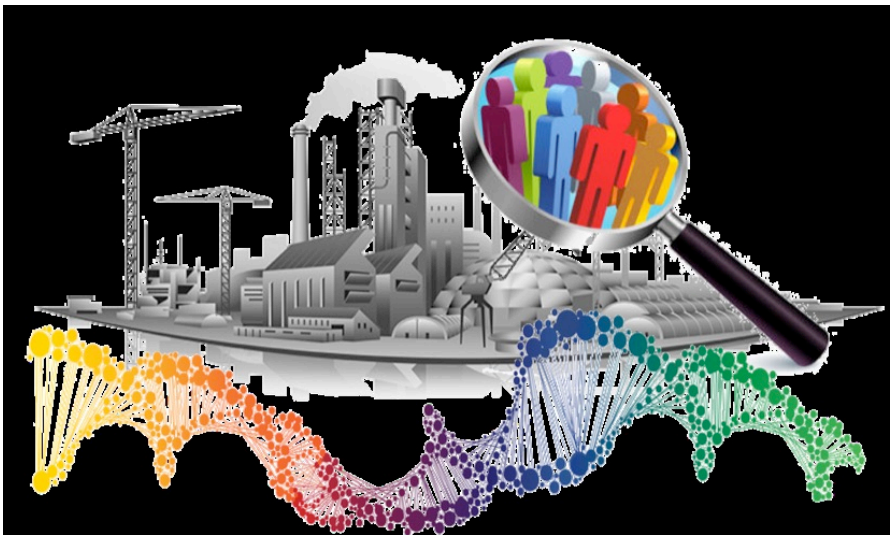

A longitudinal epidemiological study has been planned based on the recruitment of a birth cohort in order to investigate the potential risks associated with lifestyles adopted by pregnant women residing in areas with high environmental impact. The role of the placenta in mediating fetal exposure to environmental toxicants, maternal blood and cord blood, their association with placental physiology, pregnancy outcomes, and pathologies in paediatric age will be investigated. The study will focus on the possible effect of prenatal exposure on numerous health conditions, including respiratory disorders, obesity, cognitive and behavioural disorders, infectious and chronic-degenerative diseases. The project has also the purpose to communicate and disseminate the results and to perform training activities on environment and health. Dissemination and training activities are designed for a large audience (local stakeholders, teachers, students, specialized scientific communities, etc.) and can be found on the CISAS website: www.cisas.cnr.it Project Leader: Department of earth system science and environmental technologies (DSSTTA) of the National Research Council, NRC. Participating NRC Institutes: Institute for the Anthropic impacts and Sustainability in marine Environment, Institute of Clinical Physiology, Institute for the Biomedical Research and Innovation, Institute for Systems Analysis and Computer Science “A. Ruberti”.

QUADERNI di GEOFISICA

ISSN 1590-2595 http://istituto.ingv.it/it/le-collane-editoriali-ingv/quaderni-di-geofisica.html/

I QUADERNI DI GEOFISICA (QUAD. GEOFIS.) accolgono lavori, sia in italiano che in inglese, che diano particolare risalto alla pubblicazione di dati, misure, osservazioni e loro elaborazioni anche preliminari che necessitano di rapida diffusione nella comunità scientifica nazionale ed internazionale. Per questo scopo la pubblicazione on-line è particolarmente utile e fornisce accesso immediato a tutti i possibili utenti. Un Editorial Board multidisciplinare ed un accurato processo di peer-review garantiscono i requisiti di qualità per la pubblicazione dei contributi. I QUADERNI DI GEOFISICA sono presenti in "Emerging Sources Citation Index" di Clarivate Analytics, e in "Open Access Journals" di Scopus.

QUADERNI DI GEOFISICA (QUAD. GEOFIS.) welcome contributions, in Italian and/or in English, with special emphasis on preliminary elaborations of data, measures, and observations that need rapid and widespread diffusion in the scientific community. The on-line publication is particularly useful for this purpose, and a multidisciplinary Editorial Board with an accurate peer-review process provides the quality standard for the publication of the manuscripts. QUADERNI DI GEOFISICA are present in "Emerging Sources Citation Index" of Clarivate Analytics, and in "Open Access Journals" of Scopus.

RAPPORTI TECNICI INGV

ISSN 2039-7941 http://istituto.ingv.it/it/le-collane-editoriali-ingv/rapporti-tecnici-ingv.html/

I RAPPORTI TECNICI INGV (RAPP. TEC. INGV) pubblicano contributi, sia in italiano che in inglese, di tipo tecnologico come manuali, software, applicazioni ed innovazioni di strumentazioni, tecniche di raccolta dati di rilevante interesse tecnico-scientifico. I RAPPORTI TECNICI INGV sono pubblicati esclusivamente on-line per garantire agli autori rapidità di diffusione e agli utenti accesso immediato ai dati pubblicati. Un Editorial Board multidisciplinare ed un accurato processo di peer-review garantiscono i requisiti di qualità per la pubblicazione dei contributi.

RAPPORTI TECNICI INGV (RAPP. TEC. INGV) publish technological contributions (in Italian and/or in English) such as manuals, software, applications and implementations of instruments, and techniques of data collection. RAPPORTI TECNICI INGV are published online to guarantee celerity of diffusion and a prompt access to published data. A multidisciplinary Editorial Board and an accurate peer-review process provide the quality standard for the publication of the contributions.

MISCELLANEA INGV

ISSN 2039-6651 http://istituto.ingv.it/it/le-collane-editoriali-ingv/miscellanea-ingv.html

MISCELLANEA INGV (MISC. INGV) favorisce la pubblicazione di contributi scientifici riguardanti le attività svolte dall'INGV. In particolare, MISCELLANEA INGV raccoglie reports di progetti scientifici, proceedings di convegni, manuali, monografie di rilevante interesse, raccolte di articoli, ecc. La pubblicazione è esclusivamente on-line, completamente gratuita e garantisce tempi rapidi e grande diffusione sul web. L'Editorial Board INGV, grazie al suo carattere multidisciplinare, assicura i requisiti di qualità per la pubblicazione dei contributi sottomessi.

MISCELLANEA INGV (MISC. INGV) favours the publication of scientific contributions regarding the main activities carried out at INGV. In particular, MISCELLANEA INGV gathers reports of scientific projects, proceedings of meetings, manuals, relevant monographs, collections of articles etc. The journal is published online to guarantee celerity of diffusion on the internet. A multidisciplinary Editorial Board and an accurate peer-review process provide the quality standard for the publication of the contributions.

Coordinamento editoriale e impaginazione
Francesca DI STEFANO, Rossella CELI
Istituto Nazionale di Geofisica e Vulcanologia

Progetto grafico e impaginazione
Barbara ANGIONI
Istituto Nazionale di Geofisica e Vulcanologia

Istituto Nazionale di Geofisica e Vulcanologia
Via di Vigna Murata, 605
00143 Roma
tel. +39 06518601

www.ingv.it

ISTITUTO NAZIONALE DI GEOFISICA E VULCANOLOGIA